PROBLEMS IN NONLINEAR HOMOGENIZATION: BOUNDS, ESTIMATES, MACROSCOPIC INSTABILITIES, AND POST-BIFURCATION RESPONSE

Joshua Robert Furer

A DISSERTATION

in

Applied Mathematics and Computational Science

Presented to the Faculties of the University of Pennsylvania in Partial Fulfillment of the Requirements for the Degree of Doctor of Philosophy

2019

Supervisor of Dissertation

Pedro Ponte Castañeda, Raymond S. Markowitz Faculty Fellow and Professor of Mechanical Engineering and Applied Mechanics

Graduate Group Chairperson

Pedro Ponte Castañeda, Raymond S. Markowitz Faculty Fellow and Professor of Mechanical Engineering and Applied Mechanics

Dissertation Committee:
John L. Bassani, Richard H. and S.L. Gabel Professor of Mechanical Engineering and Applied Mechanics and Professor of Materials Science Engineering
Charles L. Epstein, Thomas A. Scott Professor of Mathematics

Acknowledgments

I would like to first thank my advisor, Dr. Ponte Castañeda. Through his mentoring, I have become a better researcher and mathematician, and have learned skills that I will carry with me for years to come. I am truly grateful for all that he has done for me, and thank him for guiding me to this point.

I would also like to thank Dr. Epstein and Dr. Bassani for serving on my thesis committee. Moreover, I would like to specifically thank Dr. Epstein, who when serving as the head of my graduate group in Applied Mathematics, gave me the opportunity to come study at UPenn. For that, I am exceedingly grateful.

I would like to thank my lab mates, Jose Cotelo, Christoph Kammer, and Shruvangsu Das for their time spent discussing our work, among other things, their support, but most importantly, their friendship.

I want to thank Paul and Sharon for their continuing encouragement, and I am forever grateful to Paul, Harry, Julie, Neve, and Asher for their constant support. A special thank to RS for always encouraging me to "hit the send button."

I can never express in words how grateful I am to have my mother and father always by my side. This journey would not have been possible without them. I thank them for unconditional love, and for always showing me by example how to be a better person.

Last but certainly not least, I want to thank my best friend, the love of my life, my wife Nicole. Her support has been unwavering, and her encouragement relentless. I would not have arrived at this point without her, and I count myself lucky to get to spend the rest of my life with her.

ABSTRACT

PROBLEMS IN NONLINEAR HOMOGENIZATION: BOUNDS, ESTIMATES, MACROSCOPIC INSTABILITIES, AND POST-BIFURCATION RESPONSE

Joshua Robert Furer
Pedro Ponte Castañeda

Due to the ever-growing interest in composite materials designed with complex microstructures and capable of possessing exotic properties, it has become increasingly important to be able to accurately capture the interplay between the macroscopic response and the underlying microstructure, as the former is greatly influenced by the latter. Of the different approaches available, this thesis is concerned with the use of nonlinear homogenization to study the effective response of composites. We look to illustrate the effect that constitutive assumptions have on the methods by which such estimates can be obtained, and on the actual effective, or homogenized, response of the material. For materials whose constitutive response is governed by *convex* functions, we show how the convexity itself can be utilized to obtain rigorous bounds and improved estimates. We prove the optimality of variational linear comparison bounds over the class of nonlinear anisotropic composites with linearly isotropic response and introduce a new symmetric fully optimized second-order method which is able to generate estimates for the effective response of nonlinear composites. On the other hand, convexity is often inconsistent with certain physical requirements (e.g. objectivity). Such is the case of hyperelasticity, where the lack of convexity of the stored-energy functions has long been known to lead to the development of instabilities. We present a framework for studying the post-bifurcation response of such systems and apply it to a specific class of reinforced hyperelastic composites under general three-dimensional loading conditions. We also consider the class of magneto-elastic composites, which consist of hyperelastic materials that are also magnetically susceptible. Unlike in the case of hyperelasticity, there lacks a complete mathematical framework for obtaining the effective response of such materials, and researchers have only begun to investigate the potential for instabilities in these materials. We therefore generalize the same methodology used successfully in the purely mechanical context to study the post-bifurcation behavior of magneto-elastic composites. This in part requires a rigorous generalization of the theoretical aspects that underlie the

method. We then calculate the post-bifurcation response of a magneto-elastic material under general plane-strain loading conditions with a magnetic field applied in the plane of deformation.

Contents

List of Tables

List of Figures

Chapter 1
Introduction

This thesis looks to answer questions that arise in the field of nonlinear homogenization. Specifically, we look to see how assumptions on the constitutive behavior of the underlying homogeneous phases effect both the ability to obtain bounds and estimates on the effective, or homogenized, response of composites, as well as their effect on the homogenized response itself. The problem of obtaining the effective response of composite material is most often placed in a variational setting, whereby one looks to minimize an energy functional over some set of admissible trial fields that satisfy the relevant boundary conditions. For example, in looking for the effective conductivity of a system, one minimizes the energy over all electric field potentials, while in defining the effective elasticity modulus tensor, one would minimize over all displacement fields.

In describing systems from a variational point of view, solutions are often found by solving a set of equilibrium equations which are obtained from the Euler-Lagrange equations of the corresponding energy functionals. Thus arises the major difficulty in obtaining exact solutions to (non)linear homogenization problems: as the underlying system is heterogeneous, one must solve a system of (non)linear partial differential equations with rapidly oscillating, and in some cases random, coefficients. For this reason, there has be a great deal of emphasis put on obtaining bounds and estimates

on the effective behavior of composite materials.

Many of the tools used in the nonlinear context can be traced back to results that were first obtained in the linear setting. Perhaps one of the most well known, and important, results used to bound linear heterogenous materials is the so called Hashin-Shtrikman variational principle. The basic idea is to introduce a *homogeneous* reference material, and then define the polarization as the difference between the field in the heterogeneous medium and the field in the homogeneous reference medium. One is then left to solve two boundary value problems; the first is associated with the reference medium. The second involves the polarizations, whose divergence is treated as the body force. By making use of the appropriate Green's functions, Hashin and Shtrikman (1962) were able to obtain rigorous upper and lower bounds on the effective magnetic response of random multiphase heterogeneous composites; they later extended their work to bound the response of mechanical systems (Hashin and Shtrikman, 1963).

That this variational procedure is able to produce upper and lower bounds is a consequence of the freedom one has in choosing the reference medium. We also note that bounds for material with more general two-point statistics (other than ones which are isotropic, as assumed by Hashin and Shtrikman (1962)), were developed by Willis (1977). Moreover, in this work, Willis (1977) showed how the Hashin-Shtrikman variational principle could be used to obtain the so called self-consistent estimates by choosing the reference medium to be the effective material itself; the self-consistent estimates were originally proposed by Hill (1965). In looking to use more information about the underlying microstructure, Beran (1965) generalized of the Hashin-Shtrikman variational principle to obtain bounds that make use of three-point statistics of the microstructure. The three-point bounds of Beran were later simplified by Milton (1981) through the introduction of a geometric parameter (see also Milton and Phan-Thien, 1981; Torquato, 1980, 1991).

Simultaneously, the problem of obtaining the effective response of composite ma-

terials was taken up in the mathematics community. Spagnolo (1968) introduced $G-$ convergence, while Tartar (1978) (see also Murat and Tartar, 1985) provided a framework for the related $H-$ convergence, both of which allow for a rigorous mathematical definition of the effective elasticity tensor. The books of Sanchez-Palencia (1980) and Bensoussan et al. (1978) contain general results pertaining to periodic homogenization, and a complete accounting of the available method for obtaining bounds and estimates in the linear context can be found in the monograph of Milton (2002a).

There has been much success in generalizing the classic linear bounds and estimates to the nonlinear setting. Talbot and Willis (1985) first introduced a variational principle related to that of Hashin and Shktriman which was suitable for nonlinear composites. These bounds were later improved by Ponte Castañeda (1991), who made use of a variational principle for the properties of a linear comparison composite. These bounds were later generalized by Talbot and Willis (1992), and bounds for power-law materials were independently obtained by Suquet (1993). Many of these works rely either implicitly, or explicitly, on the fact that the energy potentials of the constitutive phases are *convex*, whereby solutions to the variational problems at hand exist, and can be unique. In fact, Marcellini (1978) showed that when the potentials are strictly convex, the effective response of a nonlinear periodic composite can be obtained exactly by considering the solution to the so called unit cell problem.

However, such convexity assumptions can be physically inconsistent. This is indeed the case in elastic materials at finite strain, where both objectivity, as well as incompressibility, necessitate the need for non-convex a constitutive response. The mathematical implications on existence of solutions to variational problems in the non-convex setting are well understood, with the seminal work of Ball (1977) providing a necessary and sufficient condition for the existence to such variational problems in hyperelasticity; the condition, know as *quasiconvexity*, was first introduced by Morrey Jr. (1952). In order to define the effective response of hyperelastic compos-

ites with periodic microstructures, Müller (1987) and Braides (1985) provided results that made use of the notion of $\Gamma-$ convergence, as introduced by De Giorgi (1975). These results showed that in order to properly calculate the effective response of the composite, it was necessary to consider solutions that are periodic on not just the unit cell (as is the case when the potentials are convex (Marcellini, 1978)), but on all possible combinations of cells. As these results are difficult to implement in practice, bounds and estimates in the setting on nonlinear hyperelasticity have been developed as well (Ponte Castañeda and Tiberio, 2000; deBotton, 2005; Lopez-Pamies and Ponte Castañeda, 2006a,b; Ponte Castañeda, 1989).

A consequence of the lack of convexity of the energy potentials is that solutions may fail to be unique. In particular, the composite material may undergo an instability. Such a possibility has been known for many years, and can lead to microbuckling, as discussed by Rosen (1965). However, the wavelength of the instability, relative to the size of the unit cell, need not be finite, and indeed, in consider laminated hyperelastic composites, Triantafyllidis and Maker (1985) found that instabilities may have infinite wavelength, and that these macroscopic instabilities can occur prior to the microscopic ones. These results were later confirmed by Geymonat et al. (1993), who considered more general hyperelastic composites, and showed that the onset of macroscopic instabilities can be estimated by the loss of strong ellipticity of the principal solution, i.e. the solution before the onset of an instability. Less work has been done to understand the post-bifurcation response of these and related systems, but there are examples of works in which researchers look for ways to understand, and take advantage of, the potential non-uniqueness (Avazmohammadi and Ponte Castañeda, 2016; DeSimone and Dolzmann, 2002).

More recently, there has been an effort to extend the framework that exists for studying hyperelastic composites to magneto-elastic systems, those where (at least) one of the underlying hyperelastic phases is magnetically susceptible. These materials are of great interest due to their ability to undergo large strains and exhibit magneto-

elastic effects, making them useful in many practical applications. Some models used to predict the behavior of magneto-elastic composites are based experimental observations (Dorfmann and Ogden, 2004; Kankanala and Triantafyllidis, 2004; Danas et al., 2012), while other are based on directly on the use of homogenization. In particular Ponte Castañeda and Galipeau (2011) provided a general framework for estimating the effective response of magneto-elastic systems with *random* microstructures. In terms of unstable behavior, due to the fact that the underlying purely mechanical system can undergo an instability, it is reasonable to assume that the more general magneto-elastic composites will as well. Indeed, results of Kankanala and Triantafyllidis (2004) as well as those of Destrade and Ogden (2011) indicate that magneto-elastic composites can undergo instabilities (see also Rudykh and Bertoldi, 2013; Galipeau and Ponte Castañeda, 2013). Nonetheless, there still lacks a rigorous mathematical theory akin to what exists in the purely mechanical context (e.g. Müller, 1987) for computing the effective response of magneto-elastic composites, and people are only recently beginning to probe the possible utility of theses systems in their post-bifurcation state.

We look to address problems that arise in each of the aforementioned areas. As such, the rest of the thesis will be organized as follows. In Chapter 2-Chapter 3, we start first with the problem of obtaining bounds on the effective behavior of nonlinear materials. In particular, these chapters deals with the variational linear comparison method (VLC) due to Ponte Castañeda (1992b), one which makes explicit use of the convexity of the energy potentials in order to obtain bounds on the nonlinear response by appealing to a suitably chosen, fictitious, linear comparison composite (LCC). By bounding the *linear* behavior of the LCC using the Hashin-Shtrikman estimates, Ponte Castañeda (1992b) obtained the variational bounds of the Hashin-Shtrikman type (VHS), which are known to be rigorous bounds on the class of composites with isotropic phases and statistically isotropic microstructures. While it has long been suspected that these bounds are not optimal, in that they are not attained by a mem-

ber of this case, we show that these bounds are optimal when viewed as bounds on the class of nonlinear anisotropic composites with linearly *isotropic* response. This is achieved by appealing to finite-rank laminates, a the special class of microstructure for which the effective nonlinear response can be computed exactly. We show optimality in the context of two- and three-dimensional dielectrics, as well as two-dimensional incompressible nonlinear elasticity in Chapter 2, and in the context of porous viscoplasticity under general plane-strain loading conditions in Chapter 3. The results of these chapter indicate why the VHS bounds are not tighter when compared to estimates for the effective behavior of nonlinear composites with statistically isotropic microstructures, and yield important insight into what can be done to improve them.

One major drawback of the VHS bounds lies in the fact that they do not, explicitly, make use of all available information of the fields of the LCC. In Chapter 4, we introduce a method that looks to remedy this in order to produce improved estimates on the effective response of nonlinear composites. This symmetric, fully optimized second-order method, or the symmetric FO-SO, provides an alternate formulation of the recently proposed (nonsymmetric) FO-SO, both of which are based on a stationary variational principal. By introducing a polarization field, this method is able to capture information on both the first, and second moments of the corresponding fields, and can moreover estimate the response of the nonlinear composite directly from the behavior of the optimally chosen LCC. Both FO-SO methods are fully optimal with respect to the trial fields, and the symmetric FO-SO is able to provide more robust results. The method is applied to the class of two-phase power-law composites with fibrous microstructures subjected to plane strain loading and compared with other available bounds and estimates.

The FO-SO method featured in Chapter 4 is derived in the context of nonlinear infinitesimal elasticity, in which case the energy potentials are convex. However, as mentioned above, convexity is often incompatible with certain physical requirements. This is indeed the case in finite-strain hyperelasticity, where it is of interest to under-

stand how this lack of convexity effects the overall stability of hyperelastic composites. While it has long been known that such hyperelastic composites can undergo instabilities and bifurcate to lower energy solutions, there is less of an understanding of the post-bifurcation behavior. To that end, Chapter 5 introduces the mathematical underpinnings needed to investigate both the stability, and post-bifurcation response, of hyperelastic composites. Much of the theory laid out in this chapter will be used extensively in Chapters 6 and 7, where the post-bifurcation response of a model hyperelastic composite is computed explicitly.

While the framework outlined in Chapter 4 can be extended to obtain estimates for such nonlinear hyperelastic composites, the implementation of the FO-SO method to this setting is expected to be more difficult, due in part to complications that arise on account of objectivity. Moreover, the method for obtaining the post-bifurcation behavior, or relaxation, as given by $\widetilde{W}$ requires a (semi-)analytical expression for the principal solution $\widehat{W}$, i.e. the solution before the onset of an instability. Before the onset of an instability, $\widetilde{W} = \widehat{W}$, while afterwards, $\widetilde{W} \leqslant \widehat{W}$. With this in mind, we instead choose to investigate the the post-bifurcation response of a hyperelastic laminate, consisting of two isotropic incompressible neo-Hookean phases. Like in linear elasticity, the principal solution of a nonlinear hyperelastic laminate can be computed exactly, and we make use of such available analytical results. As such, the post-bifurcation behavior of the neo-Hookean laminate is obtained for plane-strain loading conditions in Chapter 6, and then generalized to three-dimensional loading conditions in Chapter 7. In each case, the quasiconvexification $Q\widehat{W}$ of the principal solution is computed by first calculating the the rank-one convex envelope $R\widehat{W}$, and then showing that it is polyconvex. As $\widetilde{W}$ is quasiconvex, and satisfies $\widetilde{W} \leqslant \widehat{W}$, the quasiconvexification will provide us with at least a tighter upper bound on $\widetilde{W}$ than the one given by $\widehat{W}$, whereby $\widetilde{W} \leqslant Q\widehat{W} \leqslant \widehat{W}$; the possible equality between $\widetilde{W}$ and $Q\widehat{W}$ is discussed within the chapters. Such a calculation reveals that, upon sufficient compression of the stiffer layer, the laminate undergoes a macroscopic instability, and

the relaxation is obtained via the formation of "lamellar" domains. In plane-strain, a single lamination is needed, while more generally, certain loading conditions (like axisymmetric extension) lead to a laminate-within-a-laminate microstructure.

With a better understanding of the post-bifurcation behavior of hyperelastic composites under purely mechanical loading, we conclude this thesis by turning our attention to magneto-elastic composites. In Chapter 8, we revisit the theory outlined in Chapter 4, and look to generalize it to the setting of magneto-elasticity. Indeed, results similar to those in the purely mechanical case are proven in Chapter 8, and a rigorous extension of periodic homogenization is introduced and discussed. While some of the extensions are rather straightforward, the magneto-elastic notion of rank-one convexity is novel, and crucial in allowing for the calculation of the post-bifurcation response. The tools developed in Chapter 8 are then applied in Chapter 9 to the same laminated microstructure used in previous chapters, where we now assume that the homogenous phases are magnetically susceptible. Due to the complexity of the calculation, we are unable to implement our methodology directly, and instead derive bounds on the $Q\widehat{W}$. For some loading conditions, $Q\widehat{W}$ can be obtained analytically, and more generally, we find that $R\widehat{W}$ provides an accurate approximation of $Q\widehat{W}$. Upon studying $R\widehat{W}$, it is found that, while purely mechanical compression is still a mechanism for instabilities, magneto-elastic coupling can also lead to compression, whereby properly aligned magnetic fields will also cause instabilities. Like in the purely mechanical case, unstable loading conditions are accommodated via the formation of domains.

While this thesis aims to tell a complete story, we mention that each chapter is self-contained, and corresponds to one of various projects worked on over a period of time. Each chapter contains a fuller introduction to the relevant topics, as well as concluding remarks that give a full representation of the results found therein. Nonetheless, in Chapter 10, we will summarize the findings of the thesis as a whole, and discuss the possible avenues for future research that arise as a result of the work

undertaken here. Before proceeding, we provide a reference to connect each chapter to the various works that have been published or are in preparation as a result of this research.

Chapters	**Publication**
Chapter 2	Furer, J., and Ponte Castañeda, P. *"On the Optimality of Nonlinear Variational Bounds of the Hashin-Shtrikman Type."* In preparation
Chapter 3	Furer, J., and Ponte Castañeda, P. *"Optimal Bounds for Porous Viscoplastic Nonlinear Composites."* In preparation
Chapter 4	Furer, J. and Ponte Castañeda, P. *"A Symmetric Fully Optimized Second-Order Method for Nonlinear Homogenization."* Zeitschrift f ur Angewandte Mathematik und Mechanik, **98**, 222-254, 2018
Chapters 5 and 6	Furer, J. and Ponte Castañeda, P. *"Macroscopic Instabilities and Domain Formation in Neo-Hookean Laminates."* Journal of the Mechanics and Physics of Solids, **118**, 94-114, 2018.
Chapters 5 and 7	Furer, J. and Ponte Castañeda, P. *"Reinforced Elastomers: Homogenization, macroscopic stability, and relaxation."* Journal of the Mechanics and Physics of Solids, available online, 2019
Chapter 8	Furer, J. and Ponte Castañeda, P. *"Theoretical Aspects of Periodic Homogenization and Post-Bifurcation Analysis for Magneto-Elastic Systems."* In preparation
Chapter 9	Furer, J. and Ponte Castañeda, P. *"Instabilities and the Post-Bifurcation Response of Magneto-Active Elastomers."* In preparation
Appendix A	Furer, J. and Ponte Castañeda, P. *"An exact result for the weakly nonlinear composite cylinder assemblage."* In preparation

Chapter 2

Optimality of Nonlinear Variational Bounds in Nonlinear Dielectrics and Plane-Strain Incompressible Elasticity

Abstract

In this chapter, we look to address the optimality of the nonlinear variational bounds of the Hashin-Shtrikman type (Willis, 1989; Ponte Castañeda, 1992b). These results are known to provide rigorous bounds on the effective behavior of the class of nonlinear composites with statistically isotropic microstructures, but it has long been suspected that they fail to be optimal in the sense that they are not attained by any member of this class. By using this linear comparison variational method, together with the translations bounds of Lurie and Cherkaev (1984) (see also Lurie and Cherkaev, 1986; Milton and Kohn, 1988; Murat and Tartar, 1985), we extend the bounds to the larger class of *anisotropic* nonlinear composites with linearly *isotropic* response. Then by making use of finite-rank laminates, we show that these bounds are in fact optimal. In doing so, it becomes clear that the inclusions of such "undesirable" microstructures prohibits the nonlinear variational bounds from providing tighter results when applied to composites with statistically isotropic microstructures. Moreover, we gain useful insight into what must be changed in the variational formulation in order to obtain better bounds.

2.1 Introduction

The study of the effective behavior of heterogeneous materials has long driven research in the engineering and mathematical communities. Most of the early work was concerned with describing the behavior of linear systems, while more recently, methods have been developed that leverage these linear results to better understand nonlinear systems. Due to the difficulty in finding exact results, even for linear systems, much of the focus has been placed on obtaining bounds and estimates on the effective response of certain classes of microstructures. Once a bound has been obtained, it is also important to assess the sharpness, or optimality, of the bound; in particular, the bound will be optimal for the class in question if there exists a member of the class that attains the bound.

Many methods for obtaining bounds on the effective response of random linear media have been developed by appealing to the variational definition of the effective potential energy. One of the main differences between these various results is the amount of statistical information of the microstructure that is utilized. For example, the seminal works of Hashin and Shtrikman (1962, 1963) produce results that depend on the first and second-order statistics of the microstructure, i.e. the volume fraction of the constituent phases and the two-point geometric correlations, respectively. Generalizations of the HS variational principle for microstructures with more general two-point statistics were first proposed by Willis (1977). In contrast, the bounds of Beran (1965), which were given a simpler form in terms of a geometric parameter by Milton (1981), make use of three-point statistics (see also Torquato, 1980, 1991). Other, more technical methods have been proposed to obtain bounds for general anisotropic composites. Such works include those of Francfort and Murat (1986) and Tartar (1985), who made use of the notion of compensated compactness, as well as the related works of Lurie and Cherkaev (1984, 1986), Milton and Kohn (1988) and Murat and Tartar (1985) using the translation method. In each case, optimality has

also been investigated. It is well known that the HS bounds for the shear and bulk moduli of a two-phase well-ordered composite can be attained by finite-rank laminates (Francfort and Murat, 1986), while the HS bounds for the effective conductivity (or transverse conductivity in two dimensions) can be attained by a composite sphere (or cylinder) assemblage, as introduced by Hashin and Shtrikman (1962). It should also be recalled that the effective bulk moduli can also be attained by a composite sphere assemblage (Hashin, 1962). The bounds obtained via the translation method, later generalized by Milton and Kohn (1988) and referred to as the "trace bounds," have been shown to be optimal (Grabovsky, 1993), with attainment by sequential laminates (Lurie and Cherkaev, 1984, 1986), or coated ellipsoidal assemblages (Murat and Tartar, 1985). For a more complete accounting of current results in bounding the effective response of linear composites, we refer the reader to the monograph of Milton (2002a).

Many efforts have been made to extend the linear results to the nonlinear setting. Willis (1986) and Talbot and Willis (1985) used a generalization of the HS variational principle to obtain bounds for nonlinear composites with ellipsoidal microstructures. Generalizations of the translation method in the nonlinear context have also been used successfully (Nesi et al., 1999; Peigney and Peigney, 2017). Checking the optimality of these nonlinear bounds remains a difficult problem, due in large part to the absence of exact solutions for the effective behavior of such nonlinear composites.

In this work, we focus on the nonlinear variational method of Ponte Castañeda (1992b) for nonlinear dielectrics, (as well as Ponte Castañeda, 1991, in the context of nonlinear elasticity), which can be used to obtain bounds on the effective response of nonlinear composites by instead determining the effective behavior of a suitably chosen linear comparison composite (LCC), for which bounds and estimates are readily available. In turn, the variational method extends the bounds on a given class of *linear* heterogeneous materials with specific microstructures to the class of *nonlinear* heterogeneous materials with the same microstructures. These microstructures, as

mentioned above, are usually described in terms of available statistical information, such as the volume fractions of the phases or two-point statistics. The advantage of this variational linear comparison method (VLC) over other nonlinear variational methods (e.g. Talbot and Willis, 1985) is that it can be used in conjunction with any bound on the LCC, and is therefore applicable to more general classes of microstructures.

Our main goal is to show the optimality of the variational bounds for a certain class of microstructures. As such, the rest of the chapter will be organized as follows. Section 2.2 introduces the basic concepts of effective behavior, both in the context of nonlinear dielectrics and nonlinear elasticity. Section 2.3 describes the class of microstructures known as finite-rank laminates, and describes how they can produce composites with linearly isotropic response; it is these microstructures that will be used later to show optimality. Section 2.4 describes the nonlinear variational bounds of Ponte Castañeda (1992b). Finally Section 2.5 shows how the nonlinear variational bounds of the Hashin-Shtrikman type (VHS) can be interpreted as bounds on the class of anisotropic nonlinear composites with linearly isotropic behavior, and exhibits their optimality over this larger class.

We close this section by introducing the notation that will be used throughout this work. The real $d-$dimensional space is denoted by $\mathbb{R}^d$, with the scalar product $\mathbf{u}\cdot\mathbf{v}$, and norm $|\mathbf{u}|^2 = \mathbf{u}\cdot\mathbf{u}$. We denote the set of $d\times d$ tensors by Lin, and endow it with the usual inner product $\boldsymbol{A}\cdot\boldsymbol{B} = \mathrm{tr}(\boldsymbol{A}\boldsymbol{B}^T)$, and norm $\|\boldsymbol{A}\|^2 = \boldsymbol{A}\cdot\boldsymbol{A}$. The second-order identity tensor will be denoted by $\mathbf{I}$. We fix the standard Cartesian basis $\{\mathbf{e}_i\}$, with respect to which vectors with Cartesian components b_i are represented by bold letters $\mathbf{b}$, while second-order tensors with Cartesian components A_{ij} are represented by bold italic letters $\boldsymbol{A}$. Here i,j,k,l range from 1 to d. Given two vectors $\mathbf{a},\mathbf{b}$, the dyadic product $\mathbf{a}\otimes\mathbf{b}$ is defined to be the second-order tensor with Cartesian components a_ib_j, while the symmetric dyadic product is defined by the second-order tensor $\mathbf{a}\otimes_s\mathbf{b} = \frac{1}{2}(\mathbf{a}\otimes\mathbf{b}+\mathbf{b}\otimes\mathbf{a})$. Throughout this work, the primary variables of

interest will be the electric field $\mathbf{E}$, as well as the strain $\boldsymbol{\varepsilon}$. We denote the magnitude of the electric field by $E = |\mathbf{E}|$. On the other hand, we consider the commonly used strain invariants ε_e and ε_m to describe $\boldsymbol{\varepsilon}$. Here $\varepsilon_e = \sqrt{(2/3)\boldsymbol{\varepsilon}_d \cdot \boldsymbol{\varepsilon}_d}$ is the equivalent strain, where $\boldsymbol{\varepsilon}_d = \boldsymbol{\varepsilon} - \varepsilon_m \mathbf{I}$ is the strain deviator, while $\varepsilon_m = \frac{\mathrm{tr}(\boldsymbol{\varepsilon})}{d}$ denotes the mean strain.

2.2 Effective Behavior

In what follows, we consider a $2-$phase composite occupying some region denoted by Ω, which has been chosen as a representative volume element (RVE). We assume that each phase is isotropic, and occupies a region $\Omega^{(r)} \subset \Omega$. We take $\chi^{(r)}$ to be the characteristic function of phase r, so that $\chi^{(r)}(\mathbf{x}) = 1$ when $\mathbf{x}$ is in phase r, and 0 otherwise, and assume that $\chi^{(r)}$ varies on a scale much smaller than that of the material sample. In such a way, we can look to define the effective properties of the material by taking the limit as this scale of variation vanishes; in this case, the composite can be described as a homogenous material. We define the effective properties first in the context of nonlinear dielectrics, and then in the setting of nonlinear elasticity. Although not detailed here, some knowledge of the basics of electro- and elastostatic theory is assumed.

2.2.1 Nonlinear Dielectrics

To formulate the problem at hand, we assume that each phase is characterized by a nonlinear, strictly convex potential $w^{(r)} = w^{(r)}(\mathbf{E})$. The electric displacement field in phase r is given by the constitutive equation

$$\mathbf{D} = \frac{\partial w^{(r)}}{\partial \mathbf{E}}. \tag{2.2.1}$$

If the phases are isotropic, whereby $w^{(r)}(\mathbf{E}) = \phi^{(r)}(E)$, then Eq. (2.2.1) can be written as

$$\mathbf{D} = \epsilon_s^{(r)}(E)\mathbf{E}, \tag{2.2.2}$$

where $\epsilon_s^{(r)}(E)$ is the corresponding secant dielectric coefficient given by

$$\epsilon_s^{(r)}(E) = \frac{\partial \phi^{(r)}(E)}{\partial E}\frac{1}{E}. \tag{2.2.3}$$

The local behavior of the system is described by the energy-density function

$$w(\mathbf{x}, \mathbf{E}) = \sum_{r=1}^{2} \chi^{(r)}(\mathbf{x}) w^{(r)}(\mathbf{E}). \tag{2.2.4}$$

We let $\langle \cdot \rangle$ and $\langle \cdot \rangle^{(r)}$ denote the volume averages over Ω and $\Omega^{(r)}$, respectively, so that

$$\langle w(\mathbf{x}, \mathbf{E}) \rangle = \sum_{r=1}^{2} c^{(r)} \langle w^{(r)}(\mathbf{E}) \rangle^{(r)}, \tag{2.2.5}$$

where $c^{(r)} = \langle \chi^{(r)} \rangle$ represents the volume fraction of phase r.

Following Hill (1963) we define the effective potential

$$\widetilde{w}(\overline{\mathbf{E}}) = \min_{\mathbf{E} \in \mathcal{K}(\overline{\mathbf{E}})} \langle w(\mathbf{x}, \mathbf{E}(\mathbf{x})) \rangle, \tag{2.2.6}$$

where

$$\mathcal{K}(\overline{\mathbf{E}}) = \{\mathbf{E} \,:\, \mathbf{E} = -\nabla \Phi, \text{ in } \Omega, \quad \text{and } \Phi = -\overline{\mathbf{E}} \cdot \mathbf{x}, \text{ on } \partial\Omega\} \tag{2.2.7}$$

denotes the set of admissible electric field potentials. It can then be shown that the average electric displacement field $\overline{\mathbf{D}} = \langle \mathbf{D} \rangle$ is related to the average electric field $\overline{\mathbf{E}} = \langle \mathbf{E} \rangle$ by the effective constitutive relation

$$\overline{\mathbf{D}} = \frac{\partial \widetilde{w}}{\partial \overline{\mathbf{E}}}. \tag{2.2.8}$$

2.2.2 Nonlinear Elasticity

Things become a bit more complicated in elasticity, as the primary variables, the strain $\boldsymbol{\varepsilon}$ and stress $\boldsymbol{\sigma}$, are tensorial quantities. Nonetheless, we assume that each phase is characterized by a nonlinear, strictly convex strain potential $W^{(r)} = W^{(r)}(\boldsymbol{\varepsilon})$. The stress in phase r is given by the constitutive equation

$$\boldsymbol{\sigma}^{(r)} = \frac{\partial W^{(r)}}{\partial \boldsymbol{\varepsilon}}. \tag{2.2.9}$$

In modeling material with isotropic phases, $W^{(r)}$ is often taken of the form

$$W^{(r)}(\boldsymbol{\varepsilon}) = \varphi^{(r)}(\varepsilon_e) + \frac{d^2}{2}\kappa^{(r)}\varepsilon_m^2 \quad r = 1, 2, \tag{2.2.10}$$

where here, we assume that $\varphi^{(r)}$ satisfies the square-concavity hypothesis for $r = 1, 2$. In principle, isotropy of the phases implies that $W^{(r)}$ is a function of d invariants in d dimensions. It is often commonplace to disregard the dependence of $W^{(r)}$ on $\det \boldsymbol{\varepsilon}$, and moreover, we will only be dealing with two-dimensional elasticity in what follows, and as such, it suffices to consider potentials of the form in Eq. (2.2.10) that depend only on 2 invariants. With such a potential, the constitutive relation can be written as

$$\boldsymbol{\sigma}^{(r)} = 2\mu_s^{(r)}(\varepsilon_e)\boldsymbol{\varepsilon}_d + d\kappa^{(r)}\varepsilon_m \mathbf{I}, \tag{2.2.11}$$

where $\mu_s^{(r)}(\varepsilon_e)$ is the secant modulus defined by

$$\mu_s^{(r)}(\varepsilon_e) = \frac{\partial \varphi^{(r)}(\varepsilon_e)}{\partial \varepsilon_e}\frac{1}{3\varepsilon_e}. \tag{2.2.12}$$

With a local strain energy potential is given by

$$W(\mathbf{x}, \boldsymbol{\varepsilon}) = \sum_{r=1}^{2} \chi^{(r)}(\mathbf{x}) W^{(r)}(\boldsymbol{\varepsilon}), \tag{2.2.13}$$

and by appealing again to Hill (1963), we define the effective strain energy potential

$$\widetilde{W}(\overline{\boldsymbol{\varepsilon}}) = \min_{\boldsymbol{\varepsilon}\in\mathcal{K}(\overline{\boldsymbol{\varepsilon}})} \langle W(\mathbf{x}, \boldsymbol{\varepsilon}(\mathbf{x}))\rangle, \tag{2.2.14}$$

where

$$\mathcal{K}(\overline{\boldsymbol{\varepsilon}}) = \{\boldsymbol{\varepsilon} \,:\, \boldsymbol{\varepsilon} = \frac{1}{2}\left(\nabla\mathbf{u} + (\nabla\mathbf{u})^T\right) \text{ in } \Omega, \text{and } \mathbf{u} = \overline{\boldsymbol{\varepsilon}}\mathbf{x}, \text{ on } \partial\Omega\} \tag{2.2.15}$$

denotes the set of admissible displacement fields. It can then be shown that the average stress field $\overline{\boldsymbol{\sigma}}$ is given by

$$\overline{\boldsymbol{\sigma}} = \frac{\partial\widetilde{W}}{\partial\overline{\boldsymbol{\varepsilon}}}. \tag{2.2.16}$$

2.3 Finite-Rank Laminates

In this section, we recall the notion of sequentially laminated finite-rank laminates, which were introduced in the linear context by Tartar (1985); Lurie and Cherkaev (1984, 1986), and later generalized to the nonlinear setting by Ponte Castañeda (1992b); Hariton and deBotton (2002). The basic idea can be understood by first considering a simple, or rank-1, laminate. This composite is obtained by mixing two homogenous phases in a given layering direction $\mathbf{n}_{[1]}$. A rank-2 laminate is then obtained by mixing the rank-1 laminate with either one of the two homogenous phases in a given second layering direction $\mathbf{n}_{[2]}$. This processes can be iterated, whereby a rank$-M$ laminate is obtained by mixing a rank$-(M-1)$ laminate with either one of the two homogenous phase in a given lamination direction $\mathbf{n}_{[M]}$. It is known that the effective properties of simple laminates can be computed exactly, due to the fact that the fields in each homogenous phase are constant. With this in mind, we assume that the length scale of the previous laminate is much smaller than the length scale of the current laminate. Therefore, at the M^{th} iteration, the rank$-(M-1)$ laminate is taken as a homogenous phase, so that the rank-M laminate can be treated as a

simple laminate. whereby its effective properties can also be computed exactly.

In what follows, we will assume that for each $M \geqslant 2$, a rank$-M$ laminate is obtained by layering a rank$-(M-1)$ with the same homogeneous phase. As such this phase can be regarded as the (continuous) matrix phase of rank$-M$ laminate, while the other phase is regarded as the (discontinuous) inclusion phase. Two comments are in order before we proceed. The first is that, unlike in the linear case, even when the initial homogenous phases are assumed to be isotropic, the effective behavior of a rank$-M$ laminate will, in general, be *anisotropic*. In fact, only in the limit as M tends to infinity can we expect there to be an isotropic response (Hariton and deBotton, 2002; deBotton and Hariton, 2002; deBotton, 2005). As a final comment, denote the two phases of the simple laminate as phase 1 and phase 2. Upon fixing the microstructure, it is known that the rank-M laminate with phase 1 acting as the matrix phase will have a different effective response than the rank-M laminate with phase 2 acting as the matrix phase. In order to differentiate between such cases, we will employ the following notation convention: the rank of the laminate will be indicated in square brackets as a subscript, while the phase representing the matrix will be indicated in parentheses as a superscript. For example, the effective energy potential of a rank$-M$ laminate with phase 2 as the matrix phase will be given by $\widetilde{w}^{(2)}_{[M]}$.

2.3.1 Dielectrics

Fix a unit vector $\mathbf{n}_{[1]}$. If phase 1 and phase 2 are taken in proportions $\widehat{c}_{[1]}$ and $1-\widehat{c}_{[1]}$, respectively, then, the effective potential of the simple laminate can be written as (Ponte Castañeda, 1992a; Hariton and deBotton, 2002)

$$\widetilde{w}_{[1]}(\overline{\mathbf{E}}) = \min_{a_{[1]}}\{\widehat{c}_{[1]}w^{(1)}(\overline{E} - (1-\widehat{c}_{[1]})a_{[1]}\mathbf{n}_{[1]}) + (1-\widehat{c}_{[1]})w^{(2)}(\overline{E} + \widehat{c}_{[1]}a_{[1]}\mathbf{n}_{[1]})\}. \tag{2.3.1}$$

Considering the case where phase 2 corresponds to the matrix phase, a rank-2

laminate is then constructed by layering the rank-1 laminate with phase 2 in proportions $\widehat{c}_{[2]}$ and $1-\widehat{c}_{[2]}$, respectively, in the direction $\mathbf{n}_{[2]}$. The effective potential of the rank-2 laminate is the given by

$$\begin{aligned}\widetilde{w}^{(2)}_{[2]}(\overline{\mathbf{E}}) &= \min_{a_{[2]}} \left\{\widehat{c}_{[2]}\widetilde{w}_{[1]}(\overline{\mathbf{E}} - (1-\widehat{c}_{[2]})a_{[2]}\mathbf{n}_{[2]}) + (1-\widehat{c}_{[2]})w^{(2)}(\overline{\mathbf{E}} + \widehat{c}_{[2]}a_{[2]}\mathbf{n}_{[2]})\right\} \\ &= \min_{a_{[1]},a_{[2]}} \left\{\widehat{c}_{[1]}\widehat{c}_{[2]}w^{(1)}(\overline{\mathbf{E}}^{(1)}) + (1-\widehat{c}_{[1]}\widehat{c}_{[2]}w^{(2)}(\overline{\mathbf{E}}^{(2)}_{[1]}) + (1-\widehat{c}_{[2]})w^{(2)}(\overline{\mathbf{E}}^{(2)}_{[2]})\right\},\end{aligned} \tag{2.3.2}$$

where

$$\overline{\mathbf{E}}^{(1)} = \overline{\mathbf{E}} - (1-\widehat{c}_{[1]})a_{[1]}\mathbf{n}_{[1]} - (1-\widehat{c}_{[2]})a_{[2]}\mathbf{n}_{[2]}, \tag{2.3.3}$$

$$\overline{\mathbf{E}}^{(2)}_{[1]} = \overline{\mathbf{E}} + \widehat{c}_{[1]}a_{[1]}\mathbf{n}_{[1]} - (1-\widehat{c}_{[2]})a_{[2]}\mathbf{n}_{[2]}, \tag{2.3.4}$$

$$\overline{\mathbf{E}}^{(2)}_{[2]} = \overline{\mathbf{E}} + \widehat{c}_{[2]}a_{[2]}\mathbf{n}_{[2]}. \tag{2.3.5}$$

Note that the total volume fraction of the inclusion phase, i.e. phase 1, in the rank-2 laminate is given by $c = \widehat{c}_{[1]}\widehat{c}_{[2]}$.

The lamination process can be iterated, so long as at each step we make the separation of length scale assumption discussed at the beginning of this section. In particular, upon choosing the lamination directions $\mathbf{n}_{[i]}$ and relative volume fractions $\widehat{c}_{[i]}$ at each step, for $i = 1, \ldots, M$, the effective behavior of a rank$-M$ laminate is given by

$$\widetilde{w}_{[M]}(\overline{\mathbf{E}}) = \min_{\substack{a_{[i]} \\ i=1,\ldots,M}} \left\{ cw^{(1)}(\overline{\mathbf{E}}^{(1)}) + \sum_{i=1}^{M}(1-\widehat{c}_{[i]}) \prod_{j=i+1}^{M} \widehat{c}_{[j]} w^{(2)}(\overline{\mathbf{E}}^{(2)}_{[i]}) \right\}, \tag{2.3.6}$$

where

$$\overline{\mathbf{E}}^{(1)} = \overline{\mathbf{E}} - \sum_{i=1}^{M}(1-\widehat{c}_{[i]})a_{[i]}\mathbf{n}_{[i]}, \tag{2.3.7}$$

$$\overline{\mathbf{E}}^{(2)}_{[i]} = \overline{\mathbf{E}} + \widehat{c}_{[i]}a_{[i]}\mathbf{n}_{[i]} - \sum_{j=i+1}^{M}(1-\widehat{c}_{[j]})a_{[j]}\mathbf{n}_{[j]}, \tag{2.3.8}$$

$$c = \prod_{i=1}^{M}\widehat{c}_{[i]}. \tag{2.3.9}$$

When the phases are linear and isotropic, the energy potentials take the form

$$w^{(r)}(\boldsymbol{E}) = \frac{\epsilon^{(r)}}{2}E^2, \tag{2.3.10}$$

where $\epsilon^{(r)}$ correspond to the dielectric coefficient of phase r. In this case, it is well known (Tartar, 1985), that in d-dimensions, upon fixing the volume fraction $c = c^{(1)}$ of the inclusion phase, the lamination directions $\mathbf{n}_{[1]}, \cdots, \mathbf{n}_{[d]}$ as well as the relative volume fractions $\widehat{c}_{[1]}, \cdots, \widehat{c}_{[d]}$ can be chosen in such a way that the overall response of the laminate is *isotropic*, i.e.

$$\widetilde{w}^{(r)}_{[d]}(\overline{\mathbf{E}}) = \frac{\widetilde{\epsilon}^{(r)}_{[d]}}{2}\overline{E}^2,\ r = 1, 2 \tag{2.3.11}$$

Moreover, these laminates saturate the Hashin-Shtrikman bounds on the effective dielectric coefficient, as given by

$$\widetilde{\epsilon}_{HS} = c\epsilon^{(1)} + (1-c)\epsilon^{(2)} - \frac{c(1-c)(\epsilon^{(1)}-\epsilon^{(2)})^2}{(d-1)\epsilon^{(0)} + (1-c)\epsilon^{(1)} + c\epsilon^{(2)}}. \tag{2.3.12}$$

The upper bound is identified with the choice $\epsilon^{(0)} = \max\{\epsilon^{(1)}, \epsilon^{(2)}\}$, and is attained by a rank-two laminate when the dielectric coefficient of the phase acting as the matrix is larger. Conversely, The lower bound is identified with the choice $\epsilon^{(0)} = \min\{\epsilon^{(1)}, \epsilon^{(2)}\}$, and is attained by a rank-two laminate when the dielectric coefficient of the phase acting as the matrix is smaller.

In the current setting, where phase 2 corresponds to the matrix phase, the response of the laminate can be made isotropic in two dimensions by taking $\mathbf{n}_{[i]} = \mathbf{e}_i$ for $i = 1, 2$ and

$$\widehat{c}_{[1]} = \frac{1+c}{2}, \quad \text{and} \quad \widehat{c}_{[2]} = \frac{2c}{1+c}, \tag{2.3.13}$$

while in three dimensions ($d = 3$) by taking $\mathbf{n}_{[i]} = \mathbf{e}_i$ for $i = 1, 2, 3$ and

$$\widehat{c}_{[1]} = \frac{2+c}{3}, \quad \widehat{c}_{[2]} = \frac{1+2c}{2+c}, \quad \text{and} \quad \widehat{c}_{[3]} = \frac{3c}{1+2c}. \tag{2.3.14}$$

We recall that $\{\mathbf{e}_i\}$ represents the standard Cartesian basis, and hence the layer directions needed to have a laminate with isotropic response must be orthogonal.

2.3.2 Elasticity

The same arguments used in Section 2.3.1 can be employed to show that the effective strain potential of a rank-M laminate with phase 2 acting as the matrix phase is given by

$$\widetilde{W}^{(2)}_{[M]}(\overline{\boldsymbol{\varepsilon}}) = \min_{\substack{\mathbf{a}_{[i]} \\ i=1,\dots,M}} \left\{ cW^{(1)}(\overline{\boldsymbol{\varepsilon}}^{(1)}) + \sum_{i=1}^{M}(1-\widehat{c}_{[i]}) \prod_{j=i+1}^{M} \widehat{c}_{[j]} W^{(2)}(\overline{\boldsymbol{\varepsilon}}^{(2)}_{[i]}) \right\}, \tag{2.3.15}$$

where

$$\overline{\boldsymbol{\varepsilon}}^{(1)} = \overline{\boldsymbol{\varepsilon}} - \sum_{i=1}^{M}(1-\widehat{c}_{[i]})\mathbf{a}_{[i]} \otimes_s \mathbf{n}_{[i]}, \tag{2.3.16}$$

$$\overline{\boldsymbol{\varepsilon}}^{(2)}_{[i]} = \overline{\boldsymbol{\varepsilon}} + \widehat{c}_{[i]}\mathbf{a}_{[i]} \otimes_s \mathbf{n}_{[i]} - \sum_{j=i+1}^{M}(1-\widehat{c}_{[j]})\mathbf{a}_{[j]} \otimes_s \mathbf{n}_{[j]}. \tag{2.3.17}$$

Now, extending the work Tartar (1985), Francfort and Murat (1986) showed that when

$$W^{(r)}(\boldsymbol{\varepsilon}) = \frac{3}{2}\mu^{(r)}\varepsilon_e^2 + \frac{d^2}{2}\kappa^{(r)}\varepsilon_m^2, \tag{2.3.18}$$

with $\mu^{(r)}$ and $\kappa^{(r)}$ corresponding to the shear and bulk moduli, respectively, of phase

r, then, upon fixing $c = c^{(1)}$, $\widehat{c}_{[i]}$ and $\mathbf{n}_{[i]}$, $(i = 1, \ldots, p)$ can be chosen in such a way so that

$$\widetilde{W}^{(r)}_{[p]}(\overline{\boldsymbol{\varepsilon}}) = \frac{3}{2}\widetilde{\mu}^{(r)}_{[p]}\,\overline{\varepsilon}^2_e + \frac{d^2}{2}\widetilde{\kappa}^{(r)}_{[p]}\,\overline{\varepsilon}^2_m,\ r = 1, 2, \tag{2.3.19}$$

where $p = \frac{d(d+1)}{2}$. Moreover, as above, these laminates saturate the Hashin-Shtrikman bounds on the effective shear and bulk moduli, as given by

$$\widetilde{\mu}_{HS} = c\mu^{(1)} + (1-c)\mu^{(2)} - \frac{c(1-c)(\mu^{(1)} - \mu^{(2)})^2}{(1-c)\mu^{(1)} + c\mu^{(2)} + \mu^{(0)}\frac{d^2\kappa^{(0)} + 2\mu^{(0)}(d+1)(d-2)}{2d(\kappa^{(0)} + 2\mu^{(0)})}}. \tag{2.3.20}$$

and

$$\widetilde{\kappa}_{HS} = c\kappa^{(1)} + (1-c)\kappa^{(2)} - \frac{c(1-c)(\kappa^{(1)} - \kappa^{(2)})^2}{(1-c)\kappa^{(1)} + c\kappa^{(2)} + \frac{2(d-1)}{d}\mu^{(0)}}, \tag{2.3.21}$$

respectively. Here, as above, $\mu^{(0)}$ and $\kappa^{(0)}$ can take the values $\mu^{(1)}, \mu^{(2)}$ and $\kappa^{(1)}, \kappa^{(2)}$ respectively. We remark that the original bounds of Hashin and Shtrikman (1963) on the elastic properties of two phase composites were derived in the three-dimensional case, while the two-dimensional extension was found by Hill (1965) and Hill (1964). When $d = 2$, the case that is of primary interest in this work, upon taking $\widehat{c}_{[1]}, \widehat{c}_{[2]}$ and $\widehat{c}_{[3]}$ as in Eq. (2.3.14), and letting

$$\mathbf{n}_{[1]} = \mathbf{e}_1, \quad \mathbf{n}_{[2]} = \frac{1}{2}(\mathbf{e}_1 + \sqrt{3}\mathbf{e}_2), \quad \mathbf{n}_{[3]} = \frac{1}{2}(-\mathbf{e}_1 + \sqrt{3}\mathbf{e}_2), \tag{2.3.22}$$

the resulting rank-3 laminate will have an isotropic response, and moreover, will attain the HS bound (Francfort and Murat, 1986). Now, when both phases are taken to be incompressible, whereby $\kappa^{(1)}, \kappa^{(2)} \to \infty$, the bound on effective shear modulus reduces to

$$\widetilde{\mu}_{HS} = c\mu^{(1)} + (1-c)\mu^{(2)} - \frac{c(1-c)(\mu^{(1)} - \mu^{(2)})^2}{(1-c)\mu^{(1)} + c\mu^{(2)} + \frac{d}{2}\mu^{(0)}}, \tag{2.3.23}$$

which, in $d = 2$ dimensions, is identical to the bounds for the effective dielectric coefficient (c.f. Eq. (2.3.12) with $d = 2$). Furthermore, by taking $\widehat{c}_{[1]}$ and $\widehat{c}_{[2]}$ as in

Eq. (2.3.13), and letting

$$\mathbf{n}_{[1]} = \mathbf{e}_1, \quad \mathbf{n}_{[2]} = \frac{1}{\sqrt{2}} \left(\mathbf{e}_1 + \mathbf{e}_2 \right), \tag{2.3.24}$$

it can be shown that the resulting rank-2 laminate has an isotropic response under purely deviatoric loading and attains the corresponding HS bound; the rank-2 laminate does not have an isotropic response under more general loading. This result was first observed by Lipton (1988) (see also Lipton and Kohn, 1988). Moreover, as noted by author, while the lamination directions needed to attain the HS bound in two-dimensional dielectrics must be taken to be orthogonal, in two-dimensional, incompressible, elasticity, their orientations must differ by 45^o.

2.4 Linear Comparison Variational Bounds

In general, when the phases are nonlinear, the computation of the effective potential is very difficult, due to the fact that it involves solving a set of nonlinear partial differential equations with randomly oscillating coefficients. In fact, exact results are known only in very special cases; laminates are one such case. On the other hand, computing, or at least bounding, the effective properties of a composite with linear phases is more tractable, and many results to that end exist. Motivated by this fact, we now recall the variational method of Ponte Castañeda (1992b), which converts available bounds for the effective behavior of some fictitious linear comparison composite (LCC) into bounds for the effective behavior of the nonlinear composite of interest. We spell out, explicitly, the bounds in the context of nonlinear dielectrics, and also comment on their form in nonlinear elasticity. The method for obtaining bounds works for general N-phase composites, but we consider here the case of two-phase composites. Before starting, we provide the definition of a certain technical hypothesis that is crucial in both deriving the variational bounds, as well as in our analysis to come. We state the hypothesis in the context of nonlinear dielectrics, but

note that it can be stated for nonlinear elasticity by replacing E with ε_e.

Square-Concavity Hypothesis: An isotropic function $w(\mathbf{E}) = \phi(E)$ satisfies the square-concavity hypothesis if $\phi(E) = f(p)$ with $p = E^2$, where f satisfies the following properties:

1. f is a strictly concave.
2. $f > 0$ for $p > 0$ and $f(p) = -\infty$ when $p < 0$.
3. $f(0) = 0$ and $f \to \infty$ as $p \to \infty$.

As an example, for $0 \leqslant m \leqslant 1$, $\phi(E) \sim E^{m+1}$ satisfies the square-concavity hypothesis. Note that ϕ is convex, while, $f(p) \sim p^{(m+1)/2}$ is concave.

Square-Convexity Hypothesis: An isotropic function $w(\mathbf{E}) = \phi(E)$ satisfies the square-convexity hypothesis if $\phi(E) = f(p)$ with $p = E^2$, where f satisfies the following properties:

1. f is a strictly convex.
2. $f > 0$ for $p > 0$ and $f(p) = -\infty$ when $p < 0$.
3. $f(0) = 0$ and $f \to \infty$ as $p \to \infty$.

As an example, for $1 \leqslant m \leqslant \infty$, $\phi(E) \sim E^{m+1}$ satisfies the square-convexity hypothesis. In this case, both ϕ and f are convex.

2.4.1 Dielectrics

Consider a nonlinear composite whose local potential has the form of Eq. (2.2.4), with isotropic phase energy density functions satisfying the square concavity hypothesis. Next, we introduce a heterogenous linear comparison composite (LCC) whose local energy density function takes the form $w_0(\mathbf{x}, \mathbf{E}) = \frac{1}{2}\epsilon_0(\mathbf{x})|\mathbf{E}|^2$, where $\epsilon_0(\mathbf{x})$ denotes

the arbitrary non-negative dielectric coefficient of the LCC, and will be determined later. It follows that the effective energy potential of the LCC is given by

$$\widetilde{w}_0(\overline{\mathbf{E}}) = \min_{\mathbf{E}\in\mathcal{K}(\overline{\mathbf{E}})} \langle w_0(\mathbf{x}, \mathbf{E}(\mathbf{x}))\rangle, \tag{2.4.1}$$

with $\mathcal{K}(\overline{\mathbf{E}})$ given by Eq. (2.2.7). Upon defining the "error" function

$$v(\epsilon_0) = \langle v(\mathbf{x}, \epsilon_0(\mathbf{x}))\rangle, \tag{2.4.2}$$

where

$$v(\mathbf{x}, \epsilon_0) = \sup_{\mathbf{E}} \{w(\mathbf{x}, \mathbf{E}) - w_0(\mathbf{x}, \mathbf{E})\} \tag{2.4.3}$$

it can be shown that the effective energy density of the nonlinear composite can be written as (Ponte Castañeda, 1992b)

$$\widetilde{w}(\overline{\mathbf{E}}) = \inf_{\epsilon_0(\mathbf{x})>0} \left\{\widetilde{w}_0(\overline{\mathbf{E}}) + v(\epsilon_0)\right\}. \tag{2.4.4}$$

Note that the square-concavity hypothesis ensures that w has weaker-than-quadratic growth at ∞, so that the supremum in Eq. (2.4.3) is finite.

It is difficult to calculate the infimum in Eq. (2.4.4) directly, but if we instead consider $\epsilon_0(\mathbf{x})$ that are piecewise constant per phase, we obtain the upper variational linear comparison bound (VLC):

$$\widetilde{w}(\overline{\mathbf{E}}) \leqslant \widetilde{w}_{VLC+}(\overline{\mathbf{E}}) = \inf_{\epsilon_0^{(1)},\epsilon_0^{(2)}>0} \left\{ \widetilde{w}_0(\overline{\mathbf{E}}) + \sum_{r=1}^{2} c^{(r)} v^{(r)}(\epsilon_0^{(r)}) \right\}. \tag{2.4.5}$$

Here, $\widetilde{w}_0$ now represents the effective potential of the LCC whose dielectric coefficient is given by

$$\epsilon_0(\mathbf{x}) = \epsilon_0^{(1)}\chi^{(1)}(\mathbf{x}) + \epsilon_0^{(2)}\chi^{(2)}(\mathbf{x}), \tag{2.4.6}$$

while

$$v^{(r)}(\epsilon_0^{(r)}) = \sup_{\mathbf{E}} \left\{ \phi^{(r)}(E) - \frac{1}{2}\epsilon_0^{(r)} E^2 \right\}, \tag{2.4.7}$$

where we recall that $\phi^{(r)}(E) = w^{(r)}(\mathbf{E})$ is the isotropic energy density function. Note that the LCC has the same microstructure (as defined by $\chi^{(r)}$) as the nonlinear composite. It can also be shown (Ponte Castañeda and Suquet, 1998) that the VLC bound can be written as

$$\widetilde{w}_{VLC+}(\overline{\mathbf{E}}) = \sum_{r=1}^{2} c^{(r)} \phi^{(r)} \left(\overline{\overline{E}}^{(r)} \right), \tag{2.4.8}$$

where

$$\overline{\overline{E}}^{(r)} = \sqrt{\langle |E|^2 \rangle^{(r)}}, \tag{2.4.9}$$

corresponds to the second moment of the electric field in the LCC.

It is clear from Eq. (2.4.5) that any upper bound on $\widetilde{w}_0$ will provide a corresponding upper bound on $\widetilde{w}$. By consider a nonlinear composite composed of two isotropic phases distributed with statistical isotropy, and applying the HS bounds to the corresponding LCC, Ponte Castañeda (1992a) showed that

$$\widetilde{w}_{VHS+}(\overline{\mathbf{E}}) = \max \left\{ \begin{array}{l} \inf\limits_{\omega} \left\{ c^{(1)} \phi^{(1)} \left(|1 - c^{(2)} \omega | \overline{E} \right) + c^{(2)} \phi^{(2)} \left(\sqrt{(1 + c^{(1)}\omega)^2 + (d-1) c^{(1)} \omega^2}\, \overline{E} \right) \right\} \\ \\ \inf\limits_{\omega} \left\{ c^{(1)} \phi^{(1)} \left(\sqrt{(1 - c^{(2)}\omega)^2 + (d-1) c^{(2)} \omega^2}\, \overline{E} \right) + c^{(2)} \phi^{(2)} \left(|1 + c^{(1)} \omega | \overline{E} \right) \right\} \end{array} \right\}. \tag{2.4.10}$$

Note that there exists two branches of the VHS bound. As mentioned by Ponte Castañeda (1992a), this is related to the fact that, in utilizing the HS upper bound on the effective dielectric coefficient of the LCC, it is necessary to take $\epsilon^{(0)} = \max\{\epsilon_0^{(1)}, \epsilon_0^{(2)}\}$ (see Eq. (2.3.12)). However, the maximum of $\epsilon_0^{(1)}$ and $\epsilon_0^{(2)}$ depends on

$\overline{E}$, and can therefore occur in either phase.

We comment that if $w^{(r)}$ has stronger-than-quadratic growth at ∞, the same procedure above can be reinterpreted to give lower bounds on $\widetilde{w}$. In this case, we would have that

$$\widetilde{w}(\overline{\mathbf{E}}) \geqslant \widetilde{w}_{VLC-}(\overline{\mathbf{E}}) = \sup_{\epsilon_0^{(1)},\epsilon_0^{(2)}>0} \left\{ \widetilde{w}_0(\overline{\mathbf{E}}) - \sum_{r=1}^{2} c^{(r)} v^{(r)}(\epsilon_0^{(r)}) \right\}, \tag{2.4.11}$$

where now

$$v^{(r)}(\epsilon_0^{(r)}) = \sup_{\mathbf{E}} \left\{ \frac{1}{2}\epsilon_0^{(r)} E^2 - \phi^{(r)}(E) \right\}. \tag{2.4.12}$$

Then, any lower bound on $\widetilde{w}_0$ would provide a corresponding lower bound on $\widetilde{w}$. In particular, upon changing the max to a min, the expression in Eq. (2.4.10) would correspond to the Hashin-Shtrikman lower bound $\widetilde{w}_{VHS-}(\overline{E})$.

2.4.2 Elasticity

The VLC bounds can be recast in the setting of nonlinear elasticity with relative ease (Ponte Castañeda, 1991). Due to the tensorial nature of elasticity, there are some minor differences in how the bounds are formulated. For one, the potential for the LCC used in the variational bounds now takes the form

$$W_0(\mathbf{x}, \boldsymbol{\varepsilon}) = \frac{3}{2}\mu_0(\mathbf{x})\varepsilon_e^2 + \frac{d^2}{2}\kappa_0(\mathbf{x})\varepsilon_m^2, \tag{2.4.13}$$

where $\mu_0(\mathbf{x})$ and $\kappa_0(\mathbf{x})$ are the non-negative shear and bulk moduli of the heterogeneous LCC, respectively.

As above, we find that the effective strain potential can be written as

$$\widetilde{W}(\overline{\boldsymbol{\varepsilon}}) = \inf_{\mu_0(\mathbf{x}),\kappa_0(\mathbf{x})>0} \left\{ \widetilde{W}_0(\overline{\boldsymbol{\varepsilon}}) + V(\mu_0, \kappa_0) \right\}. \tag{2.4.14}$$

In calculating the error functions, as above, we write

$$V(\mathbf{x},\mu_0,\kappa_0) = \sup_{\boldsymbol{\varepsilon}}\{W(\mathbf{x},\boldsymbol{\varepsilon}) - W_0(\mathbf{x},\boldsymbol{\varepsilon})\}$$
$$V(\mu_0,\kappa_0) = \langle V(\mathbf{x},\mu_0(\mathbf{x}),\kappa_0(\mathbf{x}))\rangle. \tag{2.4.15}$$

Upon taking $W^{(r)}$ to be as in Eq. (2.2.10), and combining the optimizing conditions with respect to both κ_0 as well as $\boldsymbol{\varepsilon}$ in Eqs. (2.4.14) and (2.4.15), respectively, we find that

$$\kappa_0(\mathbf{x}) = \kappa(\mathbf{x}) = \kappa^{(1)}\chi^{(1)}(\mathbf{x}) + \kappa^{(2)}\chi^{(2)}(\mathbf{x}) \tag{2.4.16}$$

where $\kappa^{(1)}$ and $\kappa^{(2)}$ are the bulk moduli of the nonlinear phases. Therefore, the error functions reduce to

$$V(\mathbf{x},\mu_0) = \sup_{\boldsymbol{\varepsilon}}\left\{\sum_{r=1}^{2}\chi^{(r)}(\mathbf{x})\varphi^{(r)}(\varepsilon_e) - \frac{3}{2}\mu_0(\mathbf{x})\varepsilon_e^2\right\}$$
$$V(\mu_0) = \langle V(\mathbf{x},\mu_0(\mathbf{x}))\rangle, \tag{2.4.17}$$

and $\widetilde{W}$ is given by

$$\widetilde{W}(\overline{\boldsymbol{\varepsilon}}) = \inf_{\mu_0(\mathbf{x})>0}\left\{\widetilde{W}_0(\overline{\boldsymbol{\varepsilon}}) + V(\mu_0)\right\}. \tag{2.4.18}$$

To obtain the corresponding VLC bounds, we consider an LCC with piecewise constant shear moduli of the form

$$\mu_0(\mathbf{x}) = \mu_0^{(1)}\chi^{(1)}(\mathbf{x}) + \mu_0^{(2)}\chi^{(2)}(\mathbf{x}). \tag{2.4.19}$$

Then, upon defining

$$V^{(r)}(\mu_0^{(r)}) = \sup_{\boldsymbol{\varepsilon}}\left\{\varphi^{(r)}(\varepsilon_e) - \frac{3}{2}\mu_0^{(r)}\varepsilon_e^2\right\}. \tag{2.4.20}$$

we obtain

$$\widetilde{W}(\overline{\boldsymbol{\varepsilon}}) \leqslant \widetilde{W}_{VLC+}(\overline{\boldsymbol{\varepsilon}}) = \inf_{\mu_0^{(r)}>0} \left\{ \widetilde{W}_0(\overline{\boldsymbol{\varepsilon}}) + \sum_{r=1}^{2} c^{(r)} V^{(r)}(\mu_0^{(r)}) \right\}, \tag{2.4.21}$$

where $\widetilde{W}_0$ is the effective potential of the LCC whose local strain potential takes the form Eq. (2.4.13), and whose local shear and bulk moduli are given by Eqs. (2.4.16) and (2.4.19), respectively. Moreover, by making use of the linear Hashin-Shtrikman bounds to obtain estimates for $\widetilde{W}_0$, we can similarly obtain the corresponding VHS bounds on $\widetilde{W}$. In fact, when considering purely deviatoric loading ($X \to 0$) the bounds $\widetilde{W}_{VHS+}(\overline{\boldsymbol{\varepsilon}})$ take the same form as Eq. (2.4.10), with $\phi^{(r)}$ and $\overline{E}$ replaced by $\varphi^{(r)}$ and $\overline{\varepsilon}_e$, respectively. Although, mathematically, the same trick can be played to obtain lower bounds in the case that $\varphi^{(r)}$ satisfies the square-convexity hypothesis, in practice, $\varphi^{(r)}$ is almost always taken to only be square-concave, and lower bounds are usually obtained by appealing to Legendre duality (see Ponte Castañeda, 1992b).

From here on, we refer the VLC bounds that make use of the Hashin-Shtrikman estimates on the LCC as the nonlinear variational bounds of the Hashin-Shtrikman type (VHS). Due to the assumption of statistical isotropy of the microstructure, the response of the nonlinear composite and the VHS bounds are both isotropic. It is therefore natural to assume that the VHS bounds hold only for those nonlinear composites with statistically isotropic microstructures. As we will see next, the VHS bounds are valid for a much larger class of composites.

2.5 Optimality of the Variational Bounds

By construction, the VLC bounds as given by Eqs. (2.4.5) and (2.4.21) can be applied more generally to nonlinear composites with any arbitrary microstructure, so long as their exists a bound for the effective behavior of the corresponding LCC. With this in mind, consider first the class of nonlinear anisotropic materials consisting of

two isotropic phases given in prescribed volume fractions. Having made no additional restrictions on the microstructure, we can apply the linear translation bounds to obtain bounds on the effective potential of the LCC. This in turn will produce a nonlinear variational translation bound (VT).

It is known that the linear translation bounds reduce to the linear HS bounds when the macroscopic response of the linear composite is isotropic. Therefore when applied to the subclass of nonlinear anisotropic composites that have linearly isotropic response, the VT are the same as the VHS bounds; this follows from the fact that the bounds used on the LCC are identical for this class. Hence, the VHS bounds actually hold not just for the class of two phase nonlinear composites with statistically isotropic microstructures, but for the larger class of nonlinear anisotropic composites that have linearly isotropic response. This, in part, explains why the VHS bounds, when compared to estimates on the effective behavior of composites with statistically isotropic microstructures, tend to "over-bound" these estimates, even for weak nonlinearities (see Furer and Ponte Castañeda, 2018b; Ponte Castañeda, 2001, 2016; Ponte Castañeda and Kailasam, 1997, and references therein). The VHS bounds hold over a class of composites that includes some special anisotropic microstructures (e.g. finite-rank laminates), and therefore cannot be expected to be tight when applied to composites with statistically isotropic microstructures.

Before proceeding, we comment on the interplay between nonlinearity and the isotropy of the microstructure. Recall that the linear translation bounds make no assumptions on the higher-order statistics of the microstructure, whereas the linear HS bounds were originally derived by assuming that the two-point statistics were isotropic. Nonetheless, as just mentioned, when the overall response of the linear composite is taken to be isotropic, both bounds are identical. This indicates that the procedure for obtaining bounds on materials with linearly isotropic behavior are in some sense insensitive to the microstructure. In fact, it is known that the linear HS bounds hold for materials not only with random microstructures, but also for those

with periodic microstructures, as well as finite-rank laminates, which are neither random nor periodic. On the other hand, while materials (comprised of isotropic phases) with statistically isotropic microstructures will also have nonlinear isotropic response, the same cannot be said for materials with more general microstructures; materials with linearly isotropic response will not generally have nonlinearly isotropic response. As such, it is important to incorporate any available statistical information on the microstructure in order to obtain a more accurate prediction of the nonlinear response of composites. As the VLC method only makes use of bounds on the LCC, it fails to fully incorporate such information.

In the remainder of this section, we show the VHS bounds are optimal over the class of nonlinear anisotropic composites that have linearly isotropic response by constructing a microstructure that attains them. It is clear that microstructures that have linearly isotropic responses may have nonlinear anisotropic responses. Nonetheless, the anisotropic effective energy of the nonlinear material can still be bounded by these isotropic VHS bounds. The former will depend fully on the loading variable (i.e. $\overline{\mathbf{E}}$ or $\overline{\boldsymbol{\varepsilon}}$), while the latter will depend only on certain invariants of the loading variable (i.e. $\overline{E}$ or $\overline{\varepsilon}_e$ and $\overline{\varepsilon}_m$). As such, we will show that, for fixed values of $\overline{E}$ or $\overline{\varepsilon}_e$ and $\overline{\varepsilon}_m$, there exists specific orientations of $\overline{\mathbf{E}}$ or $\overline{\boldsymbol{\varepsilon}}$ for which the effective behavior of the laminate agrees with the VHS bound.

It is easier to show optimality in the vectorial case, and in order to avoid further repetition, we spell out explicitly the optimality of the VHS bounds for two- and three-dimensional dielectrics. We will present results for two-dimensional elasticity, but will exclude a full derivation of the optimality of the VHS bounds for two-dimensional incompressible and compressible elasticity, as it can be shown in a manner identical to the case of dielectrics, *mutatis mutandis*. Moreover, for dielectrics, we prove optimality of only the VHS upper bounds, since the optimality of the VHS lower bounds can be shown, *mutatis mutandis*.

2.5.1 Dielectrics

2.5.1.1 Two-dimensional Dielectrics

We set $\mathbf{n}_{[1]} = \mathbf{e}_1$ and $\mathbf{n}_{[2]} = \mathbf{e}_2$ as the direction of lamination, and fix $\overline{E}$. We then write

$$\overline{\mathbf{E}} = \overline{E}_1 \mathbf{n}_{[1]} + \overline{E}_2 \mathbf{n}_{[2]}, \tag{2.5.1}$$

whereby $\overline{E}_1$ and $\overline{E}_2$ are related via the identity

$$\overline{E}_1^2 + \overline{E}_2^2 = \overline{E}^2. \tag{2.5.2}$$

We start our analysis by taking phase 2 to be the matrix phase, so that $c = c^{(1)}$ corresponds to the volume fraction of the inclusion phase. Then, from Eq. (2.3.2), we have

$$\widetilde{w}_{[2]}^{(2)}(\overline{\mathbf{E}}) = \min_{a_{[1]}, a_{[2]}} \left\{ \widehat{c}_{[1]} \widehat{c}_{[2]} \phi^{(1)} \left(\overline{E}^{(1)} \right) + (1 - \widehat{c}_{[1]}) \widehat{c}_{[2]} \phi^{(2)} \left(\overline{E}_{[1]}^{(2)} \right) + (1 - \widehat{c}_{[2]}) \phi^{(2)} \left(\overline{E}_{[2]}^{(2)} \right) \right\}, \tag{2.5.3}$$

where $\widehat{c}_{[1]}$ and $\widehat{c}_{[2]}$ are given by Eq. (2.3.13), and where

$$\overline{E}^{(1)} = \sqrt{(\overline{E}_1 - (1 - \widehat{c}_{[1]}) a_{[1]})^2 + (\overline{E}_2 - (1 - \widehat{c}_{[2]}) a_{[2]})^2}, \tag{2.5.4}$$

$$\overline{E}_{[1]}^{(2)} = \sqrt{(\overline{E}_1 + \widehat{c}_{[1]} a_{[1]})^2 + (\overline{E}_2 - (1 - \widehat{c}_{[2]}) a_{[2]})^2}, \tag{2.5.5}$$

$$\overline{E}_{[2]}^{(2)} = \sqrt{\overline{E}_1^2 + (\overline{E}_2 + \widehat{c}_{[2]} a_{[2]})^2}. \tag{2.5.6}$$

At this point, the microstructure, defined through $\mathbf{n}_{[1]}, \mathbf{n}_{[2]}, \widehat{c}_{[1]}$ and $\widehat{c}_{[2]}$, is completely fixed. Now, when

$$\phi^{(r)}(E) = \frac{\epsilon^{(r)}}{2} E^2, \tag{2.5.7}$$

then, as discussed above, it can be shown that

$$\widetilde{w}_{[2]}^{(2)}(\overline{\mathbf{E}}) = \frac{\widetilde{\epsilon}_{HS}}{2} \overline{E}^2, \tag{2.5.8}$$

whereby the rank-2 laminate has linearly isotropic response, and hence lies in the class of microstructures bounded by the VHS bounds. Moreover, we see that it attains the HS bounds in this linear setting.

Now, for general $\phi^{(r)}$ that satisfy the square concavity hypothesis, we know that, for a fixed value of $\overline{E}$, $\widetilde{w}^{(2)}_{[2]}(\overline{\mathbf{E}})$ changes as the orientation of $\overline{\mathbf{E}}$ varies. As such, and in order to see that the VHS bounds are attained, we maximize $\widetilde{w}^{(2)}_{[2]}(\overline{\mathbf{E}})$ with respect to $\overline{E}_1$ and $\overline{E}_2$ and treat the condition $\overline{E}^2 = \overline{E}_1^2 + \overline{E}_2^2$ as a constraint by using the method of Lagrange multipliers. In what follows,

$$\overline{\mathbf{E}}^* = \overline{E}_1^* \mathbf{n}_{[1]} + \overline{E}_2^* \mathbf{n}_{[2]} \tag{2.5.9}$$

corresponds to the optimal value of $\overline{\mathbf{E}}$ that maximizes $\widetilde{w}^{(2)}_{[2]}$, subject to the constraint $\overline{E}^2 = \overline{E}_1^{*2} + \overline{E}_2^{*2}$. More generally, given a vector-valued function f, by $f(\mathbf{a}^*)$, we mean

$$\mathbf{a}^* = \underset{\mathbf{a}:\, |\mathbf{a}| = |\overline{\mathbf{E}}|}{\operatorname{argmax}} f(\mathbf{a}), \tag{2.5.10}$$

i.e. $\mathbf{a}^*$ is value that maximizes f, subject to the constraint that $|\mathbf{a}| = |\overline{\mathbf{E}}|$. (We note that if $\phi^{(r)}$ satisfied the square convexity hypothesis, we would minimize) Taking into account the stationary conditions with respect to $a_{[i]}$, which read

$$\frac{\partial \phi^{(2)}\left(\overline{E}^{(2)}_{[1]}\right)}{\partial \overline{E}} \frac{(\overline{E}_1 + \widehat{c}_{[1]} a_{[1]})}{\overline{E}^{(2)}_{[1]}} - \frac{\partial \phi^{(1)}\left(\overline{E}^{(1)}\right)}{\partial \overline{E}} \frac{(\overline{E}_1 - (1 - \widehat{c}_{[1]}) a_{[1]})}{\overline{E}^{(1)}} = 0, \tag{2.5.11}$$

$$\begin{aligned} &\frac{\partial \phi^{(2)}\left(\overline{E}^{(2)}_{[2]}\right)}{\partial \overline{E}} \frac{(\overline{E}_2 + \widehat{c}_{[2]} a_{[2]})}{\overline{E}^{(2)}_{[2]}} \\ &- \left[\frac{\partial \phi^{(1)}\left(\overline{E}^{(1)}\right)}{\partial \overline{E}} \frac{\widehat{c}_{[1]}}{\overline{E}^{(1)}} + \frac{\partial \phi^{(2)}\left(\overline{E}^{(2)}_{[1]}\right)}{\partial \overline{E}} \frac{(1 - \widehat{c}_{[1]})}{\overline{E}^{(2)}_{[1]}} \right] (\overline{E}_2 - (1 - \widehat{c}_{[2]}) a_{[2]}) = 0, \end{aligned} \tag{2.5.12}$$

and optimizing Eq. (2.5.3) with respect to $\overline{\mathbf{E}}$, we find that $\overline{E}_1^*$ and $\overline{E}_2^*$ must satisfy

$$\begin{aligned}
&\widehat{c}_{[1]}(1-\widehat{c}_{[1]})a_{[1]}\overline{E}_2^*\left[\frac{\partial\phi^{(2)}\left(\overline{E}_{[1]}^{(2)}\right)}{\partial\overline{E}}\frac{1}{\overline{E}_{[1]}^{(2)}}-\frac{\partial\phi^{(1)}\left(\overline{E}^{(1)}\right)}{\partial\overline{E}}\frac{1}{\overline{E}^{(1)}}\right]\\
&=(1-\widehat{c}_{[2]})a_{[2]}\overline{E}_1^*\left[\frac{\partial\phi^{(2)}\left(\overline{E}_{[2]}^{(2)}\right)}{\partial\overline{E}}\frac{1}{\overline{E}_{[2]}^{(2)}}-\right.\\
&\qquad\left.\left[\frac{\partial\phi^{(1)}\left(\overline{E}^{(1)}\right)}{\partial\overline{E}}\frac{\widehat{c}_{[1]}}{\overline{E}^{(1)}}+\frac{\partial\phi^{(2)}\left(\overline{E}_{[1]}^{(2)}\right)}{\partial\overline{E}}\frac{(1-\widehat{c}_{[1]})}{\overline{E}_{[1]}^{(2)}}\right]\right],
\end{aligned}\tag{2.5.13}$$

where we implicitly take the values of $\overline{E}^{(1)}$ and $\overline{E}_{[j]}^{(2)}$, for $j=1,2$, to be evaluated at $\overline{\mathbf{E}}^*$. Upon using Eqs. (2.5.11)-(2.5.12), as well as Eq. (2.3.13) for the specific values of $\widehat{c}_{[i]}$, Eq. (2.5.13) simplifies to

$$a_{[1]}^2(1+c)\overline{E}_2^*((1+c)\overline{E}_2^*+2ca_{[2]})-4a_{[2]}^2\overline{E}_1^*(\overline{E}_1^*+ca_1)=0.\tag{2.5.14}$$

As Eq. (2.5.14) is quadratic in $a_{[1]}$ and $a_{[2]}$, there are two possible solutions. We choose the root that is consistent with the values that $a_{[1]}$ and $a_{[2]}$ take in the linear case, as given by

$$a_{[1]}^{lin}=\frac{2(\epsilon^{(1)}-\epsilon^{(2)})\overline{E}_1}{(1-c)\epsilon^{(1)}+c\epsilon^{(2)}},\quad a_{[2]}^{lin}=\frac{(1+c)(\epsilon^{(1)}-\epsilon^{(2)})\overline{E}_2}{(1-c)\epsilon^{(1)}+c\epsilon^{(2)}}.\tag{2.5.15}$$

Therefore, we conclude that

$$a_{[1]}=\frac{2a_{[2]}\overline{E}_1^*}{(1+c)\overline{E}_2^*},\tag{2.5.16}$$

a relationship that is also satisfied by $a_{[1]}^{lin}$ and $a_{[2]}^{lin}$. Combining Eq. (2.5.16) with Eq. (2.5.13), we find

$$\frac{\partial\phi^{(2)}\left(\overline{E}_{[1]}^{(2)}\right)}{\partial\overline{E}}\frac{1}{\overline{E}_{[1]}^{(2)}}=\frac{\partial\phi^{(2)}\left(\overline{E}_{[2]}^{(2)}\right)}{\partial\overline{E}}\frac{1}{\overline{E}_{[2]}^{(2)}},\tag{2.5.17}$$

which in connection to Eq. (2.2.3), states that the secant dielectric coefficient of

phase 2 is the same when evaluated at $\overline{E}^{(2)}_{[1]}$ and $\overline{E}^{(2)}_{[2]}$. Under the square concavity hypothesis, $\phi^{(2)}(E) = f^{(2)}(p)$, where $p = E^2$. Therefore

$$\frac{\partial \phi^{(2)}}{\partial E}\frac{1}{2E} = \frac{\partial f^{(2)}}{\partial p}, \tag{2.5.18}$$

so that, upon letting $p^{(2)}_{[1]} = (\overline{E}^{(2)}_{[1]})^2$ and $p^{(2)}_{[2]} = (\overline{E}^{(2)}_{[2]})^2$, Eq. (2.5.17) is equivalent to the condition that

$$\frac{\partial f^{(2)}(p^{(2)}_{[1]})}{\partial p} = \frac{\partial f^{(2)}(p^{(2)}_{[2]})}{\partial p}. \tag{2.5.19}$$

Due to the fact that $f^{(2)}$ is strictly concave, $\frac{\partial f^{(2)}}{\partial p}$ is strictly decreasing, and therefore, Eq. (2.5.19) implies that $p^{(2)}_{[1]} = p^{(2)}_{[2]}$. Hence $\overline{E}^{(2)}_{[1]} = \overline{E}^{(2)}_{[2]}$, which, from Eq. (2.5.5) and Eq. (2.5.6), shows that

$$a_{[2]} = \frac{2(1+c)\left(\overline{E}^{*2}_2 - \overline{E}^{*2}_1\right)\overline{E}^*_2}{(1-c)\overline{E}^2 - 2c\left(\overline{E}^{*2}_2 - \overline{E}^{*2}_1\right)}. \tag{2.5.20}$$

Upon letting

$$\omega = \frac{2\left(\overline{E}^{*2}_2 - \overline{E}^{*2}_1\right)}{(1-c)\overline{E}^2 - 2c\left(\overline{E}^{*2}_2 - \overline{E}^{*2}_1\right)}, \tag{2.5.21}$$

Eq. (2.5.11) can be used to write

$$\widetilde{w}^{(2)}_{[2]}(\overline{\mathbf{E}}^*) = \min_{\omega}\left\{c\phi^{(1)}\left(|1-(1-c)\omega|\overline{E}\right) + (1-c)\phi^{(2)}\left(\sqrt{(1+c\omega)^2 + c\omega^2}\,\overline{E}\right)\right\}. \tag{2.5.22}$$

Now, suppose that instead, we take phase 1 to be the matrix phase, so that $\widehat{c}_{[1]}\widehat{c}_{[2]} = c^{(2)} = 1 - c$ represents the total volume fraction of the inclusion phase.

Then,

$$\widetilde{w}_{[2]}^{(1)}(\overline{\mathbf{E}}) = \min_{a_{[1]},a_{[2]}} \left\{ (1-\widehat{c}_{[1]})\widehat{c}_{[2]}\phi^{(1)}\left(\overline{E}_{[1]}^{(1)}\right) + (1-\widehat{c}_{[2]})\phi^{(1)}\left(\overline{E}_{[2]}^{(1)}\right) + \widehat{c}_{[1]}\widehat{c}_{[2]}\phi^{(2)}\left(\overline{E}^{(2)}\right) \right\}, \tag{2.5.23}$$

where $\widehat{c}_{[1]}$ and $\widehat{c}_{[2]}$ are still given by Eq. (2.3.13) (with c replaced by $(1-c)$), and where

$$\overline{E}_{[1]}^{(1)} = \sqrt{(\overline{E}_1 + \widehat{c}_{[1]}a_{[1]})^2 + (\overline{E}_2 - (1-\widehat{c}_{[2]})a_{[2]})^2}, \tag{2.5.24}$$

$$\overline{E}_{[2]}^{(1)} = \sqrt{\overline{E}_1^2 + (\overline{E}_2 + \widehat{c}_{[2]}a_{[2]})^2}, \tag{2.5.25}$$

$$\overline{E}^{(2)} = \sqrt{(\overline{E}_1 - (1-\widehat{c}_{[1]})a_{[1]})^2 + (\overline{E}_2 - (1-\widehat{c}_{[2]})a_{[2]})^2}. \tag{2.5.26}$$

A similar analysis reveals that, upon letting

$$\omega = \frac{-2\left(\overline{E}_2^{*2} - \overline{E}_1^{*2}\right)}{c\overline{E}^2 - 2(1-c)\left(\overline{E}_2^{*2} - \overline{E}_1^{*2}\right)}, \tag{2.5.27}$$

the effective behavior can be calculated via

$$\widetilde{w}_{[2]}^{(1)}(\overline{\mathbf{E}}^*) = \min_{\omega} \left\{ c\phi^{(1)}\left(\sqrt{(1-(1-c)\omega)^2 + (1-c)\omega^2}\,\overline{E}\right) + (1-c)\phi^{(2)}\left(|1+c\omega|\overline{E}\right) \right\}. \tag{2.5.28}$$

Therefore, upon defining

$$\widetilde{w}_{[2]}(\overline{\mathbf{E}}) \equiv \max\{\widetilde{w}_{[2]}^{(1)}(\overline{\mathbf{E}}), \widetilde{w}_{[2]}^{(2)}(\overline{\mathbf{E}})\}, \tag{2.5.29}$$

we find that $\widetilde{w}_{[2]}(\overline{\mathbf{E}}^*) = \widetilde{w}_{VHS+}(\overline{\mathbf{E}}^*)$, where $\widetilde{w}_{VHS+}$ is given by Eq. (2.4.10). From this, we can conclude that the VHS bound is attained by a rank-2 laminate, proving optimality. As mentioned earlier, the VHS bound has two branches and the choice of the branch depends on $\overline{E}$. We see then that each branch is attained by a different rank-2 laminate. Now, if it is known that, without loss of generality, $\phi^{(1)}(\overline{E}) < \phi^{(2)}(\overline{E})$

for all $\overline{E}$, then the bound reduces to a single branch, whereby only one particular laminate is needed to attain the bound. This is indeed the case when the constitutive response of the phases are described by a pure power law, with each phase sharing the same nonlinearity exponent.

Further simplification is possible in the cases when the inclusion phase is taken to be either perfectly insulating or perfectly conducting. We explore such simplifications assuming that phase 2 is the matrix phase, but note that the final expressions for the effective behavior are the same when one takes phase 1 to be the matrix phase. For perfectly insulating inclusions (i.e. when $\phi^{(1)} \to 0$), we find that $\omega = -(1+c)^{-1}$, while

$$\overline{E}_1^* = \pm\frac{\sqrt{3-c}}{2}\overline{E}, \quad \text{and} \quad \overline{E}_2^* = \pm\frac{\sqrt{1+c}}{2}\overline{E}, \tag{2.5.30}$$

so that

$$\widetilde{w}_{[2]}(\overline{\mathbf{E}}^*) = (1-c)\phi^{(2)}\left(\frac{\overline{E}}{\sqrt{1+c}}\right). \tag{2.5.31}$$

On the other hand, in the case of perfectly conducting inclusions, when $\phi^{(1)}(E) = \infty$ unless $E = 0$, we find that $\omega = (1-c)^{-1}$, while

$$\overline{E}_1^* = \pm\frac{\sqrt{1+c}}{2}\overline{E}, \quad \text{and} \quad \overline{E}_2^* = \pm\frac{\sqrt{3-c}}{2}\overline{E}, \tag{2.5.32}$$

which yields

$$\widetilde{w}_{[2]}(\overline{\mathbf{E}}^*) = (1-c)\phi^{(2)}\left(\frac{\sqrt{1+c}}{1-c}\overline{E}\right). \tag{2.5.33}$$

Note that Eqs. (2.5.31) and (2.5.33) agree with the results of Ponte Castañeda (1992a), and the argument of $\phi^{(2)}$ is independent of the choice of $\phi^{(2)}$.

2.5.1.2 Three-dimensional dielectrics

Now, we fix $\mathbf{n}_{[i]} = \mathbf{e}_i$ for $i = 1, 2, 3$ so that

$$\overline{\mathbf{E}} = \overline{E}_1\mathbf{n}_{[1]} + \overline{E}_2\mathbf{n}_{[2]} + \overline{E}_3\mathbf{n}_{[3]}, \tag{2.5.34}$$

whereby

$$\overline{E}^2 = \overline{E}_1^2 + \overline{E}_2^2 + \overline{E}_3^2. \tag{2.5.35}$$

We also take $\widehat{c}_{[i]}$ as in Eq. (2.3.14), and letting phase 2 represent the matrix phase, we see that, from Eq. (2.3.6) with $M = 3$,

$$\begin{aligned}\widetilde{w}_{[3]}^{(2)}(\overline{\mathbf{E}}) = \min_{a_{[1]},a_{[2]},a_{[3]}} \Big\{ &\widehat{c}_{[1]}\widehat{c}_{[2]}\widehat{c}_{[3]}\phi^{(1)}\left(\overline{E}^{(1)}\right) + (1-\widehat{c}_{[1]})\widehat{c}_{[2]}\widehat{c}_{[3]}\phi^{(2)}\left(\overline{E}_{[1]}^{(2)}\right) \\ &+(1-\widehat{c}_{[2]})\widehat{c}_{[3]}\phi^{(2)}\left(\overline{E}_{[2]}^{(2)}\right) + (1-\widehat{c}_{[3]})\phi^{(2)}\left(\overline{E}_{[3]}^{(2)}\right)\Big\}\end{aligned} \tag{2.5.36}$$

where

$$\overline{E}^{(1)} = \sqrt{(\overline{E}_1 - (1-\widehat{c}_{[1]})a_{[1]})^2 + (\overline{E}_2 - (1-\widehat{c}_{[2]})a_{[2]})^2 + (\overline{E}_3 - (1-\widehat{c}_{[3]})a_{[3]})^2}, \tag{2.5.37}$$

$$\overline{E}_{[1]}^{(2)} = \sqrt{(\overline{E}_1 + \widehat{c}_{[1]}a_{[1]})^2 + (\overline{E}_2 - (1-\widehat{c}_{[2]})a_{[2]})^2 + (\overline{E}_3 - (1-\widehat{c}_{[3]})a_{[3]})^2}, \tag{2.5.38}$$

$$\overline{E}_{[2]}^{(2)} = \sqrt{\overline{E}_1^2 + (\overline{E}_2 + \widehat{c}_{[2]}a_{[2]})^2 + (\overline{E}_3 - (1-\widehat{c}_{[3]})a_{[3]})^2}, \tag{2.5.39}$$

$$\overline{E}_{[3]}^{(2)} = \sqrt{\overline{E}_1^2 + \overline{E}_2^2 + (\overline{E}_3 + \widehat{c}_{[3]}a_{[3]})^2}. \tag{2.5.40}$$

As mentioned earlier, it can be shown that with this choice of $\mathbf{n}_{[i]}$ and $\widehat{c}_{[i]}$, the effective behavior of the linear rank-3 laminate is isotropic. Therefore, the rank-3 laminate is a member of the class which is bounded by the VHS bounds. Additionally, it attains the linear HS bound. It therefore remains to show that the rank-3 laminate attains the VHS bound in the nonlinear case.

In a manner similar to that used in the two-dimensional case, the stationary conditions with respect to the $a_{[i]}$ $(i = 1, 2, 3)$ and $\overline{E}_j$ $(j = 1, 2, 3)$ can be combined to show that

$$\widehat{c}_{[1]}(1-\widehat{c}_{[1]})\overline{E}_2^* a_{[1]}^2(\overline{E}_2^* + \widehat{c}_{[2]}a_{[2]}) = (1-\widehat{c}_{[2]})\overline{E}_1^* a_{[2]}^2(\overline{E}_1^* - (1-2\widehat{c}_{[1]})a_{[1]}), \tag{2.5.41}$$

$$\widehat{c}_{[2]}(1-\widehat{c}_{[2]})\overline{E}_3^* a_{[2]}^2(\overline{E}_3^* + \widehat{c}_{[3]}a_{[3]}) = (1-\widehat{c}_{[3]})\overline{E}_2^* a_{[3]}^2(\overline{E}_2^* - (1-2\widehat{c}_{[2]})a_{[2]}), \tag{2.5.42}$$

from which is follows that

$$a_{[3]} = \frac{(1+2c)\overline{E}_3^* a_{[2]}}{(2+c)\overline{E}_2^*} = \frac{(1+2c)\overline{E}_3^* a_{[1]}}{3\overline{E}_1^*}, \tag{2.5.43}$$

which itself implies that

$$\frac{\partial \phi^{(2)}\left(\overline{E}_{[1]}^{(2)}\right)}{\partial \overline{E}} \frac{1}{\overline{E}_{[1]}^{(2)}} = \frac{\partial \phi^{(2)}\left(\overline{E}_{[2]}^{(2)}\right)}{\partial \overline{E}} \frac{1}{\overline{E}_{[2]}^{(2)}} = \frac{\partial \phi^{(2)}\left(\overline{E}_{[3]}^{(2)}\right)}{\partial \overline{E}} \frac{1}{\overline{E}_{[3]}^{(2)}}, \tag{2.5.44}$$

i.e. that the secant dielectric coefficient of phase 2 is the same when evaluated at $\overline{E}_{[j]}^{(2)}$ for $j = 1, 2, 3$. Here

$$\overline{\mathbf{E}}^* = \overline{E}_1^* \mathbf{n}_{[1]} + \overline{E}_2^* \mathbf{n}_{[2]} + \overline{E}_3^* \mathbf{n}_{[3]} \tag{2.5.45}$$

corresponds to the optimal value of $\overline{\mathbf{E}}$ that maximizes $\widetilde{w}_{[3]}^{(2)}$ (and more generally the value of $\overline{\mathbf{E}}$ that maximizes the function it is an argument of), subject to the constraint $\overline{E}^2 = \overline{E}_1^{*2} + \overline{E}_2^{*2} + \overline{E}_3^{*2}$.

By appealing again to the square concavity hypothesis, this implies that $\overline{E}_{[1]}^{(2)} = \overline{E}_{[2]}^{(2)} = \overline{E}_{[3]}^{(2)}$. Making use of Eqs. (2.5.38)-(2.5.40), we see that $\widetilde{w}_3^{[2]}(\overline{\mathbf{E}})$ is optimal precisely when the components of $\overline{\mathbf{E}}$ satisfy

$$\overline{E}_2^{*2} = 3(\overline{E}_1^* \overline{E}_3^*)^2. \tag{2.5.46}$$

Thus, by letting

$$\omega = \frac{2\left(\overline{E}_3^{*2} - \overline{E}_2^{*2}\right)}{(1+2c)\overline{E}_2^{*2} + (1-4c)\overline{E}_3^{*2}} = \frac{2\left(\overline{E}_2^{*2} - \overline{E}_1^{*2}\right)}{(2+c)\overline{E}_1^{*2} - 3c\overline{E}_2^{*2}}, \tag{2.5.47}$$

we find that

$$\widetilde{w}_{[3]}^{(2)}(\overline{\mathbf{E}}^*) = \min_{\omega} \left\{ c\phi^{(1)}\left(|1-(1-c)\omega|\overline{E}\right) + (1-c)\phi^{(2)}\left(\sqrt{(1+c\omega)^2 + 2c\omega^2}\,\overline{E}\right) \right\}. \tag{2.5.48}$$

By taking instead phase 1 to be the matrix phase, it can be shown, *mutatis mutandis* that

$$\widetilde{w}^{(1)}_{[3]}(\overline{\mathbf{E}}^*) = \min_{\omega}\left\{c\phi^{(1)}\left(\sqrt{(1-(1-c)\omega)^2+2(1-c)\omega^2}\,\overline{E}\right)+(1-c)\phi^{(2)}\left(|1+c\omega|\overline{E}\right)\right\}, \tag{2.5.49}$$

whereby upon taking

$$\widetilde{w}_{[3]}(\overline{\mathbf{E}}) \equiv \max\{\widetilde{w}^{(1)}_{[3]}(\overline{\mathbf{E}}), \widetilde{w}^{(2)}_{[3]}(\overline{\mathbf{E}})\}, \tag{2.5.50}$$

it follows $\widetilde{w}_{[3]}(\overline{\mathbf{E}}^*) = \widetilde{w}_{VHS+}(\overline{\mathbf{E}}^*)$, with the expression for $\widetilde{w}_{HS+}$ given by Eq. (2.4.10).

As above, further simplification is possible in two limiting cases. When phase 1 is perfectly insulating, we find that $\omega = -(2+c)^{-1}$, which can be used to show that

$$\overline{E}^*_1 = \pm\frac{\sqrt{5-2c}}{3}\overline{E}, \quad \overline{E}^*_2 = \pm\frac{\sqrt{(2+c)(5-2c)}}{3\sqrt{4-c}}\overline{E}, \quad \overline{E}^*_3 = \pm\frac{\sqrt{2+c}}{\sqrt{3(4-c)}}\overline{E}, \tag{2.5.51}$$

and

$$\widetilde{w}_{[3]}(\overline{\mathbf{E}}^*) = (1-c)\phi^{(2)}\left(\frac{\overline{E}}{\sqrt{1+\frac{c}{2}}}\right). \tag{2.5.52}$$

On the other hand, when phase 1 is perfectly conducting, we find that $\omega = (1-c)^{-1}$, so that

$$\overline{E}^*_1 = \pm\frac{\sqrt{1+2c}}{3}\overline{E}, \quad \overline{E}^*_2 = \pm\frac{\sqrt{(4-c)(1+2c)}}{3\sqrt{2+c}}\overline{E}, \quad \overline{E}^*_3 = \pm\frac{\sqrt{4-c}}{\sqrt{3(2+c)}}\overline{E}, \tag{2.5.53}$$

and

$$\widetilde{w}_{[3]}(\overline{\mathbf{E}}^*) = (1-c)\phi^{(2)}\left(\frac{\sqrt{1+2c}}{1-c}\overline{E}\right). \tag{2.5.54}$$

Again, we note that both Eqs. (2.5.52) and (2.5.54) agree with the results of Ponte Castañeda (1992a), and the argument of $\phi^{(2)}$ is independent of the choice of $\phi^{(2)}$, so long as it satisfies the square concavity (or convexity) assumption.

2.5.1.3 Further Results

It is illustrative to apply the above framework to a case when $\phi^{(r)}$ has a specific form. In particular, we assume that

$$\phi^{(r)}(E) = \frac{\epsilon^{(r)}}{m^{(r)}+1} E^{m^{(r)}+1}. \tag{2.5.55}$$

where $\epsilon^{(r)}$ is the dielectric coefficient and $m^{(r)}$ the nonlinearity of phase r. Now, when $m^{(1)} = m^{(2)} = m$, then, since $\phi^{(r)}$ are both homogeneous of degree $m+1$ in E, we can write

$$\widetilde{w}_{[2]}(\overline{\mathbf{E}}) = \frac{\widetilde{\epsilon}_{[2]}}{m+1} \overline{E}^{m+1}, \tag{2.5.56}$$

where $\widetilde{\epsilon}_{[2]} = \widetilde{\epsilon}_{[2]}(\overline{\mathbf{E}})$ is the effective nonlinear dielectric coefficient of the laminate, and is homogeneous of degree zero in $\overline{\mathbf{E}}$; in particular, it is, in general, a function of $\overline{E}_1/\overline{E}$ and $\overline{E}_2/\overline{E}$. When $0 \leqslant m \leqslant 1$, we are able to obtain upper bounds on $\widetilde{\epsilon}_{[2]}$ by using corresponding upper bounds for the LCC, while when $1 \leqslant m \leqslant \infty$, we can generate lower bounds on $\widetilde{\epsilon}_{[2]}$ by using lower bounds on the LCC (see Section 2.4 for a discussion of square concavity versus square convexity).

In what follows, we will compare the equipotential surfaces of $\widetilde{w}_{[2]}$ to $\widetilde{w}_{VHS}$. In particular, upon defining the gauge functions

$$\widetilde{\Phi}_{[2]}(\overline{\mathbf{E}}) = \frac{\widetilde{\epsilon}_{[2]}(\overline{\mathbf{E}})}{\epsilon^{(2)}} \overline{E}^{m+1} - 1, \tag{2.5.57}$$

and

$$\widetilde{\Phi}_{VHS}(\overline{\mathbf{E}}) = \frac{\widetilde{\epsilon}_{VHS}}{\epsilon^{(2)}} \overline{E}^{m+1} - 1, \tag{2.5.58}$$

we will compare corresponding gauge surfaces defined by

$$\widetilde{\Phi}_{[2]}(\overline{\mathbf{E}}) = 0, \quad \text{and} \quad \widetilde{\Phi}_{VHS}(\overline{\mathbf{E}}) = 0. \tag{2.5.59}$$

Having assumed that $w^{(r)}$ is strict convex, it follows that $\widetilde{w}^{(r)}_{[2]}$ is also strictly convex;

the same is true for $\widetilde{w}_{VHS}$ (Marcellini, 1978). This implies that the sets defined by $\{\widetilde{\Phi}_{VHS}(\overline{\mathbf{E}}) \leqslant 0\}$ and $\{\widetilde{\Phi}_{[2]}(\overline{\mathbf{E}}) \leqslant 0\}$ will be convex (Ekeland and Téman, 1976), and hence, the points $\overline{\mathbf{E}}$ for which Eq. (2.5.59) hold will form the boundaries of these convex set. It is clear that when $\widetilde{w}_{VHS}$ represents an upper bound on $\widetilde{w}^{(r)}_{[2]}$, then $\{\widetilde{\Phi}_{VHS}(\overline{\mathbf{E}}) \leqslant 0\} \subseteq \{\widetilde{\Phi}_{[2]}(\overline{\mathbf{E}}) \leqslant 0\}$; when $\widetilde{w}_{VHS}$ is a lower bound, the converse holds.

We will restrict our attention, in two-dimensions, to the two cases discussed above. Now, when $0 \leqslant m \leqslant 1$, then $\phi^{(r)}$ satisfy the square-concavity hypothesis, and as such, the VLC method produces rigorous upper bounds on the effective energy potential. We therefore compare $\widetilde{\Phi}_{[2]}$ with the gauge surface predicted VHS upper bound in the case of perfectly insulating inclusions, when $\epsilon^{(1)} \to 0$; the VHS upper bound for perfectly conducting inclusions is infinite. For composites with perfectly insulating inclusions, the gauge function takes the form (Ponte Castañeda, 1992a)

$$\widetilde{\Phi}_{VHS+}(\overline{\mathbf{E}}) = \frac{(1-c)}{(1+c)^{(m+1)/2}}\overline{E}^{m+1} - 1. \tag{2.5.60}$$

These results are presented in Figure 2.1. On the other hand, when $1 \leqslant m \leqslant \infty$ so that $\phi^{(r)}$ satisfy the square-convexity hypothesis, the VLC method produces rigorous lower bounds on the effective energy potential. In this case, we compare $\widetilde{\Phi}_{[2]}$ with the gauge surface predicted VHS lower bound in the case of perfectly conducting inclusions, when $\epsilon^{(1)} \to \infty$; the VHS lower bound for perfectly insulating inclusions is zero. Here, the gauge function takes the form (Ponte Castañeda, 1992a)

$$\widetilde{\Phi}_{VHS-}(\overline{\mathbf{E}}) = (1-c)\left(\frac{\sqrt{1+c}}{1-c}\right)^{m+1}\overline{E}^{m+1} - 1. \tag{2.5.61}$$

These results are presented in Figure 2.2.

Note that in Figures 2.1a and 2.2a, when $m = 1$, the rank-2 laminate and the VHS bounds both reduce to the linear HS upper and lower bounds, respectively. In general, as the nonlinearity increases (i.e. as m moves away from 1), the behavior of the rank-2 laminate becomes more anisotropic. Note that gauge surface of the

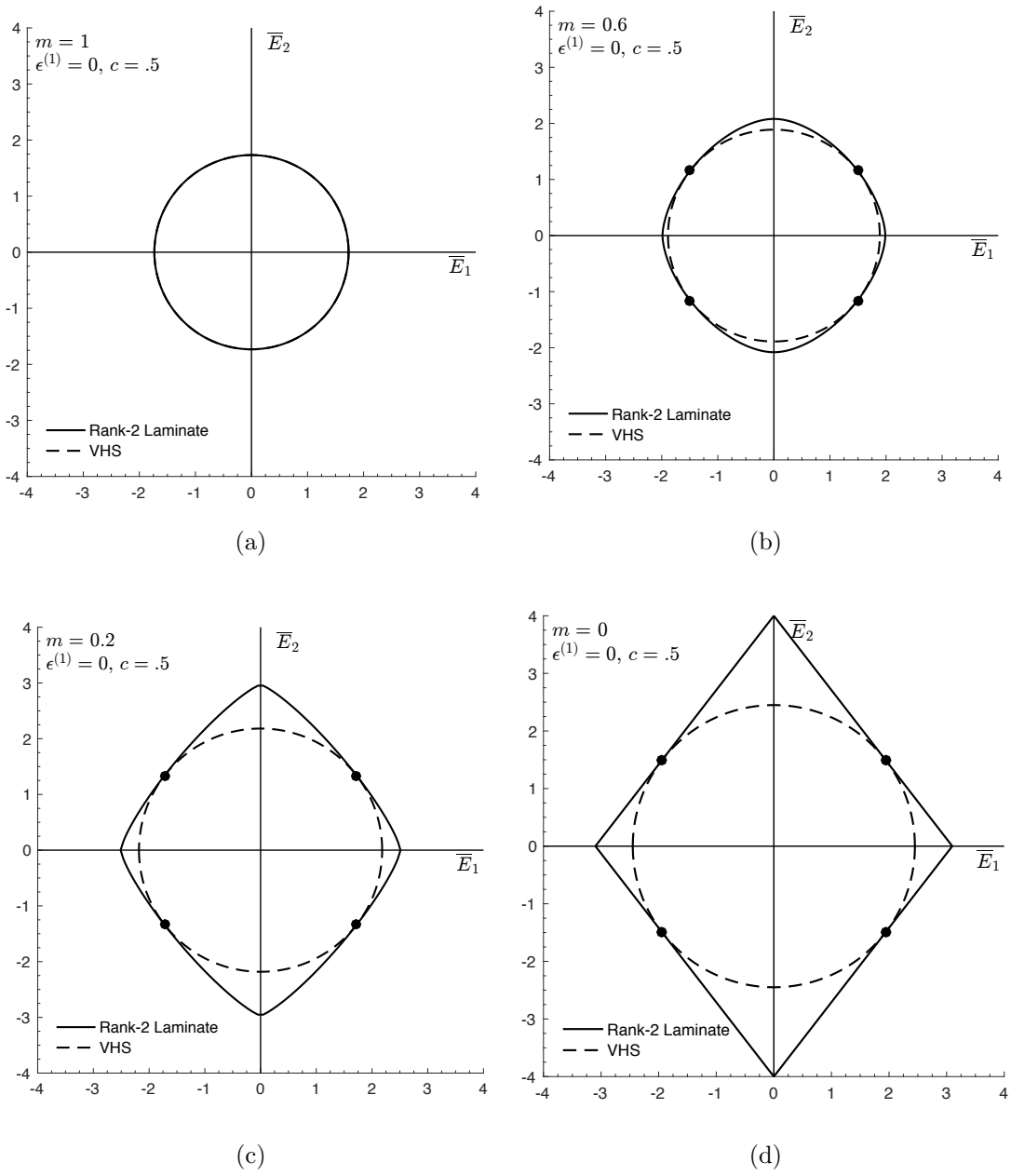

Figure 2.1: Gauge surface of a rank-2 laminate with perfectly insulating "inclusion" phase in volume fraction $c = .5$, compared to the VHS upper bound. Results are presented in the $\overline{E}_1 - \overline{E}_2$ plane. Points where the VHS bounds are attained are indicated by black dots. Results are presented for values of the nonlinearity m equal to (a) 1 (b) 0.6 (c) 0.2 and (d) 0.

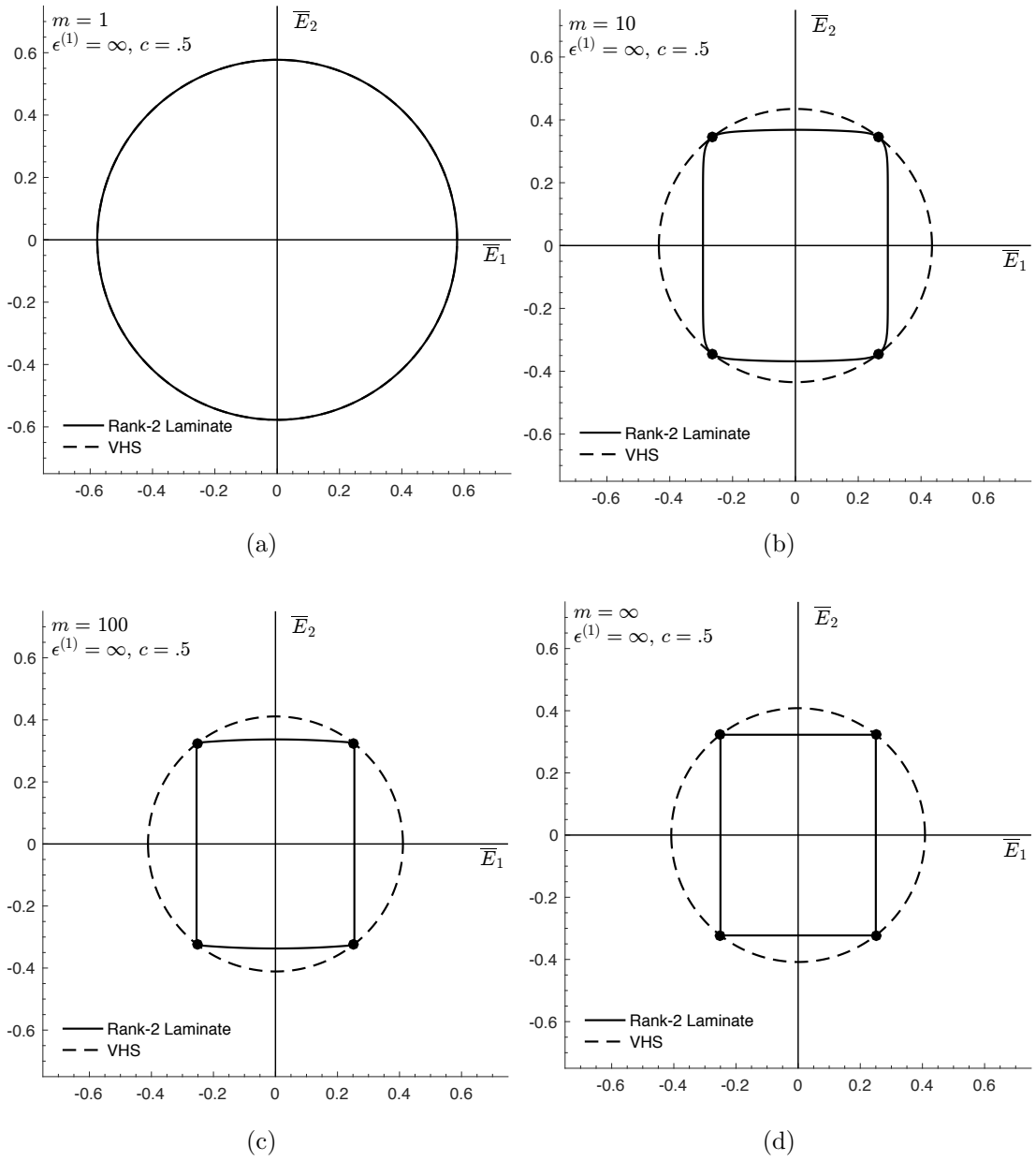

Figure 2.2: Gauge surface of a rank-2 laminate with perfectly conducting "inclusion" phase in volume fraction $c = .5$, compared to the VHS lower bound. Results are presented in the $\overline{E}_1 - \overline{E}_2$ plane. Points where the VHS bounds are attained are indicated by black dots. Results are presented for values of the nonlinearity m equal to (a) 1 (b) 5 (c) 10 and (d) ∞.

rank-2 laminate coincides with the VHS upper or lower bounds precisely when $\overline{\mathbf{E}}$ has components given by Eq. (2.5.30) or Eq. (2.5.32) respectively. It is worth reiterating that this prescription of $\overline{\mathbf{E}}$ is independent of the form of $\phi^{(r)}$, and hence is the same regardless of the nonlinearity.

2.5.2 Elasticity

The purpose of this subsection is two-fold. Firstly, we wish to discuss the optimality of the VHS bounds in the context of incompressible two-dimensional elasticity. This discussion will reveal that a rank-2 laminate, not a rank-3 laminate, attains the VHS bound. We will also examine the case of two-dimensional elasticity under more general loading conditions, and show that a rank-3 laminate attains the VHS bounds. We also consider purely hydrostatic loading conditions and show how in this case, the VHS bounds fail to be optimal.

2.5.2.1 Two-dimensional incompressible elasticity

To start, we fix $\mathbf{n}_{[1]}$ and $\mathbf{n}_{[2]}$ as in Eq. (2.3.24) and $\widehat{c}_{[1]}$ and $\widehat{c}_{[2]}$ as in Eq. (2.3.13). We assume that each phase is incompressible, so that $W^{(r)}(\boldsymbol{\varepsilon}) = \varphi^{(r)}(\varepsilon_e)$ if $\varepsilon_m = 0$, and is infinite otherwise. We also assume that $\varphi^{(r)}$ satisfies the square concavity hypothesis. Then, from Eq. (2.3.15), with $M = 2$ we have

$$\widetilde{W}^{(2)}_{[2]}(\overline{\boldsymbol{\varepsilon}}) = \min_{\mathbf{a}_{[1]},\mathbf{a}_{[2]}} \left\{ \widehat{c}_{[1]}\widehat{c}_{[2]}\varphi^{(1)}\left(\overline{\varepsilon}^{(1)}_e\right) + (1-\widehat{c}_{[1]})\widehat{c}_{[2]}\varphi^{(2)}\left(\overline{\varepsilon}^{(2)}_{e,[1]}\right) + (1-\widehat{c}_{[2]})\phi^{(2)}\left(\overline{\varepsilon}^{(2)}_{e,[2]}\right) \right\}, \tag{2.5.62}$$

where $\overline{\varepsilon}^{(1)}_e$ and $\overline{\varepsilon}^{(2)}_{e,[j]}\,(j = 1, 2)$ are the equivalent strain measures associated to the strains

$$\overline{\boldsymbol{\varepsilon}}^{(1)} = \overline{\boldsymbol{\varepsilon}} - (1-\widehat{c}_{[1]})\mathbf{a}_{[1]} \otimes_s \mathbf{n}_{[1]} - (1-\widehat{c}_{[2]})\mathbf{a}_{[2]} \otimes_s \mathbf{n}_{[2]} \tag{2.5.63}$$

$$\overline{\boldsymbol{\varepsilon}}^{(2)}_{[1]} = \overline{\boldsymbol{\varepsilon}} + \widehat{c}_{[1]}\mathbf{a}_{[1]} \otimes_s \mathbf{n}_{[1]} - (1-\widehat{c}_{[2]})\mathbf{a}_{[2]} \otimes_s \mathbf{n}_{[2]} \tag{2.5.64}$$

$$\overline{\boldsymbol{\varepsilon}}^{(2)}_{[2]} = \overline{\boldsymbol{\varepsilon}} + \widehat{c}_{[2]}\mathbf{a}_{[2]} \otimes_s \mathbf{n}_{[2]} \tag{2.5.65}$$

As discussed in Section 2.3, with this choice of $\mathbf{n}_i$ and $\widehat{c}_{[i]}$, the rank-2 laminate has linearly isotropic behavior under purely deviatoric loading, and hence is a member of the class of composites bounded by the VHS bound. Now, due to the assumed incompressibility, the composite can only support purely deviatoric loading, and it must be that $\mathrm{tr}(\overline{\boldsymbol{\varepsilon}}^{(1)}) = \mathrm{tr}(\overline{\boldsymbol{\varepsilon}}^{(2)}_{[1]}) = \mathrm{tr}(\overline{\boldsymbol{\varepsilon}}^{(2)}_{[2]}) = 0$, which, from Eqs. (2.5.63)-(2.5.65), can be used to show that $(\mathbf{a}_{[1]} \cdot \mathbf{n}_{[1]}) = (\mathbf{a}_{[2]} \cdot \mathbf{n}_{[2]}) = 0$. Therefore, we can write

$$\mathbf{a}_{[1]} = a_{[1]}\mathbf{n}^{\perp}_{[1]}, \quad \mathbf{a}_{[2]} = a_{[2]}\mathbf{n}^{\perp}_{[2]}, \tag{2.5.66}$$

where

$$\mathbf{n}^{\perp}_{[1]} = \begin{bmatrix} 0 \\ 1 \end{bmatrix}, \quad \mathbf{n}^{\perp}_{[2]} = \frac{1}{\sqrt{2}} \begin{bmatrix} 1 \\ -1 \end{bmatrix}. \tag{2.5.67}$$

Since $\overline{\varepsilon}_m = 0$, $\overline{\boldsymbol{\varepsilon}}$ can be written as

$$\overline{\boldsymbol{\varepsilon}} = \begin{bmatrix} \frac{\overline{\varepsilon}_{11} - \overline{\varepsilon}_{22}}{2} & \overline{\varepsilon}_{12} \\ \overline{\varepsilon}_{12} & \frac{\overline{\varepsilon}_{22} - \overline{\varepsilon}_{11}}{2} \end{bmatrix} \tag{2.5.68}$$

where $\frac{\overline{\varepsilon}_{11} - \overline{\varepsilon}_{22}}{2}$ and $\overline{\varepsilon}_{12}$ satisfy the condition

$$\overline{\varepsilon}^2_e = \frac{4}{3}\left(\left(\frac{\overline{\varepsilon}_{11} - \overline{\varepsilon}_{22}}{2} \right)^2 + \overline{\varepsilon}^2_{12} \right), \tag{2.5.69}$$

which will serve as a constraint when it comes time to optimize over $\overline{\boldsymbol{\varepsilon}}$.

A straightforward calculation reveals that

$$\overline{\varepsilon}^{(1)}_e = \frac{1}{\sqrt{3}} \sqrt{(2\overline{\varepsilon}_{12} - (1 - \widehat{c}_{[1]})a_{[1]})^2 + ((\overline{\varepsilon}_{11} - \overline{\varepsilon}_{22}) - (1 - \widehat{c}_{[2]})a_{[2]})^2}, \tag{2.5.70}$$

$$\overline{\varepsilon}^{(2)}_{e,[1]} = \frac{1}{\sqrt{3}} \sqrt{(2\overline{\varepsilon}_{12} + \widehat{c}_{[1]}a_{[1]})^2 + ((\overline{\varepsilon}_{11} - \overline{\varepsilon}_{22}) - (1 - \widehat{c}_{[2]})a_{[2]})^2}, \tag{2.5.71}$$

$$\overline{\varepsilon}^{(2)}_{e,[2]} = \frac{1}{\sqrt{3}} \sqrt{4\overline{\varepsilon}^2_{12} + ((\overline{\varepsilon}_{11} - \overline{\varepsilon}_{22}) + \widehat{c}_{[2]}a_{[2]})^2}. \tag{2.5.72}$$

In comparing Eqs. (2.5.4)-(2.5.6) with Eqs. (2.5.70)-(2.5.72), we see that the in-

compressible two-dimensional elasticity problem, which is in general tensorial, can be treated vectorially as in Section 2.5.1.1. In a manner similar to what was outlined above, given a tensor-valued function g, by $g(\boldsymbol{F}^*)$, we mean

$$\boldsymbol{F}^* = \underset{\boldsymbol{F}:\, F_m=\overline{\varepsilon}_m,\, F_e=\overline{\varepsilon}_e}{\operatorname{argmax}} g(\boldsymbol{F}), \tag{2.5.73}$$

i.e. $\boldsymbol{F}^*$ is value that maximizes g, subject to the constraint that $F_m \equiv \frac{1}{2}\mathrm{tr}(\boldsymbol{F}) = \overline{\varepsilon}_m$ and $F_e \equiv \sqrt{\frac{2}{3}\boldsymbol{F}_d \cdot \boldsymbol{F}_d} = \overline{\varepsilon}_e$. Therefore, upon defining

$$\widetilde{W}_{[2]}(\overline{\boldsymbol{\varepsilon}}) = \max\{\widetilde{W}^{(1)}_{[2]}(\overline{\boldsymbol{\varepsilon}}), \widetilde{W}^{(2)}_{[2]}(\overline{\boldsymbol{\varepsilon}})\}, \tag{2.5.74}$$

we find that $\widetilde{W}_{[2]}(\overline{\boldsymbol{\varepsilon}}^*) = \widetilde{W}_{VHS+}(\overline{\boldsymbol{\varepsilon}}^*)$, and hence the VHS bound is attained by a rank-two laminate, which has linearly isotropic response, (and attains the linear HS bound) can attain the nonlinear VHS bound for specific loading conditions. Moreover, we find that the VHS bound is attained precisely when $\overline{\varepsilon}^{(r)}_{e,[1]}$ and $\overline{\varepsilon}^{(r)}_{e,[2]}$ satisfy the condition

$$\frac{\partial \varphi^{(r)}(\overline{\varepsilon}^{(r)}_{e,[1]})}{\partial \varepsilon_e}\frac{1}{\overline{\varepsilon}^{(r)}_{e,[1]}} = \frac{\partial \varphi^{(r)}(\overline{\varepsilon}^{(r)}_{e,[2]})}{\partial \varepsilon_e}\frac{1}{\overline{\varepsilon}^{(r)}_{e,[2]}}, \tag{2.5.75}$$

where $r = 1$ or 2 depending on which phase is acting as the matrix.

Now, as above, simplification is possible in some special cases. In particular, in the case of a porous laminate, when phase 1 is taken to be void and phase 2 acts as the matrix phase, we find that

$$\frac{\overline{\varepsilon}^*_{11} - \overline{\varepsilon}^*_{22}}{2} = \pm\left(\frac{\sqrt{1+c}}{2}\right)\frac{\sqrt{3}\overline{\varepsilon}_e}{2}, \quad \text{and} \quad \overline{\varepsilon}^*_{12} = \pm\left(\frac{\sqrt{3-c}}{2}\right)\frac{\sqrt{3}\overline{\varepsilon}_e}{2}, \tag{2.5.76}$$

whereby

$$\widetilde{W}_{[2]}(\overline{\boldsymbol{\varepsilon}}^*) = (1-c)\varphi^{(2)}\left(\frac{\overline{\varepsilon}_e}{\sqrt{1+c}}\right), \tag{2.5.77}$$

where the argument of $\varphi^{(2)}$ is independent of the form of $\varphi^{(2)}$.

Note that the values of $\frac{\overline{\varepsilon}_{11}^* - \overline{\varepsilon}_{22}^*}{2}$ and $\overline{\varepsilon}_{12}^*$ take the same form as $\overline{E}_2^*$ and $\overline{E}_1^*$, respectively, in Eq. (2.5.32). In fact, as we will see, gauge surfaces for the rank-2 laminate in the $\frac{\overline{\varepsilon}_{11} - \overline{\varepsilon}_{22}}{2} - \overline{\varepsilon}_{12}$ plane are nothing more than the results for the rank-2 laminate in the $\overline{E}_1 - \overline{E}_2$ plane, depicted in Figure 2.2, rotated by $\frac{\pi}{2}$. This is related to the specific correspondence between two-dimensional dielectrics and two-dimensional, (incompressible) planar elasticity (Chen and Lai, 1997; Milton and Movchan, 1995; Francfort, 1992).

As indicated by Eqs. (2.5.17), (2.5.44), and (2.5.75), the VHS bound is attained by a finite-rank laminate precisely when the secant modulus of the matrix phase is the same at each iteration. Now, the effective nonlinear potential for the finite-rank laminate can also, in principle, be calculated using Eq. (2.4.4), in the context of dielectrics, and Eq. (2.4.18), in the context of elasticity. Consider in particular the rank-2 laminate that attains the VHS bounds under purely deviatoric loading; the discussion to follow holds more generally, but we fix a specific case to ease the discussion. As noted by Ponte Castañeda (1992a), the rank-2 laminate would need to be treated as a 3-phase composite when applying the VLC procedure. In particular, upon treating phase 2 as the matrix phase, the LCC would be chosen with one phase corresponding to phase 1, and two phases corresponding to phase 2, one phase for each lamination; this is necessary since, in general, the local fields of phase 2 will not have the same value at each iteration. Nonetheless, our results reveal that the optimal heterogenous shear modulus of the LCC for which equality is obtained in Eq. (2.4.18) is in fact phase-wise constant. Moreover, due to Eq. (2.5.75), the moduli in the two "phases" of the matrix phase are the same, and hence so too are the fields.

2.5.2.2 Further results

To better illustrate the attainability of the VHS bounds in the context of nonlinear elasticity, we consider the case when

$$\varphi^{(r)}(\varepsilon_e) = \frac{4\mu^{(r)}}{3(m+1)}\left(\frac{3\varepsilon_e}{2}\right)^{m+1}. \tag{2.5.78}$$

Unlike in dielectrics, the nonlinearity exponent m is restricted to takings values $0 \leqslant m \leqslant 1$, whereby, on account of $\varphi^{(r)}$ satisfying the square concavity hypothesis, the resulting variational bounds will represent an upper bound on the effective properties of the material. We continue to assume that the inclusion phase is void, whereby $\mu^{(1)} = 0$. From here on, we let $\mu = \mu^{(2)}$ correspond to the shear modulus of the matrix phase. As above, in order to best visualize our results, we define the gauge functions

$$\widetilde{\Psi}_{[2]}(\overline{\boldsymbol{\varepsilon}}) = \widetilde{W}_{[2]}(\overline{\boldsymbol{\varepsilon}}) - \frac{2\mu}{(m+1)}\left(\frac{3}{2}\right)^{m} \tag{2.5.79}$$

and

$$\widetilde{\Psi}_{VHS+}(\overline{\boldsymbol{\varepsilon}}) = \widetilde{W}_{VHS+}(\overline{\boldsymbol{\varepsilon}}) - \frac{2\mu}{(m+1)}\left(\frac{3}{2}\right)^{m} \tag{2.5.80}$$

and look to compare the gauge surfaces defined by

$$\widetilde{\Psi}_{[2]}(\overline{\boldsymbol{\varepsilon}}) = 0, \quad \text{and} \quad \widetilde{\Psi}_{VHS+}(\overline{\boldsymbol{\varepsilon}}) = 0. \tag{2.5.81}$$

In the current setting of two-dimensional incompressible elasticity, for any composite whose phases have potentials of the form (2.5.78), it follows from their homogeneity of degree $m+1$ in $\boldsymbol{\varepsilon}$, that the effective potential can be written as

$$\widetilde{W}(\overline{\boldsymbol{\varepsilon}}) = \frac{4\widetilde{\mu}_{[2]}}{3(m+1)}\left(\frac{3\overline{\varepsilon}_e}{2}\right)^{m+1}, \tag{2.5.82}$$

where $\widetilde{\mu}_{[2]} = \widetilde{\mu}_{[2]}(\overline{\boldsymbol{\varepsilon}})$ is the *anistropic* effective shear modulus, and is homogeneous of

degree zero in $\overline{\boldsymbol{\varepsilon}}$. Therefore, just as above, we can rewrite the gauge functions as

$$\widetilde{\Psi}_{[2]}(\overline{\boldsymbol{\varepsilon}}) = \frac{\widetilde{\mu}_{[2]}(\overline{\boldsymbol{\varepsilon}})}{\mu}\overline{\varepsilon}_e^2 - 1, \quad \text{and} \quad \widetilde{\Psi}_{VHS+}(\overline{\boldsymbol{\varepsilon}}) = \frac{\widetilde{\mu}_{VHS}}{\mu}\overline{\varepsilon}_e^2 - 1, \tag{2.5.83}$$

where

$$\frac{\widetilde{\mu}_{VHS}}{\mu} = \frac{(1-c)}{(1+c)^{(m+1)/2}}. \tag{2.5.84}$$

In the current setting of two-dimensional incompressible elasticity, the gauge surface is a two-dimensional surface in the plane of the strain deviator. As such, we will present cross sections of the gauge surface by finding the values $\frac{\overline{\varepsilon}_{11}-\overline{\varepsilon}_{22}}{2}$ and $\overline{\varepsilon}_{12}$ for which Eq. (2.5.81) is satisfied.

For purely deviatoric loading, we consider the gauge surface plotted in the $\frac{\overline{\varepsilon}_{11}-\overline{\varepsilon}_{22}}{2} - \overline{\varepsilon}_{12}$ plane, akin to the ones given in Figure 2.2. We do so in Figure 2.3, and we also include results for the rank-3 laminate. Recall that in the linear case, this rank-3 laminate has isotropic behavior under *general* loading (not just under purely deviatoric loading); additionally, it attains the HS bounds. Therefore, this rank-3 laminate lies in the class of microstructures bounded by the VHS bounds under purely deviatoric loading. Now, as we see in Figure 2.3, and consistent with the calculations laid out above, the rank-2 laminate attains the VHS bound precisely when $\frac{\overline{\varepsilon}_{11}-\overline{\varepsilon}_{22}}{2}$ and $\overline{\varepsilon}_{12}$ take the values in Eq. (2.5.76), independently of the value of m. We also see that the rank-3 laminate does not attain the VHS bound, with the gauge surfaces always lying strictly outside of those predicted by the bounds. Note that in the ideally plastic limit (i.e. as $m \to 0$), the corresponding gauge surface of the rank-3 laminate has hexagonal symmetry, while that of the rank-2 laminate only has orthotropic symmetry (in the $\frac{\overline{\varepsilon}_{11}-\overline{\varepsilon}_{22}}{2} - \overline{\varepsilon}_{12}$ plane).

Recall that the VHS bounds represent bounds on the class of microstructures that have linearly isotropic effective behavior. This includes, but is not restricted to, all statistically isotropic microstructures. However, the inclusions of other, "undesirable," microstructures prohibits the optimality of the VHS bounds on composites

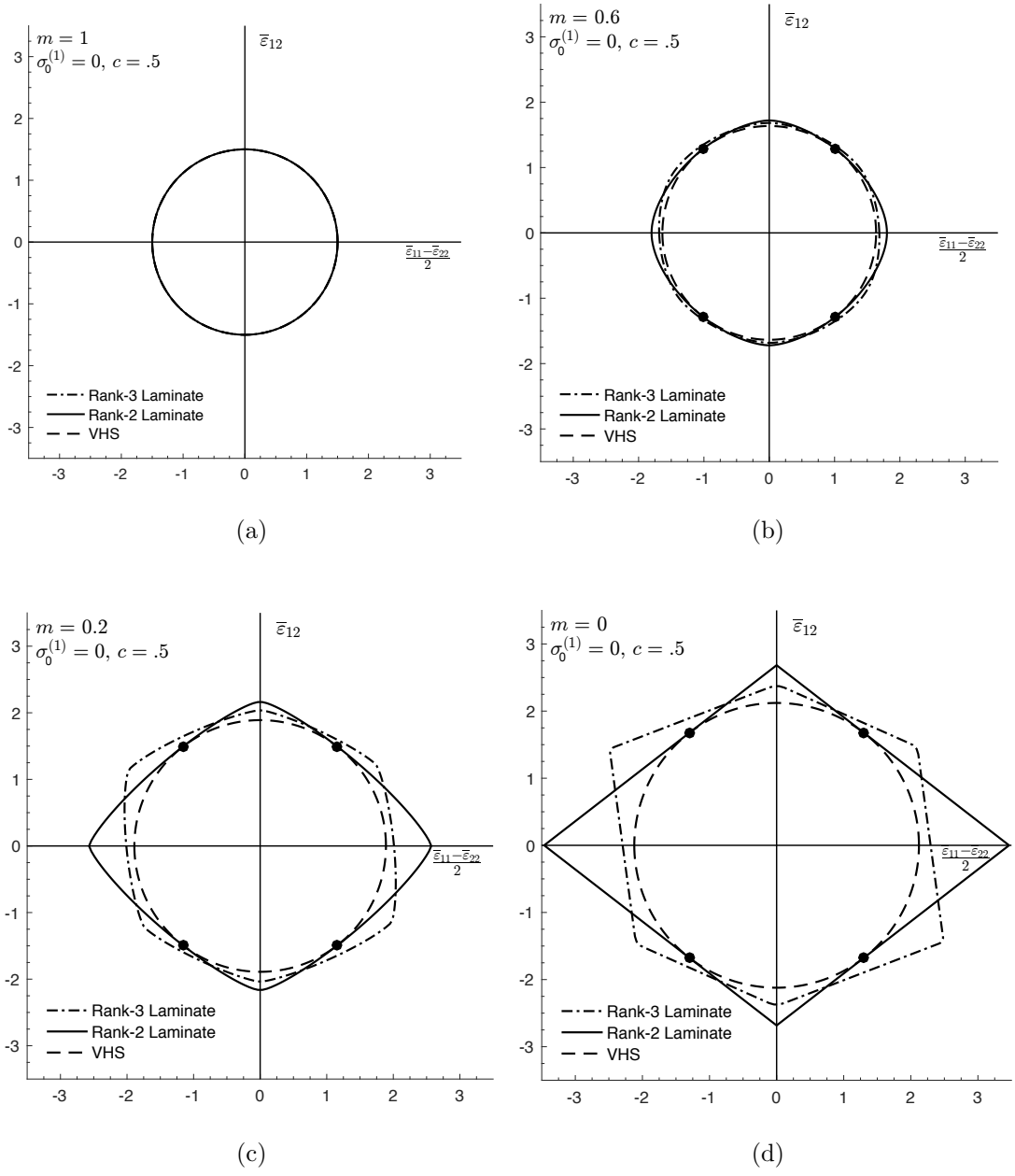

Figure 2.3: Level sets in the $\frac{\overline{\sigma}_{11}-\overline{\sigma}_{22}}{2} - \overline{\sigma}_{12}$ plane of a rank-2 laminate with porous "inclusion" phase in volume fraction $c = .5$, compared to the VHS lower bound. Results for the rank-3 laminate are included for reference, and all results are presented for values of the nonlinearity n equal to (a) 1 (b) 10 (c) 100 and (d) ∞.

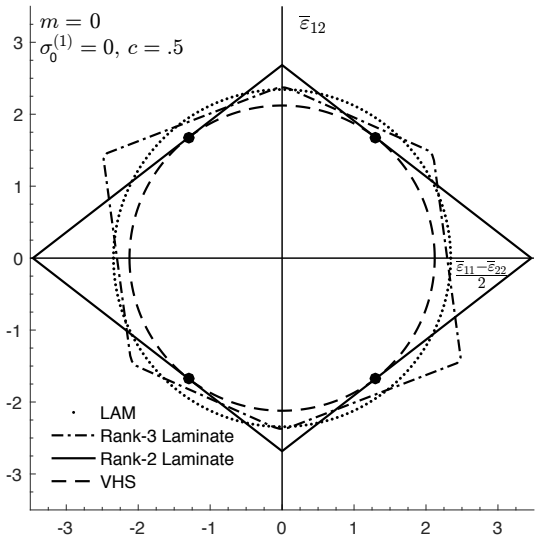

(a)

Figure 2.4: (a) Cross section of the gauge surface in the $\frac{\overline{\varepsilon}_{11}-\overline{\varepsilon}_{22}}{2} - \overline{\varepsilon}_{12}$ plane with $\overline{\varepsilon}_m = 0$ of a rank-2 laminate with porous "inclusion" phase in volume fraction $c = .5$, compared to the VHS upper bound, the rank-3 laminate, as well as the infinite rank-laminate. Points where the VHS bounds are attained are indicated by black dots.

with statistically isotropic microstructures, and illustrates the role that nonlinearity and the anisotropy of the microstructure play in determining the effective behavior. In connection with the symmetries of the rank-2 and rank-3 laminates in the ideally plastic limit, the rank-2 laminate represents a microstructure in the class bounded by the VHS bounds that, in some sense, is the most anisotropic. It is this inherent anisotropy that allows the rank-2 laminate to attain the bound. On the other hand, the rank-3 laminate's microstructure is, in the same sense, *less* anisotropic than that of the rank-2 laminate. In fact, the infinite rank-laminate (LAM) is known to have a statistically isotropic microstructure (Idiart, 2008; Idiart and Ponte Castañeda, 2013). Statistical isotropy implies that the linear, and nonlinear, behavior of the LAM is isotropic, whereby it is a member of the class of microstructures bounded by the VHS bounds. Indeed, as depicted in Figure 2.4a, the gauge surface of the LAM

lies strictly within that of the VHS bounds. Moreover, its response is generally softer than that of the lower rank laminates, and in fact the gauge surface of the LAM has the largest maximal distance from that of the VHS bounds, when compared with the rank-2 and rank-3 laminates.

2.6 Conclusion

In this chapter, we looked to answer some questions regarding the optimality of nonlinear variational bounds. We first showed that the nonlinear variational procedure, when applied to a composite with isotropic phases given in prescribed volume fractions, produces optimal bounds not on the class of two-phase isotropic composites with statistically isotropic microstructures, but rather on the class of two-phase anisotropic composites that have linearly isotropic response. We were able to show optimality in this larger class by constructing a microstructure that attains them. These optimal microstructures are created by making use of finite-rank laminates, which have, in general, anisotropic nonlinear response. Nonetheless, we showed that the effective response of the laminates attain the VHS bounds by optimizing over all loading conditions while keeping the "magnitude" of the load constant. In future work, we plan to consider nonlinear elasticity under more general loading, and investigate the attainability of the bounds.

It remains an open question whether optimal bounds for the class of nonlinear composites with statistically isotropic microstructures can be generated, either in the case of nonlinear dielectrics or elasticity. As we have seen, the VHS bounds failed to be optimal for this class because the prescription of the LCC allows for "undesirable" microstructures that are linearly isotropic, but fail to remain isotropic once nonlinear behavior is considered. In that sense, the class of microstructures with isotropic response is less selective in the linear case. Therefore, in order to improve on the nonlinear variational bounds, it is clear that the choice of LCC must be restricted in

such a way as to exclude these "undesirable" microstructures.

Another possible avenue for improved bounds for isotropic nonlinear composites may lie in the use of the translation method. Indeed, in the recent work of Peigney and Peigney (2017), the authors used this method to obtain improved bounds on the effective dielectric coefficient of two phase nonlinear composites. While these bounds are in general difficult to implement, they show that improved bounds do exist. The method by which such bounds are obtained involves the use of a "comparison" potential which must satisfy certain technical hypotheses. Peigney and Peigney (2017) considered a specific "comparison" potential, but by considering more general forms, it may be possible to obtain sharper bounds. Moreover, such bounds make use of the microstructure in such a way as to avoid the phase-wise constant moduli assumption that inhibits the VLC bounds.

Chapter 3

Optimality of Nonlinear Variational Bounds in Porous Nonlinear Viscoplasticity

Abstract

In this chapter, we look to address the optimality of the variational bounds of the Hashin-Shtrikman type (VHS), due to Ponte Castañeda (1991, 1992b), in the context of porous viscoplasticity. In Chapter 2, it was shown in the context of two- and three-dimensional dielectrics, as well as incompressible plane-strain elasticity, that the VHS bounds are optimal over the class of anisotropic composites that have linearly isotropic response. We look to extend these result by considering a porous composite under more general plane-strain loading, where the matrix phase is characterized by an incompressible, isotropic, stress energy potential. By appealing to an exact variational representation for the effective energy of a finite-rank laminate, we show that there exist certain values of the applied macroscopic stress for which the VHS bound is attained. This result is independent of the behavior of the matrix phase, so long as it satisfies a certain technical hypothesis. We then present results in the ideally plastic limit, and characterize the yield surface of the finite-rank laminates that attain the bound.

3.1 Introduction

The problem of determining the effective behavior of porous viscoplastic materials has been of great interest to the engineering community for quite some time. Due to the fact that many materials can be accurately modeled as porous viscoplastic (e.g. metals, sea ice, etc.), it is important to have accurate bounds and estimates that can be used to obtain the response of such systems.

No discussion of models used in porous viscoplasticity would be complete without mentioning the seminal work of Gurson (1977). By using the the exact solution for a spherical/cylindrical shell under hydrostatic loading and an uniform purely deviatoric field, Gurson (1977) was able to obtain estimates for the effective response of rigid-perfectly plastic porous solids. This model has been shown to provide sufficiently accurate predictions for isotropic porous solids at moderate to high stress triaxialities, and has been generalized to account for more general power-law type viscoplastic behavior (Leblond et al., 1994).

The existence of exact results (e.g. Leblond et al., 1994; Idiart, 2008, for cylindrical/spherical voids and infinite rank laminates, respectively) has been useful in testing the suitability of bounds and estimates that have been obtained over the years. The methods proposed by Ponte Castañeda (1991) (see also Willis, 1991; Michel and Suquet, 1992, for alternative approaches) have been used to obtain rigorous bounds for porous nonlinear materials by making use of a fictitious linear comparison composite (LCC), whose microstructure is the same as the nonlinear composite under consideration. This method therefore makes use of the linear estimates on the LCC to obtain corresponding estimates on the nonlinear material. In particular, by using the linear Hashin-Shtrikmann estimates, the resulting nonlinear variational bounds of the Hashin-Shtrikmann type (VHS) can account for a full range of triaxialities, pore shapes, and matrix behavior.

This work is concerned with investigating the potential optimality of these VHS

bounds in the context of viscoplasticity. While they represent rigorous bounds on the class of composites with statistically isotropic microstructures, their optimality over this class is unknown. It is known that for composites with linearly isotropic response, the linear Hashin-Shtrikman bounds and the translation bounds (Lurie and Cherkaev, 1984, 1986) coincide. Bounds obtained using the latter method only takes into account the relative volume fractions of the phases, while the Hashin-Shtrikman bounds are generated by implicitly assuming that the two-point correlation functions of the phases are isotropic. It then becomes clear that the linear bounds are in a sense degenerate in that they are seemingly independent of higher-order microstructural statistics. Using this fact, it was shown in Chapter 2, in the context of nonlinear dielectrics and incompressible plane-strain elasticity, that the VHS bounds are in fact optimal for the class of microstructures that have nonlinear anisotropic response, but are linearly isotropic. This was done by combining the degeneracy of the linear bounds with the observation that the bounds generated by using the nonlinear variational linear comparison method (VLC) can be extended to this larger class on account of the freedom one has in using any bound on the LCC. This flexibility in the VLC method should be contrasted with the bounds obtained using the nonlinear Hashin-Shtrikman method of Talbot and Willis (1985). This method is based on a generalization of the original Hashin-Shtrikman variational principle (Hashin and Shtrikman, 1962), and makes use of an uniform linear reference medium and an appropriately chosen polarization fields. Under certain technical hypotheses on the phase potentials, it is known that the Talbot-Willis bounds and the VHS bounds are the same, but like the Hashin-Shtrikman variational principle, the Talbot-Willis variational principle also assume isotropic two-point correlation functions, and therefore lacks the freedom in choosing bounds on the LCC. As we saw in Chapter 2, we were able to extend the class of functions over which the VHS bounds hold by using the translation bounds on our LCC instead of the linear HS bounds. That one cannot bound the uniform linear reference medium used in the Talbot-Willis method by the translation bounds keeps

the class of microstructures over which the Talbot-Willis bounds hold restricted. As a result, even though, in some cases, the Talbot-Willis bounds and VHS bounds are the same, the optimality of the latter over some extended class of composites will *not* imply the optimality of the former.

In looking to prove optimality to the current setting of nonlinear porous viscoplasticity, we organize the rest of the chapter as follows. Section 3.2 provides the basic definition of the effective response. Section 3.3 introduces the special class of composites known as finite-rank laminates in the linear context, and discusses their optimality as it pertains to the associated linear bounds. Next, Section 3.4 provides the framework for computing bounds for porous composites, as well as exact results for nonlinear finite-rank laminates, using the method of Ponte Castañeda (1992a). Section 3.5 shows explicitly the optimality of the VHS bounds for both purely deviatoric and more general plane strain loading conditions, while Section 3.6 presents the results in the ideally plastic limit and compares the yield surfaces and effective hydrostatic flow stresses of the optimal finite-rank laminates to the bounds obtained using the VHS method.

We close this section by introducing the notation that will be used throughout this work. We fix the standard Cartesian basis $\{\mathbf{e}_1, \mathbf{e}_2\}$, with respect to which vectors with Cartesian components b_i are represented by bold letters $\mathbf{b}$, while second-order tensors with Cartesian comnents A_{ij} are represented by bold italic letters $\boldsymbol{A}$. Here i, j, k, l range from 1 to 2. The real $2-$dimensional space is denoted by $\mathbb{R}^2$, and endowed with the scalar product $\mathbf{u} \cdot \mathbf{v}$, and norm $|\mathbf{u}|^2 = \mathbf{u} \cdot \mathbf{u}$. Similarly, we define the inner product between two second-order tensors via $\boldsymbol{A} \cdot \boldsymbol{B} = \text{tr}(\boldsymbol{A}\boldsymbol{B}^T)$, which induces the norm $\|\boldsymbol{A}\|^2 = \boldsymbol{A} \cdot \boldsymbol{A}$. The second-order identity tensor will be denoted by $\mathbf{I}$. Given two vectors $\mathbf{a}, \mathbf{b}$, the dyadic product $\mathbf{a} \otimes \mathbf{b}$ is defined to be the second-order tensor with Cartesian components $a_i b_j$, while the symmetric dyadic product is defined by the second-order tensor $\mathbf{a} \otimes_s \mathbf{b} = \frac{1}{2}(\mathbf{a} \otimes \mathbf{b} + \mathbf{b} \otimes \mathbf{a})$.

3.2 Effective Behavior for Porous Viscoplastic Composites

In what follows, we consider a 2−phase porous composite occupying some region denoted by Ω, which has been chosen as a representative volume element (RVE). We denote the matrix phase by phase 2, the porous phase by phase 1, and assume that they occupy regions $\Omega^{(r)} \subset \Omega$ for $r = 1, 2$, respectively. We assume that the local response of the matrix phase is characterized by a (strictly) convex, incompressible, isotropic stress potential $u^{(2)}(\boldsymbol{\sigma})$, while the porous phase is characterized by the stress potential $u^{(1)}(\boldsymbol{\sigma})$ which is zero when $\boldsymbol{\sigma} = 0$ and infinite otherwise. We take $\chi^{(r)}$ to be the characteristic function of phase r, so that $\chi^{(r)}(\mathbf{x}) = 1$ when $\mathbf{x}$ is in phase r, and 0 otherwise, and assume that $\chi^{(r)}$ varies on a scale much smaller than that of the material sample. In such a way, we can look to define the effective properties of the material by taking the limit as this scale of variation vanishes; in this case, the composite can be described as a homogenous material. Letting $\langle\cdot\rangle$ and $\langle\cdot\rangle^{(r)}$ denote the volume averages over Ω and $\Omega^{(r)}$, respectively, we take

$$f = \langle\chi^{(1)}\rangle = \langle 1 - \chi^{(2)}\rangle \tag{3.2.1}$$

to be the volume fraction of the porous phase; f is often referred to as the porosity.

By appealing to Hill (1963) in the linear case, and Willis (1991); Suquet (1987) in the nonlinear case, we define the effective energy potential as a function of the macroscopic average Cauchy stress $\overline{\boldsymbol{\sigma}} = \langle\boldsymbol{\sigma}\rangle$ through

$$\widetilde{u}(\overline{\boldsymbol{\sigma}}) = (1 - f) \min_{\boldsymbol{\sigma}\in\mathcal{S}(\overline{\boldsymbol{\sigma}})} \langle u^{(2)}(\boldsymbol{\sigma})\rangle^{(2)}, \tag{3.2.2}$$

where

$$\mathcal{S}(\overline{\boldsymbol{\sigma}}) = \{\boldsymbol{\sigma} \,:\, \nabla\cdot\boldsymbol{\sigma} = \mathbf{0} \text{ in } \Omega,\, \boldsymbol{\sigma}\mathbf{n} = \mathbf{0} \text{ on } \partial\Omega^{(1)},\, \langle\boldsymbol{\sigma}\rangle = \overline{\boldsymbol{\sigma}}\} \tag{3.2.3}$$

denotes the set of statistically admissible stresses. Here, $\mathbf{n}$ corresponds to the unit normal to the boundary of $\Omega^{(1)}$. It can then be shown that the average Eulerian strain rate $\overline{\boldsymbol{D}} = \langle \boldsymbol{D} \rangle$ is given by

$$\overline{\boldsymbol{D}} = \frac{\partial \widetilde{u}}{\partial \overline{\boldsymbol{\sigma}}}. \tag{3.2.4}$$

In this work, we will be interested in plane-strain loading conditions, and the primary variable of interest will be stress tensor $\boldsymbol{\sigma}$. We consider the commonly used stress invariants σ_e and σ_m to describe $\boldsymbol{\sigma}$. Here $\sigma_e = \sqrt{(3/2)\mathbf{s} \cdot \mathbf{s}}$ is the equivalent stress, where $\mathbf{s} = \boldsymbol{\sigma} - \sigma_m \mathbf{I}$ is the stress deviator, while $\sigma_m = \frac{\mathrm{tr}(\boldsymbol{\sigma})}{2}$ denotes the mean stress. Now, in plane-strain, we write $\overline{\boldsymbol{\sigma}}$ with respect to the standard Cartesian basis via

$$\overline{\boldsymbol{\sigma}} = \begin{bmatrix} \overline{\sigma}_{11} & \overline{\sigma}_{12} \\ \overline{\sigma}_{12} & \overline{\sigma}_{22} \end{bmatrix}. \tag{3.2.5}$$

One may also choose to write

$$\overline{\boldsymbol{\sigma}} = \overline{\mathbf{s}} + \overline{\sigma}_m \mathbf{I}, \tag{3.2.6}$$

where $\overline{\mathbf{s}}$ denotes the average stress deviator, whose Cartesian components are given by

$$\overline{\mathbf{s}} = \begin{bmatrix} \overline{s}_{11} & \overline{s}_{12} \\ \overline{s}_{12} & -\overline{s}_{11} \end{bmatrix} = \begin{bmatrix} \frac{\overline{\sigma}_{11} - \overline{\sigma}_{22}}{2} & \overline{\sigma}_{12} \\ \overline{\sigma}_{12} & -\frac{\overline{\sigma}_{11} - \overline{\sigma}_{22}}{2} \end{bmatrix}. \tag{3.2.7}$$

Clearly,

$$\overline{\sigma}_e = \sqrt{\frac{3}{2} \overline{\mathbf{s}} \cdot \overline{\mathbf{s}}} = \sqrt{3(\overline{s}_{11}^2 + \overline{s}_{12}^2)}, \tag{3.2.8}$$

and, as such, we define $\overline{\theta}$ via

$$\overline{s}_{11} = \frac{\overline{\sigma}_e \cos(\overline{\theta})}{\sqrt{3}}, \quad \overline{s}_{12} = \frac{\overline{\sigma}_e \sin(\overline{\theta})}{\sqrt{3}}. \tag{3.2.9}$$

We also define the stress triaxiality $X = \sigma_m / \sigma_e$.

3.3 Linear Porous Finite-Rank Laminates

In this section, we introduce the notion of finite-rank laminates in the context of porous linear materials under plane-strain loading conditions. The basic idea can be understood more generally by first considering a simple, or rank-1, laminate. This composite is obtained by mixing two homogeneous phases in a given layering direction $\mathbf{n}_{[1]}$. A rank-2 laminate is then obtained by mixing the rank-1 laminate with a homogenous phase in a second given layering direction $\mathbf{n}_{[2]}$; this phase does not have to be one of those used in the rank-1 laminate. This processes can be iterated, whereby a rank$-M$ laminate is obtained by mixing a rank$-(M-1)$ laminate with a homogenous phase in a given lamination direction $\mathbf{n}_{[M]}$. It is known that the effective properties of simple laminates (even when the behavior is nonlinear) can be computed exactly, due to the fact that the fields in each homogenous phase are constant. With this in mind, we assume that the length scale of the previous laminate is much smaller than the length scale of the current laminate. Therefore, at the M^{th} iteration, the rank$-(M-1)$ laminate is taken as a homogenous phase, so that the rank-M laminate can be treated as a simple laminate, whereby its effective properties can also be computed exactly.

In what follows, laminates will be obtained by starting with a simple porous laminate, and forming the higher-rank laminates by laminating with an isotropic, incompressible, homogeneous phase at each step. The porous phase will occupy a relative volume fraction of $\widehat{f}_{[1]}$ in the simple laminate, and in each subsequent step, the rank$-(k-1)$ laminate will be mixed with a homogenous phase in relative proportions $\widehat{f}_{[k]}$ and $1-\widehat{f}_{[k]}$ respectively, for $2 \leqslant k \leqslant M$. The resulting volume fraction of the porous phase, also known as the porosity, of the rank$-M$ laminate will be equal to

$$f = \prod_{i=1}^{M} \widehat{f}_{[i]}. \tag{3.3.1}$$

Note that the microstructure is completely determined once the values of $\{\mathbf{n}_{[i]}, \widehat{f}_{[i]}\}_{1\leqslant i\leqslant M}$ are prescribed. The porous phase is defined by a stress potential that is 0 if $\boldsymbol{\sigma} = 0$ and is infinite otherwise. The linear phases will be characterized by a stress potential of the form

$$u_0^{[r]}(\boldsymbol{\sigma}) = \frac{\sigma_e^2}{6\mu_0^{[r]}}, \tag{3.3.2}$$

where $\mu_0^{[r]}$ represents the shear modulus of the homogeneous isotropic phase used in the r^{th} iteration. On account of the phase-wise constant fields, the effective response of the rank$-M$ laminate can be calculated exactly via (deBotton and Ponte Castañeda, 1992; Danas et al., 2008; deBotton and Hariton, 2002; Idiart, 2006).

$$\widetilde{u}_{0[M]}(\overline{\boldsymbol{\sigma}}) = \min_{\substack{\omega_{[i]} \\ \overline{\boldsymbol{\sigma}}^{(1)}=\mathbf{0}}} \left\{ \sum_{i=1}^{M} \frac{(1-\widehat{f}_{[i]})}{6\mu_0^{[i]}} \prod_{j=i+1}^{M} \widehat{f}_{[j]} \left(\overline{\sigma}_e^{[i]}\right)^2 \right\}, \tag{3.3.3}$$

where $\overline{\sigma}_e^{[r]}$ is the average equivalent stress associated to the stress of the homogeneous phase added in the r^{th} iteration; the stresses are given by

$$\overline{\boldsymbol{\sigma}}^{[i]} = \overline{\boldsymbol{\sigma}} + \widehat{f}_{[i]}\omega_{[i]}\mathbf{m}_{[i]} \otimes \mathbf{m}_{[i]} - \sum_{j=i+1}^{M} (1-\widehat{f}_{[j]})\omega_{[j]}\mathbf{m}_{[j]} \otimes \mathbf{m}_{[j]}, \qquad \text{for } i = 1, \ldots, M. \tag{3.3.4}$$

Moreover, the average stress in the porous phase is given by

$$\overline{\boldsymbol{\sigma}}^{(1)} = \overline{\boldsymbol{\sigma}} - \sum_{i=1}^{M} (1-\widehat{f}_{[i]})\omega_{[i]}\mathbf{m}_{[i]} \otimes \mathbf{m}_{[i]}. \tag{3.3.5}$$

In the above, $\mathbf{m}_{[i]}$ are the unit vectors orthogonal to the layering directions $\mathbf{n}_{[i]}$. Note that in order to find $\widetilde{u}_{0[M]}$, we must solve an $M-$dimensional minimization problem, subject to the constraint that $\overline{\boldsymbol{\sigma}}^{(1)} = \mathbf{0}$.

The effective response of the $(M+1)$ phase rank$-M$ laminate, as given by $\widetilde{u}_{0[M]}$, will, in general, be *anisotropic*. For reasons which will become clear shortly, we fix

our microstructure by prescribing

$$\widehat{f}_{[1]} = \frac{2+f}{3}, \quad \widehat{f}_{[2]} = \frac{1+2f}{2+f}, \quad \widehat{f}_{[3]} = \frac{3f}{1+2f} \tag{3.3.6}$$

and

$$\mathbf{n}_{[1]} = \mathbf{e}_1, \quad \mathbf{n}_{[2]} = \frac{1}{2}(\mathbf{e}_1 + \sqrt{3}\mathbf{e}_2), \quad \mathbf{n}_{[3]} = \frac{1}{2}(-\mathbf{e}_1 + \sqrt{3}\mathbf{e}_2), \tag{3.3.7}$$

and look to find the values $\omega_{[1]}, \omega_{[2]}$ and $\omega_{[3]}$ that both minimize the expression on the right hand side of Eq. (3.3.3), and satisfy the constraint imposed by the condition $\overline{\boldsymbol{\sigma}}^{(1)} = \mathbf{0}$. In writing out these conditions, it becomes clear that the three values $\omega_{[1]}, \omega_{[2]}$ and $\omega_{[3]}$ are completely determined by the constraint, and some simple algebra reveals that

$$\begin{aligned}
\omega_{[1]} &= \frac{2}{3(1-\widehat{f}_{[1]})}\left(\overline{\sigma}_m - 2\overline{s}_{11}\right), \\
\omega_{[2]} &= \frac{2}{3(1-\widehat{f}_{[2]})}\left(\overline{\sigma}_m + \overline{s}_{11} - \sqrt{3}\overline{s}_{12}\right), \\
\omega_{[3]} &= \frac{2}{3(1-\widehat{f}_{[3]})}\left(\overline{\sigma}_m + \overline{s}_{11} + \sqrt{3}\overline{s}_{12}\right),
\end{aligned} \tag{3.3.8}$$

where we recall that $\overline{\sigma}_m$ is the average mean stress, and $\overline{s}_{ij}$ are the Cartesian components of the average stress deviator (c.f. Eqs. (3.2.6)-(3.2.7)). Plugging back into Eq. (3.3.3), and taking $\mu_0^{[1]} = \mu_0^{[2]} = \mu_0^{[3]} = \mu_0$, we recover the result of Francfort and Murat (1986) (who themselves extended the work Tartar (1985)) which indicates that this two-phase rank-3 laminate saturates the Hashin-Shtrikman (HS) bounds. In particular, with this prescription of $\{\mathbf{n}_{[i]}, \widehat{f}_{[i]}\}_{1\leqslant i\leqslant 3}$, $\widetilde{u}_{0[3]}(\overline{\boldsymbol{\sigma}})$ is equal to

$$\widetilde{u}_{0HS}(\overline{\boldsymbol{\sigma}}) = \frac{1}{6\widetilde{\mu}_{0HS}}\overline{\sigma}_e^2 + \frac{1}{2\widetilde{\kappa}_{HS}}\overline{\sigma}_m^2, \tag{3.3.9}$$

where

$$\widetilde{\mu}_{0HS} = \frac{1-f}{1+f}\mu_0, \quad \text{and} \quad \widetilde{\kappa}_{HS} = \frac{1-f}{3f}\mu_0. \tag{3.3.10}$$

On the other hand, upon considering purely deviatoric loading, we let

$$\widehat{f}_{[1]} = \frac{1+f}{2}, \quad \widehat{f}_{[2]} = \frac{2f}{1+f}, \tag{3.3.11}$$

and

$$\mathbf{n}_{[1]} = \mathbf{e}_1, \quad \mathbf{n}_{[2]} = \frac{1}{\sqrt{2}}\left(\mathbf{e}_1 + \mathbf{e}_2\right). \tag{3.3.12}$$

Solving the minimization problem defined through Eq. (3.3.3), it becomes clear that, while the constraint $\overline{\boldsymbol{\sigma}}^{(1)} = \mathbf{0}$ completely determines the values of $\omega_{[1]}$ and $\omega_{[2]}$, the rank-2 laminate can only support purely deviatoric loading. In this case, we find that

$$\begin{aligned} \omega_{[1]} &= \frac{-2\overline{s}_{11}}{1-\widehat{f}_{[1]}}, \\ \omega_{[2]} &= \frac{-2\overline{s}_{12}}{1-\widehat{f}_{[2]}}. \end{aligned} \tag{3.3.13}$$

As above, plugging these values back into Eq. (3.3.3), and taking $\mu_0^{[1]} = \mu_0^{[2]} = \mu_0$, we recover the result of Lipton (1988) (see also Lipton and Kohn, 1988), namely that the effective response of the rank-2 laminate is isotropic, and saturates the HS bounds, i.e.

$$\widetilde{u}_{0[2]}(\overline{\boldsymbol{\sigma}}) = \frac{1}{6\widetilde{\mu}_{0HS}}\overline{\sigma}_e^2. \tag{3.3.14}$$

3.4 Nonlinear Porous Materials

We turn our attention to nonlinear, two-phase, porous materials. In general, the computation of the effective potential is very difficult, due to the fact that it involves solving a set of nonlinear partial differential equations with randomly oscillating coefficients. In fact, exact results are known only in very special cases; laminates are one such case, and will be discussed next. We begin this section however by introducing a method that allows for the extraction of estimates and bounds on the effective behavior of nonlinear composites. In what follows, we take the matrix phase to be

isotropic and incompressible, whereby

$$u^{(2)}(\boldsymbol{\sigma}) = \psi(\sigma_e), \tag{3.4.1}$$

and we assume that ψ satisfies the so called "square-convexity" hypothesis, whereby the function g, defined by $g(p) = \psi(\sigma_e)$ with $p = \sigma_e^2$, is a non-negative, strictly convex function for which $g \to \infty$ as $p \to \infty$. This technical hypothesis is necessary in both obtaining the variational bounds, as well as in proving their optimality. As before, associated to the porous phase is a stress potential $u^{(1)}(\boldsymbol{\sigma})$ which is zero when $\boldsymbol{\sigma} = \mathbf{0}$ and infinite otherwise.

3.4.1 Variational Linear Comparison Bounds

Computing, or at least bounding, the effective properties of a composite with linear phases is more tractable than in the nonlinear case, and many results to that end exist. Motivated by this fact, we now recall the variational method of Ponte Castañeda (1992b), which converts available bounds on the effective behavior of some fictitious linear comparison composite (LCC) into bounds for the effective behavior of the nonlinear composite of interest. We spell out the procedure here in the context of the two-phase porous composites, but mention that method for obtaining bounds works for general N-phase composites.

In order to properly account for the porous phase, it is easiest to first treat it as, say, a linearly elastic one, with the same form as given in Eq. (3.3.2); the shear modulus, which we denote by $\mu^{(1)}$, will eventually be taken to be zero. Thus, the local potential of the nonlinear composite can be written as

$$u(\mathbf{x}, \boldsymbol{\sigma}) = \chi^{(1)}(\mathbf{x}) \frac{\sigma_e^2}{6\mu^{(1)}} + \chi^{(2)}(\mathbf{x}) \psi(\sigma_e). \tag{3.4.2}$$

Now, as a consequence of the square convexity hypothesis, it can be shown (Ponte Castañeda, 1992a) that the effective response of a two-phase material can be

written as

$$\widetilde{u}(\overline{\boldsymbol{\sigma}}) = \sup_{\mu_0(\mathbf{x})>0} \left\{ \widetilde{u}_0(\overline{\boldsymbol{\sigma}}) - \langle V(\mu_0(\mathbf{x})) \rangle \right\}. \tag{3.4.3}$$

Here, $\mu_0(\mathbf{x})$ is the local shear modulus of the LCC whose local stress potential is given by

$$u_0(\mathbf{x}, \boldsymbol{\sigma}) = \frac{\sigma_e^2}{6\mu_0(\mathbf{x})}, \tag{3.4.4}$$

while $\widetilde{u}_0(\overline{\boldsymbol{\sigma}})$ is the corresponding effective linear potential. The error function $V(\mu_0)$ is defined by

$$V(\mu_0(\mathbf{x})) = \sup_{\boldsymbol{\sigma}} \left\{ u_0(\mathbf{x}, \boldsymbol{\sigma}) - u(\mathbf{x}, \boldsymbol{\sigma}) \right\}, \tag{3.4.5}$$

where, on account of the assumed square convexity of ψ, the supremum in Eq. (3.4.5) is finite. In carrying out the optimization associated with the error function and the modulus, it becomes clear that $\mu_0(\mathbf{x}) = \mu^{(1)}$ for $\mathbf{x}$ in phase 1, whereby $V(\mu_0(\mathbf{x})) = 0$ for $\mathbf{x}$ in phase 1. As a consequence

$$\langle V(\mu_0(\mathbf{x})) \rangle = (1-f) \langle v(\mu_0(\mathbf{x})) \rangle^{(2)}, \tag{3.4.6}$$

where

$$v(\mu_0(\mathbf{x})) = \sup_{\boldsymbol{\sigma}} \left\{ \frac{\sigma_e^2}{6\mu_0(\mathbf{x})} - \psi(\sigma_e) \right\}. \tag{3.4.7}$$

At this point, only $\widetilde{u}_0(\overline{\boldsymbol{\sigma}})$ depends on $\mu^{(1)}$ through the fact that $\mu_0(\mathbf{x}) = \mu^{(1)}$ when $\mathbf{x}$ is in phase 1. Thus, we can take the limit as $\mu^{(1)} \to 0$, whereby $\mu_0(\mathbf{x})$ represents the (heterogenous) shear modulus associated to the matrix phase of a linear porous material.

The exact result in Eq. (3.4.3), although simpler to utilize than the direct calculation of $\widetilde{u}$, is still difficult due to the fact that $\mu_0(\mathbf{x})$ is heterogenous. However, upon replacing the supremum by one taken over phase-wise constant moduli, we arrive at

the nonlinear variational linear comparison lower bound,

$$\widetilde{u}(\boldsymbol{\sigma}) \geqslant \widetilde{u}_{VLC}(\overline{\boldsymbol{\sigma}}) = \sup_{\mu_0>0} \left\{ \widetilde{u}_0(\overline{\boldsymbol{\sigma}}) - (1-f)v(\mu_0) \right\}, \tag{3.4.8}$$

where $\widetilde{u}$ is the effective potential of the nonlinear composite, and $\widetilde{u}_0$ is the effective potential of the LCC whose matrix phase has constant shear modulus μ_0, and whose microstructure is the same as that of the nonlinear composite. It is clear from Eq. (3.4.8) that any lower bound on $\widetilde{u}_0$ will lead to a corresponding lower bound on $\widetilde{u}$. Therefore, we apply the Hashin-Shtrikmann lower bound to $\widetilde{u}_0$, which yields the nonlinear variational lower bound of the Hashin-Shtrikman type (VHS), and is given by

$$\widetilde{u}_{VHS-}(\overline{\boldsymbol{\sigma}}) = \sup_{\mu_0>0} \left\{ \widetilde{u}_{0HS}(\overline{\boldsymbol{\sigma}}) - (1-f)v(\mu_0) \right\}, \tag{3.4.9}$$

where $\widetilde{u}_{0HS}(\overline{\boldsymbol{\sigma}})$ is the same as in Eq. (3.3.9).

For later use, it can be shown (Ponte Castañeda and Suquet, 1998) that the VHS bound can also be written as

$$\widetilde{u}_{VHS-}(\overline{\boldsymbol{\sigma}}) = (1-f)\psi(\overline{\overline{\sigma}}_e^{(2)}), \tag{3.4.10}$$

where

$$\overline{\overline{\sigma}}_e^{(2)} = \frac{\sqrt{3f\overline{\sigma}_m^2 + (1+f)\overline{\sigma}_e^2}}{1-f}, \tag{3.4.11}$$

is the second moment of the stress field in the matrix of the LCC.

3.4.2 Nonlinear Porous Finite-Rank Laminates

The discussion regarding finite-rank laminates in the linear context can be generalized to the nonlinear setting. In particular, under the separation of length scale hypothesis, the effective response of a nonlinear finite-rank laminate can be computed exactly, and relies on the fact that the fields within each phase are constant. We are interested in the case of two-phase porous nonlinear laminates, whereby the same

incompressible, isotropic, homogeneous phase is used in each iteration. As such, the homogenous phase represents the continuous "matrix" phase of the laminate, with the pores acting as an inclusion phase.

Like the construction above, we prescribe $\{\mathbf{n}_{[i]}, \widehat{f}_{[i]}\}_{1\leqslant i\leqslant M}$, whereby the total porosity f is given by Eq. (3.3.1) as the product of the $\widehat{f}_{[i]}$. With this prescription, we can make use of the nonlinear variational procedure laid out above, whereby we introduce an LCC, and look to optimize over all shear moduli, as is done in Eq. (3.4.8). Since the fields in each copy of the matrix are constant, it can be shown that it suffices to optimize over phase-wise constant moduli, and still maintain the equality in Eq. (3.4.8). However, the fields in each copy of the matrix phase will in general be different, and it is therefore necessary to treat the LCC as a porous $(M+1)$ phase composite, with M (potentially) different moduli corresponding to the M laminations. As before, we use $\mu_0^{[r]}$ to represent the shear modulus of phase r of the LCC, which corresponds to the copy of the matrix phase added in the r^{th} lamination.

With the microstructure fixed, the effective response of the nonlinear rank$-M$ laminate, which will in general be *anisotropic*, can be calculated exactly via (Ponte Castañeda, 1992a)

$$\widetilde{u}_{[M]}(\overline{\boldsymbol{\sigma}}) = \sup_{\mu_0^{[1]},\ldots,\mu_0^{[M]}} \left\{ \widetilde{u}_{0[M]}(\overline{\boldsymbol{\sigma}}) - \sum_{i=1}^{M}(1-\widehat{f}_{[i]}) \prod_{j=i+1}^{M} \widehat{f}_{[j]} v(\mu_0^{[i]}) \right\}, \tag{3.4.12}$$

where v is the same error functions as defined by Eq. (3.4.7), and where $\widetilde{u}_{0[M]}$ is the effective potential of the linear $(M+1)-$phase rank$-M$ laminate, which can be calculated using Eq. (3.3.3).

Now, the optimality conditions from Eq. (3.4.12) and the error functions can be used to show that

$$\frac{1}{\mu_0^{[r]}} = \frac{3\psi'(\overline{\overline{\sigma}}_e^{[r]})}{\overline{\overline{\sigma}}_e^{[r]}}, \tag{3.4.13}$$

where, $\overline{\overline{\sigma}}_e^{[r]}$ is the second moment of the equivalent stress measure of the homogenous

phase in the LCC added in the r^{th} iteration, and where the prime is used to denote a derivative with respect to σ_e. However, since the fields are constant within each phase, it follows that

$$\frac{1}{\mu_0^{[r]}} = \frac{3\psi'(\overline{\sigma}_e^{[r]})}{\overline{\sigma}_e^{[r]}}. \tag{3.4.14}$$

As we will see next, this relation is necessary in determining the optimality of the bound.

3.5 Optimality of the Variational Bounds

As discussed in Chapter 2, the VHS bounds presented in Section 3.4.1 hold over the class of anisotropic nonlinear composites that are linearly isotropic. We now look to see whether these bounds are optimal in the current setting. As we saw at the end of Section 3.3, the laminates whose microstructures are given by Eqs. (3.3.6)-(3.3.7) (for general plane-strain loading), and Eqs. (3.3.11)-(3.3.12) (for purely deviatoric plane strain loading), have linearly isotropic response, and hence are members of the class of microstructures bounded by the VHS bound. Moreover, they attain the linear HS bounds, and we aim to show that in fact, this same microstructure, which is optimal in the linear setting, is also optimal in the nonlinear setting.

Suppose that, for some $\overline{\boldsymbol{\sigma}} = \overline{\boldsymbol{\sigma}}^*$, the optimal values of $\mu_0^{[r]}$ arising from the supremum in Eq. (3.4.12) are equal; we denote this optimal value by μ_0. In this case, the LCC will reduce to the porous two-phase linear composite whose effective potential $\widetilde{u}_{0[M]}$, on account of the optimality of the microstructure in the linear setting, will be identical to $\widetilde{u}_{0HS}$. Moreover, all of the error functions will be equal, whereby

$$\sum_{i=1}^{M}(1-\widehat{f}_{[i]}) \prod_{j=i+1}^{M} \widehat{f}_{[j]} v(\mu_0^{[i]}) = (1-f)v(\mu_0). \tag{3.5.1}$$

As such, $\widetilde{u}_{[M]}$, as given in Eq. (3.4.12), will be equal to $\widetilde{u}_{VHS-}$ as given by Eq. (3.4.9). Therefore, the VHS bound can be attained so long as we can find $\overline{\boldsymbol{\sigma}}^*$ for which the

optimal shear moduli of the LCC are all equal.

In order to determine conditions on $\overline{\boldsymbol{\sigma}}^*$ that will be consistent with such a condition, we note that, from Eq. (3.4.14), $\mu_0^{[1]} = \cdots = \mu_0^{[M]}$ implies

$$\frac{\psi'(\overline{\sigma}_e^{[1]})}{\overline{\sigma}_e^{[1]}} = \cdots = \frac{\psi'(\overline{\sigma}_e^{[M]})}{\overline{\sigma}_e^{[M]}}. \tag{3.5.2}$$

Due to the square convexity hypothesis, whereby $\psi(\sigma_e) = g(p)$, with $p = \sigma_e^2$, it follows that

$$\frac{\partial g}{\partial p} = \psi' \frac{\partial \sigma_e}{\partial p} = \frac{\psi'}{2\sigma_e}. \tag{3.5.3}$$

which, upon letting $\overline{p}^{[r]} = (\overline{\sigma}_e^{[r]})^2$, indicates that

$$\frac{\partial g(\overline{p}^{[1]})}{\partial p} = \cdots = \frac{\partial g(\overline{p}^{[M]})}{\partial p}. \tag{3.5.4}$$

Since g is assumed to be strictly convex, Eq. (3.5.4) implies that each $\overline{p}^{[r]}$ must be equal, which itself means that

$$\overline{\sigma}_e^{[1]} = \cdots = \overline{\sigma}_e^{[M]}, \tag{3.5.5}$$

where it is recalled that $\overline{\sigma}_e^{[r]}$ corresponds to the average equivalent stress in phase r of LCC, and can therefore be computed by making use of Eq. (3.3.4). Hence, $\overline{\boldsymbol{\sigma}}^*$ will be determined from the $(M-1)$ conditions in Eq. (3.5.5).

As such, the rest of this section is concerned with investigating the potential optimality of the VHS bounds, both for purely deviatoric, and then for more general plane-strain loading conditions. For a fixed value of $\overline{\sigma}_e$, we note that under plane-strain, purely deviatoric loading, $\overline{\boldsymbol{\sigma}}$ is completely determined by $\overline{\theta}$ (as defined in Eq. (3.2.9)), while under general plane-strain loading, $\overline{\boldsymbol{\sigma}}$ is determined by $\overline{\theta}$ as well as the stress triaxiality $X = \overline{\sigma}_m/\overline{\sigma}_e$. Therefore, in showing optimality in the former case, we use the one equation given by Eq. (3.5.5) to determine the optimal value of $\overline{\theta}^*$, while in the latter, we use the two equations given by Eq. (3.5.5) to determine the optimal

value of $\overline{\theta}^*$ and X^*.

3.5.1 Purely Deviatoric Loading

To start, we fix $\mathbf{n}_{[1]}$ and $\mathbf{n}_{[2]}$ as in Eq. (3.3.12) and $\widehat{f}_{[1]}$ and $\widehat{f}_{[2]}$ as in Eq. (3.3.11). Then, from Eq. (3.4.12), with $M = 2$,

$$\widetilde{u}_{[2]}(\overline{\boldsymbol{\sigma}}) = \sup_{\mu_0^{[1]},\mu_0^{[2]}} \left\{ \widetilde{u}_{0[2]}(\overline{\boldsymbol{\sigma}}) - (1-\widehat{f}_{[1]})\widehat{f}_{[2]} v(\mu_0^{[1]}) - (1-\widehat{f}_{[2]}) v(\mu_0^{[2]}) \right\}. \tag{3.5.6}$$

By making use of Eq. (3.3.4) for the average stresses in the various copies of the matrix, as well as Eq.(3.3.13) for the optimal values of $\omega_{[r]}$, we find that

$$\overline{\sigma}_e^{[1]} = \frac{2\sqrt{3}|\overline{s}_{11}|}{1-f}, \tag{3.5.7}$$

$$\overline{\sigma}_e^{[2]} = \frac{\sqrt{3}}{1-f}\sqrt{(1+f)^2\overline{s}_{12}^2 + (1-f)^2\overline{s}_{11}^2}. \tag{3.5.8}$$

Therefore, the bound can be attained if there exists a value of $\overline{\theta}$ for which $\overline{\sigma}_e^{[1]} = \overline{\sigma}_e^{[2]}$. Indeed, upon making use of Eqs. (3.5.7)-(3.5.8), it follows that when

$$\tan(\overline{\theta}^*) = \pm\sqrt{\frac{3-f}{1+f}}, \tag{3.5.9}$$

then

$$\overline{s}_{11}^* = \pm\frac{\sqrt{1+f}}{2\sqrt{3}}\overline{\sigma}_e, \quad \text{and} \quad \overline{s}_{12}^* = \pm\frac{\sqrt{3-f}}{2\sqrt{3}}\overline{\sigma}_e, \tag{3.5.10}$$

so that

$$\overline{\sigma}_e^{[1]} = \overline{\sigma}_e^{[2]} = \frac{\sqrt{1+f}}{1-f}\overline{\sigma}_e. \tag{3.5.11}$$

Note that the choice of the sign in the expression for $\overline{s}_{11}^*$ can be chosen independently of that in the expression for $\overline{s}_{12}^*$, and hence there are four points in the deviatoric plane at which the VHS bound is attained. For completeness, we note that, with Eq.

(3.5.11),

$$\widetilde{u}_{[2]}(\overline{\boldsymbol{\sigma}}^*) = (1-f)\psi\left(\frac{\sqrt{1+c}}{1-c}\overline{\sigma}_e\right), \tag{3.5.12}$$

a result which, when compared to Eqs. (3.4.10) and (3.4.11) (with $\overline{\sigma}_m = 0$), indicates that the bound is indeed attained by $\overline{\boldsymbol{\sigma}}^*$, as defined by Eqs. (3.5.9)-(3.5.10).

3.5.2 General Plane-Strain Loading

We fix $\mathbf{n}_{[1]}, \mathbf{n}_{[2]}, \mathbf{n}_{[3]}$ as in Eq. (3.3.7), and $\widehat{f}_{[1]}, \widehat{f}_{[2]}, \widehat{f}_{[3]}$ as in Eq. (3.3.6). Then, from Eq. (3.4.12), with $M = 3$, the effective response of the rank-3 laminate is given by

$$\begin{aligned}\widetilde{u}_{[3]}(\overline{\boldsymbol{\sigma}}) = \sup_{\mu_0^{[1]},\mu_0^{[2]},\mu_0^{[3]}} \Big\{ & \widetilde{u}_{0[3]}(\overline{\boldsymbol{\sigma}}) - (1-\widehat{f}_{[1]})\widehat{f}_{[2]}\widehat{f}_{[3]}v(\mu_0^{[1]}) \\ & -(1-\widehat{f}_{[2]})\widehat{f}_{[3]}v(\mu_0^{[2]}) - (1-\widehat{f}_{[3]})v(\mu_0^{[3]})\Big\}. \end{aligned} \tag{3.5.13}$$

In this case, $\overline{\boldsymbol{\sigma}}$ need not be purely deviatoric, and Eqs. (3.3.4) and (3.3.8) can be used to show that

$$\overline{\sigma}_e^{[1]} = \frac{\sqrt{3}\,|\overline{\sigma}_m - 2\overline{s}_{11}|}{1-f}, \tag{3.5.14}$$

$$\begin{aligned}\overline{\sigma}_e^{[2]} = \frac{1}{1-f}\Big(& (2+f)(\overline{s}_{11} - \sqrt{3}\overline{s}_{12} + \overline{\sigma}_m)(\overline{s}_{11} - \sqrt{3}\overline{s}_{12} + f\overline{\sigma}_m) \\ & +(1-f)(\overline{\sigma}_m^2 + 2f\overline{\sigma}_m\overline{s}_{11} + 4\overline{s}_{11}^2) - \frac{(1-f)(2+f)}{3}\overline{\sigma}_e^2\Big)^{1/2} \end{aligned} \tag{3.5.15}$$

$$\overline{\sigma}_e^{[3]} = \frac{1}{1-f}\left(3f(\overline{s}_{11} + \sqrt{3}\overline{s}_{12} + \overline{\sigma}_m)(\overline{s}_{11} + \sqrt{3}\overline{s}_{12} + f\overline{\sigma}_m) + (1-f)^2\overline{\sigma}_e^2\right)^{1/2}, \tag{3.5.16}$$

where we recall that $\overline{\sigma}_e$ is related to $\overline{s}_{11}$ and $\overline{s}_{12}$ through Eq. (3.2.8).

As above, we look to find $\overline{\boldsymbol{\sigma}}^*$ for which $\overline{\sigma}_e^{[1]} = \overline{\sigma}_e^{[2]} = \overline{\sigma}_e^{[3]}$. Making use of Eqs. (3.5.14)-(3.5.16), a straightforward calculation reveals that $\overline{\sigma}_e^{[r]}$ (for $r = 1, 2, 3$) are all equal (so that the VHS bound can be attained) when $\overline{s}_{11}^*, \overline{s}_{12}^*$ and $\overline{\sigma}_m^*$ are related

through the equations

$$(2\overline{s}^*_{11} - \overline{\sigma}^*_m)^2 = \frac{3f\overline{\sigma}^{*2}_m + (1+f)\overline{\sigma}^2_e}{3}, \tag{3.5.17}$$

$$\overline{s}^*_{12} = \frac{1-f}{\sqrt{3}(1+f)}\left(\overline{s}^*_{11} + \frac{\overline{\sigma}^*_m(\overline{\sigma}^*_m - 2\overline{s}^*_{11})}{2\overline{s}^*_{11} + (1+f)\overline{\sigma}^*_m}\right). \tag{3.5.18}$$

Upon using the fact that

$$\overline{\sigma}^2_e = 3\left(\overline{s}^{*2}_{11} + \overline{s}^{*2}_{12}\right), \tag{3.5.19}$$

Eqs. (3.5.17)-(3.5.18) combine to show that the VHS bound is attained whenever the stress triaxiality $X^* = \overline{\sigma}^*_m/\overline{\sigma}_e$ is a solutions to the eighth-order polynomial

$$X_8X^8 + X_6X^6 + X_4X^4 + X_2X^2 + X_0 = 0, \tag{3.5.20}$$

where

$$X_8 = 81(1-f)^2(f^4 + 2f^3 + 9f^2 + 20f + 16), \tag{3.5.21}$$

$$X_6 = 54(f^2 + f + 1)(f^4 - 3f^3 - 3f^2 - 37f - 54), \tag{3.5.22}$$

$$X_4 = 9(f^6 - 6f^5 + 4f^4 + 15f^3 + 102f^2 + 191f + 125), \tag{3.5.23}$$

$$X_2 = -3(2f^5 - 8f^4 - 3f^3 + 13f^2 + 59f + 45), \tag{3.5.24}$$

$$X_0 = (f^2 - 2f - 2)^2. \tag{3.5.25}$$

Once X^* has been obtained, it can be used in conjunction with Eqs. (3.5.17)-(3.5.18) to determine the value of $\overline{\theta}^*$. By appealing to the rules governing the zeros of a quartic polynomial, it can be checked that for any value of $0 < f < 1$, there are always four real values of X^2 that satisfy Eq. (3.5.20). When all four roots are positive (which in practice is the case for all the values of porosity we considered), there will be 8 values of X, coming in 4 pairs with the same magnitude and opposite sign, for which a rank-3 laminate attains the VHS bounds. Note that since $X_0 \neq 0$ for any value of f, 0 is never a solution of Eq. (3.5.20), and hence the rank-3 laminate cannot attain

the VHS bound under purely deviatoric loading (when $X \to 0$).

For completeness, by evaluating Eqs. (3.5.14)-(3.5.16) at $\overline{\boldsymbol{\sigma}}^*$, as defined by Eqs. (3.5.17)-(3.5.18), it follows that

$$\overline{\sigma}_e^{[1]} = \overline{\sigma}_e^{[2]} = \overline{\sigma}_e^{[3]} = \overline{\overline{\sigma}}_e^{*(2)}, \tag{3.5.26}$$

with $\overline{\overline{\sigma}}_e^{*(2)}$ given by Eq. (3.4.11) with $\overline{\sigma}_m$ replaced by $\overline{\sigma}_m^*$. Therefore

$$\widetilde{u}_{[3]}(\overline{\boldsymbol{\sigma}}^*) = (1-f)\psi\left(\overline{\overline{\sigma}}_e^{*(2)}\right) = \widetilde{u}_{VHS-}(\overline{\boldsymbol{\sigma}}^*). \tag{3.5.27}$$

3.6 Results and Discussion

In order to better visualize our results, we look to specialize to the ideally plastic limit. In general, and following Suquet (1987), we define the constitutive behavior of the phases in terms of the yield domains $\mathcal{P}^{(r)}$, which themselves are defined in terms of the convex yield functions $\Psi^{(r)}(\boldsymbol{\sigma})$, so that

$$\mathcal{P}^{(r)} = \{\boldsymbol{\sigma} \,:\, \Psi^{(r)}(\boldsymbol{\sigma}) \leqslant 0\}. \tag{3.6.1}$$

These sets can be used to define the stress potential via

$$u^{(r)}(\boldsymbol{\sigma}) = \begin{cases} 0, & \text{when } \boldsymbol{\sigma} \in \mathcal{P}^{(r)}, \\ +\infty, & \text{otherwise,} \end{cases} \tag{3.6.2}$$

and their boundaries, corresponding to the conditions $\Psi^{(r)}(\boldsymbol{\sigma}) = 0$, define the yield surface. For simplicity, we assume that each phase obeys a Von Mises type yield criterion, whereby

$$\Psi^{(r)}(\boldsymbol{\sigma}) = \sigma_e - \sigma_0^{(r)}, \tag{3.6.3}$$

where $\sigma_0^{(r)}$ corresponds to the flow stress of phase r. It can then be shown (Suquet, 1987) that one can define the effective yield domain $\widetilde{\mathcal{P}}$ as

$$\widetilde{\mathcal{P}} = \left\{ \begin{array}{c} \overline{\boldsymbol{\sigma}} \text{ such that there exists } \boldsymbol{\sigma}(\mathbf{x}) \text{ with } \langle \boldsymbol{\sigma} \rangle = \overline{\boldsymbol{\sigma}} \\ \text{div}\boldsymbol{\sigma}(\mathbf{x}) = \mathbf{0}, \text{ and } \boldsymbol{\sigma}(\mathbf{x}) \in \mathcal{P}^{(r)} \text{ for } \mathbf{x} \text{ in phase } r. \end{array} \right\}, \tag{3.6.4}$$

whereby

$$\widetilde{u}(\overline{\boldsymbol{\sigma}}) = \begin{cases} 0, & \text{when } \overline{\boldsymbol{\sigma}} \in \widetilde{\mathcal{P}}, \\ +\infty, & \text{otherwise.} \end{cases} \tag{3.6.5}$$

The effective yield domain can also be defined in terms of the effective yield function $\widetilde{\Psi}$, so that

$$\widetilde{\mathcal{P}} = \{\overline{\boldsymbol{\sigma}} \,:\, \widetilde{\Psi}(\overline{\boldsymbol{\sigma}}) \leqslant 0\}. \tag{3.6.6}$$

The boundary of this set then defines the effective yield surface, which can be characterized by the condition $\widetilde{\Psi}(\overline{\boldsymbol{\sigma}}) = 0$, and we are interested in comparing the yield surfaces of the rank$-M$ laminates to those of the VHS bounds. In the current setting of plane strain, the yield surface is three-dimensional in stress space; we will represents points on the yield surface as the triple $(\overline{s}_{11}, \overline{s}_{12}, \overline{\sigma}_m)$.

In the context of the porous viscoplastic composites, the flow stress in the porous phase is zero, while upon combining Eqs. (3.6.1)-(3.6.3), we have

$$u^{(2)}(\boldsymbol{\sigma}) = \psi(\sigma_e) = \begin{cases} 0, & \text{when } \sigma_e \leqslant \sigma_0 \\ +\infty, & \text{otherwise,} \end{cases} \tag{3.6.7}$$

where we have written σ_0 to represent the flow stress of the matrix phase. Using this expression along with Eqs. (3.4.10) and (3.6.5), it follows that

$$\widetilde{\Psi}_{VHS}(\overline{\boldsymbol{\sigma}}) = \frac{\sqrt{3f\overline{\sigma}_m^2 + (1+f)\overline{\sigma}_e^2}}{(1-f)} - \sigma_0, \tag{3.6.8}$$

whereby the yield surface of the VHS bound is spheroidal in shape, with a circular

cross section in the deviatoric plane.

A technical point is in order here. As defined, ψ is convex, but not strictly so. The expressions for $\widetilde{u}$ as well as $\widetilde{\mathcal{P}}$, as given above, are still well defined, but we recall that strict convexity of ψ was used to generate conditions on $\overline{\boldsymbol{\sigma}}^*$ to ensure that the VHS bound is attained (c.f. Eq. (3.5.5)). In particular, as demonstrated above, if we can find a value of $\overline{\boldsymbol{\sigma}}^*$ for which the optimal value of the moduli used in the LCC are all the same, then the bound will be attained. In the course of our analysis, we found that if ψ is strictly convex, and all of the moduli are the same, then Eq. (3.5.5) holds, providing us with expressions $\overline{\boldsymbol{\sigma}}^*$. However, it is clear from Eq. (3.4.14) that if Eq. (3.5.5) holds, then all of the moduli are the same, so that the VHS bound is attained independently of whether or not ψ is strictly convex. Therefore, as our intention here is to illustrate the attainment of the bound, we can proceed with using the conditions on $\overline{\boldsymbol{\sigma}}^*$ found above, and not concern ourselves further with the lack of strict convexity of ψ. We mention that Eq. (3.4.14), which is a condition involving the derivative of ψ can either be interpreted in the sense of subgradients (Ekeland and Téman, 1976), or by taking ψ to be pure power law type function, and taking the limit as the nonlinearity exponent tends to infinity.

In order to describe the yield surface of the rank$-M$ laminate, we recall that in computing $\widetilde{u}_{[M]}(\overline{\boldsymbol{\sigma}})$, we made use of the error function, as defined by Eq. (3.4.7). Using Eq. (3.6.7), we see that

$$\begin{aligned} v(\mu_0^{[r]}) &= \sup_{\boldsymbol{\sigma}} \left\{ \frac{\sigma_e^2}{6\mu_0^{[r]}} - \psi(\sigma_e) \right\} \\ &= \sup_{\boldsymbol{\sigma}\in\mathcal{P}} \frac{\sigma_e^2}{6\mu_0^{[r]}} \\ &= \frac{\sigma_0^2}{6\mu_0^{[r]}}, \end{aligned} \tag{3.6.9}$$

where $\mathcal{P}$ is the yield domain of the matrix phase, and is given by

$$\mathcal{P} = \{\boldsymbol{\sigma} \,:\, \sigma_e - \sigma_0 \leqslant 0\}. \tag{3.6.10}$$

Now, for the fixed microstructure described either through Eqs. (3.3.11)-(3.3.12) for purley deviatoric loading, or Eqs. (3.3.6)-(3.3.7) for more general plane-strain loading, the expression for $\widetilde{u}_{[M]}(\overline{\boldsymbol{\sigma}})$, given by Eq. (3.3.3), can be combined with Eq. (3.4.12) as well as Eq. (3.6.9) to show that, in the ideally plastic limit

$$\widetilde{u}_{[M]}(\overline{\boldsymbol{\sigma}}) = \sup_{\mu_0^{[r]}>0} \left\{ \sum_{i=1}^{M} (1-\widehat{f}_{[i]}) \prod_{j=i+1}^{M} \widehat{f}_{[j]} \left[\frac{\left(\overline{\sigma}_e^{[i]}\right)^2 - \sigma_0^2}{6\mu_0^{[i]}} \right] \right\}, \tag{3.6.11}$$

where $\overline{\sigma}_e^{[r]}$ for $1 \leqslant r \leqslant M$ are given by Eqs. (3.5.7)-(3.5.8) for $M = 2$ and Eqs. (3.5.14)-(3.5.16) for $M = 3$. With a slight abuse of notation, we define

$$\mathcal{P}(\mu_0^{[r]}) = \{\overline{\boldsymbol{\sigma}} \,:\, \overline{\sigma}_e^{[r]} - \sigma_0 \leqslant 0\}, \quad \text{for } r = 1, \ldots, M. \tag{3.6.12}$$

Without loss of generality, suppose that $\overline{\boldsymbol{\sigma}} \notin \mathcal{P}(\mu_0^{[1]})$. Then the term proportional to $\frac{1}{6\mu_0^{[1]}}$ in the sum on the right-hand side of Eq. (3.6.11) will be positive. Therefore, independent of whether $\overline{\boldsymbol{\sigma}} \in \mathcal{P}(\mu_0^{[r]})$ for $1 < r \leqslant M$, the supremum in Eq. (3.6.11) will equal $+\infty$; this follows by considering the limit as $\mu_0^{[1]} \to 0^+$. In light of Eq. (3.6.5), it therefore becomes clear that

$$\widetilde{\mathcal{P}}_{[M]} = \bigcap_{r=1}^{M} \mathcal{P}(\mu_0^{[r]}) \tag{3.6.13}$$

and hence the effective yield domain of the rank$-M$ laminate is defined as the intersection of M regions in stress space. We note that Eq. (3.6.13) is a specialization of a more general result given by Ponte Castañeda and Suquet (1998), who showed that when using the variational linear comparison method, the effective yield domain

is given by the intersection over all possible moduli of the yield domains of the LCC.

Now, for a fixed value of $\overline{\boldsymbol{\sigma}}$, $\overline{\sigma}_e^{[r]} \leqslant \sigma_0$ for each r (whereby $\overline{\boldsymbol{\sigma}} \in \widetilde{\mathcal{P}}_{[M]}$) if and only if $\max_{1\leqslant r\leqslant M} \overline{\sigma}_e^{[r]} \leqslant \sigma_0$. This observation allows us to define the effective yield function for the rank$-M$ laminate by

$$\widetilde{\Psi}_{[M]}(\overline{\boldsymbol{\sigma}}) = \max_{1\leqslant r\leqslant M} \overline{\sigma}_e^{[r]} - \sigma_0. \tag{3.6.14}$$

In what follows, we assume, without loss of generality, that $\sigma_0 = 1$. We first present results for purely deviatoric loading, then we consider more general loading, and finish by examining the response of the laminate under purely hydrostatic loading conditions. In the first two cases, we present cross sections of the yield surfaces in the $\frac{\overline{\sigma}_{11}-\overline{\sigma}_{22}}{2} - \overline{\sigma}_{12}$ deviatoric plane, whereby we fix a value of $\overline{\sigma}_m$, and plot the values of $\overline{s}_{11} = \frac{\overline{\sigma}_{11}-\overline{\sigma}_{22}}{2}$ and $\overline{s}_{12} = \overline{\sigma}_{12}$ for which

$$\overline{\boldsymbol{\sigma}} = \overline{\mathbf{s}} + \overline{\sigma}_m \mathbf{I} \tag{3.6.15}$$

lies on the yield surface. In what follows, $\overline{s}_{11}$ and $\frac{\overline{\sigma}_{11}-\overline{\sigma}_{22}}{2}$ are used interchangeably, as are $\overline{s}_{12}$ and $\overline{\sigma}_{12}$. For purely deviatoric loading, we will compare the yield surfaces of the rank-2 and rank-3 laminates with those predicted by the VHS bounds, while for general loading, we will consider only a comparison of the rank-3 laminate to the VHS bounds, since the rank-2 laminate is not in the class of microstructures bounded by the VHS bounds (recall that it does not have linearly isotropic response under general loading conditions). We will also, in this case, present results for the other two cross sections of the three dimensional yield surface, whereby we will fix $\overline{s}_{11}$ or $\overline{s}_{12}$ and look at the resulting cross sections in the $\overline{\sigma}_m - \overline{s}_{12}$ or $\overline{\sigma}_m - \overline{s}_{11}$ plane, respectively.

Before presenting results, it is instructive to clarify how the yield surfaces of the laminates are constructed, and we use Figure 3.1 as a guide. As discussed above, the yield domains for the rank$-M$ laminates can be described as the intersection of the

regions for which $\overline{\sigma}_e^{[i]} \leqslant 1$ for $i = 1, \ldots, M$; the corresponding yield surface is then the boundary of this intersection. Now, for the rank-2 laminate, the yield surface is two-dimensional, and lies in the deviatoric plane. Recalling Eqs. (3.5.7)-(3.5.8), and as we see in Figure 3.1a, the yield surface of the rank-2 laminate is a combination of the horizontal lines

$$\overline{s}_{11} = \pm \frac{1-f}{2\sqrt{3}}, \tag{3.6.16}$$

corresponding to $\overline{\sigma}_e^{[1]} = 1$, and the ellipse defined by the equation

$$\overline{s}_{11}^2 (1-f)^2 + \overline{s}_{12}^2 (1+f)^2 = \frac{(1-f)^2}{3}, \tag{3.6.17}$$

and corresponding to $\overline{\sigma}_e^{[2]} = 1$. In fact, upon letting

$$\overline{\theta}_{[2]}^* = \arctan\left(\sqrt{\frac{3-f}{1+f}}\right) \tag{3.6.18}$$

and recalling the parametrization of $\overline{s}_{11}$ and $\overline{s}_{12}$ introduced in Eq. (3.2.9), it follows that for $|\overline{\theta}| < \overline{\theta}_{[2]}^*$ or $|\overline{\theta} + \pi| < \overline{\theta}_{[2]}^*$ the yield surface of the rank-2 laminate is given by the lines defined in Eq. (3.6.16), while, otherwise, the yield surface is given by the part of the ellipse that is defined by the equation (3.6.17). It becomes clear then that the corners of the yield surface for the rank-2 laminate correspond to loadings conditions for which $\overline{\sigma}_e^{[1]} = \overline{\sigma}_e^{[2]} = 1$, i.e. $\overline{\theta} = \overline{\theta}^*$, simultaneously.

The description of the yield surface for the rank-3 laminate is a bit more complicated, due in part to the fact that is a three dimensional surface. To aid in its

description, we introduce the following functions:

$$h_{\pm}^{[1]}(\overline{s}_{11},\overline{s}_{12}) = \frac{2\sqrt{3}\overline{s}_{11} \pm (1-f)}{\sqrt{3}} \tag{3.6.19}$$

$$h_{\pm}^{[2]}(\overline{s}_{11},\overline{s}_{12}) = \frac{(2+f)(1+f)(\overline{s}_{11}+\sqrt{3}\overline{s}_{12}) - 4(2f+1)\overline{s}_{11}}{2(1+f+f^2)} \pm \frac{(1-f)\sqrt{4(1+f+f^2)-(2+f)^2(\sqrt{3}\overline{s}_{11}-\overline{s}_{12})^2}}{2(1+f+f^2)}, \tag{3.6.20}$$

$$h_{\pm}^{[3]}(\overline{s}_{11},\overline{s}_{12}) = \frac{-3f(1+f)(\overline{s}_{11}+\sqrt{3}\overline{s}_{12}) \pm \sqrt{3}(1-f)f\sqrt{4-3(\sqrt{3}\overline{s}_{11}-\overline{s}_{12})^2}}{6f^2}. \tag{3.6.21}$$

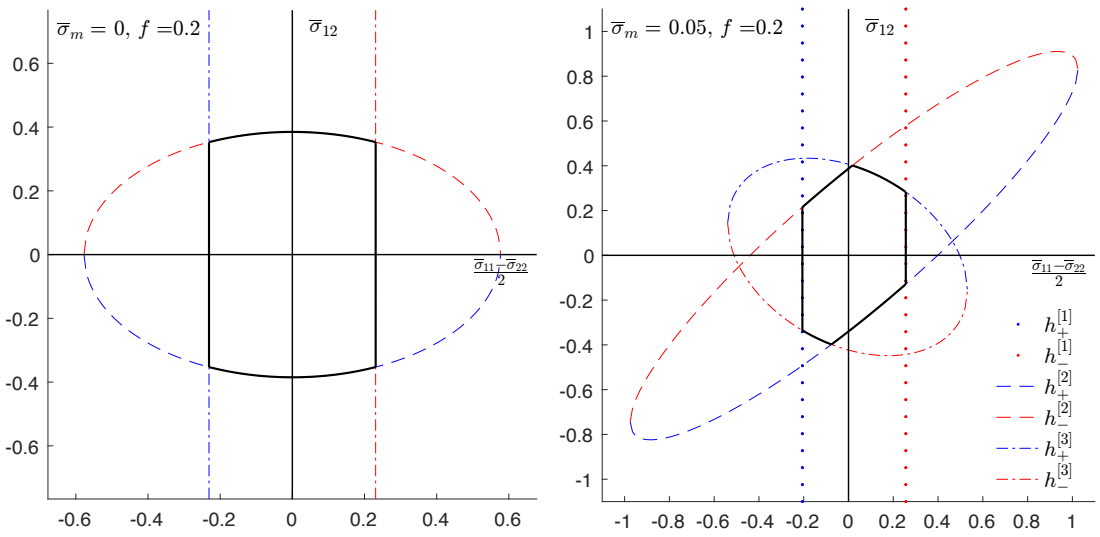

(a) (b)

Figure 3.1: Schematic of the cross section in the $\frac{\overline{\sigma}_{11}-\overline{\sigma}_{22}}{2} - \overline{\sigma}_{12}$ plane of the yield surface for the (a) rank−2 and (b) rank−3 laminate. The yield surfaces are represented by the solid black curves.

These functions are defined in such a way that $\overline{\sigma}_e^{[r]} \leqslant 1$ if and only if

$$\min\{h_+^{[r]}(\overline{s}_{11},\overline{s}_{12}), h_-^{[r]}(\overline{s}_{11},\overline{s}_{12})\} \leqslant \overline{\sigma}_m \leqslant \max\{h_+^{[r]}(\overline{s}_{11},\overline{s}_{12}), h_-^{[r]}(\overline{s}_{11},\overline{s}_{12})\}. \tag{3.6.22}$$

In connection to the discussion above, we note that

$$\mathcal{P}(\mu_0^{[r]}) = \left\{ \overline{\boldsymbol{\sigma}} \,:\, \min\{h_+^{[r]}, h_-^{[r]}\} \leqslant \overline{\sigma}_m \leqslant \max\{h_+^{[r]}, h_-^{[r]}\} \right\} \tag{3.6.23}$$

whereby $\mathcal{P}(\mu_0^{[2]})$ and $\mathcal{P}(\mu_0^{[3]})$ correspond to ellipsoids, with ellipsoidal cross sections in the deviatoric plane, while $\mathcal{P}(\mu_0^{[1]})$ is the region bounded between two planes. The effective yield domain $\widetilde{\mathcal{P}}_{[3]}$ is then the intersection of these regions, and therefore, upon fixing a value of $\overline{\sigma}_m$, the cross section of the yield surface of the rank-3 laminate in the deviatoric plane is a combination of $h_\pm^{[r]}$, corresponding to the boundary of $\widetilde{\mathcal{P}}_{[3]}$, as depicted in Figure 3.1b. For this value of $\overline{\sigma}_m$ considered, the yield domain is described using all six functions, but for larger values of $\overline{\sigma}_m$, only the "+" function or "$-$" function will be used, depending on which parts of $\mathcal{P}(\mu_0^{[r]})$, whose boundaries are determine by $h_\pm^{[r]}$, lie in $\widetilde{\mathcal{P}}_{[3]}$.

3.6.1 Purely Deviatoric Loading

For $\overline{\sigma}_m = 0$, we consider the two-dimensional subset of the yield surface plotted in the $\frac{\overline{\sigma}_{11}-\overline{\sigma}_{22}}{2} - \overline{\sigma}_{12}$ plane. We do so in Figure 3.2, and we also include results for the rank-3 laminate. Recall that in the linear case, this rank-3 laminate has isotropic behavior under *general* loading (not just under purely deviatoric loading); additionally, it attains the HS bounds. Therefore, this rank-3 laminate lies in the class of microstructures bounded by the VHS bounds under purely deviatoric loading.

Now, as we see in Figure 3.2, and consistent with the calculations laid out above, the rank-2 laminate attains the VHS bound precisely when $\overline{s}_{11}$ and $\overline{s}_{12}$ take the values $\overline{s}_{11}^*$ and $\overline{s}_{12}^*$ as given by Eq. (3.5.10). We also see that the rank-3 laminate does not attain the VHS bound for any value of $\overline{s}_{11}$ and $\overline{s}_{12}$; its yield surface always lying strictly inside of that predicted by the bound. The horizontal lines (in the $\frac{\overline{\sigma}_{11}-\overline{\sigma}_{22}}{2} - \overline{\sigma}_{12}$ plane) defined by the equations (3.6.16) for $M = 2$ and $h_\pm^{[1]} = 0$ for $M = 3$ correspond to the loading conditions for which $\overline{\sigma}_e^{[1]} - 1 = 0$, and it is therefore interesting to see

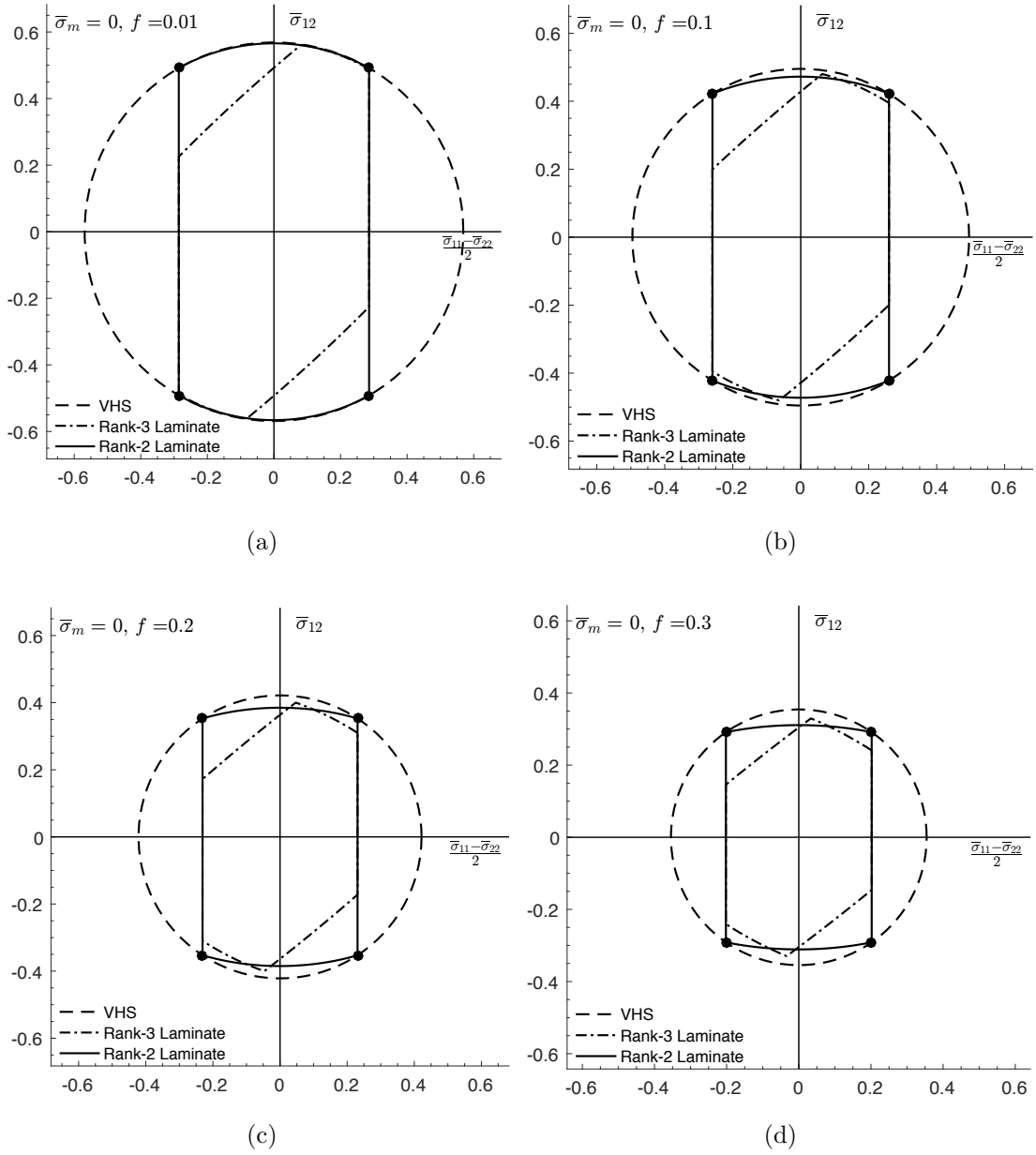

Figure 3.2: Cross section in the $\frac{\overline{\sigma}_{11}-\overline{\sigma}_{22}}{2} - \overline{\sigma}_{12}$ plane of the yield surface under purely deviatoric loading of the rank-2. laminate compared with those of the rank-3 laminate as well as the VHS bound. Results are presented for values of the porosity f equal to (a) 0.01 (b) 0.1 (c) 0.2 and (d) 0.3. Points where the VHS bound is attained are represented by black circles.

that this horizontal line lies on the boundary of the yield domain simultaneous for both the rank−2 and rank−3 laminates for a range of loading conditions. Note also that the corner points, which as discussed above correspond to loading conditions for which both $\overline{\sigma}_e^{[1]} = \overline{\sigma}_e^{[2]} = 1$ simultaneously, also corresponds to the points for which the VHS bound is attained.

3.6.2 General Plane-Strain Loading

For more general loading conditions, we now turn our attention to the yield surface of the rank−3 laminate, which we recall is defined by the equation $\widetilde{\Psi}_{[3]}(\overline{\boldsymbol{\sigma}}) = 0$. Due to the isotropy of the VHS bound, for each fixed value of $\overline{\sigma}_m$, the corresponding cross section is represented by a circle whose radius, for a fixed value of $\overline{\sigma}_m$, is proportional to

$$\overline{\sigma}_e^{VHS} = \overline{\sigma}_e^{VHS}(\overline{\sigma}_m) = \sqrt{\frac{(1-f)^2 - 3f\overline{\sigma}_m^2}{1+f}}. \tag{3.6.24}$$

On the other hand, the yield surface of the laminate is highly anisotropic, but as we saw above, there are multiple values of the stress triaxiality for which the VHS bound can be attained. In particular, it turns out that there are four positive values of X^2 that satisfy Eq. (3.5.20), and hence eight values of X for which the VHS bound is attained by the rank-3 laminate, i.e. $\pm|X|$ for each value of X^2 that solves Eq. (3.5.20). Since the yield surfaces of the rank−3 laminate and VHS bound coincide at these points, it follows that the four positive values of $\overline{\sigma}_m$ for which the VHS bound is attained will be given as the solution to the equation

$$\overline{\sigma}_m = \sqrt{\frac{(1-f)^2 - 3f\overline{\sigma}_m^2}{1+f}}|X|, \tag{3.6.25}$$

for each of the four corresponding values of $|X|$; here we used the definition of $X = \overline{\sigma}_m/\overline{\sigma}_e$ as well as Eq. (3.6.24). We denote these values by $\overline{\sigma}_{m,I}, \ldots, \overline{\sigma}_{m,IV}$, and number

them in such a way so that

$$0 < \overline{\sigma}_{m,I} < \overline{\sigma}_{m,II} < \overline{\sigma}_{m,III} < \overline{\sigma}_{m,IV}. \tag{3.6.26}$$

In the discussion to follow, we will assume that $\overline{\sigma}_m \geqslant 0$. This is done merely out of convenience, and the same trends that we will mention appear also for values of $\overline{\sigma}_m < 0$. As the results indicate, there are five regimes to consider. The first is when $0 \leqslant \overline{\sigma}_m \leqslant \overline{\sigma}_{m,I}$, and we show results in Figure 3.3. For these loading conditions, the yield surface is made up of six parts. This regime was depicted earlier in Figure 3.1. Now, each of the six corner points occur when two of the three copies of the matrix phases yield, i.e. when $\overline{\sigma}_e^{[r]} = 1$ for two values of $r \in \{1, 2, 3\}$. Note that as we approach $\overline{\sigma}_{m,I}$, one of the branches corresponding to the condition $\overline{\sigma}_e^{[3]} = 1$ shrinks, and eventually vanishes when $\overline{\sigma}_m = \overline{\sigma}_{m,I}$; this branch corresponds to $h_-^{[3]}$. Moreover, this corresponds to a loading condition for which $\overline{\sigma}_e^{[1]} = \overline{\sigma}_e^{[2]} = \overline{\sigma}_e^{[3]}$, and is a point at which the laminate attains the VHS bound.

The second regime is associated with cases when $\overline{\sigma}_{m,I} < \overline{\sigma}_m \leqslant \overline{\sigma}_{m,II}$, and we show results in Figure 3.4. The five corners occur when two of the three copies of the matrix phase yield, and now, one of the branches corresponding to the condition $\overline{\sigma}_e^{[2]} = 1$ vanishes as $\overline{\sigma}_m$ approaches $\overline{\sigma}_{m,II}$; this branch corresponds to $h_-^{[2]}$. The same trend continues in the third regime $\overline{\sigma}_{m,II} < \overline{\sigma}_m \leqslant \overline{\sigma}_{m,III}$, depicted in Figure 3.5, where, as we approach $\overline{\sigma}_{m,III}$, the right-most vertical line associated with the condition $\overline{\sigma}_e^{[1]} = 1$, and corresponding to $h_-^{[1]}$, shrinks down to a point.

Now, in the fourth regime, depicted in Figure 3.6 when $\overline{\sigma}_{m,III} < \overline{\sigma}_m \leqslant \overline{\sigma}_{m,IV}$, only three equations are needed to describe the yield surface; in this case, they correspond to $h_+^{[1]}$, $h_+^{[2]}$ and $h_+^{[3]}$. Moreover, it is here that the yield surface of the rank-3 laminate crosses the hydrostatic axis, and does so at the point

$$(\overline{s}_{11}, \overline{s}_{12}, \overline{\sigma}_m) = \left(0, 0, \frac{1-f}{\sqrt{3}}\right). \tag{3.6.27}$$

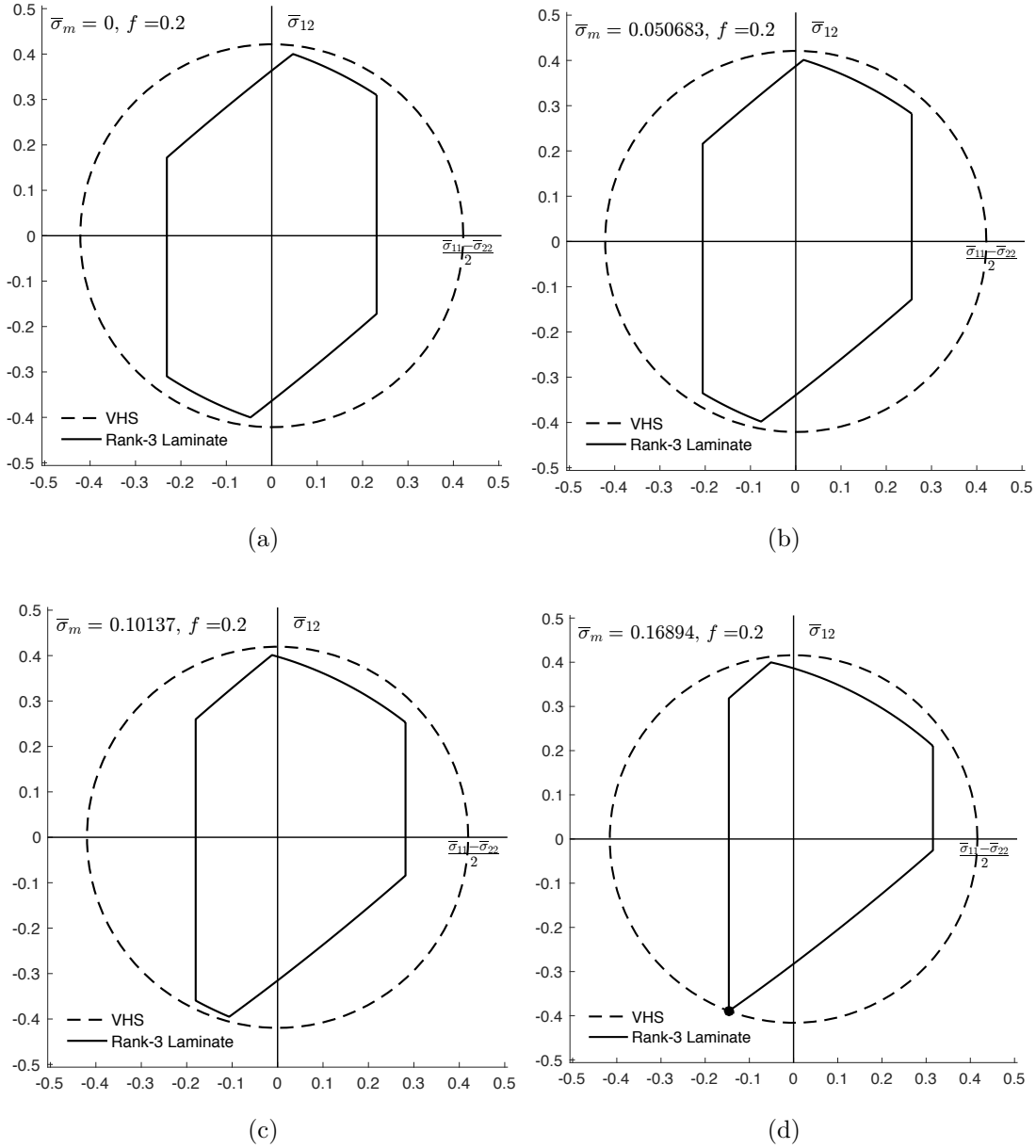

Figure 3.3: Cross sections in the $\frac{\overline{\sigma}_{11}-\overline{\sigma}_{22}}{2} - \overline{\sigma}_{12}$ plane of the yield surface of the rank-3 laminate compared with the VHS bound. Results are shown for four values in $0 \leqslant \overline{\sigma}_m \leqslant \overline{\sigma}_{m,I}$. Points where the VHS bound is attained are represented by black circles.

It can be checked that for all values of $0 \leqslant f < 1$, $\frac{1-f}{\sqrt{3}} < \overline{\sigma}_{m,IV}$, so that in particular, when $\overline{\sigma}_m = \overline{\sigma}_{m,IV}$, the yield surface of the rank-3 laminate does not lie on the hydrostatic axis. This is consistent with the fact that the VHS bound, which lies

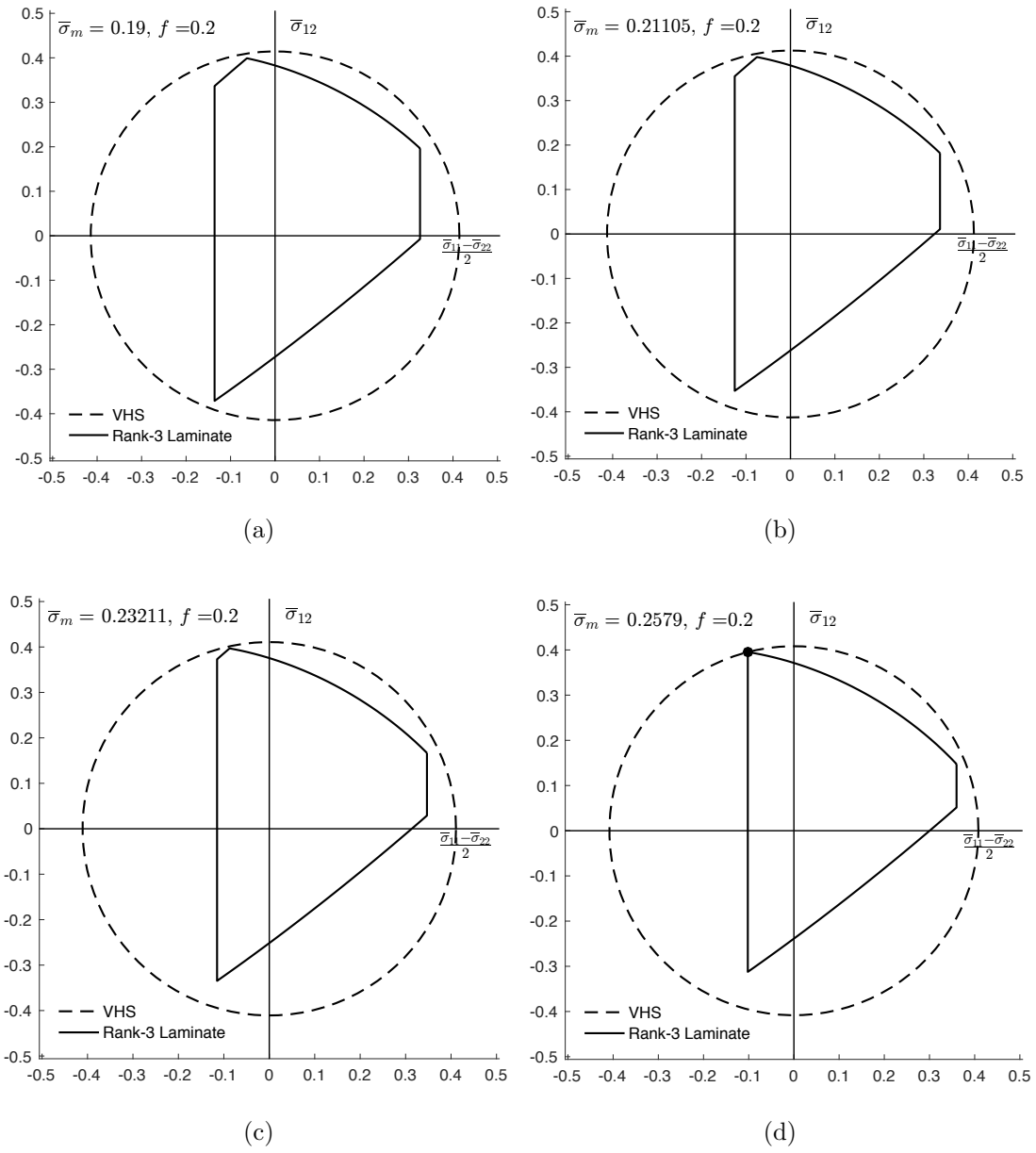

Figure 3.4: Cross sections in the $\frac{\overline{\sigma}_{11}-\overline{\sigma}_{22}}{2} - \overline{\sigma}_{12}$ plane of the yield surface of the rank-3 laminate compared with the VHS bound. Results are shown for four values in $\overline{\sigma}_{m,I} < \overline{\sigma}_m \leqslant \overline{\sigma}_{m,II}$. Points where the VHS bound is attained are represented by black circles.

off of the hydrostatic axis, (except at the hydrostatic point) is attained when $\overline{\sigma}_m = \overline{\sigma}_{m,IV}$; we will discuss this so called hydrostatic point in more detail later on. More

interestingly, as we see, not only does the rank−3 laminate attain the bound one final time when $\overline{\sigma}_m = \overline{\sigma}_{m,IV}$, but its yield surface simultaneously reaches its apex and close up. Then, in the fifth regime $\overline{\sigma}_m > \overline{\sigma}_{m,IV}$, the rank−3 laminate can no longer yield.

In order to get a clearer understanding of how the yield surface evolves in the three-dimensional stress space, we present sample results for the remaining two cross section of the yield surface. Recall that the values of $\overline{s}^*_{11}, \overline{s}^*_{12}$ and $\overline{\sigma}^*_m$ for which the VHS bound is attained can be related via Eqs. (3.5.17)-(3.5.18). The cross sections considered in Figure 3.7a and Figure 3.7b are thus obtained by fixing the value of $\overline{s}_{12} = \overline{s}^*_{12}$ and $\overline{s}_{11} = \overline{s}^*_{11}$, respectively, corresponding to those values for which the bound is attained when $\overline{\sigma}_m = \overline{\sigma}_{m,I}$. The cross sections in Figure 3.7e-Figure 3.7f are obtained similarly, with $\overline{\sigma}_m = \overline{\sigma}_{m,IV}$. On the other hand, the cross sections in Figure 3.7c-Figure 3.7d are obtained by taking cross sections along the $\overline{s}_{12} = 0$ and $\overline{s}_{11} = 0$ axes, respectively.

As we see in Figure 3.7a and Figure 3.7b, when $\overline{\sigma}_m = \overline{\sigma}_{m,I}$, the VHS bound is attained when $\overline{s}_{11}$ and $\overline{s}_{12}$ reach the optimal values $\overline{s}^*_{11}$ and $\overline{s}^*_{12}$, respectively. It is interesting to note that, $\overline{\sigma}_m = \overline{\sigma}_{m,I}$ is the largest positive value of the mean stress for which the rank−3 laminate will yield. In Figure 3.7c and Figure 3.7d, we see how, the yield surface is symmetric with respect to point symmetry about the origin, i.e. with $\overline{\boldsymbol{\sigma}} \mapsto -\overline{\boldsymbol{\sigma}}$. Finally, in Figure 3.7e and Figure 3.7f, we see how the yield surface behaves at its apex point. We recall that the yield surface closes up when $\overline{\sigma}_m = \overline{\sigma}_{m,IV}$, and as indicated in these cross sections, the yield surface closes up off of the hydrostatic axis.

While under deviatoric loading both the rank-2 and rank-3 laminates have linearly isotropic responses, and hence are members of the class of composites bounded by the VHS bounds, under the more general loading conditions considered in Figure 3.6, only the rank-3 laminate has linearly isotropic behavior, and hence we have not included any results for the rank-2 laminate. This point illustrates the interplay between microstructure and loading conditions. In fact, the rank-3 laminate is the

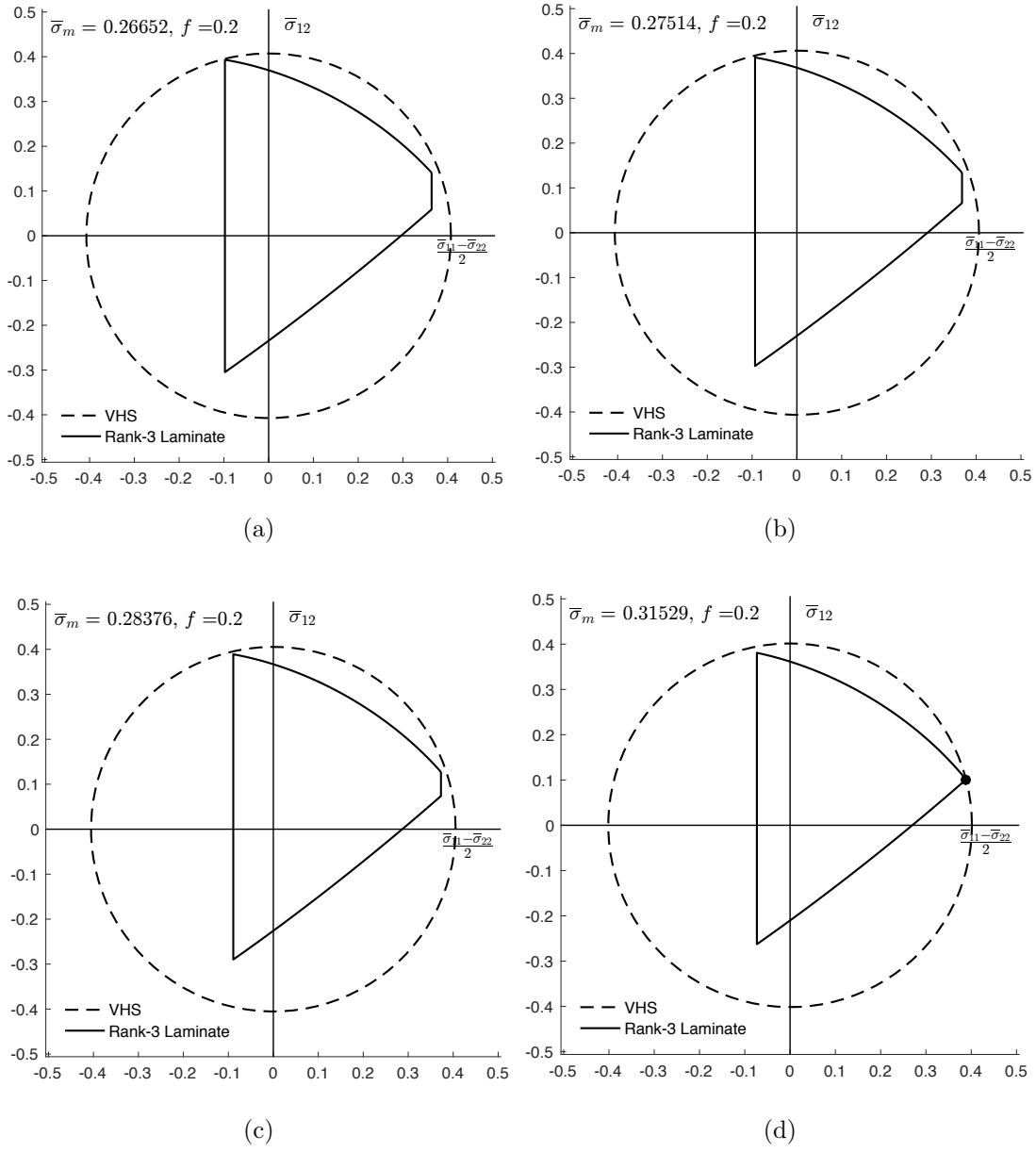

Figure 3.5: Cross sections in the $\frac{\overline{\sigma}_{11}-\overline{\sigma}_{22}}{2} - \overline{\sigma}_{12}$ plane of the yield surface of the rank-3 laminate compared with the VHS bound. Results are shown for four values in $\overline{\sigma}_{m,II} < \overline{\sigma}_m \leqslant \overline{\sigma}_{m,III}$. Points where the VHS bound is attained are represented by black circles.

lowest rank laminate that lies in the class of microstructures that are bounded by the VHS bounds under general plane-strain loading. It is also, in some sense, the most

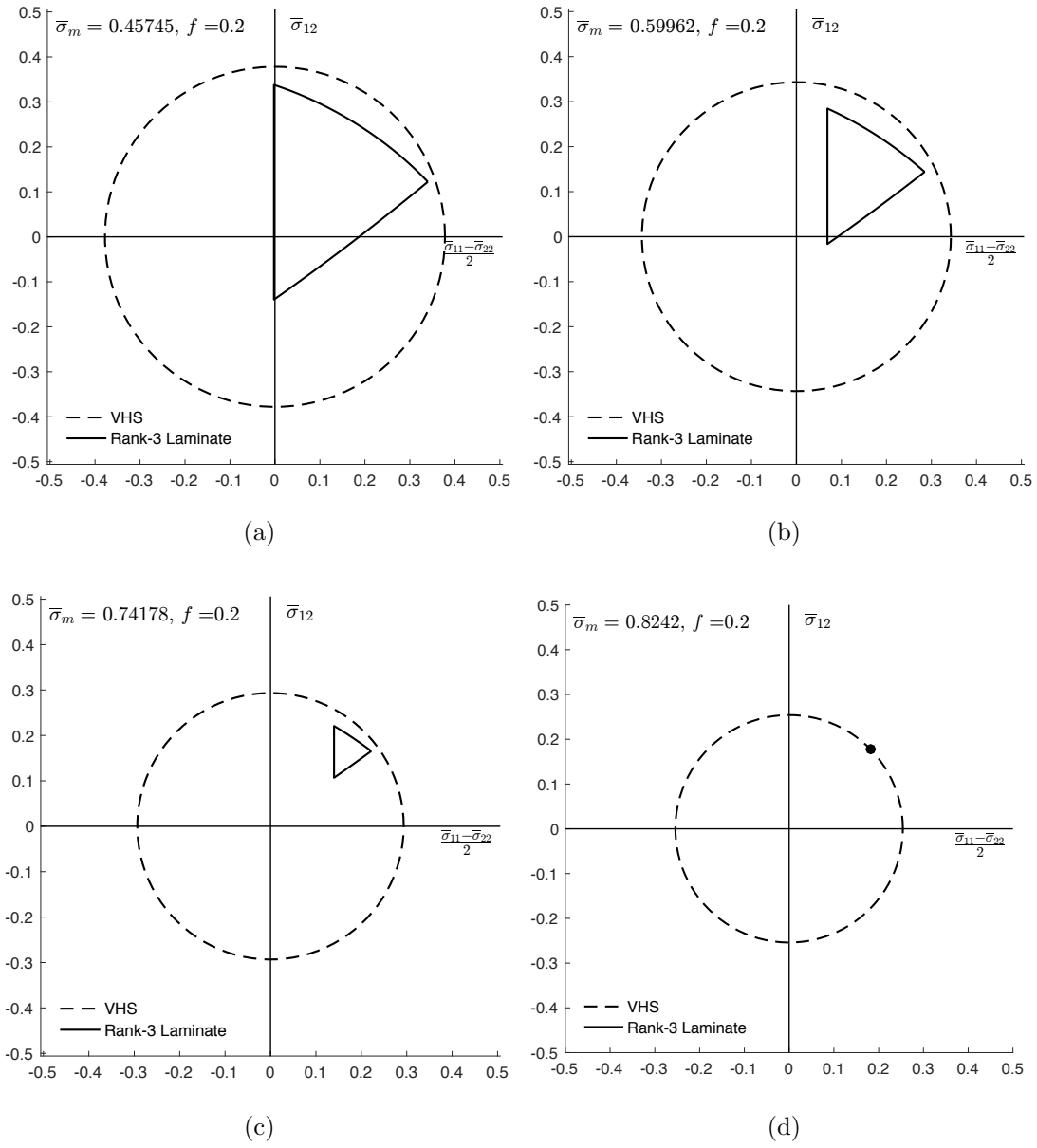

Figure 3.6: Cross sections in the $\frac{\overline{\sigma}_{11}-\overline{\sigma}_{22}}{2} - \overline{\sigma}_{12}$ plane of the yield surface of the rank-3 laminate compared with the VHS bound. Results are shown for four values in $\overline{\sigma}_{m,III} < \overline{\sigma}_m \leqslant \overline{\sigma}_{m,IV}$. Points where the VHS bound is attained are represented by black circles.

anisotropic microstructure in the class. As in the case of purely deviatoric loading, it is the anisotropy of the microstructure that allows the rank-3 laminate to attain the VHS bounds.

3.6.3 Purely Hydrostatic Loading

We close this section by discussing the VHS bounds in the context purely hydrostatic loading, when

$$\overline{\boldsymbol{\sigma}} = \overline{\sigma}_m \mathbf{I}. \tag{3.6.28}$$

As is customary, we define the effective hydrostatic flow stress $\widetilde{\sigma}^H$ to be the value of $\overline{\sigma}_m$ for which $\overline{\boldsymbol{\sigma}}$ of the form (3.6.28) lies on the yield surface. In the discussion that follows, we will also include exact results generated from the infinite rank-laminate (LAM) microstructure (Idiart, 2008; Idiart and Ponte Castañeda, 2013). This microstructure is known to statistically isotropic, implying that the linear, and nonlinear, behavior is isotropic, whereby it is a member of the class of microstructures bounded by the VHS bounds. Now, it can be shown that

$$\widetilde{\sigma}^H_{VHS} = \frac{(1-f)}{\sqrt{3f}}, \quad \widetilde{\sigma}^H_{LAM} = -\frac{\log(f)}{\sqrt{3}}, \quad \widetilde{\sigma}^H_{[3]} = \frac{(1-f)}{\sqrt{3}}, \tag{3.6.29}$$

and a comparison of $\widetilde{\sigma}^H$, is given in Figure 3.8a. Note that predictions from the VHS bound and exact LAM result are singular as $f \to 0$, while the result for the rank-3 laminate remains finite. It is known that the LAM microstructure, like the VHS bound and rank-3 laminate, attains the linear HS bound under purely hydrostatic loading. The rank-2 laminate on the other hand fails to do so, and therefore, we have not included its associated results, but mention that they lie below the other estimates for all values of porosity. It is important to mention that the LAM result given in Eq. (3.6.29) agrees exactly with the standard Gurson (1977) model prediction, as well as the viscoplastic extensions proposed by Leblond et al. (1994). As depicted in Figure 3.8a, we find that the difference between the VHS bounds, the exact LAM

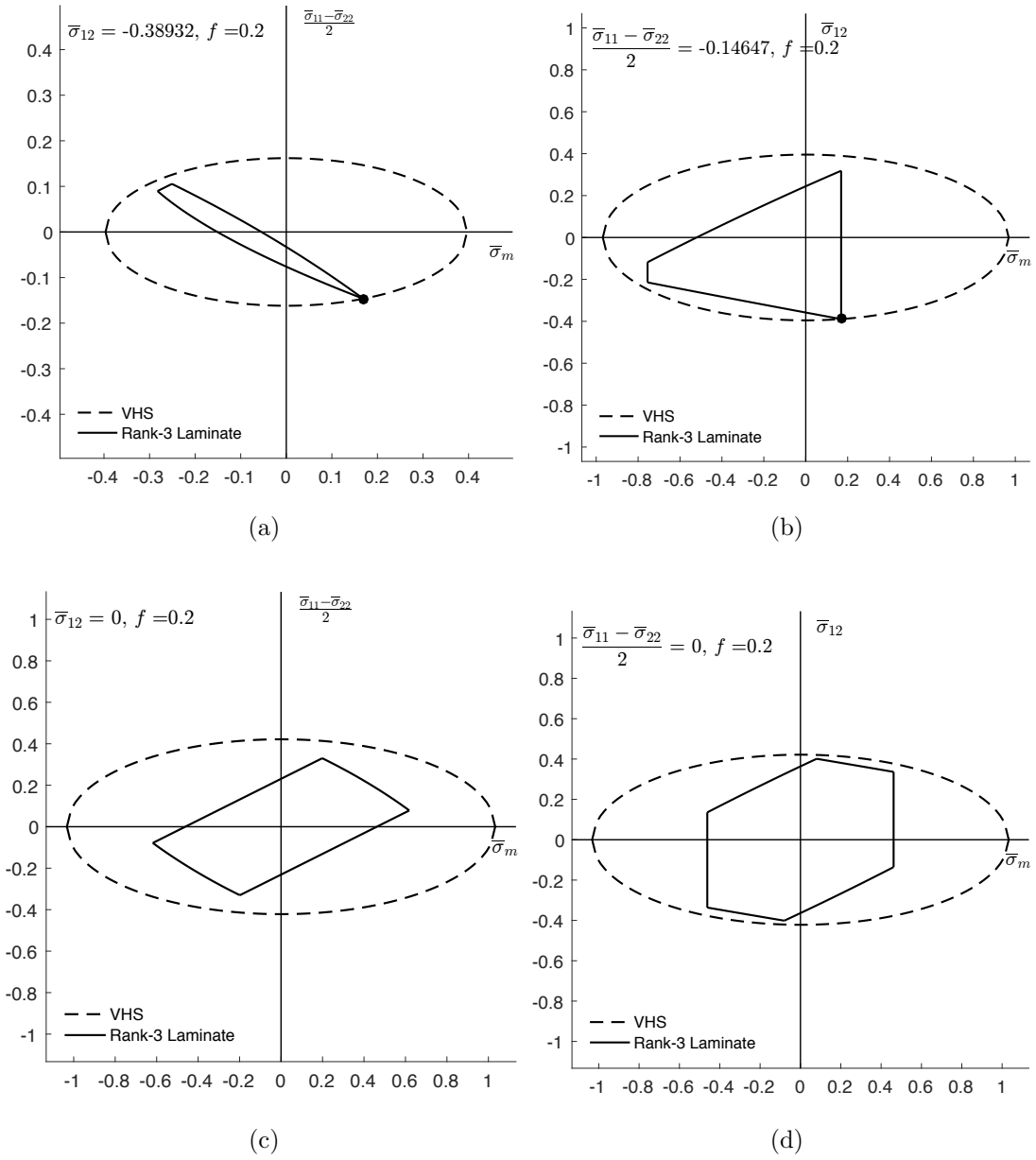

Figure 3.7: Cross sections in the (a),(c),(e) $\overline{\sigma}_m - \frac{\overline{\sigma}_{11}-\overline{\sigma}_{22}}{2}$ and (b),(d),(f) $\overline{\sigma}_m - \overline{\sigma}_{12}$ plane of the yield surface of the rank-3 laminate compared with the VHS bound. Cross sections are taken by fixing the value of $\overline{\sigma}_{12}$ on the right column, and $\frac{\overline{\sigma}_{11}-\overline{\sigma}_{22}}{2}$ in the left column. In (a)-(b), and (e)-(f), the fixed values correspond to the coordinate values of $\frac{\overline{\sigma}_{11}-\overline{\sigma}_{22}}{2}$ or $\overline{\sigma}_{12}$ at the points where VHS bound is attained when $\overline{\sigma}_m = \overline{\sigma}_{m,I}$ and $\overline{\sigma}_m = \overline{\sigma}_{m,IV}$, respectively. Points where the VHS bound is attained are represented by black circles.

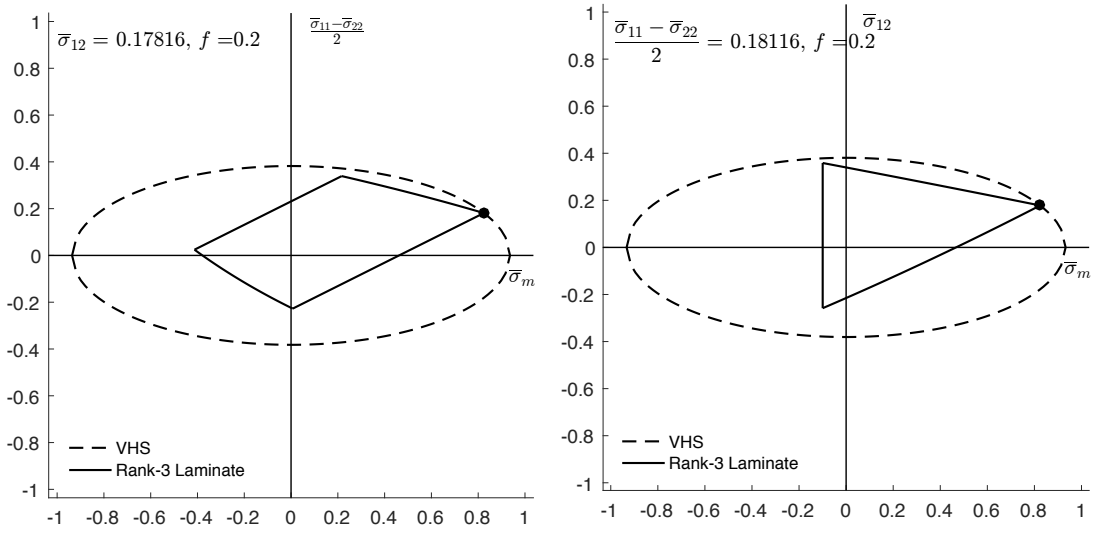

(e) (f)

Figure 3.7: Continued

results and the rank-3 laminate increases with decreasing porosity. Moreover, $\widetilde{\sigma}^H_{[3]}$ remains finite as $f \to 0$, a point which will be further discussed below.

Note that, in contrast to the trend for deviatoric loading, the predictions for $\widetilde{\sigma}^H$ from the composites with the more isotropic microstructures lie closer to the VHS bound (vis-a-vis the infinite rank laminate relative to the rank-3 laminate relative to the rank-2 laminate); it is the rank-2 laminate that attains the VHS bounds under purely deviatoric loading, not the rank-3 laminate. The effective response under purely hydrostatic loading is trivially isotropic regardless of the microstructure, as it only depends on $\overline{\boldsymbol{\sigma}}$ through $\overline{\sigma}_m$. Therefore, the class of microstructures bounded by the VHS bounds, when restricted to such loading conditions, is staggeringly large. As such, it is the anisotropy of the microstructure itself that determines effective response.

It has long been known that the VHS bounds are relatively stiffer for loading with high triaxialty, as well as for porous materials with low porosity (i.e. volume fraction of the void phase). This is related to the use of an LCC with constant-per-phase

moduli, and, as noted by Ponte Castañeda (2012), can be understood intuitively by the strong radial dependence of the fields (relative to the pores) under hydrostatic loading. In fact, by making use of iterated homogenization and the nonlinear variational method to approximate a heterogeneous LCC, Ponte Castañeda (2012) produced bounds which improve on the VHS bounds, and like the LAM microstructure, achieve the exact result under hydrostatic loading. These iterated nonlinear variational bounds of the Hashin-Shtrikman type (IHS) hold for the special class of multi-scale microstructures, but do not include the finite-rank microstructures considered in this work. This is due to the fact that the two-point correlation functions of the phases in the finite-rank laminates do not satisfy the hypotheses used in deriving the IHS bounds. In particular, the class of multi-scale microstructures is smaller than the class of linearly isotropic, nonlinearly anisotropic microstructures considered here, and hence the IHS bounds will predict a stiffer behavior than the VHS bounds. As such, one would expect that, as we increase the rank of the laminate, the effective response would approach the IHS result, never passing above it. Since both the IHS and LAM models give the excact result, this may be connected to the conjecture that the Gurson model is rigorous upper bound for all porous composites under hydrostatic loading (see Idiart, 2008, and references therein for a further discussion). Either way, these results reveal limitation of the VHS bounds, and VLC type bounds in general; although the use of a phase-wise constant LCC allows for analytical estimates, VLC bounds fail to produce accurate results for certain loading conditions and microstructures.

Now, as mentioned above, as $f \to 0$, $\widetilde{\sigma}^H_{VHS}$ tends to infinity, while $\widetilde{\sigma}^H_{[3]}$ remains finite. For nonzero values of f, the compressibility associated with the porous phase means that the yield surfaces must eventually come to a point. Due to the isotropy of the VHS bound, the associated yield surface reaches an apex and closes up on the hydrostatic axis when $\overline{\sigma}_m = \widetilde{\sigma}^H_{VHS}$; note that this corresponds to the value of for which $\overline{\sigma}^{VHS}_e$ vanishes (c.f. Eq. (3.6.24)). This value of $\overline{\sigma}_m$ is often referred to

as the "hydrostatic point," but care must be taken when defining such a point for composites with anisotropic response. As discussed above, the apex of the yield surface of the rank−3 laminate is also a point at which it attains the VHS bound, and hence is located off of the hydrostatic axis. This trend has been seen before in other anisotropic materials, specifically for systems of random viscoplastic materials with ellipsoidal voids (Agoras and Ponte Castañeda, 2013). It is therefore of interest to compare the apex points of the VHS bound with those for the rank−3 laminate.

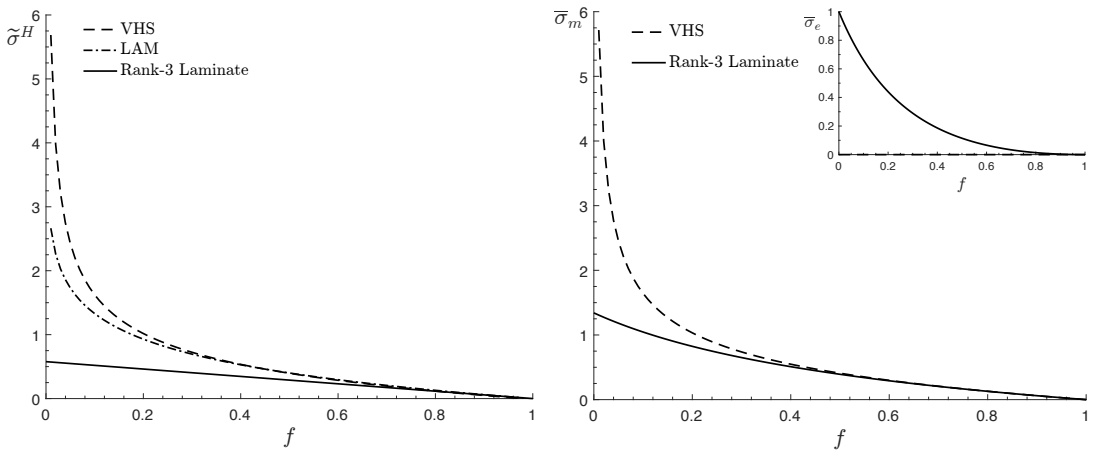

(a) (b)

Figure 3.8: (a) A comparison between the hydrostatic flow stress $\widetilde{\sigma}^H$ as predicted by the VHS bound, the exact LAM result, and the rank−3 laminate, as a function of porosity. (b) Value of $\overline{\sigma}_m$, as a function of porosity f, at which the yield surfaces of the rank−3 laminate and VHS bounds reach their apices. The corresponding values of $\overline{\sigma}_e$ are included as well.

Such a comparison is done in Figure 3.8b, where we have plotted, as a function of porosity, the value of $\overline{\sigma}_m$ for which the yield surfaces reach their apices. Inset in this plot are the corresponding values of $\overline{\sigma}_e$ for which this happens. Clearly, since the VHS bound closes up on the hydrostatic axis, the value of $\overline{\sigma}_e$ is always 0. However, we see that this is only true for the rank−3 laminate in the limit as $f \to 1$. Now, for values of f near 1, we see that the value of $\overline{\sigma}_e$ at which the rank−3 laminate reaches its apex

is small, and the difference between corresponding values of $\overline{\sigma}_m$ for the VHS bound and rank-3 laminate is small. Therefore, the apex point of the rank-3 laminate is located close to the hydrostatic axis and the VHS bound. However, as f decreases, the apex point for the laminate is located at smaller value of $\overline{\sigma}_m$ relative to those predicted by the VHS bound, and begins to move further into the deviatoric plane, as indicated by an increasing value of $\overline{\sigma}_e$. Interestingly, in the limit as $f \to 0$, whereby only the incompressible matrix phase remains, the apex point of the yield surface of the VHS bound tends towards infinity, while the value of $\overline{\sigma}_m$ for which the rank-3 laminate reaches its apex actually remains finite.

3.7 Conclusion

In this work, we looked prove optimality of the VHS bounds under general plane-strain loading conditions. Due to their interest within the engineering community, we focused our attention to porous viscoplastic materials. By taking the matrix phase to be isotropic and incompressible, we showed directly that the VHS bounds are attained under both purely deviatoric loading, as well as the more general plane-strain loading, and are hence optimal for the class of microstructures with nonlinear anisotropic response that have linearly isotropic response. Consistent with what was found for porous finite-rank laminates in the equivalent context of elasticity (as in Chapter 2), the microstructure that attains the bound depends on the type of loading applied. In particular, it is the rank-2 laminate that attains the bound under purely deviatoric loading, and the rank-3 laminate that attains the bound more generally. This is related to the fact that the microstructure that attains the bound is the most anisotropic within the class of microstructures bounded by it. The rank-2 laminate is in this sense more anisotropic than the rank-3 laminate, and as they both have linearly isotropic response under purely deviatoric loading (and are hence members of the class), the bound is attained by the former. For more general loading, the rank-2

laminate fails to have linearly isotorpic response, and therefore the rank-3 laminate is the one that attains the bound.

The method by which optimality is proven here illustrates clearly the issue with the variational linear comparison method that precludes them from being optimal over the class of statistically isotropic microstructures. In fact, the issue lies not with the VLC formulation *per se*, but with the bounds used for the LCC itself. Indeed, when the response of the linear material is isotropic, existing bounds that depend only on the volume fraction of the phases become degenerate. The Hashin-Shtrikmann bounds (which were derived under the assumption of a statistically isotropy microstructure), the translations bounds (which were derived under no assumptions on the microstructure), and the trace bounds of Milton and Kohn (1988) (which were derived under the assumption of a periodic microstructure) are all the same. Moreover, they are attained by a microstructure (i.e. finite-rank laminates) that is neither random nor periodic. This degeneracy is related to the fact that assumptions on the microstructure are irrelevant in the linear setting. This makes sense physically, as one could approximate any composite by taking a sufficiently large sample and extending it periodically; to prove this directly, one would have to make use of the notion of $G-$convergence.

Chapter 4

A Symmetric Fully Optimized Second-Order Method

Abstract

We consider an alternate formulation of a recently developed nonlinear homogenization method, which is based on a stationary variational principle for the macroscopic energy function. In this method, the trial fields are the properties of a suitably designed linear comparison composite (LCC), thus allowing for the estimation of the effective response and field statistics of the nonlinear composite in terms of available estimates for the corresponding quantities in the LCC. The formulation considered in this chapter makes use of a more symmetric choice for the linear comparison composite, which not only resolves an inconsistency that is present in the previous work, but also allows for a more robust set of estimates. The new symmetric fully optimized second-order method is applied to a class of two-phase power-law composites with fibrous microstructures subjected to plane strain loading. The resulting estimates for the effective response and field statistics are found to improve on earlier estimates, and to be in good agreement with full-field numerical simulations for nonlinear composite cylinder assemblages, as well as with available results for sequentially layered composites.

4.1 Introduction

Most materials are heterogeneous at sufficiently small length scales—well before reaching atomic length scales. Polar ice and aluminum alloys are polycrystalline aggregates of randomly oriented single-crystal grains, while metal-matrix composites and fiber-reinforced elastomers are two-phase material systems consisting of an 'inclusion' phase distributed randomly or periodically in a surrounding 'matrix' phase. In addition, when the loads applied to these materials are sufficiently large, their response is nonlinear—either due to intrinsic nonlinearities in their constitutive response (e.g., plasticity), or to geometric nonlinearities associated with finite strains and rotations. For these reasons, there is much interest in the development of homogenization methods with the objective of generating macroscopic constitutive relations for such heterogeneous materials from the constitutive properties of their constituent phases and information about their distribution in space (or microstructure). For small applied loads, the properties are linear and there is a well-developed theory of composites (see, for example, the monograph by Milton (2002b)), but for nonlinear composites much less is known. Classical extensions of the Voigt-Reuss bounds have been given, for example, by Hutchinson (1976) and Bhattacharya and Kohn (1997) to estimate the effective behavior of viscoplastic and shape-memory polycrystals, respectively. In addition, building on a nonlinear generalization (Willis, 1983) of the Hashin-Shtrikman variational principles for linear-elastic composites (Hashin and Shtrikman, 1963), rigorous bounds of the Hashin-Shtrikman type were obtained by Talbot and Willis (1985); Willis (1991). Later, new variational principles based on the use of a 'linear comparison composite' (LCC) were proposed by Ponte Castañeda (1991, 1992a), and used to generate improved bounds of the Hashin-Shtrikman and Beran-Milton (3-point) types for nonlinear composites. The idea of the method was to rewrite the local energy as the sum of the energy of the LCC plus a certain 'error' function consisting of the smallest difference between the linear and nonlinear

energies. An alternative method has been developed by Suquet (1993) by means of Hölder's inequality for special classes of pure power-law composites. In addition, bounds for nonlinear composites have also been obtained (Kohn and Little, 1998; Nesi et al., 1999; Peigney and Peigney, 2017) using appropriate extensions of the 'translation' method of Lurie and Cherkaev (1984) and Tartar (1985). The above-mentioned bounds were obtained for the effective strain-energy density function; bounds on the effective constitutive relation have also been obtained (Talbot and Willis, 2004; Peigney, 2005) using an approach developed by Milton and Serkov (2000).

While general bounds of the Hashin-Shtrikman and translation types are useful for broad classes of microstructures, they may not be as useful for more specific types of microstructures, such a particulate (matrix-inclusion) or granular (polycrystalline) microstructures. In addition, it is known that these bounds for nonlinear composites are only exact to first-order in the heterogeneity contrast, suggesting that they may not be sharp. For these reasons, it is sometimes useful to obtain estimates for more specific classes of microstructures. Building on a perturbation expansion for nonlinear composites with small contrast by Suquet and Ponte Castañeda (1993), Ponte Castañeda (1996) proposed a 'second-order' method for general composites, leading to estimates that agree with the perturbation estimates (Suquet and Ponte Castañeda, 1993) and are therefore exact to second-order in the contrast. This new method made use of a stationary variational principle (see also Ponte Castañeda and Willis (1999)) for a more general type of LCC incorporating eigenstresses or polarizations, in addition to the elasticity moduli of the phases of the LCC. More specifically, the polarizations were selected optimally in the context of the variational method, but the elastic moduli were set—in ad hoc fashion—equal to the tangent moduli of the nonlinear phases (evaluated at the phase averages of the fields in the LCC). However, it was later found (Leroy and Ponte Castañeda, 2001) that these 'tangent second-order' estimates could violate the rigorous bounds provided by the earlier 'variational' method (Ponte Castañeda, 1991) when the contrast and field fluctuations

are large, as is the case for porous materials near the percolation limit. Improved estimates satisfying the 'variational' bounds were generated by Ponte Castañeda (2002), by also making use of an LCC incorporating polarizations. However, this time the estimates were made stationary with respect to the moduli, but could not be made stationary with respect to the polarizations. Recently, Ponte Castañeda (2016) developed a fully stationary variational method which is stationary with respect to both the moduli and the polarizations of the LCC, leading to estimates that are exact to second-order in the contrast and satisfy all known bounds. In addition, as a consequence of the 'full stationarity,' this new method allows the estimation of the macroscopic response, as well as of the field statistics (first and second moments of the stress and strain fields in the phases), directly from the suitably optimized LCC.

By making use of appropriately selected LCCs, the above-mentioned variational methods can be used to estimate the macroscopic behavior and field statistics for broad classes of nonlinear composites, including polycrystalline aggregates (Ponte Castañeda, 2015). For special classes of microstructures, such as sequential laminates (consisting of laminates layered with one of the phases multiple times at different length scales, or ranks), it is sometimes possible to obtain exact estimates. Thus, for two-phase nonlinear composites with finite-rank sequentially layered microstructures, Ponte Castañeda (1992a) generated exact estimates, generalizing corresponding estimates by Maxwell for rank-three laminates in linear conductivity (see Milton (2002b)). However, while the estimates for finite-rank laminates with linear phases can be made to have overall isotropic response, this is no longer possible when the phases are nonlinear (Ponte Castañeda, 1992a). Motivated by this finding, deBotton and Hariton (2002) considered nonlinear laminates of high rank and showed that the properties could be made isotropic as the rank becomes large. More recently, Idiart (2008) considered the limit as the rank of the laminates tends to infinity and obtained an analytical characterization for its effective behavior in terms of a Hamilton-Jacobi-type partial differential equation. One important application of

such results for sequentially layered composites is that they can be used to saturate the Hashin-Shtrikman bounds for two-phase composites with linear phases (Tartar, 1985; Milton, 2002b). When the properties of the phases are nonlinear, however, the results for two-phase composites with sequentially layered microstructures do not saturate the above-mentioned nonlinear bounds of the Hashin-Shtrikman or translation types, suggesting that such bounds may not be sharp. On the other hand, Idiart and Ponte Castaneda (2013) have recently shown that the infinite-rank laminates cannot be extremal within the class of two-phase composites with isotropic two-point statistics. Clearly, things are much more complicated for nonlinear composites than for linear composites, and hence the need for further progress in this field.

This chapter is concerned with providing an alternative, more symmetric, formulation of the recently introduced fully optimized second-order (FOSO) homogenization method (Ponte Castañeda, 2016). As discussed in this reference, while there is no duality gap present in this previous method, one must be mindful of extra terms that appear when considering the energy potential and the associated dual energy potential of the LCC. In fact, it is known that the previous method may produce two estimates for the macroscopic response of the composite (each with its own, but different dual result). Thus we lay out a symmetric formulation of the FOSO method that produces only one estimate for the macroscopic response; this is achieved by choosing a different LCC potential. We show that the symmetric version of the FOSO method maintains all of the desirable properties present in the non-symmetric FOSO method. We then apply the symmetric FOSO method to a class of two-phase power-law composites with fibrous microstructures subjected to plane strain loading. We compare the resulting estimates with the corresponding estimates of the previous 'tangent second-order' (TSO) method (Ponte Castañeda, 1996), the 'variational' (VAR) bounds (Ponte Castañeda, 1991), exact results for infinite-rank laminates (LAM) (Idiart, 2008), as well as full-field simulations (Idiart et al., 2006) based on the fast Fourier transform (FFT) spectral technique (Moulinec and Suquet,

1998) for composite cylinder assemblages (CCA).

4.2 Homogenized behavior and field statistics

For the sake of exposition, the theoretical aspects of the work are presented in the setting of nonlinear infinitesimal elasticity. However, the method is fully generalizable to any number of constitutive theories; in Section 4.5, we consider a composite consisting of two nonlinear viscoplastic phases. This change, done in order to give more physical relevance to the results, does not affect the outcome of the method, as viscoplasticity and nonlinear elasticity are mathematically analogous. In the former, a constitutive model relates the Cauchy stress to the Eulerian strain rate, while in the latter, the constitutive model relates the infinitesimal stress to the infinitesimal strain. Moreover, the Eulerian strain rate is taken to be the symmetric part of the gradient of the velocity field, while the infinitesimal strain is that of the displacement field.

Thus, we consider here a heterogeneous material composed on N homogenous nonlinear elastic phases, which are distributed randomly and with statistical uniformity in an ensemble of specimens of the material. We further assume ergodicity and separation of length scales, so that ensemble averages can be replaced by volume average over a 'representative volume element' (RVE) of the composite, and 'effective' or 'homogenized' properties can be defined in terms of volume averages over the RVE (Milton, 2002b). We denote the volume occupied by the RVE by Ω and the corresponding regions occupied by the phases by $\Omega^{(r)}$ $(r = 1, \ldots, N)$, and let $\chi^{(r)}(\mathbf{x})$ be the corresponding characteristic function of phase r, such that $\chi^{(r)}(\mathbf{x}) = 1$ when x is in $\Omega^{(r)}$ and 0 otherwise. The constitutive behavior of the phases will be characterized by energy functions $w^{(r)}$ $(r = 1, \ldots, N)$, which are assumed in this work to be (strictly) convex and piecewise smooth. Then, the local stress-strain relation for the

heterogeneous material may be written as

$$\boldsymbol{\sigma} = \frac{\partial w(\mathbf{x}, \boldsymbol{\varepsilon})}{\partial \boldsymbol{\varepsilon}}, \quad w(\mathbf{x}, \boldsymbol{\varepsilon}) = \sum_{r=1}^{N} \chi^{(r)}(\mathbf{x}) w^{(r)}(\boldsymbol{\varepsilon}). \tag{4.2.1}$$

Alternatively, the constitutive behavior may be characterized by complementary energy functions $u^{(r)}$ $(r = 1, \ldots, N)$, such that

$$\boldsymbol{\varepsilon} = \frac{\partial u(\mathbf{x}, \boldsymbol{\sigma})}{\partial \boldsymbol{\sigma}}, \quad u(\mathbf{x}, \boldsymbol{\sigma}) = \sum_{r=1}^{N} \chi^{(r)}(\mathbf{x}) u^{(r)}(\boldsymbol{\sigma}). \tag{4.2.2}$$

The complementary potentials $u^{(r)}$ are related to the potentials $w^{(r)}$ via the Legendre transformation:

$$u^{(r)}(\boldsymbol{\sigma}) = \underset{\boldsymbol{\varepsilon}}{\operatorname{stat}} \left\{ \boldsymbol{\sigma} \cdot \boldsymbol{\varepsilon} - w^{(r)}(\boldsymbol{\varepsilon}) \right\}, \text{ such that } \; u(\mathbf{x}, \boldsymbol{\sigma}) = \underset{\boldsymbol{\varepsilon}}{\operatorname{stat}} \left\{ \boldsymbol{\sigma} \cdot \boldsymbol{\varepsilon} - w(\mathbf{x}, \boldsymbol{\varepsilon}) \right\}. \tag{4.2.3}$$

The stationary operation $g(y) = \underset{x}{\operatorname{stat}}\{f(x, y)\}$ acts on a function as follows. First, assuming appropriate regularity conditions on f, we compute the value of x^* for which $f(x, y)$ is stationary (i.e. $\frac{\partial f(x^*, y)}{\partial x} = 0$), and then solve for x^* as a function of y (i.e. $x^* = h(y)$). Finally, the stationary operator returns $g(y) = f(h(y), y)$. Under appropriate convexity assumptions of $w^{(r)}$, the stationary condition uniquely determines $\boldsymbol{\varepsilon}$ as a function of $\boldsymbol{\sigma}$, and it can be shown that $u^{(r)}(\boldsymbol{\sigma})$ is also convex. However, we note that the above definition still works even when w is not convex (Sewell, 1987). In this case, u becomes a multiple-valued function, as there may be multiple stationary points when evaluating Eq. (4.2.3).

We let $\langle \cdot \rangle$ and $\langle \cdot \rangle^{(r)}$ denote volume averages over Ω and $\Omega^{(r)}$, respectively, so that

$$\langle w(\mathbf{x}, \boldsymbol{\varepsilon}) \rangle = \sum_{r=1}^{N} c^{(r)} \left\langle w^{(r)}(\boldsymbol{\varepsilon}) \right\rangle^{(r)}, \quad \langle u(\mathbf{x}, \boldsymbol{\sigma}) \rangle = \sum_{r=1}^{N} c^{(r)} \left\langle u^{(r)}(\boldsymbol{\sigma}) \right\rangle^{(r)}, \tag{4.2.4}$$

where the $c^{(r)} = \left\langle \chi^{(r)} \right\rangle$ denote the volume fractions of the phases. As is well known (see Hutchinson (1976); Willis (1989); Ponte Castañeda and Suquet (1998)), the

macroscopic constitutive behavior of the composite is determined by the homogenized potential

$$\widetilde{W}(\overline{\boldsymbol{\varepsilon}}) = \min_{\boldsymbol{\varepsilon}\in\mathcal{K}} \langle w(\mathbf{x},\boldsymbol{\varepsilon})\rangle = \operatorname*{stat}_{\boldsymbol{\varepsilon}\in\mathcal{K}} \langle w(\mathbf{x},\boldsymbol{\varepsilon})\rangle\,, \tag{4.2.5}$$

where $\mathcal{K}$ is the set of *kinematically admissible* strain fields loosely defined by

$$\mathcal{K} = \left\{ \boldsymbol{\varepsilon} : \text{ there is } \mathbf{u} \text{ such that } \boldsymbol{\varepsilon} = \frac{1}{2}\left(\nabla\mathbf{u} + \nabla\mathbf{u}^T\right) \text{ in } \Omega, \text{ and } \mathbf{u} = \overline{\boldsymbol{\varepsilon}}\mathbf{x} \text{ on } \partial\Omega \right\}, \tag{4.2.6}$$

where the above strain-displacement relation must be interpreted in a weak sense across interphase boundaries. (For more mathematically precise definitions in terms of appropriate functional spaces, see, for example, Toland and Willis (1989).) It is also noted that the second equality in Eq. (4.2.5) is valid when the potentials $w^{(r)}$ are assumed to be strictly convex and to satisfy appropriate growth conditions. In this case, the unique minimum point is attained at the stationary point which in turn is determined by setting the first variational derivative equal to zero. This condition corresponds to the Euler-Lagrange equation, as given by the equilibrium equation $\nabla\cdot\boldsymbol{\sigma} = 0$ (also interpreted in a weak sense across interphase boundaries). However, in some cases, as with ideal plasticity, $w^{(r)}$ may lose strict convexity. Nonetheless, the variational problem is still well defined (see Suquet (1987)).

As with the local potentials, it is known (see Ponte Castañeda and Suquet (1998)) that the average stress $\overline{\boldsymbol{\sigma}} = \langle\boldsymbol{\sigma}\rangle$ is related to the average strain $\overline{\boldsymbol{\varepsilon}}$ via

$$\overline{\boldsymbol{\sigma}} = \frac{\partial\widetilde{W}}{\partial\overline{\boldsymbol{\varepsilon}}}. \tag{4.2.7}$$

A dual formulation making use of the complementary potential $u^{(r)}$ leads to an equivalent stress-strain relation (Suquet, 1987; Willis, 1989)

$$\overline{\boldsymbol{\varepsilon}} = \frac{\partial\widetilde{U}}{\partial\overline{\boldsymbol{\sigma}}}, \tag{4.2.8}$$

where

$$\widetilde{U}(\overline{\boldsymbol{\sigma}}) = \min_{\boldsymbol{\sigma}\in\mathcal{S}} \langle u(\mathbf{x},\boldsymbol{\sigma})\rangle = \operatorname*{stat}_{\boldsymbol{\sigma}\in\mathcal{S}} \langle u(\mathbf{x},\boldsymbol{\sigma})\rangle\,. \tag{4.2.9}$$

In this expression, $\mathcal{S}$ denotes the set of *statically admissible* stress fields

$$\mathcal{S} = \{\boldsymbol{\sigma} \,:\, \nabla\cdot\boldsymbol{\sigma} = \mathbf{0} \text{ in } \Omega, \text{ and } \langle\boldsymbol{\sigma}\rangle = \overline{\boldsymbol{\sigma}}\}\,. \tag{4.2.10}$$

Under the stated convexity assumptions, the two formulations are exactly equivalent in the sense that $\widetilde{W}^* = \widetilde{U}$. In general, $\widetilde{W}$ and $\widetilde{U}$ are difficult to compute, as they involve sets of nonlinear partial differential equations with randomly oscillating coefficients. In an attempt to facilitate this calculation, this work makes use of homogenization estimates (Willis, 1981; Milton, 2002b) for a suitably defined linear comparison composite (LCC) to generate corresponding estimates for the nonlinear composite.

It is useful at this point to recall some definitions concerning the field statistics in the composite. The averages (or first moments) of the stress and strain fields over phase r are respectively defined by $\overline{\boldsymbol{\sigma}}^{(r)} = \langle\boldsymbol{\sigma}\rangle^{(r)}$ and $\overline{\boldsymbol{\varepsilon}}^{(r)} = \langle\boldsymbol{\varepsilon}\rangle^{(r)}$, and are such that $\overline{\boldsymbol{\sigma}} = \sum_{r=1}^{N} c^{(r)}\overline{\boldsymbol{\sigma}}^{(r)}$ and $\overline{\boldsymbol{\varepsilon}}^{(r)} = \sum_{r=1}^{N} c^{(r)}\overline{\boldsymbol{\varepsilon}}^{(r)}$. The equivalent measures associated with $\overline{\boldsymbol{\sigma}}^{(r)}$ and $\overline{\boldsymbol{\varepsilon}}^{(r)}$ are defined by $\bar{\sigma}_e^{(r)} = \sqrt{\frac{3}{2}\bar{\mathbf{s}}^{(r)}\cdot\bar{\mathbf{s}}^{(r)}}$, where $\bar{\mathbf{s}}^{(r)}$ is the average stress deviator in phase r, and $\bar{\varepsilon}_e^{(r)} = \sqrt{\frac{2}{3}\bar{\boldsymbol{\varepsilon}}^{(r)}\cdot\bar{\boldsymbol{\varepsilon}}^{(r)}}$, respectively. In addition, the second moments of the stress and strain over phase r are given by $\langle\boldsymbol{\sigma}\otimes\boldsymbol{\sigma}\rangle^{(r)}$ and $\langle\boldsymbol{\varepsilon}\otimes\boldsymbol{\varepsilon}\rangle^{(r)}$, respectively, while the corresponding phase fluctuation covariance tensors are given by

$$\mathbb{C}_{\boldsymbol{\sigma}}^{(r)} = \big\langle(\boldsymbol{\sigma}-\overline{\boldsymbol{\sigma}}^{(r)})\otimes(\boldsymbol{\sigma}-\overline{\boldsymbol{\sigma}}^{(r)})\big\rangle^{(r)} = \langle\boldsymbol{\sigma}\otimes\boldsymbol{\sigma}\rangle^{(r)} - \overline{\boldsymbol{\sigma}}^{(r)}\otimes\overline{\boldsymbol{\sigma}}^{(r)}, \tag{4.2.11}$$

$$\mathbb{C}_{\boldsymbol{\varepsilon}}^{(r)} = \big\langle(\boldsymbol{\varepsilon}-\overline{\boldsymbol{\varepsilon}}^{(r)})\otimes(\boldsymbol{\varepsilon}-\overline{\boldsymbol{\varepsilon}}^{(r)})\big\rangle^{(r)} = \langle\boldsymbol{\varepsilon}\otimes\boldsymbol{\varepsilon}\rangle^{(r)} - \overline{\boldsymbol{\varepsilon}}^{(r)}\otimes\overline{\boldsymbol{\varepsilon}}^{(r)}. \tag{4.2.12}$$

In addition, use will be made here of the standard deviation of appropriate scalar quantities. For example, the standard deviation of the von Mises equivalent stress

and strain over phase r are given by

$$\mathrm{SD}^{(r)}(\sigma_e) = \sqrt{\langle \sigma_e^2 - \left(\overline{\sigma}_e^{(r)}\right)^2 \rangle^{(r)}}, \quad \text{and} \qquad \mathrm{SD}^{(r)}(\varepsilon_e) = \sqrt{\langle \varepsilon_e^2 - \left(\overline{\varepsilon}_e^{(r)}\right)^2 \rangle^{(r)}}, \quad (4.2.13)$$

and can be identified with appropriate projections of the corresponding covariance tensors $\mathbb{C}_{\boldsymbol{\sigma}}^{(r)}$ and $\mathbb{C}_{\boldsymbol{\varepsilon}}^{(r)}$, respectively. Expressions for the computation of the first and second moments of the fields in the phases of a nonlinear composite are available (Idiart and Ponte Castañeda, 2007a) and will be discussed below.

4.3 Fully stationary second-order variational estimates

4.3.1 Estimates for the Effective Potential

As mentioned earlier, the FOSO method makes use of a fictitious linear comparison composite (LCC) to estimate the properties of the nonlinear material. Given the nonlinear potential $w^{(r)}$ of phase r, we consider a corresponding linear potential $w_L^{(r)}$. Then, for some appropriate choice of weight factor $\alpha^{(r)}$, such that $0 < \alpha^{(r)} < 1$, we write our nonlinear potential $w^{(r)}(\boldsymbol{\varepsilon})$, trivially, as

$$w^{(r)}(\boldsymbol{\varepsilon}) = w_L^{(r)}(\boldsymbol{\varepsilon}) + \alpha^{(r)} \left(w^{(r)}(\boldsymbol{\varepsilon}) - w_L^{(r)}(\boldsymbol{\varepsilon}) \right) + (1 - \alpha^{(r)}) \left(w^{(r)}(\boldsymbol{\varepsilon}) - w_L^{(r)}(\boldsymbol{\varepsilon}) \right). \quad (4.3.1)$$

Here we choose the strain potential of phase r of the LCC to be of the form

$$w_L^{(r)}(\boldsymbol{\sigma}) = \frac{1}{2}\boldsymbol{\varepsilon} \cdot \mathbb{L}^{(r)}\boldsymbol{\varepsilon} + \boldsymbol{\tau}^{(r)} \cdot \boldsymbol{\varepsilon} + \frac{1}{4}\boldsymbol{\tau}^{(r)} \cdot \mathbb{M}^{(r)}\boldsymbol{\tau}^{(r)}, \quad (4.3.2)$$

where $\mathbb{L}^{(r)}$ is an elasticity tensor, $\mathbb{M}^{(r)} = (\mathbb{L}^{(r)})^{-1}$ is the corresponding compliance tensor and $\boldsymbol{\tau}^{(r)}$ is an eigenstress, all of which will be determined later as part of the

homogenization process. In addition, for added flexibility, we set

$$\boldsymbol{\tau}^{(r)} = \sum_{p=1}^{M} \beta_{(p)}^{(r)} \boldsymbol{\tau}_{(p)}^{(r)}, \tag{4.3.3}$$

where, for $p = 1, \ldots, M$, $\boldsymbol{\tau}_{(p)}^{(r)}$ are eigenstresses, and M is an arbitrary integer, to be determined later. The weight factors $\beta_{(p)}^{(r)}$ are taken to satisfy $0 < \beta_{(p)}^{(r)} < 1$ and $\sum_{p=1}^{M} \beta_{(p)}^{(r)} = 1$, and will be determined by the symmetry of the problem.

Differentiation of Eq. (4.3.2) with respect to $\boldsymbol{\varepsilon}$ shows that, in fact, the stress-strain relation is linear, i.e. $\boldsymbol{\sigma} = \mathbb{L}^{(r)}\boldsymbol{\varepsilon} + \boldsymbol{\tau}^{(r)}$. We take the LCC to have the same microstructure as the nonlinear composite we wish to approximate. The microstructure is defined via the indicator functions associated with the nonlinear composite $\chi^{(r)}(\mathbf{x})$. Using these functions, we define the local strain potential for the LCC, as in Eq. (4.2.1), via

$$w_L(\mathbf{x}, \boldsymbol{\varepsilon}) = \sum_{r=1}^{N} \chi^{(r)}(\mathbf{x}) w_L^{(r)}(\boldsymbol{\varepsilon}). \tag{4.3.4}$$

Now, the functions $\Delta w^{(r)} = w^{(r)} - w_L^{(r)}$ are in general non-convex, and can exhibit multiple stationary points; in contrast, $w^{(r)}$ and $w_L^{(r)}$ each possesses only one stationary point, corresponding to their global minimum. The hope nonetheless is to approximate the stationary point of $w^{(r)}$ with that of $w_L^{(r)}$ by suitably choosing $\mathbb{L}^{(r)}$ and $\boldsymbol{\tau}_{(p)}^{(r)}$. Building on a result for a slightly different form of the LCC (Ponte Castañeda, 2016), we have the following result:

Proposition 1:

Given a nonlinear phase potential $w^{(r)}$, we may write

$$w^{(r)}(\boldsymbol{\varepsilon}) = \underset{\boldsymbol{\tau}_{(p)}^{(r)}, \mathbb{L}^{(r)}}{\text{stat}} \left\{ w_L^{(r)}(\boldsymbol{\varepsilon}) + V^{(r)}(\mathbb{L}^{(r)}, \boldsymbol{\tau}_{(p)}^{(r)}) \right\}, \tag{4.3.5}$$

where $w_L^{(r)}$ is defined by Eq. (4.3.2), and the 'error' function $V^{(r)}(\mathbb{L}^{(r)}, \boldsymbol{\tau}_{(p)}^{(r)})$ is defined

via the relations

$$V^{(r)}(\mathbb{L}^{(r)}, \boldsymbol{\tau}_{(p)}^{(r)}) = \alpha^{(r)} \breve{V}^{(r)}(\mathbb{L}^{(r)}, \boldsymbol{\tau}_{(p)}^{(r)}) + (1 - \alpha^{(r)}) \widehat{V}^{(r)}(\mathbb{L}^{(r)}, \boldsymbol{\tau}_{(p)}^{(r)}), \tag{4.3.6}$$

with

$$\begin{aligned} \breve{V}^{(r)}(\mathbb{L}^{(r)}, \boldsymbol{\tau}_{(p)}^{(r)}) &= \sum_{r=1}^{M} \beta_{(p)}^{(r)} \breve{V}_{(p)}^{(r)}(\mathbb{L}^{(r)}, \boldsymbol{\tau}_{(p)}^{(r)}), \quad \breve{V}_{(p)}^{(r)}(\mathbb{L}^{(r)}, \boldsymbol{\tau}_{(p)}^{(r)}) = \underset{\breve{\boldsymbol{\varepsilon}}_{(p)}^{(r)}}{\text{stat}} \Delta w^{(r)}(\breve{\boldsymbol{\varepsilon}}_{(p)}^{(r)}), \\ \widehat{V}^{(r)}(\mathbb{L}^{(r)}, \boldsymbol{\tau}_{(p)}^{(r)}) &= \sum_{r=1}^{M} \beta_{(p)}^{(r)} \widehat{V}_{(p)}^{(r)}(\mathbb{L}^{(r)}, \boldsymbol{\tau}_{(p)}^{(r)}), \quad \widehat{V}_{(p)}^{(r)}(\mathbb{L}^{(r)}, \boldsymbol{\tau}_{(p)}^{(r)}) = \underset{\widehat{\boldsymbol{\varepsilon}}_{(p)}^{(r)}}{\text{stat}} \Delta w^{(r)}(\widehat{\boldsymbol{\varepsilon}}_{(p)}^{(r)}). \end{aligned} \tag{4.3.7}$$

It is recalled that the functions $\Delta w^{(r)}(\boldsymbol{\varepsilon}) = w^{(r)}(\boldsymbol{\varepsilon}) - w_L^{(r)}(\boldsymbol{\varepsilon})$ *are non-convex, in general, and the notation* $\widehat{\cdot}$ *and* $\breve{\cdot}$ *is used to distinguish between intrinsically different stationary points* $\breve{\boldsymbol{\varepsilon}}_{(p)}^{(r)}$ *and* $\widehat{\boldsymbol{\varepsilon}}_{(p)}^{(r)}$*, arising in the functions* $\breve{V}_{(p)}^{(r)}$ *and* $\widehat{V}_{(p)}^{(r)}$*, respectively. On the other hand, the subscript* p *is used to distinguish between symmetry-related versions of the same type of stationary point (*$\breve{\boldsymbol{\varepsilon}}_{(p)}^{(r)}$*, or* $\widehat{\boldsymbol{\varepsilon}}_{(p)}^{(r)}$*).*

Moreover, with respect to the stationary values of $\mathbb{L}^{(r)}$ *and* $\boldsymbol{\tau}_{(p)}^{(r)}$ *in expression* (4.3.5)*, we have that*

$$\frac{\partial w^{(r)}}{\partial \boldsymbol{\varepsilon}}(\boldsymbol{\varepsilon}) = \mathbb{L}^{(r)}\boldsymbol{\varepsilon} + \boldsymbol{\tau}^{(r)} = \frac{\partial w_L^{(r)}}{\partial \boldsymbol{\varepsilon}}(\boldsymbol{\varepsilon}). \tag{4.3.8}$$

Proof. To see that Eq. (4.3.5) is, in fact, a valid representation of the phase potential, we first note that the stationary conditions from the error functions give

$$\frac{\partial w^{(r)}}{\partial \boldsymbol{\varepsilon}}(\breve{\boldsymbol{\varepsilon}}_{(p)}^{(r)}) - \mathbb{L}^{(r)}\breve{\boldsymbol{\varepsilon}}_{(p)}^{(r)} = \boldsymbol{\tau}_{(p)}^{(r)} = \frac{\partial w^{(r)}}{\partial \boldsymbol{\varepsilon}}(\widehat{\boldsymbol{\varepsilon}}_{(p)}^{(r)}) - \mathbb{L}^{(r)}\widehat{\boldsymbol{\varepsilon}}_{(p)}^{(r)} \tag{4.3.9}$$

for each p. This implies a generalized secant condition (e.g. Figure 4.1a),

$$\frac{\partial w^{(r)}}{\partial \boldsymbol{\varepsilon}}(\breve{\boldsymbol{\varepsilon}}_{(p)}^{(r)}) - \frac{\partial w^{(r)}}{\partial \boldsymbol{\varepsilon}}(\widehat{\boldsymbol{\varepsilon}}_{(p)}^{(r)}) = \mathbb{L}^{(r)}(\breve{\boldsymbol{\varepsilon}}_{(p)}^{(r)} - \widehat{\boldsymbol{\varepsilon}}_{(p)}^{(r)}). \tag{4.3.10}$$

Now, the stationary condition with respect to $\boldsymbol{\tau}_{(p)}^{(r)}$ gives

$$\boldsymbol{\varepsilon} + \frac{1}{2}\mathbb{M}^{(r)}\boldsymbol{\tau}^{(r)} = \alpha^{(r)}\breve{\boldsymbol{\varepsilon}}_{(p)}^{(r)} + (1-\alpha^{(r)})\widehat{\boldsymbol{\varepsilon}}_{(p)}^{(r)} + \frac{1}{2}\mathbb{M}^{(r)}\boldsymbol{\tau}_{(p)}^{(r)}, \tag{4.3.11}$$

which holds for each p. Multiplying Eq. (4.3.11) by $\beta_{(p)}^{(r)}$ and summing, we find that

$$\boldsymbol{\varepsilon} = \sum_{p=1}^{M} \beta_{(p)}^{(r)} \left(\alpha^{(r)}\breve{\boldsymbol{\varepsilon}}_{(p)}^{(r)} + (1-\alpha^{(r)})\widehat{\boldsymbol{\varepsilon}}_{(p)}^{(r)} \right). \tag{4.3.12}$$

For $p \neq q$, Eq. (4.3.11) also tells us that

$$\alpha^{(r)} \left(\breve{\boldsymbol{\varepsilon}}_{(p)}^{(r)} - \breve{\boldsymbol{\varepsilon}}_{(q)}^{(r)} \right) + (1-\alpha^{(r)}) \left(\widehat{\boldsymbol{\varepsilon}}_{(p)}^{(r)} - \widehat{\boldsymbol{\varepsilon}}_{(q)}^{(r)} \right) + \frac{1}{2}\mathbb{M}^{(r)} \left(\boldsymbol{\tau}_{(p)}^{(r)} - \boldsymbol{\tau}_{(q)}^{(r)} \right) = \mathbf{0}. \tag{4.3.13}$$

The stationary condition with respect to $\mathbb{L}^{(r)}$ gives

$$\begin{aligned} &\boldsymbol{\varepsilon} \otimes \boldsymbol{\varepsilon} - \frac{1}{2}\mathbb{M}^{(r)}\boldsymbol{\tau}^{(r)} \otimes \mathbb{M}^{(r)}\boldsymbol{\tau}^{(r)} \\ &= \sum_{p=1}^{M} \beta_{(p)}^{(r)} \left(\alpha^{(r)}\breve{\boldsymbol{\varepsilon}}_{(p)}^{(r)} \otimes \breve{\boldsymbol{\varepsilon}}_{(p)}^{(r)} + (1-\alpha^{(r)})\widehat{\boldsymbol{\varepsilon}}_{(p)}^{(r)} \otimes \widehat{\boldsymbol{\varepsilon}}_{(p)}^{(r)} - \frac{1}{2}\mathbb{M}^{(r)}\boldsymbol{\tau}_{(p)}^{(r)} \otimes \mathbb{M}^{(r)}\boldsymbol{\tau}_{(p)}^{(r)} \right). \end{aligned} \tag{4.3.14}$$

We can then combine Eqs. (4.3.13) and (4.3.14) to find that

$$\begin{aligned} \boldsymbol{\varepsilon} \otimes \boldsymbol{\varepsilon} = &\sum_{p=1}^{M} \beta_{(p)}^{(r)} \left(\alpha^{(r)}\breve{\boldsymbol{\varepsilon}}_{(p)}^{(r)} + (1-\alpha^{(r)})\widehat{\boldsymbol{\varepsilon}}_{(p)}^{(r)} \right) \otimes \left(\alpha^{(r)}\breve{\boldsymbol{\varepsilon}}_{(p)}^{(r)} + (1-\alpha^{(r)})\widehat{\boldsymbol{\varepsilon}}_{(p)}^{(r)} \right) \\ &- \alpha^{(r)}(1-\alpha^{(r)}) \sum_{p=1}^{M} \beta_{(p)}^{(r)} \left(\breve{\boldsymbol{\varepsilon}}_{(p)}^{(r)} - \widehat{\boldsymbol{\varepsilon}}_{(p)}^{(r)} \right) \otimes \left(\breve{\boldsymbol{\varepsilon}}_{(p)}^{(r)} - \widehat{\boldsymbol{\varepsilon}}_{(p)}^{(r)} \right). \end{aligned} \tag{4.3.15}$$

On the other hand, from Eq. (4.3.12), we also have that

$$\boldsymbol{\varepsilon} \otimes \boldsymbol{\varepsilon} = \left[\sum_{p=1}^{M} \beta_{(p)}^{(r)} \left(\alpha^{(r)}\breve{\boldsymbol{\varepsilon}}_{(p)}^{(r)} + (1-\alpha^{(r)})\widehat{\boldsymbol{\varepsilon}}_{(p)}^{(r)} \right) \right] \otimes \left[\sum_{p=1}^{M} \beta_{(p)}^{(r)} \left(\alpha^{(r)}\breve{\boldsymbol{\varepsilon}}_{(p)}^{(r)} + (1-\alpha^{(r)})\widehat{\boldsymbol{\varepsilon}}_{(p)}^{(r)} \right) \right]. \tag{4.3.16}$$

Upon subtracting Eq. (4.3.16) from Eq. (4.3.15), we find that

$$\begin{aligned}\mathbb{O} = \alpha^{(r)}(1-\alpha^{(r)}) \sum_{p=1}^{M} \beta_{(p)}^{(r)} \left(\breve{\boldsymbol{\varepsilon}}_{(p)}^{(r)} - \widehat{\boldsymbol{\varepsilon}}_{(p)}^{(r)}\right) \otimes \left(\breve{\boldsymbol{\varepsilon}}_{(p)}^{(r)} - \widehat{\boldsymbol{\varepsilon}}_{(p)}^{(r)}\right) \\ - \sum_{1 \leqslant p < q \leqslant M} \beta_{(p)}^{(r)} \beta_{(q)}^{(r)} \left[\left(\alpha^{(r)} \breve{\boldsymbol{\varepsilon}}_{(p)}^{(r)} + (1-\alpha^{(r)}) \widehat{\boldsymbol{\varepsilon}}_{(p)}^{(r)}\right) - \left(\alpha^{(r)} \breve{\boldsymbol{\varepsilon}}_{(q)}^{(r)} + (1-\alpha^{(r)}) \widehat{\boldsymbol{\varepsilon}}_{(q)}^{(r)}\right)\right] \otimes \\ \left[\left(\alpha^{(r)} \breve{\boldsymbol{\varepsilon}}_{(p)}^{(r)} + (1-\alpha^{(r)}) \widehat{\boldsymbol{\varepsilon}}_{(p)}^{(r)}\right) - \left(\alpha^{(r)} \breve{\boldsymbol{\varepsilon}}_{(q)}^{(r)} + (1-\alpha^{(r)}) \widehat{\boldsymbol{\varepsilon}}_{(q)}^{(r)}\right)\right]. \quad (4.3.17)\end{aligned}$$

One possible solution is that $\breve{\boldsymbol{\varepsilon}}_{(p)}^{(r)} = \widehat{\boldsymbol{\varepsilon}}_{(p)}^{(r)} = \boldsymbol{\varepsilon}$ for each p. To see that this is the only solution for a given choice of $\beta_{(p)}^{(r)}$ and the optimal values of $\boldsymbol{\tau}_{(p)}^{(r)}$ and $\mathbb{L}^{(r)}$, suppose that $\breve{\breve{\boldsymbol{\varepsilon}}}_{(1)}^{(r)}, \cdots, \breve{\breve{\boldsymbol{\varepsilon}}}_{(M)}^{(r)}$ and $\widehat{\widehat{\boldsymbol{\varepsilon}}}_{(1)}^{(r)}, \cdots, \widehat{\widehat{\boldsymbol{\varepsilon}}}_{(M)}^{(r)}$ represent another set of solutions, which by necessity satisfy all the stationary conditions outlined above. In particular, from Eq. (4.3.11)

$$\begin{aligned}\boldsymbol{\varepsilon} + \frac{1}{2}\mathbb{M}^{(r)}\boldsymbol{\tau}^{(r)} &= \alpha^{(r)} \breve{\breve{\boldsymbol{\varepsilon}}}_{(p)}^{(r)} + (1-\alpha^{(r)}) \widehat{\widehat{\boldsymbol{\varepsilon}}}_{(p)}^{(r)} + \frac{1}{2}\mathbb{M}^{(r)}\boldsymbol{\tau}_{(p)}^{(r)} \\ &= \alpha^{(r)} \breve{\boldsymbol{\varepsilon}}_{(p)}^{(r)} + (1-\alpha^{(r)}) \widehat{\boldsymbol{\varepsilon}}_{(p)}^{(r)} + \frac{1}{2}\mathbb{M}^{(r)}\boldsymbol{\tau}_{(p)}^{(r)}, \quad (4.3.18)\end{aligned}$$

which implies then that

$$\alpha^{(r)} \breve{\breve{\boldsymbol{\varepsilon}}}_{(p)}^{(r)} + (1-\alpha^{(r)}) \widehat{\widehat{\boldsymbol{\varepsilon}}}_{(p)}^{(r)} = \alpha^{(r)} \breve{\boldsymbol{\varepsilon}}_{(p)}^{(r)} + (1-\alpha^{(r)}) \widehat{\boldsymbol{\varepsilon}}_{(p)}^{(r)} \quad (4.3.19)$$

for each p. Recalling that our first set of solutions was found to satisfy $\breve{\boldsymbol{\varepsilon}}_{(p)}^{(r)} = \widehat{\boldsymbol{\varepsilon}}_{(p)}^{(r)} = \boldsymbol{\varepsilon}$ for all p, we see that from Eq. (4.3.19),

$$\alpha^{(r)} \breve{\breve{\boldsymbol{\varepsilon}}}_{(p)}^{(r)} + (1-\alpha^{(r)}) \widehat{\widehat{\boldsymbol{\varepsilon}}}_{(p)}^{(r)} = \boldsymbol{\varepsilon} \quad (4.3.20)$$

for all p. Therefore the second term of Eq. (4.3.17), as applied to the new solution set, is identically the zero 4^{th} order tensor, leaving us with

$$\mathbb{O} = \alpha^{(r)}(1-\alpha^{(r)}) \sum_{p=1}^{M} \beta_{(p)}^{(r)} \left(\breve{\breve{\boldsymbol{\varepsilon}}}_{(p)}^{(r)} - \widehat{\widehat{\boldsymbol{\varepsilon}}}_{(p)}^{(r)}\right) \otimes \left(\breve{\breve{\boldsymbol{\varepsilon}}}_{(p)}^{(r)} - \widehat{\widehat{\boldsymbol{\varepsilon}}}_{(p)}^{(r)}\right). \quad (4.3.21)$$

Upon taking the suitable trace of Eq. (4.3.21), we find that

$$0 = \alpha^{(r)}(1-\alpha^{(r)}) \sum_{p=1}^{M} \beta_{(p)}^{(r)} \left| \breve{\boldsymbol{\varepsilon}}_{(p)}^{(r)} - \widehat{\boldsymbol{\varepsilon}}_{(p)}^{(r)} \right|^2, \tag{4.3.22}$$

which implies that $\breve{\boldsymbol{\varepsilon}}_{(p)}^{(r)} = \widehat{\boldsymbol{\varepsilon}}_{(p)}^{(r)}$. Combining this fact with Eq. (4.3.20), we conclude that $\breve{\boldsymbol{\varepsilon}}_{(p)}^{(r)} = \widehat{\boldsymbol{\varepsilon}}_{(p)}^{(r)} = \boldsymbol{\varepsilon}$ as well, which proves Eq. (4.3.5).

Returning to Eq. (4.3.9), we note that we may write

$$\boldsymbol{\tau}_{(p)}^{(r)} = \alpha^{(r)} \frac{\partial w^{(r)}}{\partial \boldsymbol{\varepsilon}}(\breve{\boldsymbol{\varepsilon}}_{(p)}^{(r)}) + (1-\alpha^{(r)}) \frac{\partial w^{(r)}}{\partial \boldsymbol{\varepsilon}}(\widehat{\boldsymbol{\varepsilon}}_{(p)}^{(r)}) - \mathbb{L}^{(r)} \left(\alpha^{(r)} \breve{\boldsymbol{\varepsilon}}_{(p)}^{(r)} + (1-\alpha^{(r)}) \widehat{\boldsymbol{\varepsilon}}_{(p)}^{(r)} \right). \tag{4.3.23}$$

Rearranging terms, multiplying by $\beta_{(p)}^{(r)}$ and summing, we find

$$\begin{aligned}
&\sum_{p=1}^{M} \beta_{(p)}^{(r)} \left[\alpha^{(r)} \frac{\partial w^{(r)}}{\partial \boldsymbol{\varepsilon}}(\breve{\boldsymbol{\varepsilon}}_{(p)}^{(r)}) + (1-\alpha^{(r)}) \frac{\partial w^{(r)}}{\partial \boldsymbol{\varepsilon}}(\widehat{\boldsymbol{\varepsilon}}_{(p)}^{(r)}) \right] \\
&= \mathbb{L}^{(r)} \left[\sum_{p=1}^{M} \beta_{(p)}^{(r)} \left(\alpha^{(r)} \breve{\boldsymbol{\varepsilon}}_{(p)}^{(r)} + (1-\alpha^{(r)}) \widehat{\boldsymbol{\varepsilon}}_{(p)}^{(r)} \right) \right] + \sum_{p=1}^{M} \beta_{(p)}^{(r)} \boldsymbol{\tau}_{(p)}^{(r)} \\
&= \mathbb{L}^{(r)} \boldsymbol{\varepsilon} + \boldsymbol{\tau}^{(r)} \\
&= \frac{\partial w_L^{(r)}(\boldsymbol{\varepsilon})}{\partial \boldsymbol{\varepsilon}},
\end{aligned} \tag{4.3.24}$$

where use was made of Eqs. (4.3.3) and (4.3.12) in the third line. Recalling though that $\breve{\boldsymbol{\varepsilon}}_{(p)}^{(r)} = \widehat{\boldsymbol{\varepsilon}}_{(p)}^{(r)} = \boldsymbol{\varepsilon}$ at the stationary points of Eq. (4.3.5), the first line of Eq.(4.3.24) reduces to $\frac{\partial w^{(r)}(\boldsymbol{\varepsilon})}{\partial \boldsymbol{\varepsilon}}$, showing that

$$\frac{\partial w^{(r)}(\boldsymbol{\varepsilon})}{\partial \boldsymbol{\varepsilon}} = \frac{\partial w_L^{(r)}(\boldsymbol{\varepsilon})}{\partial \boldsymbol{\varepsilon}}.$$

□

Thus, we have that $w^{(r)}$ and the right-hand side of Eq. (4.3.5) share not only the same values, but the same stationary points.

4.3.2 Fully Optimized Stationary Variational Estimates

With our new expression for $w^{(r)}$, as given by Eq. (4.3.5), we move to our next result, which gives a corresponding expression for approximating the effective potential of the nonlinear composite.

Proposition 2:

Given the definitions (4.3.7) *of the error functions* $V^{(r)}$*, and the expression* (4.3.2) *for the linear comparison composite phase potential ,the effective potential of the nonlinear composite, as defined by Eq.* (4.2.5)*, can be approximated by*

$$\widetilde{W}(\overline{\boldsymbol{\varepsilon}}) \approx \widetilde{W}_N(\overline{\boldsymbol{\varepsilon}}) = \underset{\mathbb{L}^{(s)},\boldsymbol{\tau}_{(p)}^{(s)}}{\operatorname{stat}} \left\{ \widetilde{W}_L(\overline{\boldsymbol{\varepsilon}}) + \sum_{r=1}^{N} V^{(r)}(\mathbb{L}^{(r)}, \boldsymbol{\tau}_{(p)}^{(r)}) \right\}, \tag{4.3.25}$$

where $\widetilde{W}_L(\overline{\boldsymbol{\varepsilon}})$ *is the effective potential of the LCC defined by Eq.* (4.3.4)*, and is given by*

$$\widetilde{W}_L(\overline{\boldsymbol{\varepsilon}}) = \underset{\boldsymbol{\varepsilon}\in\mathcal{K}}{\operatorname{stat}} \langle w_L(\mathbf{x}, \boldsymbol{\varepsilon}) \rangle = \underset{\boldsymbol{\varepsilon}\in\mathcal{K}}{\operatorname{stat}} \sum_{r=1}^{N} c^{(r)} \langle w_L^{(r)}(\boldsymbol{\varepsilon}) \rangle^{(r)}. \tag{4.3.26}$$

Proof. Using Proposition 1, we know that we can substitute the expression (4.3.5) for the local potentials into Eq. (4.2.5). Upon interchanging the stationary operations with integration, we find that

$$\widetilde{W}(\overline{\boldsymbol{\varepsilon}}) = \underset{\boldsymbol{\varepsilon}\in\mathcal{K}}{\operatorname{stat}} \underset{\mathbb{L}^{(s)}(\mathbf{x}),\boldsymbol{\tau}_{(p)}^{(s)}(\mathbf{x})}{\operatorname{stat}} \left\{ \sum_{r=1}^{N} c^{(r)} \left\langle w_L^{(r)}(\boldsymbol{\varepsilon}) + V^{(r)}(\mathbb{L}^{(r)}, \boldsymbol{\tau}_{(p)}^{(r)}) \right\rangle^{(r)} \right\}, \tag{4.3.27}$$

where $\mathbb{L}^{(s)}(\mathbf{x})$ and $\boldsymbol{\tau}_{(p)}^{(s)}(\mathbf{x})$ are to be interpreted as trial fields in some suitable function spaces. As there are no differential constraints on these trial fields, we merely need to assume that $\mathbb{L}^{(s)}(\mathbf{x})$ and $\boldsymbol{\tau}_{(p)}^{(s)}(\mathbf{x})$ have appropriate integrability, as it pertains to 4^{th} order, and 2^{nd} order tensors, respectively.

Interchanging the stationary operations, and noting that only the $w_L^{(r)}$ depend on

$\boldsymbol{\varepsilon}$, we find that

$$\widetilde{W}(\overline{\boldsymbol{\varepsilon}}) = \underset{\mathbb{L}^{(s)}(\mathbf{x}),\boldsymbol{\tau}_{(p)}^{(s)}(\mathbf{x})}{\text{stat}} \left\{ \underset{\boldsymbol{\varepsilon}\in\mathcal{K}}{\text{stat}} \sum_{r=1}^{N} c^{(r)} \left\langle w_L^{(r)}(\boldsymbol{\varepsilon}) \right\rangle^{(r)} + \sum_{r=1}^{N} \left\langle V^{(r)}(\mathbb{L}^{(r)}, \boldsymbol{\tau}_{(p)}^{(r)}) \right\rangle^{(r)} \right\}. \quad (4.3.28)$$

It should be noted that Eq. (4.3.28) is an exact result, since, due to the lack of differential constraints on the trial fields, the associated Euler-Lagrange equations are precisely those obtained from Eq. (4.3.5). However, the inner stationary problem cannot in general be solved for analytically, due to the non-uniformity of $\mathbb{L}^{(s)}(\mathbf{x})$ and $\boldsymbol{\tau}_{(p)}^{(s)}(\mathbf{x})$. We therefore narrow the class of trial fields to those which are piecewise uniform (i.e., uniform per phase), which gives Eq. (4.3.25). □

Remark 1:

While the 'exact' version of the estimate (4.3.28) *is valid (and gives the same value) for any choice of the interpolating parameters* $\alpha^{(r)}$*, the 'approximate' version* (4.3.25) *can give different results depending on the choice of the parameters* $\alpha^{(r)}$*.*

Remark 2:

Estimates for the homogenized response of linear composites with given types of microstructures can then be used to generate corresponding estimates for nonlinear composites. In particular, homogenization estimates of the Willis type (Ponte Castañeda and Willis, 1995) for the macroscopic response and first and second moments of the stress or strain fields in two-phase linear-elastic composites with particulate microstructures are given in Section 4.8, and will be used in Section 4.5 to obtain corresponding estimates for two-phase (nonlinear) viscoplastic composites.

Next, we spell out the stationary conditions obtained from the estimate (4.3.25) for the nonlinear composite. The inner stationary conditions, as determined from the definitions (4.3.7) of $\widehat{V}_{(p)}^{(r)}$ and $\check{V}_{(p)}^{(r)}$, are precisely the same conditions for the phase potentials, namely Eq. (4.3.9). The stationary conditions with respect to $\boldsymbol{\tau}_{(p)}^{(r)}$ now yield

$$\overline{\boldsymbol{\varepsilon}}_L^{(r)} + \frac{1}{2}\mathbb{M}^{(r)}\boldsymbol{\tau}^{(r)} = \alpha^{(r)}\check{\boldsymbol{\varepsilon}}_{(p)}^{(r)} + (1-\alpha^{(r)})\widehat{\boldsymbol{\varepsilon}}_{(p)}^{(r)} + \frac{1}{2}\mathbb{M}^{(r)}\boldsymbol{\tau}_{(p)}^{(r)} \quad (4.3.29)$$

for $p = 1, \ldots, M$ and $r = 1, \ldots, N$, where $\overline{\boldsymbol{\varepsilon}}_L^{(r)}$ is the average of the strain field over phase r in the LCC, and where use has been made of the stationarity of $\widetilde{W}_L$ with respect to the strain field $\boldsymbol{\varepsilon}(\mathbf{x})$. This implies that

$$\overline{\boldsymbol{\varepsilon}}_L^{(r)} = \sum_{p=1}^{M} \beta_{(p)}^{(r)} \left[\alpha^{(r)} \breve{\boldsymbol{\varepsilon}}_{(p)}^{(r)} + (1 - \alpha^{(r)}) \widehat{\boldsymbol{\varepsilon}}_{(p)}^{(r)} \right], \tag{4.3.30}$$

for each r, as well as

$$\alpha^{(r)} \left(\breve{\boldsymbol{\varepsilon}}_{(p)}^{(r)} - \breve{\boldsymbol{\varepsilon}}_{(q)}^{(r)} \right) + (1 - \alpha^{(r)}) \left(\widehat{\boldsymbol{\varepsilon}}_{(p)}^{(r)} - \widehat{\boldsymbol{\varepsilon}}_{(q)}^{(r)} \right) + \frac{1}{2} \mathbb{M}^{(r)} \left(\boldsymbol{\tau}_{(p)}^{(r)} - \boldsymbol{\tau}_{(q)}^{(r)} \right) = \mathbf{0} \tag{4.3.31}$$

for $p \neq q$, and each r. Similarly, the stationary condition with respect to $\mathbb{L}^{(r)}$ yields

$$\begin{aligned} &\langle \boldsymbol{\varepsilon} \otimes \boldsymbol{\varepsilon} \rangle_L^{(r)} - \frac{1}{2} \mathbb{M}^{(r)} \boldsymbol{\tau}^{(r)} \otimes \mathbb{M}^{(r)} \boldsymbol{\tau}^{(r)} \\ &= \sum_{p=1}^{M} \beta_{(p)}^{(r)} \left(\alpha^{(r)} \breve{\boldsymbol{\varepsilon}}_{(p)}^{(r)} \otimes \breve{\boldsymbol{\varepsilon}}_{(p)}^{(r)} + (1 - \alpha^{(r)}) \widehat{\boldsymbol{\varepsilon}}_{(p)}^{(r)} \otimes \widehat{\boldsymbol{\varepsilon}}_{(p)}^{(r)} - \frac{1}{2} \mathbb{M}^{(r)} \boldsymbol{\tau}_{(p)}^{(r)} \otimes \mathbb{M}^{(r)} \boldsymbol{\tau}_{(p)}^{(r)} \right), \end{aligned} \tag{4.3.32}$$

where $\langle \boldsymbol{\varepsilon} \otimes \boldsymbol{\varepsilon} \rangle_L^{(r)}$ is the second moment of the strain field over phase r in the LCC. Note that these conditions have the same general form as the stationary conditions found for the local potential $w^{(r)}(\boldsymbol{\varepsilon})$. Combining Eqs. (4.3.30), (4.3.31), and (4.3.32), we find that

$$\begin{aligned} \mathbb{C}_{\boldsymbol{\varepsilon}}^{(r)} = \alpha^{(r)}(1 - \alpha^{(r)}) \sum_{p=1}^{M} \beta_{(p)}^{(r)} \left(\breve{\boldsymbol{\varepsilon}}_{(p)}^{(r)} - \widehat{\boldsymbol{\varepsilon}}_{(p)}^{(r)} \right) \otimes \left(\breve{\boldsymbol{\varepsilon}}_{(p)}^{(r)} - \widehat{\boldsymbol{\varepsilon}}_{(p)}^{(r)} \right) \\ - \sum_{1 \leqslant p < q \leqslant M} \beta_{(p)}^{(r)} \beta_{(q)}^{(r)} \left[\alpha^{(r)} \left(\breve{\boldsymbol{\varepsilon}}_{(p)}^{(r)} - \breve{\boldsymbol{\varepsilon}}_{(q)}^{(r)} \right) + (1 - \alpha^{(r)}) \left(\widehat{\boldsymbol{\varepsilon}}_{(p)}^{(r)} - \widehat{\boldsymbol{\varepsilon}}_{(q)}^{(r)} \right) \right] \otimes \\ \left[\alpha^{(r)} \left(\breve{\boldsymbol{\varepsilon}}_{(p)}^{(r)} - \breve{\boldsymbol{\varepsilon}}_{(q)}^{(r)} \right) + (1 - \alpha^{(r)}) \left(\widehat{\boldsymbol{\varepsilon}}_{(p)}^{(r)} - \widehat{\boldsymbol{\varepsilon}}_{(q)}^{(r)} \right) \right], \end{aligned} \tag{4.3.33}$$

where $\mathbb{C}_{\boldsymbol{\varepsilon}}^{(r)}$ is the covariance tensor of the fluctuations of the strain field in phase r of the LCC.

In general, the covariance tensor is known to have full rank (Ponte Castañeda

and Suquet, 1998). This fact helps determine the value of M, which, until now, was taken to be arbitrary. Let D be the dimension of the space of 4^{th} order tensors, and note that the right hand side of Eq. (4.3.33) is a sum of dyadic products of 2^{nd} order tensors. Therefore, for the right-hand side of Eq. (4.3.33) to be of full rank, we see that M must be chosen to be at least as large as $\lceil \frac{D}{2} \rceil$; for a problem in two dimensions, $M \geqslant 2$, while for a problem in 3 dimensions, $M \geqslant 5$. Thus, it is seen that the use of the more general polarizations , as given by Eq. (4.3.3), and associated error functions defined by Eq. (4.3.7) makes it possible to generate estimates that are fully stationary with respect to both $\mathbb{L}^{(r)}$ and $\boldsymbol{\tau}^{(r)}$ in expression (4.3.25). In this context, it should be noted that this was not the case for earlier 'second-order' estimates (Ponte Castañeda, 1996, 2002) for nonlinear composites.

4.4 Additional Properties of the Stationary Variational Estimates

4.4.1 Calculation of effective behavior and field statistics

Upon substituting into Eq. (4.3.25) the stationary values of $\check{\boldsymbol{\varepsilon}}^{(r)}_{(p)}, \hat{\boldsymbol{\varepsilon}}^{(r)}_{(p)}, \mathbb{L}^{(r)}$, and $\boldsymbol{\tau}^{(r)}_{(p)}$, as determined by Eqs. (4.3.9), (4.3.29) and (4.3.32), it can be shown that

$$\widetilde{W}_N(\overline{\boldsymbol{\varepsilon}}) = \sum_{r=1}^{N} c^{(r)} \sum_{p=1}^{M} \beta^{(r)}_{(p)} \left[\alpha^{(r)} w^{(r)}(\check{\boldsymbol{\varepsilon}}^{(r)}_{(p)}) + (1-\alpha^{(r)}) w^{(r)}(\hat{\boldsymbol{\varepsilon}}^{(r)}_{(p)}) \right]. \tag{4.4.1}$$

This follows from the fact that the method produces results that are stationary with respect to both the trial fields $\mathbb{L}^{(s)}$ and $\boldsymbol{\tau}^{(s)}_{(p)}$. Therefore, any terms with linear dependence on the trial fields, both in the expression for $\widetilde{W}_L$, as well as in the error functions, will cancel out, leaving only the evaluation of the nonlinear potential at the specified critical points. Moreover, differentiating Eq. (4.3.25) with respect to $\overline{\boldsymbol{\varepsilon}}$,

we have the macroscopic stress-strain relation

$$\overline{\boldsymbol{\sigma}} = \widetilde{\mathbb{L}}\overline{\boldsymbol{\varepsilon}} + \widetilde{\boldsymbol{\tau}}, \tag{4.4.2}$$

where $\widetilde{\mathbb{L}}$ and $\widetilde{\boldsymbol{\tau}}$ are the effective elasticity tensor and eigenstress, respectively. This again follows from the stationarity of the nonlinear estimate (4.3.25) with respect to the trial fields $\mathbb{L}^{(s)}$ and $\boldsymbol{\tau}_{(p)}^{(s)}$, as well as stationarity with respect to the variables $\check{\boldsymbol{\varepsilon}}_{(p)}^{(r)}$ and $\widehat{\boldsymbol{\varepsilon}}_{(p)}^{(r)}$ in the error functions (4.3.7). It now follows (Ponte Castañeda, 1996) from this expression that the constitutive response of the nonlinear composite is exact to second-order in the heterogeneity contrast provided that the estimate for the LCC is also exact to second-order in the contrast. This will be the case, for example, for the Willis estimates given in Section 4.8.

Now, in order to calculate the field statistics of the nonlinear composite, we use a general procedure developed in Idiart and Ponte Castañeda (2007a), which gives a way to calculate the n^{th} moment of the stress or strain fields in the phases of the nonlinear composite directly from the linear composite. The calculation is made possible by considering a suitably perturbed local potential.

For example, in calculating the first moment of the strain field in phase r, we consider the perturbed local nonlinear potential

$$w_{\boldsymbol{\eta}}(\mathbf{x}, \boldsymbol{\varepsilon}) = \sum_{r=1}^{N} \chi^{(r)}(\mathbf{x}) w^{(r)}(\boldsymbol{\varepsilon}) + \chi^{(r)}(\mathbf{x}) \boldsymbol{\eta}^{(r)} \cdot \boldsymbol{\varepsilon}, \tag{4.4.3}$$

where $\boldsymbol{\eta}^{(r)}$ is a constant, symmetric, second-order tensor, and $w^{(r)}$ is the nonlinear phase potential. Let $\widetilde{W}_{\boldsymbol{\eta}}(\overline{\boldsymbol{\varepsilon}})$ be the homogenized potential associated to Eq. (4.4.3). The result in Idiart and Ponte Castañeda (2007a) states that

$$\overline{\boldsymbol{\varepsilon}}^{(r)} = \frac{1}{c^{(r)}} \left. \frac{\partial \widetilde{W}_{\boldsymbol{\eta}}(\overline{\boldsymbol{\varepsilon}})}{\partial \boldsymbol{\eta}^{(r)}} \right|_{\boldsymbol{\eta}^{(r)}=\mathbf{0}}. \tag{4.4.4}$$

Using this, we find that

$$\overline{\boldsymbol{\varepsilon}}_L^{(r)} = \frac{1}{c^{(r)}} \left. \frac{\partial \widetilde{W}_{L\boldsymbol{\eta}}(\overline{\boldsymbol{\varepsilon}})}{\partial \boldsymbol{\eta}^{(r)}} \right|_{\boldsymbol{\eta}^{(r)}=\mathbf{0}}, \tag{4.4.5}$$

where $\widetilde{W}_{L\boldsymbol{\eta}}(\overline{\boldsymbol{\varepsilon}})$ is the homogenized potential associated with the local potential

$$w_{L\boldsymbol{\eta}}(\mathbf{x}, \boldsymbol{\varepsilon}) = \sum_{r=1}^{N} \chi^{(r)}(\mathbf{x}) w_L^{(r)}(\boldsymbol{\varepsilon}) + \chi^{(r)}(\mathbf{x}) \boldsymbol{\eta}^{(r)} \cdot \boldsymbol{\varepsilon}, \tag{4.4.6}$$

and $w_L^{(r)}$ is the linear comparison potential as given by Eq. (4.3.2). Using Eqs. (4.4.3) and (4.4.6) in both Eqs. (4.2.5) and (4.3.5), respectively, we find that

$$\widetilde{W}_{\boldsymbol{\eta}}(\overline{\boldsymbol{\varepsilon}}) = \underset{\mathbb{L}^{(s)}, \boldsymbol{\tau}_{(p)}^{(s)}}{\operatorname{stat}} \left\{ \widetilde{W}_{L\boldsymbol{\eta}}(\overline{\boldsymbol{\varepsilon}}) + \sum_{r=1}^{N} V^{(r)}(\mathbb{L}^{(r)}, \boldsymbol{\tau}_{(p)}^{(r)}) \right\}. \tag{4.4.7}$$

Note that the perturbed terms cancel in the error functions, and so $V^{(r)}$ is independent of $\boldsymbol{\eta}$. Differentiating with respect to $\boldsymbol{\eta}^{(r)}$, evaluating at $\boldsymbol{\eta}^{(r)} = \mathbf{0}$, and using the stationary values of $\boldsymbol{\tau}_{(p)}^{(r)}$ and $\mathbb{L}^{(r)}$, we see that

$$\overline{\boldsymbol{\varepsilon}}^{(r)} = \frac{1}{c^{(r)}} \left. \frac{\partial \widetilde{W}_{\boldsymbol{\eta}}(\overline{\boldsymbol{\varepsilon}})}{\partial \boldsymbol{\eta}^{(r)}} \right|_{\boldsymbol{\eta}^{(r)}=\mathbf{0}} = \frac{1}{c^{(r)}} \left. \frac{\partial \widetilde{W}_{L\boldsymbol{\eta}}(\overline{\boldsymbol{\varepsilon}})}{\partial \boldsymbol{\eta}^{(r)}} \right|_{\boldsymbol{\eta}^{(r)}=\mathbf{0}} = \overline{\boldsymbol{\varepsilon}}_L^{(r)}, \tag{4.4.8}$$

that is, the phase averages over the strain field in the nonlinear composite can be estimated directly from the phase averages of the strain field in the LCC. In fact, the results in Idiart and Ponte Castañeda (2007a) can also be used to show that

$$\langle \boldsymbol{\varepsilon} \otimes \boldsymbol{\varepsilon} \rangle^{(r)} = \langle \boldsymbol{\varepsilon} \otimes \boldsymbol{\varepsilon} \rangle_L^{(r)}, \tag{4.4.9}$$

and moreover, that the same results also hold for the stress fields, namely

$$\overline{\boldsymbol{\sigma}}^{(r)} = \overline{\boldsymbol{\sigma}}_L^{(r)}, \quad \text{and} \quad \langle \boldsymbol{\sigma} \otimes \boldsymbol{\sigma} \rangle^{(r)} = \langle \boldsymbol{\sigma} \otimes \boldsymbol{\sigma} \rangle_L^{(r)}. \tag{4.4.10}$$

In the context of calculating the moments of the stress fields, we again perturb

the potentials, but now with a term of the form $w^{(r)}(\boldsymbol{\varepsilon} - \boldsymbol{\eta}^{(r)})$—see Idiart and Ponte Castañeda (2007a).

4.4.2 Duality Results

Different applications of this procedure may necessitate an approximation of either the macroscopic stress potential, or the macroscopic strain potential. We recall that, in laying out the theory in the previous sections, we chose an LCC strain potential of the form

$$w_L^{(r)}(\boldsymbol{\varepsilon}) = \frac{1}{2}\boldsymbol{\varepsilon} \cdot \mathbb{L}^{(r)}\boldsymbol{\varepsilon} + \boldsymbol{\varepsilon} \cdot \boldsymbol{\tau}^{(r)} + \frac{1}{4}\boldsymbol{\tau}^{(r)} \cdot (\mathbb{L}^{(r)})^{-1}\boldsymbol{\tau}^{(r)}. \tag{4.4.11}$$

Upon taking the Legendre transform, we find that the LCC stress potential is of the form

$$u_L^{(r)}(\boldsymbol{\sigma}) = \frac{1}{2}\boldsymbol{\sigma} \cdot \mathbb{M}^{(r)}\boldsymbol{\sigma} + \boldsymbol{\sigma} \cdot \boldsymbol{\gamma}^{(r)} + \frac{1}{4}\boldsymbol{\gamma}^{(r)} \cdot (\mathbb{M}^{(r)})^{-1}\boldsymbol{\gamma}^{(r)} \tag{4.4.12}$$

where $\boldsymbol{\gamma}^{(r)} = -\mathbb{M}^{(r)}\boldsymbol{\tau}^{(r)}$ and $\mathbb{L}^{(r)} = (\mathbb{M}^{(r)})^{-1}$. The symmetry between the forms of these two potentials, as we will see shortly, is precisely where the Symmetric FOSO method gains an extra layer of duality relative to the previous (non-symmetric) FOSO method (see Ponte Castañeda (2016)).

It is useful next to show the duality of the error functions $\check{V}_{(p)}^{(r)}$ and $\widehat{V}_{(p)}^{(r)}$, as functions of either $\mathbb{L}^{(r)}$ and $\boldsymbol{\tau}_{(p)}^{(r)}$, or $\mathbb{M}^{(r)}$ and $\boldsymbol{\gamma}_{(p)}^{(r)}$, respectively.

Making use of the Legendre duality between $w_L^{(r)}$ and $u_L^{(r)}$, we have

$$\begin{aligned}
\breve{V}_{(p)}^{(r)}(\mathbb{L}^{(r)}, \boldsymbol{\tau}_{(p)}^{(r)}) &= \operatorname*{stat}_{\breve{\boldsymbol{\varepsilon}}_{(p)}^{(r)}} \left\{ w^{(r)}(\breve{\boldsymbol{\varepsilon}}_{(p)}^{(r)}) - w_L^{(r)}(\breve{\boldsymbol{\varepsilon}}_{(p)}^{(r)}) \right\} \\
&= \operatorname*{stat}_{\breve{\boldsymbol{\varepsilon}}_{(p)}^{(r)}} \left\{ w^{(r)}(\breve{\boldsymbol{\varepsilon}}_{(p)}^{(r)}) - \operatorname*{stat}_{\breve{\boldsymbol{\sigma}}_{(p)}^{(r)}} \left[\breve{\boldsymbol{\varepsilon}}_{(p)}^{(r)} \cdot \breve{\boldsymbol{\sigma}}_{(p)}^{(r)} - u_L^{(r)}(\breve{\boldsymbol{\sigma}}_{(p)}^{(r)}) \right] \right\} \\
&= \operatorname*{stat}_{\breve{\boldsymbol{\varepsilon}}_{(p)}^{(r)}} \left\{ \operatorname*{stat}_{\breve{\boldsymbol{\sigma}}_{(p)}^{(r)}} \left[w^{(r)}(\breve{\boldsymbol{\varepsilon}}_{(p)}^{(r)}) - \breve{\boldsymbol{\varepsilon}}_{(p)}^{(r)} \cdot \breve{\boldsymbol{\sigma}}_{(p)}^{(r)} + u_L^{(r)}(\breve{\boldsymbol{\sigma}}_{(p)}^{(r)}) \right] \right\} \\
&= \operatorname*{stat}_{\breve{\boldsymbol{\sigma}}_{(p)}^{(r)}} \left\{ \operatorname*{stat}_{\breve{\boldsymbol{\varepsilon}}_{(p)}^{(r)}} \left[w^{(r)}(\breve{\boldsymbol{\varepsilon}}_{(p)}^{(r)}) - \breve{\boldsymbol{\varepsilon}}_{(p)}^{(r)} \cdot \breve{\boldsymbol{\sigma}}_{(p)}^{(r)} \right] + u_L^{(r)}(\breve{\boldsymbol{\sigma}}_{(p)}^{(r)}) \right\} \\
&= \operatorname*{stat}_{\breve{\boldsymbol{\sigma}}_{(p)}^{(r)}} \left\{ u_L^{(r)}(\breve{\boldsymbol{\sigma}}_{(p)}^{(r)}) - u^{(r)}(\breve{\boldsymbol{\sigma}}_{(p)}^{(r)}) \right\}. \qquad (4.4.13)
\end{aligned}$$

Therefore, we define

$$\breve{V}_{(p)}^{(r)}(\mathbb{M}^{(r)}, \boldsymbol{\gamma}_{(p)}^{(r)}) = \operatorname*{stat}_{\breve{\boldsymbol{\sigma}}_{(p)}^{(r)}} \left\{ u_L^{(r)}(\breve{\boldsymbol{\sigma}}_{(p)}^{(r)}) - u^{(r)}(\breve{\boldsymbol{\sigma}}_{(p)}^{(r)}) \right\}, \qquad (4.4.14)$$

where $u_L^{(r)}$ is given in terms of $\mathbb{M}^{(r)}$ and $\boldsymbol{\gamma}^{(r)}$ by expression (4.4.12), and similarly for $\widehat{V}_{(p)}^{(r)}(\mathbb{M}^{(r)}, \boldsymbol{\gamma}_{(p)}^{(r)})$. Moreover, from Eq. (4.4.13) and the corresponding equation for $\widehat{V}_{(p)}^{(r)}(\mathbb{M}^{(r)}, \boldsymbol{\gamma}_{(p)}^{(r)})$, we have that

$$\begin{aligned}
\widehat{\boldsymbol{\sigma}}_{(p)}^{(r)} &= \frac{\partial w^{(r)}}{\partial \boldsymbol{\varepsilon}}(\widehat{\boldsymbol{\varepsilon}}_{(p)}^{(r)}), & \widehat{\boldsymbol{\varepsilon}}_{(p)}^{(r)} &= \frac{\partial u^{(r)}}{\partial \boldsymbol{\sigma}}(\widehat{\boldsymbol{\sigma}}_{(p)}^{(r)}), \\
\breve{\boldsymbol{\sigma}}_{(p)}^{(r)} &= \frac{\partial w^{(r)}}{\partial \boldsymbol{\varepsilon}}(\breve{\boldsymbol{\varepsilon}}_{(p)}^{(r)}), & \breve{\boldsymbol{\varepsilon}}_{(p)}^{(r)} &= \frac{\partial u^{(r)}}{\partial \boldsymbol{\sigma}}(\breve{\boldsymbol{\sigma}}_{(p)}^{(r)}). \qquad (4.4.15)
\end{aligned}$$

Then, evaluating the Legendre transform of the approximation $\widetilde{W}_N$ of $\widetilde{W}$ in

Eq.(4.3.25), we obtain an approximation $\widetilde{U}_N$ of $\widetilde{U}$, as given by

$$\begin{aligned}
\widetilde{U}_N(\overline{\boldsymbol{\sigma}}) &= \underset{\overline{\boldsymbol{\varepsilon}}}{\text{stat}} \left\{ \overline{\boldsymbol{\sigma}} \cdot \overline{\boldsymbol{\varepsilon}} - \widetilde{W}_N(\overline{\boldsymbol{\varepsilon}}) \right\} \\
&= \underset{\overline{\boldsymbol{\varepsilon}}}{\text{stat}} \left\{ \overline{\boldsymbol{\varepsilon}} \cdot \overline{\boldsymbol{\sigma}} - \underset{\mathbb{L}^{(s)}, \boldsymbol{\tau}_{(p)}^{(s)}}{\text{stat}} \left\{ \widetilde{W}_L(\overline{\boldsymbol{\varepsilon}}) + \sum_{r=1}^{N} V^{(r)}(\mathbb{L}^{(r)}, \boldsymbol{\tau}_{(p)}^{(r)}) \right\} \right\} \\
&= \underset{\mathbb{L}^{(s)}, \boldsymbol{\tau}_{(p)}^{(s)}}{\text{stat}} \left\{ \underset{\overline{\boldsymbol{\varepsilon}}}{\text{stat}} \left\{ \overline{\boldsymbol{\sigma}} \cdot \overline{\boldsymbol{\varepsilon}} - \widetilde{W}_L(\overline{\boldsymbol{\varepsilon}}) \right\} + \sum_{r=1}^{N} V^{(r)}(\mathbb{L}^{(r)}, \boldsymbol{\tau}_{(p)}^{(r)}) \right\} \\
&= \underset{\mathbf{M}^{(s)}, \boldsymbol{\gamma}_{(p)}^{(s)}}{\text{stat}} \left\{ \widetilde{U}_L(\overline{\boldsymbol{\sigma}}) - \sum_{r=1}^{N} V^{(r)}(\mathbb{M}^{(r)}, \boldsymbol{\gamma}_{(p)}^{(r)}) \right\}, \qquad (4.4.16)
\end{aligned}$$

where we have made use of the duality between and pairs $\mathbb{L}^{(r)}, \boldsymbol{\tau}_{(p)}^{(r)}$ and $\mathbb{M}^{(r)}, \boldsymbol{\gamma}_{(p)}^{(r)}$.

While an approximation for $\widetilde{U}_N(\overline{\boldsymbol{\sigma}})$ is attainable through duality, it is here that we finally see the advantage of the symmetric choice of LCC potentials. If we start with the representation

$$u^{(r)}(\boldsymbol{\sigma}) = \underset{\boldsymbol{\gamma}_{(p)}^{(r)}, \mathbb{M}^{(r)}}{\text{stat}} \left\{ u_L^{(r)}(\boldsymbol{\sigma}) - V^{(r)}(\mathbb{M}^{(r)}, \boldsymbol{\gamma}_{(p)}^{(r)}) \right\}, \qquad (4.4.17)$$

then through arguments completely analogous to those in Proposition 1 and Proposition 2, and upon carrying out the calculations above, as applied to the stress potential, the estimate we obtain for $\widetilde{U}(\overline{\boldsymbol{\varepsilon}})$ is precisely the Legendre dual calculated in Eq. (4.4.16). As discussed in Ponte Castañeda (2016), this was not the case with the previous (non-symmetric) FOSO method.

For completeness, we spell out the stationary conditions associated with the Symmetric FOSO stress formulation. The optimality conditions from the error functions using the stress potentials are

$$\frac{\partial u^{(r)}}{\partial \boldsymbol{\sigma}}(\breve{\boldsymbol{\sigma}}_{(p)}^{(r)}) - \mathbb{M}^{(r)} \breve{\boldsymbol{\sigma}}_{(p)}^{(r)} = \boldsymbol{\gamma}_{(p)}^{(r)} = \frac{\partial u^{(r)}}{\partial \boldsymbol{\sigma}}(\widehat{\boldsymbol{\sigma}}_{(p)}^{(r)}) - \mathbb{M}^{(r)} \widehat{\boldsymbol{\sigma}}_{(p)}^{(r)} \qquad (4.4.18)$$

while the stationary conditions with respect to $\mathbb{M}^{(r)}$ and $\boldsymbol{\gamma}_{(p)}^{(r)}$ can be combined to give

$$\overline{\boldsymbol{\sigma}}_L^{(r)} = \sum_{p=1}^{M} \beta_{(p)}^{(r)} \left[\alpha^{(r)} \check{\boldsymbol{\sigma}}_{(p)}^{(r)} + (1-\alpha^{(r)}) \hat{\boldsymbol{\sigma}}_{(p)}^{(r)} \right] \tag{4.4.19}$$

and

$$\begin{aligned} \mathbb{C}_{\boldsymbol{\sigma}}^{(r)} = \alpha^{(r)}(1-\alpha^{(r)}) \sum_{p=1}^{M} \beta_{(p)}^{(r)} \left(\check{\boldsymbol{\sigma}}_{(p)}^{(r)} - \hat{\boldsymbol{\sigma}}_{(p)}^{(r)} \right) \otimes \left(\check{\boldsymbol{\sigma}}_{(p)}^{(r)} - \hat{\boldsymbol{\sigma}}_{(p)}^{(r)} \right) \\ - \sum_{1 \leqslant p < q \leqslant M} \beta_{(p)}^{(r)} \beta_{(q)}^{(r)} \left[\alpha^{(r)} \left(\check{\boldsymbol{\sigma}}_{(p)}^{(r)} - \check{\boldsymbol{\sigma}}_{(q)}^{(r)} \right) + (1-\alpha^{(r)}) \left(\hat{\boldsymbol{\sigma}}_{(p)}^{(r)} - \hat{\boldsymbol{\sigma}}_{(q)}^{(r)} \right) \right] \otimes \\ \left[\alpha^{(r)} \left(\check{\boldsymbol{\sigma}}_{(p)}^{(r)} - \check{\boldsymbol{\sigma}}_{(q)}^{(r)} \right) + (1-\alpha^{(r)}) \left(\hat{\boldsymbol{\sigma}}_{(p)}^{(r)} - \hat{\boldsymbol{\sigma}}_{(q)}^{(r)} \right) \right]. \end{aligned} \tag{4.4.20}$$

4.4.3 The Stress-Strain Relation

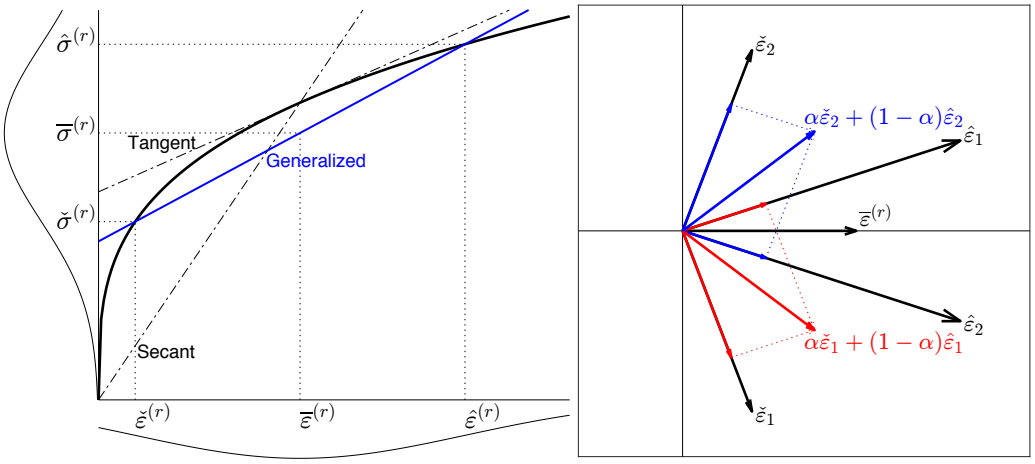

(a) (b)

Figure 4.1: (a): A one-dimensional depiction of the new 'generalized secant' linearization scheme. (b): A two-dimensional cartoon depicting the choice of stationary points in the symmetric FOSO method.

Figure 4.1a shows a one-dimensional picture of the new 'generalized secant' linearization used in this work, as well as some of the other linearization schemes that

have been used in the past, for comparison purposes. The nonlinear stress-strain curve in phase r is represented by the continuous black curve. The 'secant' linearization produces an approximation to the values of the stress at a given strain under the assumption $\overline{\boldsymbol{\sigma}}^{(r)} = \frac{\partial w^{(r)}}{\partial \boldsymbol{\varepsilon}}(\overline{\boldsymbol{\varepsilon}}^{(r)})$. However, this equality cannot hold, in general, due to the fact that for a general nonlinear function $w^{(r)}$, $\left\langle \frac{\partial w^{(r)}}{\partial \boldsymbol{\varepsilon}}(\boldsymbol{\varepsilon}) \right\rangle^{(r)} \neq \frac{\partial w^{(r)}}{\partial \boldsymbol{\varepsilon}}(\overline{\boldsymbol{\varepsilon}}^{(r)})$. Similarly, the 'tangent' linearization uses the line tangent to the curve at $\overline{\boldsymbol{\varepsilon}}^{(r)}$—albeit typically implemented in incremental form—and suffers from the same limitation as the classical secant. On the other hand, the new method makes use of the first and second moments of the fields in the phases—by means of variables $\widehat{\boldsymbol{\varepsilon}}^{(r)}$ and $\breve{\boldsymbol{\varepsilon}}^{(r)}$ (or, alternatively, dual variables $\widehat{\boldsymbol{\sigma}}^{(r)}$ and $\breve{\boldsymbol{\sigma}}^{(r)}$ related to $\widehat{\boldsymbol{\varepsilon}}^{(r)}$ and $\breve{\boldsymbol{\varepsilon}}^{(r)}$ by Eq. (4.4.15))—to define a generalized secant linearization in such a fashion that the point defined by $(\overline{\boldsymbol{\varepsilon}}^{(r)}, \overline{\boldsymbol{\sigma}}^{(r)})$ lies on this line. This produces a consistent approximation to the phase average strain, since $\overline{\boldsymbol{\sigma}}^{(r)} = \left\langle \mathbb{L}^{(r)}\boldsymbol{\varepsilon} + \boldsymbol{\tau}^{(r)} \right\rangle^{(r)} = \mathbb{L}^{(r)}\overline{\boldsymbol{\varepsilon}}^{(r)} + \boldsymbol{\tau}^{(r)}$. Moreover, we find that the stress and strain in the phase are distributed about $\overline{\boldsymbol{\sigma}}^{(r)}$ and $\overline{\boldsymbol{\varepsilon}}^{(r)}$, as depicted schematically by the curve below the strain axis and the curve to the left of the stress axis, respectively. For clarity, it is worth mentioning that this depiction is completely symmetric, and could alternatively be looked at from the perspective of applying some stress $\overline{\boldsymbol{\sigma}}^{(r)}$ and looking to approximate the average strain $\overline{\boldsymbol{\varepsilon}}^{(r)}$. For completeness, it should also be mentioned in this context that the 'variational' bound (Ponte Castañeda, 1991) lies on a 'generalized secant' line defined by the second moments of the fields (instead of the first moments), while the 'tangent second-order' includes corrections to the tangent also depending on the second moments (Ponte Castañeda and Suquet, 1998), thus avoiding the undesirable restriction of the classical secant and tangent methods (i.e., $\overline{\boldsymbol{\sigma}}^{(r)} = \frac{\partial w^{(r)}(\overline{\boldsymbol{\varepsilon}}^{(r)})}{\partial \boldsymbol{\varepsilon}}$).

Since the stress and strain fields are not one-dimensional, the picture depicted in Figure 4.1a is incomplete. For this reason, we also provide in Figure 4.1b a cartoon which elucidates the significance of the previously outlined stationary conditions. In it, we see the value of the average strain $\overline{\boldsymbol{\varepsilon}}^{(r)}$ we wish to approximate, taken, without

loss of generality, to lie on one axis in the space of deviatoric strains. Plotted next are the critical points, $\widehat{\boldsymbol{\varepsilon}}_i$ and $\breve{\boldsymbol{\varepsilon}}_i$ $(i = 1, 2)$, of $\Delta w^{(r)}$ which are used to approximate the value of $\overline{\boldsymbol{\varepsilon}}^{(r)}$. In application, certain symmetries arise between these critical points; for example, they often come in pairs, a fact which is represented here. Stationary conditions (4.3.9) and (4.3.33) show that the location of the critical points is determined not only by the field fluctuations relative to the average strain, but also by their positions relative to all other critical points.

4.4.4 Comparison with the non-symmetric FOSO

In applying the non-symmetric FOSO method of Ponte Castañeda (2016) to approximate the effective strain potential, the choice of LCC phase potentials was taken to be

$$w_L^{(r)}(\boldsymbol{\varepsilon}) = \frac{1}{2}\boldsymbol{\varepsilon} \cdot \mathbb{L}^{(r)}\boldsymbol{\varepsilon} + \boldsymbol{\varepsilon} \cdot \boldsymbol{\tau}^{(r)}, \tag{4.4.21}$$

which gives dual stress potentials of the form

$$u_L^{(r)}(\boldsymbol{\sigma}) = \frac{1}{2}\boldsymbol{\sigma} \cdot \mathbb{M}^{(r)}\boldsymbol{\sigma} + \boldsymbol{\sigma} \cdot \boldsymbol{\gamma}^{(r)} + \frac{1}{2}\boldsymbol{\gamma}^{(r)} \cdot (\mathbb{M}^{(r)})^{-1}\boldsymbol{\gamma}^{(r)}. \tag{4.4.22}$$

Note the asymmetry in the forms of the stress and strain potentials, as given by the extra quadratic term in $\boldsymbol{\gamma}^{(r)}$ for $u_L^{(r)}$. We emphasize that upon carrying out the calculations presented in Ponte Castañeda (2016), which were adopted in this chapter, one can produce a fully optimized second-order estimate for the effective strain potential, which is exact to second order in the heterogeneity. Moreover there is no duality gap in that the estimate obtained for the effective strain potential using an LCC as defined by Eq. (4.4.21) is exactly dual to the estimate obtained for the effective stress potential using an LCC defined by Eq. (4.4.22). However, the forms of the dual estimates are different, and this is why we refer to this method as being 'non-symmetric.'

As a consequence, some of the stationary conditions used to determine the optimal

values of $\mathbb{L}^{(r)}$ and $\boldsymbol{\tau}^{(r)}$ differ from the conditions spelled out in this chapter. For example, as shown in Section 4.9, expression (4.9.4) for the covariance tensor is given by only the first term in Eq. (4.3.33). Nonetheless, with respect to the optimal values of the trial fields, Eq. (4.4.1) holds in the non-symmetric FOSO version. Also, the macroscopic response is still given by Eq. (4.4.2), and it is still true that $\overline{\boldsymbol{\varepsilon}}^{(r)} = \overline{\boldsymbol{\varepsilon}}_L^{(r)}$ and $\langle \boldsymbol{\varepsilon} \otimes \boldsymbol{\varepsilon} \rangle^{(r)} = \langle \boldsymbol{\varepsilon} \otimes \boldsymbol{\varepsilon} \rangle_L^{(r)}$, etc.

Now, using the non-symmetric FOSO method to approximate the effective stress potential, it is natural to choose

$$u_L^{(r)}(\boldsymbol{\sigma}) = \frac{1}{2}\boldsymbol{\sigma} \cdot \mathbb{M}^{(r)}\boldsymbol{\sigma} + \boldsymbol{\sigma} \cdot \boldsymbol{\gamma}^{(r)}, \tag{4.4.23}$$

which gives dual strain potentials of the form

$$w_L^{(r)}(\boldsymbol{\varepsilon}) = \frac{1}{2}\boldsymbol{\varepsilon} \cdot \mathbb{L}^{(r)}\boldsymbol{\varepsilon} + \boldsymbol{\varepsilon} \cdot \boldsymbol{\tau}^{(r)} + \frac{1}{2}\boldsymbol{\tau}^{(r)} \cdot (\mathbb{L}^{(r)})^{-1}\boldsymbol{\tau}^{(r)}. \tag{4.4.24}$$

Once again, upon implementing the method, one will obtain estimates for the effective stress potential which are fully stationary, and share all the properties mentioned above, as they pertain to the homogenized response and the first and second moments of the stress fluctuations.

It is here where the asymmetry of the LCC in the previous FOSO version becomes an issue. This method produces two different estimates for, say, the effective strain potential: one estimate is obtained using an LCC of the form (4.4.21), and another is obtained by using Eq.(4.4.24). By contrast, the current symmetric FOSO method produces only one result for the effective behavior. It is interesting to notice that the choice Eq. (4.4.11) of LCC for the symmetric version is the average of Eqs. (4.4.21) and (4.4.24). In general, the symmetric and asymmetric methods using Eq. (4.4.11), or (4.4.21)/(4.4.24), respectively, will produce different results, although the differences turn out to be relatively small. In addition, it should be noted that the choice of critical points for the non-symmetric FOSO version is more constrained by

symmetry requirements. The increased flexibility in the choice of critical points for the symmetric FOSO method is expected to lead, in general, to a more robust set of results. Therefore, it is not just that the symmetric FOSO method provides an additional layer of duality, but also that it uses the given field statistics more fully than its predecessor.

4.5 Application to two-phase, isotropic, power-law viscoplastic material in plane strain

The general results of Section 4.3 are specialized to fibrous two-phase composites with incompressible phases subjected to plane strain (or anti-plane strain) loading. The infinitely long fibers are assumed to be aligned and perfectly bonded to the matrix, and to have a circular cross-section with diameter much smaller than the dimensions of the whole composite. Moreover, they are distributed with statistical isotropy in the matrix phase. This assumption leads to transversely isotropic overall properties for the composite. We denote the fibrous inclusions as phase 2, and the matrix as phase 1; the inclusions occupy a region with volume fraction $c^{(2)} = c$, while the matrix occupies a region with volume fraction $c^{(1)} = 1-c$. For simplicity, only deviatoric plane strain loading transverse to the fibers is considered, so that the problem becomes two-dimensional, and the hydrostatic component of the macroscopic stress vanishes. We assume further power-law phase potentials, so that the microscopic and macroscopic strain potentials can be written in the form

$$w^{(r)}(\boldsymbol{\varepsilon}) = \frac{\sigma_0^{(r)}\varepsilon_0}{m+1}\left(\frac{\varepsilon_e}{\varepsilon_0}\right)^{m+1}, \quad \text{and} \quad \widetilde{W}(\overline{\boldsymbol{\sigma}}) = \frac{\widetilde{\sigma}_0\varepsilon_0}{m+1}\left(\frac{\bar{\varepsilon}_e}{\varepsilon_0}\right)^{m+1} \tag{4.5.1}$$

and the stress potentials written as

$$u^{(r)}(\boldsymbol{\sigma}) = \frac{\sigma_0^{(r)}}{n+1}\left(\frac{\sigma_e}{\sigma_0^{(r)}}\right)^{n+1}, \quad \text{and} \quad \widetilde{U}(\overline{\boldsymbol{\sigma}}) = \frac{\widetilde{\sigma}_0}{n+1}\left(\frac{\bar{\sigma}_e}{\widetilde{\sigma}_0}\right)^{n+1}, \tag{4.5.2}$$

where $n = 1/m$ (with $0 \leqslant n < \infty$) is the nonlinearity exponent, and $\sigma_0^{(r)}$ (r=1,2) and $\widetilde{\sigma}_0$ are the phase and macroscopic flow stresses, respectively.

To implement the new method, we take the LCC to be characterized by a viscosity tensor of the form

$$\mathbb{L}^{(r)} = 2\lambda^{(r)}\mathbb{E} + 2\mu^{(r)}\mathbb{F}, \tag{4.5.3}$$

where $\mathbb{E}$ and $\mathbb{F}$ are the loading-dependent projection operators (Ponte Castañeda, 1996). We recall that

$$\mathbb{E} = \frac{2}{3\overline{\varepsilon}_e^2}\bar{\mathbf{e}} \otimes \bar{\mathbf{e}}, \quad \mathbb{F} = \mathbb{K} - \mathbb{E}, \tag{4.5.4}$$

where $\bar{\mathbf{e}}$ is the deviatoric part of $\overline{\boldsymbol{\varepsilon}}$, and $\mathbb{K}$ is the standard 4^{th}- order, isotropic, shear projection tensor.

Use will be made of the Willis estimates (Ponte Castañeda and Willis, 1995) to describe the effective behavior of the LCC. In this context, it should be noted that the shape of the (transversely isotropic) fiber distribution and fiber cross-section are both circular, and as a consequence, the Willis estimates will take the precisely the same form as the Hashin-Shtrikman-Willis bounds (Willis, 1977) for two-phase composites. It should be emphasized that only first- and second-order statistics of the microstructure are used in these types of estimates. The first-order statistics are characterized by the volume fraction of the phases, while the second-order statistics are accounted for by a two-point probability function (which is assumed to be known and is used implicitly in the estimates). The implementation of these estimates for general two-phase linear composites is described in Section 4.8, where explicit expressions are also given for the macroscopic constitutive relation and field statistics (of the LCC).

Due to isotropy of the phases, and the statistical isotropy of the distribution of inclusions in the transverse plane, it is reasonable to assume that the average strains in the phases are aligned with the macroscopic applied strain, i.e. $\bar{\mathbf{e}}^{(r)} = \frac{\overline{\varepsilon}_e^{(r)}}{\overline{\varepsilon}_e}\bar{\mathbf{e}}$. Under

this assumption, we note that

$$\bar{\varepsilon}_e = (1-c)\bar{\varepsilon}_e^{(1)} + c\bar{\varepsilon}_e^{(2)}. \tag{4.5.5}$$

The eigenstresses are taken to be of the form

$$\boldsymbol{\tau}^{(r)} = \frac{1}{2}\left(\boldsymbol{\tau}_{(1)}^{(r)} + \boldsymbol{\tau}_{(2)}^{(r)}\right) \tag{4.5.6}$$

where symmetry requires that $\beta_{(p)}^{(r)} = \frac{1}{2}$ for $p = 1, 2$ and $r = 1, 2$. For simplicity, we also will take $\alpha^{(r)} = \frac{1}{2}$ for $r = 1, 2$ in what follows.

It is next useful to take up the notation in Ponte Castañeda (2016) by introducing 'parallel' and 'perpendicular' components (relative to the loading direction) of $\check{\boldsymbol{\varepsilon}}_{(p)}^{(r)}, \widehat{\boldsymbol{\varepsilon}}_{(p)}^{(r)}$ and $\boldsymbol{\tau}_{(p)}^{(r)}$. For example, we take $(\widehat{\varepsilon}_{(p)}^{(r)})_{\parallel} = \left(\frac{2}{3}\widehat{\boldsymbol{\varepsilon}}_{(p)}^{(r)} \cdot \mathbb{E}\widehat{\boldsymbol{\varepsilon}}_{(p)}^{(r)}\right)^{1/2}$ and $(\widehat{\varepsilon}_{(p)}^{(r)})_{\perp} = \left(\frac{2}{3}\widehat{\boldsymbol{\varepsilon}}_{(p)}^{(r)} \cdot \mathbb{F}\widehat{\boldsymbol{\varepsilon}}_{(p)}^{(r)}\right)^{1/2}$, so that $(\widehat{\varepsilon}_e)_{(p)}^{(r)} = \sqrt{(\widehat{\varepsilon}_{(p)}^{(r)})_{\parallel}^2 + (\widehat{\varepsilon}_{(p)}^{(r)})_{\perp}^2}$. We make use of the symmetry of the problem by setting $(\widehat{\varepsilon}_{(1)}^{(r)})_{\parallel} = (\widehat{\varepsilon}_{(2)}^{(r)})_{\parallel} = \widehat{\varepsilon}_{\parallel}^{(r)}$, $(\widehat{\varepsilon}_{(1)}^{(r)})_{\perp} = -(\widehat{\varepsilon}_{(2)}^{(r)})_{\perp} = \widehat{\varepsilon}_{\perp}^{(r)}, (\check{\varepsilon}_{(1)}^{(r)})_{\parallel} = (\check{\varepsilon}_{(2)}^{(r)})_{\parallel} = \check{\varepsilon}_{\parallel}^{(r)}$, and $(\check{\varepsilon}_{(1)}^{(r)})_{\perp} = -(\check{\varepsilon}_{(2)}^{(r)})_{\perp} = \check{\varepsilon}_{\perp}^{(r)}$.

With these symmetries, we find that the components of $\boldsymbol{\tau}_{(p)}^{(r)}$ must satisfy $(\tau_{(1)}^{(r)})_{\parallel} = (\tau_{(2)}^{(r)})_{\parallel} \equiv \tau_{\parallel}^{(r)}$ and $(\tau_{(1)}^{(r)})_{\perp} = -(\tau_{(2)}^{(r)})_{\perp} \equiv \tau_{\perp}^{(r)}$, where, from Eq. (4.3.9),

$$\frac{2\sigma_0^{(r)}}{3\varepsilon_0^m}(\widehat{\varepsilon}_e^{(r)})^{m-1}\widehat{\varepsilon}_{\parallel}^{(r)} - 2\lambda^{(r)}\widehat{\varepsilon}_{\parallel}^{(r)} = \tau_{\parallel}^{(r)} = \frac{2\sigma_0^{(r)}}{3\varepsilon_0^m}(\check{\varepsilon}_e^{(r)})^{m-1}\check{\varepsilon}_{\parallel}^{(r)} - 2\lambda^{(r)}\check{\varepsilon}_{\parallel}^{(r)} \tag{4.5.7}$$

$$\frac{2\sigma_0^{(r)}}{3\varepsilon_0^m}(\widehat{\varepsilon}_e^{(r)})^{m-1}\widehat{\varepsilon}_{\perp}^{(r)} - 2\mu^{(r)}\widehat{\varepsilon}_{\perp}^{(r)} = \tau_{\perp}^{(r)} = \frac{2\sigma_0^{(r)}}{3\varepsilon_0^m}(\check{\varepsilon}_e^{(r)})^{m-1}\check{\varepsilon}_{\perp}^{(r)} - 2\mu^{(r)}\check{\varepsilon}_{\perp}^{(r)}. \tag{4.5.8}$$

Applying Eq. (4.3.33) yields

$$\frac{2}{3}\mathbb{C}_{\boldsymbol{\varepsilon}}^{(r)} \cdot \mathbb{E} = \left(\frac{\widehat{\varepsilon}_{\parallel}^{(r)} - \check{\varepsilon}_{\parallel}^{(r)}}{2}\right)^2, \quad \frac{2}{3}\mathbb{C}_{\boldsymbol{\varepsilon}}^{(r)} \cdot \mathbb{F} = -\check{\varepsilon}_{\perp}^{(r)}\widehat{\varepsilon}_{\perp}^{(r)}, \tag{4.5.9}$$

while use of Eqs. (4.3.30) and (4.3.31) gives

$$\bar{\varepsilon}_e^{(r)} = \frac{1}{2}\left(\check{\varepsilon}_{\parallel}^{(r)} + \hat{\varepsilon}_{\parallel}^{(r)}\right), \quad 0 = \frac{1}{2}\left(\check{\varepsilon}_{\perp}^{(r)} + \hat{\varepsilon}_{\perp}^{(r)}\right) + \frac{\tau_{\perp}^{(r)}}{4\mu^{(r)}}. \tag{4.5.10}$$

Now, an important feature of the Willis estimates is that there are no field fluctuations in the inclusion phase, so that $\mathbb{C}_{\boldsymbol{\varepsilon}}^{(2)} = \mathbb{O}$. Therefore $\hat{\varepsilon}_{(p)}^{(2)}$ and $\check{\varepsilon}_{(p)}^{(2)}$ are determined by means of the results in Proposition 1, i.e. $\hat{\boldsymbol{\varepsilon}}_{(p)}^{(2)} = \check{\boldsymbol{\varepsilon}}_{(p)}^{(2)} = \overline{\boldsymbol{\varepsilon}}^{(2)}$, so that $\hat{\varepsilon}_{\parallel}^{(2)} = \check{\varepsilon}_{\parallel}^{(2)} = \bar{\varepsilon}_e^{(2)}$, $\hat{\varepsilon}_{\perp}^{(2)} = \check{\varepsilon}_{\perp}^{(2)} = 0$, and $\tau_{\parallel}^{(2)} = \tau_{\perp}^{(2)} = 0$. Thus, we find that the viscosity tensor in the inclusion simplifies to $\mathbb{L}^{(2)} = 2\lambda^{(2)}\mathbb{K}$, where

$$2\lambda^{(2)} = 2\mu^{(2)} = \frac{2\sigma_0^{(2)}}{3(\varepsilon_0)^m}\left(\bar{\varepsilon}_e^{(2)}\right)^{m-1} = \frac{2\sigma_0^{(2)}}{3(\varepsilon_0)^m}\left(\frac{\bar{\varepsilon}_e - (1-c)\bar{\varepsilon}_e^{(1)}}{c}\right)^{m-1}. \tag{4.5.11}$$

With the use of Eqs. (4.5.7)-(4.5.11), together with expression (4.8.23) (from Section 4.8.1) for the covariance of the fields in the matrix , we can solve for $\hat{\varepsilon}_{\parallel}^{(1)}$, $\check{\varepsilon}_{\parallel}^{(1)}$, $\hat{\varepsilon}_{\perp}^{(1)}$ and $\check{\varepsilon}_{\perp}^{(1)}$ in terms of k and $\bar{\varepsilon}_e^{(1)}$ to find that

$$\begin{aligned}
\hat{\varepsilon}_{\parallel}^{(1)} &= \bar{\varepsilon}_e^{(1)} - \left(\bar{\varepsilon}_e^{(1)} - \bar{\varepsilon}_e\right)\frac{k^{-1/4}}{\sqrt{2c}}, \\
\check{\varepsilon}_{\parallel}^{(1)} &= \bar{\varepsilon}_e^{(1)} + \left(\bar{\varepsilon}_e^{(1)} - \bar{\varepsilon}_e\right)\frac{k^{-1/4}}{\sqrt{2c}}, \\
\hat{\varepsilon}_{\perp}^{(1)} &= -\left(\bar{\varepsilon}_e^{(1)} - \bar{\varepsilon}_e\right)\frac{k^{1/4}}{\sqrt{2c}}\left(\frac{\sqrt{\Delta} + \left(\bar{\varepsilon}_e^{(1)} - \bar{\varepsilon}_e\right)k^{3/4}}{\sqrt{2c}\bar{\varepsilon}_e^{(1)} + \left(\bar{\varepsilon}_e^{(1)} - \bar{\varepsilon}_e\right)k^{-1/4}}\right)^{1/2}, \\
\check{\varepsilon}_{\perp}^{(1)} &= \left(\bar{\varepsilon}_e^{(1)} - \bar{\varepsilon}_e\right)\frac{k^{1/4}}{\sqrt{2c}}\left(\frac{\sqrt{\Delta} - \left(\bar{\varepsilon}_e^{(1)} - \bar{\varepsilon}_e\right)k^{3/4}}{\sqrt{2c}\bar{\varepsilon}_e^{(1)} - \left(\bar{\varepsilon}_e^{(1)} - \bar{\varepsilon}_e\right)k^{-1/4}}\right)^{1/2},
\end{aligned} \tag{4.5.12}$$

where $\Delta = \left(\bar{\varepsilon}_e^{(1)} - \bar{\varepsilon}_e\right)^2\left(k^{3/2} - k^{-1/2}\right) + 2c\left(\bar{\varepsilon}_e^{(1)}\right)^2$. At this point, we are left with two unknowns: the anisotropy ratio $k = \frac{\lambda^{(1)}}{\mu^{(1)}}$ and the average von Mises equivalent strain in the matrix, $\bar{\varepsilon}_e^{(1)}$. These unknowns can be obtained from two nonlinear algebraic

equations. The first, which reads

$$\frac{\sigma_0^{(2)}}{\sigma_0^{(1)}}\left(\frac{1-(1-c)\bar{\varepsilon}_e^{(1)}/\bar{\varepsilon}_e}{c}\right)^m = \frac{1}{2}\left[\left(\widehat{\varepsilon}_e^{(1)}\right)^{m-1}\widehat{\varepsilon}_{\parallel}^{(1)}\left(1-\sqrt{\frac{2}{c}}k^{-1/4}\right)\right.$$
$$\left.+\left(\breve{\varepsilon}_e^{(1)}\right)^{m-1}\breve{\varepsilon}_{\parallel}^{(1)}\left(1+\sqrt{\frac{2}{c}}k^{-1/4}\right)\right], \quad (4.5.13)$$

is derived from the LCC estimate (4.8.22) (from Section 4.8.1) for $\bar{\varepsilon}_e^{(1)}$. The second comes from combining Eqs. (4.5.7) and (4.5.8):

$$\frac{\left(\widehat{\varepsilon}_e^{(1)}\right)^{m-1}\widehat{\varepsilon}_{\parallel}^{(1)}-\left(\breve{\varepsilon}_e^{(1)}\right)^{m-1}\breve{\varepsilon}_{\parallel}^{(1)}}{\left(\widehat{\varepsilon}_e^{(1)}\right)^{m-1}\widehat{\varepsilon}_{\perp}^{(1)}-\left(\breve{\varepsilon}_e^{(1)}\right)^{m-1}\breve{\varepsilon}_{\perp}^{(1)}} = k\frac{\widehat{\varepsilon}_{\parallel}^{(1)}-\breve{\varepsilon}_{\parallel}^{(1)}}{\widehat{\varepsilon}_{\perp}^{(1)}-\breve{\varepsilon}_{\perp}^{(1)}}. \quad (4.5.14)$$

Once k and $\bar{\varepsilon}_e^{(1)}$ are determined, we can then calculate the effective flow stress from Eq. (4.4.1). The result as a function of the nonlinearity $n = 1/m$, fiber concentration c, and heterogeneity contrast $\sigma_0^{(2)}/\sigma_0^{(1)}$, is given by

$$\frac{\widetilde{\sigma}_0}{\sigma_0^{(1)}} = \frac{1-c}{2}\left[\left(\frac{\widehat{\varepsilon}_e^{(1)}}{\bar{\varepsilon}_e}\right)^{m+1}+\left(\frac{\widehat{\varepsilon}_e^{(2)}}{\bar{\varepsilon}_e}\right)^{m+1}\right]+c\frac{\sigma_0^{(2)}}{\sigma_0^{(1)}}\left(\frac{1-(1-c)\bar{\varepsilon}_e^{(1)}/\bar{\varepsilon}_e}{c}\right)^{m+1}. \quad (4.5.15)$$

Alternatively, by means of the dual formulation for the stress potential, a second, equivalent equation is obtained for the effective flow stress:

$$\frac{\widetilde{\sigma}_0}{\sigma_0^{(1)}} = \left[\frac{1-c}{2}\left[\left(\frac{\widehat{\sigma}_e^{(1)}}{\bar{\sigma}_e}\right)^{n+1}+\left(\frac{\widehat{\sigma}_e^{(2)}}{\bar{\sigma}_e}\right)^{n+1}\right]+c\frac{\sigma_0^{(2)}}{\sigma_0^{(1)}}\left(\frac{\sigma_0^{(1)}}{\sigma_0^{(2)}}\frac{1-(1-c)\bar{\sigma}_e^{(1)}/\bar{\sigma}_e}{c}\right)^{n+1}\right]^{-\frac{1}{n}} \quad (4.5.16)$$

where a separate set of nonlinear equations must be solved for k and $\bar{\sigma}_e^{(1)}$, while $\widehat{\sigma}_{\parallel}^{(r)}$, $\breve{\sigma}_{\parallel}^{(r)}$, $\widehat{\sigma}_{\perp}^{(r)}$, $\breve{\sigma}_{\perp}^{(r)}(r=1,2)$ can similarly be written as functions of the unknowns.

Both Eqs. (4.5.15) and (4.5.16) generate the same results, and as a consequence of duality, the stress variables can be related to the strain variables. However, one

must take care in choosing the appropriate sign when solving for the appropriate dual variables. The sign convention is chosen so that duality relations (4.4.15) hold, which, when applied in the current setting, read

$$\frac{\widehat{\varepsilon}_{\parallel}^{(r)}}{\widehat{\varepsilon}_{e}^{(r)}} = \frac{\widehat{\sigma}_{\parallel}^{(r)}}{\widehat{\sigma}_{e}^{(r)}}, \quad \frac{\breve{\varepsilon}_{\parallel}^{(r)}}{\breve{\varepsilon}_{e}^{(r)}} = \frac{\breve{\sigma}_{\parallel}^{(r)}}{\breve{\sigma}_{e}^{(r)}}, \quad \frac{\widehat{\varepsilon}_{\perp}^{(r)}}{\widehat{\varepsilon}_{e}^{(r)}} = \frac{\widehat{\sigma}_{\perp}^{(r)}}{\widehat{\sigma}_{e}^{(r)}}, \quad \frac{\breve{\varepsilon}_{\perp}^{(r)}}{\breve{\varepsilon}_{e}^{(r)}} = \frac{\breve{\sigma}_{\perp}^{(r)}}{\breve{\sigma}_{e}^{(r)}}. \tag{4.5.17}$$

We close this section by discussing the weight factors, $\beta_{(p)}^{(r)}$ and $\alpha^{(r)}$, which appear in this method. As mentioned above, symmetry dictates the value of $\beta_{(p)}^{(r)}$. In our two-dimensional example, it was found that the critical points of the functions $\Delta w^{(r)}$ came in pairs. This therefore necessitated the use of two eigenstresses $\tau_{(1)}^{(r)}$ and $\tau_{(2)}^{(r)}$, to account for the 4 critical points which are located symmetrically about $\overline{\boldsymbol{\varepsilon}}^{(r)}$, for $r = 1, 2$. It is necessary to give these pairs of points equal weight, and so the value of $\beta_{(p)}^{(r)} = \frac{1}{2}$ was chosen. As for the choice of $\alpha^{(r)} = \frac{1}{2}$, this decision was made for the sake of simplicity. With this value, we were able to find explicit equations for the components of $\widehat{\boldsymbol{\varepsilon}}_{(p)}^{(r)}$ and $\breve{\boldsymbol{\varepsilon}}_{(p)}^{(r)}$. As will be discussed later, while there is no condition yet available to determine the 'optimal' value of $\alpha^{(r)}$, it is possible that different values of $\alpha^{(r)}$ could produce more accurate results for different specific microstructures (with different higher-point statistics).

4.6 Results and Discussion

The results of the previous section will now be presented for specific values of the material and microstructural parameters and compared to results obtained in the literature for special types of microstructures, including infinite-rank sequential laminates (LAM) (Idiart, 2008), as well as composite cylinder assemblages (CCA) (Hashin and Rosen, 1964). It should be mentioned that, in this particular application, the FOSO and LAM estimates agree in the linear limit ($m = 1$), since the sequentially laminated microstructures saturate the Hashin-Shtrikman bounds and

therefore the Willis estimate. On the contrary, for nonlinear cases, the FOSO is not expected to agree with the LAM estimates. This is because the LCC that would be required to recover the LAM estimate would involve an infinite-rank sequentially layered microstructure with different viscosities at each layering operation (cf. Eq. (4.3.28)), while in this work we will restrict our attention only to two-phase LCCs. As a consequence, the comparisons between the FOSO and LAM estimates will allow us to gauge the approximations that are introduced by taking the phases of the LCC to be constant (at least for this somewhat special type of microstructure).

On the other hand, the results for the CCA microstructures were obtained by means of FFT full-field simulations (Idiart et al., 2006). For certain types of loading conditions, such as anti-plane strain, it is known that, in the linear case, the CCA model gives exact results that saturate the Hashin-Shtrikman bounds and therefore the Willis estimates. However, for plane strain loading, the CCA is only an approximation for the Willis estimates. Moreover, the CCA model requires an infinite number of sizes for the 'composite cylinders' to fill the entire domain. However, the FFT calculations (Idiart et al., 2006) were carried out for an approximation of the CCA making use of only three different composite-cylinder sizes. It is also for this reason that the FFT results can only be regarded as approximations of the exact CCA results, and therefore do not agree exactly with the FOSO estimates even in the linear case. In addition, due to the need of taking ensemble averages of calculations for several different realizations of the microstructure, as well as the fact that each realization used a different total number of inclusions, the fiber concentration in each calculation was never exactly the same (see Idiart et al. (2006)). Therefore, when presenting results, the average fiber concentration, $c = 0.20626$ was used; in order to compare with the FFT results, this fiber concentration has been used in the FOSO calculations as well as the LAM calculations (Idiart and Ponte Castañeda, 2007b).

In most instances, we will also include the 'variational' bounds of the Hashin-Shtrikman (HS) type (Ponte Castañeda, 1991). The variational method, upon which

the current method builds, makes use of an LCC in order to estimate the effective behavior of nonlinear composites. However, unlike the current method, the 'variational' method makes use of an LCC with isotropic phases, with properties determined by suitable extremal conditions. While the choice of isotropy of the linear phase potentials is much more restrictive, the 'variational' approach provides an upper bound for the nonlinear estimates. In addition, we also include some results obtained by means of the 'tangent second-order' (TSO) method, in order to illustrate how the new FOSO method improves on earlier 'second-order' methods. The TSO method was itself introduced (Ponte Castañeda, 1996) in an attempt to improve upon the earlier 'variational' method. (Recall that the 'variational" bounds are only exact to first order in the contrast.) However, the lack of stationarity with respect to the modulus tensor in the TSO method leads to difficulties in computing the field statistics of the LCC, and also introduces a duality gap. For this reason, the estimates obtained by applying the TSO method to the stress potential $u(\boldsymbol{\sigma})$ (TSO(U)) are different from those obtained by applying the TSO method to the strain potential $w(\boldsymbol{\varepsilon})$ (TSO(W)). While the results of TSO(U) and TSO(W) for the effective behavior agree in the weakly nonlinear case, this agreement deteriorates in the strongly nonlinear regime. This is due to the fact that the TSO method does not fully account for the field fluctuations, which in general tend to become progressively more significant with increasing nonlinearity.

We also include the Voigt-Reuss bounds for the effective behavior of the composite (see Milton (2002b)). The Voigt bound is known to be an upper bound on the effective behavior, while the Reuss bound is known to be a lower bound on the effective behavior. In our application, we find that

$$\left((1-c)(\sigma_0^{(1)})^{-\frac{1}{m}}+c(\sigma_0^{(2)})^{-\frac{1}{m}}\right)^{-m}=\sigma_0^R\leqslant\widetilde{\sigma}_0\leqslant\sigma_0^V=(1-c)\sigma_0^{(1)}+c\sigma_0^{(2)}. \quad (4.6.1)$$

The results of this section are presented as functions of the nonlinearity $m=1/n$, the fiber concentration c, and the heterogeneity contrast $\sigma_0^{(2)}/\sigma_0^{(1)}$. The contrast can

be chosen for any value $0 \leqslant \sigma_0^{(2)}/\sigma_0^{(1)} \leqslant \infty$, where $\sigma_0^{(2)}/\sigma_0^{(1)} = 0$ corresponds to void inclusions (porous composites), and $\sigma_0^{(2)}/\sigma_0^{(1)} = \infty$ corresponds to rigid particles. We say that the composite is fiber-weakened when $\sigma_0^{(2)}/\sigma_0^{(1)} < 1$, while we call a composite fiber-strengthened, or fiber-reinforced, when $\sigma_0^{(2)}/\sigma_0^{(1)} \geqslant 1$.

4.6.1 Fiber-Weakened Composites

In order to be able to compare with numerical results available from the literature, all the results in this section will be for a heterogeneity contrast of $\sigma_0^{(2)}/\sigma_0^{(1)} = 0.2$.

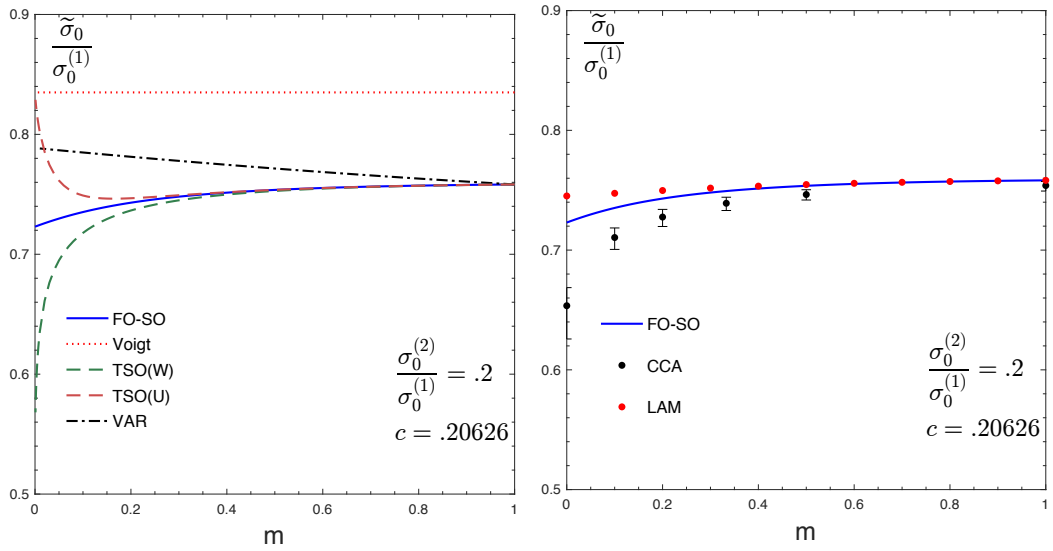

Figure 4.2: Effective flow stress $\widetilde{\sigma}_0$ normalized by the flow stress of the matrix $\sigma_0^{(1)}$ for fiber concentration $c = .20626$, and contrast $\sigma_0^{(2)}/\sigma_0^{(1)} = .2$, as a function of the nonlinearity m. (a): Comparisons of the new second-order (FO-SO) estimates with the Voigt upper bound, 'tangent second-order' (TSO) estimates, and 'variational' (VAR) bounds of the Hashin-Shtrikman type. (b): Comparison between new second-order (FO-SO) estimates, Composite Cylinder Assemblage (CCA) results, and the infinite-rank laminates (LAM).

In Figure 4.2a the various results for the normalized effective flow stress $\widetilde{\sigma}_0/\sigma_0^{(1)}$ are plotted as functions of m. The FOSO estimates obey both the Voigt and variational

(VAR) upper bounds of the HS type. Moreover, the FOSO results agree quite well with both TSO results for weak to moderate nonlinearity, when the field fluctuations are not expected to be significant. In the highly nonlinear range ($0 \leqslant m \leqslant 0.2$), however, this agreement deteriorates, with the TSO(W) and TSO(U) results diverging from each other, but with the FOSO remaining roughly in between the two. These observations are consistent with the existence of a duality gap for the TSO estimates, but no duality gap for the FOSO estimates.

In Figure 4.2b, we plot the FOSO results and compare them with the CCA results, as well as the LAM results. All results are in close agreement for weak nonlinearities. While the LAM and FOSO results agree exactly in the linear case ($m = 1$), we see that the CCA results give slightly lower predictions. This is due in part to the fact that, as mentioned earlier, the CCA results are merely approximations, having used only a finite number of sizes of inclusions. In any case, the FOSO results always tend to remain above the CCA results and below the LAM results. This becomes especially apparent in the high-nonlinearity regime, where all estimates tend to show a reduction in the effective flow stress with decreasing m.

Estimates for phase averages and standard deviations of the stress and strain fields are given in Figure 4.3. As we see in Figure 4.3a, the FOSO estimates for the average stresses in the phases match very closely with all other results. In fact, it can be shown that in the porous limit, the FOSO estimate recovers the exact result ($\bar{\sigma}_e^{(1)}/\bar{\sigma}_e = 1/(1-c)$), and therefore it is not surprising that we have such good agreement. We see also that all results seem to improve on the VAR results. Figure 4.3b shows the standard deviation of parallel and perpendicular components of the stress field in the matrix phase, $\mathrm{SD}^{(1)}(\sigma_\parallel)$ and $\mathrm{SD}^{(1)}(\sigma_\perp)$, respectively. (These quantities are obtained by replacing σ_e by $\sigma_\parallel$ and $\sigma_\perp$, respectively, in expression $(4.2.13)_1$.) We first note that the VAR results predict isotropic fluctuations for all nonlinearities. This is due to the fact that the VAR method makes use of an isotropic LCC. In fact, in this plane strain case, all results predict isotropic fluctuations in

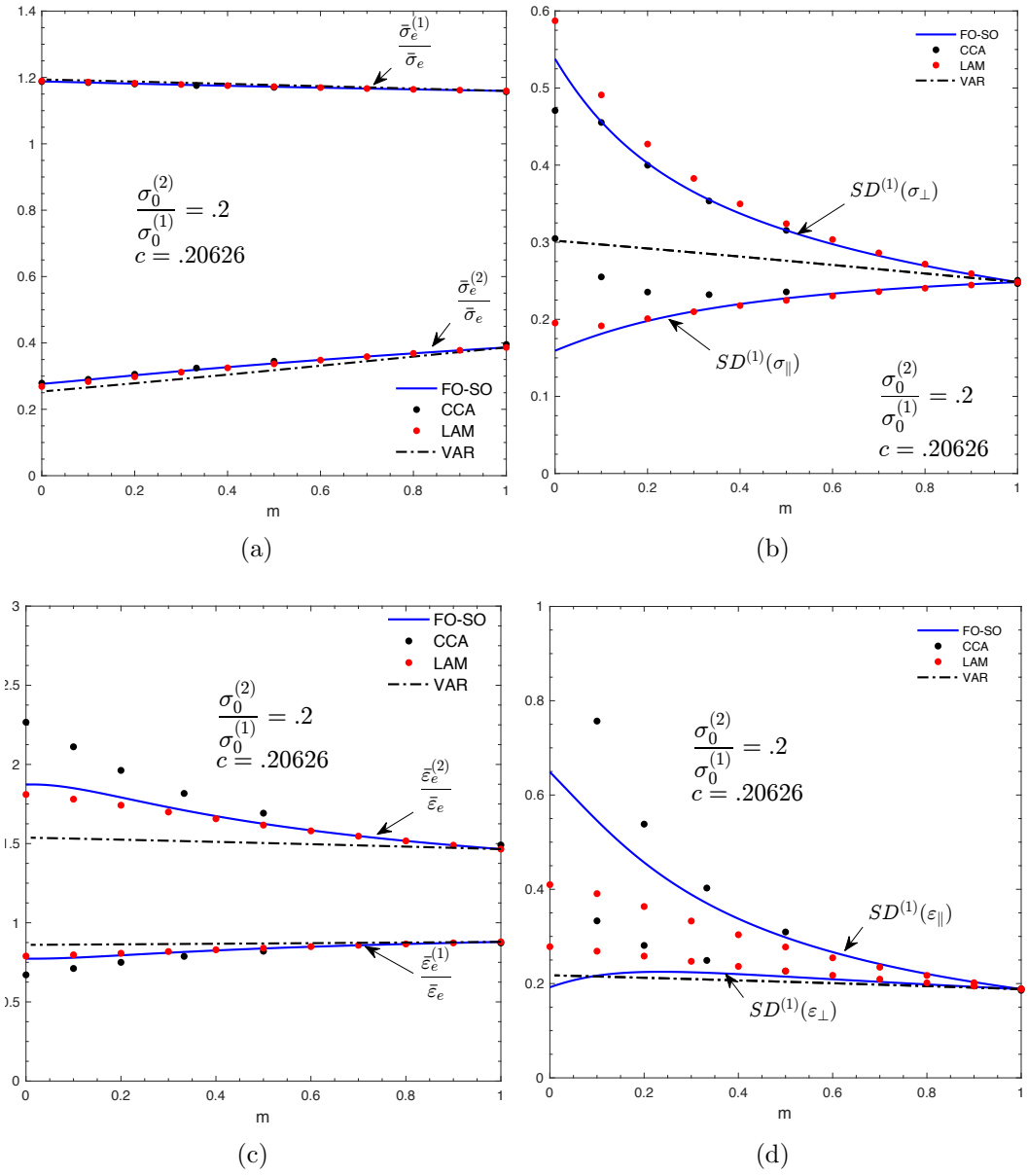

Figure 4.3: Statistics of the stress and strain fields for the case of fiber weakened composites. (a): The equivalent average stress of the matrix $\bar{\sigma}_e^{(1)}$ and the fibers $\bar{\sigma}_e^{(2)}$. (b): The standard deviation of the 'parallel' and 'perpendicular' components of the stress field in the matrix $\mathrm{SD}^{(1)}(\sigma_\parallel)$ and $\mathrm{SD}^{(1)}(\sigma_\perp)$. All results are normalized by $\bar{\sigma}_e$. (c): The equivalent average stress of the matrix $\bar{\varepsilon}_e^{(1)}$ and the fibers $\bar{\varepsilon}_e^{(2)}$. (d): The standard deviation of the 'parallel' and 'perpendicular' components of the stress field in the matrix.

the linear limit. Upon entering the nonlinear regime, it can be seen that the FOSO, CCA, and LAM methods give different predictions for the parallel and perpendicular components of the stress fluctuations, which become more anisotropic as m decreases. For nonlinearities as low as $m = 0.2$, we see that all results for the parallel and perpendicular stress fluctuations are in fairly close agreement. However, for stronger nonlinearities, differences between the methods become more apparent, especially for the parallel components. In fact, for $m \leqslant 0.5$, while the FOSO results predict a monotonically decreasing behavior for the parallel components, the CCA results indicate to the contrary that the fluctuations parallel to the applied field tend to reach a minimum value, and then start to increase again as $m \to 0$. The LAM results also predict this type of behavior, but the trend is less significant.

In Figure 4.3c, we have plotted the average equivalent strains in the matrix and fibers. As with the average equivalent stress results, the FOSO, CCA, and LAM all agree in the linear cases. As the nonlinearity increases, and m gets smaller, all the results predict an increase (decrease) in the average equivalent strain in the inclusions (matrix). In Figure 4.3d, we see that, consistent with CCA results, the FOSO estimates predict a significant rise in the parallel (to the applied macroscopic field) fluctuations of the strain fields in the matrix as m tends to zero (i.e., in the ideally plastic limit). This prediction, along with those regarding the average strains, are consistent with the notion of strain localization. As already discussed in Idiart et al. (2006), in the limit as m goes to 0, the strain will tend to seek out the softer fibers by localizing the deformation in the matrix along bands that tend to be aligned with the applied field. Therefore, within the matrix, the strain tends to remain parallel to the applied field, with smaller perpendicular fluctuations present. Thus, the FOSO results seem to capture this strongly nonlinear behavior, consistent with the CCA observations.

4.6.2 Fiber-Reinforced Composites

Again, in order to be able to compare with numerical results available from the literature, all the results in this section will be for a heterogeneity contrast of $\sigma_0^{(2)}/\sigma_0^{(1)} = 5$. The results for the effective flow stress, normalized by $\sigma_0^{(1)}$, are plotted

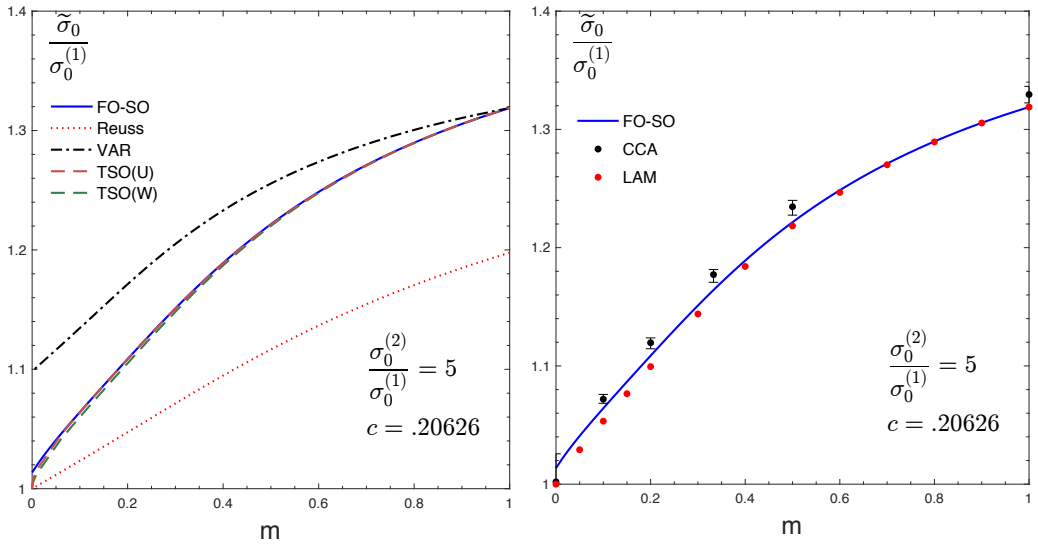

Figure 4.4: Effective flow stress $\widetilde{\sigma}_0$ normalized by flow stress of the matrix $\sigma_0^{(1)}$ for fiber concentration $c = .20626$, and contrast $\sigma_0^{(2)}/\sigma_0^{(1)} = 5$, as a function of the nonlinearity m. (a): Comparisons of the new second-order (FO-SO) estimates with the Reuss lower bound bound, 'variational' (VAR) estimates of the Willis type, and 'tangent second-order' (TSO) estimates. (b): Comparison of the new second-order (FO-SO) estimates with the Composite Cylinder Assemblage (CCA) results, and the infinite-rank laminates (LAM).

in Figure 4.4a. The FOSO results satisfy the Reuss lower bound, and the variational upper bound, and match closely with the TSO(U) and TSO(W) estimates, which exhibit a finite, but fairly small duality gap in this case. Figure 4.4b shows the FOSO results plotted against the CCA and LAM results. Again, we find that the FOSO estimates agree with the LAM results in the linear limit ($m = 1$), which is consistent with the fact that the two estimates reduce to the corresponding Hashin-Shtrikman

estimate in this limit. On the other hand, the CCA results are found to be a bit higher than the HS estimate in the linear case, which again is due to the fact that these results are for approximations of the CCA microstructures. In addition, we see that the FOSO results remain in between the CCA and LAM results, with one exception: the ideally plastic limit. When $m \to 0$, the FOSO method predicts that in fact strengthening in the matrix occurs, that is $\widetilde{\sigma}_0 > \sigma_0^{(1)}$. This behavior has not been captured before by any second-order method, but is consistent with the notion of shear banding. One could imagine that for a low fiber concentration, it would be possible for a straight shear band to form in the softer matrix phase, avoiding any of the more rigid fibers. However, for the fiber concentration of about 20% considered here, it seems unlikely that such a flat plane would exist. Instead, the shear band would be expected to curve around the strong fibers, leading to an overall behavior for the composite that will be stiffer than the matrix. In other words, a finite enhancement of the effective flow stress should be produced by a relatively large volume fraction of rigid fibers. This is consistent with the CCA results, but not with the more idealized LAM model, which, by construction, does allow for such plane bands. In turn, this again shows that, in the highly nonlinear limit, the effective behavior becomes more sensitive to the specific microstructures—and microstructures with the same first- and second-order statistics (e.g., the LAM and CCA) may exhibit effective behaviors that are qualitatively different (as a consequence of the difference in the microstructures beyond the two-point statistics).

Figure 4.5a shows the average equivalent stress plotted as a function of the nonlinearity. Note that, unlike in the fiber-weakened case, the stress in the inclusions is larger than the stress in the matrix. In comparison with the effective behavior, the FOSO results again tend to remain in-between the LAM and CCA results, except in the ideally plastic limit. Figure 4.5b depicts the stress field fluctuations as a function of m. It can be seen that, while the stress fluctuations are isotropic in the linear case, they tend to become anisotropic as the nonlinearity increases—with the CCA and

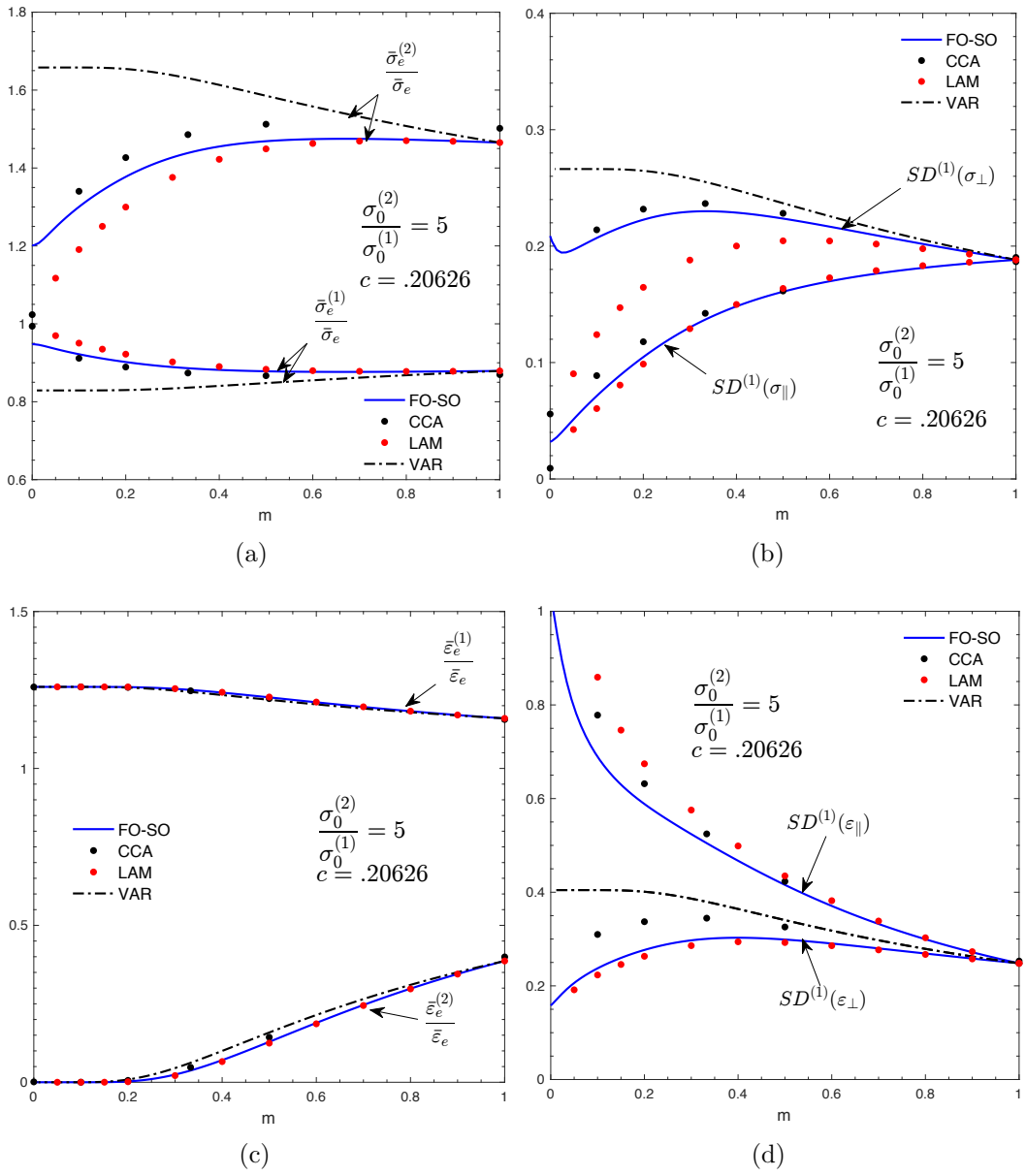

Figure 4.5: Statistics of the stress and strain fields for the case of fiber weakened composites. (a): The equivalent average stress of the matrix $\bar{\sigma}_e^{(1)}$ and the fibers $\bar{\sigma}_e^{(2)}$. (b): The standard deviation of the 'parallel' and 'perpendicular' components of the stress field in the matrix. All results are normalized by $\bar{\sigma}_e$. (c): The equivalent average stress of the matrix $\bar{\varepsilon}_e^{(1)}$ and the fibers $\bar{\varepsilon}_e^{(2)}$. (d): The standard deviation of the 'parallel' and 'perpendicular' components of the stress field in the matrix.

FOSO generally becoming more strongly anisotropic than the LAM. However, the FOSO predications for both the parallel and perpendicular stress fluctuations tend to remain in between the corresponding CCA and LAM results, with the exception once again of the ideally plastic limit. In this limit, the CCA results show a dramatic reduction of the fluctuations in both the parallel and perpendicular directions, with the fluctuations in the parallel direction nearly vanishing. On the other hand, the FOSO and LAM results predict a less dramatic drop in the fluctuations parallel to the applied field as m goes to 0.

Figure 4.5c shows the average equivalent strain plotted as a function of the non-linearity. All methods are in very close agreement. Even at a finite contrast of 5, all methods predict that the fibers tend to behave as rigid inclusions, with the average strain field in the inclusion decreasing and eventually vanishing in the ideally plastic limit. Figure 4.5d shows the strain fluctuations in the matrix. While isotropic in the linear case, we see that all methods predict increasing anisotropy with decreasing m, with the fluctuations showing their largest anisotropy in the ideally plastic limit. As discussed above, strain localization into shear bands account for the increased anisotropy of the parallel and perpendicular components of the strain fields. In contrast with the fiber weakened case, the strain will now tend to localize in the softer matrix, avoiding the more rigid fibers. The flow will accommodate the random distribution of fibers by curving and bending around them. When such a maneuver is necessary, the perpendicular component of the strain comes into play, which is why we do not see a complete vanishing of the fluctuations in the perpendicular direction.

4.7 Concluding Remarks

The goal of this work was twofold: to introduce a more symmetric formulation of the new FOSO method, and to apply this formulation to a special class of two-phase composites in order to compare with other results. As we saw, when applying the earlier 'non-symmetric' FOSO method (Ponte Castañeda, 2016), there was a difference between starting with the strain- or stress-energy function. The new approach outlined here makes the choice of formulation inconsequential. By introducing a more symmetric choice of LCC potential, we can generate results that possess all the properties of the fully optimized method—and have an extra layer of duality in that one formulation is precisely dual to the other. Moreover, due in part to a more general use of the field fluctuations, we actually loosen the restrictions imposed by the corresponding stationary conditions, leading to more freedom in the selection of the stationary points.

For the application of the new (symmetric) FOSO method, we considered two-dimensional power-law composites with microstructures consisting of statistically isotropic distributions of circular inclusions in a matrix phase, and made use of the Willis estimates (Ponte Castañeda and Willis, 1995) to characterize the macroscopic response and field statistics of the appropriately chosen LCC. It is known that the Willis estimates agree with the Hashin-Shtrikman (HS) bounds in this case, and for that reason the FOSO estimates agree with the HS upper bound for the case of fiber-weakened composites, as well as with the corresponding HS lower bound for the case of fiber-reinforced composites, in the (trivial) linear limit as the nonlinearity $n = 1/m \to 1$. For more general values of the nonlinearity, the FOSO estimates were compared with the classical Voigt-Reuss bounds, as well as with the nonlinear bounds of the HS type (Ponte Castañeda, 1991), and were found to satisfy all the bounds. In addition, the FOSO estimates were also compared with (numerically) exact estimates for two special types of particulate microstructures, namely, infinite-rank laminates

(LAM) (Idiart, 2008) and composite cylinder assemblages (CCA) (Idiart et al., 2006), and it was found that the FOSO results generally fall somewhere between the LAM results and the CCA results.

It is interesting to remark that, in the linear case (and under plane-strain loading), while the LAM and the CCA correspond to quite different microstructures, they have very similar effective behaviors. In fact, under anti-plane strain, it can be shown that the estimates agree exactly and saturate the HS bounds (Milton, 2002b). However, as the results revealed, any agreement between the LAM and CCA methods for linear and weakly nonlinear composites deteriorates in the strongly nonlinear regime. This observation, coupled with the fact that the LAM and CCA results rely on the *same* first- and second-order statistics for their microstructures, suggests that not only do higher-order statistics play a role in determining the effective behavior of nonlinear composites, but this role becomes more important with increasing nonlinearity. The fact that the FOSO estimates lie more or less in between the two estimates is encouraging. However, in order to achieve more accurate results for highly nonlinear behavior, it seems that more information about the microstructure is needed. As the FOSO method can make use of any estimate for the LCC, one may try to use the Beran-Milton three-point estimates. This was not attempted here, in particular, because we are not aware of any numerical results for nonlinear composites with prescribed three-point statistics. We simply suggest this as a possible starting point for future research.

Finally, we turn to an issue that arises in the applications of the new second-order method. Recalling from Remark Remark 1 that while the 'exact' version of the estimate (4.3.28) is independent of the weight factors $\alpha^{(r)}$, the value of the discretized (approximate) version (4.3.25) used in applications is dependent on the $\alpha^{(r)}$. In this work, we have chosen the value of $\frac{1}{2}$ out of convenience, and found that this choice produces results which are in fairly good agreement with exact (or numerically exact) estimates for two different types of microstructures. However, the choice of the $\alpha^{(r)}$

merits further investigation. It is reasonable to think that different values of $\alpha^{(r)}$ could produce improved results for specific microstructures. While we have not been able to find a general scheme to select the 'optimal' values of $\alpha^{(r)}$ for a specific microstructure, it could be that, at the very least, empirical choices could be made for such values. In other words, it is conceivable that different values of $\alpha^{(r)}$ could be used to obtain better 'fits' with the LAM and CCA results. This is again something that will be pursued in future work [1].

In any case, regardless of the specific choice of the $\alpha^{(r)}$, the new FO-SO method produces estimates for the macroscopic behavior and field statistics that agree quite well with full-field simulations, at least from a qualitative point of view. Moreover, the method is able to capture the consequences of complex physical phenomena, such as strain localization and shear banding (see also Idiart (2008)). In future work, we hope to apply the method to other cases, specifically three-dimensional applications, to test the accuracy of the method in predicting behaviors consistent with available experimental and numerical observations. Finally, we conclude by mentioning that the above-mentioned 'exact' version of the FOSO method could also be exploited in the context of full-field numerical simulations for nonlinear composites with completely general types of microstructures. In particular, the FOSO approach making use of an appropriately discretized LCC could be used to attempt to accelerate other numerical schemes, such as FEM-based numerical methods.

[1] In Appendix A, it is found that $\alpha^{(r)}$ can be chosen so that the FOSO result recovers the exact result in the weakly nonlinear limit. The optimal value of $\alpha^{(r)}$ depends on the volume fraction, but is found to be close to .5

4.8 Appendix I: General estimates for two-phase linear composites with particulate microstructures

We consider a general two-phase composite made of two linear, isotropic phases with strain potentials of the form

$$w_L^{(r)}(\boldsymbol{\varepsilon}) = \frac{1}{2}\boldsymbol{\varepsilon}\cdot\mathbb{L}^{(r)}\boldsymbol{\varepsilon} + \boldsymbol{\tau}^{(r)}\cdot\boldsymbol{\varepsilon} + \frac{1}{4}\boldsymbol{\tau}^{(r)}\cdot\left(\mathbb{L}^{(r)}\right)^{-1}\boldsymbol{\tau}^{(r)}. \tag{4.8.1}$$

Making use of duality, we may also write the corresponding stress potential as

$$u_L^{(r)}(\boldsymbol{\sigma}) = \frac{1}{2}\boldsymbol{\sigma}\cdot\mathbb{M}^{(r)}\boldsymbol{\sigma} + \boldsymbol{\gamma}^{(r)}\cdot\boldsymbol{\sigma} + \frac{1}{4}\boldsymbol{\gamma}^{(r)}\cdot\left(\mathbb{M}^{(r)}\right)^{-1}\boldsymbol{\gamma}^{(r)}, \tag{4.8.2}$$

where $\mathbb{M}^{(r)} = \left(\mathbb{L}^{(r)}\right)^{-1}$ and $\boldsymbol{\gamma}^{(r)} = -\mathbb{M}^{(r)}\boldsymbol{\tau}^{(r)}$. Denoting $g^{(r)} = \frac{1}{2}\boldsymbol{\gamma}^{(r)}\cdot\left(\mathbb{M}^{(r)}\right)^{-1}\boldsymbol{\gamma}^{(r)}$ and $f^{(r)} = \frac{1}{2}\boldsymbol{\tau}^{(r)}\cdot\left(\mathbb{L}^{(r)}\right)^{-1}\boldsymbol{\tau}^{(r)}$, it is well known (see Laws (1973); Willis (1981)) that we may write

$$\widetilde{W}_L(\overline{\boldsymbol{\varepsilon}}) = \frac{1}{2}\overline{\boldsymbol{\varepsilon}}\cdot\widetilde{\mathbb{L}}\overline{\boldsymbol{\varepsilon}} + \widetilde{\boldsymbol{\tau}}\cdot\overline{\boldsymbol{\varepsilon}} + \frac{1}{2}\widetilde{f} \tag{4.8.3}$$

and

$$\widetilde{U}_L(\overline{\boldsymbol{\sigma}}) = \frac{1}{2}\overline{\boldsymbol{\sigma}}\cdot\widetilde{\mathbb{M}}\overline{\boldsymbol{\sigma}} + \widetilde{\boldsymbol{\gamma}}\cdot\overline{\boldsymbol{\sigma}} + \frac{1}{2}\widetilde{g}, \tag{4.8.4}$$

where $\widetilde{\mathbb{L}}$, $\widetilde{\boldsymbol{\tau}}$ and $\widetilde{f}$ are the effective modulus, effective eigenstrain, and effective potential at zero stress, respectively, and $\widetilde{\mathbb{M}}$, $\widetilde{\boldsymbol{\gamma}}$ and $\widetilde{g}$ are their respective dual variables. The values of these effective variables depend not only on the properties of the specific phases, but also on the microstructure.

Making use of the estimates of Ponte Castañeda and Willis (Ponte Castañeda and Willis, 1995) for two-phase composites with particulate microstructures, as well as the Levin relations (Levin, 1967), letting $\Delta\cdot = (\cdot)^{(1)} - (\cdot)^{(2)}$, and taking phase 1 to be

the matrix phase, we can represent Eqs. (4.8.3) and (4.8.4) as

$$\widetilde{W}_L(\overline{\boldsymbol{\varepsilon}}) = \frac{1}{2}\overline{\boldsymbol{\varepsilon}}\cdot\langle\mathbb{L}\rangle\,\overline{\boldsymbol{\varepsilon}} + \langle\boldsymbol{\tau}\rangle\cdot\overline{\boldsymbol{\varepsilon}} + \frac{1}{2}\left(\overline{\boldsymbol{\varepsilon}} + (\Delta\mathbb{L})^{-1}\,\Delta\boldsymbol{\tau}\right)\cdot\left(\widetilde{\mathbb{L}} - \langle\mathbb{L}\rangle\right)\left(\overline{\boldsymbol{\varepsilon}} + (\Delta\mathbb{L})^{-1}\,\Delta\boldsymbol{\tau}\right) + \frac{1}{2}\bar{f} \tag{4.8.5}$$

and

$$\widetilde{U}_L(\overline{\boldsymbol{\sigma}}) = \frac{1}{2}\overline{\boldsymbol{\sigma}}\cdot\langle\mathbb{M}\rangle\,\overline{\boldsymbol{\sigma}} + \langle\boldsymbol{\gamma}\rangle\cdot\overline{\boldsymbol{\sigma}} + \frac{1}{2}\left(\overline{\boldsymbol{\sigma}} + (\Delta\mathbb{M})^{-1}\,\Delta\boldsymbol{\gamma}\right)\cdot\left(\widetilde{\mathbb{M}} - \langle\mathbb{M}\rangle\right)\left(\overline{\boldsymbol{\sigma}} + (\Delta\mathbb{M})^{-1}\,\Delta\boldsymbol{\gamma}\right) + \frac{1}{2}\bar{g} \tag{4.8.6}$$

respectively, where

$$\widetilde{\mathbb{L}} = \mathbb{L}^{(1)} + c^{(2)}\left[c^{(1)}\mathbb{P}^{(1)} - (\Delta\mathbb{L})^{-1}\right]^{-1}, \tag{4.8.7}$$

$$\widetilde{\mathbb{M}} = \mathbb{M}^{(1)} + c^{(2)}\left[c^{(1)}\mathbb{Q}^{(1)} - (\Delta\mathbb{M})^{-1}\right]^{-1}, \tag{4.8.8}$$

$$\bar{f} = \sum_{r=1}^{2} c^{(r)}\frac{1}{2}\boldsymbol{\tau}^{(r)}\cdot\left(\mathbb{L}^{(r)}\right)^{-1}\boldsymbol{\tau}^{(r)}, \tag{4.8.9}$$

$$\bar{g} = \sum_{r=1}^{2} c^{(r)}\frac{1}{2}\boldsymbol{\gamma}^{(r)}\cdot\left(\mathbb{M}^{(r)}\right)^{-1}\boldsymbol{\gamma}^{(r)}. \tag{4.8.10}$$

Here, $\mathbb{P}^{(1)} = \frac{1}{c^{(1)}}\left(\mathbb{P}_i - c^{(2)}\mathbb{P}_d\right)$, where $\mathbb{Q}^{(1)} = \left(\mathbb{M}^{(1)}\right)^{-1} - \left(\mathbb{M}^{(1)}\right)^{-1}\mathbb{P}^{(1)}\left(\mathbb{M}^{(1)}\right)^{-1}$ is a microstructural tensor related to the Eshelby tensor, which takes into account the matrix properties, the shape and orientation of the inclusions, as well as the shape and orientation of the distribution of the inclusions, through second-order tensors $\mathbf{Z}_i$ and $\mathbf{Z}_d$. We assume that the shape and orientation of the inclusions is the same as the shape and orientation of the distribution of inclusions, so that $\mathbf{Z}_i = \mathbf{Z}_d \equiv \mathbf{Z}$, implying that $\mathbb{P}_i = \mathbb{P}_d$. Then, with $H^{(1)}_{ijkl}(\boldsymbol{\xi}) = \left[L^{(1)}_{ipkq}\xi_p\xi_q\right]^{-1}\xi_j\xi_l\Big|_{(ij)(kl)}$, we can write

$$\mathbb{P}^{(1)} = \frac{1}{4\pi\det\mathbf{Z}}\int_{|\boldsymbol{\xi}|=1}\mathbb{H}^{(1)}(\boldsymbol{\xi})|\mathbf{Z}^{-1}\boldsymbol{\xi}|^{-3}dS(\boldsymbol{\xi}).$$

Now, we have the well known result (Bobeth and Diener, 1987; Parton and Buryachenko, 1990; Ponte Castañeda and Suquet, 1998) that, given phase potentials of

the form (4.8.1) and (4.8.2),

$$\langle \boldsymbol{\varepsilon} \rangle^{(r)} = \frac{1}{c^{(r)}} \frac{\partial (\widetilde{W}_L - \frac{1}{2}\widetilde{f})}{\partial \boldsymbol{\tau}^{(r)}}, \quad \text{and} \quad \langle \boldsymbol{\varepsilon} \otimes \boldsymbol{\varepsilon} \rangle^{(r)} = \frac{2}{c^{(r)}} \frac{\partial (\widetilde{W}_L - \frac{1}{2}\widetilde{f})}{\partial \mathbb{L}^{(r)}} \tag{4.8.11}$$

$$\langle \boldsymbol{\sigma} \rangle^{(r)} = \frac{1}{c^{(r)}} \frac{\partial (\widetilde{U}_L - \frac{1}{2}\widetilde{g})}{\partial \boldsymbol{\gamma}^{(r)}}, \quad \text{and} \quad \langle \boldsymbol{\sigma} \otimes \boldsymbol{\sigma} \rangle^{(r)} = \frac{2}{c^{(r)}} \frac{\partial (\widetilde{U}_L - \frac{1}{2}\widetilde{g})}{\partial \mathbb{M}^{(r)}}. \tag{4.8.12}$$

Using Eqs. (4.8.11) and (4.8.12), together with expressions (4.8.5) and (4.8.6) for $\widetilde{W}_L$ and $\widetilde{U}_L$, respectively, it can be shown that the phase averages of the strain and stress are given by

$$\overline{\boldsymbol{\varepsilon}}^{(1)} = \overline{\boldsymbol{\varepsilon}} + \frac{1}{c^{(1)}} \mathbb{Y} \left(\Delta \mathbb{L} \overline{\boldsymbol{\varepsilon}} + \Delta \boldsymbol{\tau} \right), \qquad \overline{\boldsymbol{\varepsilon}}^{(2)} = \overline{\boldsymbol{\varepsilon}} - \frac{1}{c^{(2)}} \mathbb{Y} \left(\Delta \mathbb{L} \overline{\boldsymbol{\varepsilon}} + \Delta \boldsymbol{\tau} \right), \tag{4.8.13}$$

$$\overline{\boldsymbol{\sigma}}^{(1)} = \overline{\boldsymbol{\sigma}} + \frac{1}{c^{(1)}} \mathbb{X} \left(\Delta \mathbb{M} \overline{\boldsymbol{\sigma}} + \Delta \boldsymbol{\gamma} \right), \qquad \overline{\boldsymbol{\sigma}}^{(2)} = \overline{\boldsymbol{\sigma}} - \frac{1}{c^{(2)}} \mathbb{X} \left(\Delta \mathbb{M} \overline{\boldsymbol{\sigma}} + \Delta \boldsymbol{\gamma} \right), \tag{4.8.14}$$

where $\mathbb{X} = (\Delta \mathbb{M})^{-1} \left(\widetilde{\mathbb{M}} - \langle \mathbb{M} \rangle \right) (\Delta \mathbb{M})^{-1}$ and $\mathbb{Y} = (\Delta \mathbb{L})^{-1} \left(\widetilde{\mathbb{L}} - \langle \mathbb{L} \rangle \right) (\Delta \mathbb{L})^{-1}$.

It can also be shown that the covariance of the strain and stress fluctuations in the phases are given by

$$\begin{aligned}
\mathbb{C}_{\boldsymbol{\varepsilon}}^{(1)} &= -\frac{1}{c^{(2)}} (\overline{\boldsymbol{\varepsilon}}^{(1)} - \overline{\boldsymbol{\varepsilon}}) \otimes (\overline{\boldsymbol{\varepsilon}}^{(1)} - \overline{\boldsymbol{\varepsilon}}) \\
&\quad - \frac{1}{c^{(2)}} \left[(\mathbb{P}^{(1)})^{-1} (\overline{\boldsymbol{\varepsilon}}^{(1)} - \overline{\boldsymbol{\varepsilon}}) \right] \cdot \frac{\partial \mathbb{P}^{(1)}}{\partial \mathbb{L}^{(1)}} \left[(\mathbb{P}^{(1)})^{-1} (\overline{\boldsymbol{\varepsilon}}^{(1)} - \overline{\boldsymbol{\varepsilon}}) \right], \\
\mathbb{C}_{\boldsymbol{\varepsilon}}^{(2)} &= \mathbb{O},
\end{aligned} \tag{4.8.15}$$

$$\begin{aligned}
\mathbb{C}_{\boldsymbol{\sigma}}^{(1)} &= -\frac{1}{c^{(2)}} (\overline{\boldsymbol{\sigma}}^{(1)} - \overline{\boldsymbol{\sigma}}) \otimes (\overline{\boldsymbol{\sigma}}^{(1)} - \overline{\boldsymbol{\sigma}}) \\
&\quad - \frac{1}{c^{(2)}} \left[(\mathbb{Q}^{(1)})^{-1} (\overline{\boldsymbol{\sigma}}^{(1)} - \overline{\boldsymbol{\sigma}}) \right] \cdot \frac{\partial \mathbb{Q}^{(1)}}{\partial \mathbb{M}^{(1)}} \left[(\mathbb{Q}^{(1)})^{-1} (\overline{\boldsymbol{\sigma}}^{(1)} - \overline{\boldsymbol{\sigma}}) \right], \\
\mathbb{C}_{\boldsymbol{\sigma}}^{(2)} &= \mathbb{O}
\end{aligned} \tag{4.8.16}$$

In the above, quantities such as $\frac{\partial \mathbb{P}^{(1)}}{\partial \mathbb{L}^{(1)}}$ represent eight-order tensors and the products in the last term of Eq. $(4.8.15)_1$ should be interpreted as

$$\left[(\mathbb{P}^{(1)})^{-1} (\overline{\boldsymbol{\varepsilon}}^{(1)} - \overline{\boldsymbol{\varepsilon}}) \right]_{pq} \frac{\partial P_{pqrs}^{(1)}}{\partial \mathbb{L}^{(1)}} \left[(\mathbb{P}^{(1)})^{-1} (\overline{\boldsymbol{\varepsilon}}^{(1)} - \overline{\boldsymbol{\varepsilon}}) \right]_{rs} \tag{4.8.17}$$

where repeated indices are summed over. The same convention holds when evaluation the dot product in Eq. $(4.8.16)_1$.

We note that in the case of rigid inclusions

$$\overline{\boldsymbol{\varepsilon}}^{(1)} = \frac{1}{c^{(1)}}\overline{\boldsymbol{\varepsilon}}, \quad \text{and} \quad \widetilde{\mathbb{L}} = \mathbb{L}^{(1)} + \frac{c^{(2)}}{c^{(1)}}\left(\mathbb{P}^{(1)}\right)^{-1}, \tag{4.8.18}$$

while in the case of porous inclusions

$$\overline{\boldsymbol{\sigma}}^{(1)} = \frac{1}{c^{(1)}}\overline{\boldsymbol{\sigma}}, \quad \text{and} \quad \widetilde{\mathbb{M}} = \mathbb{M}^{(1)} + \frac{c^{(2)}}{c^{(1)}}\left(\mathbb{Q}^{(1)}\right)^{-1}. \tag{4.8.19}$$

4.8.1 Willis estimates for 2D incompressible two-phase composites

While it is often difficult to find an explicit representation for $\mathbb{P}^{(1)}$, under the assumptions made in this application, it can be shown that (see Ponte Castañeda (1996))

$$\mathbb{P}^{(1)} = \frac{1}{2\mu^{(1)}\sqrt{k}(\sqrt{k}+1)}\mathbb{E} + \frac{1}{2\mu^{(1)}(\sqrt{k}+1)}\mathbb{F}. \tag{4.8.20}$$

where $k = \lambda^{(1)}/\mu^{(1)}$ is the anisotropy ratio of the homogenous reference medium. Then

$$\mathbb{Q}^{(1)} = \frac{2\lambda^{(1)}}{\sqrt{k}+1}\mathbb{E} + \frac{2\mu^{(1)}\sqrt{k}}{\sqrt{k}+1}\mathbb{F} \tag{4.8.21}$$

Using Eqs. (4.8.13)-(4.8.14), we find that the average equivalent strain and stress in the matrix to be

$$\overline{\varepsilon}_e^{(1)} = \frac{(\sqrt{k}\mu^{(1)} + \lambda^{(2)})\overline{\varepsilon}_e - \frac{c^{(2)}}{2}\tau_{\parallel}^{(1)}}{\mu^{(1)}\sqrt{k} + c^{(2)}\lambda^{(1)} + c^{(1)}\lambda^{(2)}}, \quad \bar{\sigma}_e^{(1)} = \frac{(\lambda^{(1)} + \lambda^{(2)}\sqrt{k})\bar{\sigma}_e - 2c^{(2)}\lambda^{(1)}\lambda^{(2)}\gamma_{\parallel}^{(1)}}{\langle\lambda\rangle + \lambda^{(2)}\sqrt{k}}, \tag{4.8.22}$$

where $\langle\lambda\rangle = c^{(1)}\lambda^{(1)} + c^{(2)}\lambda^{(2)}$, and both $\gamma_{\parallel}^{(1)}$ and $\tau_{\parallel}^{(1)}$ are determined from the appro-

priate stationary conditions. Also, from Eqs. (4.8.15)-(4.8.16), we find

$$\frac{2}{3}\mathbb{C}_{\boldsymbol{\varepsilon}}^{(1)} = \frac{\left(\overline{\varepsilon}_e^{(1)} - \overline{\varepsilon}_e\right)^2 \sqrt{\lambda^{(1)}\mu^{(1)}}}{c^{(2)}}(\mathbb{L}^{(1)})^{-1}, \quad \frac{3}{2}\mathbb{C}_{\boldsymbol{\sigma}}^{(1)} = \frac{\left(\bar{\sigma}_e^{(1)} - \bar{\sigma}_e\right)^2}{4c^{(2)}\sqrt{\lambda^{(1)}\mu^{(1)}}}(\mathbb{M}^{(1)})^{-1}, \quad (4.8.23)$$

while $\boldsymbol{C}_{\boldsymbol{\sigma}}^{(2)} = \boldsymbol{C}_{\boldsymbol{\varepsilon}}^{(2)} = \mathbb{O}$.

4.9 Appendix II: On applying the non-symmetric FOSO method to a 2D example

We outline the general procedure for applying the non-symmetric FOSO method to our 2D example. We illustrate the method by applying the produce to the stress potential. We use the same symmetries as laid out in Section 4.5. The main difference with the non-symmetric method arises from the way that the moments are calculated. In general, the inner stationary conditions read

$$\frac{\partial u^{(r)}}{\partial \boldsymbol{\sigma}}(\breve{\boldsymbol{\sigma}}_{(p)}^{(r)}) - \mathbb{M}^{(r)}\breve{\boldsymbol{\sigma}}_{(p)}^{(r)} = \boldsymbol{\gamma}_{(p)}^{(r)} = \frac{\partial u^{(r)}}{\partial \boldsymbol{\sigma}}(\widehat{\boldsymbol{\sigma}}_{(p)}^{(r)}) - \mathbb{M}^{(r)}\widehat{\boldsymbol{\sigma}}_{(p)}^{(r)} \quad (4.9.1)$$

for each $r = 1, \ldots, N$ and each $p = 1, \ldots, M$. The stationary conditions with respect to $\boldsymbol{\gamma}_{(p)}^{(r)}$ give

$$\overline{\boldsymbol{\sigma}}^{(r)} = \sum_{r=1}^{M} \beta_{(p)}^{(r)} \left[\alpha^{(r)}\breve{\boldsymbol{\sigma}}_{(p)}^{(r)} + (1-\alpha^{(r)})\widehat{\boldsymbol{\sigma}}_{(p)}^{(r)}\right], \quad (4.9.2)$$

$$\mathbf{0} = \alpha^{(r)}(\breve{\boldsymbol{\sigma}}_{(p)}^{(r)} - \breve{\boldsymbol{\sigma}}_{(q)}^{(r)}) + (1-\alpha^{(r)})(\widehat{\boldsymbol{\sigma}}_{(p)}^{(r)} - \widehat{\boldsymbol{\sigma}}_{(q)}^{(r)}), \quad (4.9.3)$$

while

$$\mathbb{C}_{\boldsymbol{\sigma}}^{(r)} = \alpha^{(r)}(1-\alpha^{(r)}) \sum_{p=1}^{M} \beta_{(p)}^{(r)} \left(\breve{\boldsymbol{\sigma}}_{(p)}^{(r)} - \widehat{\boldsymbol{\sigma}}_{(p)}^{(r)}\right) \otimes \left(\breve{\boldsymbol{\sigma}}_{(p)}^{(r)} - \widehat{\boldsymbol{\sigma}}_{(p)}^{(r)}\right). \quad (4.9.4)$$

Taking $M = 2$, $\beta_{(p)}^{(r)} = \alpha^{(r)} = \frac{1}{2}$, these equations, reduce to

$$\bar{\sigma}_e^{(r)} = \frac{\breve{\sigma}_{\parallel}^{(r)} + \widehat{\sigma}_{\parallel}^{(r)}}{2}, \qquad 0 = \breve{\sigma}_{\perp}^{(r)} + \widehat{\sigma}_{\perp}^{(r)}, \tag{4.9.5}$$

$$\frac{3}{2}\mathbb{C}_{\boldsymbol{\sigma}}^{(r)} \cdot \mathbb{E} = \left(\frac{\widehat{\sigma}_{\parallel}^{(r)} - \breve{\sigma}_{\parallel}^{(r)}}{2} \right)^2, \qquad \frac{3}{2}\mathbb{C}_{\boldsymbol{\sigma}}^{(r)} \cdot \mathbb{F} = \left(\frac{\widehat{\sigma}_{\perp}^{(r)} - \breve{\sigma}_{\perp}^{(r)}}{2} \right)^2. \tag{4.9.6}$$

Combining the above, we find that

$$\widehat{\sigma}_{\parallel}^{(1)} = \bar{\sigma}_e^{(1)} + \left(\bar{\sigma}_e^{(1)} - \bar{\sigma}_e \right) \frac{k^{1/4}}{\sqrt{2c^{(2)}}}, \tag{4.9.7}$$

$$\breve{\sigma}_{\parallel}^{(1)} = \bar{\sigma}_e^{(1)} - \left(\bar{\sigma}_e^{(1)} - \bar{\sigma}_e \right) \frac{k^{1/4}}{\sqrt{2c^{(2)}}}, \tag{4.9.8}$$

$$\widehat{\sigma}_{\perp}^{(1)} = \left(\bar{\sigma}_e^{(1)} - \bar{\sigma}_e \right) \frac{k^{-1/4}}{\sqrt{2c^{(2)}}}, \tag{4.9.9}$$

$$\breve{\sigma}_{\perp}^{(1)} = -\left(\bar{\sigma}_e^{(1)} - \bar{\sigma}_e \right) \frac{k^{-1/4}}{\sqrt{2c^{(2)}}}. \tag{4.9.10}$$

It remains to solve two equations for the unknowns k and $\bar{\sigma}_e^{(1)}$. The first equation comes from the LCC estimate $(4.8.22)_1$ as given in Section 4.8.1:

$$\left(\frac{\sigma_0^{(1)}}{\sigma_0^{(2)}} \frac{\bar{\sigma}_e - c^{(1)}\bar{\sigma}_e^{(1)}}{c^{(2)}} \right)^n = \frac{1}{2}(\widehat{\sigma}_e^{(1)})^{n-1}\widehat{\sigma}_{\parallel}^{(1)} \left(1 + \sqrt{\frac{2}{c^{(2)}}} k^{1/4} \right) + \frac{1}{2}(\breve{\sigma}_e^{(1)})^{n-1}\breve{\sigma}_{\parallel}^{(1)} \left(1 - \sqrt{\frac{2}{c^{(2)}}} k^{1/4} \right) \tag{4.9.11}$$

The second comes from combining the equations for the parallel and perpendicular components of $\boldsymbol{\gamma}_{(p)}^{(r)}$ obtained from Eq. (4.9.1), and reduce to

$$(\widehat{\sigma}_e)^{n-1}(\sqrt{k}\widehat{\sigma}_{\parallel}^{(1)} - \widehat{\sigma}_{\perp}^{(1)}) = (\breve{\sigma}_e^{(1)})^{n-1}(\sqrt{k}\breve{\sigma}_{\parallel}^{(1)} - \breve{\sigma}_{\perp}^{(1)}). \tag{4.9.12}$$

Once we have determined k and $\bar{\sigma}_e^{(1)}$, we can compute the effective flow stress using Eq. (4.5.16).

It is helpful to also outline the procedure for calculating the dual version of this method. This introduces terms to the strain potentials that are quadratic in the $\boldsymbol{\tau}_{(p)}^{(r)}$.

The general stationary conditions with respect to $\boldsymbol{\tau}_{(p)}^{(r)}$ give by

$$\overline{\boldsymbol{\varepsilon}}^{(r)} = \sum_{r=1}^{M} \beta_{(p)}^{(r)} \left[\alpha^{(r)} \breve{\boldsymbol{\varepsilon}}_{(p)}^{(r)} + (1-\alpha^{(r)}) \widehat{\boldsymbol{\varepsilon}}_{(p)}^{(r)} \right], \tag{4.9.13}$$

$$\mathbf{0} = \alpha^{(r)} (\breve{\boldsymbol{\varepsilon}}_{(p)}^{(r)} - \breve{\boldsymbol{\varepsilon}}_{(q)}^{(r)}) + (1-\alpha^{(r)}) (\widehat{\boldsymbol{\varepsilon}}_{(p)}^{(r)} - \widehat{\boldsymbol{\varepsilon}}_{(q)}^{(r)}) + \mathbb{M}^{(r)} (\boldsymbol{\tau}_{(p)}^{(r)} - \boldsymbol{\tau}_{(q)}^{(r)}). \tag{4.9.14}$$

Interestingly enough, despite the presence of the extra term, we still find that

$$\mathbb{C}_{\boldsymbol{\varepsilon}}^{(r)} = \alpha^{(r)} (1-\alpha^{(r)}) \sum_{p=1}^{M} \beta_{(p)}^{(r)} \left(\breve{\boldsymbol{\varepsilon}}_{(p)}^{(r)} - \widehat{\boldsymbol{\varepsilon}}_{(p)}^{(r)} \right) \otimes \left(\breve{\boldsymbol{\varepsilon}}_{(p)}^{(r)} - \widehat{\boldsymbol{\varepsilon}}_{(p)}^{(r)} \right). \tag{4.9.15}$$

Taking $M = 2$, $\beta_{(p)}^{(r)} = \alpha^{(r)} = \frac{1}{2}$, these equations, again using the same symmetries as outlined in Section 4.5 (as applied to strains) yield

$$\overline{\varepsilon}_e^{(r)} = \frac{\breve{\varepsilon}_{\parallel}^{(r)} + \widehat{\varepsilon}_{\parallel}^{(r)}}{2}, \qquad 0 = \frac{\breve{\varepsilon}_{\perp}^{(r)} + \widehat{\varepsilon}_{\perp}^{(r)}}{2} + \frac{\tau_{\perp}^{(r)}}{2\mu^{(r)}}, \tag{4.9.16}$$

$$\frac{2}{3} \mathbb{C}_{\boldsymbol{\varepsilon}}^{(r)} \cdot \mathbb{E} = \left(\frac{\widehat{\varepsilon}_{\parallel}^{(r)} - \breve{\varepsilon}_{\parallel}^{(r)}}{2} \right)^2, \qquad \frac{2}{3} \mathbb{C}_{\boldsymbol{\varepsilon}}^{(r)} \cdot \mathbb{F} = \left(\frac{\widehat{\varepsilon}_{\perp}^{(r)} - \breve{\varepsilon}_{\perp}^{(r)}}{2} \right)^2. \tag{4.9.17}$$

Now, the symmetries of the problem give $(\tau_{(1)}^{(r)})_{\parallel} = (\tau_{(2)}^{(r)})_{\parallel} = \tau_{\parallel}^{(r)}$ and $(\tau_{(1)}^{(r)})_{\perp} = -(\tau_{(2)}^{(r)})_{\perp} = \tau_{\perp}^{(r)}$, while the stationary conditions from the error functions are the same as Eqs. (4.5.7) and (4.5.8). Using results from Section 4.8.1, we find that $\widehat{\varepsilon}_{\parallel}^{(2)} = \breve{\varepsilon}_{\parallel}^{(2)} = \overline{\varepsilon}_e^{(2)}$, $\widehat{\varepsilon}_{\perp}^{(2)} = \breve{\varepsilon}_{\perp}^{(2)} = 0$ and

$$2\mu^{(2)} = 2\lambda^{(2)} = \frac{2\sigma_0^{(2)}}{3\left(\varepsilon_0\right)^m} \left(\frac{\overline{\varepsilon}_e - c^{(1)} \overline{\varepsilon}_e^{(1)}}{c^{(2)}} \right)^{m-1}, \tag{4.9.18}$$

while

$$\widehat{\varepsilon}_{\parallel}^{(1)} = \overline{\varepsilon}_e^{(1)} - \left(\overline{\varepsilon}_e^{(1)} - \overline{\varepsilon}_e\right) \frac{k^{-1/4}}{\sqrt{2c^{(2)}}}, \tag{4.9.19}$$

$$\overset{\times}{\varepsilon}_{\parallel}^{(1)} = \overline{\varepsilon}_e^{(1)} + \left(\overline{\varepsilon}_e^{(1)} - \overline{\varepsilon}_e\right) \frac{k^{-1/4}}{\sqrt{2c^{(2)}}}, \tag{4.9.20}$$

$$\widehat{\varepsilon}_{\perp}^{(1)} = -\left(\overline{\varepsilon}_e^{(1)} - \overline{\varepsilon}_e\right) \frac{k^{1/4}}{\sqrt{2c^{(2)}}} - \frac{\overline{\varepsilon}_e^{(1)} - \sqrt{\left(\overline{\varepsilon}_e^{(1)}\right)^2 - \frac{2}{c^{(2)}}\left(\overline{\varepsilon}_e^{(1)} - \overline{\varepsilon}_e\right)^2 \sqrt{k}(1-k)}}{2\sqrt{k}}, \tag{4.9.21}$$

$$\overset{\times}{\varepsilon}_{\perp}^{(1)} = \left(\overline{\varepsilon}_e^{(1)} - \overline{\varepsilon}_e\right) \frac{k^{1/4}}{\sqrt{2c^{(2)}}} - \frac{\overline{\varepsilon}_e^{(1)} - \sqrt{\left(\overline{\varepsilon}_e^{(1)}\right)^2 - \frac{2}{c^{(2)}}\left(\overline{\varepsilon}_e^{(1)} - \overline{\varepsilon}_e\right)^2 \sqrt{k}(1-k)}}{2\sqrt{k}}. \tag{4.9.22}$$

It then remains to solve two equations for k and $\overline{\varepsilon}_e^{(1)}$. As in the case of the stress formulation, the first is generated from the LCC estimate $(4.8.22)_1$ for $\overline{\varepsilon}_e^{(1)}$, as given in Section 4.8.1, and reads

$$\frac{\sigma_0^{(2)}}{\sigma_0^{(1)}} \left(\frac{\overline{\varepsilon}_e - c^{(1)}\overline{\varepsilon}_e^{(1)}}{c^{(2)}}\right)^m = \left(\overset{\times}{\varepsilon}^{(1)}\right)^{m-1} \left(\frac{1}{2}\overset{\times}{\varepsilon}_{\parallel}^{(1)} + \frac{k^{1/4}}{\sqrt{2p}}\overset{\times}{\varepsilon}_{\perp}^{(1)}\right) + \left(\widehat{\varepsilon}^{(1)}\right)^{m-1} \left(\frac{1}{2}\widehat{\varepsilon}_{\parallel}^{(1)} - \frac{k^{1/4}}{\sqrt{2p}}\widehat{\varepsilon}_{\perp}^{(1)}\right), \tag{4.9.23}$$

while the second comes from combining Eqs. (4.5.7) and (4.5.8), and is given by

$$\left(\widehat{\varepsilon}_e^{(1)}\right)^{m-1} \left(\widehat{\varepsilon}_{\parallel}^{(1)} - \sqrt{k}\widehat{\varepsilon}_{\perp}^{(1)}\right) = \left(\overset{\times}{\varepsilon}_e^{(1)}\right)^{m-1} \left(\overset{\times}{\varepsilon}_{\parallel}^{(1)} - \sqrt{k}\overset{\times}{\varepsilon}_{\perp}^{(1)}\right). \tag{4.9.24}$$

Once k and $\overline{\varepsilon}_e^{(1)}$ are determined, we can use Eq. (4.5.15) to calculate the effective flow stress.

Chapter 5

Theoretical Aspects of Periodic Homogenization and Post-Bifurcation Analysis for Finite Elasticity

Abstract

In this chapter, we introduce the relevant tools needed to carry out our analysis in the chapters to come. Some of the discussion is a review of well founded results from the theory of the calculus of variations, as well as the theory of homogenization, but we also present novel results regarding the rank-one convexification procedure. The general framework for obtaining the effective behavior of periodic hyperelastic composites is also introduced.

5.1 Introduction

A general framework for describing the macroscopic response of hyperelastic composites undergoing finite strains was first given by Hill (1972), who made use of the principal of minimum potential energy to define the effective potential through the minimization of some energy functional. Due to physical requirements of objectivity and incompressibility, the stored-energy functions in (nonlinear) hyperelasticity, which act as integrands of these energy functionals, are generally non-convex. In order to make use of more realistic constitutive models, Ball (1977) introduced generalized

notions of convexity, e.g. polyconvexity, that allowed for a more mathematically rigorous variational formulation of hyperelasticity.

Due to the general nonconvexity of the energy potentials, it is possible for such composites to undergo both microscopic and macroscopic instabilities. In order to account for this, Braides (1985) and Müller (1987) made use of Γ-convergence to derive expressions for the effective stored-energy function of composites whose phases are modeled by more realistic non-convex constitutive responses. Building on these works, Geymonat et al. (1993) carried out a rigorous analysis for the possible development of instabilities in hyperelastic composites with *periodic* microstructures. By consideration of the *incremental* (linearized) problem for the homogenized energy, criteria were developed for the possible onset of microscopic instabilities, where the one-cell periodic solution near the undeformed configuration gives way to lower energy multi-cell solutions. The theory also allows for the onset of macroscopic instabilities, i.e. instabilities which occur at an infinite wavelength.

One main goal of this thesis to extract the post bifurcation behavior of hyperelastic composites after the onset of a macroscopic instability. The methodology we plan on utilizing was first proposed by Avazmohammadi and Ponte Castañeda (2016). It makes use of results from theory of the calculus of variations, as well as the abstract theory of homogenization. Since this method will be used multiple times in this work, we look to summarize it here. As such, Section 5.2 provides a review of the results from the calculus of variations that are used extensively throughout the thesis. It also includes novel results regarding the calculation of the rank-one convex envelope; this quantity is needed in order to extract the post-bifurcation response. Section 5.3 discusses the general framework used in finding the effective behavior of hyperelastic composites, as well as the method by which the relaxation is obtained. This chapter is meant to supplement Chapter 5 and Chapter 6, and results stated here are referenced throughout the next two chapters.

5.2 Mathematical Preliminaries

In this section, we review some definitions and results that are needed in our analysis (see Ball, 1977; Dacorogna, 1989, for more details). We also prove new results that are helpful in interpreting our findings.

Definition 1:
A function $W : \mathbb{R}^{d\times d} \to \mathbb{R}$ is *polyconvex* at $\boldsymbol{F}_0$ if there exists a convex function g that depends on the vector $T(\boldsymbol{F}_0)$ of all the minors of $\boldsymbol{F}_0$, such that $W(\boldsymbol{F}_0) = g(T(\boldsymbol{F}_0))$.

Remark 3:
In the case that $d = 2$, $W(\boldsymbol{F}_0) = g(\boldsymbol{F}_0, \det \boldsymbol{F}_0)$ *where* $g : \mathbb{R}^5 \to \mathbb{R} \cup \{+\infty\}$ *is convex, while for* $d = 3$, $W(\boldsymbol{F}_0) = g(\boldsymbol{F}_0, \boldsymbol{F}_0^*, \det \boldsymbol{F}_0)$ *where* $g : \mathbb{R}^{19} \to \mathbb{R} \cup \{+\infty\}$ *is convex, and* $\boldsymbol{F}_0^*$ *denotes the adjugate of* $\boldsymbol{F}_0$.

Definition 2:
A function $W : \mathbb{R}^{d\times d} \to \mathbb{R}$ is *quasiconvex* (in the sense of Morrey Jr. (1952)) if

$$W(\boldsymbol{F}_0) \leqslant \frac{1}{|D|} \int_D W(\boldsymbol{F}_0 + \nabla\varphi(\mathbf{x}))d\mathbf{x}, \tag{5.2.1}$$

for every constant $\boldsymbol{F}_0$, for every open bounded region $D \subset \mathbb{R}^d$ and for every $\varphi \in W_0^{1,\infty}(D)$.

Definition 3:
A function $W : \mathbb{R}^{d\times d} \to \mathbb{R}$ is said to be *rank-one convex* if for any $t \in (0, 1)$ and any $\boldsymbol{F}_1, \boldsymbol{F}_2$ with $\operatorname{rank}(\boldsymbol{F}_1 - \boldsymbol{F}_2) \leqslant 1$,

$$W((1-t)\boldsymbol{F}_1 + t\boldsymbol{F}_2) \leqslant (1-t)W(\boldsymbol{F}_1) + tW(\boldsymbol{F}_2). \tag{5.2.2}$$

If the above inequality is strict for all $t \in (0, 1)$ and any $\boldsymbol{F}_1, \boldsymbol{F}_2$ with $\operatorname{rank}(\boldsymbol{F}_1 - \boldsymbol{F}_2) \leqslant 1$, then W is said to be *strictly rank-one convex*.

Definition 4:

For $W : \mathbb{R}^{d\times d} \to \mathbb{R}$, the *convex, polyconvex, quasiconvex, and rank-one convex envelope* (or the *convexification*, *polyconvexification*, etc., respectively) of a function W are given by

$$CW(\boldsymbol{F}) = \sup\{g(\boldsymbol{F}) \,:\, g \leqslant W,\, g \text{ is convex}\}, \tag{5.2.3}$$

$$PW(\boldsymbol{F}) = \sup\{g(\boldsymbol{F}) \,:\, g \leqslant W,\, g \text{ is polyconvex}\}, \tag{5.2.4}$$

$$QW(\boldsymbol{F}) = \sup\{g(\boldsymbol{F}) \,:\, g \leqslant W,\, g \text{ is quasiconvex}\}, \tag{5.2.5}$$

$$RW(\boldsymbol{F}) = \sup\{g(\boldsymbol{F}) \,:\, g \leqslant W,\, g \text{ is rank one convex}\}, \tag{5.2.6}$$

respectively.

The next result is crucial in the arguments used to calculate the relaxation.

Theorem 1 (Theorem 5.3 (i) Dacorogna (1989))**:**
For a function taking finite values,

$$W \text{ convex} \implies W \text{ polyconvex} \implies W \text{ quasiconvex} \implies W \text{ rank-one convex}. \tag{5.2.7}$$

In light of (5.2.7), we have

$$CW(\boldsymbol{F}) \leqslant PW(\boldsymbol{F}) \leqslant QW(\boldsymbol{F}) \leqslant RW(\boldsymbol{F}) \leqslant W(\boldsymbol{F}). \tag{5.2.8}$$

We note here that if W takes values in the extended real numbers $\mathbb{R} \cup \{+\infty\}$, polyconvexity implies both quasiconvexity and rank-one convexity, but quasiconvexity does not generally imply rank-one convexity. In the cases of interest in this work, $W(\boldsymbol{F}) < \infty$ on some subset of $\mathbb{R}^{3\times 3}$ which is determined by a condition on $\det \boldsymbol{F}$. By appealing to the result of Conti (2008), it is known that quasiconvex function with

such volumetric constraints are in fact rank-one convex. Therefore, the inequality

$$PW \leqslant QW \leqslant RW \tag{5.2.9}$$

is still valid in such cases.

Rank-one convexity plays an important role in much of the analysis used in this work, and therefore requires further discussion. Unlike quasiconvexity, rank-one convexity can be interpreted as a local property. Since rank-one convexity of a function W is equivalent to the convexity of the scalar function $\varphi(t) = W(\boldsymbol{F}_0 + t\mathbf{a} \otimes \mathbf{b})$, for any $\mathbf{a}, \mathbf{b} \in \mathbb{R}^d$, and every $\boldsymbol{F}_0$, we can discuss *local* rank-one convexity, or rank-one convexity at $\boldsymbol{F}_0$, by considering the convexity of W along all rank-one paths going through $\boldsymbol{F}_0$.

Notation:
We write $\langle t, \boldsymbol{F}_1, \boldsymbol{F}_2 \rangle_{\boldsymbol{F}_0}$ to signify that $\boldsymbol{F}_0 = (1-t)\boldsymbol{F}_1 + t\boldsymbol{F}_2$ for $t \in (0,1)$ and $\operatorname{rank}(\boldsymbol{F}_1 - \boldsymbol{F}_2) \leqslant 1$. In other literature, $\boldsymbol{F}_0$ is said to be the *barycenter* between $\boldsymbol{F}_1$ and $\boldsymbol{F}_2$.

Definition 5:
A function $W : \mathbb{R}^{d\times d} \to \mathbb{R} \cup \{+\infty\}$ is *locally rank-one convex*, or simply rank-one convex at $\boldsymbol{F}_0$, if

$$W(\boldsymbol{F}_0) \leqslant (1-t)tW(\boldsymbol{F}_1) + tW(\boldsymbol{F}_2) \tag{5.2.10}$$

for any $\langle t, \boldsymbol{F}_1, \boldsymbol{F}_2 \rangle_{\boldsymbol{F}_0}$.

Replacing $\leqslant$ with $<$ provides the definition strict rank-one convexity at $\boldsymbol{F}_0$ Moreover, if W is locally rank-one convex at every $\boldsymbol{F}_0$, then W is rank-one convex, in the usual sense of the definition.

Now, if W is twice continuously differentiable, then W is rank-one convex at $\boldsymbol{F}_0$ if and only if W satisfies the so called *Legendre-Hadamard* condition:

$$\frac{\partial^2 W(\boldsymbol{F}_0)}{\partial F_{ij} \partial F_{kl}} a_i b_j a_k b_l \geqslant 0 \quad \forall\, \mathbf{a},\, \mathbf{b}. \tag{5.2.11}$$

In this setting, W is strictly rank-one convex at $\boldsymbol{F}_0$ if

$$\frac{\partial^2 W(\boldsymbol{F}_0)}{\partial F_{ij}\partial F_{kl}} a_i b_j a_k b_l > 0 \quad \forall\, \mathbf{a},\, \mathbf{b}, \tag{5.2.12}$$

a condition oftentimes referred to as the *strong ellipticity* condition.

Next, we provide a definition which allows for the description of the rank-one connectedness of a set of tensors.

Notation:

For any $I \in \mathbb{N}$, we define the set Λ_I to be

$$\Lambda_I = \{\lambda = (\lambda_1, \ldots, \lambda_I) \,:\, \lambda_i \geqslant 0 \text{ and } \sum_{i=1}^{I} \lambda_i = 1\}. \tag{5.2.13}$$

Definition 6:

For $I \in \mathbb{N}$, $\lambda \in \Lambda_I$, and a collection of $\boldsymbol{F}_i \in \mathbb{R}^{d\times d}$ for $1 \leqslant i \leqslant I$, we say that $(\lambda_i, \boldsymbol{F}_i)_{1\leqslant i\leqslant I}$ satisfy (H_I) if

(i) when $I = 2$, then $\operatorname{rank}(\boldsymbol{F}_1 - \boldsymbol{F}_2) \leqslant 1$;

(ii) when $I > 2$, then, up to a permutation, $\operatorname{rank}(\boldsymbol{F}_1 - \boldsymbol{F}_2) \leqslant 1$, and if, for every $2 \leqslant i \leqslant I-1$, we define

$$\begin{cases} \mu_1 = \lambda_1 + \lambda_2, & \boldsymbol{G}_1 = \frac{\lambda_1 \boldsymbol{F}_1 + \lambda_2 \boldsymbol{F}_2}{\lambda_1 + \lambda_2} \\ \mu_i = \lambda_{i+1}, & \boldsymbol{G}_i = \boldsymbol{F}_{i+1} \end{cases} \tag{5.2.14}$$

then $(\mu_i, \boldsymbol{G}_i)_{1\leqslant i\leqslant I-1}$ satisfy (H_{I-1})

Finally, we recall the result of Kohn and Strang (1986), which will play an important roll in the construction of the relaxation.

Theorem 2:

Let $W : \mathbb{R}^{d\times d} \to \mathbb{R} \cup \{+\infty\}$, *and let* $g : \mathbb{R}^{d\times d} \to \mathbb{R} \cup \{+\infty\}$ *be a rank-one convex*

function such that

$$W(\boldsymbol{F}) \geqslant g(\boldsymbol{F}) \quad \forall \boldsymbol{F}.$$

Define $R_0 W = W$ *and, for each* $k \in \mathbb{N}$ *define*

$$R_{k+1}W(\boldsymbol{F}) = \inf_{\langle \lambda, \boldsymbol{F}_1, \boldsymbol{F}_2 \rangle_{\boldsymbol{F}}} \left\{ (1-\lambda) R_k W(\boldsymbol{F}_1) + \lambda R_k W(\boldsymbol{F}_2) \right\}. \tag{5.2.15}$$

Then

$$RW(\boldsymbol{F}) = \lim_{k \to \infty} R_k W(\boldsymbol{F}) = \inf_{k \in \mathbb{N}} R_k W(\boldsymbol{F}). \tag{5.2.16}$$

We are now in a position to state and prove results that allow for a more complete description of the relaxation in the case that it is obtained through a finite number of laminations. We will use these results to better explain the nature of the Kohn-Strang lamination procedure, thereby allowing us to fully describe the rank-one convex envelope when it is obtained by a finite number of laminations. We start with two definitions:

Definition 7:

Given a function $W : \mathbb{R}^{d \times d} \to \mathbb{R} \cup \{+\infty\}$, we define

$$\mathcal{R}_0(W) = \left\{ \boldsymbol{F} \,:\, W \text{ is strictly rank-one convex at } \boldsymbol{F} \right\}. \tag{5.2.17}$$

$$\mathcal{R}_k(W) = \left\{ \boldsymbol{F} \,:\, R_k W \text{ is strictly rank-one convex at } \boldsymbol{F} \right\}, \; k \geqslant 1. \tag{5.2.18}$$

When the argument of $\mathcal{R}_k(W)$ is understood, we will simply write $\mathcal{R}_k$. The next result relates to the rank-one connected matrices needed when computing $R_k W$ from $R_{k-1} W$ in the Kohn-Strang formula.

Proposition 3:

Let $\boldsymbol{F} \in \mathcal{R}_1$, *and suppose that the infimum in Eq.* (5.2.15) *which determines* $R_1 W(\boldsymbol{F})$ *is obtained at* $\langle t_0, \boldsymbol{F}_1, \boldsymbol{F}_2 \rangle_{\boldsymbol{F}}$. *Then* $\boldsymbol{F}_1, \boldsymbol{F}_2 \in \mathcal{R}_0$.

Proof:

We note that if $\boldsymbol{F} \in \mathcal{R}_1 \cap \mathcal{R}_0$, *the infimum which determines* $R_1 W$ *is trivially attained*

at $\boldsymbol{F}_1 = \boldsymbol{F}_2 = \boldsymbol{F}$. *To see this, we assume, by way of contradiction, that* $\boldsymbol{F}_1 \neq \boldsymbol{F}$ *and* $\boldsymbol{F}_2 \neq \boldsymbol{F}$. *Then*

$$R_1 W(\boldsymbol{F}) = (1 - t_0) W(\boldsymbol{F}_1) + t_0 W(\boldsymbol{F}_2) > W(\boldsymbol{F}) \tag{5.2.19}$$

which is a contradiction, since $R_1 W \leqslant W$. *Hence,* $\boldsymbol{F}_1 = \boldsymbol{F}_2 = \boldsymbol{F} \in \mathcal{R}_0$. *This also shows that if* $\boldsymbol{F} \in \mathcal{R}_0$, *then* $R_1 W(\boldsymbol{F}) = W(\boldsymbol{F})$. *Now, suppose that* $\boldsymbol{F} \in \mathcal{R}_1 \backslash \mathcal{R}_0$. *By the assumption made on* $\langle t_0, \boldsymbol{F}_1, \boldsymbol{F}_2 \rangle_{\boldsymbol{F}}$, *we know that*

$$R_1 W(\boldsymbol{F}) = (1 - t_0) W(\boldsymbol{F}_1) + t_0 W(\boldsymbol{F}_2). \tag{5.2.20}$$

Now, by way of contradiction, suppose that $\boldsymbol{F}_1, \boldsymbol{F}_2 \notin \mathcal{R}_0$. *Then, we know that* $\boldsymbol{F}_1, \boldsymbol{F}_2 \neq \boldsymbol{F} \in \mathcal{R}_0$, *and we can find* $\langle t_1, \boldsymbol{G}_1, \boldsymbol{G}_2 \rangle_{\boldsymbol{F}_1}$ *and* $\langle t_2, \boldsymbol{H}_1, \boldsymbol{H}_2 \rangle_{\boldsymbol{F}_2}$ *such that*

$$\begin{aligned} (1 - t_1) W(\boldsymbol{G}_1) + t_1 W(\boldsymbol{G}_2) &\leqslant W(\boldsymbol{F}_1), \\ (1 - t_2) W(\boldsymbol{H}_1) + t_2 W(\boldsymbol{H}_2) &\leqslant W(\boldsymbol{F}_2). \end{aligned} \tag{5.2.21}$$

On the other hand, using the definition of $R_1 W$, *we know that*

$$\begin{aligned} R_1 W(\boldsymbol{F}_1) &\leqslant (1 - t_1) W(\boldsymbol{G}_1) + t_1 W(\boldsymbol{G}_2), \\ R_1 W(\boldsymbol{F}_2) &\leqslant (1 - t_2) W(\boldsymbol{H}_1) + t_2 W(\boldsymbol{H}_2). \end{aligned} \tag{5.2.22}$$

Upon combining Eqs. (5.2.20)-(5.2.22), *we see that that*

$$(1 - t_0) R_1 W(\boldsymbol{F}_1) + t_0 R_1 W(\boldsymbol{F}_2) \leqslant R_1 W(\boldsymbol{F}). \tag{5.2.23}$$

contradicting the fact that $\boldsymbol{F} \in \mathcal{R}_1$. *Therefore we can conclude that* $\boldsymbol{F}_1, \boldsymbol{F}_2 \in \mathcal{R}_0$. □

Corollary:

Let $\boldsymbol{F} \in \mathcal{R}_k$, *and suppose that the infimum in Eq.* (5.2.15) *which determines* $R_k W(\boldsymbol{F})$

is obtained at $\langle \lambda_k, \boldsymbol{F}_1, \boldsymbol{F}_2 \rangle_{\boldsymbol{F}}$. *Then* $\boldsymbol{F}_1, \boldsymbol{F}_2 \in \mathcal{R}_{k-1}$.

Proof:

The proof proceeds exactly as it does for Proposition 3, mutatis mutandis. □

In practice, Eqs. (5.2.15)-(5.2.16) prove to be more useful than Eq. (5.2.6), as it is often possible to obtain, analytically, expressions for $R_k W$. Moreover, if there exists some K for which $R_K W$ is rank-one convex, then $R_K W = RW$. To gain a physical insight into the motivation for Eq. (5.2.15), we note that, given any $\langle \lambda, \boldsymbol{F}_1, \boldsymbol{F}_2 \rangle_{\boldsymbol{F}_0}$, we can find two vectors $\mathbf{a}, \mathbf{N}$ such that

$$\boldsymbol{F}_2 - \boldsymbol{F}_1 = \mathbf{a} \otimes \mathbf{N}, \tag{5.2.24}$$

and

$$\boldsymbol{F}_0 = (1-\lambda)\boldsymbol{F}_1 + \lambda \boldsymbol{F}_2 \implies \begin{cases} \boldsymbol{F}_1 = \boldsymbol{F}_0 - \lambda \mathbf{a} \otimes \mathbf{N} \\ \boldsymbol{F}_2 = \boldsymbol{F}_0 + (1-\lambda)\mathbf{a} \otimes \mathbf{N} \end{cases} . \tag{5.2.25}$$

Therefore, we can redefine

$$\begin{aligned} R_k W(\boldsymbol{F}_0) = \inf_{\mathbf{a}, \mathbf{N}_k, c_k} \{ & (1-c_k) R_{k-1} W(\boldsymbol{F}_0 - c_k \mathbf{a} \otimes \mathbf{N}_k) \\ & + c_k R_{k-1} W(\boldsymbol{F}_0 + (1-c_k)\mathbf{a} \otimes \mathbf{N}_k) \} , \end{aligned} \tag{5.2.26}$$

which proves to be a more useful form for calculating $R_k W$. Interpreted from the perspective of continuum mechanics, we see that Eq. (5.2.24) relates to the jump condition that must be satisfied by a deformation gradient at an interface boundary with unit normal $\mathbf{N}$. Thus Eq. (5.2.26) can be interpreted as the procedure by which domains are formed. In the first iteration, two copies of the composite described by the principal solution W are laminated together in a direction with normal $\mathbf{N}_1$. If $\boldsymbol{F}_1$ and $\boldsymbol{F}_2$ fail to be stable deformations, i.e. if $\boldsymbol{F}_1, \boldsymbol{F}_2 \notin \mathcal{R}_0(W)$, the composite breaks up again in a second lamination procedure. When the process terminates, we are left a material composed of copies of the principal solution laminated together in such

a way as to support the original applied deformation $\boldsymbol{F}_0$. It is unknown, for $d \geqslant 2$, if RW can be obtained through a finite number of iterations. Furthermore, in the search for the relaxation, there is no way to know, *a priori*, whether RW will in fact turn out to be polyconvex.

If, however, RW is polyconvex, whereby $QW = RW$, and if $RW = R_k W$ for some finite k, this final result allows for a more explicit representation of the relaxation.

Proposition 4:

Suppose that there exists a k such that $R_k W(\boldsymbol{F}) = RW(\boldsymbol{F})$ for all $\boldsymbol{F}$. Then, for $\boldsymbol{F}_0 \in \mathcal{R}_k$, there exists an integer I, and tensors $\boldsymbol{F}_i$, where $\{\lambda_i, \boldsymbol{F}_i\}_{i=1}^I$ satisfy (H_I), and such that

$$\boldsymbol{F}_0 = \sum_{i=1}^{I} \lambda_i \boldsymbol{F}_i, \text{ and } RW(\boldsymbol{F}_0) = \sum_{i=1}^{I} \lambda_i W(\boldsymbol{F}_i). \tag{5.2.27}$$

Moreover, $\boldsymbol{F}_i \in \mathcal{R}_0(W)$.

Proof:

The proof follows by repeated use of Section 5.2. We prove the result only for the case where $k = 2$. The proof for general k follows by an analogous argument. Thus, given $\boldsymbol{F}_0 \in \mathcal{R}_2$, we may write

$$RW(\boldsymbol{F}_0) = R_2 W(\boldsymbol{F}_0) = (1 - \mu_2) R_1 W(\boldsymbol{H}_1) + \mu_2 R_1 W(\boldsymbol{H}_2) \tag{5.2.28}$$

where $\operatorname{rank}(\boldsymbol{H}_1 - \boldsymbol{H}_2) \leqslant 1$, $\boldsymbol{F}_0 = (1 - \mu_2)\boldsymbol{H}_1 + \mu_2 \boldsymbol{H}_2$ *and* $\boldsymbol{H}_1, \boldsymbol{H}_2 \in \mathcal{R}_1$. *Applying Proposition 3 to $\boldsymbol{H}_1$ and $\boldsymbol{H}_2$ gives the existence of ν_1, ξ_1, $\boldsymbol{F}_1$, $\boldsymbol{F}_2$, $\boldsymbol{F}_3$ and $\boldsymbol{F}_4$ such that*

$$R_1 W(\boldsymbol{H}_1) = (1 - \nu_1) W(\boldsymbol{F}_1) + \nu_1 W(\boldsymbol{F}_2), \tag{5.2.29}$$

$$R_1 W(\boldsymbol{H}_2) = (1 - \chi_1) W(\boldsymbol{F}_3) + \chi_1 W(\boldsymbol{F}_4), \tag{5.2.30}$$

where $\operatorname{rank}(\boldsymbol{F}_1 - \boldsymbol{F}_2) \leqslant 1$, $\operatorname{rank}(\boldsymbol{F}_3 - \boldsymbol{F}_4) \leqslant 1$, $\boldsymbol{H}_1 = (1 - \nu_1)\boldsymbol{F}_1 + \nu_1 \boldsymbol{F}_2$, $\boldsymbol{H}_2 = (1 -$

$\xi_1)\boldsymbol{F}_3 + \xi_3\boldsymbol{F}_4$ *and* $\boldsymbol{F}_i \in \mathcal{R}_0$. *By taking*

$$\lambda_1 = (1-\mu_2)(1-\nu_1), \quad \lambda_2 = (1-\mu_2)\nu_1, \quad \lambda_3 = \mu_2(1-\chi_1), \quad \lambda_4 = \mu_2\chi_1, \quad (5.2.31)$$

we see that $\{\lambda_i, \boldsymbol{F}_i\}_{i=1}^4$ *satisfy* (H_4), *and Eq.* (5.2.27) *is satisfied.* □

5.3 Homogenization Framework for Hyperelastic Composites

In the context of periodic homogenization, upon fixing the standard Cartesian basis $\{\mathbf{e}_i\}$, we start by introducing the unit cell Y_0, which is composed of two homogeneous materials: a soft elastomeric matrix and stiffer elastomeric inclusion, denoted by phase 1 and 2, respectively. These materials are assumed to be in a stress-free state, and we fill $\mathbb{R}^3$ with a periodic repetition of Y_0, and from this infinite medium, we select some sufficiently large region Ω_0, which in the homogenization limit can be identified with a *representative volume element* (RVE) of the composite elastomer. If we let $\Omega_0^{(r)} \subset \Omega_0$ denote the regions occupied by phase r, then the distribution of the phases can be determined by the Y_0-periodically extended functions $\chi_0^{(r)}\,(r = 1, 2)$, where $\chi_0^{(r)}(\mathbf{X}) = 1$ if $\mathbf{X}$ lies in phase r and 0 otherwise. Moreover, we make use of the notation $\langle\cdot\rangle$ to denote volume averages over the RVE and assume that the initial volume fractions of the phases, $c^{(r)} = \left\langle \chi_0^{(r)} \right\rangle$, are known.

Next, we define the deformation $\mathbf{x} : \Omega_0 \to \Omega$ as a mapping from the undeformed configuration, Ω_0, to the deformed configuration, Ω. Such a deformation is characterized by the deformation gradient $\boldsymbol{F} = \operatorname{Grad}\mathbf{x}$. As to preserve material impenetrability, $\boldsymbol{F}$ is assumed to satisfy the constraint $\det \boldsymbol{F}(\mathbf{X}) > 0$ for every $\mathbf{X} \in \Omega_0$. The constitutive behavior of each phase is determined by *non-convex* stored-energy functions $W^{(r)}$. These functions are taken to be objective, so that $W^{(r)}(\boldsymbol{Q}\boldsymbol{F}) = W^{(r)}(\boldsymbol{F})$ for orthogonal $\boldsymbol{Q}$. Other technical hypotheses, including smoothness and boundedness

assumptions on $W^{(r)}$, will be discussed below.

The local stored-energy function of the hyperelastic composite can then be written as

$$W(\mathbf{X}, \boldsymbol{F}) = \chi_0^{(1)}(\mathbf{X})W^{(1)}(\boldsymbol{F}) + \chi_0^{(2)}(\mathbf{X})W^{(2)}(\boldsymbol{F}), \tag{5.3.1}$$

so that the local constitutive relation for the composite is given by

$$\boldsymbol{S} = \frac{\partial W}{\partial \boldsymbol{F}}(\mathbf{X}, \boldsymbol{F}), \tag{5.3.2}$$

where $\boldsymbol{S}$ denotes the first Piola-Kirchhoff stress tensor. We also define the local elasticity tensor of the composite by

$$\mathbb{L}(\mathbf{X}, \boldsymbol{F}) = \frac{\partial^2 W}{\partial \boldsymbol{F} \partial \boldsymbol{F}}(\mathbf{X}, \boldsymbol{F}). \tag{5.3.3}$$

It was Hill (1972) who first provided a definition of the effective behavior of hyperelastic composites by appealing to the principle of minimum potential energy. More robust definitions for hyperelastic composites with periodic microstructures, accounting for the non-convexity of the stored-energy functions, were developed by Braides (1985) and Müller (1987) making use of Γ-convergence. In particular, Müller (1987) obtained a representation formula for effective or homogenized stored-energy function $\widetilde{W}$. Thus, by letting

$$\widehat{W}_k(\overline{\boldsymbol{F}}) = \inf_{\boldsymbol{\varphi} \in W^{1,p}_{\#}(kY_0)} \frac{1}{|kY_0|} \int_{kY_0} W(\boldsymbol{Y}, \overline{\boldsymbol{F}} + \mathrm{Grad}\boldsymbol{\varphi}(\boldsymbol{Y}))d\boldsymbol{Y}, \quad k = 1, 2, ..., \tag{5.3.4}$$

it follows that, under certain technical hypotheses on the domain of definition, as well as coercivity and growth conditions on $W(\mathbf{X}, \cdot)$, the effective potential is given by

$$\widetilde{W}(\overline{\boldsymbol{F}}) = \inf_k \widehat{W}_k(\overline{\boldsymbol{F}}). \tag{5.3.5}$$

In the definition of $\widehat{W}_k$, $W^{1,p}_{\#}(kY_0)$ corresponds to the Sobolev space of weakly dif-

ferentiable functions with periodic boundary conditions on kY_0. As such, in order to calculate the effective potential, one must consider fluctuations about $\overline{\boldsymbol{F}}$ which are periodic over kY_0, for every value of k. The use of the Sobolev space allows for piecewise affine solutions that satisfy the equilibrium equations of hyperelasticity (in some appropriately weak sense).

Noting that $\langle \boldsymbol{F} \rangle = \overline{\boldsymbol{F}}$ is the average deformation gradient over the RVE, it follows from the above definition of $\widetilde{W}$ (assumed to be sufficiently smooth) that the macroscopic first Piola-Kirchhoff stress $\overline{\boldsymbol{S}} = \langle \boldsymbol{S} \rangle$ is given by

$$\overline{\boldsymbol{S}} = \frac{\partial \widetilde{W}}{\partial \overline{\boldsymbol{F}}}(\overline{\boldsymbol{F}}). \tag{5.3.6}$$

As $W(\mathbf{X}, \cdot)$ need not be convex in expressions (5.3.4) to (5.3.5), this definition of $\widetilde{W}$ allows for the possible development of "microscopic" instabilities, i.e. instabilities at wavelengths on the scale of the unit cell (Geymonat et al., 1993). Before the onset of any instability, the effective behavior of the composite can be fully characterized by the solution on the unit cell Y_0. We refer to the solution to Eq. (5.3.4) for $k = 1$ as the "principal" solution, and denote the corresponding effective potential as $\widehat{W} = \widehat{W}_1$. Upon the initiation of a microscopic instability, the principal solution, which is periodic on a single unit cell, gives way to solutions which are periodic on $N \times M \times L$ "super-cells" at sufficiently large deformations. Physically, this is due to the fact that solutions involving interactions between several unit cells may lead to lower macroscopic energies.

The theory also predicts the possible development of "macroscopic" instabilities corresponding to long-wavelength instabilities which are not periodic at finite wavelengths. As defined by Eq. (5.3.5), $\widetilde{W}$ is quasiconvex, and hence rank-1 convex. However, $\widetilde{W}$ need not be *strictly* rank-1 convex. Indeed, Geymonat et al. (1993) showed that long-wavelength instabilities, as indicated by the loss strong ellipticity of the incremental modulus $\widehat{\mathbb{L}}$ of the (one-cell periodic) principal solution $\widehat{W}$, lead to

the loss of strict rank-1 convexity of $\widetilde{W}$. By adopting rather strong hypotheses, the authors showed that the instability analysis, which was carried out on the linearized system (i.e. using the incremental moduli), would extend to the fully nonlinear setting. In other words, it was assumed that homogenization and linearization commute. It has been shown rigorously that commutability can hold in a neighborhood of $\overline{\boldsymbol{F}} = \boldsymbol{I}$ (Müller and Neukamm, 2011; Neukamm and Schäffner, 2018). For larger deformations, however, $\widehat{W}$ may not even remain rank-1 convex (Barchiesi and Gloria, 2010), in which case $\widehat{W}$ would only serve as an upper bound on $\widetilde{W}$. Moreover, there is no physically motivated reason to adopt the hypotheses used by Geymonat et al. (1993) to ensure commutability will hold for large deformations. Therefore, checking strict rank-1 convexity of $\widehat{W}$ directly should give a more reliable estimate for stability than using the tangent modulus tensor $\widehat{\mathbb{L}}$ associated with $\widehat{W}$ to check for loss of strong ellipticity (Avazmohammadi and Ponte Castañeda, 2016).

In order to avoid the possible development of instabilities within the homogeneous phases, we assume that the $W^{(r)}\,(r = 1, 2)$ are strictly polyconvex, and hence strongly elliptic. Nonetheless, these assumptions do not preclude the possibility of the aforementioned macroscopic instabilities of the composite, and a primary goal of this work is to describe the effective response of periodic hyperelastic laminates after the development of these macroscopic instabilities; this behavior will be referred to as the "post-bifurcation," or "relaxed" response. In general, it is not known *a priori* whether the critical wavelength corresponding to the initiation of the first instability will be finite or infinite; the former would indicate a microscopic instability, while the latter, a macroscopic instability. In fact, for the examples considered by Triantafyllidis and Maker (1985) and Geymonat et al. (1993), in the context of layered materials, it was shown that such a determination depends on the choice of material and geometric parameters (i.e., elasticities and volume fractions of the phases). Similar observations have been made for more general periodic elastomeric composites (Triantafyllidis et al., 2006; Michel et al., 2007, 2010; Bertoldi et al., 2008).

In what follows, we assume that the primary mode of instability will be macroscopic. For the laminated composites to be considered in this work, this is known to be the case when the volume fraction of the stiffer phase is sufficiently large (Triantafyllidis and Maker, 1985; Geymonat et al., 1993). We also remark that composites with *random* microstructures cannot accommodate microscopic instabilities, and hence all instabilities will be macroscopic (Lopez-Pamies and Ponte Castañeda, 2006a; Michel et al., 2007, 2010). Motivated by the findings of Furer and Ponte Castañeda (2018a), who considered laminated composites under plane strain loading conditions, we anticipate that the instability will then manifest itself via the formation of domains to accommodate the applied deformation; such domains will exist on a scale much larger than the unit cell, but still small compared to the composite itself. In order to estimate the macroscopic energy $\widetilde{W}$ in these cases, our approach, as proposed by Avazmohammadi and Ponte Castañeda (2016), is to calculate the quasiconvexification $Q\widehat{W}$ of the principal solution. Recall that $Q\widehat{W}$ is defined as the largest quasiconvex function less than or equal to $\widehat{W}$. When $\widehat{W}$ takes finite values, $Q\widehat{W}$ is given by (Dacorogna, 1989)

$$Q\widehat{W}(\overline{\boldsymbol{F}}) = \inf_{\boldsymbol{\varphi}\in W_0^{1,p}(D)} \frac{1}{D}\int_D \widehat{W}(\overline{\boldsymbol{F}} + \text{Grad}\boldsymbol{\varphi}(\boldsymbol{Y}))d\boldsymbol{Y}, \tag{5.3.7}$$

which is independent of the domain D. We mention that, in general, Eq. (5.3.7) is not guaranteed to hold when $\widehat{W}$ can be infinite. Nonetheless, under suitable growth conditions, Conti and Dolzmann (2015) showed that Eq. (5.3.7) is still valid for incompressible materials, i.e. for those materials which are finite so long as $\det \overline{\boldsymbol{F}} = 1$.

Since the homogenized energy $\widetilde{W}$ is quasiconvex, it follows by taking the quasiconvex envelopes of both sides of the inequality $\widetilde{W} \leqslant \widehat{W}$ that

$$\widetilde{W} \leqslant Q\widehat{W}. \tag{5.3.8}$$

In general, we are unaware of any rigorous results that would ensure equality to hold in Eq. (5.3.8). Certainly, since the quasiconvexification $Q\widehat{W}$ would not account for

periodic solutions on any super-cell, the inequality in Eq. (5.3.8) will be strict when the primary mode of instability is microscopic; in this case, neither $\widehat{W}$ nor $Q\widehat{W}$ can be used to describe the macroscopic behavior beyond the initiation of the instability, and the calculation of the effective energy must be carried out as in Eq. (5.3.5). On the other hand, assuming that the primary mode of instability is macroscopic, we anticipate that $Q\widehat{W}$ will give a very good, and in some cases exact, estimate of $\widetilde{W}$ (see Avazmohammadi and Ponte Castañeda, 2016, for some further arguments on this point). At the very least, the calculation of $Q\widehat{W}$ will still provide an upper bound on the effective energy $\widetilde{W}$ that is tighter than that given by $\widehat{W}$.

Unfortunately, the calculation of $Q\widehat{W}$ is, in general, also a very difficult problem. However, there is a well-established procedure (Ball, 1977; Kohn and Strang, 1986; Dacorogna, 1989) that, when it works, can lead to $Q\widehat{W}$ exactly. It is based on the inequalities

$$P\widehat{W} \leqslant Q\widehat{W} \leqslant R\widehat{W}, \tag{5.3.9}$$

where $R\widehat{W}$ and $P\widehat{W}$ are the rank-1 and polyconvex envelopes of $\widehat{W}$, respectively. The calculation of $R\widehat{W}$ is facilitated by the well-known formula of Kohn and Strang (1986), and involves the iterative use of a generalized lamination procedure. Once $R\widehat{W}$ is computed, if we can show that $R\widehat{W}$ is polyconvex, it would follow that $R\widehat{W} = Q\widehat{W}$. Even if $R\widehat{W}$ is not polyconvex, it would still provide an upper bound for $Q\widehat{W}$. In this context, it is important to recall that Eq. (5.3.9) holds strictly when $\widehat{W}$ takes finite values. In the setting on incompressibility, it is possible for $\widehat{W}$ to take infinite values, but this only occurs if $\det \overline{\boldsymbol{F}} \neq 1$. Nonetheless, it has been shown that quasiconvex functions incorporating volumetric constraints are still rank-1 convex (Conti, 2008). Therefore, the inequalities (5.3.9) for computing $Q\widehat{W}$ still hold for incompressible materials.

5.4 Concluding Remarks

This chapter laid the groundwork for the next two chapters to come. Many of the theorems and definitions stated here will be utilized quite often, and it was therefore helpful summarize them separately. On the other hand, as we saw, by making use of the methodology for obtaining the post-bifurcation by way of calculating the rank-one convexification, we were able to prove that the quasiconvexification corresponds to the formation of domains, within which the average deformation is stable. It will therefore be of interest to confirm this finding when we apply our methodology.

Chapter 6

Application to Neo-Hookean Hyperelastic Laminates Under Plane-Strain Loading Conditions

Abstract

This work is concerned with the characterization of the macroscopic response of soft elastomeric composites following the onset of 'macroscopic' (long wavelength) instabilities. For this purpose, the special case of laminated composites made of two neo-Hookean phases of different stiffnesses subjected to plane strain loading is considered. Indeed, it is known that the macroscopic response of such elastic composites can lose strong ellipticity when the stiff layers are subjected to sufficiently high compressive loads and their volume fraction is large enough. However, their post-bifurcation response is not yet known. Here it will be shown that the laminates can in fact lose (global) strict rank-one convexity, and do so well before losing (local) strong ellipticity. This will be accomplished by first constructing the rank-one convexification of the 'principal' solution for the stored-energy function at finite strains. It will then be shown that the rank-one convexification of the energy is polyconvex, and therefore corresponds to the quasiconvexification or 'relaxation' of the energy. Consequently, the post-bifurcation response corresponds to the formation of lamellar or 'striped' domains, which, in turn, gives rise to 'soft modes' of deformation. One important implication of this work for more general soft elastic composites is that the commonly accepted practice of using loss of strong ellipticity to predict the onset of macroscopic instabilities can significantly overestimate their

stability. Instead, the relaxation of the energy should be computed in order to get more accurate (and conservative) estimates for their macroscopic stability, as well as the correct post-bifurcation response.

6.1 Introduction

Reinforced elastomers are commonplace in numerous applications from tires and conveyor belts to hoses and couplings. Examples include carbon-black-filled elastomers, fiber-reinforced elastomers, fabric-reinforced rubbers and thermoplastic elastomers (TPEs). Due to the pervasiveness of these and other elastomeric composites, it is important to develop homogenization methods to describe their macroscopic constitutive response accounting for the properties of their constituent phases and their distribution, or microstructure. However, the characterization of such macroscopic or homogenized behavior is complicated by the possible development of instabilities, including microbuckling (Rosen, 1965). Moreover, it has been recognized recently that these instabilities can be harnessed in numerous other applications, such as for the development of artificial muscles in robotic applications, and for band-gap materials in acoustic applications. Our objective in this work is to investigate the instabilities and 'post-bifurcation' response of elastomeric composites in the simplest possible context of neo-Hookean laminated elastomers, for which exact analytical estimates are available for the 'pre-bifurcation' response.

The study of nonlinear elastic composites can be traced back to the work of Hill (1972), who advanced a theoretical framework for estimating the macroscopic response of such composites in the finite-strain regime, generalizing earlier work for infinitesimal strains. Building on this, Odgen (1978) proposed a variational formulation and generated Voigt-type upper bounds for the macroscopic stored-energy function of hyperelastic composites. This author also proposed Reuss-type lower bounds based on a complementary energy principle that made use of rather strong convexity assumptions for the stored-energy functions of the phases. However, the stored-energy

functions in (nonlinear) hyperelasticity are generally non-convex, in particular, due to the physical requirements of objectivity and incompressibility. By appealing to generalized notions of convexity, such as polyconvexity (see next section for detailed definitions), Ball (1977) was able to consider more realistic constitutive assumptions and developed mathematically rigorous variational formulations for hyperelasticity. In later work, Triantafyllidis and Maker (1985) considered hyperelastic laminates with periodic microstructures and showed that such composites can undergo 'microscopic' (finite wavelength) and 'macroscopic' (infinite wavelength) instabilities. In addition, they showed that the latter instabilities correspond to the loss of ellipticity of the homogenized macroscopic response of the laminates. Braides (1985) and Müller (1987) made use of Γ-convergence to generate variational expressions for the homogenized stored-energy function under realistic (non-convex) constitutive hypotheses for the constituent phases, thereby allowing for the possible development of such instabilities in periodic hyperelastic composites. Also, improved bounds on the homogenized stored-energy function of hyperelastic composites have been obtained by Ponte Castañeda (1989) by exploiting the notion of polyconvexity.

A systematic investigation of the possible development of instabilities in hyperelastic composites with *periodic* microstructures has been carried out by Geymonat et al. (1993). By consideration of the *incremental* (linearized) problem for the homogenized energy, criteria were developed for the possible onset of microscopic instabilities, where the one-cell periodic solution near the undeformed configuration gives way to lower energy multi-cell solutions. Consistent with the results obtained by Triantafyllidis and Maker (1985) for laminates, it was also found that the long wavelength (macroscopic) instabilities, corresponding to solutions involving large (infinite) numbers of cells, could often occur before the microscopic instabilities and are captured by loss of ellipticity of the homogenized constitutive relation (Triantafyllidis et al., 2006; Michel et al., 2007). For composites with *random* microstructures, there are no corresponding simplifications for calculating the effective behavior vis-a-vis the

unit cell problem in the periodic case, and the theory concerning instabilities is less developed. However, it was argued by Lopez-Pamies and Ponte Castañeda (2006a,b) that, while microscopic instabilities cannot be supported in such random systems, macroscopic instabilities can still be detected by loss of ellipticity of the homogenized response.

The question then becomes what is the post-bifurcation homogenized response beyond such macroscopic instabilities—and how to compute it? Recently, Avazmohammadi and Ponte Castañeda (2016) proposed a strategy to address this question. In this context, it is recalled (Geymonat et al., 1993) that the homogenized stored-energy function is quasiconvex and therefore rank-one convex, but not necessarily strictly so. Therefore, the possible development of macroscopic instabilities is related to loss of *strict* rank-one convexity. Given an estimate for the homogenized energy before the onset of a macroscopic instability, which we will refer to here as the 'principal' solution, a corresponding estimate for the post-bifurcation response can be obtained by computing the quasiconvexification of the principal estimate for the energy, which we will refer to here as the 'relaxation.' Thus, Avazmohammadi and Ponte Castañeda (2016) made use of the homogenization estimates of Lopez-Pamies and Ponte Castañeda (2006a,b) for the principal solution for the energy of elastomers reinforced by random distributions of aligned elliptical rigid fibers to obtain the corresponding relaxation by first computing the rank-one convexification, and then showing that it is polyconvex. This type of construction was pioneered by Ball and James (1987) to describe solid-solid phase transformations in martensitic materials (see also Bhattacharya, 2003). For the particular case considered by Avazmohammadi and Ponte Castañeda (2016), the rank-one convexification turns out to be a simple laminate, consisting of layers of the original composite material with alternating orientation of the fibers. Thus, these authors provided an example where the post-bifurcation response involved the formation of (lamellar) domains. Lamellar domains have also been predicted theoretically (DeSimone and Dolzmann, 2000;

Conti et al., 2002) in the context of liquid crystal elastomers, though the macroscopic response of these materials is quite different. An important observation from the work of Avazmohammadi and Ponte Castañeda (2016) is that macroscopic instabilities may develop well before loss of (local) strong ellipticity, due to loss of *global* strict rank-one convexity.

However, the example of Avazmohammadi and Ponte Castañeda (2016) made use of an *approximation* for the homogenized (principal) response of the elastomer reinforced by short fibers. In this work, we consider neo-Hookean laminates, for which deBotton (2005) has provided an *exact analytical* estimates for the homogenized (principal) response. As already mentioned, such hyperelastic laminates with periodic microstructures are also found to undergo macroscopic instabilities and, furthermore, these instabilities are triggered before any microscopic instabilities when the volume fraction and stiffness of the stiffer phase are sufficiently large (Triantafyllidis and Maker, 1985; Geymonat et al., 1993). Therefore, they provide an ideal test case for the application of the above-mentioned strategy (Avazmohammadi and Ponte Castañeda, 2016) to generate estimates for the 'relaxed' energy describing the post-bifurcation response beyond the onset of such macroscopic instabilities. Assuming for simplicity plane strain loading conditions, in Section 6.2 we proceed with the calculation of the 'principal' solution for neo-Hookean laminates, and discuss the conditions under which instabilities for this specific material model occur. In Section 6.3, the relaxation is derived by first computing the rank-one convexification, and then by showing that it is polyconvex—so that it corresponds to the quasiconvexification of the energy. Finally, we conclude in Section 6.4 by showing some explicit results for specific values of the various microstructural parameters (i.e. volume fraction, heterogeneity contrast) to display, in particular, the 'soft modes of deformation' associated with the relaxed solution, as well as by making comparisons with appropriate bounds.

Here we make use of standard notation in the continuum mechanics literature, and let $d = 2$ or $d = 3$ be the dimension of the space, so that $\mathbb{R}^d$ is the usual real

$d-$dimensional space. We fix the standard Cartesian basis $\{\mathbf{e}_i\}$, with respect to which vectors with Cartesian components a_i or A_i are represented by bold letters $\mathbf{a}$ or $\mathbf{A}$, respectively. Second-order tensors with Cartesian components F_{ij} are represented by bold italic letters $\boldsymbol{F}$, while fourth-order tensors with Cartesian components L_{ijkl} are denoted by barred letters $\mathbb{L}$. Here i, j, k, l range from 1 to d. The Einstein summation convention will be utilized, so that repeated indices are summed over. For example, the product $\boldsymbol{F}\mathbf{X}$ has Cartesian components $F_{ij}X_j$. Given two vectors $\mathbf{a}, \mathbf{b}$, the quantity $\mathbf{a}\otimes\mathbf{b}$ is defined to be in second-order tensor with Cartesian components $a_i b_j$. We denote by Lin (Lin^+) the set of all second-order tensors (with positive determinant).

6.2 Neo-Hookean laminates under plane-strain (2D) conditions

Here, we consider a simple laminate consisting of two phases, which are layered periodically in a direction with unit normal $\mathbf{N}_0$, in prescribed volume fractions $c^{(r)}$ $(r = 1, 2)$. For simplicity, the phases are assumed to be incompressible Neo-Hookean materials, with stored-energy functions of the form

$$W^{(r)}(\boldsymbol{F}) = \frac{\mu^{(r)}}{2}\text{tr}(\boldsymbol{F}^T\boldsymbol{F} - \boldsymbol{I}) + K(\det \boldsymbol{F}), \tag{6.2.1}$$

where $\mu^{(r)} > 0$ represents the shear modulus of phase r, and where

$$K(J) = \begin{cases} 0, & J = 1, \\ \infty & \text{otherwise} \end{cases} \tag{6.2.2}$$

serves to enforce the incompressibility constraint. In addition, we restrict ourselves to plane strain loading conditions, so that $d = 2$ and the deformation gradient $\boldsymbol{F} \in \text{Lin}^+$ has Cartesian components (with respect to the laboratory coordinates defined by

$\{\mathbf{e}_i\}$)

$$[F_{ij}] = \begin{bmatrix} F_{11} & F_{12} \\ F_{21} & F_{22} \end{bmatrix}. \tag{6.2.3}$$

While it is generally very difficult to derive analytical expressions for the effective macroscopic behavior of hyperelastic composites, for the special case of laminated materials it is possible to derive, using a lamination formula similar to Eq. (5.2.26), the following expression, due to deBotton (2005), for the 'principal' solution for the homogenized stored-energy function:

$$\widehat{W}(\overline{\boldsymbol{F}}) = \frac{\overline{\mu}}{2}\mathrm{tr}(\overline{\boldsymbol{F}}^T\overline{\boldsymbol{F}} - \boldsymbol{I}) + \frac{\breve{\mu} - \overline{\mu}}{2}\frac{\left[(\overline{\boldsymbol{F}}\mathbf{N}_0)\cdot(\overline{\boldsymbol{F}}\mathbf{M}_0)\right]^2}{|\overline{\boldsymbol{F}}\mathbf{M}_0|^2} + K(\det\overline{\boldsymbol{F}}), \tag{6.2.4}$$

where $\mathbf{M}_0$ is a unit vector orthogonal to $\mathbf{N}_0$ ($\mathbf{N}_0 \cdot \mathbf{M}_0 = 0$) in the plane of the deformation, and

$$\overline{\mu} = c^{(1)}\mu^{(1)} + c^{(2)}\mu^{(2)} \quad \text{and} \quad \breve{\mu} = \left(\frac{c^{(1)}}{\mu^{(1)}} + \frac{c^{(2)}}{\mu^{(2)}}\right)^{-1} \tag{6.2.5}$$

represent, respectively, the arithmetic and harmonic means of the phase shear moduli.

By making use of the following alternative form of this estimate for $\widehat{W}$,

$$\widehat{W}(\overline{\boldsymbol{F}}) = \frac{\breve{\mu}}{2}|\overline{\boldsymbol{F}}\mathbf{N}_0|^2 + \frac{\overline{\mu}}{2}\left(|\overline{\boldsymbol{F}}\mathbf{M}_0|^2 - 2\right) + \frac{\overline{\mu} - \breve{\mu}}{2}\frac{1}{|\overline{\boldsymbol{F}}\mathbf{M}_0|^2} + K(\det\overline{\boldsymbol{F}}), \tag{6.2.6}$$

a straightforward calculation then shows that the average Cauchy stress $\overline{\boldsymbol{T}} = \overline{\boldsymbol{S}}\,\overline{\boldsymbol{F}}^T$ is given by

$$\overline{\boldsymbol{T}} = \breve{\mu}\left(\overline{\boldsymbol{F}}\mathbf{N}_0\right)\otimes\left(\overline{\boldsymbol{F}}\mathbf{N}_0\right) + \overline{\mu}\left(\overline{\boldsymbol{F}}\mathbf{M}_0\right)\otimes\left(\overline{\boldsymbol{F}}\mathbf{M}_0\right) - \frac{\overline{\mu} - \breve{\mu}}{|\overline{\boldsymbol{F}}\mathbf{M}_0|^4}\left(\overline{\boldsymbol{F}}\mathbf{M}_0\right)\otimes\left(\overline{\boldsymbol{F}}\mathbf{M}_0\right) - p\boldsymbol{I}, \tag{6.2.7}$$

where p is an arbitrary hydrostatic pressure.

Next, we consider the application of the strong ellipticity condition in the context of expression (5.2.12) for the *incompressible* laminate with stored-energy function $\widehat{W}$.

Thus, following Ogden (1997), strong ellipticity at $\overline{\boldsymbol{F}}$ requires that

$$\widehat{L}^{c}_{ijkl}(\overline{\boldsymbol{F}})m_i n_j m_k n_l = \bar{F}_{jp}\bar{F}_{lq}\frac{\partial^2 \widehat{W}}{\partial \bar{F}_{ip}\partial \bar{F}_{kq}}(\overline{\boldsymbol{F}})m_i n_j m_k n_l > 0, \tag{6.2.8}$$

for all non-zero unit vectors $\mathbf{m}$ and $\mathbf{n}$ such that $\mathbf{m}\cdot\mathbf{n} = 0$, which can be shown to reduce to

$$\breve{\mu}\left[(\overline{\boldsymbol{F}}\mathbf{N}_0)\cdot\mathbf{n}\right]^2 + \overline{\mu}\left[(\overline{\boldsymbol{F}}\mathbf{M}_0)\cdot\mathbf{n}\right]^2 - (\overline{\mu}-\breve{\mu})\frac{\left[(\overline{\boldsymbol{F}}\mathbf{M}_0)\cdot\mathbf{n}\right]^2}{|\overline{\boldsymbol{F}}\mathbf{M}_0|^4}\left\{1 - 4\frac{\left[(\overline{\boldsymbol{F}}\mathbf{M}_0)\cdot\mathbf{m}\right]^2}{|\overline{\boldsymbol{F}}\mathbf{M}_0|^2}\right\} > 0. \tag{6.2.9}$$

For simplicity, we assume that $\mathbf{N}_0$ is aligned with $\mathbf{e}_1$ while $\mathbf{M}_0$ is aligned with $\mathbf{e}_2$, where it is recalled that $\{\mathbf{e}_1, \mathbf{e}_2\}$ provide a Cartesian basis in the plane of the deformation, and introduce (Avazmohammadi and Ponte Castañeda, 2016) the plane strain invariants α and γ defined by

$$\alpha = \sqrt{\frac{I_4}{\bar{J}}}, \quad \text{and} \quad \gamma = \begin{cases} \sqrt{\frac{I_1}{\bar{J}} - \frac{I_4}{\bar{J}} - \frac{\bar{J}}{I_4}} & \overline{F}_{11}\overline{F}_{12} + \overline{F}_{21}\overline{F}_{22} \geqslant 0, \\ -\sqrt{\frac{I_1}{\bar{J}} - \frac{I_4}{\bar{J}} - \frac{\bar{J}}{I_4}} & \overline{F}_{11}\overline{F}_{12} + \overline{F}_{21}\overline{F}_{22} \leqslant 0, \end{cases} \tag{6.2.10}$$

where $I_1 = \mathrm{tr}(\overline{\boldsymbol{F}}^T\overline{\boldsymbol{F}})$, $I_4 = |\overline{\boldsymbol{F}}\mathbf{N}_0|^2$ and $\bar{J} = \det(\overline{\boldsymbol{F}}) > 0$ are the corresponding classical invariants. Then, using objectivity and incompressibility, and without loss of generality, we can restrict our attention to deformation gradients of the form

$$\left[\overline{F}_{ij}\right] = \begin{bmatrix} \alpha & \gamma \\ 0 & \alpha^{-1} \end{bmatrix}, \tag{6.2.11}$$

so that $\bar{J} = 1$ and expression (6.2.4) for $\widehat{W}$ can be rewritten, in terms of α and γ, in the form

$$\widehat{W}(\overline{\boldsymbol{F}}) = \widehat{\Psi}(\alpha,\gamma) = \frac{\breve{\mu}}{2}\alpha^2 + \frac{\overline{\mu}}{2}\left(\gamma^2 + \alpha^{-2} - 2\right) + \frac{\overline{\mu}-\breve{\mu}}{2}\left(\frac{\alpha^2}{1+\alpha^2\gamma^2}\right). \tag{6.2.12}$$

Now, for the special case of pure shear loading ($\gamma = 0$), the critical stretch α_{se} at which the composite first loses strong ellipticity (SE) is found to be given by

$$\alpha_{se} = \left(1 - \frac{\breve{\mu}}{\overline{\mu}}\right)^{-1/4}, \tag{6.2.13}$$

which agrees exactly with the result of Triantafyllidis and Maker (1985). More generally, Eq. (6.2.9) can be used to show that $\widehat{W}$ satisfies the SE condition in the region $\mathcal{S}_{se}$, defined by

$$\mathcal{S}_{se} = \{\, (\alpha, \gamma) \in (0, \infty) \times \mathbb{R} \,:\, \alpha < \alpha_{se} \text{ or } \alpha \geqslant \alpha_{se} \text{ and } |\gamma| > \gamma_{se}\}, \tag{6.2.14}$$

where γ_{se} can be obtained, as a function of α, from the solution of an explicit equation, which is omitted here due to its complexity and length.

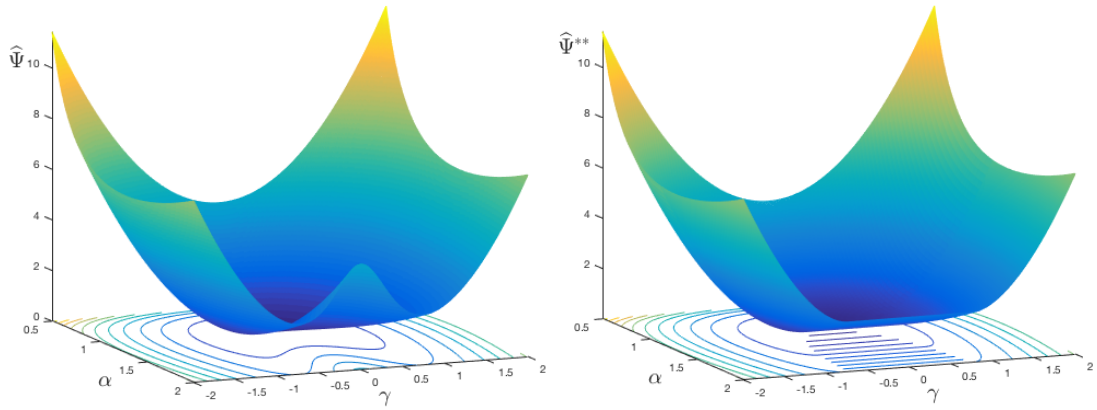

(a) (b)

Figure 6.1: A three-dimensional depiction of the energy landscapes for the (a) 'principal' and (b) 'relaxed' solutions for a fixed volume fraction of $c = c^{(2)} = 0.3$ and contrast of $\mu^{(2)}/\mu^{(1)} = 10$. Corresponding curves of α vs. γ along which the 'principal' solution loses both strong ellipticity and global (strict) rank-one convexity for varying (c) contrasts and (d) volume fractions.

In order to visualize the 'principal' solution for the energy function, we show in Figure 6.1a plots of $\widehat{\Psi}$, as defined by (6.2.12) in terms of the variables α and γ, for a

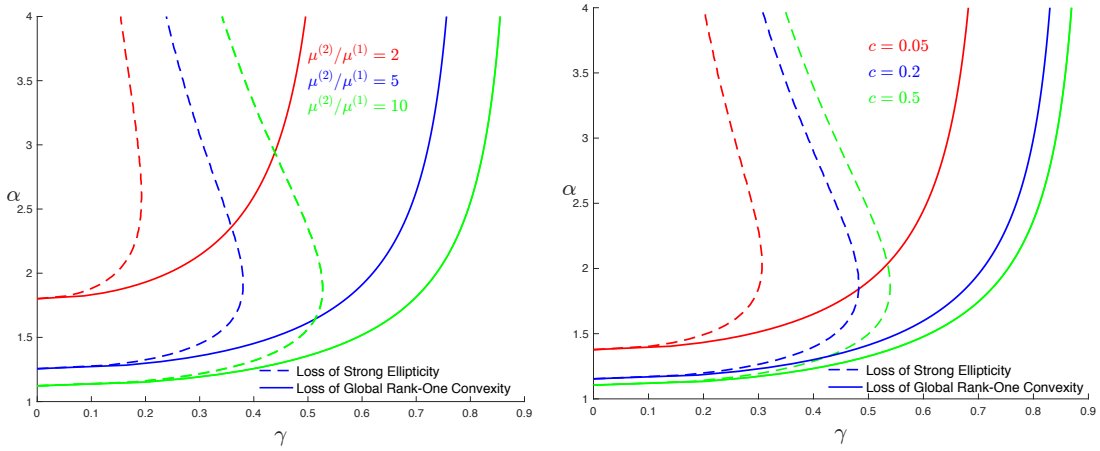

(c) (d)

fixed volume fraction of $c = c^{(2)} = 0.3$ and contrast of $\mu^{(2)}/\mu^{(1)} = 10$. It is observed that $\widehat{\Psi}$ exhibits a 'crease' in the vicinity of the $\gamma = 0$ axis for $\alpha > \alpha_{se}$, where it can be seen to lose convexity as a function of γ (for fixed α). Correspondingly, Figure 6.1c and Figure 6.1d show (in dashed lines) plots of the onset of loss of strong ellipticity, which occurs according to expression (6.2.14) when $\alpha \geqslant \alpha_{se}$ and $|\gamma| = \gamma_{se}$, for different values of the moduli contrast and volume fractions, respectively. (The continuous lines in Figure 6.1c and Figure 6.1d will be discussed further below in connection with Figure 6.1b). Interestingly, we can see that the loss of strong ellipticity takes place within the creased region, suggesting that the loss of rank-one convexity of $\widehat{W}$ should be related to the loss of convexity of $\widehat{\Psi}$ in the variables α and γ characterizing the class of isochoric deformations.

6.3 Relaxation

As discussed earlier, our goal here is the calculation of the quasiconvexification $Q\widehat{W}$ of the 'principal' solution $\widehat{W}$, which, at a minimum, will provide an upper bound on the homogenized potential $\widetilde{W}$, and, in some cases, may even correspond exactly to $\widetilde{W}$. In turn, the calculation of $Q\widehat{W}$ will proceed in two steps: we will first compute

$R\widehat{W}$ and then show that it is polyconvex. It should be recalled in this context that while $\widehat{W}$ can take infinite values due to incompressibility constraint $\det \boldsymbol{F} = 1$ in (6.2.6), Conti (2008) has shown that quasiconvex functions with constraints on the determinant are rank-one convex, and therefore the inequalities $P\widehat{W} \leqslant Q\widehat{W} \leqslant R\widehat{W}$ implicit in the above argument for computing $Q\widehat{W}$ still hold.

We will calculate $R\widehat{W}$ by making use of Eq. (5.2.26) for $R_k\widehat{W}$ for $k = 1$, 2, etc.. Since we do not know, *a priori*, how many iterations will need to be performed, we will check, for each k, whether or not $R_k\widehat{W}$ is in fact rank-one convex. Because our underlying functions are smooth enough, this is accomplished by checking the *Legendre-Hadamard* condition (5.2.12) as it pertains to $R_k\widehat{W}$. Once we find a k for which $R_k\widehat{W}$ is in fact rank-one convex, we can conclude that $R_k\widehat{W} = R\widehat{W}$. Thus, we start by computing $R_1\widehat{W}$ from Eq. (5.2.26) with $k = 1$. However, because of incompressibility, $\widehat{W}(\overline{\boldsymbol{F}})$ returns an infinite value for $\overline{\boldsymbol{F}}$ with $\det \overline{\boldsymbol{F}} \neq 1$, and, as noted by deBotton (2005), we can restrict our attention to values of $\mathbf{a}$ and $\mathbf{N}_1$ in the infimum such that

$$1 = \det(\overline{\boldsymbol{F}} - c_1 \mathbf{a} \otimes \mathbf{N}_1) = \det \overline{\boldsymbol{F}} \det(\boldsymbol{I} - c_1 \overline{\boldsymbol{F}}^{-1} \mathbf{a} \otimes \mathbf{N}_1) = (1 - c_1 \overline{\boldsymbol{F}}^{-1} \mathbf{a} \cdot \mathbf{N}_1), \quad (6.3.1)$$

implying that $\overline{\boldsymbol{F}}^{-1}\mathbf{a} \perp \mathbf{N}_1$. Therefore, upon defining $\omega_1 = |\overline{\boldsymbol{F}}^{-1}\mathbf{a}|$ and $\mathbf{M}_1 = \frac{1}{\omega_1}\overline{\boldsymbol{F}}^{-1}\mathbf{a}$, we obtain the result that

$$\begin{aligned} R_1\widehat{W}(\overline{\boldsymbol{F}}) = \inf_{\omega_1, c_1, \mathbf{N}_1} \Big\{ & (1 - c_1)\widehat{W}(\overline{\boldsymbol{F}}[\boldsymbol{I} - c_1\omega_1 \mathbf{M}_1 \otimes \mathbf{N}_1]) \\ & + c_1 \widehat{W}(\overline{\boldsymbol{F}}[\boldsymbol{I} + (1 - c_1)\omega_1 \mathbf{M}_1 \otimes \mathbf{N}_1]) \Big\}, \end{aligned} \quad (6.3.2)$$

where $\mathbf{N}_1 \cdot \mathbf{M}_1 = 0$. Moreover, because of the assumption of plane strain conditions, we can take $\mathbf{N}_1 = [\cos\varphi, \sin\varphi]^T$, so that $\mathbf{M}_1 = [\sin\varphi, -\cos\varphi]^T$. Then, the expression for $R_1\widehat{W}$ reduces to a three-dimensional minimization problem in the scalar variables

ω_1, c_1 and φ:

$$R_1\widehat{W}(\overline{\boldsymbol{F}}) = \inf_{\omega_1,c_1,\varphi}\Big\{(1-c_1)\widehat{W}(\overline{\boldsymbol{F}}[\boldsymbol{I}-c_1\omega_1\mathbf{M}_1\otimes\mathbf{N}_1]) \\ +c_1\widehat{W}(\overline{\boldsymbol{F}}[\boldsymbol{I}+(1-c_1)\omega_1\mathbf{M}_1\otimes\mathbf{N}_1])\Big\}. \tag{6.3.3}$$

The stationary conditions corresponding the infimum in Eq. (6.3.3) can be solved explicitly, and we find that

$$\omega_1 = -\frac{2\gamma_{rc}}{\alpha} \qquad c_1 = \frac{1}{2}\left(1-\frac{\gamma}{\gamma_{rc}}\right), \qquad \varphi = \frac{\pi}{2}, \tag{6.3.4}$$

where

$$\gamma_{rc}(\alpha) = \pm\alpha^{-1}\sqrt{\left(\frac{\alpha}{\alpha_{se}}\right)^2 - 1} \tag{6.3.5}$$

is associated with the condition that

$$\frac{\partial\widehat{\Psi}}{\partial\gamma}(\alpha,\gamma_{rc}(\alpha)) = 0. \tag{6.3.6}$$

Thus, we find that, for a fixed $\alpha \geqslant \alpha_{se}$, γ_{rc} corresponds to the location of the local minima of the corresponding cross-section of the function $\widehat{\Psi}$ in Figure 6.1a. In addition, as depicted in Figure 6.1, $R_1\widehat{W}$ physically corresponds to a simple laminate of two identical (anisotropic) phases, with the same energy function $\widehat{W}$, but with alternating orientations. Moreover, the 'mesolayers' in this laminate have volume fractions c_1 and $1-c_1$ and are layered in the direction normal to $\mathbf{N}_1$. Recalling that the minimizing angle above is $\varphi = \frac{\pi}{2}$, we can see that $\mathbf{N}_1\cdot\mathbf{N}_0 = 0$, so that the layering direction (in the reference configuration) in the rank-one lamination $R_1\widehat{W}$ is orthogonal to the layering direction in the original laminate (i.e., $\mathbf{N}_1 = \mathbf{M}_0$).

It is also important to note that the average deformation gradient within the mesolayers of type I and II, as given by $\overline{\boldsymbol{F}}^{(I)} = \overline{\boldsymbol{F}}[\boldsymbol{I}-c_1\omega_1\mathbf{M}_1\otimes\mathbf{N}_1]$ and $\overline{\boldsymbol{F}}^{(II)} =$

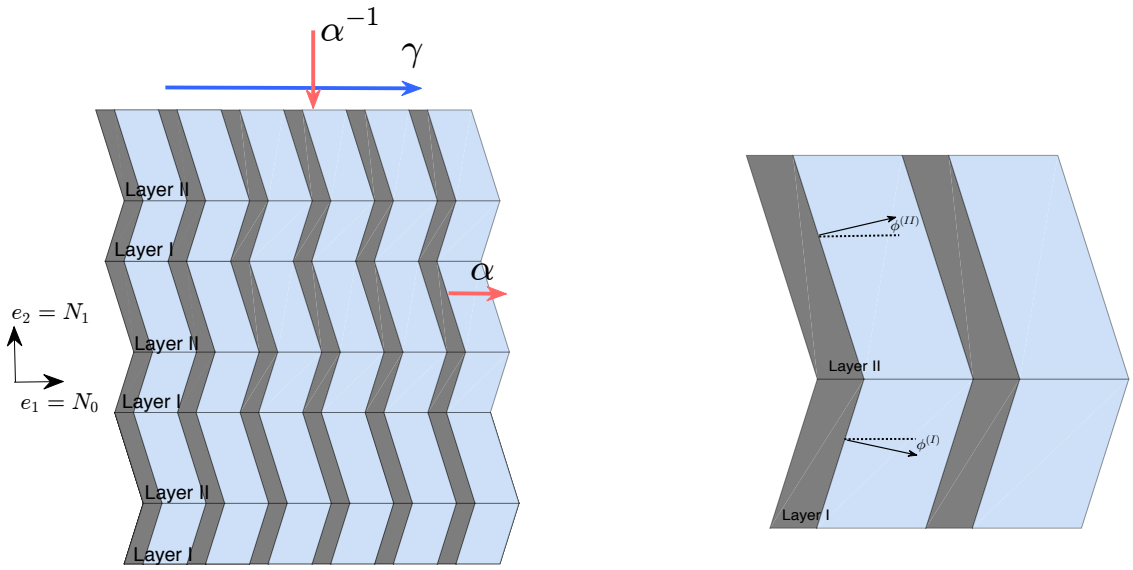

(a) (b)

Figure 6.1: A schematic for how the rank-one convex lamination procedure produces the 'mesolayers'. (a) Under the application of compression and shear, the composite breaks up into 'mesolayers' to accommodate the deformation. (b) With each layer, the original phases are subjected to a deformation which rotates these phases by an amount of $\phi^{(I)}$ or $\phi^{(II)}$.

$\overline{\boldsymbol{F}}[\boldsymbol{I} + (1-c_1)\omega_1 \mathbf{M}_1 \otimes \mathbf{N}_1]$ in Eq. (6.3.2), have Cartesian components of the form

$$\left[\bar{F}_{ij}^{(I,II)}\right] = \begin{bmatrix} \alpha & \pm\gamma_{rc} \\ 0 & \alpha^{-1} \end{bmatrix}, \tag{6.3.7}$$

and are therefore independent of γ. In addition, recalling (Lopez-Pamies and Ponte Castañeda, 2009) that the rotation of the layers in a hyperelastic laminate is controlled by Nanson's relation, it follows that the rotation of the mesolayers of type I and II in the rank-one lamination $R_1\widehat{W}$ is determined by $(\overline{\boldsymbol{F}}^{(I)})^{-T}\mathbf{N}_0$ and $(\overline{\boldsymbol{F}}^{(II)})^{-T}\mathbf{N}_0$, respectively. In the plane of the deformation, this corresponds to rotations by angles $\phi^{(I)}$ and $\phi^{(II)}$, respectively, as depicted in Figure 6.1b.

Next, observing from Eq. (6.3.4) that $c_1 = 0$ when $\gamma = \pm\gamma_{rc}$, so that $R_1\widehat{W} = \widehat{W}$

at $\gamma = \pm\gamma_{rc}$, it follows that, in fact,

$$R_1\widehat{W}(\overline{\boldsymbol{F}}) = \widehat{\Psi}^{**}(\alpha, \gamma), \tag{6.3.8}$$

where $\widehat{\Psi}^{**}$ is the convexification of the function $\widehat{\Psi}$, defined by (6.2.12), and is given by

$$\widehat{\Psi}^{**}(\alpha, \gamma) = \begin{cases} \widehat{\Psi}(\alpha, \gamma), & \text{when } (\alpha, \gamma) \in \mathcal{S}_{rc}, \\ \frac{\breve{\mu}}{2}\alpha^2 + \overline{\mu}(\alpha_{se}^{-2} - 1), & \text{when } (\alpha, \gamma) \in \mathcal{S}_{rc}^c, \end{cases} \tag{6.3.9}$$

with

$$\mathcal{S}_{rc} = \{\, (\alpha, \gamma) \in (0, \infty) \times \mathbb{R} \,:\, \alpha < \alpha_{se} \text{ or } \alpha \geqslant \alpha_{se} \text{ and } |\gamma| > \gamma_{rc}\}, \tag{6.3.10}$$

so that $\mathcal{S}_{rc}^c$ corresponds to the set of values of α and γ where the function $\widehat{\Psi}$ is no longer globally convex. Note that, as a consequence, $R_1\widehat{W}$ is independent of γ for $\overline{\boldsymbol{F}} \in \mathcal{S}_{rc}^c$, and that

$$\mathcal{S}_{rc} \subset \mathcal{S}_{se}. \tag{6.3.11}$$

Having obtained an analytical expression for $R_1\widehat{W}$ in terms of $\overline{\boldsymbol{F}}$, it is easy to show that $R_1\widehat{W}$ is globally rank-one convex, and must therefore be equal to the rank-one convex envelope of $\widehat{W}$. To see this, we first consider the case where $\overline{\boldsymbol{F}} \in \mathcal{S}_{rc}$, so that, from expressions (6.3.8) and (6.3.9), $R_1\widehat{W} = \widehat{W}$. In addition, it follows from the inclusion (6.3.11) that $\widehat{W}$—and therefore $R_1\widehat{W}$—must satisfy the (SE) condition in $\mathcal{S}_{rc}$, ensuring that $R_1\widehat{W}$ satisfies the Legendre-Hadamard condition and is thus locally rank-one convex (in fact, strictly so) everywhere inside $\mathcal{S}_{rc}$. Next, we consider the case where $\overline{\boldsymbol{F}} \in \mathcal{S}_{rc}^c$. Using the chain rule in expression $(6.3.9)_2$, together with expression $(6.2.10)_1$, it can be shown that, for $\overline{\boldsymbol{F}} \in \mathcal{S}_{rc}^c$,

$$\overline{F}_{jp}\overline{F}_{lq}\frac{\partial^2 R_1\widehat{W}(\overline{\boldsymbol{F}})}{\partial \overline{F}_{ip}\partial \overline{F}_{kq}} m_i n_j m_k n_l = \breve{\mu}\left[(\overline{\boldsymbol{F}}\mathbf{N}_0)\cdot\mathbf{n}\right]^2 \geqslant 0, \tag{6.3.12}$$

and hence $R_1\widehat{W}$ is *locally* rank-one convex for every $\overline{\boldsymbol{F}}$, implying that it is *globally* rank-one convex, so that $R_1\widehat{W} = R\widehat{W}$. Thus, as depicted in Figure 6.1b, the rank-one convex envelope of $\widehat{W}$ (which will be shown shortly to be identical to the quasiconvexification $Q\widehat{W}$) corresponds to the convexification of the function $\hat{\Psi}$ (in the variables α and γ). However, we note that while $R\widehat{W}$ is *globally* rank-one convex, it is not strongly elliptic, as can be seen by taking $\mathbf{n}$ orthogonal to $\overline{\boldsymbol{F}}\mathbf{N}_0$ in (6.3.12). This result corresponds to the fact that the 'push forward' transverse shear modulus $\hat{L}^c_{1212}$—as defined by expression (6.2.8)—vanishes (i.e., $\hat{L}^c_{1212} = 0$) for all $\overline{\boldsymbol{F}} \in \mathcal{S}^c_{rc}$.

At this point, it is important to emphasize that—consistent with the inclusion (6.3.11)—the principal solution $\widehat{W}$ loses global (strict) rank-one convexity before losing (local) strong ellipticity. This can be seen in Figure 6.1c and Figure 6.1d, where the values of γ for which the 'principal' solution $\widehat{W}$ loses strong ellipticity (γ_{se}) and rank-one convexity (γ_{rc}) are plotted versus α. Figure 6.1c shows results for a fixed volume fraction and varying contrasts, while Figure 6.1d does the same but for a fixed contrast, and varying volume fractions. In both cases, we find that the 'principal' solution satisfies the (SE) condition and, hence, is (*locally*) stable for all $\alpha < \alpha_{se}$. For values of $\alpha \geqslant \alpha_{se}$, the 'principal' solution is strongly elliptic and therefore *locally* rank-one convex for all sufficiently large γ. However, as we approach the state of pure shear ($\gamma = 0$), the 'principal' solution loses *global* rank-one convexity before losing strong ellipticity. In fact, the only time that strong ellipticity and *local* rank-one convexity are lost simultaneously is when $\alpha = \alpha_{se}$ and $\gamma = \gamma_{se} = \gamma_{rc} = 0$.

Having shown that $R\widehat{W} = R_1\widehat{W}$, we now look to show that $R\widehat{W}$ is polyconvex. Toward that end, we first observe that $R\widehat{W} = R_1\widehat{W}$, as given by Eq. (6.3.8), can be rewritten in the form

$$R\widehat{W}(\overline{\boldsymbol{F}}) = g(\overline{\boldsymbol{F}}) + K(\det \overline{\boldsymbol{F}}), \tag{6.3.13}$$

where K is defined by (6.2.2),

$$g(\overline{\boldsymbol{F}}) = \begin{cases} \frac{\breve{\mu}}{2}|\overline{\boldsymbol{F}}\mathbf{N}_0|^2 + \frac{\overline{\mu}}{2}\left(|\overline{\boldsymbol{F}}\mathbf{M}_0|^2 - 2\right) + \frac{\overline{\mu}-\breve{\mu}}{2}\frac{1}{|\overline{\boldsymbol{F}}\mathbf{M}_0|^2}, & \text{if} \quad \overline{\boldsymbol{F}} \in \mathcal{S}_{rc}, \\ \frac{\breve{\mu}}{2}|\overline{\boldsymbol{F}}\mathbf{N}_0|^2 + \overline{\mu}(\alpha_{se}^{-2} - 1), & \text{if} \quad \overline{\boldsymbol{F}} \in \mathcal{S}_{rc}^c, \end{cases} \tag{6.3.14}$$

and where $\mathcal{S}_{rc}$ can also be rewritten explicitly in terms of $\overline{\boldsymbol{F}}$ via

$$\mathcal{S}_{rc} = \left\{\overline{\boldsymbol{F}} \,:\, |\overline{\boldsymbol{F}}\mathbf{N}_0| < \alpha_{se} \text{ or } |\overline{\boldsymbol{F}}\mathbf{N}_0| \geqslant \alpha_{se} \text{ and } |\overline{\boldsymbol{F}}\mathbf{M}_0| > \alpha_{se}^{-1}\right\}. \tag{6.3.15}$$

Next, in order to show that $R\widehat{W}$ is polyconvex, we must show that $R\widehat{W}$ can be written as a convex function of $\overline{\boldsymbol{F}}$ and $\det \overline{\boldsymbol{F}}$. Making use of Corollary 3.2 of the work of Schröder and Neff (2003) for additive polyconvex functions and noting that $K(\det \overline{\boldsymbol{F}})$ is a convex function in $\det \overline{\boldsymbol{F}}$, it is seen that, in order to prove polyconvexity, it suffices to show that $g(\overline{\boldsymbol{F}})$ is a convex function in $\overline{\boldsymbol{F}}$, which can be accomplished directly by showing that the Hessian of g is positive semidefinite. A direct calculation shows that, for any $\boldsymbol{H}$,

$$\begin{aligned} \boldsymbol{H} \cdot \frac{\partial^2 g(\overline{\boldsymbol{F}})}{\partial \overline{\boldsymbol{F}} \partial \overline{\boldsymbol{F}}} \boldsymbol{H} = \breve{\mu}|\boldsymbol{H}\mathbf{N}_0|^2 + \frac{4(\overline{\mu} - \breve{\mu})}{|\overline{\boldsymbol{F}}\mathbf{M}_0|^6}\left[(\overline{\boldsymbol{F}}\mathbf{M}_0) \cdot (\boldsymbol{H}\mathbf{M}_0)\right]^2 \\ + \overline{\mu}\left[1 - \frac{1}{(\alpha_{se}\,|\overline{\boldsymbol{F}}\mathbf{M}_0|)^4}\right]|\boldsymbol{H}\mathbf{M}_0|^2 \end{aligned} \tag{6.3.16}$$

if $\overline{\boldsymbol{F}} \in \mathcal{S}_{rc}$ and

$$\boldsymbol{H} \cdot \frac{\partial^2 g(\overline{\boldsymbol{F}})}{\partial \overline{\boldsymbol{F}} \partial \overline{\boldsymbol{F}}} \boldsymbol{H} = \breve{\mu}|\boldsymbol{H}\mathbf{N}_0|^2 \tag{6.3.17}$$

if $\overline{\boldsymbol{F}} \in \mathcal{S}_{rc}^c$. That the Hessian is positive semidefinite for $\overline{\boldsymbol{F}} \in \mathcal{S}_{rc}^c$ is trivial from the second expression above. On the other hand, for $\overline{\boldsymbol{F}} \in \mathcal{S}_{rc}$, it can be seen that every term in the first expression for the Hessian is non-negative—including the last one (since $\alpha_{se}\,|\overline{\boldsymbol{F}}\mathbf{M}_0| > 1$). Therefore, g is a convex function of $\overline{\boldsymbol{F}}$, and it is concluded

that $R\widehat{W}$ is polyconvex and

$$Q\widehat{W}(\overline{\boldsymbol{F}}) = R\widehat{W}(\overline{\boldsymbol{F}}) = P\widehat{W}(\overline{\boldsymbol{F}}). \tag{6.3.18}$$

Now, it is recalled from expression (5.3.8) that $Q\widehat{W}$ is, in general, only an upper bound for the homogenized energy $\widetilde{W}$ of the hyperelastic laminate, and the question then arises as to whether this bound can correspond exactly to the homogenized energy and, if so, under which conditions. In this connection, it should be first recalled from the work of Triantafyllidis and Maker (1985) that when the volume fraction of the stiff layers is sufficiently small, the first instability is expected to be a *microscopic* one (exhibiting a wavelength that is commensurate with the unit cell size). Therefore, under such conditions, the actual post-bifurcation solutions is expected to be one exhibiting *microbuckling*, and $Q\widehat{W}$ would then not be equal to $\widetilde{W}$ (i.e., $\widetilde{W} < Q\widehat{W}$). On the other hand, when the volume fraction of the stiff layers is sufficiently large, the first instability is a *macroscopic* one (exhibiting a wavelength that is large compared to the unit cell size). In this case, it may be expected that the long wavelength modes will indeed evolve into a pattern of lamellar domains, where the lamellar domains are made up of a large (infinite) number of unit cells, but are still small compared to the overall size of the RVE. In addition, because of the relaxation process that is involved in this construction, it is reasonable that the 'mesoscopic' response of these lamellar domains should be captured by the principal solution $\widehat{W}$ for the homogenized energy, and therefore we would conclude that $\widetilde{W} = Q\widehat{W}$ in this case. (Note that Avazmohammadi and Ponte Castañeda (2016) have suggested that the homogenized energy $\widetilde{W}$ can also be estimated directly from $Q\widehat{W}$ for a similar two-dimensional problem consisting of aligned short rigid fibers distributed randomly in an elastomeric matrix—where microscopic instabilities are excluded by the randomness of the microstructures.) In any event, while this remains to be shown rigorously, in the discussions that follow it will be assumed that *the volume fraction of the stiff layers is sufficiently large* so that the homogenized energy is well approximated by

the relaxation of the principal solution for the energy, that is,

$$\widetilde{W}(\overline{\boldsymbol{F}}) = Q\widehat{W}(\overline{\boldsymbol{F}}) = R\widehat{W}(\overline{\boldsymbol{F}}), \tag{6.3.19}$$

where $R\widehat{W}$ is given by (6.3.13) and (6.3.14). In this case, it can be concluded that the homogenized energy $\widetilde{W}$ for the neo-Hookean laminates corresponds to the formation of lamellar (or striped) domains. Thus, the macroscopic instabilities in this case do not lead to shear localization, but to domain formation. Furthermore, it should be emphasized that these instabilities are triggered by loss of *global* (strict) rank-one convexity, which—depending on the loading—can take place *well before* loss of *local* (strict) rank-one convexity (or strong ellipticity).

Finally, for completeness and use below, it is noted that the Cauchy stress associated with the relaxed solution is still given by expressions (6.2.7) if $\overline{\boldsymbol{F}} \in \mathcal{S}_{rc}$, while it is given by

$$\overline{\boldsymbol{T}} = \breve{\mu}\left(\overline{\boldsymbol{F}}\mathbf{N}_0\right) \otimes \left(\overline{\boldsymbol{F}}\mathbf{N}_0\right) - p\boldsymbol{I}, \quad \text{if } \overline{\boldsymbol{F}} \in \mathcal{S}_{rc}^c, \tag{6.3.20}$$

where p is an arbitrary hydrostatic pressure.

6.4 Results and discussion

We present next the results of the previous sections for the homogenized energy and associated stresses in more detail and investigate their dependence on material and microstructural parameters. When present, a diamond (⧫) represents the point where the 'principal' solution loses global (strict) rank-one convexity, while a circle (•) represents the point where the solution first violates the (SE) condition. Moreover, the 'principal' solution, represented by dashed curves, is provided for reference. Figure 6.2a shows various fixed-α cross-sections of the homogenized energy $\widetilde{W}(\overline{\boldsymbol{F}}) = \widehat{\Psi}^{**}(\alpha, \gamma)$ for fixed volume fraction of the stiffer phase ($c = 0.3$) and heterogeneity contrast ($\mu^{(2)}/\mu^{(1)} = 10$). Note that, in each case, loss of global rank-one

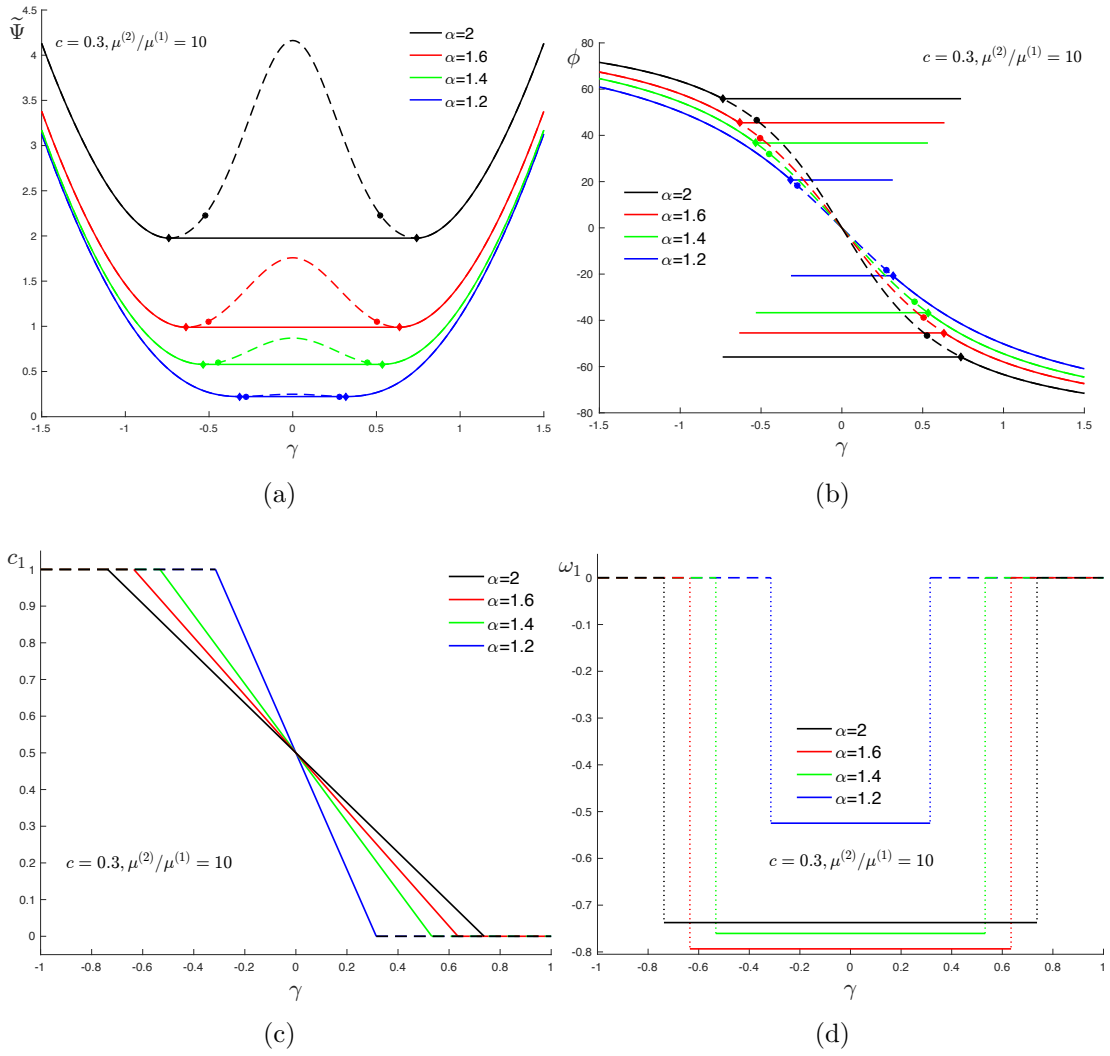

Figure 6.2: Relaxed results for (a) the effective energy, (b) the rotation of the mesolayers, (c) the volume fraction of the 'mesolayer', and (d) the amplitude factor associated with the rank-one convexification. Results are plotted as a function of γ for a fixed volume fraction $c = 0.3$, contrast of $\mu^{(2)}/\mu^{(1)} = 10$ and for various values of α. The 'principal' estimates are also included for comparison (dashed lines).

convexity occurs at the local minima of each cross section. Moreover, moving from large values of $|\gamma|$ towards $\gamma = 0$, we see that the 'principal' solution always loses rank-one convexity before strong ellipticity. Figure 6.2b shows the macroscopic rotation of the domains. In the rank-one convex region ($\overline{\boldsymbol{F}} \in \mathcal{S}_{rc}$), the solution is macroscopically

uniform and the rotation of the layers takes on a single value, which can be positive or negative, depending on whether γ is negative or positive, respectively. On the other hand, as illustrated in Figure 6.1b, the relaxed or post-bifurcation solution (for $\overline{\boldsymbol{F}} \in \mathcal{S}^c_{rc}$) is no longer macroscopically uniform and forms lamellar domains at the mesoscopic scale. These mesolayers undergo alternating rotations by equal and opposite amounts, i.e. $\phi^{(I)} = -\phi^{(II)}$. Thus in Figure 6.2b, the constant positive value of ϕ corresponds to the rotation of 'mesolayer' II, while the corresponding negative value corresponds to the rotation of 'mesolayer' I. Although the rotation of the mesolayers remains constant for fixed $\alpha > \alpha_{se}$ and $|\gamma| < \gamma_{rc}$, the relaxed solution compensates for the increased/decreased macroscopic shearing by changing the volume fractions of the 'mesolayers'. This change is linear, as depicted Figure 6.2c, and the solution in the remaining 'mesolayer' agrees precisely with the 'principal' solution as the value of c_1 reaches 1 or 0. In Figure 6.2d, the amplitude factor ω_1 is plotted as a function of γ. Unlike c_1, ω_1 remains constant in the unstable region, with its value depending only on α. Finally, it should be noted that the orientation of the layers in the relaxed region for the principal solution, also shown (in dashed lines) in Figure 6.1b, varies smoothly and is uniquely determined—just as for the corresponding layer orientation in the rank-one convex region. On the other hand, the corresponding values of c_1 and ω_1 are trivial ($c_1 = 1$ or 0 and $\omega_1 = 0$) and are shown in dashed lines in Figure 6.2c and Figure 6.2d, respectively, for reference.

Figure 6.3 shows the corresponding macroscopic stresses as functions of γ for the same values of volume fraction ($c = 0.3$) and contrast ($\mu^{(2)}/\mu^{(1)} = 10$). On account of the incompressibility of the composite, Figure 6.3a shows the results for the difference in the normal Cauchy stress ($T_{11} - T_{22}$). Note that—similar to the results for the relaxed energy—the 'principal' solution also produces a 'creased' region for the values of $T_{11} - T_{22}$ for $|\gamma| < \gamma_{rc}$ and for each (depicted) fixed value of α. Moreover, as α increases, the value of $T_{11} - T_{22}$ for the 'principal' solution in the creased region increases dramatically reaching a maximum at $\gamma = 0$. As for the

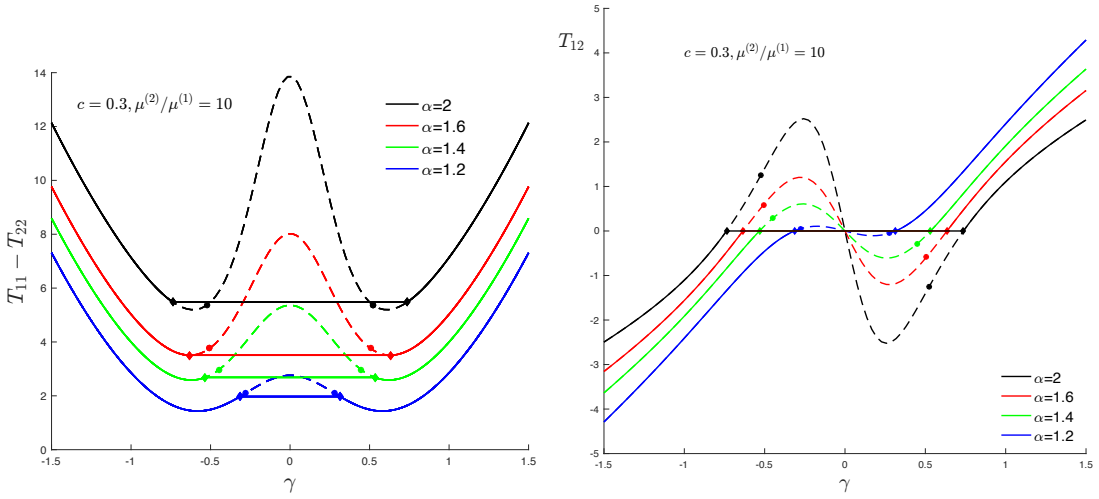

(a) (b)

Figure 6.3: Relaxed results for the macroscopic (a) normal Cauchy stress difference $T_{11} - T_{22}$ and (b) Cauchy shear stress T_{12}. Results are plotted as a function of γ for a fixed volume fraction of $c = 0.3$, contrast of $\mu^{(2)}/\mu^{(1)} = 10$ and for various values of α. The 'principal' solutions are also included for comparison (dashed lines).

relaxed solution, we see that $T_{11} - T_{22}$ remains constant (and is much smaller that the above-mentioned maximum) for fixed α and $|\gamma| < \gamma_{rc}$. This is to be expected, as the difference in the normal Cauchy stresses can be related to derivatives of the effective energy with respect to α. Therefore, as the relaxed solution for the energy is independent of γ, it is no surprise that the corresponding stresses are also independent of γ. Figure 6.3b shows the relaxed results for the Cauchy shear stress (T_{12}). It is interesting to note that for all depicted values of α, the results for the relaxed shear stress vanish identically for $|\gamma| < \gamma_{rc}$. Similar to the normal stress difference, the shear stress T_{12} can be related to derivatives of the effective energy with respect to γ. Since, as depicted in Figure 6.1b and Figure 6.2a, the relaxed solution is constant in γ for fixed α and $|\gamma| < \gamma_{rc}$, derivatives with respect to γ will be zero. In connection to Figure 6.1a, the vanishing of the shear stress is related to the fact that, as γ goes from, say $-\gamma_{rc}$ to γ_{rc}, the composite breaks up into the 'mesolayers' with volume fractions ranging from $c_1 = 1$ to $c_1 = 0$, respectively. In this way, the laminate

accommodates the deformation by splitting the effect on the shearing component γ between the two 'mesolayers.' In fact, the shear stress in one 'mesolayer' is equal and opposite in sign to the shear stress in the other 'mesolayer' (as can be deduced from Eq. (6.3.7)); hence the shear stresses cancel out. This phenomenon is analogous to the Maxwell-type construction, but only for the shear stress.

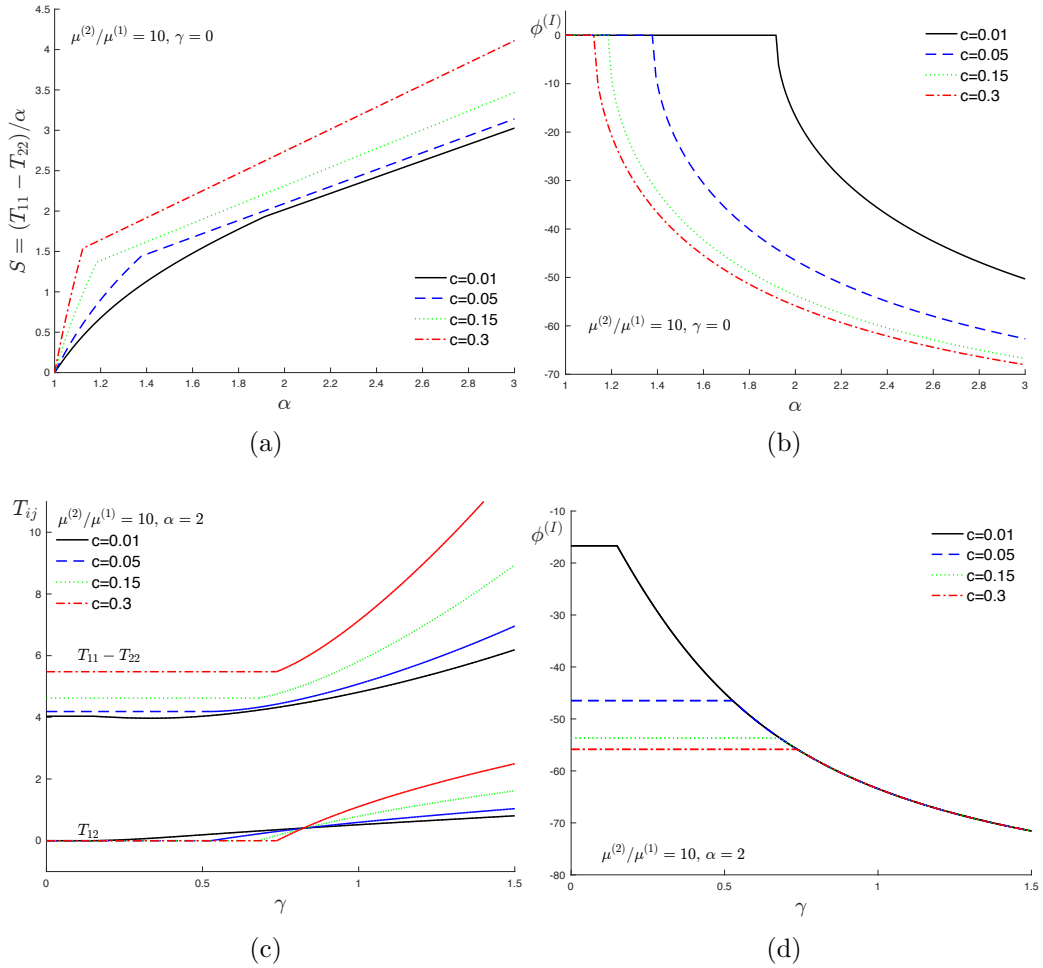

Figure 6.4: Relaxed results for the macroscopic stresses, and 'mesolayer' rotations, for various values of the volume fraction c and a fixed contrast of $\mu^{(2)}/\mu^{(1)} = 10$. (a) and (b) depict results for pure-shear loading ($\gamma = 0$) as a function of α. (c) and (d) depict results plotted as a function of γ for a fixed value of $\alpha = 2$.

Figure 6.4 shows results for the stress measures associated with the relaxed so-

lution, as well as for the corresponding 'mesolayer' rotation for a fixed value of the stiffness ratio $\mu^{(2)}/\mu^{(1)} = 10$ and for various values of the volume fraction of the stiffer phase ($c = 0.01, 0.05, 0.15$ and 0.3). In connection with these results, it should be noted that, for the smaller values of c, microscopic instabilities leading to microbuckling post-bifurcation responses would be expected to occur before any macroscopic instabilities, and therefore the corresponding relaxed solutions shown in the figure would only be upper bound estimates for the homogenized response in those cases. Figures 6.4a and 6.4b depicts these results for pure shear loading as functions of α, while Figures 6.4c and 6.4d show the corresponding results for transverse shear loading as functions of γ. Figure 6.4a shows that the nominal stress difference measure $S = (T_{11} - T_{22})/\alpha$ initially (i.e., for small values of α) becomes stiffer with increasing concentration. However, at $\alpha = \alpha_{se}$, the slope of the stress measure changes quite abruptly leading to a softer response, which also becomes stiffer with increasing values of c. As shown in Figure 6.4b, the softening is triggered by a sudden change in the layer orientation in the 'mesolayers' (only orientation I is shown in the figure). Figure 6.4c shows results for the normal Cauchy stress difference $T_{11} - T_{22}$ and transverse shear stress T_{12}, as functions of γ, for a fixed value of $\alpha = 2$. Consistent with earlier observations, it can be seen that, in the 'relaxed' region, $T_{11} - T_{22}$ is constant while T_{12} is zero. Note that larger volume fractions generally lead to higher stresses, but not always. Figure 6.4d shows the corresponding constant rotations $\phi^{(1)}$ in the layers for the various volume fractions. Beyond the relaxed region, the stresses increase with the strain γ, and are stiffer for higher values of c. However, it is seen from Figure 6.4d that, for large enough values of γ, the rotation of the 'mesolayers' is the same regardless of volume fraction, consistent with the fact that the rotation of the layers in the principal solution is controlled by the macroscopic deformation and hence independent of c. Finally, it should be noted that macroscopic stresses in the laminate tend to those in a homogeneous elastomer made up of the softer phase as the volume fraction of the stiff layers tends to zero.

Although not shown for brevity, it should be noted that very similar results are obtained by fixing the volume fraction c and varying the contrast $\mu^{(2)}/\mu^{(1)}$. Noting that $\mu^{(2)}/\mu^{(1)} = 1$ (for any c) and $c = 0$ (for any $\mu^{(2)}/\mu^{(1)}$) both correspond to the special case of a homogeneous elastomer, the trends for a fixed value of c and increasing values of $\mu^{(2)}/\mu^{(1)}$ are very similar to the above-mentioned trends for a fixed value of $\mu^{(2)}/\mu^{(1)}$ and increasing values of c. This follows from the fact that the dependence on the variables c and $\mu^{(2)}/\mu^{(1)}$ appears only through $\overline{\mu}$ and $\breve{\mu}$, which have similar dependence on both c and $\mu^{(2)}/\mu^{(1)}$.

It is also of interest to compare the new estimates for neo-Hookean laminates with available bounds. As already mentioned, bounds of the Voigt and Reuss types are available for hyperelastic composites. For the special case of interest here, these bounds reduce to

$$\frac{\breve{\mu}}{2}\left(\alpha^2+\alpha^{-2}+\gamma^2-2\right) \leqslant \widetilde{\Psi}(\alpha,\gamma) \leqslant \frac{\overline{\mu}}{2}\left(\alpha^2+\alpha^{-2}+\gamma^2-2\right), \tag{6.4.1}$$

where it is recalled that $\widetilde{W}(\overline{\boldsymbol{F}}) = \widetilde{\Psi}(\alpha,\gamma)$. The upper (Voigt) bound is due to Odgen (1978), while the lower bound is a refinement of the Reuss-type lower bounds obtained by Ponte Castañeda (1989) exploiting polyconvexity. A proof of both of these bounds is found in Section 6.6. Thus, Figure 6.5 presents a comparison of the 'principal' and 'post-bifurcation' or 'relaxed' estimates with the bounds (6.4.1) for the homogenized energy as functions of α and γ. Interestingly, while both the principal and relaxed solutions always satisfy the bounds, it can be seen that the bounds are saturated for special values of α and γ. In particular, as can be seen in Figure 6.5a, the principal solution attains the Voigt upper bound for $\gamma = 0$ and all α, while the relaxed solution is much closer to the Reuss lower bound for all $\alpha \geqslant \alpha_{se}$. Similar observations can be made in Figure 6.5b for another fixed value of γ, although the Voigt bound is only attained asymptotically as α tends to zero, while the Reuss bound is tangent to the principal solution for a value of α greater than 1. Moreover, we find that, as indicated by the black diamond, the principal solution and relaxed solution agree until $\alpha \approx 1.5$,

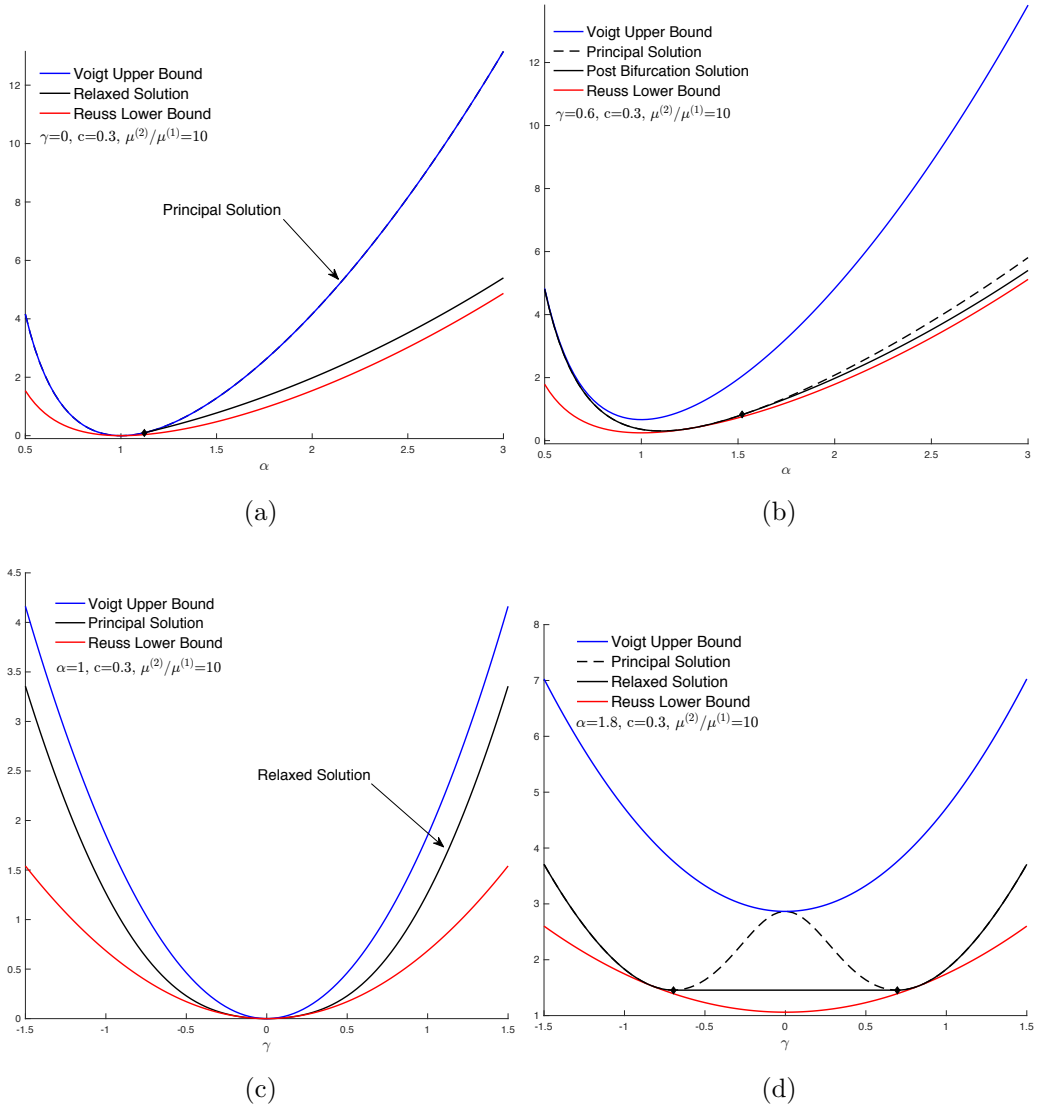

Figure 6.5: Comparison of the relaxed estimates for the homogenized energy $\widetilde{\Psi}$ with the Voigt upper bound and Reuss-type polyconvex lower bound. Parts (a) and (b) depict results for pure-shear loading ($\gamma = 0$) and non-aligned loading ($\gamma = .6$), respectively, as a function of α. Parts (c) and (d) depict results plotted as a function of γ for fixed values of $\alpha = 1$ and $\alpha = 1.8$ (respectively). The principal solution is also included for reference.

at which point, the deformation, as determined by the pair (α, γ), falls into the region $\mathcal{S}^c_{rc}$. On the other hand, as can be seen in Figure 6.5c and Figure 6.5d, the plots for fixed values of α show that the principal solution is tangent to the Reuss bound for small values of γ ($\gamma = 0$ for $\alpha = 1$, and $\gamma \sim 0.85$ for $\alpha = 1.8$), while it tends to the Voigt bound for large values of γ. In connection with Figure 6.5c, it should be mentioned that, since $\alpha = 1 < \alpha_{se}$, the principal solution never bifurcates to a lower energy solution, and hence agrees exactly with the relaxed solution, regardless of the value of γ. It should also be noted that, while closer to the Reuss bound than the principal solution, the relaxed solution never violates the Reuss lower bound.

At this point, it is useful to make contact with the recent work of Avazmohammadi and Ponte Castañeda (2016) for composites consisting of aligned elliptical fibers distributed randomly in an elastomer matrix, and also subjected to plane strain deformations. While the fibers in that work were taken to be rigid and discontinuous (in the plane of the deformation)—in contrast with the stiff, but deformable continuous layers in the present work—it is found that the results for both the instabilities and the post-bifurcation macroscopic response are remarkably similar—provided that the aspect ratio of the fibers in the earlier work and the stiffness of the stiffer layers in the present work are both taken to be sufficiently large. In fact, it has been verified that the results agree exactly in the limits as the aspect ratio of the elliptical fibers in the earlier work tends to infinity (i.e., to layers) and as the shear modulus of the stiff layers in the present work tends to infinity (i.e., become rigid). In this context, it is important to emphasize, however, that while the results for the principal solution of the earlier work (Avazmohammadi and Ponte Castañeda, 2016) for aligned elliptical fibers were based on the *approximate* 'linear comparison' variational estimates of Lopez-Pamies and Ponte Castañeda (2006b), the results in the present work are based on the *exact* homogenization estimates of deBotton (2005) for the principal solution. Indirectly, this suggests that the 'linear comparison' homogenization method (Lopez-Pamies and Ponte Castañeda, 2006a) should be quite accurate and could be used to

carry out similar investigations for more general classes of hyperelastic composites, such as random distributions of aligned ellipsoidal particles (Avazmohammadi and Ponte Castañeda, 2014a,b), for which exact analytical solutions would not otherwise be possible.

In addition, it is also relevant to discuss here the possible effects of the constitutive response of the phases on the relaxation. Indeed, the recent work of d'Avila M. P. et al. (2016) for periodic hyperelastic laminates subjected to uniaxial compression along the layers suggests that the constitutive behavior of the layers should have crucial implications for the relaxed response of the laminates. In fact, these authors have shown that, when at least one of the phases has a shear modulus that decreases sufficiently fast with the strain (i.e., exhibits softening akin to deformation theory of plasticity), the post-bifurcation (beyond loss of ellipticity) macroscopic response of the laminate is 'subcritical' (decreasing stress and strain), leading to localization of the deformation and to unstable response. On the other hand, for neo-Hookean behavior for both phases, the post-bifurcation response is 'supercritical' (increasing stress and strain) and therefore stable. While these authors did not compute the relaxation of the energy (and therefore found no domain formation), restricting their attention to uniaxial compression along the layers of the laminates, the solution for the special case of neo-Hookean laminates can be shown to correspond exactly to the solution in the 'mesolayers' of the rank-one convexification $R_1\widehat{W}$, as given by (6.3.8), for the special case when $\gamma = 0$. In addition, based on the results of Avazmohammadi and Ponte Castañeda (2016) for fiber-reinforced elastomers with Gent-type behavior, it would be expected that laminates consisting of Gent and other types of commonly used constitutive models for elastomers, which tend to stiffen with stretch, would exhibit a post-bifurcation response also leading to domain formation. In fact, Gent-type laminates have been found (Lopez-Pamies and Ponte Castañeda, 2009) to lose strong ellipticity in much the same way the neo-Hookean laminates, suggesting also similar post-bifurcation responses.

6.5 Concluding Remarks

The focus of this chapter has been on the 'post-bifurcation' response following the onset of 'macroscopic' (long-wavelength) instabilities in soft hyperelastic composites. For analytical simplicity, two-phase neo-Hookean laminates under general plane strain loading conditions have been considered. Due to the existence of a simple expression for the 'principal' solution for the homogenized stored-energy function of these materials, it was possible to derive a correspondingly simple analytical expression for the rank-one convex envelope $R\widehat{W}$ of the 'principal' solution $\widehat{W}$. By appealing to the notion of polyconvexity, it was also possible to show that $R\widehat{W}$ is in fact quasiconvex and hence should correspond to the 'relaxation' of the energy $\widetilde{W}$—at least when the volume fraction and stiffness of the stiffer layers is sufficiently large to ensure that the first instability is a macroscopic one. In this connection, it should be kept in mind that periodic laminates are also susceptible to 'microscopic' (finite wavelength) instabilities leading to a microbuckling post-bifurcation response when the volume fraction of the stiffer layers is small enough (Triantafyllidis and Maker, 1985; Geymonat et al., 1993). One important consequence of the results of this work (cf. Figures 6.1c and 6.1d) is that *global* strict rank-one convexity can be lost prior to *local* strict rank-one convexity (strong ellipticity). This strongly suggests that, in general, 'macroscopic' instabilities in these hyperelastic laminates should correspond to loss of *global* rank-one convexity and not to loss of strong ellipticity—as it has been commonly assumed (Triantafyllidis and Maker, 1985; Geymonat et al., 1993). It also suggests that the post-bifurcated macroscopic response takes place by the formation of (stable) 'lamellar domain' microstructures—and not by shear localization. In addition, it has been found that 'soft' modes of deformation are associated with the development of these domain microstructures. However, unlike the 'perfectly soft' (i.e., zero elastic moduli) modes of deformation associated with certain types of shape-memory alloys (Ball and James, 1987; Bhattacharya, 2003) and liquid crystal

elastomers (DeSimone and Dolzmann, 2000; Conti et al., 2002), the post-bifurcation response of the neo-Hookean laminates is only perfectly soft in the shear direction transverse to the layers, while it has a reduced but finite elasticity modulus in the direction of compression along the layers.

Finally, it should be noted that the formation of domain microstructures should also be possible following the onset of 'macroscopic' instabilities in hyperelastic composites with more general periodic microstructures (Triantafyllidis et al., 2006; Michel et al., 2007, 2010), as has also been found for composites with random microstructures (Avazmohammadi and Ponte Castañeda, 2016). However, it should be kept in mind that such macroscopic instabilities could also be excited in these more general periodic composites well before loss of strong ellipticity, at least for some loading paths. In fact, the same could also be the case for the microscopic instabilities; thus, it is conceivable that periodic hyperelastic composites may find it energetically favorable to transform from a solution that is periodic on one cell to a solution that is periodic on multiple cells, before reaching the appropriate bifurcation condition based on the incremental (linearized) elasticity problem, again at least for some loading paths. Thus, caution should be exercised when making use of the *incremental* elasticity problem to generate estimates for the relaxation of the homogenized elastic energy—since the linearization and homogenization procedures may not commute, in general, for these materials with non-convex phase energies (contrary to what has been shown by Geymonat et al. (1993) for convex energies). In any event, the formation of domain microstructures after the onset of macroscopic instabilities is entirely consistent with the formation of period solutions on $N \times M \times L$ 'super-cells' following the onset of microscopic instabilities. Indeed, from this more general point of view, the post-bifurcation response of hyperelastic composites with periodic microstructures would alway corresponds to relaxation by domain formation, where the domain size is either commensurate with the unit-cell size for the microscopic instabilities, or much larger than the cell size for the macroscopic instabilities (assuming, of course, that the

constitutive behavior of the constituent phases is consistent with a macroscopically stable post-bifurcation response).

6.6 Appendix I: Derivation of the bounds on $\widetilde{W}$

In this appendix, we look to derive the lower and upper bounds on the relaxation of a two phase, incompressible Neo-Hookean hyperelastic composite under general plane-strain loading conditions. To do this, we must first consider a compressible composite, and then take the limit as $J = \det \overline{\boldsymbol{F}} \to 1$. To set up the derivation of the bounds, we suppose that our composite, which occupies some region Ω_0, which we take as our RVE, is comprised of two isotropic phases whose constitutive behavior is governed by

$$W^{(r)}(\boldsymbol{F}) = \frac{\mu^{(r)}}{2}(|\boldsymbol{F}|^2 - 2) - \mu^{(r)}(J-1). \tag{6.6.1}$$

Normally, the second term takes the form $\ln(J)$, but as we will be interested in taking the limit as $J \to 1$, and since

$$\ln(J) = \ln(1 + (J-1)) \approx (J-1), \tag{6.6.2}$$

we use the form given in Eq. (6.6.1). Now, the distribution of the phases is described by the characteristic functions $\chi^{(r)}(\mathbf{X})$ of each phase, whereby the local constitutive behavior is given by

$$W(\mathbf{X}, \boldsymbol{F}) = \chi^{(1)}(\mathbf{X})W^{(1)}(\boldsymbol{F}) + \chi^{(2)}(\mathbf{X})W^{(2)}(\boldsymbol{F}), \tag{6.6.3}$$

and we assume that the initial volume fraction of the phases $c^{(r)} = \langle \chi^{(r)} \rangle$ is known. By using the definition of $\widetilde{W}$ due to Hill (1972), we may write

$$\widetilde{W}(\overline{\boldsymbol{F}}) = \inf_{\overline{\boldsymbol{F}} \in \mathcal{K}(\overline{\boldsymbol{F}})} \langle W(\mathbf{X}, \boldsymbol{F}(\mathbf{X})) \rangle, \tag{6.6.4}$$

where

$$\mathcal{K}(\overline{\boldsymbol{F}}) = \{\mathbf{x} \,:\, \boldsymbol{F} = \mathrm{Grad}\mathbf{x},\, \det \boldsymbol{F} > 0 \text{ in } \Omega_0, \text{ and } \mathbf{x} = \overline{\boldsymbol{F}}\mathbf{X} \text{ on } \partial\Omega_0\}. \tag{6.6.5}$$

Note that $\mathbf{x} = \overline{\boldsymbol{F}}\mathbf{X} \in \mathcal{K}(\overline{\boldsymbol{F}})$, and hence, we immediately arrive at the upper bound

$$\widetilde{W}(\overline{\boldsymbol{F}}) \leqslant \langle W(\mathbf{X}, \overline{\boldsymbol{F}})\rangle = \frac{\overline{\mu}}{2}(|\boldsymbol{F}|^2 - 2) - \overline{\mu}(J-1). \tag{6.6.6}$$

In order to derive the lower bound, we modify the method used by Ponte Castañeda (1989). This procedure relies on the notion of polyconvexity, and we first require some definitions and results, which we take from Dacorogna (1989), and specify to our particular case; we mention that the method we will lay out holds in far more generality in higher dimensions. To start, consider a function $f : \mathbb{R}^{2\times 2} \to \mathbb{R}$. We define the polyconvex polar, $f^p : \mathbb{R}^{2\times 2} \times \mathbb{R} \to \mathbb{R}$ as

$$f^p(\boldsymbol{S}, p) = \sup_{\boldsymbol{F}} \{\boldsymbol{S} \cdot \boldsymbol{F} + pJ - f(\boldsymbol{F})\}. \tag{6.6.7}$$

We then define the polyconvex biconjugate of f as

$$f^{pp}(\boldsymbol{F}) = \sup_{S,p} \{\boldsymbol{S} \cdot \boldsymbol{F} + pJ - f^p(\boldsymbol{S}, p)\}. \tag{6.6.8}$$

It then follows that if W is polyconvex, $f = f^{pp}$. An important hypothesis needed to use this result is that W takes finite values. This is why we cannot simply assume that our material is incompressible, since in that case, the stored energy functions $W^{(r)}$ are infinite whenever $\det \boldsymbol{F} \neq 1$.

Next, let us define

$$\mathcal{K}'(\overline{\boldsymbol{F}}) = \{\mathbf{x} \,:\, \boldsymbol{F} = \mathrm{Grad}\mathbf{x} \text{ and } \mathbf{x} = \overline{\boldsymbol{F}}\mathbf{X} \text{ on } \partial\Omega_0\}, \tag{6.6.9}$$

which is similar to $\mathcal{K}(\overline{\boldsymbol{F}})$, but we have removed the highly nonlinear constraint

$\det \boldsymbol{F} > 0$. Due to the inclusion $\mathcal{K}'(\overline{\boldsymbol{F}}) \subset \mathcal{K}(\overline{\boldsymbol{F}})$, we see that

$$\inf_{\overline{\boldsymbol{F}} \in \mathcal{K}'(\overline{\boldsymbol{F}})} \langle W(\mathbf{X}, \boldsymbol{F}(\mathbf{X})) \rangle \leqslant \widetilde{W}(\overline{\boldsymbol{F}}). \tag{6.6.10}$$

Now, as defined, $W(\mathbf{X}, \boldsymbol{F})$ is polyconvex, so we know that $W = W^{pp}$. Next, note that for each $\mathbf{X}$ and $\boldsymbol{F}$ we have

$$\boldsymbol{S} \cdot \boldsymbol{F} + pJ - W^p(\mathbf{X}, \boldsymbol{S}, p) \leqslant W(\mathbf{X}, \boldsymbol{F}) \tag{6.6.11}$$

for every $\boldsymbol{S}$ and p, where

$$W^p(\mathbf{X}, \boldsymbol{S}, p) = \chi^{(1)}(\mathbf{X})(W^{(1)})^p(\boldsymbol{S}, p) + \chi^{(2)}(\mathbf{X}))(W^{(2)})^p(\boldsymbol{S}, p), \tag{6.6.12}$$

and where $(W^{(r)})^p(\boldsymbol{S}, p)$ the polyconvex polar of $W^{(r)}$. Therefore, upon noting that W^p is independent of $\boldsymbol{F}$, we see that

$$\inf_{\overline{\boldsymbol{F}} \in \mathcal{K}'(\overline{\boldsymbol{F}})} \{\langle \boldsymbol{S} \cdot \boldsymbol{F} + pJ \rangle\} - \langle W^p(\mathbf{X}, \boldsymbol{S}, p) \rangle \leqslant \widetilde{W}(\overline{\boldsymbol{F}}). \tag{6.6.13}$$

Upon considering $\boldsymbol{S} = \overline{\boldsymbol{S}}$ and $p = \overline{p}$ to be uniform, and owing to the fact that the integrand in the first integral is a null Lagrangian, we find that

$$\overline{\boldsymbol{S}} \cdot \overline{\boldsymbol{F}} + \overline{p}\, \overline{J} - \langle W^p(\mathbf{X}, \overline{\boldsymbol{S}}, \overline{p}) \rangle \leqslant \widetilde{W}(\overline{\boldsymbol{F}}). \tag{6.6.14}$$

Upon denoting $\overline{W}^p(\overline{\boldsymbol{S}}, \overline{p}) = \langle W^p(\mathbf{X}, \overline{\boldsymbol{S}}, \overline{p}) \rangle$, optimizing Eq. (6.6.14) over $\overline{\boldsymbol{S}}$ and $\overline{p}$, and using Eq (6.6.8), we arrive at the lower bound

$$(\overline{W}^p)^p(\overline{\boldsymbol{F}}) \leqslant \widetilde{W}(\overline{\boldsymbol{F}}). \tag{6.6.15}$$

We now proceed in calculating $(\overline{W}^p)^p$. To start, we must calculate $(W^{(r)})^p$. Dropping

the superscript r for the time being, we must therefore find

$$W^p(\boldsymbol{S}, p) = \sup_{\boldsymbol{F}} \left\{ \boldsymbol{S} \cdot \boldsymbol{F} + pJ - \frac{\mu}{2}|\boldsymbol{F}| + \mu J \right\}. \tag{6.6.16}$$

The optimality conditions yield

$$\boldsymbol{S} = \mu \boldsymbol{F} - (\mu + p)\boldsymbol{F}^*, \tag{6.6.17}$$

where $\boldsymbol{F}^* = \overline{\boldsymbol{F}}^{-T} \det \boldsymbol{F}$. Now, in two dimensions, we recall that

$$f_{\boldsymbol{A}}(\lambda) = \det(\lambda \boldsymbol{I} - A) = \lambda^2 - \operatorname{tr}(\boldsymbol{A})\lambda + \det(\boldsymbol{A}) \tag{6.6.18}$$

is the characteristic polynomial of $\boldsymbol{A}$, which, by the Cayley-Hamilton Theorem, has the eigenvalues of $\boldsymbol{A}$ as its roots. As a consequence, it follows that a matrix satisfies its own characteristic equation. As such,

$$\boldsymbol{0} = \boldsymbol{C}^2 - I_1 \boldsymbol{C} + I_3 \boldsymbol{I}, \tag{6.6.19}$$

where $\boldsymbol{C} = \boldsymbol{F}^T \boldsymbol{F}$, $I_1 = \operatorname{tr}(\boldsymbol{C}) = |\boldsymbol{F}|^2$ and $I_3 = \det(\boldsymbol{C}) = J^2$. Therefore, upon multiplying Eq. (6.6.19) by $\boldsymbol{C}^{-1}$ and taking the trace, we find that

$$|\overline{\boldsymbol{F}}|^2 = |\overline{\boldsymbol{F}}^*|^2. \tag{6.6.20}$$

We also record the fact that $\boldsymbol{F} \cdot \boldsymbol{F}^{-T} = 2$. Now, from Eq. (6.6.17), we find that

$$\boldsymbol{S} \cdot \boldsymbol{F} = \mu |\boldsymbol{F}|^2 - 2(\mu + p)J \tag{6.6.21}$$

$$|\boldsymbol{S}|^2 = (\mu^2 + (\mu + p)^2)|\boldsymbol{F}|^2 - 4\mu(\mu + p)J \tag{6.6.22}$$

$$\det \boldsymbol{S} = (\mu^2 + (\mu + p)^2)J - \mu(\mu + p)|\boldsymbol{F}|^2 \tag{6.6.23}$$

where we used Eqs. (6.6.20) and (6.6.18) to obtain Eqs. (6.6.22) and (6.6.23), re-

spectively. Moreover, Eqs. (6.6.22) and (6.6.23) may be used to find that

$$|\boldsymbol{F}|^2 = \frac{1}{p^2(p+2\mu)^2}\left((\mu^2+(\mu+p)^2)|\boldsymbol{S}|^2 + 4\mu(\mu+p)\det\boldsymbol{S}\right) \tag{6.6.24}$$

$$J = \frac{1}{p^2(p+2\mu)^2}\left(\mu(\mu+p)\boldsymbol{S}|^2 + (\mu^2+(\mu+p)^2)\det\boldsymbol{S}\right). \tag{6.6.25}$$

Combining this all, and plugging back in Eq. (6.6.16), we find that

$$W^p(S,p) = -\frac{\mu}{2p(p+2\mu)}|\boldsymbol{S}|^2 - \frac{\mu+p}{p(p+2\mu)}\det\boldsymbol{S}. \tag{6.6.26}$$

It can be confirmed, as expected, that

$$W^{pp}(\boldsymbol{F}) = \sup_{S,p}\{\boldsymbol{S}\cdot\boldsymbol{F} + pJ - W^p(\boldsymbol{S},p)\} = W(\boldsymbol{F}). \tag{6.6.27}$$

Upon defining

$$a_0 = a_0(p) = \sum_{r=1}^{2}\frac{c^{(r)}\mu^{(r)}}{p(p+2\mu^{(r)})}, \quad a_1 = a_1(p) = \sum_{r=1}^{2}\frac{c^{(r)}(p+\mu^{(r)})}{p(p+2\mu^{(r)})}, \tag{6.6.28}$$

we have found that

$$\overline{W}^p(\overline{\boldsymbol{S}},\overline{p}) = -\frac{a_0(\overline{p})}{2}|\overline{\boldsymbol{S}}|^2 - a_1(\overline{p})\det\overline{\boldsymbol{S}}, \tag{6.6.29}$$

and it therefore remains to calculate

$$(\overline{W}^p)^p(\overline{\boldsymbol{F}}) = \sup_{\overline{\boldsymbol{S}},\overline{p}}\{\overline{\boldsymbol{S}}\cdot\overline{\boldsymbol{F}} + \overline{p}\,\overline{J} - \overline{W}^p(\overline{\boldsymbol{S}},\overline{p})\}. \tag{6.6.30}$$

It can be shown that

$$c_0 = \frac{\overline{\mu}\,\overline{p} + 2\mu^{(1)}\mu^{(2)}}{\overline{p}(\overline{p}+2\mu^{(1)})(\overline{p}+2\mu^{(2)})} \tag{6.6.31}$$

$$c_1 = \frac{\overline{p}^2 + (\overline{\mu} + 2\mu^{(1)}\mu^{(2)}\breve{\mu}^{-1})\overline{p} + 2\mu^{(1)}\mu^{(2)}}{\overline{p}(\overline{p}+2\mu^{(1)})(\overline{p}+2\mu^{(2)})}, \tag{6.6.32}$$

whereby

$$c_1 - c_0 = \frac{\overline{p} + 2\mu^{(1)}\mu^{(2)}\breve{\mu}^{-1}}{(\overline{p} + 2\mu^{(1)})(\overline{p} + 2\mu^{(2)})}, \quad c_1 + c_0 = \frac{1}{\overline{p}}. \tag{6.6.33}$$

The optimality conditions indicate that $p \neq -2\mu^{(r)}$ for $r = 1, 2$, else $(\bar{W}^{\,p})^p(\overline{\boldsymbol{F}}) = -\infty$, and that

$$\overline{\boldsymbol{F}} = -a_0\overline{\boldsymbol{S}} - a_1\overline{\boldsymbol{S}}^*, \tag{6.6.34}$$

$$\overline{J} = -\frac{1}{2}\frac{\partial a_0}{\partial \overline{p}}|\overline{\boldsymbol{S}}|^2 - \frac{\partial a_1}{\partial \overline{p}}\det\overline{\boldsymbol{S}}. \tag{6.6.35}$$

Now, from Eq. (6.6.34), as above, we find that

$$\overline{\boldsymbol{S}} \cdot \overline{\boldsymbol{F}} = -a_0|\overline{\boldsymbol{S}}|^2 - 2a_1\det\overline{\boldsymbol{S}} \tag{6.6.36}$$

$$|\overline{\boldsymbol{F}}|^2 = (a_0^2 + a_1^2)|\overline{\boldsymbol{S}}|^2 + 4a_0a_1\det\overline{\boldsymbol{S}} \tag{6.6.37}$$

$$\overline{J} = a_0a_1|\overline{\boldsymbol{S}}|^2 + (a_0^2 + a_1^2)\det\overline{\boldsymbol{S}}. \tag{6.6.38}$$

Note that in order to obtain an expression for $(\overline{W}^{\,p})^p$, it suffices to solve for $|\overline{\boldsymbol{S}}|^2$, $\det\overline{\boldsymbol{S}}$ and $\overline{p}$ in terms of $|\overline{\boldsymbol{F}}|^2$ and $\overline{J}$. Eqs. (6.6.37) and (6.6.38) constitute two equations in the unknowns, which can be used to show that

$$|\overline{\boldsymbol{S}}|^2 = \frac{1}{(a_0^2 - a_1^2)^2}\left((a_0^2 + a_1^2)|\overline{\boldsymbol{F}}|^2 - 4a_0a_1\overline{J}\right) \tag{6.6.39}$$

$$\det\overline{\boldsymbol{S}} = \frac{1}{(a_0^2 - a_1^2)^2}\left(-a_0a_1|\overline{\boldsymbol{F}}|^2 + (a_0^2 + a_1^2)\overline{J}\right). \tag{6.6.40}$$

From this, we can immediately simplify our expression for $(\overline{W}^{p})^p(\overline{\boldsymbol{F}})$ to read

$$\begin{aligned}(\overline{W}^{p})^p(\overline{\boldsymbol{F}}) =& \frac{\breve{\mu}}{\breve{\mu}\overline{p} + 2\mu^{(1)}\mu^{(2)}}\left[\frac{\overline{\mu}\,\overline{p} + 2\mu^{(1)}\mu^{(2)}}{2}|\overline{\boldsymbol{F}}|^2\right. \\ &\left. - \frac{\breve{\mu}(\overline{p})^2 + (\overline{\mu}\breve{\mu} + 2\mu^{(1)}\mu^{(2)})\overline{p} + 2\breve{\mu}\mu^{(1)}\mu^{(2)}}{\breve{\mu}}\overline{J}\right],\end{aligned} \tag{6.6.41}$$

The third equation, which is needed to determine $\overline{p}$ is obtained by combining Eqs.

(6.6.35) and (6.6.38), leading to the requirement that

$$\left(a_0 a_1 + \frac{1}{2}\frac{\partial a_0}{\partial \overline{p}}\right)|\overline{\boldsymbol{S}}|^2 + \left((a_0^2 + a_1^2) + \frac{\partial a_1}{\partial \overline{p}}\right)\det \overline{\boldsymbol{S}} = 0. \tag{6.6.42}$$

A rather tedious calculation reveals that Eq. (6.6.42) is equivalent to the condition that

$$|\overline{\boldsymbol{S}}|^2 - 2\det \overline{\boldsymbol{S}} = 0, \tag{6.6.43}$$

which, from Eqs. (6.6.37) and (6.6.38), it follows that $|\overline{\boldsymbol{S}}|^2 = \overline{p}^2|\overline{\boldsymbol{F}}|^2$ and $\det \overline{\boldsymbol{S}} = \overline{p}^2\overline{J}$. However, in order for Eq. (6.6.43) to remain true, it must be that

$$\overline{p}^2(|\overline{\boldsymbol{F}}|^2 - 2\overline{J}) = 0. \tag{6.6.44}$$

Since, in general, $(|\overline{\boldsymbol{F}}|^2 - 2\overline{J}) \geqslant 0$, with equality only in a few cases (for example when $\overline{\boldsymbol{F}} = \boldsymbol{I}$), for our result to hold in general, we see that we require $\overline{p} = 0$. Using this in Eq. (6.6.41), gives us our final result, namely that

$$(\overline{W}^{p})^{p}(\overline{\boldsymbol{F}}) = \frac{\breve{\mu}}{2}(|\overline{\boldsymbol{F}}|^2 - 2) - (\breve{\mu} - 1)\overline{J}. \tag{6.6.45}$$

Chapter 7

Application to Neo-Hookean Hyperelastic Laminates Under General 3D Loading Conditions

Abstract

This paper deals with the stability and post-bifurcation response of reinforced hyperelastic composites under general loading conditions. It has long been known that these types of materials can undergo both microscopic and macroscopic instabilities. In the latter case, when the instability does not result in material failure, the behavior of the composite after the onset of the instability is less well understood. Recent work (Avazmohammadi and Ponte Castañeda, 2016) indicates that it is possible for the "principal" solution, i.e. the solution before the onset of any instability, to bifurcate into a lower energy solution via the formation of domains. These domains form on a scale much larger than that of the heterogeneity, but still smaller than that of the macroscopic specimen. This work is concerned with such domain formation in Neo-Hookean laminates under general three-dimensional loading. In order to obtain the post-bifurcation behavior, the quasiconvexification or relaxation of the principal solution is computed explicitly. In addition, it is shown that the macroscopic instabilities are triggered not by the loss of strong ellipticity, but rather by the loss of global rank-1 convexity of the principal solution, which, in general, happens first. The calculation also reveals that the relaxation requires, in general, a rank-2 "laminate-within-a-laminate" microstructure and allows for multiple "perfectly soft" modes of deformation.

7.1 Introduction

Reinforced elastomers are an important class of composite materials in many industrial applications. They include traditional types, such as fiber-reinforced elastomers, but also thermoplastic elastomers (TPEs), which are a special class of block copolymers consisting of "hard" (glassy or crystalline) and "soft" (rubbery) blocks that *self-assemble* at the nanometer scale into a wide range of microstructures (Fredrickson and Bates, 1996), including periodic arrangements of spherical particles (Prasman and Thomas, 1998), cylindrical fibers (Honeker et al., 2000) and layers (Cohen et al., 2000). Interestingly, highly oriented TPEs samples with layered and cylindrical microstructures are known to undergo instabilities for certain special loading configurations (Honeker et al., 2000). For example, highly oriented layered TPEs subjected to large stretches perpendicular to the layers undergo instabilities leading to a relatively soft macroscopic mechanical response. These instabilities at the macroscopic level are associated with the formation of "chevron" microstructures or lamellar domains (see Fig. 8 of Cohen et al., 2000) at the microscopic scale—similar to those observed in shape memory alloys.

This paper is concerned with the possible development of "material instabilities" in reinforced elastomeric composites and, more specifically, with their homogenized or macroscopic response beyond the onset of such instabilities. In particular, we are interested in the response of the composite after loss of strong ellipticity of the "principal" macroscopic response (or homogenized response *before* the onset of any instabilities). In this context, it is useful to recall (e.g., Truesdell and Toupin, 1960) that strong ellipticity is a sufficient condition for uniqueness of the elasticity boundary value problem of place (for a material with uniform properties). For metals and other materials exhibiting rate-independent plastic response, loss of strong ellipticity typically leads to localization of the deformation into bands and eventual failure of the material (Rice, 1976). For reinforced elastomeric composites, it has recently be

shown (Avazmohammadi and Ponte Castañeda, 2016) that loss of strong ellipticity can also lead to the formation of lamellar domains with associated "soft" (but stable) deformation modes. In this work, which builds on earlier work by Furer and Ponte Castañeda (2018a) for plane strain loading of layered composites, the macroscopic response of such layered elastomeric composites is investigated under more general three-dimensional loading conditions leading to loss of ellipticity of the principal homogenized response.

A general framework for describing the macroscopic response of hyperelastic composites undergoing finite strains was first given by Hill (1972). For hyperelastic composites with periodic microstructures, mathematically rigorous formulations incorporating the possible development of instabilities were developed by Braides (1985) and Müller (1987). These authors showed that the effective, or homogenized, stored-energy function of the composite can be computed by considering solutions that are periodic on multiple cells of the composite's microstructure and choosing the one that leads to the smallest overall energy. Exact results for the principal macroscopic response of layered composites under specific loading conditions were obtained by Triantafyllidis and Maker (1985). More significantly, these authors found that the principal solution could become unstable either by microbuckling of the layers (see also Rosen, 1965), or by long-wavelength buckling modes, which could be captured by loss of ellipticity of the principal macroscopic response. Building on these earlier works, Geymonat et al. (1993) considered more general periodic microstructures and provided conditions under which such *microscopic* and *macroscopic* instabilities can occur. In particular, they showed that the loss of strong ellipticity of the incremental problem associated with the homogenized energy function generally corresponds to the onset of macroscopic or long-wavelength instabilities. Applications to porous and rigidly reinforced elastomers with periodic microstructures were given by Triantafyllidis et al. (2006), Michel et al. (2007) and Michel et al. (2010). For the porous elastomers, Bertoldi et al. (2008) confirmed experimentally the existence

of the microscopic instabilities and also characterized the post-bifurcation response, which was found to exhibit soft modes of deformation. Bounds for hyperelastic composites with more general random microstructures have been given by Odgen (1978) and Ponte Castañeda (1989), while various estimates for the macroscopic response and onset of instabilities for such more general microstructures have been developed over the last 20 years (e.g., Ponte Castañeda and Tiberio, 2000; Lahellec et al., 2004; deBotton, 2005; Lopez-Pamies and Ponte Castañeda, 2006a,b; deBotton et al., 2006; Agoras et al., 2009a; Avazmohammadi and Ponte Castañeda, 2014a,b).

As already mentioned, this work is concerned with describing the effective response of hyperelastic composite materials after the onset of macroscopic instabilities. For this purpose, following Avazmohammadi and Ponte Castañeda (2016), we propose to make use of the *quasiconvexification*, or *relaxation*, of the principal solution for the energy, which can be viewed as a generalized Maxwell construction, where solutions are interpreted as (minimizing) sequences of deformations whose energies converge (in some appropriate sense) to a minimum value. The computation of the relaxation is in general a very difficult problem, and it is usually only possible to compute upper and lower bounds, as given by the *rank-1 convexification* and the *polyconvexification*, respectively (Ball, 1977; Kohn and Strang, 1986; Dacorogna, 1989). This methodology was developed and utilized by Ball and James (1987) to describe solid-solid phase transformations in martensitic materials. More recently, DeSimone and Dolzmann (2000, 2002) made use of this methodology to compute exactly the relaxation of the energy for a class of nematic liquid crystal elastomers (LCEs). In fact, they provided one of the first examples of the successful computation of the relaxation by first computing the rank-1 convexification and then showing that it is identical to its polyconvexification. In the context of hyperelastic composites, Avazmohammadi and Ponte Castañeda (2016) investigated the class of two-dimensional fiber-reinforced composites considered earlier by Lopez-Pamies and Ponte Castañeda (2006b), and used their estimate for the principal homogenized response to generate a correspond-

ing estimate for the relaxed energy, by first computing the rank-1 convexification and then showing that it is polyconvex. In turn, in Chapter 6, we made use of the same general approach—together with an exact estimate for the principal solution for the homogenized energy function—to generate exact estimates for the relaxation (or post-bifurcation) of the energy function for laminated composites subjected to plane strain loading conditions. One important finding in these works was that the principal solution generally loses global (strict) rank-1 convexity before loss of strong ellipticity, which suggests that the estimates for the onset of macroscopic instabilities based on loss of strong ellipticity of the principal solution (Geymonat et al., 1993) are, in general, only upper bounds for such instabilities.

Our primary focus here is to calculate the relaxation of the homogenized energy for a class of Neo-Hookean laminates under general three-dimensional loadings. Secondary to the calculation is an investigation of the relation between strict (global) rank-1 convexity of the homogenized energy and loss of ellipticity. As such, the rest of the paper is laid out as follows. Section 7.2 presents some basic results regarding laminated elastomer composites: Section 7.2.1 provides a brief review of transversely isotropic materials, and introduces new invariants that will turn out to be useful in the calculation of the relaxation, while Section 7.2.2 recalls some results for the principal solution. Then, Section 7.3 details the calculation of the relaxation, leading to the analytical expression (7.3.41) for the quasiconvexification $Q\widehat{W}$ in terms of the rank-1 convexification $R\widehat{W}$, as given by (7.3.32) with (7.3.29). Finally, Section 7.4 describes further the physical implications of the relaxation construction, and highlights the distinguishing features of the relaxed energy. While some of the important definitions relating to the calculus of variations are assumed to be known to the reader and recalled in the text, a more complete discussion of the relevant concepts needed in carrying out our analysis is given in Chapter 5.

We close the introduction by commenting on the notation that will be used in this work. We fix the standard Cartesian basis $\{\mathbf{e}_i\}$, with respect to which vectors with

Cartesian components a_i or A_i are represented by bold letters $\mathbf{a}$ or $\mathbf{A}$, respectively. Second-order tensors with Cartesian components F_{ij} are represented by bold italic letters $\boldsymbol{F}$, while fourth-order tensors with Cartesian components L_{ijkl} are denoted by barred letters $\mathbb{L}$. Here i, j, k, l range from 1 to 3. When appropriate, use will be made of the standard notation in continuum mechanics literature. Specifically, the Einstein summation convention will be utilized, so that repeated indices are summed over. Given two vectors $\mathbf{a}, \mathbf{b}$, the scalar product $\mathbf{a} \cdot \mathbf{b}$ is defined by $a_i b_i$, while the dyadic product $\mathbf{a} \otimes \mathbf{b}$ is defined to be the (rank-1) second-order tensor with Cartesian components $a_i b_j$. Similarly, the inner product of two second-order tensors is given by $\boldsymbol{H} \cdot \boldsymbol{G} = \text{tr}(\boldsymbol{H}\boldsymbol{G}^T) = H_{ij}G_{ij}$.

7.2 Preliminary Results for Laminates

7.2.1 Transverse Isotropy

By construction, a laminated composite consisting of isotropic phases exhibits transverse isotropy, where the direction of transverse isotropy, denoted by the unit vector $\mathbf{N}$, is normal to the layers and corresponds to the direction of lamination. Therefore, it is helpful to discuss the invariants that will be used in describing the constitutive behavior of these transversely isotropic materials.

Without loss of generality we take $\mathbf{N} = \mathbf{e}_1$, and choose $\mathbf{e}_2$ and $\mathbf{e}_3$ to be so that $\{\mathbf{e}_i\}$ represents the standard Cartesian basis. Now, given a macroscopic deformation gradient $\overline{\boldsymbol{F}}$, we define the associated right Cauchy-Green tensor as $\overline{\boldsymbol{C}} = \overline{\boldsymbol{F}}^T\overline{\boldsymbol{F}}$, and consider the following set of independent transversely isotropic invariants (e.g., Steigmann, 2003):

$$I_1 = \text{tr}(\overline{\boldsymbol{C}}),\ I_2 = \text{tr}(\overline{\boldsymbol{C}}^*),\ I_3 = \det(\overline{\boldsymbol{C}}),\ I_4 = \mathbf{N} \cdot (\overline{\boldsymbol{C}}\mathbf{N}),\ I_5 = \mathbf{N} \cdot (\overline{\boldsymbol{C}}^*\mathbf{N}), \qquad (7.2.1)$$

where $\overline{\boldsymbol{C}}^* = [\det(\overline{\boldsymbol{C}})]\overline{\boldsymbol{C}}^{-T}$ denotes the adjugate of $\overline{\boldsymbol{C}}$.

In the context of the laminates of interest in this work, the invariants I_4 and I_5 have simple physical interpretations. Note that $I_4 = \mathbf{N} \cdot \overline{\boldsymbol{C}}\mathbf{N} = |\overline{\boldsymbol{F}}\mathbf{N}|^2$, and hence, by taking

$$\lambda_n = |\overline{\boldsymbol{F}}\mathbf{N}| = \sqrt{I_4}, \tag{7.2.2}$$

we see that I_4 is related to λ_n, which represents the amount of stretch of a material line element that is aligned with $\mathbf{N}$ in the undeformed configuration.

Next, we recall Nanson's Formula:

$$\mathbf{n}da = \overline{\boldsymbol{F}}^{*}\mathbf{N}dA, \tag{7.2.3}$$

where dA represents the area of a material surface element with unit normal $\mathbf{N}$ in the undeformed configuration, while da represents the area of a material surface element with unit normal $\mathbf{n}$ in the deformed configuration. Thus, it follows that

$$\frac{da}{dA} = |\overline{\boldsymbol{F}}^{*}\mathbf{N}| = \sqrt{\mathbf{N} \cdot (\overline{\boldsymbol{C}}^{*}\mathbf{N})} = \sqrt{I_5}, \tag{7.2.4}$$

whereby it is seen that I_5 is related to the local change in area of a material surface element with outward normal $\mathbf{N}$ in the undeformed configuration.

As noted by Ericksen and Rivlin (1954), the list of invariants $I_1, \ldots, I_5$ is not unique. In fact, as we will see later, the sets of invariants that are needed to provide a concise description of the principal solution and relaxation of the incompressible laminated composite are different, and it is useful to introduce such alternative sets of invariants at this point. For this purpose, we define the symmetric (semi-positive definite) tensor

$$\boldsymbol{D} \equiv \overline{\boldsymbol{F}}\,\overline{\boldsymbol{F}}^{T} - (\overline{\boldsymbol{F}}\mathbf{N}) \otimes (\overline{\boldsymbol{F}}\mathbf{N}), \tag{7.2.5}$$

which, as shown in Section 7.6, is a transversely isotropic tensor function of $\overline{\boldsymbol{F}}$ and

can be diagonalized in the form

$$\boldsymbol{D} = d_2^2\,\mathbf{t}_2 \otimes \mathbf{t}_2 + d_3^2\,\mathbf{t}_3 \otimes \mathbf{t}_3 \tag{7.2.6}$$

where $0 = d_1^2 < d_2^2 \leqslant d_3^3$ represent the eigenvalues of $\boldsymbol{D}$, and where the set $\{\mathbf{t}_1, \mathbf{t}_2, \mathbf{t}_3\}$ are the corresponding eigenvectors, defined by

$$\mathbf{t}_1 = \frac{1}{\sqrt{I_5}}\overline{\boldsymbol{F}}^*\mathbf{N},\ \mathbf{t}_2 = \frac{1}{d_2}\overline{\boldsymbol{F}}\widehat{\mathbf{e}}_2,\ \mathbf{t}_3 = \frac{1}{d_3}\overline{\boldsymbol{F}}\widehat{\mathbf{e}}_3. \tag{7.2.7}$$

Here, as described in Section 7.6, $\widehat{\mathbf{e}}_2, \widehat{\mathbf{e}}_3$ are orthogonal unit vectors (also orthogonal to $\mathbf{N} = \mathbf{e}_1$), whose orientations depend on $\overline{\boldsymbol{F}}$. As also demonstrated in Section 7.6, $d_2 = |\boldsymbol{F}\widehat{\mathbf{e}}_2|$ and $d_3 = |\boldsymbol{F}\widehat{\mathbf{e}}_3|$ are transversely isotropic invariants of $\overline{\boldsymbol{F}}$ and straightforward calculations show that

$$d_2 = \sqrt{\frac{(I_1 - I_4) - \sqrt{(I_1 - I_4)^2 - 4I_5}}{2}}, \quad d_3 = \sqrt{\frac{(I_1 - I_4) + \sqrt{(I_1 - I_4)^2 - 4I_5}}{2}}, \tag{7.2.8}$$

with I_1, I_4 and I_5 as defined above. Further note that

$$d_2^2 + d_3^2 = I_1 - I_4, \quad d_2 d_3 = \sqrt{I_5}, \tag{7.2.9}$$

and, since $d_2 \leqslant d_3$, that $d_2^2 \leqslant \sqrt{I_5} \leqslant d_3^2$. Physically, d_2 and d_3 are the stretches of material line elements respectively aligned with the $\widehat{\mathbf{e}}_2$ and $\widehat{\mathbf{e}}_3$ directions within the layers. More precisely, $\boldsymbol{D}^{1/2}$ is a two-dimensional stretch tensor projected on the plane of the layers, while d_2 and d_3 are the associated principal stretches. However, in general, neither λ_n, nor d_2, d_3, are principal stretches.

In addition, we introduce invariants $\psi_k\,(k = 1, 2, 3)$, defined by

$$\cos\psi_k = \mathbf{t}_k \cdot \left(\frac{1}{|\overline{\boldsymbol{F}}\mathbf{N}|}\overline{\boldsymbol{F}}\mathbf{N}\right), \tag{7.2.10}$$

whereby ψ_k represents the angle between $\mathbf{t}_k$, defined in Eq. (7.2.7), and $\overline{\boldsymbol{F}}\mathbf{N}$. In particular, upon recalling (see Lopez-Pamies and Ponte Castañeda, 2009) that the rotation of the layers in a hyperelastic laminate is controlled by Nanson's formula, it is seen that ψ_1 is a measure of the amount of rotation of the layers in the current configuration relative to the orientation of a material line element initially aligned with the lamination direction $\mathbf{N}$ in the undeformed configuration.

It follows from expressions $(7.2.7)_1$ and (7.2.10) that

$$\cos\psi_1 = \sqrt{\frac{I_3}{I_4 I_5}} = \frac{\det\overline{\boldsymbol{F}}}{\lambda_n d_2 d_3}, \tag{7.2.11}$$

which, in the incompressible limit ($\det\overline{\boldsymbol{F}} = 1$), can be used to express λ_n in terms of d_2 and d_3, i.e.,

$$\lambda_n = \frac{1}{d_2 d_3 \cos\psi_1}. \tag{7.2.12}$$

Due to the impenetrability constraint $\det\overline{\boldsymbol{F}} > 0$, we see that $\cos\psi_1 > 0$, implying $-\frac{\pi}{2} < \psi_1 < \frac{\pi}{2}$. Since the vectors $\mathbf{t}_k$ form an orthonormal basis, we find that

$$\cos^2\psi_1 + \cos^2\psi_2 + \cos^2\psi_3 = 1, \tag{7.2.13}$$

which implies only two of the three angles are independent. Note that if $\psi_1 = 0$, then automatically $\psi_2 = \psi_3 = \frac{\pi}{2}$, by Eq. (7.2.13). Moreover, since $\cos\psi_1 > 0$, ψ_2 and ψ_3 cannot simultaneously take the value $\frac{\pi}{4}$, and neither ψ_2 nor ψ_3 can ever take the value 0.

As already noted, for the transversely isotropic materials, five invariants are required to completely describe $\overline{\boldsymbol{F}}$. As such, instead of using the classic transversely isotropic invariants $I_1, \ldots, I_5$, defined in Eq. (7.2.1), it is possible to alternatively use $d_2, d_3, \lambda_n, \psi_1$ and either ψ_2 or ψ_3. In terms of this choice of invariants, $I_1, \ldots, I_5$ can

be expressed as

$$I_1 = d_2^2 + d_3^2 + \lambda_n^2, \quad I_2 = \lambda_n^2(d_2^2 \sin^2\psi_2 + d_3^2 \sin^2\psi_3) + d_2^2 d_3^2,$$
$$I_3 = \lambda_n^2 d_2^2 d_3^2 \cos^2\psi_1, \quad I_4 = \lambda_n^2, \quad I_5 = d_2^2 d_3^2, \tag{7.2.14}$$

where it is recalled that ψ_1, ψ_2 and ψ_3 are related by (7.2.13). As shown in Proposition 9 of Section 7.6, when $\overline{\boldsymbol{F}}$ is such that the layers do not rotate relative to $\overline{\boldsymbol{F}}\mathbf{N}$ ($\psi_1 = 0$), λ_n, d_2 and d_3 become the principal stretches. More generally, if ψ_2 or ψ_3 takes the value $\frac{\pi}{2}$, then d_2 or d_3 becomes a principal stretch.

Finally, for use in the proof of polyconvexity, we introduce the invariants $i_3 = \sqrt{I_3} = \det(\overline{\boldsymbol{F}})$, $i_4 = |\overline{\boldsymbol{F}}\mathbf{N}| = \sqrt{I_4}$, $i_5 = |\overline{\boldsymbol{F}}^*\mathbf{N}| = \sqrt{I_5}$, $i_6 = d_3^2$, where we have attempted to make the notation consistent (except for i_6) with that of Steigmann (2003). Further details on the derivation of these results involving the various invariants, as well as other useful properties, are given in Section 7.6. To close this section, the above results for the sets of invariants that will be used going forward are summarized in Table 7.1.

Set	**Description**
(I_1, I_3, I_4, I_5)	$I_1 = \mathrm{tr}(\overline{\boldsymbol{C}})$, $I_3 = \det(\overline{\boldsymbol{C}})$, $I_4 = \mathbf{N}\cdot(\overline{\boldsymbol{C}}\mathbf{N})$, $I_5 = \mathbf{N}\cdot(\overline{\boldsymbol{C}}^*\mathbf{N})$.
$(\lambda_n, \psi_1, d_2, d_3)$	$\lambda_n = \sqrt{I_4}, \quad \cos^2\psi_1 = \dfrac{I_3}{I_4 I_5},$ $d_{2,3} = \sqrt{\dfrac{I_1 - I_4 \pm \sqrt{(I_1 - I_4)^2 - 4I_5}}{2}}.$
(i_3, i_4, i_5, i_6)	$i_3 = \det(\overline{\boldsymbol{F}})$, $i_4 = \lvert\overline{\boldsymbol{F}}\mathbf{N}\rvert$, $i_5 = \lvert\overline{\boldsymbol{F}}^*\mathbf{N}\rvert$, $i_6 = d_3^2$.

Table 7.1: This table summarizes the different sets of invariants, together with their definitions, used in various parts of the paper. Note that I_2 will not be needed and is therefore omitted from the table.

7.2.2 Principal solution $\widehat{W}$

Here, we consider a simple laminate consisting of two phases, which are layered in a direction with unit normal $\mathbf{N}$, in prescribed volume fractions $c^{(r)}$ $(r = 1, 2)$. For simplicity, the phases are assumed to be incompressible Neo-Hookean materials, with stored-energy functions of the form

$$W^{(r)}(\boldsymbol{F}) = \frac{\mu^{(r)}}{2}\mathrm{tr}(\boldsymbol{F}^T\boldsymbol{F} - \boldsymbol{I}) + K(\det \boldsymbol{F}), \tag{7.2.15}$$

where $\mu^{(r)}$ represents the shear modulus of phase r, and where

$$K(J) = \begin{cases} 0, & J = 1, \\ \infty, & J \neq 1 \end{cases} \tag{7.2.16}$$

serves to enforce the incompressibility condition.

For such laminated materials, the following expression, due to Agoras et al. (2009b) (see also deBotton, 2005), for the "principal" solution for the homogenized stored-energy function is known:

$$\widehat{W}(\overline{\boldsymbol{F}}) = \frac{\overline{\mu}}{2}(I_1 - 3) - \frac{\overline{\mu} - \breve{\mu}}{2}\left(I_4 - I_5^{-1}\right) + K(I_3), \tag{7.2.17}$$

where

$$\overline{\mu} = c^{(1)}\mu^{(1)} + c^{(2)}\mu^{(2)} \quad \text{and} \quad \breve{\mu} = \left(\frac{c^{(1)}}{\mu^{(1)}} + \frac{c^{(2)}}{\mu^{(2)}}\right)^{-1} \tag{7.2.18}$$

represent, respectively, the arithmetic and harmonic means of the shear moduli.

A straightforward calculation shows that the average Cauchy stress $\overline{\boldsymbol{T}} = \overline{\boldsymbol{S}}\,\overline{\boldsymbol{F}}^T$ is given by

$$\overline{\boldsymbol{T}} = \overline{\mu}\overline{\boldsymbol{F}}\,\overline{\boldsymbol{F}}^T - (\overline{\mu} - \breve{\mu})(\overline{\boldsymbol{F}}\mathbf{N}) \otimes (\overline{\boldsymbol{F}}\mathbf{N}) + \frac{(\overline{\mu} - \breve{\mu})}{|\overline{\boldsymbol{F}}^{-T}\mathbf{N}|^4}(\overline{\boldsymbol{F}}^{-T}\mathbf{N}) \otimes (\overline{\boldsymbol{F}}^{-T}\mathbf{N}) - p\boldsymbol{I}, \tag{7.2.19}$$

where p is an arbitrary Lagrange multiplier associated with incompressibility.

Next, we consider the application of the strong ellipticity condition for the laminate with stored-energy function $\widehat{W}$. However, due to incompressibility, the strong ellipticity condition at $\overline{\boldsymbol{F}}$ should be checked on the push-forward of the associated elasticity tensor $\widehat{\mathbb{L}}$ (Ogden, 1997), requiring that

$$\bar{F}_{jp}\bar{F}_{lq}\widehat{L}_{ipkq}(\overline{\boldsymbol{F}})m_i n_j m_k n_l = \bar{F}_{jp}\bar{F}_{lq}\frac{\partial^2\widehat{W}(\overline{\boldsymbol{F}})}{\partial\bar{F}_{ip}\partial\bar{F}_{kq}}m_i n_j m_k n_l > 0, \tag{7.2.20}$$

for all non-zero unit vectors $\mathbf{m}$ and $\mathbf{n}$ such that $\mathbf{m}\cdot\mathbf{n} = 0$. This condition can be shown (Agoras et al., 2009b) to reduce to

$$\begin{aligned}\overline{\mu}(\mathbf{n}\cdot\overline{\boldsymbol{F}}\,\overline{\boldsymbol{F}}^{T}\mathbf{n}) - (\overline{\mu}-\breve{\mu})[(\overline{\boldsymbol{F}}\mathbf{N})\cdot\mathbf{n}]^2 \\ + \frac{(\overline{\mu}-\breve{\mu})[(\overline{\boldsymbol{F}}^{-T}\mathbf{N})\cdot\mathbf{m}]^2}{|\overline{\boldsymbol{F}}^{-T}\mathbf{N}|^4}\left\{\frac{4[(\overline{\boldsymbol{F}}^{-T}\mathbf{N})\cdot\mathbf{n}]^2}{|\overline{\boldsymbol{F}}^{-T}\mathbf{N}|^2} - 1\right\} > 0.\end{aligned} \tag{7.2.21}$$

To properly check whether $\widehat{W}$ is strongly elliptic at a given $\overline{\boldsymbol{F}}$, it is useful to introduce the quantity

$$\widehat{\Lambda}(\overline{\boldsymbol{F}}) = \inf_{\substack{|\mathbf{n}|=|\mathbf{m}|=1\\ \mathbf{n}\cdot\mathbf{m}=0}} \bar{F}_{jp}\bar{F}_{lq}\frac{\partial^2\widehat{W}}{\partial\bar{F}_{ip}\partial\bar{F}_{kq}}(\overline{\boldsymbol{F}})m_i n_j m_k n_l, \tag{7.2.22}$$

which is often referred to as the best ellipticity constant (Geymonat et al., 1993). The constraints in the minimization problem defined in Eq. (7.2.22) are accounted for by making use of Lagrange multipliers. By writing out the stationary conditions, these multipliers can be solved for, and it can be shown that $\overline{\boldsymbol{F}}^{-T}\mathbf{N} \in \text{span}\{\mathbf{n},\mathbf{m}\}$, so that, in particular, $[(\overline{\boldsymbol{F}}^{-T}\mathbf{N})\cdot\mathbf{m}]^2 = |\overline{\boldsymbol{F}}^{-T}\mathbf{N}|^2 - [(\overline{\boldsymbol{F}}^{-T}\mathbf{N})\cdot\mathbf{n}]^2$. Therefore, we can write

$$\widehat{\Lambda}(\overline{\boldsymbol{F}}) = \inf_{|\mathbf{n}|=1}\mathcal{F}(\overline{\boldsymbol{F}},\mathbf{n}), \tag{7.2.23}$$

where

$$\mathcal{F}(\overline{\boldsymbol{F}},\mathbf{n}) = \overline{\mu}(\mathbf{n}\cdot\overline{\boldsymbol{F}}\,\overline{\boldsymbol{F}}^{T}\mathbf{n}) - (\overline{\mu}-\breve{\mu})[(\overline{\boldsymbol{F}}\mathbf{N})\cdot\mathbf{n}]^2 + \frac{\overline{\mu}-\breve{\mu}}{|\overline{\boldsymbol{F}}^{-T}\mathbf{N}|^2}\left\{1-\frac{[(\overline{\boldsymbol{F}}^{-T}\mathbf{N})\cdot\mathbf{n}]^2}{|\overline{\boldsymbol{F}}^{-T}\mathbf{N}|^2}\right\}\left\{\frac{4[(\overline{\boldsymbol{F}}^{-T}\mathbf{N})\cdot\mathbf{n}]^2}{|\overline{\boldsymbol{F}}^{-T}\mathbf{N}|^2}-1\right\}. \tag{7.2.24}$$

The minimization in Eq. (7.2.23) can be carried out numerically, but there are some cases in which the calculation can be done explicitly. We discuss two such special cases next. In what follows, we make use of the quantity $\widetilde{\lambda}$, defined by

$$0<\widetilde{\lambda}\equiv 1-\frac{\breve{\mu}}{\overline{\mu}}<1. \tag{7.2.25}$$

Pure Shear: In pure shear, the deformation gradient takes the form

$$\overline{\boldsymbol{F}} = \lambda_n\mathbf{e}_1\otimes\mathbf{e}_1+\mathbf{e}_2\otimes\mathbf{e}_2+\lambda_n^{-1}\mathbf{e}_3\otimes\mathbf{e}_3, \tag{7.2.26}$$

and the laminate loses strong ellipticity when

$$\lambda_n=\lambda_{se}^{ps}=\widetilde{\lambda}^{-1/4}>1, \tag{7.2.27}$$

which corresponds to sufficiently large tension in the direction normal to the layers and agrees with the result of Triantafyllidis and Maker (1985).

Axisymmetric Compression/Extension: For the case of axisymmetric compression/extension, the deformation gradient takes the form

$$\overline{\boldsymbol{F}} = \lambda_n\mathbf{e}_1\otimes\mathbf{e}_1+\lambda_n^{-1/2}\mathbf{e}_2\otimes\mathbf{e}_2+\lambda_n^{-1/2}\mathbf{e}_3\otimes\mathbf{e}_3, \tag{7.2.28}$$

and the Neo-Hookean laminate loses strong ellipticity under axisymmetric extension when

$$\lambda_n=\lambda_{se}^{axi}=\widetilde{\lambda}^{-1/3}>1, \tag{7.2.29}$$

which agrees exactly with the findings of Agoras et al. (2009b). Note that

$$1 < \lambda_{se}^{ps} \leqslant \lambda_{se}^{axi}, \tag{7.2.30}$$

with equality if and only if $\mu^{(1)} \to \mu^{(2)}$ (in which case $\lambda_{se}^{axi} = \lambda_{se}^{ps} \to \infty$).

7.3 Relaxation of the energy

7.3.1 Rank-1 convexification of $\widehat{W}$

We calculate $R\widehat{W}$ by making use of the Kohn-Strang formula (Kohn and Strang, 1986). Thus, upon defining $R_0\widehat{W} = \widehat{W}$, and

$$R_k\widehat{W}(\overline{\boldsymbol{F}}) = \inf_{\mathbf{a},\mathbf{N}_k,c_k} \Big\{(1-c_k)R_{k-1}\widehat{W}(\overline{\boldsymbol{F}} - c_k\mathbf{a}\otimes\mathbf{N}_k) + c_kR_{k-1}\widehat{W}(\overline{\boldsymbol{F}} + (1-c_k)\mathbf{a}\otimes\mathbf{N}_k)\Big\}, \tag{7.3.1}$$

for $k = 1, 2, ...$, it follows that

$$R\widehat{W}(\overline{\boldsymbol{F}}) = \lim_{k\to\infty} R_k\widehat{W}(\overline{\boldsymbol{F}}). \tag{7.3.2}$$

As will be seen later, for the neo-Hookean laminates of interest here, it will be necessary to perform two iterations of the lamination procedure to obtain the rank-1 convexification.

In addition, as will also be seen later, the relaxation of the energy of the laminate is best expressed in terms of the invariants $\lambda_n, \psi_1, d_2, d_3$, defined in the previous section and listed in Table 7.1. For this reason, it is convenient to also rewrite the expression for the principal solution of the energy $\widehat{W}$ in terms of these invariants. Thus, using the identities (7.2.9), it can be readily shown that expression (7.2.17) for $\widehat{W}$ can be alternatively written in the form

$$\widehat{W}(\overline{\boldsymbol{F}}) = \frac{\breve{\mu}}{2}\lambda_n^2 + g_0(d_2, d_3) + K(d_2d_3\lambda_n\cos\psi_1), \tag{7.3.3}$$

where

$$g_0(d_2, d_3) = \frac{\overline{\mu}}{2}\left(d_2^2 + d_3^2 - 3 + \frac{\widetilde{\lambda}}{(d_2 d_3)^2}\right), \tag{7.3.4}$$

and the function K, defined by (7.2.16), serves to enforce the incompressibility condition given by (7.2.12). Note that the result is symmetric in d_2 and d_3, as expected, in spite of our labeling convention that $d_2 \leqslant d_3$. Moreover, the principal solution is written in this fashion because the relaxation procedure described below will only affect the "hard" part of the energy defined by the function g_0 and proportional to $\overline{\mu}$. Indeed, the relaxation procedure will essentially correspond to the "softening" of certain modes of deformation associated with g_0 by the formation of suitably oriented domains.

7.3.1.1 Calculation of $R_1\widehat{W}$

We start by making use of Eq. (7.3.1) with $k = 1$. On account of incompressibility, $\widehat{W}(\overline{\boldsymbol{F}})$ returns an infinite value for $\overline{\boldsymbol{F}}$ with $\det \overline{\boldsymbol{F}} \neq 1$, and, as noted by deBotton (2005) in his work on sequentially layered elastomers, we can restrict our attention to values of $\mathbf{a}$ and $\mathbf{N}_1$ in the infima of Eq. (7.3.1) that satisfy

$$1 = \det(\overline{\boldsymbol{F}} - c_1 \mathbf{a} \otimes \mathbf{N}_1) = \det \overline{\boldsymbol{F}} \det(\boldsymbol{I} - c_1 \overline{\boldsymbol{F}}^{-1} \mathbf{a} \otimes \mathbf{N}_1) = (1 - c_1 \overline{\boldsymbol{F}}^{-1} \mathbf{a} \cdot \mathbf{N}_1), \tag{7.3.5}$$

implying that $(\overline{\boldsymbol{F}}^{-1}\mathbf{a}) \cdot \mathbf{N}_1 = 0$. Therefore, upon defining $\omega_1 = |\overline{\boldsymbol{F}}^{-1}\mathbf{a}|$ and $\mathbf{M}_1 = \frac{1}{\omega_1}\overline{\boldsymbol{F}}^{-1}\mathbf{a}$, we look to calculate

$$\begin{aligned} R_1\widehat{W}(\overline{\boldsymbol{F}}) = \inf_{\substack{\omega_1, c_1, \mathbf{N}_1, \mathbf{M}_1 \\ |\mathbf{N}_1|=|\mathbf{M}_1|=1,\, \mathbf{N}_1 \cdot \mathbf{M}_1 = 0}} \Big\{ & (1 - c_1)\widehat{W}(\overline{\boldsymbol{F}}[\boldsymbol{I} - c_1 \omega_1 \mathbf{M}_1 \otimes \mathbf{N}_1]) \\ & + c_1 \widehat{W}(\overline{\boldsymbol{F}}[\boldsymbol{I} + (1 - c_1)\omega_1 \mathbf{M}_1 \otimes \mathbf{N}_1]) \Big\}. \end{aligned} \tag{7.3.6}$$

By construction, $|\mathbf{M}_1| = 1$, and, without loss of generality, we have assumed that $|\mathbf{N}_1| = 1$. Then, the orthogonality constraint reduces the number of scalar unknowns

needed to determine the optimal values of $\mathbf{N}_1$ and $\mathbf{M}_1$ down to three, which we represent as the three angles ϕ_1, θ_1 and β_1. As such, we look to solve the 5-dimensional minimization problem

$$R_1\widehat{W}(\overline{\boldsymbol{F}}) = \inf_{\omega_1,c_1,\phi_1,\theta_1,\beta_1} \Big\{(1-c_1)\widehat{W}(\overline{\boldsymbol{F}}[\boldsymbol{I} - c_1\omega_1\mathbf{M}_1\otimes\mathbf{N}_1]) \\ +c_1\widehat{W}(\overline{\boldsymbol{F}}[\boldsymbol{I} + (1-c_1)\omega_1\mathbf{M}_1\otimes\mathbf{N}_1]\Big\}, \tag{7.3.7}$$

where, with respect to the Cartesian basis $\{\mathbf{e}_i\}$,

$$\mathbf{N}_1 = \begin{bmatrix} \cos\phi_1 \\ \sin\phi_1\cos\theta_1 \\ -\sin\phi_1\sin\theta_1 \end{bmatrix},\ \mathbf{M}_1 = \cos\beta_1 \begin{bmatrix} -\sin\phi_1 \\ \cos\phi_1\cos\theta_1 \\ -\cos\phi_1\sin\theta_1 \end{bmatrix} + \sin\beta_1 \begin{bmatrix} 0 \\ \sin\theta_1 \\ \cos\theta_1 \end{bmatrix}. \tag{7.3.8}$$

From the associated stationary conditions, we find that $\phi_1 = \frac{\pi}{2}$, and

$$\tan(2\theta_1) = \frac{2\overline{C}_{23}}{\overline{C}_{33} - \overline{C}_{22}}, \tag{7.3.9}$$

where $\overline{C}_{ij}$ are the Cartesian components of $\overline{\boldsymbol{C}} = \overline{\boldsymbol{F}}^T\,\overline{\boldsymbol{F}}$. In particular, we observe that $\mathbf{N}_1\cdot\mathbf{N} = 0$, so that the direction of lamination in this rank-1 lamination procedure is orthogonal to the direction of lamination of the original layered material. It is interesting to note that $\theta_1 = \widehat{\theta}$, where $\widehat{\theta}$ is given by Equation (7.6.8) in the definition of the eigenvectors of $\boldsymbol{D} = \overline{\boldsymbol{F}}\,\overline{\boldsymbol{F}}^T - (\overline{\boldsymbol{F}}\mathbf{N})\otimes(\overline{\boldsymbol{F}}\mathbf{N})$. In fact, we have $\mathbf{N}_1 = \widehat{\mathbf{e}}_2$, while

$$\tan(\beta_1) = \frac{(\overline{\boldsymbol{F}}\widehat{\mathbf{e}}_3)\cdot(\overline{\boldsymbol{F}}\mathbf{N})}{d_3^2}, \tag{7.3.10}$$

$$\omega_1 = \pm\frac{2}{\cos(\beta_1)|\overline{\boldsymbol{F}}^{-T}\widehat{\mathbf{e}}_2|^2}\sqrt{\sqrt{\widetilde{\lambda}}d_3|\overline{\boldsymbol{F}}^{-T}\widehat{\mathbf{e}}_2|^2 - d_3^2}, \tag{7.3.11}$$

and

$$c_1 = \frac{1}{2}\left(1 \pm \frac{(\overline{\boldsymbol{F}}^{-T}\mathbf{N})\cdot(\overline{\boldsymbol{F}}^{-T}\widehat{\mathbf{e}}_2)}{\sqrt{\sqrt{\widetilde{\lambda}}d_3|\overline{\boldsymbol{F}}^{-T}\widehat{\mathbf{e}}_2|^2 - d_3^2}}\right). \tag{7.3.12}$$

It is clear that from Eq. (7.3.7) that $R\widehat{W}(\overline{\boldsymbol{F}})$ is not identically $\widehat{W}(\boldsymbol{F})$ so long as $c_1 \neq 0$ or 1, or $\omega_1 \neq 0$; in any of these cases, neither $\overline{\boldsymbol{F}}[\boldsymbol{I} - c_1\omega_1\mathbf{M}_1 \otimes \mathbf{N}_1]$ nor $\overline{\boldsymbol{F}}[\boldsymbol{I} + (1-c_1)\omega_1\mathbf{M}_1 \otimes \mathbf{N}_1]$ will equal $\overline{\boldsymbol{F}}$. Moreover, Eqs. (7.3.10)-(7.3.12) can be used to show that the above requirement boils down to

$$0 \leqslant c_1(1-c_1)\omega_1^2 = \frac{1}{\cos^2(\beta_1)|\overline{\boldsymbol{F}}^{-T}\widehat{\mathbf{e}}_2|^2}\left(\sqrt{\widetilde{\lambda}}d_3 - (d_2d_3)^2\right), \tag{7.3.13}$$

where it is recalled that d_2 has been assumed to be less than d_3. It thus follows that, in order for $R\widehat{W}(\overline{\boldsymbol{F}})$ to be different from $\widehat{W}(\boldsymbol{F})$, the condition

$$d_2 < \frac{\widetilde{\lambda}^{1/4}}{d_3^{1/2}} \tag{7.3.14}$$

must be satisfied.

Then, defining

$$g_1(d_2, d_3) = \frac{\overline{\mu}}{2}\left(d_3^2 + 2\frac{\widetilde{\lambda}^{1/2}}{d_3} - 3\right), \tag{7.3.15}$$

it can be shown that the energy (7.3.6) of the rank-1 lamination can be expressed in the form (cf. (7.3.3) with (7.3.4))

$$R_1\widehat{W}(\overline{\boldsymbol{F}}) = \frac{\breve{\mu}}{2}\lambda_n^2 + g(d_2, d_3) + K(d_2d_3\lambda_n\cos\psi_1), \tag{7.3.16}$$

where

$$g(d_2, d_3) = \begin{cases} g_0(d_2, d_3) & d_2 \geqslant \widetilde{\lambda}^{1/4}/d_3^{1/2}, \\ g_1(d_2, d_3) & d_2 < \widetilde{\lambda}^{1/4}/d_3^{1/2}. \end{cases} \tag{7.3.17}$$

Having obtained an analytical expression for $R_1\widehat{W}$ in terms of $\overline{\boldsymbol{F}}$, we now check to see whether or not it is rank-1 convex. To do this, we simply check the Legendre-Hadamard condition, as given by Eq. (7.2.20) (with the inequality $>$ replaced by $\geqslant$), as it pertains to $R_1\widehat{W}$. Clearly, in the region where $R_1\widehat{W}(\overline{\boldsymbol{F}}) = \widehat{W}(\overline{\boldsymbol{F}})$, we know that $\widehat{W}$ is rank-1 convex already. Therefore, $R_1\widehat{W}$ is globally rank-1 convex if and only

if its associated elasticity tensor $\widehat{\mathbb{L}}^{R1}$ satisfies the Legendre-Hadamard condition for $d_2 < \widetilde{\lambda}^{1/4}/d_3^{1/2}$. We find that, in this region,

$$\bar{F}_{jp}\bar{F}_{lq}\widehat{L}^{R1}_{ipkq}m_i n_j m_k n_l = \breve{\mu}[(\overline{\boldsymbol{F}}\mathbf{N})\cdot\mathbf{n}]^2 + \frac{3\overline{\mu}}{4}\sqrt{\widetilde{\lambda}}d_3^{-5}\left[\mathbf{m}\cdot\left(\frac{\partial d_3^2}{\partial\overline{\boldsymbol{F}}}\overline{\boldsymbol{F}}^T\mathbf{n}\right)\right]^2 + \frac{\overline{\mu}}{2}\left(1-\sqrt{\widetilde{\lambda}}d_3^{-3}\right)\bar{F}_{jp}\bar{F}_{lq}\frac{\partial^2 d_3^2}{\partial\bar{F}_{ip}\partial\bar{F}_{kq}}m_i n_j m_k n_l, \tag{7.3.18}$$

where expressions for $\frac{\partial d_3^2}{\partial\overline{\boldsymbol{F}}}$ as well as $\frac{\partial^2 d_3^2}{\partial\overline{\boldsymbol{F}}\partial\overline{\boldsymbol{F}}}$ are given by Proposition 7 in Section 7.6. Note that the first two terms are certainly always positive, as is the factor involving $\frac{\partial^2 d_3^2}{\partial\overline{\boldsymbol{F}}\partial\overline{\boldsymbol{F}}}$ in the last term, on account of the convexity of the mapping $\overline{\boldsymbol{F}} \mapsto d_3^2[\overline{\boldsymbol{F}}]$ (see Section 7.6). However, the factor $\left(1-\sqrt{\widetilde{\lambda}}d_3^{-3}\right)$ in the last term need not be positive. In fact, by taking $\mathbf{m} = \mathbf{t}_2$ and $\mathbf{n} = \mathbf{t}_3$, and choosing $\overline{\boldsymbol{F}}$ for which

$$d_2 < \widetilde{\lambda}^{1/4}/d_3^{1/2} \quad \text{and} \quad d_3 < \widetilde{\lambda}^{1/6}, \tag{7.3.19}$$

the expression in Eq. (7.3.18) can be shown to reduce to

$$\bar{F}_{jp}\bar{F}_{lq}\widehat{L}^{R1}_{ipkq}m_i n_j m_k n_l = \breve{\mu}[(\overline{\boldsymbol{F}}\mathbf{N})\cdot\mathbf{t}_3]^2 + \overline{\mu}\left(1-\sqrt{\widetilde{\lambda}}d_3^{-3}\right)\frac{d_3^4}{d_3^2-d_2^2}, \tag{7.3.20}$$

which is less than zero whenever $[(\overline{\boldsymbol{F}}\mathbf{N})\cdot\mathbf{t}_3]^2$—an expression for which is given by (7.6.49) in Section 7.6—is small enough. For definiteness, we remark that there exist deformations satisfying Eq. (7.3.19) and $[(\overline{\boldsymbol{F}}\mathbf{N})\cdot\mathbf{t}_3]^2 = 0$. Hence, $R_1\widehat{W}$ fails to be rank-1 convex in this part of the domain, and we must perform (at least) a second lamination procedure in order to find $R\widehat{W}$.

7.3.1.2 Calculation of $R_2\widehat{W}$

Following the sequential lamination procedure, and making use of Eq. (7.3.1), with $k = 2$, we now look to compute

$$R_2\widehat{W}(\overline{\boldsymbol{F}}) = \inf_{\omega_2,c_2,\phi_2,\theta_2,\beta_2} \Big\{(1-c_2)R_1\widehat{W}(\overline{\boldsymbol{F}}[\boldsymbol{I} - c_2\omega_2\mathbf{M}_2\otimes\mathbf{N}_2]) \\ +c_2R_1\widehat{W}(\overline{\boldsymbol{F}}[\boldsymbol{I} + (1-c_2)\omega_2\mathbf{M}_2\otimes\mathbf{N}_2])\Big\}, \tag{7.3.21}$$

where $\mathbf{N}_2$ and $\mathbf{M}_2$ are expressed in terms of ϕ_2, θ_2 and β_2 in the same way as $\mathbf{N}_1$ and $\mathbf{M}_1$ are in terms of ϕ_1, θ_1 and β_1 in Eq. (7.3.8). The stationary conditions reveal that $\phi_2 = \frac{\pi}{2}$, which implies $\mathbf{N}_2 \cdot \mathbf{N} = 0$. Moreover, for any choice of θ_2 and β_2, upon defining

$$A_1 = \widetilde{\lambda}^{1/3}(\overline{\boldsymbol{F}}\mathbf{M}_2)\cdot(\overline{\boldsymbol{F}}\mathbf{N}_2) - \cos(\beta_2)(\overline{\boldsymbol{F}}^{-T}\mathbf{N}_2)\cdot(\overline{\boldsymbol{F}}^{-T}\mathbf{N}), \tag{7.3.22}$$

$$A_2 = \widetilde{\lambda}^{1/3}|\overline{\boldsymbol{F}}\mathbf{M}_2|^2 - \cos^2(\beta_2)|\overline{\boldsymbol{F}}^{-T}\mathbf{N}_2|, \tag{7.3.23}$$

we find that

$$\omega_2 = \pm\frac{2}{A_2}\sqrt{A_1^2 + [\widetilde{\lambda}^{2/3} - (I_1 - I_4)\widetilde{\lambda}^{1/3} + I_5]A_2} \tag{7.3.24}$$

and

$$c_2 = \frac{1}{2}\left(1 \pm \frac{A_1}{\sqrt{A_1^2 + [\widetilde{\lambda}^{2/3} - (I_1 - I_4)\widetilde{\lambda}^{1/3} + I_5]A_2}}\right). \tag{7.3.25}$$

Eqs. (7.3.24)-(7.3.25) are direct consequences of the fact that

$$d_3\left[\overline{\boldsymbol{F}}(\boldsymbol{I} - c_2\omega_2\mathbf{M}_2\otimes\mathbf{N}_2)\right] = d_3\left[\overline{\boldsymbol{F}}(\boldsymbol{I} + (1-c_2)\omega_2\mathbf{M}_2\otimes\mathbf{N}_2)\right] = \widetilde{\lambda}^{1/6}. \tag{7.3.26}$$

As was the case for $R_1\widehat{W}$, $R_2\widehat{W}$ is not identically $R_1\widehat{W}$ as long as $c_2 \neq 0$ or 1, or $\omega_2 \neq 0$. Analogous to Eq. (7.3.13), we find that this requirement reduces to

$$0 \leqslant c_2(1-c_2)\omega_2^2 = \frac{\widetilde{\lambda}^{2/3} - (I_1 - I_4)\widetilde{\lambda}^{1/3} + I_5}{A_2}, \tag{7.3.27}$$

where it is noted that the numerator $\widetilde{\lambda}^{2/3} - (I_1 - I_4)\widetilde{\lambda}^{1/3} + I_5$ is nothing more than the part of the characteristic polynomial of $\boldsymbol{D}$ that determines its nonzero eigenvalues, evaluated at $\widetilde{\lambda}^{1/3}$ (see Eq. (7.6.9) in Section 7.6 for details). Therefore, the first time that this expression is identically zero is precisely when $\overline{\boldsymbol{F}}$ is such that $d_3 = \widetilde{\lambda}^{1/6}$. As a consequence, it can be shown that the rank-2 lamination can be expressed in the form

$$R_2\widehat{W}(\overline{\boldsymbol{F}}) = \frac{\breve{\mu}}{2}\lambda_n^2 + g_r(d_2, d_3) + K(d_2 d_3 \lambda_n \cos\psi_1), \tag{7.3.28}$$

where (recall that $d_2 \leqslant d_3$)

$$g_r(d_2, d_3) = \begin{cases} g_0(d_2, d_3) & d_2 \geqslant \widetilde{\lambda}^{1/4}/d_3^{1/2}, \\ g_1(d_2, d_3) & d_2 < \widetilde{\lambda}^{1/4}/d_3^{1/2} \text{ and } d_3 \geqslant \widetilde{\lambda}^{1/6}, \\ g_2(d_2, d_3) & d_3 < \widetilde{\lambda}^{1/6}. \end{cases} \tag{7.3.29}$$

and where

$$g_2(d_2, d_3) = \frac{3\overline{\mu}}{2}(\widetilde{\lambda}^{1/3} - 1). \tag{7.3.30}$$

A simple calculation then shows that

$$\overline{F}_{jp}\overline{F}_{lq}\frac{\partial^2 g_2}{\partial \overline{F}_{ip}\partial \overline{F}_{kq}} m_i n_j m_k n_l = \breve{\mu}\left[(\overline{\boldsymbol{F}}\mathbf{N}_0)\cdot\mathbf{n}\right]^2 \geqslant 0. \tag{7.3.31}$$

Therefore, g_2 is rank-1 convex whenever $d_2 \leqslant d_3 < \widetilde{\lambda}^{1/6}$. Moreover, g_1 is rank-1 convex in the region where $d_2 < \widetilde{\lambda}^{1/4}/d_3^{1/2}$ and $d_3 \geqslant \widetilde{\lambda}^{1/6}$ (see Eq. (7.3.18)), while $g_0(\overline{\boldsymbol{F}})$ is rank-1 convex when $d_2 \geqslant \widetilde{\lambda}^{1/4}/d_3^{1/2}$. In conclusion, $R_2\widehat{W}$ is rank-1 convex, and it must therefore be the rank-1 convexification of the principal solution $\widehat{W}$, so that

$$R\widehat{W}(\overline{\boldsymbol{F}}) = R_2\widehat{W}(\overline{\boldsymbol{F}}) = \frac{\breve{\mu}}{2}\lambda_n^2 + g_r(d_2, d_3) + K(d_2 d_3 \lambda_n \cos\psi_1), \tag{7.3.32}$$

where g_r is given by expressions (7.3.29). It should be remarked that the final expression for $R\widehat{W}$ is not symmetric in d_2 and d_3, due to the lack of symmetry of g_1,

as defined by (7.3.15). This is a consequence of the labeling convention that $d_2 \leqslant d_3$. However, it is clear from the derivation that an identical result would be obtained with d_2 and d_3 interchanged, had d_2 been assumed to be greater than d_3. Therefore, the result for $R\widehat{W}$ could be rewritten for general values of d_2 and d_3 by symmetrizing g_r, which would involve symmetrizing only g_1 in d_2 and d_3, since g_0 and g_2 are already symmetric.

We close this section by recording expressions for the Cauchy stresses associated with $R\widehat{W}$. A straightforward calculation gives

$$\overline{\boldsymbol{T}} = \breve{\mu}(\overline{\boldsymbol{F}}\mathbf{N}) \otimes (\overline{\boldsymbol{F}}\mathbf{N}) + \overline{\mu}\,\overline{\boldsymbol{T}}_r - p\boldsymbol{I}, \tag{7.3.33}$$

where p is an arbitrary hydrostatic stress associated with the incompressibility constraint, and where

$$\overline{\boldsymbol{T}}_r = \begin{cases} \dfrac{\widetilde{\lambda}}{(d_2 d_3)^2}\,\mathbf{t}_1 \otimes \mathbf{t}_1 + d_2^2 \mathbf{t}_2 \otimes \mathbf{t}_2 + d_3^2 \mathbf{t}_3 \otimes \mathbf{t}_3, & d_2 \geqslant \widetilde{\lambda}^{1/4}/d_3^{1/2}, \\ \left(d_3^2 - \sqrt{\widetilde{\lambda}} d_3^{-1}\right) \mathbf{t}_3 \otimes \mathbf{t}_3, & d_2 < \widetilde{\lambda}^{1/4}/d_3^{1/2} \text{ and } d_3 \geqslant \widetilde{\lambda}^{1/6}, \\ \mathbf{0}, & d_3 < \widetilde{\lambda}^{1/6}. \end{cases} \tag{7.3.34}$$

Written in this form, it is seen that the stress component $\breve{\mu}(\overline{\boldsymbol{F}}\mathbf{N}) \otimes (\overline{\boldsymbol{F}}\mathbf{N})$ corresponds to the "soft" part of the principal solution for the energy $(\breve{\mu}/2)\lambda_n^2$, while $\overline{\boldsymbol{T}}_r$ corresponds to the relaxation g_r of the "hard" part of the energy g_0, as given by expression (7.3.29) and (7.3.4), respectively. It should be recalled that λ_n is related to the layer in-plane stretches d_2 and d_3 by the incompressibility constraint $\lambda_n d_2 d_3 \cos\psi_1 = 1$. In connection with (7.3.34), it is seen that, with each lamination, there are fewer such hard modes of deformation, and, in fact, after a second lamination procedure, none are left. More specifically, the macroscopic Cauchy stress $\overline{\boldsymbol{T}}$ is given by the "relaxed" stress contribution $\overline{\boldsymbol{T}}_r$ superimposed on a (soft) uniaxial stress $\breve{\mu}(\overline{\boldsymbol{F}}\mathbf{N}) \otimes (\overline{\boldsymbol{F}}\mathbf{N})$ (and an arbitrary pressure associated with the incompressibility constraint). Moreover,

the relaxed stress, which initially has three independent "hard" modes (in the unrelaxed region), loses 2 such modes in the rank-1 lamination region and all 3 in the rank-2 region. This means, for example, that in the rank-2 region, the relaxed stress is identically zero, making all the components of the total stress vanish and leading to perfectly soft (liquid-like) response—except for the uniaxial state associated with $(\overline{\boldsymbol{F}}\mathbf{N})\otimes(\overline{\boldsymbol{F}}\mathbf{N})$ (and the arbitrary hydrostatic pressure). In particular, this also means that the stress will be constant if the quantity $\overline{\boldsymbol{F}}\mathbf{N}$ is left unchanged; in other words, the remaining deformation will be accommodated by changing the structure (e.g., the volume fractions) of the domains. This was also found to be the case for plane strain loading, as was discussed by Furer and Ponte Castañeda (2018a). In fact, it can be shown that Eqs. (7.3.28)-(7.3.29), and hence Eqs. (7.3.33)-(7.3.34), reduce to the results obtained by Furer and Ponte Castañeda (2018a) for plane strain conditions. It should also be noted that—just like the expression (7.3.32) for $R\widehat{W}$—the above expressions for $\overline{\boldsymbol{T}}$ (specifically the part given by $\overline{\boldsymbol{T}}_r$, which is valid for $d_2 \leqslant d_3$) can also be generalized for arbitrary values of d_2 and d_3 by symmetrizing the second expression in (7.3.34) for $\overline{\boldsymbol{T}}_r$ with respect to d_2 and d_3.

7.3.2 Polyconvexity of $R\widehat{W}$

To establish the polyconvexity of $R\widehat{W}$, we start by rewriting the expression (7.3.32) together with (7.3.29), as functions of i_3, i_4, i_5 and i_6, as defined in Table 7.1. Indeed, it is straightforward to see that

$$R\widehat{W}(\overline{\boldsymbol{F}}) = f(\overline{\boldsymbol{F}}) + K(\det \overline{\boldsymbol{F}}) = w(i_4, i_5, i_6) + K(i_3), \tag{7.3.35}$$

where

$$w(i_4,i_5,i_6) = \begin{cases} w_0(i_4,i_5,i_6) = \frac{\breve{\mu}}{2}i_4^2 + \frac{\overline{\mu}}{2}\left(i_6 + i_5^2 i_6^{-1} + \widetilde{\lambda} i_5^{-2} - 3\right), & i_6 \leqslant \widetilde{\lambda}^{-1} i_5^4, \\ w_1(i_4,i_5,i_6) = \frac{\breve{\mu}}{2}i_4^2 + \frac{\overline{\mu}}{2}\left(i_6 + 2\sqrt{\widetilde{\lambda} i_6^{-1}} - 3\right), & \widetilde{\lambda}^{-1} i_5^4 < i_6 \text{ and } \widetilde{\lambda}^{1/3} \leqslant i_6, \\ w_2(i_4,i_5,i_6) = \frac{\breve{\mu}}{2}i_4^2 + \frac{3\overline{\mu}}{2}\left(\widetilde{\lambda}^{1/3} - 1\right), & i_6 < \widetilde{\lambda}^{1/3}. \end{cases} \tag{7.3.36}$$

Now, $K(i_3)$ is certainly convex in $i_3 = \det \overline{\boldsymbol{F}}$. Therefore, by the result of Schröder and Neff (2003) pertaining to additive polyconvex functions, it will then follow that $R\widehat{W}$ is polyconvex provided that we can show that w is also polyconvex. On the other hand, Proposition 10 states that $f(\overline{\boldsymbol{F}}) = w(i_4,i_5,i_6)$ is polyconvex if w can be shown to be a continuously differentiable function that is convex and nondecreasing in each of its arguments.

It is easy to see that $w_0(i_4,(\widetilde{\lambda} i_6)^{1/4},i_6) = w_1(i_4,(\widetilde{\lambda} i_6)^{1/4},i_6)$ and $w_1(i_4,i_5,\widetilde{\lambda}^{1/3}) = w_2(i_4,i_5,\widetilde{\lambda}^{1/3})$, hence w is continuous. Next, by defining the operator

$$D[\cdot] \mapsto \left[\tfrac{\partial \cdot}{\partial i_4}, \quad \tfrac{\partial \cdot}{\partial i_5}, \quad \tfrac{\partial \cdot}{\partial i_6}\right]^T,$$

we calculate

$$Dw_0 = \begin{bmatrix} \breve{\mu} i_4 \\ \overline{\mu} i_5 \left(i_6^{-1} - \widetilde{\lambda} i_5^{-4}\right) \\ \frac{\overline{\mu}}{2}\left(1 - i_5^2 i_6^{-2}\right) \end{bmatrix}, \quad Dw_1 = \begin{bmatrix} \breve{\mu} i_4 \\ 0 \\ \frac{\overline{\mu}}{2}\left(1 - \sqrt{\widetilde{\lambda} i_6^{-3}}\right) \end{bmatrix}, \quad Dw_2 = \begin{bmatrix} \breve{\mu} i_4 \\ 0 \\ 0 \end{bmatrix}. \tag{7.3.37}$$

First, we note that $Dw_0(i_4,(\widetilde{\lambda} i_6)^{1/4},i_6) = Dw_1(i_4,(\widetilde{\lambda} i_6)^{1/4},i_6)$ and $Dw_1(i_4,i_5,\widetilde{\lambda}^{1/3}) = Dw_2(i_4,i_5,\widetilde{\lambda}^{1/3})$, so that w is continuously differentiable. To see

that w is nondecreasing, it suffices to show that each entry of Dw_k is non-negative, for $k = 0, 1, 2$. From Eqs. (7.3.36)-(7.3.37), we see that

$$\begin{aligned}
\frac{\partial w_0}{\partial i_5} \geqslant 0 &\iff \widetilde{\lambda}^{-1} i_5^4 \geqslant i_6, \\
\frac{\partial w_0}{\partial i_6} \geqslant 0 &\iff i_6 \geqslant i_5, \\
\frac{\partial w_1}{\partial i_6} \geqslant 0 &\iff i_6 \geqslant \widetilde{\lambda}^{1/3}.
\end{aligned} \tag{7.3.38}$$

Now, the first and third inequalities are always satisfied within the domains of definition of w_0 and w_1, respectively, and the second inequality follows from the fact that $d_2^2 \leqslant \sqrt{I_5} \leqslant d_3^2$. Therefore, w is nondecreasing.

It remains to show that w is a convex function. Since w_2 is a quadratic function of only i_4 and is therefore clearly convex, we only need to look at the convexity of w_0 and w_1. To that end, we calculate that

$$D^2 w_0(i_4, i_5, i_6) = \begin{bmatrix} \breve{\mu} & 0 & 0 \\ 0 & \overline{\mu}\left(i_6^{-1} + 3\widetilde{\lambda} i_5^{-4}\right) & -\overline{\mu} i_5 i_6^{-2} \\ 0 & -\overline{\mu} i_5 i_6^{-2} & \overline{\mu} i_5^2 i_6^{-3} \end{bmatrix} \tag{7.3.39}$$

and

$$D^2 w_1(i_4, i_5, i_6) = \begin{bmatrix} \breve{\mu} & 0 & 0 \\ 0 & 0 & 0 \\ 0 & 0 & \frac{3\overline{\mu}}{4}\sqrt{\widetilde{\lambda} i_6^{-5}} \end{bmatrix}. \tag{7.3.40}$$

Now, all diagonal entries of $D^2 w_0$ are non-negative and, moreover, $\det D^2 w_0 = 3\overline{\mu}^2 \breve{\mu} \widetilde{\lambda} i_5^{-2} i_6^{-3} \geqslant 0$, so that $D^2 w_0$ is positive semi-definite and w_0 convex. The same conclusion holds true for w_1. It follows that $w(i_4, i_5, i_6)$ is convex and hence $R\widehat{W}$ is polyconvex. Finally, from the arguments laid out at the end of Chapter 5 in connection with the inequalities (5.3.9), it is concluded that

$$Q\widehat{W} = R\widehat{W}, \tag{7.3.41}$$

where $R\widehat{W}$ is given by Eqs. (7.3.28) and (7.3.29) or, equivalently by (7.3.35) and (7.3.36).

7.3.3 Further properties of the relaxation construction

We now take a closer look at the implications of the relaxation construction. As we see, depending on the value of $\overline{\boldsymbol{F}}$, the relaxation is obtained either via a single lamination or by a-laminate-within-a-laminate microstructure, and results in the formation of two or four types of domains, respectively. In the latter case, by letting $\overline{\boldsymbol{F}}^s$ $(s = I, \ldots, IV)$ denote the average deformation gradient within each domain, we find that there exist volume fractions $c_I, \cdots, c_{IV}$ so that

$$\overline{\boldsymbol{F}} = c_I \overline{\boldsymbol{F}}^I + c_{II} \overline{\boldsymbol{F}}^{II} + c_{III} \overline{\boldsymbol{F}}^{III} + c_{IV} \overline{\boldsymbol{F}}^{IV}, \tag{7.3.42}$$

and

$$Q\widehat{W}(\overline{\boldsymbol{F}}) = \sum_{s=I}^{IV} c_s \widehat{W}(\overline{\boldsymbol{F}}^s). \tag{7.3.43}$$

A similar result holds when $Q\widehat{W}$ is obtained via a single lamination, in which case there are only two average domain deformation gradients. Moreover, in either case, although $\widehat{W}$ fails to be (strictly) rank-1 convex at $\overline{\boldsymbol{F}}$, it can be shown that $\widehat{W}$ will be rank-1 convex at $\overline{\boldsymbol{F}}^s$. We note further that such a decomposition is a direct consequence of the fact that $Q\widehat{W} = R\widehat{W} = R_k\widehat{W}$ for some k.

Using the calculations from Section 7.3.1.1 and Section 7.3.1.2, we can derive analytical expressions for $\overline{\boldsymbol{F}}^s$ to obtain further information about the relaxation. Once domain formation has been initiated, we find that the average domain deformation gradients are on the boundary of the set of deformations for which $\widehat{W}$ is (strictly) rank-1 convex, so that

$$d_2[\overline{\boldsymbol{F}}^s] = \frac{\widetilde{\lambda}^{1/4}}{\sqrt{d_3[\overline{\boldsymbol{F}}^s]}}, \tag{7.3.44}$$

for each s, where $d_2\left[\overline{\boldsymbol{F}}^{\,s}\right]$ and $d_3\left[\overline{\boldsymbol{F}}^{\,s}\right]$ denote the values of d_2 and d_3 evaluated at $\overline{\boldsymbol{F}}^{\,s}$, respectively. In fact, by considering the right Cauchy-Green tensor associated to each domain, it can be shown that the domain deformations each share the same transversely isotropic invariants I_k. In particular, they have the same principal stretches, but do not share the same principal axes. As a consequence, we find that the energy in each domain is the same, and is given by $Q\widehat{W}(\overline{\boldsymbol{F}})$.

More can be said when the relaxation is obtained via the formation of a-laminate-within-a-laminate microstructure. In this case, it has already been observed that the lamination direction $\mathbf{N}_2$ in the rank-2 lamination procedure, satisfying $\mathbf{N}_2 \cdot \mathbf{N} = 0$, is not fully specified (θ_2 is arbitrary, except that it cannot be equal to θ_1). Therefore, there are, in principle, infinitely many ways to form the domains, all of which will lead to the *same* macroscopic response. Moreover, in relation to Eq. (7.3.44), we can show that

$$d_2[\overline{\boldsymbol{F}}^{\,s}] = d_3[\overline{\boldsymbol{F}}^{\,s}] = \widetilde{\lambda}^{1/6}, \;\; s = I, \ldots, IV, \tag{7.3.45}$$

whereby $\overline{\boldsymbol{F}}^{\,s}$ are on the boundaries of the sets of deformations for which $\widehat{W}$ and $R_1\widehat{W}$ are (strictly) rank-1 convex. The derivation of these results can be found in Section 7.9.

7.4 Discussion of the results

As we have seen, the relaxation can be completely described in terms of the invariants d_2, d_3, ψ_1 and λ_n, where it is recalled that λ_n measures the stretch of material line elements initially aligned with the layering direction, ψ_1 measures the rotation of the layers (relative to such material line elements), and d_2 and d_3 are the principal stretches associated with the tensor $\boldsymbol{D}^{1/2}$, defined by (7.2.5), which is a two-dimensional "projection" of the deformation on the plane of the layers. The analysis carried out in the previous section revealed that all deformations fall into one of three regimes, within which no laminations, a single, or a double lamination is required to

obtain the relaxation. Moreover, the relaxed energy $Q\widehat{W} = R\widehat{W}$, as given by (7.3.32), can be decomposed into two parts: one associated with the "soft" modes of deformation that depends only on λ_n, and another associated with the "hard" modes of deformation, defined by expression (7.3.29) for g_r and depending on d_2 and d_3. By observing the corresponding form of the Cauchy stress given by Eq. (7.3.34), it is clear that with each lamination, additional "perfectly soft" modes of deformation become activated, in such a way that the zeroth, first, and second order laminations can be associated to different "states" or "phases" of the composite. Most interestingly, from the conditions delineating these regimes, it is seen that deformations satisfying the conditions

$$d_2 = d_3 = \widetilde{\lambda}^{1/6} \tag{7.4.1}$$

correspond to some sort of "triple point," where the 3 phases coexist.

In the rest of this section, we discuss results that are presented in Figure 7.1 and have been calculated with a fixed heterogeneity contrast of $\mu^{(2)}/\mu^{(1)} = 10$ and volume fraction $c = 0.3$. For ease of presentation, we eschew the convention previously made that $d_2 \leqslant d_3$ in favor of a more complete presentation where the results have been extended symmetrically about the line $d_2 = d_3$, in such a way that d_2 can be either larger or smaller than d_3.

Figure 7.1a shows the "phase diagram" for the relaxed energy $Q\widehat{W}$. Regions in which zero, single and double laminations are required are indicated by progressively darker shades of gray. Furthermore, in this diagram, the important special cases of plane strain and axisymmetric loadings are depicted by the dash-dot blue curve and the dashed red curve, respectively. For simplicity, we discuss these results assuming that $d_2 \leqslant d_3$. (The discussion of the corresponding results for $d_2 \geqslant d_3$ is identical with d_2 and d_3 interchanged.) Thus, it is recalled that the principal solution $\widehat{W}$ loses global rank-1 convexity when $d_2 = \widetilde{\lambda}^{1/4}/d_3^{1/2}$ and the relaxation is obtained by a rank-1 laminate for $d_2 < \widetilde{\lambda}^{1/4}/d_3^{1/2}$ and $d_3 \geqslant \widetilde{\lambda}^{1/6}$, while the rank-1 lamination $R_1\widehat{W}$ loses strict rank-1 convexity when $d_3 = \widetilde{\lambda}^{1/6}$, and the relaxation is obtained by a double

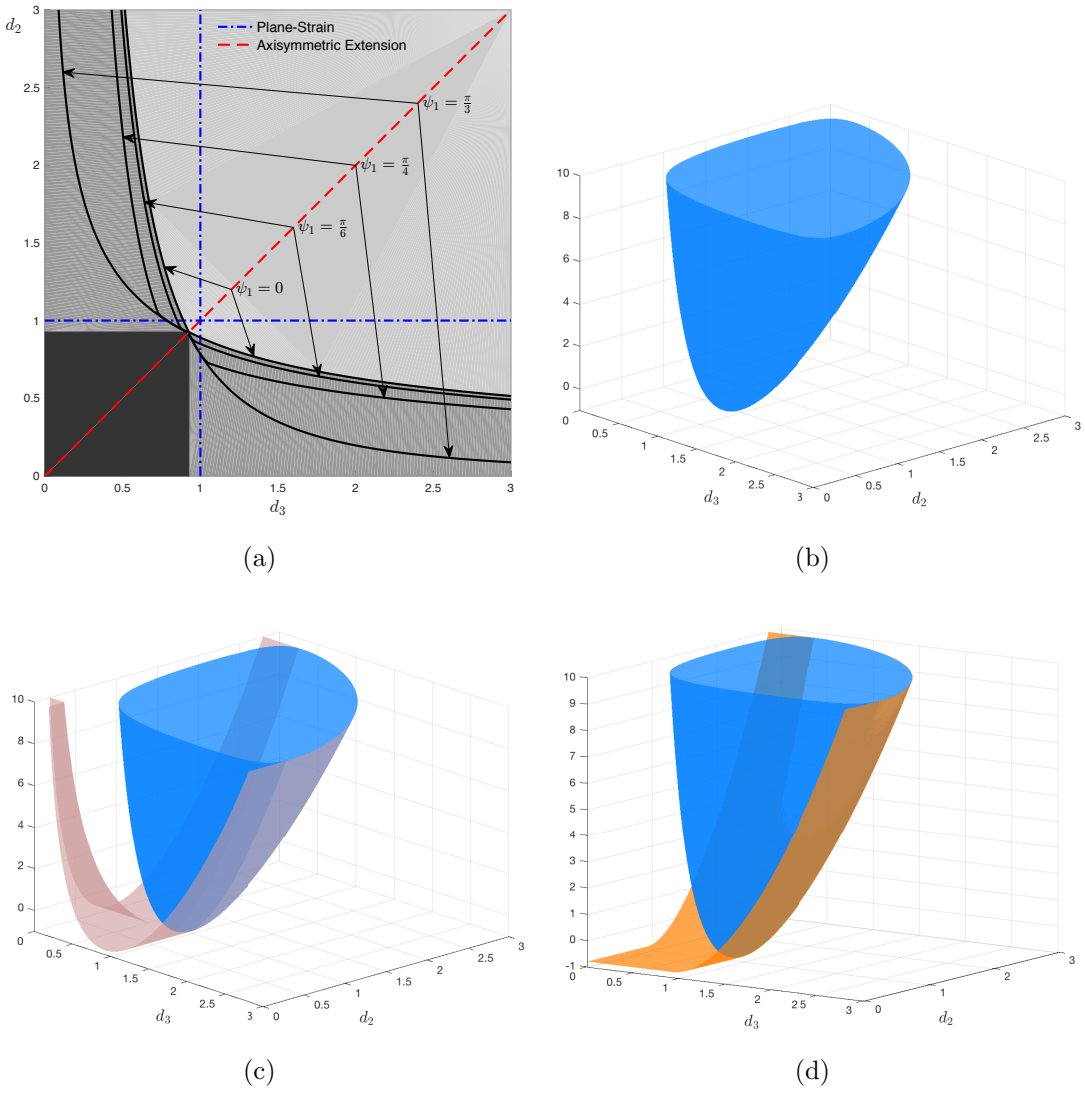

Figure 7.1: (a) Phase diagram of the relaxation construction showing in progressively darker shades of gray the regions for which zero, single and double laminations are required. Curves are also shown for the loss of ellipticity for values of $\psi_1 = 0$, $\frac{\pi}{6}$, $\frac{\pi}{4}$ and $\frac{\pi}{3}$ (see discussion for more details). Energy landscape for (b) $g_0(d_2, d_3)$ (c) $g_1(d_2, d_3)$ and (d) $g_r(d_2, d_3)$. Results are plotted in the $d_3 - d_2$ plane, and have been extended symmetrically about the line $d_2 = d_3$. The contrast is $\mu^{(2)}/\mu^{(1)} = 10$ and the volume fraction $c = 0.3$.

lamination when $d_3 < \widetilde{\lambda}^{1/6}$.

Now, for *plane strain* loading conditions, $d_3 = 1 > \widetilde{\lambda}^{1/6}$ (since $\widetilde{\lambda} < 1$) and hence, as can be seen in Figure 7.1a, and consistent with the findings of Furer and Ponte Castañeda (2018a), the relaxed solution exhibits a single family of lamellar domains for $d_2 < \widetilde{\lambda}^{1/4}$ or, equivalently, $\lambda_n > \widetilde{\lambda}^{-1/4}$, and double lamination is never required. On the other hand, for *axisymmetric loading*, the principal solution gives way directly to a rank-2 lamination, and the relaxed solution develops a "laminate-within-a-laminate" microstructure with two families of domains, when $d_2 = d_3 < \widetilde{\lambda}^{1/6}$ or, alternatively, when $\lambda_n > \widetilde{\lambda}^{-1/3}$. As such, the path corresponding to axisymmetric extension in Figure 7.1a never intersects the region of single lamination. Of course, for more general loadings, the principal solution would normally give way to a relaxed solution with one set of layers for sufficiently small values of d_2 and then to a relaxed solution with two families of layers if d_3 also becomes sufficiently small. In contrast, for sufficiently large values of both d_2 and d_3, corresponding to loadings resulting in elongations along both directions (along the layers of the neo-Hookean laminate), $Q\widehat{W}$ is identical to the principal solution, and no domain formation can take place.

Next, we would like to compare the predictions for loss of strong ellipticity, as determined by expression (7.2.23) of Section 7.2.2, with the above-discussed conditions for loss of (global) strict rank-1 convexity. For this purpose, it is useful to remark that the loss of (global) strict rank-1 convexity coincides exactly with loss of strong ellipticity for both *pure shear* loading conditions (i.e., $\lambda_n = \widetilde{\lambda}^{-1/4} = \lambda_{se}^{ps} \approx 1.123$), as well as for *axisymmetric* loading conditions (i.e., $\lambda_n = \widetilde{\lambda}^{-1/3} = \lambda_{se}^{axi} \approx 1.167$). It is recalled that, for these cases, the invariant angle ψ_1 is exactly zero. To address what happens for other more general loading conditions, some results are also presented in Figure 7.1a for loss of strong ellipticity of the principal solution $\widehat{W}$ for the following special class of loading conditions: $\psi_3 = \pi/2$, so that $\psi_2 = \pi/2 - \psi_1$ when $d_2 \leqslant d_3$ (and $\psi_2 = \pi/2$, etc., when $d_3 \leqslant d_2$), where ψ_1 is allowed to take the fixed values $(0,\ \pi/6, \pi/4, \pi/3)$. It is recalled that ψ_2 and ψ_3, which are defined by Eq. (7.2.10),

correspond to the angle between $\overline{\boldsymbol{F}}\mathbf{N}$ and the eigenvectors $\mathbf{t}_2$ and $\mathbf{t}_3$ of $\boldsymbol{D}$, respectively. Thus, it is seen that strong ellipticity and strict rank-1 convexity are lost simultaneously when $\psi_1 = 0$. (This case, of course, includes both aligned pure shear and axisymmetric loading, but is more general.) For other values of ψ_1, when the layers rotate relative to the $\overline{\boldsymbol{F}}\mathbf{N}$ direction, loss of strong ellipticity takes place strictly after loss of global (strict) rank-1 convexity, and this delay increases with the value of the reorientation of the layers ψ_1. This is entirely consistent with what was found by Furer and Ponte Castañeda (2018a) for plane strain loadings of the neo-Hookean laminates, where it was observed that strong ellipticity and strict rank-1 convexity are lost simultaneously only for (aligned) pure shear loading. In fact, as shown in Section 7.8 for completely general three-dimensional loadings, strong ellipticity and strict rank-1 convexity are lost simultaneously whenever the smallest nonzero eigenvalue of $\boldsymbol{D}^{1/2}$ is also a principal stretch. This turns out to be equivalent to the condition that $\overline{\boldsymbol{F}}\mathbf{N}$ is perpendicular to the eigenvector of $\boldsymbol{D}$ corresponding to the smallest nonzero eigenvalue; for example, when $d_2 \leqslant d_3$, this happens when $\psi_2 = \pi/2$. It is interesting to note that this condition includes, but is not limited to, all those deformations for which $\psi_1 = 0$, so that it is possible for loss of ellipticity and loss of rank-1 convexity to occur simultaneously even when $\psi_1 \neq 0$. (Note that the results shown in the figure—with $d_2 \leqslant d_3$—are for $\psi_3 = \pi/2$ and not for $\psi_2 = \pi/2$.)

Finally, Figures 7.1b to 7.1d show results for the various parts of the soft energy g_r, namely, g_0, g_1 and g_2, respectively; g_0, corresponding to the principal solution, is also included in the last two plots for reference. As can be seen in Figure 7.1b, for large values of d_2 and d_3, g_0 grows quadratically, while it exhibits singular behavior as d_2 and/or d_3 approach 0. Upon undergoing the first lamination, it is observed from Figure 7.1c that g_1 is still singular at the origin, but can now accommodate deformations for which *either* d_2 or d_3 becomes progressively smaller. (However, note that λ_n grows as either d_2 or d_3 gets smaller, so that the total relaxed energy (7.3.32) still blows up as d_2 or d_3 decrease toward zero.) Moreover, for a fixed value of d_3,

g_1 is constant as a function of d_2 for all values of d_2 satisfying $d_2 < \widetilde{\lambda}^{1/4}/d_3^{1/2}$ and $d_2 < d_3$; the same is true for g_1 as a function of d_3 when $d_3 < \widetilde{\lambda}^{1/4}/d_2^{1/2}$ and $d_3 < d_2$. This indicates the existence of a soft mode of deformation. In fact, as can be seen from Eq. (7.3.34), not one but two soft modes of deformation become activated in this case. For small enough values of both d_2 and d_3, the relaxation then involves a second lamination procedure. It can then be seen, from Figure 7.1d, that g_r is no longer singular at the origin. In fact, it is constant with respect to both d_2 and d_3 for values that lie in the black square region of the phase diagram. As such, there are no longer any hard modes associated with g_r, although, once again, the total relaxed energy (7.3.32) does blow up as d_2 or d_3 tend to zero, due to the fact that λ_n increases as either d_2 or d_3 becomes smaller.

7.5 Concluding Remarks

In this work we set out to characterize the post-bifurcation behavior of reinforced elastomeric composites undergoing macroscopic or long-wavelength instabilities under general three-dimensional loading conditions. Thus, we were able to compute analytically the relaxation of the homogenized stored-energy function of a Neo-Hookean laminate by means of the quasiconvexification $Q\widehat{W}$ of the "principal" solution $\widehat{W}$, as originally proposed by Avazmohammadi and Ponte Castañeda (2016). The calculation involves the computation of the rank-1 convexification of $\widehat{W}$, which is then shown to be polyconvex, and indicates that the laminate can lower its energy by the formation of domains, when subjected to sufficient compression of the stiff layers.

Different from the two-dimensional plane strain loading case considered by Furer and Ponte Castañeda (2018a), where the neo-Hookean laminates can develop only one family of lamellar or striped domains, we find that, for more general three-dimensional types of loading involving sufficient compression of the layers along two orthogonal directions (e.g., axisymmetric extension along the direction of lamination),

the relaxation construction requires two sequential lamination procedures leading to a "laminate-within-a-laminate" microstructure with two families of domains. This more general type of microstructure allows for multiple "perfectly soft" (liquid-like) modes of deformation—which are associated with the relaxation of the "hard" modes of the principal solution that are controlled by the Voigt (or arithmetic) average of the phase shear moduli—where the deformation can be accommodated solely by the rearrangement of the domain microstructure. However, this is only possible under certain special loading configurations; more generally, the response of the neo-Hookean laminates in the post-bifurcation regime is soft, but with a finite elasticity modulus that is proportional to the Reuss (or harmonic) average of the phase shear moduli. As a consequence of the different domains microstructures that are possible in these laminated reinforced elastomers, we were led to the definition of distinct "phases" in the deformation space exhibiting different behaviors with different number of perfectly soft modes.

It is important to emphasize that, in our relaxation framework, the macroscopic instabilities associated with the formation of domains are triggered, in general, by loss of strict *global* rank-1 convexity of the principal homogenized solution—and *not* by loss of strong ellipticity, which is a *local* condition typically occurring later. In fact, Section 7.8 provides explicitly the special conditions under which strict rank-1 convexity and strong ellipticity are lost simultaneously for the laminates. We posit that this new way of defining macroscopic instabilities is more robust and consistent with the definition of the relaxation of the energy $Q\widehat{W}$ than the use of loss of strong ellipticity (of the incremental problem associated with the principal homogenized solution), as proposed in the work of Geymonat et al. (1993). This is because (with our definition) loss of strict *global* rank-1 convexity leads directly to domain formation, whereas (with the earlier definition) loss of ellipticity in general takes place strictly after domain formation has begun (see the "phase diagram" in Figure 7.1a). As already mentioned, the difference between these two definitions of macroscopic instabilities is

due to the lack of commutativity of the homogenization and linearization procedures, which was assumed in the work of Geymonat et al. (1993). One important mathematical question that remains to be addressed rigorously is under which hypotheses can the relaxation $Q\widehat{W}$ be shown to correspond exactly to the homogenized energy function $\widetilde{W}$, as defined by expression (5.3.5) together with (5.3.4), for the case when the first instabilities are of the long-wavelength ($k \to \infty$) or macroscopic type.

Although it may not be possible to compute analytically the exact principal solution for the homogenized stored-energy function of elastomeric composites with more complex microstructures and more general constitutive models, approximate estimates are already available for the principal homogenized solution in many cases, such as, for example, continuous-fiber-reinforced elastomers (Agoras et al., 2009a,b) and short-fiber-reinforced elastomers (Avazmohammadi and Ponte Castañeda, 2014a,b). Moreover, it has been shown in these works that the principal homogenized solution loses strong ellipticity under appropriate three-dimensional loadings, suggesting similar post-bifurcation responses by the formation of appropriate domain microstructures. While it may not be feasible to compute analytically the quasiconvexification for these more complex energy functions, at the very least it should be possible to compute their rank-1 convexification, which would provide an upper bound on the relaxation. It remains to be seen whether such upper bound estimates correspond exactly to the relaxation, as has been shown to be the case in this work for the neo-Hookean laminates.

7.6 Appendix I: The tensor $\boldsymbol{D}$

There exist some novel quantities that arise as a consequence of the relaxation construction. In what follows, we give a full accounting of the properties of these quantities, which are crucial in much of the analysis in this paper. These quantities will be defined in terms of some tensor $\boldsymbol{F}$, but when they appear in the rest of the

paper, it will be understood that they are defined in terms of $\overline{\boldsymbol{F}}$, where appropriate. Here, we take GL(3) to represent the set of invertible second-order tensors, while $\mathrm{GL}^+(3)$ represents the set of invertible second-order tensors with positive determinant. SO(3) is the subset of orthogonal second-order tensors which have determinant 1. We begin with the following definition.

Definition 8:
Given $\boldsymbol{F} \in \mathrm{GL}(3)$, we define

$$\boldsymbol{D} \equiv \boldsymbol{D}[\boldsymbol{F}] = \boldsymbol{F}\boldsymbol{F}^T - (\boldsymbol{F}\mathbf{N}) \otimes (\boldsymbol{F}\mathbf{N}). \tag{7.6.1}$$

We will write $\boldsymbol{D}$ instead of $\boldsymbol{D}[\boldsymbol{F}]$ when the dependence on $\boldsymbol{F}$ is understood. Note that $\boldsymbol{F} \mapsto \boldsymbol{D}$ is invariant under right multiplication of $\boldsymbol{Q} \in \mathcal{G}$, where

$$\mathcal{G} = \{\boldsymbol{Q} \in \mathrm{SO}(3) \,:\, \boldsymbol{Q}\mathbf{N} = \mathbf{N}\} \tag{7.6.2}$$

represents the transversely isotropic symmetry group of the composite. Moreover, $\boldsymbol{D}$ is a symmetric, semi-positive definite tensor, so any non-zero eigenvalues will be positive. We now present the main result of this section.

Proposition 5:
Take $\{\mathbf{e}_1, \mathbf{e}_2, \mathbf{e}_3\}$ *to be the standard Cartesian basis, and let* $\boldsymbol{F} \in \mathrm{GL}(3)$. *By taking* $\mathbf{N} = \mathbf{e}_1 = \widehat{\mathbf{e}}_1$, *there exists unit vectors* $\widehat{\mathbf{e}}_2$ *and* $\widehat{\mathbf{e}}_3$ *such that* $\{\widehat{\mathbf{e}}_1, \widehat{\mathbf{e}}_2, \widehat{\mathbf{e}}_3\}$ *is a basis of* $\mathbb{R}^3$, *and* $\{\boldsymbol{F}^*\mathbf{N}, \boldsymbol{F}\widehat{\mathbf{e}}_2, \boldsymbol{F}\widehat{\mathbf{e}}_3\}$ *are mutually orthogonal. Moreover,*

$$\boldsymbol{D} = \boldsymbol{F}\widehat{\mathbf{e}}_2 \otimes \boldsymbol{F}\widehat{\mathbf{e}}_2 + \boldsymbol{F}\widehat{\mathbf{e}}_3 \otimes \boldsymbol{F}\widehat{\mathbf{e}}_3, \tag{7.6.3}$$

which can alternatively be written in the form (7.2.6) *in terms of its eigenvalues* $0 = d_1^2 < d_2^2 \leqslant d_3^2$ *and its eigenvectors* $\{\mathbf{t}_1, \mathbf{t}_2, \mathbf{t}_3\}$; *in this context,* $|\boldsymbol{F}\widehat{\mathbf{e}}_i| = d_i$ *for* $i = 2, 3$ *and satisfy* (7.2.8), *while the eigenvectors are defined by expressions* (7.2.7).

Proof:

The proof is constructive and, to begin, we consider a new basis $\{\widehat{\mathbf{e}}_i\}$*, where*

$$\widehat{\mathbf{e}}_1 = \mathbf{N}, \quad \widehat{\mathbf{e}}_2 = \cos(\widehat{\theta})\mathbf{e}_2 - \sin(\widehat{\theta})\mathbf{e}_3, \quad \widehat{\mathbf{e}}_3 = \sin(\widehat{\theta})\mathbf{e}_2 + \cos(\widehat{\theta})\mathbf{e}_3, \tag{7.6.4}$$

for some $\widehat{\theta}$ *to be determined later. Therefore,*

$$\boldsymbol{I} = \widehat{\mathbf{e}}_1 \otimes \widehat{\mathbf{e}}_1 + \widehat{\mathbf{e}}_2 \otimes \widehat{\mathbf{e}}_2 + \widehat{\mathbf{e}}_3 \otimes \widehat{\mathbf{e}}_3 \implies \boldsymbol{I} - \mathbf{N} \otimes \mathbf{N} = \widehat{\mathbf{e}}_2 \otimes \widehat{\mathbf{e}}_2 + \widehat{\mathbf{e}}_3 \otimes \widehat{\mathbf{e}}_3. \tag{7.6.5}$$

Now, since $\boldsymbol{D} = \boldsymbol{F}(\boldsymbol{I} - \mathbf{N} \otimes \mathbf{N})\boldsymbol{F}^T$*, Eq.* (7.6.5) *gives us Eq.* (7.6.3).

As defined, it is clear that

$$\boldsymbol{D}(\boldsymbol{F}^*\mathbf{N}) = \mathbf{0}, \tag{7.6.6}$$

whereby $d_1^2 = 0$ *is the eigenvalue corresponding to the eigenvector* $\boldsymbol{F}^*\mathbf{N}$*. Moreover, Eq.* (7.6.3)*, along with the fact that, clearly,* $(\boldsymbol{F}^*\mathbf{N}) \cdot (\boldsymbol{F}\widehat{\mathbf{e}}_i) = 0$ *for* $i = 2, 3$*, suggest that, if*

$$(\boldsymbol{F}\widehat{\mathbf{e}}_2) \cdot (\boldsymbol{F}\widehat{\mathbf{e}}_3) = 0, \tag{7.6.7}$$

then $\boldsymbol{F}^*\mathbf{N}, \boldsymbol{F}\widehat{\mathbf{e}}_2$*, and* $\boldsymbol{F}\widehat{\mathbf{e}}_3$ *would represent an orthogonal basis of eigenvectors of* $\boldsymbol{D}$*, with the eigenvalue* $0 = d_1^2 < d_2^2 \leqslant d_3^2$*, respectively, where* $d_i = |\boldsymbol{F}\widehat{\mathbf{e}}_i|$ *for* $i = 2, 3$*. By taking*

$$\widehat{\theta} = \frac{1}{2} \arctan\left(\frac{2C_{23}}{C_{33} - C_{22}}\right), \tag{7.6.8}$$

a straightforward calculation reveals that Eq. (7.6.7) *is satisfied. Here,* C_{ij} *are the components of the right Cauchy-Green tensor* $\boldsymbol{C} = \boldsymbol{F}^T\boldsymbol{F}$*. Then, by either calculating directly* $|\boldsymbol{F}\widehat{\mathbf{e}}_i|$*, or by making use of the fact that the characteristic polynomial of* $\boldsymbol{D}$ *takes the form*

$$p_{\boldsymbol{D}}(\omega) = \omega(\omega^2 - (I_1 - I_4)\omega + I_5), \tag{7.6.9}$$

we find that d_2 *and* d_3 *are given as in Eq.* (7.2.8). □

We comment here that Eq. (7.2.9), which states that $d_2 d_3 = \sqrt{I_5}$, can be de-

rived from a purely geometric argument as well. Recall that material line elements transform with $\boldsymbol{F}$, while material surface elements transform according to Nanson's Formula (*cf.* Eq. (7.2.3)). In the undeformed configuration, $\mathbf{N}$ lies perpendicular to the layers. Since $\{\mathbf{N}, \widehat{\mathbf{e}}_2, \widehat{\mathbf{e}}_3\}$ are mutually orthogonal, the material area element with sides parallel to $\widehat{\mathbf{e}}_2$ and $\widehat{\mathbf{e}}_3$ lies completely in the plane of the layers in the undeformed configuration. Moreover, since $\widehat{\mathbf{e}}_2 \cdot \widehat{\mathbf{e}}_3 = 0$, this material area element is rectangular. As discussed above, we have

$$d_2 = |\boldsymbol{F}\widehat{\mathbf{e}}_2|, \quad \text{and} \quad d_3 = |\boldsymbol{F}\widehat{\mathbf{e}}_3|, \tag{7.6.10}$$

so that d_2 and d_3 represent the stretches of material line elements aligned with $\widehat{\mathbf{e}}_2$ and $\widehat{\mathbf{e}}_3$, respectively. Since $\{\boldsymbol{F}^*\mathbf{N}, \boldsymbol{F}\widehat{\mathbf{e}}_2, \boldsymbol{F}\widehat{\mathbf{e}}_3\}$ are also mutually orthogonal, and since $\boldsymbol{F}^*\mathbf{N}$ is perpendicular to the layers in the deformed configuration, we see that $\boldsymbol{F}\widehat{\mathbf{e}}_2$ and $\boldsymbol{F}\widehat{\mathbf{e}}_3$ still lie perpendicular to one another in the plane of the layers in the deformed configuration. Therefore, the material area element with sides parallel to $\widehat{\mathbf{e}}_2$ and $\widehat{\mathbf{e}}_3$ and with normal $\mathbf{N}$ in the undeformed configuration has sides parallel to $\boldsymbol{F}\widehat{\mathbf{e}}_2$ and $\boldsymbol{F}\widehat{\mathbf{e}}_3$ and has normal $\boldsymbol{F}^*\mathbf{N}$, in the deformed configuration. As in the undeformed configuration, this material area element is also rectangular in the deformed configuration, due to the fact that $(\boldsymbol{F}\widehat{\mathbf{e}}_2) \cdot (\boldsymbol{F}\widehat{\mathbf{e}}_3) = 0$. On the one hand, the change in area of the such a material area element is equal to the change in length times the change in width, and is found to be $|\boldsymbol{F}\widehat{\mathbf{e}}_2||\boldsymbol{F}\widehat{\mathbf{e}}_3| = d_2 d_3$. On the other hand, from Nanson's Formula, the change in area is given directly by $\sqrt{I_5} = |\boldsymbol{F}^*\mathbf{N}|$. Hence, we have Eq. (7.2.9).

We now present our next result, which is helpful in proving polyconvexity of the rank-one convex envelope.

Proposition 6:

The mapping $\boldsymbol{F} \mapsto d_3^2[\boldsymbol{F}]$ is convex.

Proof:

Upon defining the Rayleigh-Ritz quotient of a symmetric tensor $\boldsymbol{A}$ *as*

$$R_{\boldsymbol{A}}(\mathbf{x}) = \frac{\mathbf{x}\cdot\boldsymbol{A}\mathbf{x}}{\mathbf{x}\cdot\mathbf{x}}, \tag{7.6.11}$$

it is known that if $\lambda_{max}(\boldsymbol{A})$ *denotes the largest eigenvalue of* $\boldsymbol{A}$*, then*

$$\lambda_{max} = \max_{\mathbf{x}\neq\mathbf{0}} R_{\boldsymbol{A}}(\mathbf{x}). \tag{7.6.12}$$

A straightforward calculations shows that for any $0 < t < 1$ *and any* $\boldsymbol{F}, \boldsymbol{G} \in \mathrm{GL}(3)$ *with* $\boldsymbol{F} \neq \boldsymbol{G}$

$$\boldsymbol{D}[t\boldsymbol{F} + (1-t)\boldsymbol{G}] = t\boldsymbol{D}[\boldsymbol{F}] + (1-t)\boldsymbol{D}[\boldsymbol{G}] - t(1-t)\boldsymbol{D}[\boldsymbol{F}-\boldsymbol{G}]. \tag{7.6.13}$$

Therefore, we see that

$$\begin{aligned} R_{\boldsymbol{D}[t\boldsymbol{F}+(1-t)\boldsymbol{G}]}(\mathbf{x}) &= tR_{\boldsymbol{D}[\boldsymbol{F}]}(\mathbf{x}) + (1-t)R_{\boldsymbol{D}[\boldsymbol{G}]}(\mathbf{x}) - t(1-t)R_{\boldsymbol{D}[\boldsymbol{F}-\boldsymbol{G}]}(\mathbf{x}), \\ &\leqslant tR_{\boldsymbol{D}[\boldsymbol{F}]}(\mathbf{x}) + (1-t)R_{\boldsymbol{D}[\boldsymbol{G}]}(\mathbf{x}), \end{aligned} \tag{7.6.14}$$

having used the fact that $\boldsymbol{D}[\boldsymbol{F}-\boldsymbol{G}]$ *is positive semi-definite. Since* d_3^2 *is the largest eigenvalue of* $\boldsymbol{D}$*, taking the maximum over all* $\mathbf{x} \neq \mathbf{0}$*, Eq.* (7.6.12) *allows us to conclude that*

$$d_3^2[t\boldsymbol{A} + (1-t)\boldsymbol{B}] \leqslant td_3^2[\boldsymbol{A}] + (1-t)d_3^2[\boldsymbol{B}], \tag{7.6.15}$$

and hence the mapping $\boldsymbol{A} \mapsto d_3^2[\boldsymbol{A}]$ *is convex.* □

These next results give the derivatives of d_2^2 and d_3^2 with respect to $\boldsymbol{F}$, and are needed in deriving expressions for the stresses of the relaxation.

Proposition 7:
Given d_2^2 *and* d_3^2 *as defined above, we have*

$$\frac{\partial d_2^2}{\partial \boldsymbol{F}} = 2(\boldsymbol{F}\widehat{\mathbf{e}}_2)\otimes\widehat{\mathbf{e}}_2, \quad \frac{\partial d_3^2}{\partial \boldsymbol{F}} = 2(\boldsymbol{F}\widehat{\mathbf{e}}_3)\otimes\widehat{\mathbf{e}}_3, \tag{7.6.16}$$

while, upon defining

$$P_{ijkl} = \frac{1}{d_3^2 - d_2^2}[\boldsymbol{F}\widehat{\mathbf{e}}_2 \otimes \widehat{\mathbf{e}}_3 + \boldsymbol{F}\widehat{\mathbf{e}}_3 \otimes \widehat{\mathbf{e}}_2]_{ij}[\boldsymbol{F}\widehat{\mathbf{e}}_2 \otimes \widehat{\mathbf{e}}_3 + \boldsymbol{F}\widehat{\mathbf{e}}_3 \otimes \widehat{\mathbf{e}}_2]_{kl}, \tag{7.6.17}$$

we have that, for $p = 2, 3$,

$$\frac{\partial^2 d_p^2}{\partial F_{ij}\partial F_{kl}} = \begin{cases} 2\delta_{ik}(\widehat{\mathbf{e}}_p)_j(\widehat{\mathbf{e}}_p)_l, & \text{when } \widehat{\theta} = \frac{\pi}{4}, \\ 2\left(\delta_{ik}(\widehat{\mathbf{e}}_p)_j(\widehat{\mathbf{e}}_p)_l + (-1)^{p+1}P_{ijkl}\right), & \text{otherwise.} \end{cases} \tag{7.6.18}$$

Proof:

To start, we note that

$$\begin{aligned} \frac{\partial D_{pq}}{\partial F_{ij}} &= \delta_{ip}(F_{qj} - N_j(\boldsymbol{F}\mathbf{N})_q) + \delta_{iq}(F_{pj} - N_j(\boldsymbol{F}\mathbf{N})_p) \\ &= \delta_{ip}(\boldsymbol{F}^{-1}\boldsymbol{D})_{jq} + \delta_{iq}(\boldsymbol{F}^{-1}\boldsymbol{D})_{jp}. \end{aligned} \tag{7.6.19}$$

Next, we recall (Magnus, 1985) that if λ *is an eigenvalue of a tensor* $\boldsymbol{A}$ *with corresponding unit eigenvector* $\mathbf{u}$, *(i.e. that* $\boldsymbol{A}\mathbf{u} = \lambda\mathbf{u}$, $|\mathbf{u}| = 1$*), then*

$$\frac{\partial \lambda}{\partial \boldsymbol{A}} = \mathbf{u} \otimes \mathbf{u}. \tag{7.6.20}$$

Thus, upon using the chain rule, we find that

$$\begin{aligned} \frac{\partial d_3^2}{\partial F_{ij}} &= \frac{\partial d_3^2}{\partial D_{pq}}\frac{\partial D_{pq}}{\partial F_{ij}} \\ &= \left[\frac{1}{|\boldsymbol{F}\widehat{\mathbf{e}}_3|}(\boldsymbol{F}\widehat{\mathbf{e}}_3)_p\frac{1}{|\boldsymbol{F}\widehat{\mathbf{e}}_3|}(\boldsymbol{F}\widehat{\mathbf{e}}_3)_q\right]\left[\delta_{ip}(\boldsymbol{F}^{-1}\boldsymbol{D})_{jq} + \delta_{iq}(\boldsymbol{F}^{-1}\boldsymbol{D})_{jp}\right] \\ &= \frac{2}{d_3^2}(\boldsymbol{F}\widehat{\mathbf{e}}_3)_i(\boldsymbol{F}^{-1}\boldsymbol{D}\boldsymbol{F}\widehat{\mathbf{e}}_3)_j \\ &= 2(\boldsymbol{F}\widehat{\mathbf{e}}_3)_i(\boldsymbol{F}^{-1}\boldsymbol{F}\widehat{\mathbf{e}}_3)_j \\ &= 2(\boldsymbol{F}\widehat{\mathbf{e}}_3)_i(\widehat{\mathbf{e}}_3)_j, \end{aligned} \tag{7.6.21}$$

having used the fact, in the third line, that $|\boldsymbol{F}\widehat{\mathbf{e}}_3| = d_3$. *A similar calculation gives the result for* $\frac{\partial d_2^2}{\partial \boldsymbol{F}}$, mutatis mutandis.

To calculate the second derivatives of the eigenvalues, we start by assuming that $\widehat{\theta} \neq \frac{\pi}{4}$, *and we note that* $\frac{\partial \widehat{\mathbf{e}}_3}{\partial \widehat{\theta}} = \widehat{\mathbf{e}}_2$ *while* $\frac{\partial \widehat{\mathbf{e}}_2}{\partial \widehat{\theta}} = -\widehat{\mathbf{e}}_3$. *Therefore, upon differentiating the equation*

$$(\boldsymbol{F}\widehat{\mathbf{e}}_2) \cdot (\boldsymbol{F}\widehat{\mathbf{e}}_3) = 0, \tag{7.6.22}$$

with respect to $\boldsymbol{F}$, *we see that*

$$0 = (\boldsymbol{F}\widehat{\mathbf{e}}_2) \otimes \widehat{\mathbf{e}}_3 + (\boldsymbol{F}\widehat{\mathbf{e}}_3) \otimes \widehat{\mathbf{e}}_2 + \frac{\partial \widehat{\theta}}{\partial \boldsymbol{F}} \left(|\boldsymbol{F}\widehat{\mathbf{e}}_2|^2 - |\boldsymbol{F}\widehat{\mathbf{e}}_3|^2 \right), \tag{7.6.23}$$

so that

$$\frac{\partial \widehat{\theta}}{\partial \boldsymbol{F}} = \frac{1}{d_3^2 - d_2^2} \left[(\boldsymbol{F}\widehat{\mathbf{e}}_2) \otimes \widehat{\mathbf{e}}_3 + (\boldsymbol{F}\widehat{\mathbf{e}}_3) \otimes \widehat{\mathbf{e}}_2 \right]. \tag{7.6.24}$$

Use of the chain rule yields

$$\frac{\partial (\widehat{\mathbf{e}}_3)_p}{\partial F_{kl}} = \frac{\partial (\widehat{\mathbf{e}}_3)_p}{\partial \widehat{\theta}} \frac{\partial \widehat{\theta}}{\partial F_{kl}} = (\widehat{\mathbf{e}}_2)_p \frac{\partial \widehat{\theta}}{\partial F_{kl}}. \tag{7.6.25}$$

Therefore, directly from Eq. (7.6.21), *we have that*

$$\begin{aligned} \frac{\partial^2 d_3^2}{\partial F_{ij} \partial F_{kl}} &= 2 \left(\delta_{ik} (\widehat{\mathbf{e}}_3)_j (\widehat{\mathbf{e}}_3)_l + [\boldsymbol{F}\widehat{\mathbf{e}}_2 \otimes \widehat{\mathbf{e}}_3 + \boldsymbol{F}\widehat{\mathbf{e}}_3 \otimes \widehat{\mathbf{e}}_2]_{ij} \frac{\partial \widehat{\theta}}{\partial F_{kl}} \right) \\ &= 2 \big(\delta_{ik} (\widehat{\mathbf{e}}_3)_j (\widehat{\mathbf{e}}_3)_l \\ &\qquad \frac{1}{d_3^2 - d_2^2} [\boldsymbol{F}\widehat{\mathbf{e}}_2 \otimes \widehat{\mathbf{e}}_3 + \boldsymbol{F}\widehat{\mathbf{e}}_3 \otimes \widehat{\mathbf{e}}_2]_{ij} [\boldsymbol{F}\widehat{\mathbf{e}}_2 \otimes \widehat{\mathbf{e}}_3 + \boldsymbol{F}\widehat{\mathbf{e}}_3 \otimes \widehat{\mathbf{e}}_2]_{kl} \big). \end{aligned} \tag{7.6.26}$$

If $\widehat{\theta} = \frac{\pi}{4}$, *then* $|\boldsymbol{F}\widehat{\mathbf{e}}_2|^2 = |\boldsymbol{F}\widehat{\mathbf{e}}_3|^2$, *and so from Eq.* (7.6.23),

$$0 = (\boldsymbol{F}\widehat{\mathbf{e}}_2) \otimes \widehat{\mathbf{e}}_3 + (\boldsymbol{F}\widehat{\mathbf{e}}_3) \otimes \widehat{\mathbf{e}}_2. \tag{7.6.27}$$

Therefore, while Eq. (7.6.24) *becomes indeterminate, we can make use of the first line of Eq.* (7.6.26) *to obtain the result* (7.6.18) *with* $p = 3$. *A similar calculation gives Eq.* (7.6.18) *with* $p = 2$. □

As an immediate consequence of Eq. (7.6.18), we see that for any tensor $\boldsymbol{H}$,

$$\frac{\partial^2 d_3^2}{\partial F_{ij} F_{kl}} H_{ij} H_{kl} = 2 \left\{ |\boldsymbol{H}\widehat{\mathbf{e}}_3|^2 + \frac{1}{d_3^2 - d_2^2} [(\boldsymbol{F}\widehat{\mathbf{e}}_2) \cdot (\boldsymbol{H}\widehat{\mathbf{e}}_3) + (\boldsymbol{F}\widehat{\mathbf{e}}_3) \cdot (\boldsymbol{H}\widehat{\mathbf{e}}_2)]^2 \right\} \geqslant 0, \tag{7.6.28}$$

which serves as a second proof of convexity of d_3^2 as a function of $\boldsymbol{F}$.

We now state a result that eases the computation of d_2 and d_3 for "plane-strain" loading conditions. We recall that:

Definition 9:

A tensor $\boldsymbol{F} \in \mathrm{GL}(3)$ is a plane-strain load with respect to the unit vector $\mathbf{N}$ if the corresponding right Cauchy-Green tensor $\boldsymbol{C} = \boldsymbol{F}^T \boldsymbol{F}$ has 1 as an eigenvalue with corresponding eigenvector $\mathbf{v}$ satisfying $\mathbf{v} \cdot \mathbf{N} = 0$.

Proposition 8:

Suppose $\boldsymbol{F} \in \mathrm{GL}(3)$ *is a plane-strain load with respect to the unit vector* $\mathbf{N}$. *Then*

$$d_2 = \min\{1, \sqrt{I_5}\}, \quad d_3 = \max\{1, \sqrt{I_5}\} \tag{7.6.29}$$

Proof:

As $\boldsymbol{C}$ *is symmetric positive definite, we can find an orthonormal basis of eigenvectors* $\mathbf{v}_1, \mathbf{v}_2, \mathbf{v}_3$ *with corresponding eigenvalues* $\lambda_1, \lambda_2, \lambda_3$. *Due to the plane-strain load hypothesis, we have, without loss of generality,* $\lambda_3 = 1$, *so that* $\mathbf{N} \cdot \mathbf{v}_3 = 0$. *Using the fact that each eigenvalue must satisfy*

$$\lambda^3 - I_1 \lambda^2 + I_2 \lambda - I_3 = 0, \tag{7.6.30}$$

we find that

$$1 - I_1 + I_2 - I_3 = 0. \tag{7.6.31}$$

Moreover, with respect to the eigenvalues, we have

$$I_1 = \lambda_1 + \lambda_2 + 1, \quad I_2 = \lambda_2\lambda_3 + \lambda_2 + \lambda_3, \quad I_3 = \lambda_2\lambda_3. \tag{7.6.32}$$

Using Eq. (7.6.31) *and the Cayley-Hamilton Theorem, we see that* $\boldsymbol{C}$ *must satisfy*

$$\boldsymbol{C}^3 - I_1\boldsymbol{C}^2 + I_2\boldsymbol{C} + I_3\boldsymbol{I} = (\boldsymbol{C} - \boldsymbol{I})(\boldsymbol{C}^2 - (I_1 - 1)\boldsymbol{C} + I_3\boldsymbol{I}) = \boldsymbol{0} \tag{7.6.33}$$

$$\implies \boldsymbol{C}^3 - (I_1 - 1)\boldsymbol{C}^2 + I_3\boldsymbol{C} = \boldsymbol{C}^2 - (I_1 - 1)\boldsymbol{C} + I_3\boldsymbol{I} \tag{7.6.34}$$

Multiplying both sides of Eq. (7.6.34) *by* $\boldsymbol{C}^{-1}$, *and then taking the inner product with* $\mathbf{N} \otimes \mathbf{N}$, *we find that*

$$|\boldsymbol{C}\mathbf{N}|^2 - (I_1 - 1)I_4 + I_3 = I_5 + 1 - (I_1 - I_4). \tag{7.6.35}$$

Since $\mathbf{N} \cdot \mathbf{v}_3 = 0$, *we can write*

$$\mathbf{N} = \mathbf{v}_1(\mathbf{v}_1 \cdot \mathbf{N}) + \mathbf{v}_2(\mathbf{v}_2 \cdot \mathbf{N}), \tag{7.6.36}$$

which, along with the fact that $|\mathbf{N}| = 1$, *implies that*

$$1 = (\mathbf{v}_1 \cdot \mathbf{N})^2 + (\mathbf{v}_2 \cdot \mathbf{N})^2. \tag{7.6.37}$$

Using Eq. (7.6.36), *along with the fact that* $\mathbf{v}_i$ *are eigenvectors or* $\boldsymbol{C}$ *shows that*

$$\boldsymbol{C}\mathbf{N} = \lambda_1\mathbf{v}_1(\mathbf{v}_1 \cdot \mathbf{N}) + \lambda_2\mathbf{v}_2(\mathbf{v}_2 \cdot \mathbf{N}), \tag{7.6.38}$$

which can be used to show that

$$I_4 = \lambda_1(\mathbf{v}_1 \cdot \mathbf{N})^2 + \lambda_2(\mathbf{v}_2 \cdot \mathbf{N})^2, \tag{7.6.39}$$

$$|\boldsymbol{C}\mathbf{N}|^2 = \lambda_1^2(\mathbf{v}_1 \cdot \mathbf{N})^2 + \lambda_2^2(\mathbf{v}_2 \cdot \mathbf{N})^2. \tag{7.6.40}$$

Combining Eqs. (7.6.32), (7.6.37) *and* (7.6.39), *we see that*

$$\begin{aligned}|\boldsymbol{C}\mathbf{N}|^2 - (I_1 - 1)I_4 + I_3 &= \lambda_1^2(\mathbf{v}_1 \cdot \mathbf{N})^2 + \lambda_2^2(\mathbf{v}_2 \cdot \mathbf{N})^2 \\ &\quad - (\lambda_1 + \lambda_2)\left(\lambda_1(\mathbf{v}_1 \cdot \mathbf{N})^2 + \lambda_2(\mathbf{v}_2 \cdot \mathbf{N})^2\right) + \lambda_1\lambda_2 \\ &= \lambda_1\lambda_2\left(1 - (\mathbf{v}_1 \cdot \mathbf{N})^2 - (\mathbf{v}_2 \cdot \mathbf{N})^2\right) \\ &= 0. \end{aligned} \tag{7.6.41}$$

Therefore, by Eq. (7.6.35), *we have*

$$I_1 - I_4 = I_5 + 1, \tag{7.6.42}$$

so that

$$\sqrt{(I_1 - I_4)^2 - 4I_5} = |I_5 - 1|. \tag{7.6.43}$$

The result then follows by using Eqs. (7.6.42) *and* (7.6.43) *in the formulae for* d_2 *and* d_3, *as given in Eq.* (7.2.8). □

We close this section with a final result which shows that d_2, d_3, and λ_n correspond to the principal stretches for certain types of loading. Before stating and proving the result, we first recall that if λ_i is a principal stretch, then there exists some unit vector $\mathbf{u}_i$, which defines the principal direction associated to λ_i, such that

$$\boldsymbol{U}\mathbf{u}_i = \lambda_i\mathbf{u}_i, \tag{7.6.44}$$

where $\boldsymbol{F} = \boldsymbol{R}\boldsymbol{U}$, with $\boldsymbol{U}$ being the right-stretch tensor. Moreover, upon defining the characteristic polynomial of $\boldsymbol{C} = \boldsymbol{U}^2$ as

$$p_{\boldsymbol{C}}(\lambda) = \lambda^3 - I_1\lambda^2 + I_2\lambda - I_3, \tag{7.6.45}$$

then, by the Cayley-Hamilton theorem, $f_{\boldsymbol{C}}(\lambda_i^2) = 0$ and

$$I_1 = \lambda_1^2 + \lambda_2^2 + \lambda_3^2, \quad I_2 = \lambda_1^2\lambda_2^2 + \lambda_1^2\lambda_3^2 + \lambda_2^2\lambda_3^2, \quad I_3 = (\lambda_1\lambda_2\lambda_2)^2. \tag{7.6.46}$$

We also recall that the invariant ψ_1 is defined by

$$\cos\psi_1 = \mathbf{t}_1 \cdot \left(\frac{1}{|\boldsymbol{F}\mathbf{N}|}\boldsymbol{F}\mathbf{N}\right) = \frac{\det \boldsymbol{F}}{|\boldsymbol{F}^*\mathbf{N}||\boldsymbol{F}\mathbf{N}|}. \tag{7.6.47}$$

Although not needed in the body of the text, and assuming that $d_2 \neq d_3$, one can also show that

$$\cos(\psi_2) = \mathbf{t}_2 \cdot \left(\frac{1}{|\boldsymbol{F}\mathbf{N}|}\boldsymbol{F}\mathbf{N}\right) = \sqrt{\frac{d_2^2(|\boldsymbol{C}\mathbf{N}|^2 - I_4^2) + I_3 - I_4 I_5}{\lambda_n^2(d_2^4 - I_5)}}, \tag{7.6.48}$$

$$\cos(\psi_3) = \mathbf{t}_3 \cdot \left(\frac{1}{|\boldsymbol{F}\mathbf{N}|}\boldsymbol{F}\mathbf{N}\right) = \sqrt{\frac{d_3^2(|\boldsymbol{C}\mathbf{N}|^2 - I_4^2) + I_3 - I_4 I_5}{\lambda_n^2(d_3^4 - I_5)}}. \tag{7.6.49}$$

We note that, by the Cayley-Hamilton Theorem, $\boldsymbol{C}$ satisfies its own characteristic polynomial, $p_{\boldsymbol{C}}(\boldsymbol{C}) = \mathbf{0}$. As such, the term $|\boldsymbol{C}\mathbf{N}|^2$ can be shown to be related to the invariants $I_1, \ldots, I_5$ through by equation

$$|\boldsymbol{C}\mathbf{N}|^2 = I_1 I_4 + I_5 - I_2. \tag{7.6.50}$$

We now present our final result.

Proposition 9:

1. *If ψ_2 or ψ_3 takes the value $\frac{\pi}{2}$, then d_2 or d_3 is a principal stretch.*
2. *The invariants d_2, d_3 and λ_n are the principal stretches of $\boldsymbol{U}$ if and only if $\psi_1 = 0$.*

Proof:

1. *Note that*

$$\begin{aligned} p_{\boldsymbol{C}}(\lambda) &= \lambda^3 - I_1\lambda^2 + I_2\lambda - I_3 \\ &= \lambda(\lambda^2 - (I_1 - I_4)\lambda + I_5) - (I_4\lambda^2 - (I_2 - I_5)\lambda + I_3) \\ &= p_{\boldsymbol{D}}(\lambda) - (I_4\lambda^2 - (I_2 - I_5)\lambda + I_3), \end{aligned} \tag{7.6.51}$$

where $p_{\boldsymbol{D}}$ *is the characteristic polynomial of* $\boldsymbol{D}$*, as defined by Eq.* (7.6.9)*. Therefore, upon using Eqs.* (7.6.48)-(7.6.50)*, together with the fact that* $p_{\boldsymbol{D}}(d_k^2) = 0$*, a straightforward calculation reveals that*

$$p_{\boldsymbol{C}}(d_k^2) = \lambda_n^2(I_5 - d_k^4)\cos^2(\psi_k) \text{ for } k = 2, 3. \tag{7.6.52}$$

It then follows directly that, for $k = 2$ *or* 3*, if* $\psi_k = \frac{\pi}{2}$*,* d_k^2 *satisfies the characteristic polynomial of* $\boldsymbol{C}$*, implying that* d_k *is a principal stretch.* □

2. *First suppose that* λ_n, d_2 *and* d_3 *are principal stretches. Use of Eq.* $(7.6.46)_3$ *shows that*

$$I_3 = \lambda_n^2 d_2^2 d_3^2 = I_4 I_5, \tag{7.6.53}$$

which, from the definition of ψ_1*, implies that* ψ_1 *must equal 0.*

Now, suppose that $\psi_1 = 0$*. Due to the fact that* ψ_1, ψ_2 *and* ψ_3 *satisfy*

$$\cos^2(\psi_1) + \cos^2(\psi_2) + \cos^2(\psi_3) = 1, \tag{7.6.54}$$

it must be that $\psi_2 = \psi_3 = \frac{\pi}{2}$*, which from the first part of this proposition, implies that* d_2 *and* d_3 *are principal stretches. It then follows from Eqs.* (7.6.47) *and* $(7.6.46)_3$ *that* λ_n *is the third principal stretch.* □

7.7 Appendix II: A polyconvexity result

Here, we provide a polyconvexity result for transversely isotropic functions that makes use of the previous convexity result for $i_6 = d_3^2$ in $\overline{\boldsymbol{F}}$ (Proposition 6), together with known corresponding convexity results for i_4 and i_5 (see Table 7.1). The result is a variant of a polyconvexity result of Steigmann (2003) for transversely isotropic functions and makes use of similar arguments.

Proposition 10:

Suppose that there exists a continuously differentiable function $w : \mathbb{R}^+ \times \mathbb{R}^+ \times \mathbb{R}^+ \to \mathbb{R}$, *which is convex, and nondecreasing in each of its arguments, such that* $f : \mathrm{GL}^+(d) \to \mathbb{R}$ *can be written as*

$$f(\overline{\boldsymbol{F}}) = w(i_4(\overline{\boldsymbol{F}}), i_5(\overline{\boldsymbol{F}}^*), i_6(\overline{\boldsymbol{F}})), \tag{7.7.1}$$

where i_4, i_5 *and* i_6 *are defined in Table 7.1. Then, the function* f *is polyconvex.*

Proof:

To see this, we follow closely the proof of Steigmann's, and start by writing Δi_4, Δi_5, Δi_6 *to mean* $i_4(\Delta\overline{\boldsymbol{F}})$, $i_5(\Delta\overline{\boldsymbol{F}}^*)$, $i_6(\Delta\overline{\boldsymbol{F}})$. *It has been proven (Steigmann, 2003) that* $\boldsymbol{F} \mapsto i_4$ *and* $\boldsymbol{F}^* \mapsto i_5$ *are convex, and as shown above (Proposition 6),* $\overline{\boldsymbol{F}} \mapsto i_6$ *is convex. Therefore,*

$$\Delta i_4 \geqslant \frac{\partial i_4}{\partial \overline{\boldsymbol{F}}} \cdot \Delta\overline{\boldsymbol{F}}, \quad \Delta i_5 \geqslant \frac{\partial i_5}{\partial \overline{\boldsymbol{F}}^*} \cdot \Delta\overline{\boldsymbol{F}}^*, \quad \Delta i_6 \geqslant \frac{\partial i_6}{\partial \overline{\boldsymbol{F}}} \cdot \Delta\overline{\boldsymbol{F}}. \tag{7.7.2}$$

Since w *is convex, and nondecreasing in each of its arguments, so that in particular its first order partial derivatives are all non-negative, we find that*

$$\begin{aligned} f(\overline{\boldsymbol{F}} + \Delta\overline{\boldsymbol{F}}) &= w(i_4 + \Delta i_4, i_5 + \Delta i_5, i_6 + \Delta i_6), \\ &\geqslant w(i_4, i_5, i_6) + \frac{\partial w}{\partial i_4}\Delta i_4 + \frac{\partial w}{\partial i_5}\Delta i_5 + \frac{\partial w}{\partial i_6}\Delta i_6, \\ &\geqslant f(\overline{\boldsymbol{F}}) + \left(\frac{\partial w}{\partial i_4}\frac{\partial i_4}{\partial \overline{\boldsymbol{F}}} + \frac{\partial w}{\partial i_6}\frac{\partial i_6}{\partial \overline{\boldsymbol{F}}}\right) \cdot \Delta\overline{\boldsymbol{F}} + \frac{\partial w}{\partial i_5}\frac{\partial i_5}{\partial \overline{\boldsymbol{F}}^*} \cdot \Delta\overline{\boldsymbol{F}}^*. \end{aligned} \tag{7.7.3}$$

It then follows from the work of Ball (1977) that Eq. (7.7.3) *implies that* f *is polyconvex. Indeed, Eq.* (7.7.3)*, which is of the same form as Eq. (4.7) in Theorem 4.4 (Ball, 1977), is a necessary and sufficient conditions for polyconvexity.* □

7.8 Appendix III: Loss of strict rank-one convexity vs. strong ellipticity

In this section, we look to characterize the deformations for which strict rank-one convexity of the principal solution $\widehat{W}$ is lost prior to strong ellipticity. In particular, we will provide a condition under which strict rank-one convexity and strong ellipticity are lost simultaneously.

Before proceeding, we recall that, due to the polar decomposition theorem, the average deformation gradient can be written as $\overline{\boldsymbol{F}} = \overline{\boldsymbol{R}}\,\overline{\boldsymbol{U}}$, where $\overline{\boldsymbol{R}}$ is a rotation, and $\overline{\boldsymbol{U}}$ is a positive definite second order tensor. As discussed in Section 7.6, $\overline{\boldsymbol{U}}$ is often referred to as the right-stretch tensor, and is related to the right Cauchy-Green tensor via $\overline{\boldsymbol{C}} = \overline{\boldsymbol{U}}^2$. Moreover, the eigenvectors of $\overline{\boldsymbol{U}}$ are called principal stretches, while the correspond eigenvectors are called principal axes. Finally, in what follows, we uphold the convention set forth in Section 7.6 that $d_2 \leqslant d_3$. With this, we can state and prove our result.

Proposition 11:

Strong ellipticity and strict rank-one convexity of the principal solution $\widehat{W}$ *are lost simultaneously whenever the smallest nonzero eigenvalue of* $\boldsymbol{D}^{1/2}$ *is a principal stretch. In all other cases, strict rank-one convexity is lost prior to strong ellipticity.*

Proof:

To start, we assume that $\overline{\boldsymbol{F}}$ *is such that*

$$d_2 = \widetilde{\lambda}^{1/4} d_3^{-1/2} \implies d_2^2 = \frac{\widetilde{\lambda}}{(d_2 d_3)^2}, \tag{7.8.1}$$

i.e. that $\widehat{W}$ has just lost strict rank-one convexity.

Recall that $\widehat{W}$ is strongly elliptic whenever

$$\widehat{\Lambda}(\overline{\boldsymbol{F}}) = \inf_{|\mathbf{n}|=1} \mathcal{F}(\overline{\boldsymbol{F}}, \mathbf{n}) > 0, \tag{7.8.2}$$

where $\mathcal{F}$ is given by Eq. (7.2.24)*. A simple manipulation reveals that*

$$\mathcal{F}(\overline{\boldsymbol{F}}, \mathbf{n}) = \mathbf{n} \cdot (\boldsymbol{T}_0 \mathbf{n}) - \overline{\mu} \frac{\widetilde{\lambda}}{(d_2 d_3)^2} (1 - 2(\mathbf{n} \cdot \mathbf{t}_1)^2)^2, \tag{7.8.3}$$

where

$$\boldsymbol{T}_0 = \breve{\mu}(\overline{\boldsymbol{F}}\mathbf{N}) \otimes (\overline{\boldsymbol{F}}\mathbf{N}) + \overline{\mu} \left(\frac{\widetilde{\lambda}}{(d_2 d_3)^2} \mathbf{t}_1 \otimes \mathbf{t}_1 + d_2^2 \mathbf{t}_2 \otimes \mathbf{t}_2 + d_3^2 \mathbf{t}_3 \otimes \mathbf{t}_3 \right). \tag{7.8.4}$$

Note that $\boldsymbol{T}_0$ is nothing more than the determinate part of the Cauchy stress of the principal solution (see Eqs. (7.3.33) *and* (7.3.34)*). Now, by letting*

$$\breve{\boldsymbol{T}}_0 = \frac{\widetilde{\lambda}}{(d_2 d_3)^2} \mathbf{t}_1 \otimes \mathbf{t}_1 + d_2^2 \mathbf{t}_2 \otimes \mathbf{t}_2 + d_3^2 \mathbf{t}_3 \otimes \mathbf{t}_3, \tag{7.8.5}$$

we see that

$$\begin{aligned} \widehat{\Lambda}(\overline{\boldsymbol{F}}) &\geqslant \inf_{|\mathbf{n}|=1} \mathbf{n} \cdot (\boldsymbol{T}_0 \mathbf{n}) - \overline{\mu} \frac{\widetilde{\lambda}}{(d_2 d_3)^2} \sup_{|\mathbf{n}|=1} (1 - 2(\mathbf{n} \cdot \mathbf{t}_1)^2)^2, \\ &\geqslant \breve{\mu} \inf_{|\mathbf{n}|=1} ((\overline{\boldsymbol{F}}\mathbf{N}) \cdot \mathbf{n})^2 + \overline{\mu} \inf_{|\mathbf{n}|=1} \mathbf{n} \cdot (\breve{\boldsymbol{T}}_0 \mathbf{n}) - \overline{\mu} \frac{\widetilde{\lambda}}{(d_2 d_3)^2} \sup_{|\mathbf{n}|=1} (1 - 2(\mathbf{n} \cdot \mathbf{t}_1)^2)^2, \end{aligned} \tag{7.8.6}$$

where equality holds precisely when the optimal value of $\mathbf{n}$ is the same for each optimization. It is easy to see that

$$\sup_{|\mathbf{n}|=1} (1 - 2(\mathbf{n} \cdot \mathbf{t}_1)^2)^2 = 1, \tag{7.8.7}$$

and is attained by $\mathbf{n} = \mathbf{t}_1$ *or* $\mathbf{n} \in \{\mathbf{t}_1\}^\perp$. *Moreover, it is clear that*

$$\inf_{|\mathbf{n}|=1} ((\overline{\boldsymbol{F}}\mathbf{N}) \cdot \mathbf{n})^2 = 0, \tag{7.8.8}$$

and is attained by $\mathbf{n} \in \{\boldsymbol{F}\mathbf{N}\}^\perp$. *Finally*

$$\inf_{|\mathbf{n}|=1} \mathbf{n} \cdot (\breve{\boldsymbol{T}}_0)\mathbf{n} = d_2^2 = \frac{\widetilde{\lambda}}{(d_2 d_3)^2}, \tag{7.8.9}$$

is attained by $\mathbf{n} \in \operatorname{span}\{\mathbf{t}_1, \mathbf{t}_2\} = \{\mathbf{t}_3\}^\perp$. *This follows from the fact that since* $\breve{\boldsymbol{T}}_0$ *is symmetric, this optimization is nothing more than the smallest eigenvalue of* $\breve{\boldsymbol{T}}_0$, *and is attained by the corresponding eigenvector.* $\breve{\boldsymbol{T}}_0$ *is already diagonalized (with respect to the basis* $\{\mathbf{t}_1, \mathbf{t}_2, \mathbf{t}_3\}$*), so Eq.* (7.8.1) *implies Eq.* (7.8.9), *for this choice of* $\overline{\boldsymbol{F}}$.

Combining Eq. (7.8.6)-(7.8.9), *it follows that* $\widehat{\Lambda}(\overline{\boldsymbol{F}}) \geqslant 0$, *and moreover that*

$$\widehat{\Lambda}(\overline{\boldsymbol{F}}) = 0, \tag{7.8.10}$$

precisely when the optimal value of $\mathbf{n}$ *is the same for all three optimizations. In other words, strong ellipticity and strict rank-one convexity are lost simultaneously whenever there exists a unit vector* $\mathbf{n}$ *for which Eqs.* (7.8.7)-(7.8.9) *are obtained simultaneously. This condition can be written as*

$$\big(\{\mathbf{t}_1\} \cup \{\mathbf{t}_1\}^\perp\big) \cap \{\overline{\boldsymbol{F}}\mathbf{N}\}^\perp \cap \{\mathbf{t}_3\}^\perp \neq \varnothing. \tag{7.8.11}$$

Now, we recall from Section 7.6, Eqs. (7.6.47)-(7.6.49), *that*

$$((\overline{\boldsymbol{F}}\mathbf{N}) \cdot \mathbf{t}_1)^2 = I_5^{-1}, \tag{7.8.12}$$

$$((\overline{\boldsymbol{F}}\mathbf{N}) \cdot \mathbf{t}_2)^2 = \lambda_n^2 \cos^2(\psi_2), \tag{7.8.13}$$

$$((\overline{\boldsymbol{F}}\mathbf{N}) \cdot \mathbf{t}_3)^2 = \lambda_n^2 \cos^2(\psi_3), \tag{7.8.14}$$

which, together with the associative and distributive properties of intersections and unions, can be used to simplify the condition in Eq. (7.8.11). *Since* $I_5 > 0$, *Eq.* (7.8.12) *implies that* $((\overline{\boldsymbol{F}}\mathbf{N}) \cdot \mathbf{t}_1) > 0$, *and hence* $\{\mathbf{t}_1\} \cap \{\overline{\boldsymbol{F}}\mathbf{N}\}^{\perp} = \varnothing$. *As such, we only need to look at whether* $\{\mathbf{t}_1\}^{\perp} \cap \{\overline{\boldsymbol{F}}\mathbf{N}\}^{\perp} \cap \{\mathbf{t}_3\}^{\perp}$ *is nonempty. In fact, since the only unit vector which lies in* $\{\mathbf{t}_1\}^{\perp} \cap \{\mathbf{t}_3\}^{\perp}$ *is* $\mathbf{t}_2$, *the condition in Eq.* (7.8.11), *which ensures that strong ellipticity and strict rank-one convexity are lost simultaneously, is equivalent to*

$$\{\mathbf{t}_2\} \cap \{\overline{\boldsymbol{F}}\mathbf{N}\}^{\perp} \neq \varnothing. \tag{7.8.15}$$

From Eq. (7.8.13), *this is equivalent to requiring that* $\psi_2 = \frac{\pi}{2}$, *which, from Proposition 9, is equivalent to* d_2, *the smallest nonzero eigenvector of* $\boldsymbol{D}^{1/2}$, *being a principal stretch of* $\overline{\boldsymbol{U}}$, *and hence the first part of the result is proven. On the other hand, when* d_2 *is not a principal stretch, whereby* $\psi_2 \neq \frac{\pi}{2}$, *there can be no equality in Equation* (7.8.10), *and we conclude that* $\widehat{W}$ *will remain strongly elliptic.* □

7.9 Appendix IV: Further results for the properties of the relaxation construction.

Here, we provide a complete derivation for the results discussed in Section 7.3 of the paper. In particular, we prove a result that describes the behavior of the domains formed during the relaxation construction. We recall that for certain values of $\overline{\boldsymbol{F}}$, $Q\widehat{W}$ is obtained either via a single lamination, or by a-laminate-within-a-laminate microstructure. In order to discuss these situations, it is helpful to first define

$$\boldsymbol{A}_{[k]}^{(1)} = \boldsymbol{I} - c_k \omega_k \mathbf{M}_k \otimes \mathbf{N}_k, \quad \boldsymbol{A}_{[k]}^{(2)} = \boldsymbol{I} + (1 - c_k)\omega_k \mathbf{M}_k \otimes \mathbf{N}_k, \tag{7.9.1}$$

where

$$\mathbf{M}_k = -\cos(\beta_k)\begin{bmatrix}1\\0\\0\end{bmatrix} + \sin(\beta_k)\begin{bmatrix}0\\\cos(\theta_k)\\-\sin(\theta_k)\end{bmatrix}, \quad \mathbf{N}_k = \begin{bmatrix}0\\\sin(\theta_k)\\\cos(\theta_k)\end{bmatrix}. \tag{7.9.2}$$

(7.9.3)

Now, θ_2 and β_2 can be chosen arbitrarily, so long as $\theta_2 \neq \theta_1$, while, upon defining

$$A_1 = \widetilde{\lambda}^{1/3}(\overline{\boldsymbol{F}}\mathbf{M}_2)\cdot(\overline{\boldsymbol{F}}\mathbf{N}_2) - \cos(\beta_2)(\overline{\boldsymbol{F}}^{-T}\mathbf{N}_2)\cdot(\overline{\boldsymbol{F}}^{-T}\mathbf{N}), \tag{7.9.4}$$

$$A_2 = \widetilde{\lambda}^{1/3}|\overline{\boldsymbol{F}}\mathbf{M}_2|^2 - \cos^2(\beta_2)|\overline{\boldsymbol{F}}^{-T}\mathbf{N}_2|, \tag{7.9.5}$$

we have

$$\omega_2 = \pm\frac{2}{A_2}\sqrt{A_1^2 + [\widetilde{\lambda}^{2/3} - (I_1 - I_4)\widetilde{\lambda}^{1/3} + I_5]A_2} \tag{7.9.6}$$

and

$$c_2 = \frac{1}{2}\left(1 \pm \frac{A_1}{\sqrt{A_1^2 + [\widetilde{\lambda}^{2/3} - (I_1 - I_4)\widetilde{\lambda}^{1/3} + I_5]A_2}}\right). \tag{7.9.7}$$

On the other hand,

$$\mathbf{N}_1 = \widehat{\mathbf{e}}_2, \quad \mathbf{M}_1 = -\cos(\beta_1)\mathbf{N} + \sin(\beta_1)\widehat{\mathbf{e}}_3, \tag{7.9.8}$$

with $\widehat{\mathbf{e}}_2$ and $\widehat{\mathbf{e}}_3$ given by

$$\widehat{\mathbf{e}}_2 = \cos(\theta_1)\mathbf{e}_2 - \sin(\theta_1)\mathbf{e}_3, \quad \widehat{\mathbf{e}}_3 = \sin(\theta_1)\mathbf{e}_2 + \cos(\theta_1)\mathbf{e}_3, \tag{7.9.9}$$

and

$$\tan(\beta_1) = \frac{(\overline{\boldsymbol{F}}\widehat{\mathbf{e}}_3)\cdot(\overline{\boldsymbol{F}}\mathbf{N})}{d_3^2}, \tag{7.9.10}$$

$$\omega_1 = \frac{-2}{\cos(\beta_1)|\overline{\boldsymbol{F}}^{-T}\widehat{\mathbf{e}}_2|^2}\sqrt{\sqrt{\widetilde{\lambda}}d_3|\overline{\boldsymbol{F}}^{-T}\widehat{\mathbf{e}}_2|^2 - d_3^2}, \tag{7.9.11}$$

$$c_1 = \frac{1}{2}\left(1 - \frac{(\overline{\boldsymbol{F}}^{-T}\widehat{\mathbf{e}}_2)\cdot(\overline{\boldsymbol{F}}^{-T}\mathbf{N})}{\sqrt{\sqrt{\widetilde{\lambda}}d_3|\overline{\boldsymbol{F}}^{-T}\widehat{\mathbf{e}}_2|^2 - d_3^2}}\right), \tag{7.9.12}$$

as applied to $\overline{\boldsymbol{F}}\boldsymbol{A}^{(i)}_{[2]}$, for $i = 1, 2$, if a double lamination is required, or as applied just to $\overline{\boldsymbol{F}}$, when a single lamination is required. In going forward, we denote the dependence of an invariant on its argument by using square brackets, so that I_1 calculated for $\overline{\boldsymbol{F}}\boldsymbol{A}^{(1)}_{[1]}$ is denoted by $I_1\left[\overline{\boldsymbol{F}}\boldsymbol{A}^{(1)}_{[1]}\right]$. The invariant corresponds to $\overline{\boldsymbol{F}}$ when no arguments appears. We will always assume that $d_2 < d_3$, and will comment briefly at the end of the proof how to handle the case when $d_2 = d_3$. For reference, we also recall that $I_4 = \lambda_n^2$ and

$$Q\widehat{W}(\overline{\boldsymbol{F}}) = \frac{\breve{\mu}}{2}\lambda_n^2 + g_r(d_2, d_3) + K(d_2 d_3 \lambda_n \cos\psi_1), \tag{7.9.13}$$

where

$$g_r(d_2, d_3) = \begin{cases} g_0(d_2, d_3) & d_2 \geqslant \widetilde{\lambda}^{1/4}/d_3^{1/2}, \\ g_1(d_2, d_3) & d_2 < \widetilde{\lambda}^{1/4}/d_3^{1/2} \text{ and } d_3 \geqslant \widetilde{\lambda}^{1/6}, \\ g_2(d_2, d_3) & d_3 < \widetilde{\lambda}^{1/6}, \end{cases} \tag{7.9.14}$$

and where

$$g_0(d_2, d_3) = \frac{\overline{\mu}}{2}\left(d_2^2 + d_3^2 + \frac{\widetilde{\lambda}}{(d_2 d_3)^2} - 3\right), \tag{7.9.15}$$

$$g_1(d_2, d_3) = \frac{\overline{\mu}}{2}\left(d_3^2 + 2\frac{\widetilde{\lambda}^{1/2}}{d_3} - 3\right), \tag{7.9.16}$$

$$g_2(d_2, d_3) = \frac{3\overline{\mu}}{2}(\widetilde{\lambda}^{1/3} - 1). \tag{7.9.17}$$

Also,

$$\widehat{W}(\overline{\boldsymbol{F}}) = \frac{\breve{\mu}}{2}\lambda_n^2 + g_0(d_2, d_3) + K(d_2 d_3 \lambda_n \cos\psi_1) \tag{7.9.18}$$

Finally, throughout this section, we rely on the basic facts that

$$(\mathbf{a}\cdot\mathbf{b})^2 = |\mathbf{a}|^2|\mathbf{b}|^2 - |\mathbf{a}\times\mathbf{b}|^2, \tag{7.9.19}$$

$$|(\boldsymbol{F}\mathbf{a})\times(\boldsymbol{F}\mathbf{b})|^2 = |\boldsymbol{F}^*(\mathbf{a}\times\mathbf{b})|^2. \tag{7.9.20}$$

With this, we are ready to state and prove our result.

Proposition 12:

1. *Suppose that*

$$d_2 \leqslant \widetilde{\lambda}^{1/4} d_3^{-1/2} \quad \text{and} \quad \widetilde{\lambda}^{1/6} \leqslant d_3. \tag{7.9.21}$$

Then, there exists c_I, c_{II}, $\overline{\boldsymbol{F}}^I$ *and* $\overline{\boldsymbol{F}}^{II}$ *such that* $c_I + c_{II} = 1$,

$$\overline{\boldsymbol{F}} = c_I \overline{\boldsymbol{F}}^I + c_{II}\overline{\boldsymbol{F}}^{II}, \tag{7.9.22}$$

$$Q\widehat{W}(\overline{\boldsymbol{F}}) = c_I \widehat{W}(\overline{\boldsymbol{F}}^I) + c_{II}\widehat{W}(\overline{\boldsymbol{F}}^{II}). \tag{7.9.23}$$

Moreover, for $s = I, II$,

$$d_2\left[\overline{\boldsymbol{F}}^s\right] = \frac{\widetilde{\lambda}^{1/4}}{\sqrt{d_3\left[\overline{\boldsymbol{F}}^s\right]}}, \tag{7.9.24}$$

$$\widehat{W}(\overline{\boldsymbol{F}}^s) = Q\widehat{W}(\overline{\boldsymbol{F}}), \tag{7.9.25}$$

and

$$I_1\left[\overline{\boldsymbol{F}}^s\right] = I_1 + \frac{\sqrt{\widetilde{\lambda}}d_3 - I_5}{d_3^2}, \tag{7.9.26}$$

$$I_2\left[\overline{\boldsymbol{F}}^s\right] = I_2 + \frac{\sqrt{\widetilde{\lambda}}d_3 - I_5}{d_3^2}\left(d_3^2 + \left[\left(\overline{\boldsymbol{F}}\mathbf{N}\right)\cdot t_3\right]^2\right), \tag{7.9.27}$$

$$I_3\left[\overline{\boldsymbol{F}}^s\right] = 1, \tag{7.9.28}$$

$$I_4\left[\overline{\boldsymbol{F}}^s\right] = I_4, \tag{7.9.29}$$

$$I_5\left[\overline{\boldsymbol{F}}^s\right] = \sqrt{\widetilde{\lambda}}d_3. \tag{7.9.30}$$

2. *Suppose that*

$$d_3 < \widetilde{\lambda}^{1/6}. \tag{7.9.31}$$

Then, there exists $c_I, \ldots, c_{IV}$, $\overline{\boldsymbol{F}}^I, \ldots, \overline{\boldsymbol{F}}^{IV}$ *such that* $c_I + c_{II} + c_{III} + c_{IV} = 1$,

$$\overline{\boldsymbol{F}} = c_I\overline{\boldsymbol{F}}^I + c_{II}\overline{\boldsymbol{F}}^{II} + c_{III}\overline{\boldsymbol{F}}^{III} + c_{IV}\overline{\boldsymbol{F}}^{IV}, \tag{7.9.32}$$

$$Q\widehat{W}(\overline{\boldsymbol{F}}) = c_I\widehat{W}(\overline{\boldsymbol{F}}^I) + c_{II}\widehat{W}(\overline{\boldsymbol{F}}^{II}) + c_{III}\widehat{W}(\overline{\boldsymbol{F}}^{III}) + c_{IV}\widehat{W}(\overline{\boldsymbol{F}}^{IV}). \tag{7.9.33}$$

Moreover, for $s = I, \ldots, IV$,

$$d_2\left[\overline{\boldsymbol{F}}^s\right] = d_3\left[\overline{\boldsymbol{F}}^s\right] = \widetilde{\lambda}^{1/6}, \tag{7.9.34}$$

$$\widehat{W}(\overline{\boldsymbol{F}}^s) = Q\widehat{W}(\overline{\boldsymbol{F}}), \tag{7.9.35}$$

and

$$I_1\left[\overline{\boldsymbol{F}}^{\,s}\right] = 2\widetilde{\lambda}^{1/3} + I_4, \tag{7.9.36}$$

$$I_2\left[\overline{\boldsymbol{F}}^{\,s}\right] = \widetilde{\lambda}^{2/3} + \widetilde{\lambda}^{1/3} I_4 + \widetilde{\lambda}^{-1/3}, \tag{7.9.37}$$

$$I_3\left[\overline{\boldsymbol{F}}^{\,s}\right] = 1, \tag{7.9.38}$$

$$I_4\left[\overline{\boldsymbol{F}}^{\,s}\right] = I_4, \tag{7.9.39}$$

$$I_5\left[\overline{\boldsymbol{F}}^{\,s}\right] = \widetilde{\lambda}^{2/3}. \tag{7.9.40}$$

Remark 4:

Interestingly, in the latter case, we can find the principle stretches of $\overline{\boldsymbol{U}}^{\,s}$ *analytically; here* $\overline{\boldsymbol{U}}^{\,s}$ *is the corresponding right stretch tensor associated to* $\overline{\boldsymbol{F}}^{\,s}$*. From the Cayley-Hamilton Theorem, we know that the principal stretches, which we denote* $\lambda_1 < \lambda_2 < \lambda_3$*, must satisfy the equation*

$$\begin{aligned} 0 &= \lambda^6 - I_1\left[\overline{\boldsymbol{F}}^{\,s}\right]\lambda^4 + I_2\left[\overline{\boldsymbol{F}}^{\,s}\right]\lambda^2 - I_3\left[\overline{\boldsymbol{F}}^{\,s}\right] \\ &= \lambda^6 - (2\widetilde{\lambda}^{1/3} + I_4)\lambda^4 + (\widetilde{\lambda}^{2/3} + \widetilde{\lambda}^{1/3} I_4 + \widetilde{\lambda}^{-1/3})\lambda^2 - 1 \\ &= (\lambda^2 - \widetilde{\lambda}^{1/3})(\lambda^4 - (I_4 + \widetilde{\lambda}^{1/3})\lambda^2 + \widetilde{\lambda}^{-1/3}). \end{aligned} \tag{7.9.41}$$

Therefore, the principal stretches are

$$\lambda_1 = \sqrt{\frac{I_4 + \widetilde{\lambda}^{1/3} - \sqrt{(I_4 + \widetilde{\lambda}^{1/3})^2 - 4\widetilde{\lambda}^{-1/3}}}{2}}, \tag{7.9.42}$$

$$\lambda_2 = \widetilde{\lambda}^{1/6}, \tag{7.9.43}$$

$$\lambda_3 = \sqrt{\frac{I_4 + \widetilde{\lambda}^{1/3} + \sqrt{(I_4 + \widetilde{\lambda}^{1/3})^2 - 4\widetilde{\lambda}^{-1/3}}}{2}}. \tag{7.9.44}$$

Proof:

Before proceeding, we record the following identities which will be useful going

forward

$$|\overline{\boldsymbol{F}}^{-T}\widehat{\mathbf{e}}_2|^2 = \frac{d_3^2(I_2 - I_5) - (I_4 I_5 + 1)}{d_3^2 - d_2^2}, \tag{7.9.45}$$

$$|\overline{\boldsymbol{F}}^{-T}\widehat{\mathbf{e}}_3|^2 = \frac{(I_4 I_5 + 1) - d_2^2(I_2 - I_5)}{d_3^2 - d_2^2}, \tag{7.9.46}$$

$$(\overline{\boldsymbol{F}}\mathbf{M}_1) \cdot (\overline{\boldsymbol{F}}\mathbf{N}_1) = -\cos(\beta_1)(\overline{\boldsymbol{F}}\mathbf{N}) \cdot (\overline{\boldsymbol{F}}\widehat{\mathbf{e}}_2), \tag{7.9.47}$$

$$|\overline{\boldsymbol{F}}\mathbf{M}_1|^2 = \frac{\cos^2(\beta_1)|\overline{\boldsymbol{F}}^{-T}\widehat{\mathbf{e}}_2|^2}{d_3^2}, \tag{7.9.48}$$

$$\left[(\overline{\boldsymbol{F}}\mathbf{N}) \cdot (\overline{\boldsymbol{F}}\widehat{\mathbf{e}}_2)\right]\left[(\overline{\boldsymbol{F}}^{-T}\mathbf{N}) \cdot (\overline{\boldsymbol{F}}^{-T}\widehat{\mathbf{e}}_2)\right] = \frac{d_3^2\left(d_2^2(|\overline{\boldsymbol{C}}\mathbf{N}|^2 - I_4^2) + 1 - I_4 I_5\right)}{d_3^2 - d_2^2}. \tag{7.9.49}$$

We know that from the Cayley Hamilton Theorem

$$I_5 = I_2 - I_1 I_4 + |\overline{\boldsymbol{C}}\mathbf{N}|^2. \tag{7.9.50}$$

We also prove the following identity:

$$\left[(\overline{\boldsymbol{F}}\mathbf{N}) \cdot (\overline{\boldsymbol{F}}\widehat{\mathbf{e}}_2)\right] d_3^2 + \left[(\overline{\boldsymbol{F}}^{-T}\mathbf{N}) \cdot (\overline{\boldsymbol{F}}^{-T}\widehat{\mathbf{e}}_2)\right] = 0. \tag{7.9.51}$$

To do this, we use the various properties of d_2 and d_3, as outlined in Appendix A, and make use of Eqs. (7.9.19) *along with Eqs.* (7.9.45)-(7.9.50). *Therefore upon square*

the left hand side of Eq. (7.9.51)*, find that*

$$\begin{aligned}
&\left[(\overline{\boldsymbol{F}}\mathbf{N})\cdot(\overline{\boldsymbol{F}}\widehat{\mathbf{e}}_2)\right]^2 d_3^4 + 2\left[(\overline{\boldsymbol{F}}\mathbf{N})\cdot(\overline{\boldsymbol{F}}\widehat{\mathbf{e}}_2)\right]\left[(\overline{\boldsymbol{F}}^{-T}\mathbf{N})\cdot(\overline{\boldsymbol{F}}^{-T}\widehat{\mathbf{e}}_2)\right] d_3^2 \\
&\qquad + \left[(\overline{\boldsymbol{F}}^{-T}\mathbf{N})\cdot(\overline{\boldsymbol{F}}^{-T}\widehat{\mathbf{e}}_2)\right]^2 \\
&= d_3^4\left(I_4 d_2^2 - |\overline{\boldsymbol{F}}^{-T}\widehat{\mathbf{e}}_3|^2\right) + \frac{2d_3^4\left(d_2^2(|\overline{\boldsymbol{C}}\mathbf{N}|^2 - I_4^2) + 1 - I_4 I_5\right)}{d_3^2 - d_2^2} + I_5|\overline{\boldsymbol{F}}^{-T}\widehat{\mathbf{e}}_2|^2 - d_3^2 \\
&= \frac{2I_5\left(d_3^2(|\overline{\boldsymbol{C}}\mathbf{N}|^2 - I_4^2 + I_2 - I_5) - I_4(d_3^4 + I_5)\right)}{d_3^2 - d_2^2} \\
&= \frac{-2I_5 I_4\left(d_3^4 - (I_1 - I_4)d_3^2 + I_5\right)}{d_3^2 - d_2^2} \\
&= 0. \qquad (7.9.52)
\end{aligned}$$

1. *Now, from Eq.* (7.9.21)*, we know that*

$$Q\widehat{W}(\overline{\boldsymbol{F}}) = (1-c_1)\widehat{W}(\overline{\boldsymbol{F}}\boldsymbol{A}_{[1]}^{(1)}) + c_1\widehat{W}(\overline{\boldsymbol{F}}\boldsymbol{A}_{[1]}^{(2)}) \qquad (7.9.53)$$

which, upon letting $c_I = 1 - c_1$, $c_{II} = c_1$, $\overline{\boldsymbol{F}}^I = \overline{\boldsymbol{F}}\boldsymbol{A}_{[1]}^{(1)}$ *and* $\overline{\boldsymbol{F}}^{II} = \overline{\boldsymbol{F}}\boldsymbol{A}_{[1]}^{(2)}$*, proves Eq.* (7.9.22)*.*

From Eq. (7.9.2)*, it is clear that* $\boldsymbol{A}_{[1]}^{(k)}\mathbf{N} = \mathbf{N}$*, and hence*

$$I_4\left[\overline{\boldsymbol{F}}^s\right] = I_4, \qquad (7.9.54)$$

for $s = I, II$*. Next we claim that*

$$I_5\left[\overline{\boldsymbol{F}}^s\right] = \sqrt{\widetilde{\lambda}}d_3, \qquad (7.9.55)$$

for $s = I, II$. To see this, we take $s = I$, and calculate directly

$$\begin{aligned} I_5[\overline{\boldsymbol{F}}^I] &= I_5 + 2c_1\omega_1\cos(\beta_1)(\overline{\boldsymbol{F}}^{-T}\mathbf{N})\cdot(\overline{\boldsymbol{F}}^{-T}\widehat{\mathbf{e}}_2) + c_1^2\omega_1^2\cos(\beta_1)^2|\overline{\boldsymbol{F}}^{-T}\widehat{\mathbf{e}}_2|^2 \\ &= I_5 + \frac{\sqrt{\widetilde{\lambda}}d_3|\overline{\boldsymbol{F}}^{-T}\widehat{\mathbf{e}}_2|^2 - [(\overline{\boldsymbol{F}}^{-T}\mathbf{N})\cdot(\overline{\boldsymbol{F}}^{-T}\widehat{\mathbf{e}}_2)]^2 - d_3^2}{|\overline{\boldsymbol{F}}^{-T}\widehat{\mathbf{e}}_2|^2} \\ &= I_5 + \frac{(\sqrt{\widetilde{\lambda}}d_3 - I_5)|\overline{\boldsymbol{F}}^{-T}\widehat{\mathbf{e}}_2|^2}{|\overline{\boldsymbol{F}}^{-T}\widehat{\mathbf{e}}_2|^2} \\ &= \sqrt{\widetilde{\lambda}}d_3. \end{aligned} \tag{7.9.56}$$

An identical calculations holds for $\overline{\boldsymbol{F}}^{II}$. Similarly, upon letting

$$\Delta = \sqrt{\sqrt{\widetilde{\lambda}}d_3|\overline{\boldsymbol{F}}^{-T}\widehat{\mathbf{e}}_2|^2 - d_3^2}, \tag{7.9.57}$$

we find directly that

$$\begin{aligned} I_1\left[\overline{\boldsymbol{F}}^I\right] &= I_1 - 2c_1\omega_1(\overline{\boldsymbol{F}}\mathbf{M}_1)\cdot(\overline{\boldsymbol{F}}\mathbf{N}_1) + c_1^2\omega_1^2|\overline{\boldsymbol{F}}\mathbf{M}_1|^2 \\ &= I_1 - \frac{2[(\overline{\boldsymbol{F}}\mathbf{N})\cdot(\overline{\boldsymbol{F}}\mathbf{e}_2)]}{|\overline{\boldsymbol{F}}^{-T}\widehat{\mathbf{e}}_2|^2}\left(\Delta - \left[(\overline{\boldsymbol{F}}^{-T}\mathbf{N})\cdot(\overline{\boldsymbol{F}}^{-T}\widehat{\mathbf{e}}_2)\right]\right) \\ &\quad + \frac{\Delta^2 + \left[(\overline{\boldsymbol{F}}^{-T}\mathbf{N})\cdot(\overline{\boldsymbol{F}}^{-T}\widehat{\mathbf{e}}_2)\right]^2 - 2\left[(\overline{\boldsymbol{F}}^{-T}\mathbf{N})\cdot(\overline{\boldsymbol{F}}^{-T}\widehat{\mathbf{e}}_2)\right]\Delta}{d_3^2|\overline{\boldsymbol{F}}^{-T}\widehat{\mathbf{e}}_2|^2} \\ &= I_1 + \frac{\sqrt{\widetilde{\lambda}}d_3 - I_5}{d_3^2}, \end{aligned} \tag{7.9.58}$$

having used Eq. (7.9.51). The same holds for $\overline{\boldsymbol{F}}^{II}$. Therefore, recalling that $d_2^2 + d_3^2 = I_1 - I_4$ and $(d_2d_3)^2 = I_5$, Eq. (7.9.54) and (7.9.58) combine to give

$$I_1\left[\overline{\boldsymbol{F}}^s\right] - I_4\left[\overline{\boldsymbol{F}}^s\right] = d_3^2 + \frac{\sqrt{\widetilde{\lambda}}}{d_3}, \tag{7.9.59}$$

for $s = I, II$. From Eq. (7.9.56), *this implies that*

$$d_3\left[\overline{\boldsymbol{F}}^{s}\right] = \sqrt{\frac{I_1\left[\overline{\boldsymbol{F}}^{s}\right] - I_4\left[\overline{\boldsymbol{F}}^{s}\right] + \sqrt{\left(I_1\left[\overline{\boldsymbol{F}}^{s}\right] - I_4\left[\overline{\boldsymbol{F}}^{s}\right]\right)^2 - 4I_5\left[\overline{\boldsymbol{F}}^{s}\right]}}{2}} = d_3, \tag{7.9.60}$$

which, in combination with the fact that and the fact that $(d_2\left[\overline{\boldsymbol{F}}^{s}\right] d_3\left[\overline{\boldsymbol{F}}^{s}\right])^2 = I_5\left[\overline{\boldsymbol{F}}^{s}\right]$ *shows Eq.* (7.9.24). *Moreover*

$$\begin{aligned}
\widehat{W}\left(\overline{\boldsymbol{F}}^{s}\right) &= \frac{\breve{\mu}}{2} I_4\left[\overline{\boldsymbol{F}}^{s}\right] + \frac{\overline{\mu}}{2}\left(\left(d_2\left[\overline{\boldsymbol{F}}^{s}\right]\right)^2 + \left(d_3\left[\overline{\boldsymbol{F}}^{s}\right]\right)^2 + \frac{\widetilde{\lambda}}{\left(\left(d_2\left[\overline{\boldsymbol{F}}^{s}\right] d_3\left[\overline{\boldsymbol{F}}^{s}\right]\right)\right)^2} - 3\right) \\
&= \frac{\breve{\mu}}{2} I_4 + \frac{\overline{\mu}}{2}\left(d_3^2 + 2\frac{\sqrt{\widetilde{\lambda}}}{d_3} - 3\right) \\
&= Q\widehat{W}(\overline{\boldsymbol{F}}).
\end{aligned} \tag{7.9.61}$$

Since $\det \overline{\boldsymbol{F}} = \det \boldsymbol{A}^{(k)}_{[1]} = 1$ *it is obvious that* $I_3\left[\overline{\boldsymbol{F}}^{s}\right] = 1$ *for* $s = I, II$. *It therefore remains only to calculate* $I_2\left[\overline{\boldsymbol{F}}^{s}\right]$. *To do this, we make use of Eq.* (7.9.50), *and note that a direction calculation yields*

$$|(\overline{\boldsymbol{F}}^{s})^T \overline{\boldsymbol{F}}^{s} \mathbf{N}|^2 = |\overline{\boldsymbol{C}}\mathbf{N}|^2 + \frac{\left(\sqrt{\widetilde{\lambda}} d_3 - I_5\right) |\overline{\boldsymbol{F}}^{-T} \hat{\mathbf{e}}_2|^2}{d_3^4}, \tag{7.9.62}$$

from which it follows that

$$I_2\left[\overline{\boldsymbol{F}}^{s}\right] = I_2 + \frac{\sqrt{\widetilde{\lambda}} d_3 - I_5}{d_3^2}\left(d_3^2 + \left[(\overline{\boldsymbol{F}}\mathbf{N}) \cdot (\mathbf{t}_3)\right]^2\right). \tag{7.9.63}$$

2. *Now, from Eq.* (7.9.31), *we know that*

$$\begin{aligned} Q\widehat{W}(\overline{\boldsymbol{F}}) &= (1-c_1)R_1\widehat{W}(\overline{\boldsymbol{F}}\boldsymbol{A}_{[2]}^{(1)}) + c_2R_1\widehat{W}(\overline{\boldsymbol{F}}\boldsymbol{A}_{[2]}^{(2)}) \\ &= (1-c_2)\left((1-c_{1,1})\widehat{W}(\overline{\boldsymbol{F}}\boldsymbol{A}_{[2]}^{(1)}\boldsymbol{A}_{[1,1]}^{(1)}) + c_{1,1}\widehat{W}(\overline{\boldsymbol{F}}\boldsymbol{A}_{[2]}^{(1)}\boldsymbol{A}_{[1,1]}^{(2)})\right) \\ &+ c_2\left((1-c_{1,2})\widehat{W}(\overline{\boldsymbol{F}}\boldsymbol{A}_{[2]}^{(2)}\boldsymbol{A}_{[1,2]}^{(1)}) + c_{1,2}\widehat{W}(\overline{\boldsymbol{F}}\boldsymbol{A}_{[2]}^{(2)}\boldsymbol{A}_{[1,2]}^{(2)})\right). \end{aligned} \tag{7.9.64}$$

Upon letting $c_I = (1-c_2)(1-c_{1,1})$, $c_{II} = (1-c_2)c_{1,1}$, $c_{III} = c_2(1-c_{1,2})$, $c_{IV} = c_2c_{1,2}$, *and*

$$\boldsymbol{F}_1 = \overline{\boldsymbol{F}}\boldsymbol{A}_{[2]}^{(1)}\boldsymbol{A}_{[1,1]}^{(1)}, \quad \boldsymbol{F}_2 = \overline{\boldsymbol{F}}\boldsymbol{A}_{[2]}^{(1)}\boldsymbol{A}_{[1,1]}^{(2)}, \quad \boldsymbol{F}_3 = \overline{\boldsymbol{F}}\boldsymbol{A}_{[2]}^{(2)}\boldsymbol{A}_{[1,2]}^{(1)}, \quad \boldsymbol{F}_4 = \overline{\boldsymbol{F}}\boldsymbol{A}_{[2]}^{(2)}\boldsymbol{A}_{[1,2]}^{(2)}, \tag{7.9.65}$$

Eq. (7.9.32) *follows directly. Here,* $c_{1,1}$ *for example, is used to indicate that the value of* $c_{1,k}$ *is given by Eq.* (7.9.12), *with* $\overline{\boldsymbol{F}}$ *replaced by* $\overline{\boldsymbol{F}}\boldsymbol{A}_{[2]}^{(k)}$, *for* $k = 1, 2$. *Many of the calculations carried out here are identical to those in the case considered above, expect the invariants in the expressions are, at times, evaluated not at* $\overline{\boldsymbol{F}}$, *but at* $\overline{\boldsymbol{F}}\boldsymbol{A}_{[2]}^{(k)}$. *Now, from the results derived in Section 4.1.2, we know that*

$$d_3\left[\overline{\boldsymbol{F}}\boldsymbol{A}_{[2]}^{(k)}\right] = \widetilde{\lambda}^{1/6}. \tag{7.9.66}$$

for $k = 1, 2$. *Therefore, using Eq.* (7.9.55), *we find that*

$$I_5\left[\overline{\boldsymbol{F}}^s\right] = \sqrt{\widetilde{\lambda}}d_3\left[\overline{\boldsymbol{F}}\boldsymbol{A}_{[2]}^{(k)}\right] = \widetilde{\lambda}^{2/3}, \tag{7.9.67}$$

for $s = I, \ldots, IV$. *Since* $\boldsymbol{A}_{[2]}^{(k)}\mathbf{N} = \boldsymbol{A}_{[1]}^{(k)}\mathbf{N} = \mathbf{N}$, *it follows immediately that*

$$I_4\left[\overline{\boldsymbol{F}}^s\right] = I_4. \tag{7.9.68}$$

Using Eq. (7.9.58)*, we note that*

$$I_1\left[\overline{\boldsymbol{F}}^s\right] = I_1\left[\overline{\boldsymbol{F}}\boldsymbol{A}^{(k)}_{[2]}\right] + \frac{\sqrt{\widetilde{\lambda}}d_3\left[\overline{\boldsymbol{F}}\boldsymbol{A}^{(k)}_{[2]}\right] - I_5\left[\overline{\boldsymbol{F}}\boldsymbol{A}^{(k)}_{[2]}\right]}{d_3\left[\overline{\boldsymbol{F}}\boldsymbol{A}^{(k)}_{[2]}\right]^2}$$
$$= \widetilde{\lambda}^{1/3} + \widetilde{\lambda}^{-1/3}\left(\widetilde{\lambda}^{1/3}I_1\left[\overline{\boldsymbol{F}}\boldsymbol{A}^{(k)}_{[2]}\right] - I_5\left[\overline{\boldsymbol{F}}\boldsymbol{A}^{(k)}_{[2]}\right]\right). \tag{7.9.69}$$

Since $d_3\left[\overline{\boldsymbol{F}}\boldsymbol{A}^{(k)}_{[2]}\right]$ *must satisfy the equation*

$$d_3\left[\overline{\boldsymbol{F}}\boldsymbol{A}^{(k)}_{[2]}\right]^4 - \left(I_1\left[\overline{\boldsymbol{F}}\boldsymbol{A}^{(k)}_{[2]}\right] - I_4\left[\overline{\boldsymbol{F}}\boldsymbol{A}^{(k)}_{[2]}\right]\right)d_3\left[\overline{\boldsymbol{F}}\boldsymbol{A}^{(k)}_{[2]}\right]^2 + I_5\left[\overline{\boldsymbol{F}}\boldsymbol{A}^{(k)}_{[2]}\right] = 0, \tag{7.9.70}$$

we find that

$$I_1\left[\overline{\boldsymbol{F}}^s\right] = 2\widetilde{\lambda}^{1/3} + I_4, \tag{7.9.71}$$

for $s = I, \ldots, IV$*. From all of this, we may conclude that*

$$d_2\left[\overline{\boldsymbol{F}}^s\right] = d_3\left[\overline{\boldsymbol{F}}^s\right] = \widetilde{\lambda}^{1/6}, \tag{7.9.72}$$

which, in particular, also shows that

$$d_2\left[\overline{\boldsymbol{F}}^s\right] = \frac{\widetilde{\lambda}^{1/4}}{\sqrt{d_3\left[\overline{\boldsymbol{F}}^s\right]}} \tag{7.9.73}$$

and

$$\widehat{W}\left(\overline{\boldsymbol{F}}^s\right) = \frac{\breve{\mu}}{2}I_4\left[\overline{\boldsymbol{F}}^s\right] + \frac{\overline{\mu}}{2}\left(\left(d_2\left[\overline{\boldsymbol{F}}^s\right]\right)^2 + \left(d_3\left[\overline{\boldsymbol{F}}^s\right]\right)^2 + \frac{\widetilde{\lambda}}{\left(\left(d_2\left[\overline{\boldsymbol{F}}^s\right]d_3\left[\overline{\boldsymbol{F}}^s\right]\right)\right)^2} - 3\right)$$
$$= \frac{\breve{\mu}}{2}I_4 + \frac{3\overline{\mu}}{2}\left(\widetilde{\lambda}^{1/3} - 1\right)$$
$$= Q\widehat{W}(\overline{\boldsymbol{F}}). \tag{7.9.74}$$

The same argument used in the first part of the proof shows that $I_3\left[\overline{\boldsymbol{F}}^s\right] = 1$*,*

and Eq. (7.9.63)*, as it pertains to* $\overline{\boldsymbol{F}}\boldsymbol{A}^{(k)}_{[2]}$*, can be used to show that*

$$I_2\left[\overline{\boldsymbol{F}}^{\,s}\right] = \widetilde{\lambda}^{2/3} + \widetilde{\lambda}^{1/3} I_4 + \widetilde{\lambda}^{-1/3}. \tag{7.9.75}$$

Note that $d_2 = d_3$ *whenever* $\widehat{\theta} = \frac{\pi}{4}$*. In these cases, the same results still hold, but the analysis needed to show this must be done without the use of the identities in equations Eq.* (7.9.45)-(7.9.49)*. Instead, such quantities can be calculated directly by taking* $\widehat{\theta} = \frac{\pi}{4}$*.*

□

Chapter 8

Theoretical Aspects of Periodic Homogenization and Post-Bifurcation Analysis for Magneto-Elastic Systems

Abstract

Magneto-elastic materials have attracted significant attention in recent years due to their ability to undergo large strains upon the application of a magnetic field. While such behavior has been seen experimentally, there still lacks a complete mathematical framework capable of describing magneto-elastic systems from a theoretical point of view. In this work, we look to build towards such a mathematical theory for determining the effective response, or relaxation, of magneto-elastic composites. We provide a rigorous treatment of the preliminaries needed to do so from the perspective of the calculus of variations and homogenization. We also describe the methodology by which the effective behavior of such a composite can be estimated in the event that it undergoes an instability and provide results that will allow for such a calculation.

8.1 Introduction

A theoretical treatment of magneto-elasticity from the perspective of continuum mechanics was developed in the works of Truesdell and Toupin (1960), Tiersten (1964), and Maugin and Eringen (1972) and has since been extended by Bustamante

et al. (2008), Dorfmann and Ogden (2004), Kankanala and Triantafyllidis (2004), and Steigmann (2004). Most of these treatments are indeed concerned with the continuum scale, and are less suited for describing a "microscopic" theory of magnetism (Brown, 1966), which can account for magnetic domain formation in ferromagnetic materials. Nonetheless, a continuum description of magneto-elasticity is useful when looking to model inhomogeneous materials on a macroscopic scale. Moreover, it is sufficient for capturing possible unstable behavior due the existence of microscopic and macroscopic instabilities.

Much progress has been made in determining the stability of homogeneous magneto-elastic systems. The well known conditions ensuring stability for purely mechanical systems, namely the Legendre-Hadamard condition and the associated strong ellipticity condition, have been generalized to the magneto-elastic setting by appealing to principles of minimum potential energy (Kankanala and Triantafyllidis, 2004), or by making use of incremental formulations of the equilibrium equations (Ottènio et al., 2008; Destrade and Ogden, 2011). Much less exists in the way of results regarding stability of magneto-elastic composite materials. Certainly, the results mentioned above can be used to test stability of the homogenized energy density, but it is only recently that research has been conducted to test the interplay between micro- and macroscopic instabilities (see Bertoldi and Gei, 2011; Rudykh et al., 2014, in the context of layered electro-elastic and magneto-elastic materials); in particular, rigorous results akin to those of Geymonat et al. (1993) are lacking.

The sparsity of investigations into the stability of magneto-elastic composites coincides with only a recent advancement in obtaining estimates for the macroscopic response, or relaxation. Galipeau and Ponte Castañeda (2013); Ponte Castañeda and Galipeau (2011) proposed methods for obtaining the effective response of magnetorheological elastomers with random microstructures, while materials with periodic microstructures have been considered both in the context of electro-elasticity (Ponte Castañeda and Siboni, 2012), as well as magneto-electro-elasticity (Miehe

et al., 2015a,b). However, to our knowledge, few rigorous results like those of Müller (1987) and Braides (1985) for purely mechanical systems exist (see Pisante, 2004; Conti et al., 2018, for an example in the context of micromagnetics, and magnetic-shape-memory polymers, respectively). Moreover, we are unaware of a theory that can predict the macroscopic response of such composites after the onset of an instability.

The purpose of this work is to provide a basis for a more robust treatment of determining the macroscopic response of magneto-elastic composite materials. This requires, in part, a generalization of many of the well-known tools from the calculus of variations that have been used successfully for purely mechanical systems. Moreover, we aim to provide a methodology by which the "principal" solution, i.e. the solution before the onset of an instability, as well as the post-bifurcation behavior, of the magneto-elastic materials can be estimated. As such, the rest of this chapter will be organized as follows. In Section 8.2, we provide a rigorous extension of the generalized notions of convexity that are crucial in developing a complete variational formulation of finite magneto-elasticity. We define the notions of polyconvexity, quasiconvexity, and rank-one convexity in the magneto-elastic setting and prove one of the main results of this work:

$$\text{polyconvexity} \implies \text{quasiconvexity} \implies \text{rank-one convexity}. \tag{8.1.1}$$

This section also contains additional results that will be necessary for analyzing the stability of magneto-elastic composites. In Section 8.3, we provide a framework for computing the homogenized potential, or relaxation, of a periodic magneto-elastic composite. We then introduce the methodology by which one can estimate the relaxation in the case where the composite has undergone a macroscopic instability. This method relies on the ansatz that macroscopic instabilities are triggered by the loss of strict rank-one convexity of the principal solution, and result in the formation of domains which exist on a length scale larger than the unit cell (of the associated mi-

crostructure), but smaller than the material sample. It is here that results obtained in the previous section will be necessary for carrying out any further analysis. We mention that much of what is proven here is done so in anticipation of considering a specific physical model and applying our analysis to describe its behavior. We choose however to keep this work self contained, and an application of these results will appear in a future work.

We close the introduction by discussing the notation to be used in this chapter. The real $n-$dimensional space is denoted by $\mathbb{R}^n$, with the scalar product $\mathbf{u} \cdot \mathbf{v}$, and norm $|\mathbf{u}|^2 = \mathbf{u} \cdot \mathbf{u}$. We denote the set of $n \times n$ matrices by $\mathbb{R}^{n\times n}$, and endow it with the usual inner product $\boldsymbol{F} \cdot \boldsymbol{G} = \operatorname{tr}(\boldsymbol{F}\boldsymbol{G}^T)$, and norm $\|\boldsymbol{F}\|^2 = \boldsymbol{F} \cdot \boldsymbol{F}$. When it exists, we define the adjugate matrix of $\boldsymbol{F} \in \mathbb{R}^{n\times n}$ by $\boldsymbol{F}^* = (\det \boldsymbol{F})\boldsymbol{F}^{-T}$. We fix the standard Cartesian basis $\{\mathbf{e}_i\}$, with respect to which vectors with Cartesian components b_i or B_i are represented by bold letters $\mathbf{b}$ or $\mathbf{B}$, respectively. Second-order tensors with Cartesian components F_{ij} are represented by bold italic letters $\boldsymbol{F}$. Here i, j, k, l range from 1 to n. Given two vectors $\mathbf{a}, \mathbf{b}$, the dyadic product $\mathbf{a} \otimes \mathbf{b}$ is defined to be the second-order tensor with Cartesian components $a_i b_j$. As the primary goal of this chapter is to facilitate the description of magneto-elastic composites, we will take the primary variables of a function $W : \mathbb{R}^{n\times n} \times \mathbb{R}^n \to \overline{\mathbb{R}}$ to be $\boldsymbol{F}$ and $\mathbf{B}$, where the former represents the deformation gradient, and the latter represents the magnetic induction field (in the undeformed configuration). Standard notation from the calculus of variations will be used, as well as some basic notation regarding Sobolev spaces. We refer those unfamiliar with these concepts to Dacorogna (1989).

8.2 Generalized Notions of Convexity

The notions of *polyconvexity, quasiconvexity,* and *rank-one convexity*, as they pertain to purely mechanical situations, have been deeply investigated and are well understood. In what follows, we lay the framework for the development of a rigorous

treatment of the calculus of variations when there is functional dependence on both first and second order tensors that are independent of one another. In particular, we consider the case when $W : \mathbb{R}^{n\times N} \times \mathbb{R}^n \to \overline{\mathbb{R}}$ with $W = W(\boldsymbol{F}, \boldsymbol{B})$ where, when viewed from the perspective of magneto-elasticity, the second-order tensor $\boldsymbol{F} = \nabla \mathbf{u}$ corresponds to the deformation gradient, and the first-order tensor, i.e. the vector, $\boldsymbol{B}$ corresponds to the induction magnetic field (in the undeformed configuration). We start by defining the extended notions of convexity, and restrict ourselves to the case where $N = n$.

Definition 10:

1. A function $W : \mathbb{R}^{n\times n} \times \mathbb{R}^n \to \overline{\mathbb{R}}$ is *polyconvex* if there exists a convex function $g : \mathbb{R}^{\tau(n,n)+2n} \to \overline{\mathbb{R}}$ such that

$$W(\boldsymbol{F}, \mathbf{B}) = g(T(\boldsymbol{F}), \mathbf{B}, \boldsymbol{F}\mathbf{B}) \tag{8.2.1}$$

   for every $\boldsymbol{F} \in \mathbb{R}^{n\times n}$, $\mathbf{B} \in \mathbb{R}^n$, where $T : \mathbb{R}^{n\times n} \to \mathbb{R}^{\tau(n,n)}$ is the vector of all $s \times s$ minors of $\boldsymbol{F}$, and where

$$\tau(n, n) = \sum_{s=1}^{n} \binom{n}{s}^2. \tag{8.2.2}$$

2. A function $W : \mathbb{R}^{n\times n} \times \mathbb{R}^n \to \mathbb{R}$ is *quasiconvex* if

$$W(\boldsymbol{F}, \mathbf{B}) \leqslant \frac{1}{|D|} \int_D W(\boldsymbol{F} + \nabla \boldsymbol{\varphi}(\mathbf{x}), \mathbf{B} + \nabla \times \boldsymbol{\phi}(\mathbf{x}))d\mathbf{x} \tag{8.2.3}$$

   for every bounded domain $D \subset \mathbb{R}^n$, every $\boldsymbol{F} \in \mathbb{R}^{n\times n}$, $\mathbf{B} \in \mathbb{R}^n$ and $\boldsymbol{\varphi}, \boldsymbol{\phi} \in W_0^{1,\infty}(D; \mathbb{R}^n)$.

3. A function $f : \mathbb{R}^{n\times n} \times \mathbb{R}^n \to \overline{\mathbb{R}}$ is *rank-one convex* at $(\boldsymbol{F}, \mathbf{B})$ if

$$W(\lambda \boldsymbol{F}_1 + (1-\lambda)\boldsymbol{F}_2, \lambda \mathbf{B}_1 + (1-\lambda)\mathbf{B}_2) \leqslant \lambda W(\boldsymbol{F}_1, \mathbf{B}_1) + (1-\lambda)W(\boldsymbol{F}_2, \mathbf{B}_2) \tag{8.2.4}$$

for every $\lambda \in [0,1]$, $\boldsymbol{F}_1, \boldsymbol{F}_2 \in \mathbb{R}^{n\times n}$, $\mathbf{B}_1, \mathbf{B}_2 \in \mathbb{R}^n$, such that $\operatorname{rank}(\boldsymbol{F}_1 - \boldsymbol{F}_2) \leqslant 1$ and $(\mathbf{B}_1 - \mathbf{B}_2) \in \ker(\boldsymbol{F}_1 - \boldsymbol{F}_2)$ and where $\boldsymbol{F} = \lambda\boldsymbol{F}_1 + (1-\lambda)\boldsymbol{F}_2$, $\mathbf{B} = \lambda\mathbf{B}_1 + (1-\lambda)\mathbf{B}_2$. If W is rank-one convex at every $(\boldsymbol{F}, \mathbf{B})$, we say that W is *(globally) rank-one convex*. Moreover, replacing "$\leqslant$" with "$<$" defines *strict rank-one convexity*.

A generalization of polyconvexity was first seen in the work of Fonseca et al. (1994), but in the context of materials whose constitutive behavior was determined by the deformation gradient and a scalar chemical potential. A similar generalization was given by Rogers (1988), who used it to prove existence results similar to those of Ball (1977). The definition of polyconvexity given above is consistent with the one given by Silhavý (2018) and Ortigosa and Gil (2016b,a), who both considered electro-magneto-elastic materials. In fact Silhavý (2018) proved that the definition is optimal, in the sense that it accounts for all the possible combinations of $\boldsymbol{F}$ and $\mathbf{B}$ that satisfy a sufficient condition for a generalization of weak lower semicontinuity. In contrast, Miehe et al. (2015a) considered a less general definition of polyconvexity that makes use of only $T(\boldsymbol{F})$ and $\mathbf{B}$. When $n = 3$, f is polyconvex if there exists a convex function $g : \mathbb{R}^{25} \to \mathbb{R}$ such that

$$W(\boldsymbol{F}, \mathbf{B}) = g(\boldsymbol{F}, \boldsymbol{F}^*, \det \boldsymbol{F}, \mathbf{B}, \boldsymbol{F}\mathbf{B}), \tag{8.2.5}$$

while for $n = 2$, f is polyconvex if there exists a convex function $g : \mathbb{R}^9 \to \mathbb{R}$ such that

$$W(\boldsymbol{F}, \mathbf{B}) = g(\boldsymbol{F}, \det \boldsymbol{F}, \mathbf{B}, \boldsymbol{F}\mathbf{B}). \tag{8.2.6}$$

The generalization of quasiconvexity is rather straightforward, and has appeared in the other works (e.g., Kankanala and Triantafyllidis, 2004). Like in the purely mechanical context (Ball, 1977), the definition can be given a physical interpretation as well. Consider a homogeneous material occupying some domain D, in the absence of any body force. Then W is quasiconvex if the state of uniform strain and uniform induction magnetic field are an absolute minimizer of the total energy. In defining

rank-one convexity, the requirement that $(\boldsymbol{B}_1 - \boldsymbol{B}_2) \in \ker(\boldsymbol{F}_1 - \boldsymbol{F}_2)$ can also be understood from a physical point of view. Consider two regions $D_1, D_2 \subset D$, whose boundaries intersect along an interphase with unit normal $\mathbf{N}$. Let $\boldsymbol{F}_i, \mathbf{B}_i$ be the deformation gradient and induction magnetic field, respectively, in region i. Kinematics require that $\boldsymbol{F}_i$ satisfy $\boldsymbol{F}_1 - \boldsymbol{F}_2 = \mathbf{a} \otimes \mathbf{N}$, for some vector $\mathbf{a}$, while Gauss' Law implies that $(\mathbf{B}_1 - \mathbf{B}_2) \cdot \mathbf{N} = 0$. Therefore, we see that $(\mathbf{B}_1 - \mathbf{B}_2) \in \ker(\boldsymbol{F}_1 - \boldsymbol{F}_2)$, and hence, the requirements made in defining rank-one convexity allow for consistency in modeling physical problems.

Next, we recall the following lemma:

Lemma 1 (Lemma 5.5 Dacorogna (1989))**:**
Let $\boldsymbol{F} \in \mathbb{R}^{n\times n}$ and $T(\boldsymbol{F})$ be defined as above.

1. *For every $\boldsymbol{F}_1, \boldsymbol{F}_2 \in \mathbb{R}^{n\times n}$ with $\operatorname{rank}\{\boldsymbol{F}_1 - \boldsymbol{F}_2\} \leqslant 1$ and for every $\lambda \in [0,1]$, then*

$$T(\lambda \boldsymbol{F}_1 + (1-\lambda)\boldsymbol{F}_2) = \lambda T(\boldsymbol{F}_1) + (1-\lambda) T(\boldsymbol{F}_2). \tag{8.2.7}$$

2. *For every bounded domain $D \subset \mathbb{R}^n$, every $\boldsymbol{F} \in \mathbb{R}^{n\times n}$, $\boldsymbol{\varphi} \in W_0^{1,\infty}(D;\mathbb{R}^n)$*

$$T(\boldsymbol{F}) = \frac{1}{|D|}\int_D T(\boldsymbol{F} + \nabla \boldsymbol{\varphi}(\mathbf{x}))d\mathbf{x}. \tag{8.2.8}$$

With the lemma, we are able to prove the first major result, which is analogous to the result for purely mechanical systems.

Theorem 3:

1. *Let $W : \mathbb{R}^{n\times n} \times \mathbb{R}^n \to \mathbb{R}$, then*

$$W \text{ convex} \implies W \text{ polyconvex} \implies W \text{ quasiconvex} \implies W \text{ rank-one convex}. \tag{8.2.9}$$

2. *Let* $W : \mathbb{R}^{n\times n} \times \mathbb{R}^n \to \overline{\mathbb{R}}$, *then*

$$W \text{ polyconvex} \implies W \text{ rank-one convex.} \tag{8.2.10}$$

Proof:

1. W convex $\implies$ W polyconvex*:*

   This implication is trivial.

   W polyconvex $\implies$ W quasiconvex*:*

   By polyconvexity, there exists a convex function g *such that* $W(\boldsymbol{F}, \mathbf{B}) = g(T(\boldsymbol{F}), \mathbf{B}, \boldsymbol{F}\mathbf{B})$. *We must show that for every* $\boldsymbol{F} \in \mathbb{R}^{n\times n}$, $\mathbf{B} \in \mathbb{R}^n$, $\boldsymbol{\varphi}, \boldsymbol{\phi} \in W_0^{1,\infty}(D;\mathbb{R}^n)$, *Eq.* (8.2.3) *holds. Since* $C_0^\infty(D;\mathbb{R}^n) \subseteq W_0^{1,\infty}(D;\mathbb{R}^n)$ *is dense, it suffices to check this condition for* $\boldsymbol{\varphi}, \boldsymbol{\phi} \in C_0^\infty(D;\mathbb{R}^n)$. *By making use Jensen's inequality, we see that*

$$\begin{aligned}
&\frac{1}{|D|}\int_D W(\boldsymbol{F} + \nabla\boldsymbol{\varphi}(\mathbf{x}), \mathbf{B} + \nabla \times \boldsymbol{\phi}(\mathbf{x}))d\mathbf{x} \\
&= \frac{1}{|D|}\int_D g(T(\boldsymbol{F} + \nabla\boldsymbol{\varphi}(\mathbf{x})), \mathbf{B} + \nabla \times \boldsymbol{\phi}(\mathbf{x}), [\boldsymbol{F} + \nabla\boldsymbol{\varphi}(\mathbf{x})][\mathbf{B} + \nabla \times \boldsymbol{\phi}(\mathbf{x})])d\mathbf{x} \\
&\geqslant g\left(\frac{1}{|D|}\int_D T(\boldsymbol{F} + \nabla\boldsymbol{\varphi}(\mathbf{x}))d\mathbf{x}, \frac{1}{|D|}\int_D \mathbf{B} + \nabla \times \boldsymbol{\phi}(\mathbf{x})d\mathbf{x}, \right. \\
&\qquad\qquad \left. \frac{1}{|D|}\int_D [\boldsymbol{F} + \nabla\boldsymbol{\varphi}(\mathbf{x})][\mathbf{B} + \nabla \times \boldsymbol{\phi}(\mathbf{x})]d\mathbf{x}\right).
\end{aligned} \tag{8.2.11}$$

   Now, from (8.2.8), *we see that*

$$\frac{1}{|D|}\int_D T(\boldsymbol{F} + \nabla\boldsymbol{\varphi}(\mathbf{x}))d\mathbf{x} = T(\boldsymbol{F}). \tag{8.2.12}$$

   On the other hand, since $\boldsymbol{\phi} = \mathbf{0}$ *on* ∂D, *the integral of* $\nabla \times \boldsymbol{\phi}$ *vanishes, due to*

the divergence theorem. Finally, we note that

$$\begin{aligned}
&\frac{1}{|D|}\int_D [\boldsymbol{F}+\nabla\boldsymbol{\varphi}(\mathbf{x})][\mathbf{B}+\nabla\times\boldsymbol{\phi}(\mathbf{x})]d\mathbf{x}\\
&=\frac{1}{|D|}\int_D \left(\boldsymbol{F}\mathbf{B}+[\nabla\boldsymbol{\varphi}(\mathbf{x})]\mathbf{B}+\boldsymbol{F}[\nabla\times\boldsymbol{\phi}(\mathbf{x})]+[\nabla\boldsymbol{\varphi}(\mathbf{x})][\nabla\times\boldsymbol{\phi}(\mathbf{x})]\right)d\mathbf{x}\\
&=\boldsymbol{F}\mathbf{B}, \qquad (8.2.13)
\end{aligned}$$

having made use of the divergence theorem, the fact that $\boldsymbol{\phi}=\boldsymbol{\varphi}=\mathbf{0}$ *on the boundary, as well as the fact that* $\nabla\cdot[\nabla\times\boldsymbol{\phi}(\mathbf{x})]=\mathbf{0}$*. Therefore, we are left with*

$$\begin{aligned}
&\frac{1}{|D|}\int_D W(\boldsymbol{F}+\nabla\boldsymbol{\varphi}(\mathbf{x}),\mathbf{B}+\nabla\times\boldsymbol{\phi}(\mathbf{x}),[\boldsymbol{F}+\nabla\boldsymbol{\varphi}(\mathbf{x})][\mathbf{B}+\nabla\times\boldsymbol{\phi}(\mathbf{x})])d\mathbf{x}\\
&\geqslant g(T(\boldsymbol{F}),\mathbf{B},\boldsymbol{F}\mathbf{B})\\
&=W(\boldsymbol{F},\mathbf{B}), \qquad (8.2.14)
\end{aligned}$$

from which we can conclude that W *is quasiconvex.*

f quasiconvex $\implies$ f rank-one convex:

Let $\lambda\in[0,1]$, $\boldsymbol{F}_1,\boldsymbol{F}_2\in\mathbb{R}^{n\times n}$, $\mathbf{B}_1,\mathbf{B}_2\in\mathbb{R}^n$, *such that* $\operatorname{rank}(\boldsymbol{F}_1-\boldsymbol{F}_2)\leqslant 1$ *and* $(\mathbf{B}_1-\mathbf{B}_2)\in\ker(\boldsymbol{F}_1-\boldsymbol{F}_2)$*. For any bounded set* D*, fix* $\epsilon>0$*. By making use of the same arguments in Lemmas 3.10 and 3.11 of Chapter 3 (Dacorogna, 1989), as well as the approximation lemmas given by Dacorogna and Fonseca (2002), we can construct functions* $\boldsymbol{\varphi},\boldsymbol{\phi}\in W_0^{1,\infty}(D;\mathbb{R}^n)$*, for which that there exist* $D_1,D_2\subset D$ *with* $D_1\cap D_2=\varnothing$*, and*

$$
\begin{aligned}
&||D_1| - \lambda|D|| \leqslant \epsilon, \quad ||D_2| - (1-\lambda)|D|| \leqslant \epsilon, \\
&\nabla\boldsymbol{\varphi} = \begin{cases} (1-\lambda)(\boldsymbol{F}_1 - \boldsymbol{F}_2) & \text{for } \mathbf{x} \in D_1, \\ -\lambda(\boldsymbol{F}_1 - \boldsymbol{F}_2) & \text{for } \mathbf{x} \in D_2, \end{cases} \\
&\nabla \times \boldsymbol{\phi} = \begin{cases} (1-\lambda)(\mathbf{B}_1 - \mathbf{B}_2) & \text{for } \mathbf{x} \in D_1, \\ -\lambda(\mathbf{B}_1 - \mathbf{B}_2) & \text{for } \mathbf{x} \in D_2, \end{cases} \\
&\|\nabla\boldsymbol{\varphi}\|_\infty \leqslant K, \quad \|\nabla \times \boldsymbol{\phi}\|_\infty \leqslant L,
\end{aligned}
\tag{8.2.15}
$$

where K depends only on $\boldsymbol{F}_1$ and $\boldsymbol{F}_2$, and where L depends only on $\mathbf{B}_1$ and $\mathbf{B}_2$. By quasiconvexity, we know that for this particular choice of $\boldsymbol{\varphi}$ and $\boldsymbol{\phi}$, that

$$
\begin{aligned}
&W(\lambda\boldsymbol{F}_1 + (1-\lambda)\boldsymbol{F}_2,\, \lambda\mathbf{B}_1 + (1-\lambda)\mathbf{B}_2) \leqslant \\
&\qquad \frac{1}{|D|}\int_D W(\lambda\boldsymbol{F}_1 + (1-\lambda)\boldsymbol{F}_2 + \nabla\boldsymbol{\varphi}(\mathbf{x}), \lambda\mathbf{B}_1 + (1-\lambda)\mathbf{B}_2 + \nabla \times \boldsymbol{\phi}(\mathbf{x}))d\mathbf{x}.
\end{aligned}
\tag{8.2.16}
$$

On the other hand, we note that

$$
\lambda\boldsymbol{F}_1 + (1-\lambda)\boldsymbol{F}_2 + \nabla\boldsymbol{\varphi}(\mathbf{x}) = \begin{cases} \boldsymbol{F}_1 & \text{for } \mathbf{x} \in D_1, \\ \boldsymbol{F}_2 & \text{for } \mathbf{x} \in D_2, \end{cases}
\tag{8.2.17}
$$

and

$$
\mathbf{B}_1 + (1-\lambda)\mathbf{B}_2 + \nabla \times \boldsymbol{\phi}(\mathbf{x}) = \begin{cases} \mathbf{B}_1 & \text{for } \mathbf{x} \in D_1, \\ \mathbf{B}_2 & \text{for } \mathbf{x} \in D_2. \end{cases}
\tag{8.2.18}
$$

Therefore,

$$\begin{aligned}
&\frac{1}{|D|}\int_D W(\lambda \boldsymbol{F}_1 + (1-\lambda)\boldsymbol{F}_2 + \nabla\boldsymbol{\varphi}(\mathbf{x}), \lambda \mathbf{B}_1 + (1-\lambda)\mathbf{B}_2 + \nabla \times \boldsymbol{\phi}(\mathbf{x}))d\mathbf{x} \\
&\quad = \frac{1}{|D|}\int_{D_1} W(\boldsymbol{F}_1, \mathbf{B}_1)d\mathbf{x} + \frac{1}{|D|}\int_{D_2} W(\boldsymbol{F}_2, \mathbf{B}_2)d\mathbf{x} \\
&\quad + \frac{1}{|D|}\int_{D-(D_1\cup D_2)} W(\lambda \boldsymbol{F}_1 + (1-\lambda)\boldsymbol{F}_2 + \nabla\boldsymbol{\varphi}(\mathbf{x}), \lambda \mathbf{B}_1 + (1-\lambda)\mathbf{B}_2 + \nabla \times \boldsymbol{\phi}(\mathbf{x}))d\mathbf{x} \\
&\quad = \frac{|D_1|}{|D|}W(\boldsymbol{F}_1, \mathbf{B}_1) + \frac{|D_2|}{|D|}W(\boldsymbol{F}_2, \mathbf{B}_2) + I. \qquad (8.2.19)
\end{aligned}$$

Now, by (8.2.15)*, we see that*

$$\frac{|D_1|}{|D|}W(\boldsymbol{F}_1, \mathbf{B}_1) + \frac{|D_2|}{|D|}W(\boldsymbol{F}_2, \mathbf{B}_2) \leqslant \lambda W(\boldsymbol{F}_1, \mathbf{B}_1) + (1-\lambda)W(\boldsymbol{F}_2, \mathbf{B}_2) + \frac{2\epsilon}{|D|}. \qquad (8.2.20)$$

On the other hand, since $\nabla\boldsymbol{\varphi}$ *and* $\nabla \times \boldsymbol{\phi}$ *are essentially bounded, and* W *only takes finite values, we see that*

$$|I| \leqslant C\frac{|D - (D_1 \cup D_2)|}{|D|} \leqslant \frac{2\epsilon C}{|D|}, \qquad (8.2.21)$$

where C *is some constant independent of* $|D|$*. Thus, since* ϵ *was chosen arbitrarily, we can conclude, from* (8.2.16)-(8.2.21) *that*

$$W(\lambda \boldsymbol{F}_1 + (1-\lambda)\boldsymbol{F}_2, \lambda \mathbf{B}_1 + (1-\lambda)\mathbf{B}_2) \leqslant \lambda W(\boldsymbol{F}_1, \mathbf{B}_1) + (1-\lambda)W(\boldsymbol{F}_2, \mathbf{B}_2). \qquad (8.2.22)$$

2. *Using* (8.2.7)*, and noting that for every* $\lambda \in [0,1]$*,* $\boldsymbol{F}_1, \boldsymbol{F}_2 \in \mathbb{R}^{n\times n}$*,* $\mathbf{B}_1, \mathbf{B}_2 \in \mathbb{R}^n$*, such that* $\operatorname{rank}(\boldsymbol{F}_1 - \boldsymbol{F}_2) \leqslant 1$ *and* $(\mathbf{B}_1 - \mathbf{B}_2) \in \ker(\boldsymbol{F}_1 - \boldsymbol{F}_2)$*, we have*

$$\begin{aligned}
[\lambda \boldsymbol{F}_1 + (1-\lambda)\boldsymbol{F}_2][\lambda \mathbf{B}_1 + (1-\lambda)\mathbf{B}_2] =& \lambda \boldsymbol{F}_1\mathbf{B}_1 + (1-\lambda)\boldsymbol{F}_2\mathbf{B}_2 \\
&- \lambda(1-\lambda)(\boldsymbol{F}_1 - \boldsymbol{F}_2)(\mathbf{B}_1 - \mathbf{B}_2) \\
=& \lambda \boldsymbol{F}_1\mathbf{B}_1 + (1-\lambda)\boldsymbol{F}_2\mathbf{B}_2, \qquad (8.2.23)
\end{aligned}$$

which, from the polyconvexity of f, implies that

$$
\begin{aligned}
&W(\lambda \boldsymbol{F}_1 + (1-\lambda)\boldsymbol{F}_2, \lambda \mathbf{B}_1 + (1-\lambda)\mathbf{B}_2) \\
&= g(T(\lambda \boldsymbol{F}_1 + (1-\lambda)\boldsymbol{F}_2), \lambda \mathbf{B}_1 + (1-\lambda)\mathbf{B}_2, [\lambda \boldsymbol{F}_1 + (1-\lambda)\boldsymbol{F}_2][\lambda \mathbf{B}_1 + (1-\lambda)\mathbf{B}_2]) \\
&= g(\lambda T(\boldsymbol{F}_1) + (1-\lambda)T(\boldsymbol{F}_2), \lambda \mathbf{B}_1 + (1-\lambda)\mathbf{B}_2, \lambda \boldsymbol{F}_1\mathbf{B}_1 + (1-\lambda)\boldsymbol{F}_2\mathbf{B}_2) \\
&\leqslant \lambda g(T(\boldsymbol{F}_1), \mathbf{B}_1, \boldsymbol{F}_1\mathbf{B}_1) + (1-\lambda) g(T(\boldsymbol{F}_2), \mathbf{B}_2, \boldsymbol{F}_2\mathbf{B}_2) \\
&= \lambda W(\boldsymbol{F}_1, \mathbf{B}_1) + (1-\lambda) W(\boldsymbol{F}_2, \mathbf{B}_2). \qquad (8.2.24)
\end{aligned}
$$

□

Given Definition 10, we now generalize the notion of the various convex envelopes.

Definition 11:
Let $W : \mathbb{R}^{n\times n} \times \mathbb{R}^n \to \mathbb{R}$. Then

$$CW = \sup\{g \,:\, g \leqslant W,\, g \text{ is convex}\}, \qquad (8.2.25)$$

$$PW = \sup\{g \,:\, g \leqslant W,\, g \text{ is polyconvex}\}, \qquad (8.2.26)$$

$$QW = \sup\{g \,:\, g \leqslant W,\, g \text{ is quasiconvex}\}, \qquad (8.2.27)$$

$$RW = \sup\{g \,:\, g \leqslant W,\, g \text{ is rank one convex}\}, \qquad (8.2.28)$$

are the convex, polyconvex, quasiconvex, and rank-one convex envelope respectively (or the *convexification*, *polyconvexification*, etc., respectively) of W.

We comment that the definition of PW and RW hold when W takes values in the extended real numbers. Also, in light of Theorem 3, we have the following result.

Proposition 13:
Let $W : \mathbb{R}^{n\times n} \times \mathbb{R}^n \to \mathbb{R}$. Then

$$CW \leqslant PW \leqslant QW \leqslant RW \leqslant W. \qquad (8.2.29)$$

Proof:

The result follows trivially as a corollary to Theorem 3 and Definition 11.

□

8.2.1 Further Properties of Rank-One Convex Functions

As will be discussed in Section 8.3, the method by which we plan to calculate the post-bifurcation behavior of magneto-elastic composites relies on calculating the rank-one convex envelope of the principal solution of the homogenized energy. Therefore, we present results that will facilitate this calculation. We start with by introducing notation related to the "rank-one compatibility" of a set of second- and first-order tensors $(\boldsymbol{F}_i, \mathbf{B}_i)$, and recall that for $I \in \mathbb{N}$

$$\Lambda_I = \{\boldsymbol{\lambda} = (\lambda_1, \dots, \lambda_I) \,:\, \lambda_i > 0, \sum_{i=1}^{I} \lambda_i = 1\}. \tag{8.2.30}$$

Definition 12:

We say $(\lambda_i, \boldsymbol{F}_i, \mathbf{B}_i)_{1 \leqslant i \leqslant I}$ satisfy (H_I) if

1. $I = 2$, $\mathrm{rank}\{\boldsymbol{F}_1 - \boldsymbol{F}_2\} \leqslant 1$ and $(\mathbf{B}_1 - \mathbf{B}_2) \in \ker\{\boldsymbol{F}_1 - \boldsymbol{F}_2\}$

2. $I > 2$, then, up to permutation, $\mathrm{rank}\{\boldsymbol{F}_1 - \boldsymbol{F}_2\} \leqslant 1$ and $(\mathbf{B}_1 - \mathbf{B}_2) \in \ker\{\boldsymbol{F}_1 - \boldsymbol{F}_2\}$, and upon defining, for $2 \leqslant i \leqslant I$

$$\begin{cases} \mu_1 = \lambda_1 + \lambda_2, & \boldsymbol{G}_1 = \frac{\lambda_1}{\lambda_1+\lambda_2}\boldsymbol{F}_1 + \frac{\lambda_2}{\lambda_1+\lambda_2}\boldsymbol{F}_2, & \mathbf{C}_1 = \frac{\lambda_1}{\lambda_1+\lambda_2}\mathbf{B}_1 + \frac{\lambda_2}{\lambda_1+\lambda_2}\mathbf{B}_2, \\ \mu_i = \lambda_{i+1}, & \boldsymbol{G}_i = \boldsymbol{F}_{i+1}, & \mathbf{C}_i = \mathbf{B}_{i+1}, \end{cases}$$

$(\mu_i, \boldsymbol{G}_i, \mathbf{C}_i)_{1 \leqslant i \leqslant I-1}$ satisfy (H_{I-1}).

With this definition, we have the following:

Proposition 14:

Let $W : \mathbb{R}^{n \times n} \times \mathbb{R}^n \to \overline{\mathbb{R}}$. The following are equivalent.

1. *W is rank-one convex.*

2. *For every $(\lambda_i, \boldsymbol{F}_i, \mathbf{B}_i)_{1\leqslant i\leqslant I}$ which satisfy* (H_I)

$$W\left(\sum_{i=1}^{I}\lambda_i\boldsymbol{F}_i, \sum_{i=1}^{I}\lambda_i\mathbf{B}_i\right) \leqslant \sum_{i=1}^{I}\lambda_i W(\boldsymbol{F}_i, \mathbf{B}_i). \tag{8.2.31}$$

Proof:

2. $\implies$ 1. : *By taking $I = 2$,* (8.2.31) *is precisely the definition of rank-one convexity.*

1. $\implies$ 2. : *We proceed via induction on I. Rank-one convexity of W implies* (8.2.62) *holds for $I = 2$. Thus, we assume that the result holds for $I - 1$. Suppose $(\lambda_i, \boldsymbol{F}_i, \mathbf{B}_i)_{1\leqslant i\leqslant I}$ satisfy* (H_I)*. Then, by defintion*

$$\left(\lambda_1 + \lambda_2,\ \frac{\lambda_1\boldsymbol{F}_1 + \lambda_2\boldsymbol{F}_2}{\lambda_1 + \lambda_2},\ \frac{\lambda_1\mathbf{B}_1 + \lambda_2\mathbf{B}_2}{\lambda_1 + \lambda_2}\right)\bigcup(\lambda_i, \boldsymbol{F}_i, \mathbf{B}_i)_{3\leqslant i\leqslant I} \tag{8.2.32}$$

satisfy (H_{I-1})*, and so by the induction hypothesis*

$$\begin{aligned} W\left(\sum_{i=1}^{I}\lambda_i\boldsymbol{F}_i, \sum_{i=1}^{I}\lambda_i\mathbf{B}_i\right) &= W\left(\frac{\lambda_1\boldsymbol{F}_1 + \lambda_2\boldsymbol{F}_2}{\lambda_1 + \lambda_2} + \sum_{i=3}^{I}\lambda_i\boldsymbol{F}_i, \frac{\lambda_1\mathbf{B}_1 + \lambda_2\mathbf{B}_2}{\lambda_1 + \lambda_2} + \sum_{i=3}^{I}\lambda_i\mathbf{B}_i\right) \\ &\leqslant (\lambda_1 + \lambda_2)W\left(\frac{\lambda_1\boldsymbol{F}_1 + \lambda_2\boldsymbol{F}_2}{\lambda_1 + \lambda_2}, \frac{\lambda_1\mathbf{B}_1 + \lambda_2\mathbf{B}_2}{\lambda_1 + \lambda_2}\right) + \sum_{i=3}^{I}\lambda_i W(\boldsymbol{F}_i, \mathbf{B}_i) \\ &\leqslant \sum_{i=1}^{I}\lambda_i W(\boldsymbol{F}_i, \mathbf{B}_i), \end{aligned} \tag{8.2.33}$$

where we used the fact that f is rank-one convex to go from the the penultimate to the last line.

□

The next result gives two representation formulae for the pointwise calculation of the rank-one convex envelope. The first relates to Proposition 14, while the second is a generalization of the well known Kohn-Strang lamination formula (Kohn and Strang, 1986).

Theorem 4:

Let $W : \mathbb{R}^{n\times n} \times \mathbb{R}^n \to \overline{\mathbb{R}}$. *Let* $g : \mathbb{R}^{n\times n} \times \mathbb{R}^n \to \overline{\mathbb{R}}$ *be rank-one convex such that*

$$W(\boldsymbol{F}, \mathbf{B}) \geqslant g(\boldsymbol{F}, \mathbf{B}) \;\; \forall \boldsymbol{F} \in \mathbb{R}^{n\times n},\, \mathbf{B} \in \mathbb{R}^n. \tag{8.2.34}$$

Part 1:

$$RW(\boldsymbol{F}, \mathbf{B}) = \inf \left\{ \begin{array}{c} \sum_{i=1}^I \lambda_i W(\boldsymbol{F}_i, \mathbf{B}_i) \,:\, \boldsymbol{\lambda} \in \Lambda_I,\, \boldsymbol{F} = \sum_{i=1}^I \lambda_i \boldsymbol{F}_i,\; \mathbf{B} = \sum_{i=1}^I \lambda_i \mathbf{B}_i \\ (\lambda_i, \boldsymbol{F}_i, \mathbf{B}_i)_{1\leqslant i\leqslant I} \text{ satisfy } (\mathrm{H}_I) \end{array} \right\}. \tag{8.2.35}$$

Part 2: *Let* $R_0 W = W$, *and for every* $k \geqslant 0$, *define*

$$R_{k+1}W(\boldsymbol{F}, \mathbf{B}) = \inf \left\{ \begin{array}{c} \lambda R_k W(\boldsymbol{F}_1, \mathbf{B}_1) + (1-\lambda) R_k W(\boldsymbol{F}_2, \mathbf{B}_2) : \\ \boldsymbol{F} = \lambda \boldsymbol{F}_1 + (1-\lambda)\boldsymbol{F}_2,\, \mathbf{B} = \lambda \mathbf{B}_1 + (1-\lambda)\mathbf{B}_2 \\ \operatorname{rank}\{\boldsymbol{F}_1 - \boldsymbol{F}_2\} \leqslant 1,\, (\mathbf{B}_1 - \mathbf{B}_2) \in \ker\{\boldsymbol{F}_1 - \boldsymbol{F}_2\} \end{array} \right\}. \tag{8.2.36}$$

Then

$$RW(\boldsymbol{F}, \mathbf{B}) = \lim_{k\to\infty} R_k W(\boldsymbol{F}, \mathbf{B}) = \inf_k R_k W(\boldsymbol{F}, \mathbf{B}). \tag{8.2.37}$$

Before proceeding, we'll require the following lemma:

Lemma 2:

Suppose that for $\boldsymbol{\lambda} \in \Lambda_I$, $\boldsymbol{\mu} \in \Lambda_J$, $(\lambda_i, \boldsymbol{F}_i, \mathbf{B}_i)_{1\leqslant i\leqslant I}$ *satisfy* (H_I) *and* $(\mu_j, \boldsymbol{G}_j, \mathbf{C}_j)_{1\leqslant j\leqslant J}$ *satsify* (H_J). *Let* $\boldsymbol{F} = \sum_{i=1}^I \lambda_i \boldsymbol{F}_i,\; \mathbf{B} = \sum_{i=1}^I \lambda_i \mathbf{B}_i$, $\boldsymbol{G} = \sum_{j=1}^J \mu_j \boldsymbol{G}_j,\; \mathbf{C} = \sum_{j=1}^J \mu_j \mathbf{C}_j$, *and suppose that* $\operatorname{rank}\{\boldsymbol{F} - \boldsymbol{G}\} \leqslant 1$, $(\mathbf{B} - \mathbf{C}) \in \ker\{\boldsymbol{F} - \boldsymbol{G}\}$. *Then for any* $0 < t < 1$

$$((t\lambda_i, \boldsymbol{F}_i, \mathbf{B}_i), ((1-t)\mu_j, \boldsymbol{G}_j, \mathbf{C}_j))_{1\leqslant i\leqslant I,\, 1\leqslant j\leqslant J} \text{ satisfy } (H_{I+J}). \tag{8.2.38}$$

Proof:

We proceed via induction on $I + J$, *and note that the proof follows closely that for the result when* $\mathbf{B}_i,\, \mathbf{C}_j = \mathbf{0}$. *The case of* $I + J = 2$ *is trivial, since this implies that* $I = J = 1$, *whereby Eq.* (8.2.38) *is equivalent to the hypotheses of the lemma.*

Therefore, we assume that the result holds for all $n \geqslant I + J - 1$. *Now for* $n = I + J$, *we assume, without loss of generality, that* $I \geqslant 2$. *Then,*

$$\operatorname{rank}(\boldsymbol{F}_1 - \boldsymbol{F}_2) \leqslant 1, \quad \textit{and} \quad (\mathbf{B}_1 - \mathbf{B}_2) \in \ker\{\boldsymbol{F}_1 - \boldsymbol{F}_2\} \tag{8.2.39}$$

and upon letting

$$\begin{cases} \nu_1 = \lambda_1 + \lambda_2, & \boldsymbol{H}_1 = \frac{\lambda_1 \boldsymbol{F}_1 + \lambda_2 \boldsymbol{F}_2}{\lambda_1 + \lambda_2}, & \mathbf{D}_1 = \frac{\lambda_1 \mathbf{B}_1 + \lambda_2 \mathbf{B}_2}{\lambda_1 + \lambda_2}, \\ \nu_i = \lambda_{i+1}, & \boldsymbol{H}_i = \boldsymbol{A}_{i+1}, & \mathbf{D}_i = \mathbf{B}_{i+1}, \end{cases}$$

for $2 \leqslant i \leqslant I - 1$, *it follows that* $(\nu_i, \boldsymbol{H}_i, \mathbf{D}_i)_{1 \leqslant i \leqslant I-1}$ *satisfy* (H_{I-1}). *Moreover, taking*

$$\boldsymbol{H} = \sum_{i=1}^{I-1} \nu_i \boldsymbol{H}_i = \boldsymbol{F}, \quad \textit{and} \quad \mathbf{D} = \sum_{i=1}^{I-1} \nu_i \mathbf{D}_i = \mathbf{B}, \tag{8.2.40}$$

we see that $\operatorname{rank}\{\boldsymbol{G} - \boldsymbol{H}\} \leqslant 1$ *and* $(\mathbf{C} - \mathbf{D}) \in \ker\{\boldsymbol{G} - \boldsymbol{H}\}$, *so that by the induction hypothesis,*

$$((t\nu_i, \boldsymbol{G}_i, \mathbf{C}_i), ((1-t)\mu_j, \boldsymbol{H}_j, \mathbf{D}_j))_{1 \leqslant i \leqslant I-1,\, 1 \leqslant j \leqslant J} \ \textit{satisfy} \ (H_{I+J-1}). \tag{8.2.41}$$

Combining this with the Eq. (8.2.39) *yields the desired result.* □

Proof (Theorem 4)**:**

Part 1: *Let*

$$R'W(\boldsymbol{F}, \mathbf{B}) = \inf \left\{ \begin{array}{c} \sum_{i=1}^{I} \lambda_i W(\boldsymbol{F}_i, \mathbf{B}_i) \ : \ \boldsymbol{\lambda} \in \Lambda_I, \ \boldsymbol{F} = \sum_{i=1}^{I} \lambda_i \boldsymbol{F}_i, \ \mathbf{B} = \sum_{i=1}^{I} \lambda_i \mathbf{B}_i \\ (\lambda_i, \boldsymbol{F}_i, \mathbf{B}_i)_{1 \leqslant i \leqslant I} \ \textit{satisfy} \ (\mathrm{H}_I) \end{array} \right\}. \tag{8.2.42}$$

We aim to show that $R'W = RW$, *with* RW *defined by Eq.* (8.2.28) *as the supremum over all rank-one convex functions less than* W. *Since* $g \leqslant W$ *is rank-one convex, we can make use of Proposition 14 to show for any* $\boldsymbol{F} = \sum_{i=1}^{I} \lambda_i \boldsymbol{F}_i$, $\mathbf{B} =$

$\sum_{i=1}^{I} \lambda_i \mathbf{B}_i$, $(\lambda_i, \boldsymbol{F}_i, \mathbf{B}_i)_{1 \leqslant i \leqslant I}$ *satisfying* (H_I),

$$g(\boldsymbol{F}, \mathbf{B}) = g\left(\sum_{i=1}^{I} \lambda_i \boldsymbol{F}_i, \sum_{i=1}^{I} \lambda_i \mathbf{B}_i\right) \leqslant \sum_{i=1}^{I} \lambda_i g(\boldsymbol{F}_i, \mathbf{B}_i) \leqslant \sum_{i=1}^{I} \lambda_i W(\boldsymbol{F}_i, \mathbf{B}_i). \tag{8.2.43}$$

Hence, $g(\boldsymbol{F}, \mathbf{B}) \leqslant R'W(\boldsymbol{F}, \mathbf{B})$ *which implies that the infimum on the right hand side of Eq.* (8.2.42) *will be bounded away from* $-\infty$.

Next, we look to show that $R'W$ *is rank-one convex. Now, let* $\boldsymbol{F}, \boldsymbol{G}, \mathbf{B}$ *and* $\mathbf{C}$ *be such that* $\operatorname{rank}\{\boldsymbol{F} - \boldsymbol{G}\} \leqslant 1$, $(\mathbf{B} - \mathbf{C}) \in \ker\{\boldsymbol{F} - \boldsymbol{G}\}$. *Then, for every* $\epsilon > 0$, *there exists and* I, J, $(\lambda_i, \boldsymbol{F}_i, \mathbf{B}_i)_{1 \leqslant i \leqslant I}$ *which satisfy* (H_I), $(\mu_j, \boldsymbol{G}_j, \mathbf{C}_j)_{1 \leqslant j \leqslant J}$ *which satisfy* (H_J), *with* $\boldsymbol{F} = \sum_{i=1}^{I} \lambda_i \boldsymbol{F}_i$, $\mathbf{B} = \sum_{i=1}^{I} \lambda_i \mathbf{B}_i$, $\boldsymbol{G} = \sum_{j=1}^{J} \mu_j \boldsymbol{G}_j$, $\mathbf{C} = \sum_{j=1}^{J} \mu_j \mathbf{C}_j$, *so that*

$$\begin{aligned} &\sum_{i=1}^{I} \lambda_i W(\boldsymbol{F}_i, \mathbf{B}_i) \leqslant R'W(\boldsymbol{F}, \mathbf{B}) + \epsilon, \\ &\sum_{j=1}^{I} \mu_j W(\boldsymbol{G}_j, \mathbf{C}_j) \leqslant R'W(\boldsymbol{G}, \mathbf{C}) + \epsilon. \end{aligned} \tag{8.2.44}$$

$$\tag{8.2.45}$$

Making use of Lemma 2, we find that

$$\begin{aligned} R'W(t\boldsymbol{F} + (1-t)\boldsymbol{G}, t\mathbf{B} + (1-t)\mathbf{C}) &\leqslant \sum_{i=1}^{I} t\lambda_i W(\boldsymbol{F}_i, \mathbf{B}_i) + \sum_{j=1}^{I} (1-t)\mu_j W(\boldsymbol{G}_j, \mathbf{C}_j) \\ &\leqslant tR'W(\boldsymbol{F}, \mathbf{B}) + (1-t)R'W(\boldsymbol{G}, \mathbf{C}) + \epsilon. \end{aligned} \tag{8.2.46}$$

Since ϵ *is arbitrary, we can conclude that* $R'f$ *is rank-one convex.*

Now, since $R'W \leqslant W$ *is rank-one convex, by definition,* $R'W \leqslant RW$. *To show the reverse inequality, fix* $\boldsymbol{F}$ *and* $\mathbf{B}$ *and let* $\epsilon > 0$. *Then, we can find* $(\lambda_i, \boldsymbol{F}_i, \mathbf{B}_i)_{1 \leqslant i \leqslant I}$

satisfying (H_I) *with* $\boldsymbol{F} = \sum_{i=1}^{I} \lambda_i \boldsymbol{F}_i,\ \mathbf{B} = \sum_{i=1}^{I} \lambda_i \mathbf{B}_i$ *such that*

$$\sum_{i=1}^{I} \lambda_i W(\boldsymbol{F}_i, \mathbf{B}_i) \leqslant R'W(\boldsymbol{F}, \mathbf{B}) + \epsilon. \tag{8.2.47}$$

Therefore, the rank-one convexity of $RW \leqslant W$ *implies that*

$$\begin{aligned} RW(\boldsymbol{F}, \mathbf{B}) &\leqslant \sum_{i=1}^{I} \lambda_i RW(\boldsymbol{F}_i, \mathbf{B}_i) \\ &\leqslant \sum_{i=1}^{I} \lambda_i W(\boldsymbol{F}_i, \mathbf{B}_i) \\ &\leqslant R'W(\boldsymbol{F}, \mathbf{B}) + \epsilon. \end{aligned} \tag{8.2.48}$$

Since ϵ *is arbitrary, we can conclude that* $RW \leqslant R'W$*, and therefore the two must be equal.*

Part 2:

By making the trivial choice of $\boldsymbol{F}_1 = \boldsymbol{F}_2 = \boldsymbol{F}, \mathbf{B}_1 = \mathbf{B}_2 = \mathbf{B}$*, we see that* $R_1 W(\boldsymbol{F}, \mathbf{B}) \leqslant W(\boldsymbol{F}, \mathbf{B})$*. In a similar fashion, we find that in fact*

$$R_{k+1} W(\boldsymbol{F}, \mathbf{B}) \leqslant R_k W(\boldsymbol{F}, \mathbf{B}) \quad \forall\, k \geqslant 1. \tag{8.2.49}$$

We define

$$R''W(\boldsymbol{F}, \mathbf{B}) \equiv \lim_{k \to \infty} R_k W(\boldsymbol{F}, \mathbf{B}) = \inf_k R_k W(\boldsymbol{F}, \mathbf{B}), \tag{8.2.50}$$

and as above, look to show that $R''W = RW$*. It is clear that* $g \leqslant R_{k+1} W$*, and therefore, we can conclude that*

$$-\infty < R''W(\boldsymbol{F}, \mathbf{B}) \tag{8.2.51}$$

In order to prove the result, we will first show that $RW \leqslant R''W$*, and then show* $R''W$ *is rank-one convex. It will then follow from the definition in* (8.2.28) *that*

$R''W \leqslant RW$, and hence the two must be equal.

To that end, suppose that some arbitrary function h is rank-one convex. It is always the case that $R_1 h \leqslant h$. On the other hand, for any $\epsilon > 0$, there exists $\lambda, \boldsymbol{F}_1, \boldsymbol{F}_2, \mathbf{B}_1$ and $\mathbf{B}_2$ such that $\mathrm{rank}\{\boldsymbol{F}_1 - \boldsymbol{F}_2\} \leqslant 1$, $(\mathbf{B}_1 - \mathbf{B}_2) \in \ker\{\boldsymbol{F}_1 - \boldsymbol{F}_2\}$, *and,*

$$\begin{aligned} & h(\lambda \boldsymbol{F}_1 + (1-\lambda)\boldsymbol{F}_2, \lambda \mathbf{B}_1 + (1-\lambda)\mathbf{B}_2) \\ & \leqslant \lambda h(\boldsymbol{F}_1, \mathbf{B}_1) + (1-\lambda) h(\boldsymbol{F}_2, \mathbf{B}_2) \\ & \leqslant R_1 h(\lambda \boldsymbol{F}_1 + (1-\lambda)\boldsymbol{F}_2, \lambda \mathbf{B}_1 + (1-\lambda)\mathbf{B}_2) + \epsilon, \end{aligned} \tag{8.2.52}$$

having used the rank-one convexity of h. Since ϵ is arbitrary, it follows that $h = R_1 h$. This proof can be iterated, mutatis mutandis, *to show that if h is rank-one convex, $h = R_k h$ for every k, and hence that $h = R'' h$. Upon replacing h with RW, we find that*

$$RW = R''(RW) \leqslant R''W. \tag{8.2.53}$$

It now remains to show that $R''W$ is rank-one convex. To that end, for any $\boldsymbol{F}_1, \boldsymbol{F}_2, \mathbf{B}_1, \mathbf{B}_2$ such that $\mathrm{rank}\{\boldsymbol{F}_1 - \boldsymbol{F}_2\} \leqslant 1$, $(\mathbf{B}_1 - \mathbf{B}_2) \in \ker\{\boldsymbol{F}_1 - \boldsymbol{F}_2\}$, *and for any $\epsilon > 0$, there exists an I and J such that*

$$R''W(\boldsymbol{F}_1, \mathbf{B}_1) \geqslant -\epsilon + R_i W(\boldsymbol{F}_1, \mathbf{B}_1), \tag{8.2.54}$$

$$R''W(\boldsymbol{F}_2, \mathbf{B}_2) \geqslant -\epsilon + R_j W(\boldsymbol{F}_2, \mathbf{B}_2), \tag{8.2.55}$$

for every $i > I$, $j > J$. We assume, without loss of generality, that $i > j$, whereby from Eq. (8.2.49), *$R_i W(\boldsymbol{F}_2, \mathbf{B}_2) \leqslant R_j W(\boldsymbol{F}_2, \mathbf{B}_2)$. Combining this with Eqs.* (8.2.54)

and (8.2.55)*, we see that for any* $0 \leqslant \lambda \leqslant 1$

$$\begin{aligned}
&\lambda R''W(\boldsymbol{F}_1, \mathbf{B}_1) + (1-\lambda)R''W(\boldsymbol{F}_2, \mathbf{B}_2) \\
&\geqslant -\epsilon + \lambda R_i W(\boldsymbol{F}_1, \mathbf{B}_1) + (1-\lambda)R_i W(\boldsymbol{F}_2, \mathbf{B}_2) \\
&\geqslant -\epsilon + R_{i+1} W(\lambda \boldsymbol{F}_1 + (1-\lambda)\boldsymbol{F}_2, \lambda \mathbf{B}_1 + (1-\lambda)\mathbf{B}_2) \\
&\geqslant -\epsilon + R''W(\lambda \boldsymbol{F}_1 + (1-\lambda)\boldsymbol{F}_2, \lambda \mathbf{B}_1 + (1-\lambda)\mathbf{B}_2). \qquad (8.2.56)
\end{aligned}$$

Since ϵ *is arbitrary, we conclude that in* $R''W$ *is rank-one convex, and the proof is complete.*

□

We close this section by presenting results that allow for the generalization of the Legendre-Hadamard condition, and also plays an important role in checking for rank-one convexity of functions which lack sufficient smoothness.

Proposition 15:
A function $W : \mathbb{R}^{n\times n} \times \mathbb{R}^n \to \mathbb{R}$ *is rank-one convex if and only if the function* $\varphi : \mathbb{R}^2 \to \mathbb{R}$*, as defined by*

$$\varphi(t, s) = W(\boldsymbol{F} + t\mathbf{m} \otimes \mathbf{n}, \mathbf{B} + s\mathbf{n}^{\perp}) \qquad (8.2.57)$$

is convex for any choice of $\mathbf{n}, \mathbf{m}$ *and* $\mathbf{n}^{\perp}$*, where* $\mathbf{n} \cdot \mathbf{n}^{\perp} = 0$*.*

Proof:
Let $\lambda \in (0, 1)$*,* $t_1, t_2, s_1, s_2 \in \mathbb{R}$ *and* $\mathbf{n}, \mathbf{m}, \mathbf{n}^{\perp} \in \mathbb{R}^n$ *where* $\mathbf{n} \cdot \mathbf{n}^{\perp} = 0$*, be arbitrary. Upon letting* $\boldsymbol{F}_i = \boldsymbol{F} + t_i \mathbf{m} \otimes \mathbf{n}$ *and* $\mathbf{B}_i = \mathbf{B} + s_i \mathbf{n}^{\perp}$ *for* $i = 1, 2$ *we see that* $\operatorname{rank}\{\boldsymbol{F}_1 - \boldsymbol{F}_2\} = 1$ *and* $(\mathbf{B}_1 - \mathbf{B}_2) \in \ker(\boldsymbol{F}_1 - \boldsymbol{F}_2)$*. Moreover, we find that*

$$\varphi(\lambda t_1 + (1-\lambda)t_2, \lambda s_1 + (1-\lambda)s_2) = W(\lambda \boldsymbol{F}_1 + (1-\lambda)\boldsymbol{F}_2, \lambda \mathbf{B}_1 + (1-\lambda)\mathbf{B}_2), \qquad (8.2.58)$$

$$\lambda\varphi(t_1, s_1) + (1-\lambda)\varphi(t_2, s_2) = \lambda W(\boldsymbol{F}_1, \mathbf{B}_1) + (1-\lambda)W(\boldsymbol{F}_2, \mathbf{B}_2). \qquad (8.2.59)$$

Therefore, we see that φ is convex if and only if W is rank-one convex. $\square$

In the case that W is only continuously differentiable, we first define

$$\begin{aligned} g(\boldsymbol{F}, \mathbf{B}, t, s, \mathbf{n}, \mathbf{m}, \mathbf{n}^{\perp}) =& W(\boldsymbol{F} + t\mathbf{m} \otimes \mathbf{n}, \mathbf{B} + s\mathbf{n}^{\perp}) - W(\boldsymbol{F}, \mathbf{B}) \\ & - t\mathbf{m} \cdot \left(\frac{\partial W(\boldsymbol{F}, \mathbf{B})}{\partial \boldsymbol{F}} \mathbf{n} \right) - s \frac{\partial W(\boldsymbol{F}, \mathbf{B})}{\partial \mathbf{B}} \mathbf{n}^{\perp}. \end{aligned} \tag{8.2.60}$$

It is not hard to see that

$$g(\boldsymbol{F}, \mathbf{B}, t, s, \mathbf{n}, \mathbf{m}, \mathbf{n}^{\perp}) = \varphi(t, s) - \varphi(0, 0) - \nabla \varphi(0, 0) \cdot \begin{bmatrix} t \\ s \end{bmatrix} \tag{8.2.61}$$

Then, generalizing the work of Dacorogna and Haiberly (1998), we have the following result.

Proposition 16:

A continuously differentiable function function $W : \mathbb{R}^{n \times n} \times \mathbb{R}^n \to \mathbb{R}$ is rank-one convex if and only if

$$\inf_{t, s, \mathbf{n}, \mathbf{m}, \mathbf{n}^{\perp}} g(\boldsymbol{F}, \mathbf{B}, t, s, \mathbf{n}, \mathbf{m}, \mathbf{n}^{\perp}) = 0, \quad \forall (\boldsymbol{F}, \mathbf{B}). \tag{8.2.62}$$

Proof:

We first note that since W is continuously differentiable, so too is φ. Clearly, $g(\boldsymbol{F}, \mathbf{B}, 0, 0, \mathbf{n}, \mathbf{m}, \mathbf{n}^{\perp}) = 0$, and hence we must prove that W is rank-one convex if and only if g is nonnegative. To that end, from Proposition 15, W is rank one-convex if and only if φ is convex if and only if

$$\varphi(t_1, s_1) \geqslant \varphi(t_2, s_2) + \nabla \varphi(t_2, s_2) \cdot \begin{bmatrix} t_1 - t_2 \\ s_1 - s_2 \end{bmatrix} \quad \forall\, t_1, t_2, s_1, s_2 \in \mathbb{R}. \tag{8.2.63}$$

In fact, φ is convex if and if Eq. (8.2.63) holds for all $t = t_1, s = s_1$ and $t_2 = s_2 = 0$; this follows replacing $\boldsymbol{F}$ and $\boldsymbol{B}$ with $\boldsymbol{F}' = \boldsymbol{F} + t_1 \mathbf{m} \otimes \mathbf{n}$, $\boldsymbol{B}' = \boldsymbol{B} + s_1 \mathbf{n}^{\perp}$. Hence, in

light of Eq. (8.2.61)*, the result follows.*

□

Finally, we consider the case when W is twice continuously differentiable, and provide a generalization to the well known Legendre-Hadamard condition. This generalization can also be derived independently by appealing to the incremental equilibrium equations of magneto-elasticity (Destrade and Ogden, 2011; Kankanala and Triantafyllidis, 2004).

Proposition 17:

Suppose that W is twice continuously differentiable. Then W is rank-one convexity if and only if

$$D^2\varphi(t,s) = \begin{bmatrix} \frac{\partial^2 W}{\partial F_{ij}\partial F_{kl}} m_i n_j m_k n_l & \frac{\partial^2 W}{\partial F_{ij}\partial B_k} m_i n_j n_k^{\perp} \\ \frac{\partial^2 W}{\partial B_i \partial F_{jk}} n_i^{\perp} m_j n_k & \frac{\partial^2 W}{\partial B_i \partial B_j} n_i^{\perp} n_j^{\perp} \end{bmatrix}_{(\boldsymbol{F}+t\mathbf{m}\otimes\mathbf{n},\mathbf{B}+s\mathbf{n}^{\perp})} \tag{8.2.64}$$

is positive semidefinite.

Proof:

This result follows immediately from Proposition 15. □

By requiring that $D^2\varphi$ be positive definite, we obtain a necessary and sufficient condition for W to be strictly rank-one convex.

8.3 Homogenization in Finite Magneto-Elasticity

We now turn our attention to the problem of describing the effective properties of magneto-elastic composites under finite strain and arbitrary magnetic field. The general idea for defining the effective behavior of such composites, which we give below, is not new, and has been considered in the context of magneto-elasticity (Ponte Castañeda and Galipeau, 2011), electro-elasticity (Ponte Castañeda and Siboni, 2012; Ortigosa and Gil, 2016b,a), as well as magneto-electro-elasticity (Miehe

et al., 2015a,b). After presenting the basic definition of the effective behavior, or relaxation, we consider the steps that would need to be taken in order to prove the validity of such a definition. From there, we focus on the issue of unstable behavior under finite magneto-elastic loadings, and introduce a methodology, which has been used used successfully in the purely mechanical context (Furer and Ponte Castañeda, 2018a, 2019; Avazmohammadi and Ponte Castañeda, 2016), for describing the behavior of magneto-elastic composites after the onset of an instability. We skip a full review of the basics of magneto-elastostatics, and refer the interested reading to the work of Dorfmann and Ogden (2014).

Consider a material occupying some region Ω_0 in the undeformed configuration, and assume that this material is heterogenous, whereby there are N homogeneous phases, occupying regions $\Omega_0^{(r)}\,(r = 1, \ldots, N)$ that partition Ω_0. Each phase is described by an energy density $W^{(r)}$, which determines the constitutive response of phase r. In particular, for our purposes, we suppose that $W^{(r)} = W^{(r)}(\boldsymbol{F}, \mathbf{B})$, where $\boldsymbol{F}$ denotes the deformation gradient, and $\mathbf{B}$ denotes the induction magnetic field in the undeformed configuration. Upon letting $\chi_0^{(r)}$ denote the characteristic function of phase r, we see that the local energy density of the composite is given by

$$W(\mathbf{X}, \boldsymbol{F}, \mathbf{B}) = \sum_{r=1}^{N} \chi_0^{(r)}(\mathbf{X}) W^{(r)}(\boldsymbol{F}, \mathbf{B}). \tag{8.3.1}$$

Then the local first Piola-Kirchoff stress $\boldsymbol{S}$, and local true magnetic field $\boldsymbol{H}$, are given by

$$\boldsymbol{S} = \frac{\partial W}{\partial \boldsymbol{F}}, \quad \text{and} \quad \boldsymbol{H} = \frac{\partial W}{\partial \mathbf{B}}, \tag{8.3.2}$$

respectively. At this point, it is helpful to recall that in the absence of any body forces, current density, or electric field, and in the (quasi-)static limit, $\boldsymbol{S}$, $\mathbf{B}$ and $\mathbf{H}$ must satisfy the equilibrium equations, Gauss' Law, and Ampere's Law, respectively. In other words,

$$\nabla \cdot \boldsymbol{S} = 0, \quad \nabla \cdot \boldsymbol{B} = 0, \quad \nabla \times \boldsymbol{H} = 0. \tag{8.3.3}$$

While the microstructure, as described through $\chi_0^{(r)}$, can be random, in what follows, we consider the case where it is periodic, and identify the unit cell Y_0 to this microstructure. For a treatment of the homogenized response of magneto-elastic composites with random microstructures, we refer the reader to the work of Ponte Castañeda and Galipeau (2011) in the current setting of magneto-elasticity and Ponte Castañeda and Siboni (2012) in the mathematically equivalent context of electro-elasticity. Following the work of Miehe et al. (2015a), who based their extensions on the findings of Müller (1987), we define

$$\widehat{W}_k(\overline{\boldsymbol{F}}, \overline{\mathbf{B}}) = \inf_{\mathbf{u}\in\mathcal{K}_k} \inf_{\boldsymbol{A}\in\mathcal{H}_k} \frac{1}{|kY_0|} \int_{kY_0} W(\mathbf{x}, \overline{\boldsymbol{F}} + \nabla\mathbf{u}(\mathbf{x}), \overline{\mathbf{B}} + \nabla \times \mathbf{A}(\mathbf{x}))d\mathbf{x}, \tag{8.3.4}$$

where

$$\mathcal{K}_k = \{\mathbf{u} \,:\, \mathbf{u} \text{ is periodic on } kY_0\}\,, \tag{8.3.5}$$

and

$$\mathcal{H}_k = \{\mathbf{A} \,:\, \nabla \cdot \mathbf{A} = 0 \text{ and } \mathbf{A} \text{ is periodic on } kY_0\}\,. \tag{8.3.6}$$

The condition that $\nabla \cdot \mathbf{A} = 0$ ensures a unique solution to the Euler-Lagrange equations, and is referred to in the literature as the Coulomb gauge. We then define the effective potential, or relaxation, via

$$\widetilde{W}(\overline{\boldsymbol{F}}, \overline{\mathbf{B}}) = \inf_k \widehat{W}_k(\overline{\boldsymbol{F}}, \overline{\mathbf{B}}). \tag{8.3.7}$$

In order to rigorously establish Eq. (8.3.7), it would first be necessary to more precisely define $\mathcal{K}_k$ and $\mathcal{H}_k$. In the purely mechanical context, $\mathcal{K}_k$ is usually taken to be a subspace of the Sobolev space of weakly differentiable functions with periodic boundary conditions; indicentally, Müller (1987) showed that one can equivalently consider functions that vanish on the boundary. The integrability of these functions is determined by the associated growth and coercivity conditions imposed on the potential W. One major complication in determining the proper functional setting

is the use of the vector potential $\mathbf{A}$. Indeed, $\mathcal{H}_k$ will need to be a function space that allows for integrability and (weak) differentiability not only of $\mathbf{A}$, but of $\nabla \times \mathbf{A}$. For purely magnetic systems, it often suffices to consider $\mathbf{A}, \nabla \times \mathbf{A} \in L^2(\Omega_0)$ (Wellander, 2001, 2002; Serrano, 2011), but due to the need to consider terms of the form $(\nabla \mathbf{u})(\nabla \times \mathbf{A})$, this may be overly restrictive. On the other hand, the use of the vector potential means that Gauss' Law, Eq. $(8.3.3)_2$, is satisfied, in some weak sense, *a priori*, and moreover, that the Euler-Lagrange equations associated with the variational problems defined in Eq. (8.3.4) correspond to the equilibrium equations, Eq. $(8.3.3)_1$, and Ampere's Law, Eq. $(8.3.3)_3$.

With the proper function space set, it would be possible to describe the topology over which weak (sequential) lower semicontinuity of functionals of the form

$$I(\mathbf{u}, \mathbf{A}) = \int_\Omega W(\mathbf{x}, \nabla \mathbf{u}(\mathbf{x}), \nabla \times \mathbf{A}(\mathbf{x})) d\mathbf{x} \tag{8.3.8}$$

could be defined. Moreover, with such a topology, a straightforward generalization of $\Gamma-$convergence, a necessary ingredient in proving (8.3.7), could be obtained. In particular, suppose that we have fixed our function space $\mathcal{F}$, which consists of elements of the form $(\mathbf{u}, \mathbf{A})$. We'll let $\rightharpoonup$ denote weak convergence with respect to the topology of $\mathcal{F}$, and define the following:

Definition 13:

A functional I on $\mathcal{F}$ is *weakly lower semicontinuous* if and only if for any $(\mathbf{u}^\epsilon, \mathbf{A}^\epsilon) \in \mathcal{F}$ such that $(\mathbf{u}^\epsilon, \mathbf{A}^\epsilon) \rightharpoonup (\mathbf{u}, \mathbf{A})$ as $\epsilon \to 0$,

$$\liminf_{\epsilon \to 0} I(\mathbf{u}^\epsilon, \mathbf{A}^\epsilon) \geqslant I(\mathbf{u}, \mathbf{A}). \tag{8.3.9}$$

Definition 14:

Let $\{I^\epsilon\}$ be a family of functionals on $\mathcal{F}$. Then $\{I^\epsilon\}_{\epsilon > 0}$ is $\Gamma-$*convergent* to I with respect to the weak topology of $\mathcal{F}$ if the following two conditions hold:

1. If $(\mathbf{u}^\epsilon, \mathbf{A}^\epsilon) \rightharpoonup (\mathbf{u}, \mathbf{A})$ as $\epsilon \to 0$, then

$$\liminf_{\epsilon \to 0} I^\epsilon(\mathbf{u}^\epsilon, \mathbf{A}^\epsilon) \geqslant I(\mathbf{u}, \mathbf{A}). \tag{8.3.10}$$

2. For every $(\mathbf{u}, \mathbf{A}) \in \mathcal{F}$ there exists $(\mathbf{u}^\epsilon, \mathbf{A}^\epsilon) \rightharpoonup (\mathbf{u}, \mathbf{A})$ such that

$$I(\mathbf{u}, \mathbf{A}) = \lim_{\epsilon \to 0} I^\epsilon(\mathbf{u}^\epsilon, \mathbf{A}^\epsilon). \tag{8.3.11}$$

By construction, the $\Gamma-$limit of a sequence of functionals is weakly lower semi-continuous (Braides, 1985). In the purely mechanical context, this is necessary and sufficient for the integrand of the $\Gamma-$limit to be quasiconvex (Morrey Jr., 1952; Ball, 1977). A generalization of this result for magneto-elastic materials is beyond the scope of this work, but has been proven in other multi-physical settings (Conti et al., 2018). Indeed, the equivalence between weak lower semicontinuity of an integral functional and the quasiconvexity of its integrand has been extended to include cases where the admissible fields satisfy certain linear differential constraints. Thus, the Coulomb gauge, as well as the fact that $\boldsymbol{F} = \nabla \mathbf{u}$, can be treated within the framework of $\mathcal{A}-$quasiconvexity (Fonseca and Müller, 1999), and the related $\mathcal{A}-\mathbb{B}-$quasiconvexity (Dacorogna and Fonseca, 2002). Moreover, in this context of $\mathcal{A}-$quasiconvexity, Braides et al. (2000) provided a homogenization results similar to the one given above, and consistent with the results of Müller (1987). As such, we anticipate that $\widetilde{W}$, the integrand of the $\Gamma-$limit of the sequence of functionals associated with $\widehat{W}_k$, will be quasiconvex in the sense of Definition 10. By the results of Section 8.2, this then implies that $\widetilde{W}$ is rank-one convex, but not necessarily strictly so. Now, for $\overline{\boldsymbol{F}}$ close to the identity, and $|\overline{\mathbf{B}}|$ small, assuming that each $W^{(r)}$ is strictly polyconvex, we expect that the minimization problem in Eq. (8.3.4), with $k = 1$, will have a unique solution (see Rogers, 1988; Silhavý, 2018, for proofs of existence to such variational problems), and hence the relaxation $\widetilde{W}$ will correspond to this one-cell period solution. Indeed, this is known to be the case when $\overline{\mathbf{B}} = \mathbf{0}$ (Müller and Neukamm, 2011; Neukamm and

Schäffner, 2018), and we call this the "principal" solution, and denote the effective energy associated with it by $\widehat{W}$.

On the other hand, under finite magneto-elastic effects, by the definition of $\widetilde{W}$, it is possible that solutions that are periodic on $N \times M \times L$ "super-cells" may exhibit lower energy than the energy of the principal solution, whereby $\widetilde{W}$ is given by $\widehat{W}_k$ for some $k > 1$. This behavior corresponds to the initiation of instability, and which point $\widehat{W}$ will only serve to provide an upper bound on $\widetilde{W}$. In the purely mechanical context, Geymonat et al. (1993) showed rigorously that the composite can indeed develop these "microscopic" instabilities. The development of "macroscopic" instabilities, corresponding to long-wavelength instabilities that are not periodic at finite wavelengths, is also possible, and Geymonat et al. (1993) showed that they can be detected by the loss strong ellipticity of the incremental moduli of the (one-cell periodic) principal solution. Moreover, such instabilities lead to the loss of strict rank-one convexity of $\widetilde{W}$.

Both types of instabilities have been predicted theoretically for magneto-elastic materials (Destrade and Ogden, 2011; Rudykh and Bertoldi, 2013), and in the equivalent context of electro-elasticity (Siboni et al., 2014; Rudykh and deBotton, 2011; Bertoldi and Gei, 2011). The onset of microscopic instabilities has been studied by making use of Bloch-Floquet type analyses (see Bertoldi and Gei, 2011; Rudykh et al., 2014, for examples in the context of electro-elasticity), while the onset of macroscopic instabilities has been attributed to failure of the generalized strong ellipticity condition, where the (electro-)magneto-elastic moduli are calculated from the principal solution $\widehat{W}$ (Rudykh and Bertoldi, 2013; Goshkoderia and Rudykh, 2017). In addressing the interplay between microscopic and macroscopic instabilities, Bertoldi and Gei (2011) and Rudykh et al. (2014) made use of layered electro-elastic composites, for which the principal solution can be calculated analytically. Consistent with the findings of Geymonat et al. (1993) and Triantafyllidis and Maker (1985) in the purely mechanical context, it was found that microscopic stability implies macroscopic sta-

bility, and moreover, when the volume fraction of the stiffer phase is large enough, the primary mode of instability has infinite wavelength, and hence corresponds to a macroscopic instability.

We are interested in the case when the first instability is macroscopic. When the instability does not result in material failure, we anticipate that the composite will break up into domains in order to accommodate the combined loading from $\overline{\boldsymbol{F}}$ and $\overline{\mathbf{B}}$. Such domain formation has been predicted for both fiber-reinforced (Avazmohammadi and Ponte Castañeda, 2016) and layered (Furer and Ponte Castañeda, 2018a, 2019) elastomers under purely mechanical loading, and can be described in those settings by means of the quasiconvexification of the principal solution. Moreover, as discussed in these works, the onset of a macroscopic instability will, in general, be initiated not by the loss strong ellipticity condition, but rather by the loss of strict rank-one convexity of the principal solution. This is related to the fact that, under finite strain, linearization and homogenization do not commute (Müller and Neukamm, 2011; Neukamm and Schäffner, 2018). As this will remain true in the more complex magneto-elastic setting, it is clear that using the magneto-elastic moduli associated with $\widehat{W}$ to predict the behavior of $\widetilde{W}$ will overestimate stability; checking strict rank-one convexity of $\widehat{W}$ directly will give a more reliable estimate.

When the primary mode of instability is macroscopic, we look to calculate $\widetilde{W}$ after the onset of such an instability. As mentioned above, in order to account for the formation of domains on a scale larger than that of the unit cell, but still small compared to the material sample, we turn our attention to the quasiconvexification $Q\widehat{W}$ of the principal solution. As $\widetilde{W}$ is quasiconvex and since $\widetilde{W} \leqslant \widehat{W}$, then from the definition of the quasiconvex envelope we know that

$$\widetilde{W} \leqslant Q\widehat{W} \leqslant \widehat{W}, \tag{8.3.12}$$

and we anticipate that $Q\widehat{W}$ will give an accurate description of the post-bifurcation behavior, and in certain cases, correspond directly to $\widetilde{W}$. In particular, we look to

calculate $R\widehat{W}$ by making use of Part 2 of Theorem 4. If we can show that $R\widehat{W}$ is polyconvex, then by Proposition 13, and Equation (8.2.27), it will follow that $R\widehat{W} = Q\widehat{W}$.

8.4 Concluding Remarks

In this work, we set out to provide rigorous generalizations to concepts that arise in the calculus of variations, so that the same machinery used in describing the macroscopic behavior of hyperelastic composites under purely mechanical loads could be reformulated to allow for the description of these composites undergoing magneto-elastic loading. Having proved that the notions of "weak" convexities generalize accordingly, we generalized the methodology for assessing the stability of periodic magneto-elastic composites based on strict rank-one convexity, as well as for extracting the post-bifurcation behavior once the composite has undergone a macroscopic instability. Some of the arguments rely on assumptions which need to be investigated further (e.g. that the relaxation is in fact quasiconvex), but the conclusions drawn are all consistent in that they agree with the well established results in the case that $\overline{\mathbf{B}} = \mathbf{0}$.

In future work, we plan on using the results obtained here to guide our calculation of the post-bifurcation behavior of magneto-elastic composites by way of the quasiconvexification of the principal solution. This requires, in particular, the evaluation of rank-one convex envelope by making use of the generalized Kohn-Strang lamination formula. Based on the findings for purely mechanical systems (Furer and Ponte Castañeda, 2018a; Avazmohammadi and Ponte Castañeda, 2016), we anticipate that, at least for certain loading conditions, the relaxation will be obtained via the formation of lamellar domains, as indicated by the construction set forth here for computing the quasiconvex envelope.

Chapter 9

Application to Neo-Hookean Magneto-Elastic Laminates Under Plane-Strain Loading Conditions

Abstract

In Chapter 8, we provided the tools needed for obtaining estimates on the relaxation of magneto-elastic composites under finite strain. In particular, we introduced a methodology for calculating the post-bifurcation behavior of such systems after the onset of a macroscopic instability by means of the quasiconvexification of the principal solution, i.e. the solution prior to the instability. This work is concerned with applying these tools to obtain estimates for the post-bifurcation behavior of a two-phase magnetically active laminate under plane-strain loading conditions and a magnetic field in the plane of deformation. We obtain bounds on the post-bifurcation behavior, and in certain cases, we are able to compute the quasiconvexification explicitly. We then apply the bounds to the two specific cases where the magnetic field is applied both parallel and perpendicular to the layers, and investigate the physical implications on the relaxation construction. In particular, we find that the magneto-elastic coupling can cause sufficient compression of the layers, leading to an instability. The laminate then forms lamellar domains in order to accommodate such unstable magneto-elastic loading.

9.1 Introduction

Magneto-elastic composites refer, in general, to a class of composite materials that can undergo deformations due to coupled magneto-elastic loading. Magnetorheological elastomers (MRE's) are a well known examples of magneto-elastic composites, and are materials consisting of magnetically susceptible particles embedded in an elastomeric matrix. These materials have sparked a recent flurry of investigations due in part to their ability to undergo finite strains, making them prime candidates for use as smart materials.

Nearly all continuum-based models of magneto-elasticity rely on the use of an energy density that is a function of the deformation gradient $\boldsymbol{F}$, as well as one of any of the magnetic variables associated with the system; in particular, constitutive models that make use of $\mathbf{B}, \mathbf{H}$, $\mathbf{M}$, the induced magnetic field, true magnetic field, and magnetization, all in the undeformed configuration, as well as their counterparts in the deformed configuration, have all been considered (see, e.g., Bustamante et al., 2008; Dorfmann and Ogden, 2004; Kankanala and Triantafyllidis, 2004; Miehe et al., 2015a; Steigmann, 2004). However, many of these works deal with homogeneous magneto-elastic composites, whereas it has been seen experimentally that much of the exotic macroscopic behavior displayed by these materials is strongly tied to the underlying microstructure.

Motivated by this, researchers have sought to understand the effective response of magneto-elastic composites by making use of homogenization. When finite strain effects are taken into account, homogenization even in the purely mechanical case is a very difficult problem. For one, the dependence on $\boldsymbol{F}$ of the energy density is non-convex, leading to the possible development of both microscopic and macroscopic instabilities (Geymonat et al., 1993). In some cases, homogenization methods in the magneto-elastic context have been proposed by using of a variety of simplifying assumptions (e.g. Yin and Sun, 2006; Borcea and Bruno, 2001, for particles

aligned in chains, and in small strain limit, respectively). For large deformations, Ponte Castañeda and Galipeau (2011) provided a homogenization-based model for obtaining the effective response of MRE's that itself relied on a "partial-decoupling" approximation.

In looking to model magneto-elastic composites undergoing large strains, one must always be aware of the potential for unstable behavior. There have been a number studies, both experimental and theoretical, that seek to generalize the work of (Geymonat et al., 1993) to the magneto-elastic context (e.g. Galipeau and Ponte Castañeda (2013); Rudykh and Bertoldi (2013); Kankanala and Triantafyllidis (2004). See Ponte Castañeda and Siboni (2012); Bertoldi and Gei (2011) for an analogous treatment in the context of electro-elasticity). Such studies, as well as those conducted in the related context of electro-elasticity, have found that magneto-elastic materials do indeed undergo both microscopic and macroscopic instabilities. Many of the methods used for checking stability of the composite are based on a generalized strong ellipticity condition as applied to the incremental magneto-elastic moduli of the principal solution. However, it has been seen recently, in the purely mechanical context, that use of the incremental magneto-elastic moduli tends to overestimate the stability of the composite Avazmohammadi and Ponte Castañeda (2016); Furer and Ponte Castañeda (2018a, 2019). Moreover, as in the purely-mechanical context, very little work has been done to describe the behavior of magneto-elastic composites after the onset of an instabilities.

Chapter 8 introduced an extension of a method, originally proposed by Avazmohammadi and Ponte Castañeda (2016), for extracting the post-bifurcation behavior of a magneto-elastic composite after the onset of a macroscopic instability. The method relies on the computation of $Q\widehat{W}$, the quasiconvex envelope of the principal solution $\widehat{W}$. Much of the theoretical machinery on which this methodology is based has roots in the calculus of variations and homogenization theory. In this work, we are interested in the application of these results to the model problem. We forgo a full review

of the relevant results used in this chapter and refer to interested reader to Chapter 8. As indicated by the findings in Chapters 6 and 7 in the purely mechanical context, the calculation of $Q\widehat{W}$ is greatly facilitated by the existence of a (semi-)analytical expression for $\widehat{W}$. The estimates for $\widehat{W}$ obtained using the model of Ponte Castañeda and Galipeau (2011) are rather complicated, and in testing this methodology for the first time, we look to apply it to a system for which estimates on $\widehat{W}$ are more tractable; in particular, we will consider a two-phase laminated composite, a material for which the estimates for $\widehat{W}$ can be given exactly. As such, the rest of this work will be laid out as follows. Section 9.2 gives a brief review of the continuum theory of magneto-elasticity, and discusses the extension of the strong ellipticity condition for magneto-elastic materials. Section 9.3 provides preliminary results regarding the magneto-elastic laminate under plane-strain loading conditions to be studied in this work, and introduces the invariants that will be used in studying them. In Section 9.4, the bounds on the quasiconvexification of the principal solution are derived, and then compared to assess their reliability. Finally, Section 9.6 provides an analysis of the physical implications of the relaxation construction by investigating the post-bifurcation response of the laminate under a range of loading conditions.

Throughout this work, we make use of standard notation in the continuum mechanics literature. We fix the standard Cartesian basis $\{\mathbf{e}_i\}$, with respect to which vectors with Cartesian components a_i or A_i are represented by bold letters $\mathbf{a}$ or $\mathbf{A}$, respectively. Second-order tensors with Cartesian components F_{ij} are represented by bold italic letters $\boldsymbol{F}$, while fourth-order tensors with Cartesian components L_{ijkl} are denoted by barred letters $\mathbb{L}$. Here i, j, k, l range from 1 to 2. The Einstein summation convention will be utilized, so that repeated indices are summed over. For example, the product $\boldsymbol{F}\mathbf{X}$ has Cartesian components $F_{ij}X_j$. Given two vectors $\mathbf{a}, \mathbf{b}$, the quantity $\mathbf{a}\otimes\mathbf{b}$ is defined to be in second-order tensor with Cartesian components a_ib_j. We denote by Lin (Lin^+) the set of all second-order tensors (with positive determinant).

9.2 Magneto-Elasticity

In this section, we will review the theory of finite magneto-elasticity from the perspective of continuum mechanics. We consider a magneto-elastic body in a stress free configuration, and will refer to this state as the reference, or Lagrangian, configuration, and denote the region in space occupied by this body as $\Omega_0 \subset \mathbb{R}^2$. Under the combined action of mechanical and magnetic loading, material at a point $\mathbf{X} \in \Omega_0$ will move to a new point $\mathbf{x} \in \Omega$, where Ω is the current, or Eulerian, configuration. This defines a mapping $\mathbf{x} : \Omega_0 \to \Omega$, which is assumed to be continuous, (weakly) differentiable, and one-to-one. Now, the deformation is characterized by the deformation gradient tensor $\boldsymbol{F} = \text{Grad}\mathbf{x}$. To ensure no interpenetration of the material, we require that

$$J = \det \boldsymbol{F} > 0. \tag{9.2.1}$$

Moreover, while $\mathbf{x}$ is continuous, $\boldsymbol{F}$ may be discontinuous across material interfaces. However, Hadamard's compatibility condition (Gurtin et al., 2010) requires that $[[\boldsymbol{F}]] = \mathbf{a} \otimes \mathbf{N}$, where $\mathbf{N}$ is the unit vector normal to the interface in the reference configuration, and $\mathbf{a}$ is an arbitrary vector.

We let ρ_0 and ρ be the material densities in the reference and deformed configurations, respectively. Conservation of mass requires that

$$\rho_0 = \rho J. \tag{9.2.2}$$

It is next useful to introduce two notions of stress. For the Lagrangian description of stress, we use the first Piola-Kirchhoff stress $\boldsymbol{S}$. The Eulerian counterpart of stress is the total Cauchy stress $\boldsymbol{T}$, which is related to $\boldsymbol{S}$ by $\boldsymbol{S} = J\boldsymbol{T}\boldsymbol{F}^{-T}$. Conservation of angular momentum requires that $\boldsymbol{T} = \boldsymbol{T}^T$, which implies $\boldsymbol{S}\boldsymbol{F}^T = \boldsymbol{F}\boldsymbol{S}^T$. If $\mathbf{f}_0$ and $\mathbf{f}$ are the mechanical body forces in the undeformed and deformed configurations,

respectively, then the stresses are assumed to satisfy the equilibrium equations

$$\mathrm{Div}\boldsymbol{S} + \rho_0 \mathbf{f}_0 = \mathbf{0}, \tag{9.2.3}$$

or

$$\mathrm{div}\boldsymbol{T} + \rho \mathbf{f} = \mathbf{0}. \tag{9.2.4}$$

Like $\boldsymbol{F}$, $\boldsymbol{S}$ (or $\boldsymbol{T}$) may exhibit discontinuities, but they are still required to satisfy the jump conditions $[[\boldsymbol{S}]]\mathbf{N} = \mathbf{0}$ (or $[[\boldsymbol{T}]]\mathbf{n} = \mathbf{0}$), where $\mathbf{N}$ (or $\mathbf{n}$) denotes the normal to the interface in the undeformed (deformed) configuration. These conditions arise from the mass and momentum balance equations.

The equations of magnetostatics are usually written in Eulerian form in terms of the magnetic induction field $\mathbf{b}$ and the (true) magnetic field $\mathbf{h}$. Assuming that the current density $\mathbf{j} = \mathbf{0}$, these fields satisfy Gauss' and Ampere's laws

$$\mathrm{div}\mathbf{b} = 0, \quad \text{and} \quad \mathrm{curl}\mathbf{h} = \mathbf{0}, \tag{9.2.5}$$

respectively. Like $\boldsymbol{F}$, these fields may be discontinuous across a material interface, but nonetheless must satisfy the jump conditions

$$[[\mathbf{b}]] \cdot \mathbf{n} = 0, \quad \text{and} \quad [[\mathbf{h}]] \times \mathbf{n} = \mathbf{0}. \tag{9.2.6}$$

It is also useful to introduce the (Eulerian) magnetization $\mathbf{m}$, which is related to $\mathbf{b}$ and $\mathbf{h}$ via

$$\mathbf{b} = \mu_0(\mathbf{h} + \mathbf{m}), \tag{9.2.7}$$

where μ_0 is the magnetic permeability of a vacuum. We remark that equations in (9.2.5) are nothing more than the time independent Maxwell equations in the absence of an electric field.

It will prove more helpful to describe these equations in the Lagrangian form.

Following Dorfmann and Ogden (2004); Kankanala and Triantafyllidis (2004), we have that

$$\text{Div}\mathbf{B} = 0, \quad \text{and} \quad \text{Curl}\mathbf{H} = \mathbf{0} \tag{9.2.8}$$

where

$$\mathbf{B} = J\boldsymbol{F}^{-1}\mathbf{b}, \quad \text{and} \quad \mathbf{H} = \boldsymbol{F}^{T}\mathbf{h} \tag{9.2.9}$$

are the Lagrangian counterparts to $\mathbf{b}$ and $\mathbf{h}$, respectively. The corresponding jump conditions in the reference configuration become

$$[[\mathbf{B}]] \cdot \mathbf{N} = 0, \quad \text{and} \quad [[\mathbf{H}]] \times \mathbf{N} = \mathbf{0}. \tag{9.2.10}$$

In order to describe the constitutive behavior of a magneto-elastic material, we choose an energy formulation based on the deformation gradient $\boldsymbol{F}$ and the magnetic induction field in the reference configuration $\mathbf{B}$, as proposed by Dorfmann and Ogden (2004). As such, the constitutive behavior of the magneto-elastic phases, at constant temperature and ignoring dissipative effects, is characterized by energy-density function $W^{(r)} = W^{(r)}(\boldsymbol{F}, \boldsymbol{B})$, and defined by

$$\boldsymbol{S} = \frac{\partial W^{(r)}}{\partial \boldsymbol{F}}(\boldsymbol{F}, \mathbf{B}), \quad \text{and} \quad \mathbf{H} = \frac{\partial W^{(r)}}{\partial \mathbf{B}}(\boldsymbol{F}, \mathbf{B}). \tag{9.2.11}$$

When the phases are incompressible, the first Piola-Kirchhoff takes the form

$$\boldsymbol{S} = \frac{\partial W^{(r)}}{\partial \boldsymbol{F}}(\boldsymbol{F}, \mathbf{B}) - p\boldsymbol{F}^{-T}, \tag{9.2.12}$$

where p is an arbitrary Lagrange multiplier associated with the incompressibility condition $\det \boldsymbol{F} = 1$. These potentials are assumed to satisfy the property of material frame indifference, so that for $\boldsymbol{Q} \in \text{Orth}^{+}$, and any $\boldsymbol{F}$ and $\boldsymbol{B}$, $W^{(r)}(\boldsymbol{QF}, \boldsymbol{B}) = W^{(r)}(\boldsymbol{F}, \boldsymbol{B})$. Therefore, using the polar decompositions theorem to write $\boldsymbol{F} = \boldsymbol{RU}$, we see that $W^{(r)}(\boldsymbol{F}, \boldsymbol{B}) = W^{(r)}(\boldsymbol{U}, \boldsymbol{B})$.

As laid out above, the Cauchy stress $\boldsymbol{T}$ includes contributions from both the mechanical and magnetic body forces. Indeed, it is known (Dorfmann and Ogden, 2004; Kankanala and Triantafyllidis, 2004; Dorfmann and Ogden, 2014) that, in the context of incompressible materials, that the total Cauchy stress $\boldsymbol{T}$ can be written as

$$\boldsymbol{T} = \boldsymbol{\sigma} + \boldsymbol{T}^M + (\mathbf{m} \cdot \mathbf{b})\mathbf{I} - \mathbf{b} \otimes \mathbf{m} - p\mathbf{I}, \tag{9.2.13}$$

where $\boldsymbol{\sigma}$ is a measure of the stress, p is the pressure associated with the incompressibility condition, and

$$\boldsymbol{T}^M = \frac{1}{\mu_0}\mathbf{b} \otimes \mathbf{b} - \frac{1}{2\mu_0}|\mathbf{b}|^2\,\mathbf{I} \tag{9.2.14}$$

is the Maxwell stress. The symmetry of $\boldsymbol{T}$ requires that $\boldsymbol{\sigma} + \mathbf{m} \otimes \mathbf{b}$ be symmetric. Moreover, recalling Eq. (9.2.7), we can write

$$\boldsymbol{T} = \boldsymbol{\sigma} + \mathbf{b} \otimes \mathbf{h} + \frac{\mu_0}{2}(|\mathbf{m}|^2 - |\mathbf{h}|^2)\mathbf{I}. \tag{9.2.15}$$

We note that $\boldsymbol{\sigma}$ will in general depend both of $\boldsymbol{F}$ and $\boldsymbol{B}$, and going forward, we define

$$\boldsymbol{T}^{mag} \equiv \mathbf{b} \otimes \mathbf{h} + \frac{\mu_0}{2}(|\mathbf{m}|^2 - |\mathbf{h}|^2)\mathbf{I} \tag{9.2.16}$$

The problem of the existence and regularity of solutions to the equilibrium equations has been studied extensively in the purely mechanical context Ball (1977); Müller (1987); Dacorogna (1989); Geymonat et al. (1993). Moreover, conditions on the (purely mechanical) energy potential that ensure smooth solutions are well known; in particular, strong ellipticity of the energy potential ensures that any solution to the equilibrium equation will be continuous. There has been progress made in establishing generalizations of the strong ellipticity condition in the case of magneto-elasticity. One approach appeals to the principle of minimum potential energy, and uses a variational formulation to derive the equilibrium equations and jump conditions outlined above. In particular, the equilibrium equations are nothing more than the Euler-

Lagrange equations of the energy functional. In order to ensure that the solution is a minimizer, one then checks to see whether the second variation of the functional, when evaluated at a solution to the Euler-Lagrange equations, is positive (semi-)definite. Kankanala and Triantafyllidis (2004) introduced one such variational principle by consider an free energy function that depends on the deformation gradient $\boldsymbol{F}$ and the (Lagrangian) magnetization $\mathbf{M}$. By appealing to the positive-definiteness of the second variation, and making use of the Fourier transform, they derived sufficient pointwises conditions for their definition of "quasiconvexity," which is similar to the one given in Chapter 8 and ensures the existence of continuous solutions. Other generalizations, some even in the case of electro-magneto-elasticity, have been derived from variational formulations as well, and all rely on the positive definiteness of either the second variation of the energy functional or the generalized Hessian of the associated energy potential (see Ortigosa and Gil, 2016a; Miehe et al., 2015b, and references therein for examples).

Another approach for establishing conditions that ensure the existence of continuous solutions is to appeal directly to the equilibrium equations, but in their incremental form. Destrade and Ogden (2011) derived a generalization of the strong ellipticity condition when the energy potential W is a function of $\boldsymbol{F}$ and $\mathbf{B}$. This condition, which was derived for an incompressible material, takes the same form of the condition derived by Kankanala and Triantafyllidis (2004). In particular, Destrade and Ogden (2011) showed that solutions will remain continuous so long as

$$\mathbf{m}\cdot\left(\left(\widehat{\boldsymbol{Q}^c}-\widehat{\boldsymbol{R}^c}\widehat{\boldsymbol{E}^c}^{-1}\widehat{\boldsymbol{R}^c}^{T}\right)\mathbf{m}\right)>0\quad\forall\,\mathbf{n},\,\mathbf{m}\text{ such that }|\mathbf{n}|=|\mathbf{m}|=1,\text{ and }\mathbf{m}\cdot\mathbf{n}=0. \tag{9.2.17}$$

Here

$$Q^c_{ik}(\mathbf{n})=L^c_{ipkq}n_pn_q,\qquad\text{and}\qquad R^c_{ik}(\mathbf{n})=M^c_{ijk}n_j, \tag{9.2.18}$$

where

$$L^c_{ijkl} = \frac{\partial^2 W}{\partial F_{ip} \partial F_{kq}} F_{jp} F_{lq}, \quad M^c_{ijk} = \frac{\partial^2 W}{\partial F_{ip} \partial B_q} F_{jp} F^{-1}_{qk}, \quad \text{and} \quad E^c_{ij} = \frac{\partial^2 W}{\partial B_p \partial B_q} F^{-1}_{pi} F^{-1}_{qj}, \tag{9.2.19}$$

are the push forward of the magnetoelastic moduli, and $\widehat{(\cdot)} = \overline{\boldsymbol{I}}(\cdot)\overline{\boldsymbol{I}}$ where $\overline{\boldsymbol{I}} = \boldsymbol{I} - \mathbf{n} \otimes \mathbf{n}$. By making use of the same analysis as Destrade and Ogden (2011), it can be shown that an equivalent generalized strong ellipticity condition is given by

$$\begin{aligned} &\left(\mathbf{m} \cdot (\widehat{\boldsymbol{Q}^c}\mathbf{m})\right)\left(\mathbf{n}^\perp \cdot (\widehat{\boldsymbol{E}^c}\mathbf{n}^\perp)\right) - (\mathbf{n}^\perp \cdot \widehat{\boldsymbol{R}^c}^T \mathbf{m})^2 > 0 \\ &\qquad \forall\, \mathbf{n}, \mathbf{m}, \mathbf{n}^\perp \text{ such that } |\mathbf{n}| = |\mathbf{m}| = |\mathbf{n}^\perp| = 1, \text{ and } \mathbf{m} \cdot \mathbf{n} = \mathbf{n}^\perp \cdot \mathbf{n} = 0. \end{aligned} \tag{9.2.20}$$

An exactly analogous expression has been found by Rudykh and Bertoldi (2013), who studied stability in the context of laminated composites. Making use of the general homogenization framework of Ponte Castañeda and Galipeau (2011), Galipeau and Ponte Castañeda (2013) have also made use of an expression akin to Eq. (9.2.20) to study the stability of magneto-elastic composites with more general microstructures. In particular, they considered composites with a random distribution of ellipsoidal inclusions; upon taking taking the limit as the aspect ratio of these inclusions tends to infinity, their results recover the exact results for the laminate considered by Rudykh and Bertoldi (2013), and the one to be considered in this work. In connection to the theory presented in Chapter 8, Eq. (9.2.20) is equivalent to the condition that W is strictly rank-one convex, when interpreted in the context of incompressibility.

9.3 Principal Solution for a two-phase Neo-hookean magneto-elastic laminate

Here, we consider a simple laminate consisting of two isotropic phases, which are layered periodically in a direction with unit normal $\mathbf{N}_0$, and in prescribed volume fractions $c^{(r)}$ $(r = 1, 2)$. For simplicity, the phases are assumed to be incompressible, Neo-Hookean materials, with stored-energy functions of the form

$$W^{(r)}(\boldsymbol{F}, \mathbf{B}) = \frac{\mu^{(r)}}{2}\mathrm{tr}(\boldsymbol{F}^T\boldsymbol{F} - \boldsymbol{I}) + \frac{\chi^{(r)}}{2\mu_0}|\boldsymbol{F}\mathbf{B}|^2 + K(\det \boldsymbol{F}), \tag{9.3.1}$$

where $\mu^{(r)} > 0$ represents the shear modulus of phase r, $\chi^{(r)} > 0$ is a measure of the magnetic permeability of phase r, μ_0 is the magnetic permeability of free space, and where

$$K(J) = \begin{cases} 0, & J = 1, \\ \infty & \text{otherwise} \end{cases} \tag{9.3.2}$$

serves to enforce the incompressibility constraint. The parameter $\chi^{(r)}$ used in this work can be related to the more traditional measure of permeability via $\chi^{(r)} = (\mu_m^{(r)})^{-1}$, where $\mu_m^{(r)} > 0$ is a measure of the relative magnetic permeability of phase r. Note that the first Piola-Kirchoff stress and true magnetic field in the undeformed configuration in phase r are given by

$$\boldsymbol{S}^{(r)} = \mu^{(r)}\boldsymbol{F} + \frac{\chi^{(r)}}{\mu_0}(\boldsymbol{F}\mathbf{B}) \otimes \mathbf{B} - p\boldsymbol{F}^{-T}, \quad \mathbf{H}^{(r)} = \frac{\chi^{(r)}}{\mu_0}\boldsymbol{F}^T\boldsymbol{F}\mathbf{B}, \tag{9.3.3}$$

respectively. Recall that p is an arbitrary hydrostatic pressure account for incompressibility. It then follows that the Cauchy-Stress and true magnetic field the deformed configuration in phase r are respectively given by

$$\boldsymbol{T}^{(r)} = \mu^{(r)}\boldsymbol{F}\boldsymbol{F}^T + \frac{\chi^{(r)}}{\mu_0}(\boldsymbol{F}\mathbf{B}) \otimes (\boldsymbol{F}\mathbf{B}) - p\boldsymbol{I}, \quad \mathbf{h}^{(r)} = \frac{\chi^{(r)}}{\mu_0}\mathbf{b}, \tag{9.3.4}$$

where it is recalled that $\mathbf{b} = \boldsymbol{F}\mathbf{B}$ is the induction field in the deformed configuration (c.f. Eq. (9.2.9) with $\overline{J} = 1$). Therefore, we see that the magnetic constitutive response of the phases is linear, and when $\chi^{(r)} = 1$, the magnetization in phase r is zero.

Now, upon letting $\mathbf{M}_0$ perpendicular to $\mathbf{N}_0$, Bertoldi and Gei (2011); Rudykh and Bertoldi (2013) showed that the principal solution for the effective response of the laminate takes the form

$$\widehat{W}(\overline{\boldsymbol{F}}, \overline{\mathbf{B}}) = G(\overline{\boldsymbol{F}}, \overline{\mathbf{B}}) + K(\det \overline{\boldsymbol{F}}), \tag{9.3.5}$$

where

$$\begin{aligned} G(\overline{\boldsymbol{F}}, \overline{\mathbf{B}}) =& \frac{\overline{\mu}}{2}\mathrm{tr}(\overline{\boldsymbol{F}}^T\overline{\boldsymbol{F}} - \boldsymbol{I}) + \frac{\overline{\chi}}{2}|\overline{\boldsymbol{F}}\,\overline{\mathbf{B}}|^2 + \frac{\breve{\mu} - \overline{\mu}}{2}\frac{\left[(\overline{\boldsymbol{F}}\mathbf{N}_0)\cdot(\overline{\boldsymbol{F}}\mathbf{M}_0)\right]^2}{|\overline{\boldsymbol{F}}\mathbf{M}_0|^2} \\ &+ \frac{\breve{\chi} - \overline{\chi}}{2}\frac{\left[(\overline{\boldsymbol{F}}\,\overline{\mathbf{B}})\cdot(\overline{\boldsymbol{F}}\mathbf{M}_0)\right]^2}{|\overline{\boldsymbol{F}}\mathbf{M}_0|^2}. \end{aligned} \tag{9.3.6}$$

Here,

$$\overline{\mu} = c^{(1)}\mu^{(1)} + c^{(2)}\mu^{(2)} \quad \text{and} \quad \breve{\mu} = \left(\frac{c^{(1)}}{\mu^{(1)}} + \frac{c^{(2)}}{\mu^{(2)}}\right)^{-1} \tag{9.3.7}$$

represent, respectively, the arithmetic and harmonic means of the phase shear moduli, and

$$\overline{\chi} = (c^{(1)}\chi^{(1)} + c^{(2)}\chi^{(2)})\mu_0^{-1} \quad \text{and} \quad \breve{\chi} = \left(\frac{c^{(1)}}{\chi^{(1)}} + \frac{c^{(2)}}{\chi^{(2)}}\right)^{-1}\mu_0^{-1} \tag{9.3.8}$$

represent, respectively the the arithmetic and harmonic means of the phase permeability measures; note that we have included the factor μ_0^{-1} in defining $\overline{\chi}$ and $\breve{\chi}$.

Upon making use of the Cayley-Hamilton Theorem, as well as incompressibility, Eq. (9.3.6) can be written in an alternative form

$$G(\overline{\boldsymbol{F}}, \overline{\mathbf{B}}) = \frac{\breve{\mu}}{2}|\overline{\boldsymbol{F}}\,\mathbf{N}_0|^2 + \frac{\overline{\mu}}{2}\left(|\overline{\boldsymbol{F}}\,\mathbf{M}_0|^2 - 2\right) + \frac{\breve{\chi}}{2}|\overline{\boldsymbol{F}}\,\overline{\mathbf{B}}|^2 + \frac{\widetilde{\mu} + \widetilde{\chi}(\overline{\mathbf{B}}\cdot\mathbf{N}_0)^2}{|\overline{\boldsymbol{F}}\,\mathbf{M}_0|^2}, \tag{9.3.9}$$

where $\widetilde{\mu} = \overline{\mu} - \breve{\mu}$ and $\widetilde{\chi} = \overline{\chi} - \breve{\chi}$. A straightforward calculation then shows that the average Cauchy stress $\overline{\boldsymbol{T}} = \overline{\boldsymbol{S}}\,\overline{\boldsymbol{F}}^T$ is given by

$$\begin{aligned}\overline{\boldsymbol{T}} =& \breve{\mu}\left(\overline{\boldsymbol{F}}\mathbf{N}_0\right)\otimes\left(\overline{\boldsymbol{F}}\mathbf{N}_0\right) + \overline{\mu}\left(\overline{\boldsymbol{F}}\mathbf{M}_0\right)\otimes\left(\overline{\boldsymbol{F}}\mathbf{M}_0\right) + \breve{\chi}\left(\overline{\boldsymbol{F}}\,\overline{\mathbf{B}}\right)\otimes\left(\overline{\boldsymbol{F}}\,\overline{\mathbf{B}}\right) \\ & - \frac{\widetilde{\mu} + \widetilde{\chi}(\overline{\mathbf{B}}\cdot\mathbf{N}_0)^2}{|\overline{\boldsymbol{F}}\mathbf{M}_0|^4}\left(\overline{\boldsymbol{F}}\mathbf{M}_0\right)\otimes\left(\overline{\boldsymbol{F}}\mathbf{M}_0\right) - p\boldsymbol{I},\end{aligned} \tag{9.3.10}$$

where p is an arbitrary hydrostatic pressure. The average magnetic field $\overline{\mathbf{H}}$ in the undeformed configuration is given by

$$\overline{\mathbf{H}} = \breve{\chi}\overline{\boldsymbol{C}}\,\overline{\mathbf{B}} + \frac{(\overline{\chi} - \breve{\chi})(\overline{\mathbf{B}}\cdot\mathbf{N}_0)}{|\overline{\boldsymbol{F}}\mathbf{M}_0|^2}\mathbf{N}_0, \tag{9.3.11}$$

where $\overline{\boldsymbol{C}} = \overline{\boldsymbol{F}}^T\overline{\boldsymbol{F}}$ denotes the right Cauchy-Green tensor. It then follows that average magnetic field $\overline{\mathbf{h}}$ in the current configuration is

$$\overline{\mathbf{h}} = \breve{\chi}\overline{\mathbf{b}} + \frac{(\overline{\chi} - \breve{\chi})(\overline{\mathbf{b}}\cdot(\overline{\boldsymbol{F}}^{-T}\mathbf{N}_0))}{|\overline{\boldsymbol{F}}\mathbf{M}_0|^2}\overline{\boldsymbol{F}}^{-T}\mathbf{N}_0, \tag{9.3.12}$$

which shows that the macroscopic magnetic constitutive response of the laminate will be linear precisely when

$$\overline{\mathbf{b}}\cdot\overline{\boldsymbol{F}}^{-T}\mathbf{N}_0 = (\overline{\mathbf{B}}\cdot\mathbf{N}_0) = 0. \tag{9.3.13}$$

Moreover, keeping in mind the definitions of $\overline{\chi}$ and $\breve{\chi}$ from Eq. (9.3.8), we see that the average magnetization in the current configuration is given by

$$\overline{\mathbf{m}} = \left(\frac{1}{\mu_0} - \breve{\chi}\right)\overline{\mathbf{b}} - \frac{(\overline{\chi} - \breve{\chi})(\overline{\mathbf{b}}\cdot(\overline{\boldsymbol{F}}^{-T}\mathbf{N}_0))}{|\overline{\boldsymbol{F}}\mathbf{M}_0|^2}\overline{\boldsymbol{F}}^{-T}\mathbf{N}_0. \tag{9.3.14}$$

In order to account for the magneto-elastic interactions fully, we also introduce the magnetic torque $\overline{\boldsymbol{\tau}}$, which, as discussed by Galipeau and Ponte Castañeda (2013), can be related to $\overline{\mathbf{m}}\times\overline{\mathbf{b}}$. Keeping in mind the relationsh ip between $\overline{\mathbf{m}}$, $\overline{\mathbf{b}}$. and $\overline{\mathbf{h}}$, we see

that

$$\overline{\boldsymbol{\tau}} = \overline{\mathbf{b}} \times \overline{\mathbf{h}}. \tag{9.3.15}$$

On the other hand, and in connection to the discussion above, we note that the average total Cauchy stress $\overline{\boldsymbol{T}}$ has contributions from both mechanical and magnetic forces. Part of the contribution to $\overline{\boldsymbol{T}}$ comes from a term of the form

$$\overline{\boldsymbol{T}}^{mag} = \overline{\mathbf{b}} \otimes \overline{\mathbf{h}} + \frac{\mu_0}{2}(|\overline{\mathbf{m}}|^2 - |\overline{\mathbf{h}}|^2)\mathbf{I}, \tag{9.3.16}$$

(c.f. Eqs. (9.2.15)-(9.2.16)), which is certainly nonsymmetric. Note then that $\overline{\boldsymbol{\tau}}$ is the axial vector corresponding to the antisymmetric second-order tensor $(\overline{\boldsymbol{T}}^{mag}) - (\overline{\boldsymbol{T}}^{mag})^T$, whereby $\overline{\boldsymbol{\tau}}$ can be thought of as a measure of the asymmetric of $\overline{\boldsymbol{T}}^{mag}$. As the cross product of $\overline{\mathbf{b}}$ and $\overline{\mathbf{h}}$, it is also related to the orientation of $\overline{\mathbf{h}}$ relative of $\overline{\mathbf{b}}$. In the plane-strain setting, the cross product is interpreted as $\mathbf{a} \times \mathbf{b} = a_1 b_2 - a_2 b_1$, with a_i and b_i representing the Cartesian components of $\mathbf{a}$ and $\mathbf{b}$, respectively.

As mentioned earlier ,we will consider only plane-strain loading in the $\mathbf{e}_1 - \mathbf{e}_2$ plane and assume that $\overline{\mathbf{B}}$ is applied in the plane of deformation. In order to describe the deformation gradient $\overline{\boldsymbol{F}}$, we make use of the set of transversely isotropic invariants that were introduced in Chapter 7. Under plane-strain loading, and recalling that each phase is taken to be incompressible, $\overline{\boldsymbol{F}}$ can be described by the invariants $\{\lambda_n, d, \psi\}$. Here

$$\lambda_n = |\overline{\boldsymbol{F}}\mathbf{N}_0|, \tag{9.3.17}$$

correspond to the amount of stretch of a material line element initially aligned with $\mathbf{N}_0$ in the undeformed configuration, while

$$d = |\overline{\boldsymbol{F}}^*\mathbf{N}_0|, \tag{9.3.18}$$

where $\overline{\boldsymbol{F}}^* = (\det \overline{\boldsymbol{F}})\overline{\boldsymbol{F}}^{-T}$ denotes the adjugate of $\overline{\boldsymbol{F}}$. We recall that (Lopez-Pamies and Ponte Castañeda, 2009) the rotation of the layers in a hyperelastic laminate is

controlled by Nanson's relation:

$$\mathbf{n}da = \overline{\boldsymbol{F}}^{*}\mathbf{N}_0 dA. \tag{9.3.19}$$

As such, $\overline{\boldsymbol{F}}^{*}\mathbf{N}_0$ denotes the normal to the layers in the deformed configuration, and $d = |\overline{\boldsymbol{F}}^{*}\mathbf{N}_0|$ corresponds to the local change in area of a material surface element with unit normal $\mathbf{N}_0$ in the undeformed configuration. Finally ψ is given by the relationship

$$\cos(\psi) = \frac{1}{\lambda_n d}(\overline{\boldsymbol{F}}\mathbf{N}_0) \cdot (\overline{\boldsymbol{F}}^{*}\mathbf{N}_0) \tag{9.3.20}$$

whereby ψ is the angles between $\overline{\boldsymbol{F}}\mathbf{N}_0$ and $\overline{\boldsymbol{F}}^{*}\mathbf{N}_0$. By definition, $-\frac{\pi}{2} < \psi < \frac{\pi}{2}$, and upon noting that $(\overline{\boldsymbol{F}}\mathbf{N}_0) \cdot (\overline{\boldsymbol{F}}^{*}\mathbf{N}_0) = \det \overline{\boldsymbol{F}}$, we see that, in the incompressible limit, λ_n, d and ψ must satisfy the incompressibility condition

$$\cos(\psi)\lambda_n d = 1. \tag{9.3.21}$$

For simplicity, we assume that $\mathbf{N}_0$ is aligned with $\mathbf{e}_1$ while $\mathbf{M}_0$ is aligned with $\mathbf{e}_2$. With respect to this choice, we write

$$\overline{\mathbf{B}} = \overline{B}\begin{bmatrix}\cos(\beta)\\ \sin(\beta)\\ 0\end{bmatrix} = \begin{bmatrix}\overline{B}_x\\ \overline{B}_y\\ 0\end{bmatrix}, \tag{9.3.22}$$

where $\overline{B} = |\overline{\mathbf{B}}|$ is the magnitude of the average induction magnetic field, and β is used to describe its orientation in the $\mathbf{e}_1 - \mathbf{e}_2$ plane. Throughout the rest of the paper, we will mostly work with $\overline{B}$ and β, but note that at times, we interchange this with $\overline{B}_x$ and $\overline{B}_y$, mostly for expositional ease. As depicted in Figure 9.1a, we see that, with this choice, $\overline{B}_x$ corresponds to the component of $\overline{\mathbf{B}}$ aligned with $\mathbf{N}_0$, and perpendicular to the layers, while $\overline{B}_y$ corresponds to the component of $\overline{\mathbf{B}}$ aligned with the layers themselves.

Now, upon using the fact that in plane-strain

$$|\overline{\boldsymbol{F}}\,\mathbf{M}_0| = |\overline{\boldsymbol{F}}^*\mathbf{N}_0|, \tag{9.3.23}$$

it follows directly from Eq. (9.3.9) that $\widehat{W}$ can be wriitten in terms of $\lambda_n, d, \psi, \overline{B}_x$ and $\overline{B}_y$ via

$$\widehat{W}(\overline{\boldsymbol{F}}, \overline{\mathbf{B}}) = \widehat{\Psi}(d, \psi, \overline{B}_x, \overline{B}_y) + K(\lambda_n d\cos(\psi)), \tag{9.3.24}$$

where

$$\begin{aligned}\widehat{\Psi}(d, \psi, \overline{B}_x, \overline{B}_y) =& \frac{\breve{\mu} + \breve{\chi}\overline{B}_x^2}{2}\frac{1}{d^2\cos^2(\psi)} + \frac{\overline{\mu} + \breve{\chi}\overline{B}_y^2}{2}d^2 \\ &+ \frac{\widetilde{\mu} + \widetilde{\chi}\overline{B}_x^2}{2}\frac{1}{d^2} + \breve{\chi}\overline{B}_x\overline{B}_y\tan(\psi) - \overline{\mu}.\end{aligned} \tag{9.3.25}$$

Note that one could alternatively write $\widehat{\Psi}$ as a function of, say, $d, \lambda_n, \overline{B}_x$ and $\overline{B}_y$ by making use of the incompressibility condition.

In order to facilitate the discussion to follow, we look now to represent certain quantities in terms of the invariants we have just introduced. To start, we note that the orientation of $\overline{\mathbf{b}}$, relative to $\{\mathbf{e}_1, \mathbf{e}_2\}$, which we denote by the angle $\beta_{\overline{\mathbf{b}}}$, can be written asf

$$\tan(\beta_{\overline{\mathbf{b}}}) = \frac{\tan(\beta)}{\lambda_n^2 + \tan(\beta)\tan(\psi)}, \tag{9.3.26}$$

while the orientation of $\overline{\mathbf{h}}$, as predicted by the principal solution, which we denote by the angle $\beta_{\overline{\mathbf{h}}}$, is given by

$$\tan(\beta_{\overline{\mathbf{h}}}) = \tan(\beta_{\overline{\mathbf{b}}})\left(\frac{\breve{\chi}\tan(\beta) - \widetilde{\chi}\lambda_n^2\cos^2(\psi)\tan(\psi)}{\breve{\chi}\tan(\beta) + \widetilde{\chi}\lambda_n^2\cos^2(\psi)\tan(\beta_{\overline{\mathbf{b}}})}\right). \tag{9.3.27}$$

and is calculated using Eq. (9.3.12). Making use of Eq. (9.3.14), we find that the

principal solution gives an estimate for the torque that can be written as

$$\overline{\tau} = \frac{(\breve{\chi} - \overline{\chi})\overline{B}^2}{2}\left(\lambda_n^2 \cos^2(\beta)\sin(2\psi) + \sin(2\beta)\right) \tag{9.3.28}$$

$$= \frac{(\breve{\chi} - \overline{\chi})\overline{B}^2 \cos^2(\beta)\tan(\psi + \beta_{\overline{\mathbf{b}}})}{d^2}. \tag{9.3.29}$$

Finally, keeping in mind the incompressibility of the material, we record expressions for the two determinate measures of the stress. The first is the normal stress difference, which can be written as

$$\begin{aligned}
\overline{T}_{11} - \overline{T}_{22} &= \breve{\mu}\lambda_n^2 + (\tan^2(\psi) - 1)\lambda_n^{-2}\left(\overline{\mu} - \frac{\widetilde{\mu}}{d^4}\right) + \overline{\tau}\sin(2\psi) + \overline{T}_{11}^{mag} - \overline{T}_{22}^{mag}, \\
\overline{T}_{11}^{mag} - \overline{T}_{22}^{mag} &= \frac{\overline{B}^2 \sin(2\beta)(\cot(\beta_{\overline{\mathbf{b}}})\cot(\beta_{\overline{\mathbf{h}}}) - 1)}{4\lambda_n^2}\left(2\breve{\chi}\tan(\beta) - \widetilde{\chi}\lambda_n^2\sin(2\psi)\right),
\end{aligned} \tag{9.3.30}$$

while the second is the shear stress, which can be written as

$$\begin{aligned}
\overline{T}_{12} &= \frac{\tan(\psi)}{\lambda_n^2}\left(\overline{\mu} - \frac{\widetilde{\mu}}{d^4}\right) - \overline{\tau}\sin^2(\psi) + \overline{T}_{12}^{mag}. \\
\overline{T}_{12}^{mag} &= \frac{\overline{B}^2 \sin(2\beta)\cot(\beta_{\overline{\mathbf{b}}})}{4\lambda_n^2}\left(2\breve{\chi}\tan(\beta) - \widetilde{\chi}\lambda_n^2\sin(2\psi)\right).
\end{aligned} \tag{9.3.31}$$

Before proceeding, and in order to make contact with available results for purely mechanical loading conditions, we recall the alternative plane strain invariants α and γ, proposed by Avazmohammadi and Ponte Castañeda (2016), and used in Chapters 6 and 7. These invariants are related to λ_n, d and ψ via the relations

$$\alpha = \lambda_n, \quad \gamma^2 = d^2\sin^2(\psi) = \frac{\tan^2(\psi)}{\lambda_n^2}, \tag{9.3.32}$$

and the Cartesian components of $\overline{\boldsymbol{F}}$ can be written as

$$[\overline{F}_{ij}] = \begin{bmatrix} \lambda_n & \gamma \\ 0 & \lambda_n^{-1} \end{bmatrix} = \begin{bmatrix} \lambda_n & d\sin(\psi) \\ 0 & \lambda_n^{-1} \end{bmatrix} = \begin{bmatrix} \lambda_n & \lambda_n^{-1}\tan(\psi) \\ 0 & \lambda_n^{-1} \end{bmatrix}. \tag{9.3.33}$$

As such, we see that from Eq. (9.3.33), the amount of rotation of the layers, as measured by $\overline{\boldsymbol{F}}^*\mathbf{N}_0$, is given by $-\psi$. We also record the following expression for the principal solution as written in terms of $\lambda_n, \gamma, \overline{B}_x$ and $\overline{B}_y$ (c.f. Eq. (9.3.25)):

$$\widehat{W}(\overline{\boldsymbol{F}}, \overline{\mathbf{B}}) = \widehat{\Phi}(\lambda_n, \gamma, \overline{B}_x, \overline{B}_y) + K(\det \overline{\boldsymbol{F}}), \tag{9.3.34}$$

where

$$\begin{aligned} \widehat{\Phi}(\lambda_n, \gamma, \overline{B}_x, \overline{B}_y) =& \frac{\breve{\mu} + \breve{\chi}\overline{B}_x^2}{2}\lambda_n^2 + \frac{\overline{\mu} + \breve{\chi}\overline{B}_y^2}{2}(\lambda_n^{-2} + \gamma^2) \\ &+ \frac{\widetilde{\mu} + \widetilde{\chi}\overline{B}_x^2}{2}\frac{1}{\lambda_n^{-2} + \gamma^2} + \breve{\chi}\overline{B}_x\overline{B}_y\lambda_n\gamma - \overline{\mu}. \end{aligned} \tag{9.3.35}$$

To close this section, we look to apply the generalized loss of strong ellipticity condition, as given by Eq. (9.2.20), to the principal solution $\widehat{W}$. The full details are given in Section 9.9. Now, under pure-shear loading ($\psi = 0$), with $\overline{\mathbf{B}} = \mathbf{0}$, as shown in Chapter 6, strong ellipticity is lost precisely when λ_n reaches the critical value of

$$\lambda_{se}^{me} = \left(1 - \frac{\breve{\mu}}{\overline{\mu}}\right)^{-1/4}. \tag{9.3.36}$$

This is exactly the result of Triantafyllidis and Maker (1985). More generally, using the analysis in Section 9.9, it can be shown that under pure-shear loading, the principal solution is strongly elliptic so long as

$$\inf_{\theta} f(\lambda_n, \overline{B}_x, \overline{B}_y, \theta) > 0, \tag{9.3.37}$$

where

$$f(\lambda_n, \overline{B}_x, \overline{B}_y, \theta) = f_2(\overline{B}_x, \overline{B}_y, \theta)\lambda_n^4 + f_1(\overline{B}_x, \overline{B}_y, \theta)\lambda_n^2 + f_0(\overline{B}_x, \overline{B}_y, \theta), \tag{9.3.38}$$

with

$$\begin{aligned} f_2(\overline{B}_x, \overline{B}_y, \theta) &= \breve{\mu}\breve{\chi}\cos^2(\theta) - \overline{\chi}(\widetilde{\mu} + \widetilde{\chi}\overline{B}_x^2)\sin^2(\theta) + \widetilde{\chi}(\overline{\mu} + \overline{\chi}\overline{B}_x)\sin^2(\theta)\cos^2(\theta) \\ &\quad + \widetilde{\mu}\widetilde{\chi}\sin^2(2\theta)\sin^2(\theta) + \breve{\chi}\widetilde{\mu}\sin^2(2\theta), \end{aligned} \tag{9.3.39}$$

$$f_1(\overline{B}_x, \overline{B}_y, \theta) = -\breve{\chi}\widetilde{\chi}\overline{B}_x\overline{B}_y\sin(2\theta)\sin^2(\theta), \tag{9.3.40}$$

$$f_0(\overline{B}_x, \overline{B}_y, \theta) = \overline{\mu}\breve{\chi}\sin^2(\theta) + \widetilde{\chi}(\overline{\mu} + \breve{\chi}\overline{B}_y^2)\sin^4(\theta). \tag{9.3.41}$$

We define λ_{se} to be the smallest value of λ_n for which

$$\inf_{\theta} f(\lambda_{se}, \overline{B}_x, \overline{B}_y, \theta) = 0. \tag{9.3.42}$$

We mention that the angle θ characterizes the vector $\mathbf{n}$ that arises in calculating the strong ellipticity condition (9.2.20). In general, computing λ_{se} must be carried out numerically. However, there are two cases in which λ_{se} can be given explicitly. In particular, when $\overline{B}_y = 0$, we find that Eq. (9.3.37) is first violated when λ_n takes the value

$$\lambda_{se}^x = \lambda_{se}^{me}\left(1 + \frac{(\overline{\chi} - \breve{\chi})\overline{B}_x^2}{(\overline{\mu} - \breve{\mu})}\right)^{-1/4}. \tag{9.3.43}$$

On the other hand, when $\overline{B}_x = 0$, Eq. (9.3.37) is first violated when λ_n takes the value

$$\lambda_{se}^y = \lambda_{se}^{me}\left(1 + \frac{\breve{\chi}(\overline{\chi} - \breve{\chi})\overline{B}_y^2}{\overline{\chi}\,\overline{\mu}}\right)^{1/4}. \tag{9.3.44}$$

Both of these results agree exactly with the expressions found by Rudykh and Bertoldi (2013), and reduce to the λ_{se}^{me} as $\overline{B} \to 0$, as expected.

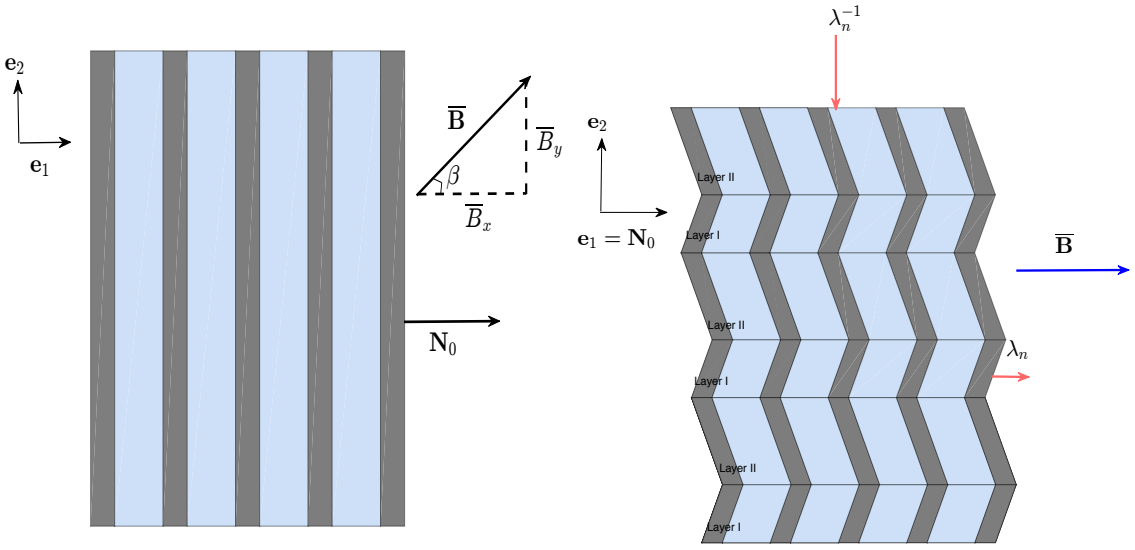

(a) (b)

Figure 9.1: (a) A visualization of the laminated microstructure. (b) A schematic for how the rank-one convex lamination procedure produces the lamellar domains. The construction is depicted for the specific case of pure-shear and a magnetic field perpendicular to the layers, and shows how the composite breaks up into layers to accommodate the deformation.

9.4 Post-bifurcation estimates: Upper and Lower Bounds

In this section, we will apply the methodology proposed Chapter 8 to our two-dimensional sample problem. The procedure is as follows. We first look to calculate the rank-one convexification $R\widehat{W}$ of the principal solution. We do so by making use of the results that states that, upon setting $R_0\widehat{W} = \widehat{W}$, and for every $k \geqslant 0$, defining

$$R_{k+1}\widehat{W}(\overline{\boldsymbol{F}}, \overline{\mathbf{B}}) = \inf \left\{ \begin{array}{c} \lambda R_k\widehat{W}(\boldsymbol{F}_1, \mathbf{B}_1) + (1-\lambda) R_k\widehat{W}(\boldsymbol{F}_2, \mathbf{B}_2) : \\ \overline{\boldsymbol{F}} = \lambda \boldsymbol{F}_1 + (1-\lambda)\boldsymbol{F}_2,\ \overline{\mathbf{B}} = \lambda \mathbf{B}_1 + (1-\lambda)\mathbf{B}_2 \\ \operatorname{rank}\{\boldsymbol{F}_1 - \boldsymbol{F}_2\} \leqslant 1,\ (\mathbf{B}_1 - \mathbf{B}_2) \in \ker\{\boldsymbol{F}_1 - \boldsymbol{F}_2\} \end{array} \right\}, \quad (9.4.1)$$

it follows that

$$R\widehat{W}(\overline{\boldsymbol{F}},\overline{\mathbf{B}}) = \lim_{k\to\infty} R_k\widehat{W}(\overline{\boldsymbol{F}},\overline{\mathbf{B}}) = \inf_k R_k\widehat{W}(\overline{\boldsymbol{F}},\overline{\mathbf{B}}). \tag{9.4.2}$$

It is helpful to spell out the result in more detail by consider the case of $k = 1$. To start, for a fixed $\overline{\boldsymbol{F}}$, we consider $c_1, \boldsymbol{F}_1, \boldsymbol{F}_2, \mathbf{B}_1, \mathbf{B}_2$ which satisfy

$$\overline{\boldsymbol{F}} = (1-c_1)\boldsymbol{F}_1 + c_2\boldsymbol{F}_2, \quad \text{and} \quad \overline{\mathbf{B}} = (1-c_1)\mathbf{B}_1 + c_1\mathbf{B}_2 \tag{9.4.3}$$

as well as

$$\operatorname{rank}(\boldsymbol{F}_1 - \boldsymbol{F}_2) \leqslant 1, \quad \text{and} \quad (\mathbf{B}_1 - \mathbf{B}_2) \in \ker\{\boldsymbol{F}_1 - \boldsymbol{F}_2\}. \tag{9.4.4}$$

Now, Eq. $(9.4.4)_1$ implies that there exist two vectors $\mathbf{a}, \mathbf{N}_1 \in \mathbb{R}^2$, such that

$$\boldsymbol{F}_1 - \boldsymbol{F}_2 = \mathbf{a} \otimes \mathbf{N}_1. \tag{9.4.5}$$

We assume, without loss of generality, that $|\mathbf{N}_1| = 1$, and parametrize $\mathbf{N}_1$ by some angle ϕ_1, so that $\mathbf{N}_1 = [\cos(\phi_1), \sin(\phi_1)]^T$. Therefore, we can use Eq. $(9.4.3)_1$ to write

$$\boldsymbol{F}_1 = \overline{\boldsymbol{F}} - c_1\mathbf{a} \otimes \mathbf{N}_1, \tag{9.4.6}$$

$$\boldsymbol{F}_2 = \overline{\boldsymbol{F}} + (1-c_1)\mathbf{a} \otimes \mathbf{N}_1. \tag{9.4.7}$$

Due to the incompressibility constraint, whereby $\widehat{W}(\overline{\boldsymbol{F}}) = \infty$ if $\det\overline{\boldsymbol{F}} \neq 1$, as first noted by deBotton (2005), we can restrict ourselves to values of $\mathbf{a}$ and $\mathbf{N}_1$ satisfying

$$\begin{aligned} 1 &= \det(\boldsymbol{F}_1) \\ &= \det(\overline{\boldsymbol{F}} - c_1\mathbf{a} \otimes \mathbf{N}_1) \\ &= \det(\overline{\boldsymbol{F}})\det(\boldsymbol{I} - c_1(\overline{\boldsymbol{F}}^{-1}\mathbf{a}) \otimes \mathbf{N}_1) \\ &= 1 - c_1(\overline{\boldsymbol{F}}^{-1}\mathbf{a}) \cdot \mathbf{N}_1. \end{aligned} \tag{9.4.8}$$

Therefore, $(\overline{\boldsymbol{F}}^{-1}\mathbf{a})\cdot\mathbf{N}_1 = 0$. Upon letting $\omega_1^{me} = |\overline{\boldsymbol{F}}^{-1}\mathbf{a}|$, it is clear from the form of $\mathbf{N}_1$ that $\overline{\boldsymbol{F}}^{-1}\mathbf{a} = \omega_1^{me}\mathbf{M}_1$ where $\mathbf{M}_1 = [\sin(\phi_1), -\cos(\phi_1)]^T$. Finally, taking into account Eqs. $(9.4.3)_2$ and $(9.4.4)_2$, it follows that

$$\mathbf{B}_1 = \overline{\mathbf{B}} - c_1\omega_1^{mag}\mathbf{M}_1, \tag{9.4.9}$$

$$\mathbf{B}_2 = \overline{\mathbf{B}} + (1-c_1)\omega_1^{mag}\mathbf{M}_1. \tag{9.4.10}$$

Therefore, at least in two dimensions, $R_1\widehat{W}$ can be obtained from the solution to a four dimensional minimization problem defined by

$$\begin{aligned} R_1\widehat{W}(\overline{\boldsymbol{F}},\overline{\mathbf{B}}) = \inf_{\omega_1^{me},\omega_1^{mag},c_1,\phi_1} \Big\{ &(1-c_1)\widehat{W}(\overline{\boldsymbol{F}}[\boldsymbol{I} - c_1\omega_1^{me}\mathbf{M}_1\otimes\mathbf{N}_1], \overline{\mathbf{B}} - c_1\omega_1^{mag}\mathbf{M}_1) \\ &+c_1\widehat{W}(\overline{\boldsymbol{F}}[\boldsymbol{I} + (1-c_1)\omega_1^{me}\mathbf{M}_1\otimes\mathbf{N}_1], \overline{\mathbf{B}} + (1-c_1)\omega_1^{mag}\mathbf{M}_1)\Big\}, \end{aligned} \tag{9.4.11}$$

Written in this way, we see that Eq. (9.4.11) represents a lamination procedure, in which materials, both of whose properties are determined by $\widehat{W}$, are layered in the direction defined by $\mathbf{N}_1$. For later use, it is helpful to also define

$$\boldsymbol{F}_1^{(I)} = \overline{\boldsymbol{F}}[\boldsymbol{I} - c_1\omega_1^{me}\mathbf{M}_1\otimes\mathbf{N}_1], \quad \boldsymbol{F}_1^{(II)} = \overline{\boldsymbol{F}}[\boldsymbol{I} + (1-c_1)\omega_1^{me}\mathbf{M}_1\otimes\mathbf{N}_1], \tag{9.4.12}$$

$$\mathbf{B}_1^{(I)} = \overline{\mathbf{B}} - c_1\omega_1^{mag}\mathbf{M}_k, \quad \mathbf{B}_1^{(II)} = \overline{\mathbf{B}} + (1-c)\omega_1^{mag}\mathbf{M}_1, \tag{9.4.13}$$

whereby $\boldsymbol{F}_1^{(q)}$ and $\boldsymbol{B}_1^{(q)}$ denote the average deformation gradient and induction magnetic field, respectively, in phase $q\,(q = I, II)$.

The hope is that there exists a K for which $R_k\widehat{W}(\overline{\boldsymbol{F}},\overline{\mathbf{B}})$ is rank-one convex. It would then follow that $R\widehat{W} = R_K\widehat{W}$. Once $R\widehat{W}$ has been calculated, we then aim to prove that it is polyconvex, i.e. that it can be written as a convex function of $\overline{\boldsymbol{F}}$, $\det\overline{\boldsymbol{F}}$, $\overline{\mathbf{B}}$ and $\overline{\boldsymbol{F}}\,\overline{\mathbf{B}}$. Then, due to the result that

$$P\widehat{W} \leqslant Q\widehat{W} \leqslant R\widehat{W}, \tag{9.4.14}$$

and by definition of the various convex envelopes, it will follow that $R\widehat{W} = Q\widehat{W}$.

The method laid out above for computing $Q\widehat{W}$ relies on a major, as yet unstated, assumption: that $R\widehat{W}$ can be computed (semi-)analytically. In order to check for polyconvexity, it is necessary to have some knowledge of how $R\widehat{W}$ depends on $\overline{\boldsymbol{F}}$, $\det \overline{\boldsymbol{F}}$, $\overline{\mathbf{B}}$ and $\overline{\boldsymbol{F}}\,\overline{\mathbf{B}}$. As we will see, due to the added complexity of the coupling between $\overline{\boldsymbol{F}}$ and $\overline{\mathbf{B}}$, it is not possible, in general, to obtain an analytical expression for $R_1\widehat{W}$. While we can still confirm that $R_1\widehat{W}$ is rank-one convex numerically, and hence corresponds to $R\widehat{W}$, without any knowledge of even the general form of $R\widehat{W}$, it becomes untenable to check for polyconvexity. Therefore, we have no way of obtaining an estimate for $P\widehat{W}$ from $R\widehat{W}$. However, if we can find a polyconvex function satisfying $P_L\widehat{W} \leqslant \widehat{W}$, then, by definition of the polyconvex envelope as the supremum over all polyconvex lower bounds on $\widehat{W}$, it follows that $P_L\widehat{W} \leqslant P\widehat{W}$. Combining this with Eq. (9.4.14), we will have

$$P_L\widehat{W} \leqslant Q\widehat{W} \leqslant R\widehat{W}. \tag{9.4.15}$$

As such, the rest of this section will be dedicated to calculating the upper and lower bounds in Eq. (9.4.15). $P_L\widehat{W}$ will be obtained by exploiting the rank-one lamination procedure, while $R\widehat{W}$ will be obtained by using this procedure directly. In what follows, we denote the set of $(\overline{\boldsymbol{F}}, \overline{\mathbf{B}})$ for which $\widehat{W}$ is (strictly) rank-one convex and polyconvex by $\mathcal{S}_{rc}$ and $\mathcal{S}_{pc}$, respectively.

9.4.1 Lower bound on $Q\widehat{W}$ via polyconvexity

Consider the new function defined by

$$\breve{W}(\overline{\boldsymbol{F}}, \overline{\mathbf{B}}) = \widehat{W}(\overline{\boldsymbol{F}}, \overline{\mathbf{B}}) - \frac{\breve{\chi}}{2}|\overline{\boldsymbol{F}}\,\overline{\mathbf{B}}|^2. \tag{9.4.16}$$

It is clear that $|\overline{\boldsymbol{F}}\,\overline{\mathbf{B}}|^2$ is polyconvex, and hence rank-one convex. Therefore, $R_1[|\overline{\boldsymbol{F}}\,\overline{\mathbf{B}}|^2] = R[|\overline{\boldsymbol{F}}\,\overline{\mathbf{B}}|^2] = |\overline{\boldsymbol{F}}\,\overline{\mathbf{B}}|^2$, so that, in evaluating $R_1\widehat{W}$ using Eq. (9.4.11), we

have

$$R_1\breve{W}(\overline{\boldsymbol{F}},\overline{\mathbf{B}})+\frac{\breve{\chi}}{2}|\overline{\boldsymbol{F}}\,\overline{\mathbf{B}}|^2\leqslant R_1\left[\breve{W}(\overline{\boldsymbol{F}},\overline{\mathbf{B}})+\frac{\breve{\chi}}{2}|\overline{\boldsymbol{F}}\,\overline{\mathbf{B}}|^2\right]=R_1\widehat{W}(\overline{\boldsymbol{F}},\overline{\mathbf{B}})\leqslant\widehat{W}(\overline{\boldsymbol{F}},\overline{\mathbf{B}}). \tag{9.4.17}$$

Proceeding *mutatis mutandis*, it then follows that

$$R_k\breve{W}(\overline{\boldsymbol{F}},\overline{\mathbf{B}})+\frac{\breve{\chi}}{2}|\overline{\boldsymbol{F}}\,\overline{\mathbf{B}}|^2\leqslant R_k\widehat{W}(\overline{\boldsymbol{F}},\overline{\mathbf{B}})\leqslant\widehat{W}(\overline{\boldsymbol{F}},\overline{\mathbf{B}}), \tag{9.4.18}$$

from which we may conclude, using Eq. (8.2.37) that

$$R\breve{W}(\overline{\boldsymbol{F}},\overline{\mathbf{B}})+\frac{\breve{\chi}}{2}|\overline{\boldsymbol{F}}\,\overline{\mathbf{B}}|^2\leqslant R\widehat{W}(\overline{\boldsymbol{F}},\overline{\mathbf{B}})\leqslant\widehat{W}(\overline{\boldsymbol{F}},\overline{\mathbf{B}}). \tag{9.4.19}$$

Therefore, if we can show that $R\breve{W}(\overline{\boldsymbol{F}},\overline{\mathbf{B}})$ is polyconvex, then $R\breve{W}(\overline{\boldsymbol{F}},\overline{\mathbf{B}})+\frac{\breve{\chi}}{2}|\overline{\boldsymbol{F}}\,\overline{\mathbf{B}}|^2$, as the sum of two polyconvex functions, will be polyconvex, less than or equal to $\widehat{W}$, and hence will correspond to our polyconvex lower bound

$$P_L\widehat{W}(\overline{\boldsymbol{F}},\overline{\mathbf{B}})=R\breve{W}(\overline{\boldsymbol{F}},\overline{\mathbf{B}})+\frac{\breve{\chi}}{2}|\overline{\boldsymbol{F}}\,\overline{\mathbf{B}}|^2\leqslant P\widehat{W}\leqslant Q\widehat{W} \tag{9.4.20}$$

As such, we look to apply the rank-one convexification procedure to $\breve{W}$. The stationary conditions corresponding to the infimum in Eq. (9.4.11), as applied to $\breve{W}$, can be solved for explicitly, and yield

$$\phi_1=\frac{\pi}{2},\quad c_1=\frac{1}{2}\left(1-\frac{d\sin(\psi)}{\sqrt{(\lambda^x_{se})^{-2}-\lambda_n^{-2}}}\right),\quad \omega_1^{me}=\frac{2\sqrt{(\lambda^x_{se})^{-2}-\lambda_n^{-2}}}{\lambda_n},\quad \omega_1^{mag}=0, \tag{9.4.21}$$

where λ^x_{se} is given by Eq. (9.3.43). With Eq. (9.4.21), we find that

$$R_1\breve{W}(\overline{\boldsymbol{F}},\overline{\mathbf{B}})=h(\overline{\boldsymbol{F}},\overline{\mathbf{B}},\overline{\boldsymbol{F}}\,\overline{\mathbf{B}})+K(\det\boldsymbol{F}) \tag{9.4.22}$$

where

$$h(\overline{\boldsymbol{F}},\overline{\mathbf{B}},\overline{\boldsymbol{F}}\,\overline{\mathbf{B}}) = \begin{cases} \frac{\breve{\mu}}{2}|\overline{\boldsymbol{F}}\mathbf{N}_0|^2 + \frac{\overline{\mu}}{2}\left(|\overline{\boldsymbol{F}}\mathbf{M}_0|^2 - 2\right) + \frac{\widetilde{\mu}+\widetilde{\chi}\overline{B}_x^2}{2}\frac{1}{|\overline{\boldsymbol{F}}\mathbf{M}_0|^2} & \text{when } (\overline{\boldsymbol{F}},\overline{\mathbf{B}}) \in \mathcal{S}_{pcl} \\ \frac{\breve{\mu}}{2}|\overline{\boldsymbol{F}}\mathbf{N}_0|^2 + \overline{\mu}\left(\sqrt{\frac{(\widetilde{\mu}+\widetilde{\chi}\overline{B}_x^2)}{\overline{\mu}}} - 1\right) & \text{when } (\overline{\boldsymbol{F}},\overline{\mathbf{B}}) \in \mathcal{S}_{pcl}^c \end{cases}, \tag{9.4.23}$$

and where

$$\mathcal{S}_{pcl} = \left\{(d,\overline{B}_x) \,:\, d > (\lambda_{se}^x)^{-1}\right\}. \tag{9.4.24}$$

Therefore, $\mathcal{S}_{pcl}$ is independent of λ_n, ψ and $\overline{B}_y$. Note that we have suppressed the dependence of λ_{se}^x on $\overline{B}_x$ for compositional ease. It is interesting to note that when $\overline{\mathbf{B}} = \mathbf{0}$, $P_L\widehat{W}$ is precisely the quasiconvexification of the principal solution in the purely mechanical case, as found in Chapter 6.

While we can check directly whether $R_1\widetilde{W}$ is rank-one convex, since polyconvexity implies rank-one convexity, it suffices to check if it is polyconvex. Moreover, if $R_1\widetilde{W}$ turns out to be polyconvex, then we can simultaneous conclude that $R_1\widetilde{W} = R\widetilde{W} = P\widetilde{W}$. Now, it is clear that $K(\det\overline{\boldsymbol{F}})$ is convex in $\det\overline{\boldsymbol{F}}$, so checking whether $R_1\widetilde{W}$ is polyconvex amounts to checking whether h is polyconvex. To do this we calculate the generalized Hessian of h, given by

$$D^2h = \begin{bmatrix} h_{\overline{\boldsymbol{F}},\overline{\boldsymbol{F}}} & h_{\overline{\boldsymbol{F}},\overline{\mathbf{B}}} & h_{\overline{\boldsymbol{F}},\overline{\boldsymbol{F}}\,\overline{\mathbf{B}}} \\ h_{\overline{\mathbf{B}},\overline{\boldsymbol{F}}} & h_{\overline{\mathbf{B}},\overline{\mathbf{B}}} & h_{\overline{\mathbf{B}},\overline{\boldsymbol{F}}\,\overline{\mathbf{B}}} \\ h_{\overline{\boldsymbol{F}}\,\overline{\mathbf{B}},\overline{\boldsymbol{F}}} & h_{\overline{\boldsymbol{F}}\,\overline{\mathbf{B}},\overline{\mathbf{B}}} & h_{\overline{\boldsymbol{F}}\,\overline{\mathbf{B}},\overline{\boldsymbol{F}}\,\overline{\mathbf{B}}} \end{bmatrix}, \tag{9.4.25}$$

and check that it is positive semi-definite; here $h_{(\cdot)} = \frac{\partial h}{\partial(\cdot)}$. For any second order tensor $\boldsymbol{A}$, and any first order tensors $\mathbf{a}$ and $\mathbf{b}$, we let $\mathbf{p} = \begin{bmatrix}\boldsymbol{A} & \mathbf{a} & \mathbf{b}\end{bmatrix}^T$, so that, with a slight abuse of notation, the positive semi-definiteness of D^2h is equivalent to showing that the inequality

$$\mathbf{p}\cdot[D^2h]\mathbf{p} \geqslant 0 \tag{9.4.26}$$

holds. By making use of the calculation carried out in Section 9.8, we find that

$$\begin{aligned}\mathbf{p}\cdot[D^2h]\mathbf{p} = {}& \breve{\mu}|\boldsymbol{A}\mathbf{N}_0|^2 + \frac{4(\overline{\mu}-\breve{\mu})}{d^6}[(\overline{\boldsymbol{F}}\mathbf{M}_0)\cdot(\boldsymbol{A}\mathbf{M}_0)]^2 \\ & + \frac{(\overline{\chi}-\breve{\chi})}{d^2}\left[(\mathbf{a}\cdot\mathbf{N}_0)d^2 - 2[(\overline{\boldsymbol{F}}\mathbf{M}_0)\cdot(\boldsymbol{A}\mathbf{M}_0)](\overline{\mathbf{B}}\cdot\mathbf{N}_0)\right]^2 \\ & + \overline{\mu}\left[1-(\lambda^x_{se}d)^{-4}\right]|\boldsymbol{A}\mathbf{M}_0|^2, \end{aligned} \tag{9.4.27}$$

when $(\overline{\boldsymbol{F}},\overline{\mathbf{B}}) \in \mathcal{S}_{pcl}$, and

$$\mathbf{p}\cdot[D^2h]\mathbf{p} = \breve{\mu}|\boldsymbol{A}\mathbf{N}_0|^2 + (\overline{\chi}-\breve{\chi})(\lambda^x_{se})^6(\mathbf{a}\cdot\mathbf{N}_0)^2 \tag{9.4.28}$$

when $(\overline{\boldsymbol{F}},\overline{\mathbf{B}}) \in \mathcal{S}^c_{pcl}$. Positive semi-definiteness of D^2h is clear in the latter case, while in the former, all terms except the last in Eq. (9.4.27) are nonnegative for all $(\overline{\boldsymbol{F}},\overline{\mathbf{B}})$. However, $[1-(\lambda^x_{se}d)^{-4}]$ is also nonnegative so long as $(\overline{\boldsymbol{F}},\overline{\mathbf{B}}) \in \mathcal{S}_{pcl}$, and hence, D^2h is positive definite in both $\mathcal{S}_{pcl}$ and $\mathcal{S}^c_{pcl}$, from which we can conclude that $R_1\breve{W}$ is polyconvex.

9.4.2 Upper bound on $Q\widehat{W}$ via $R\widehat{W}$

We now look to compute $R\widehat{W}$ directly, which, like above, we do by starting with $R_1\widehat{W}$. Now, in general, we can write

$$R_1\widehat{W}(\overline{\boldsymbol{F}},\overline{\mathbf{B}}) = \begin{cases} \widehat{W}(\overline{\boldsymbol{F}},\overline{\mathbf{B}}) & \text{when } (\overline{\boldsymbol{F}},\overline{\mathbf{B}}) \in \mathcal{S}_{rc}, \\ \overline{W}(\overline{\boldsymbol{F}},\overline{\mathbf{B}}) & \text{when } (\overline{\boldsymbol{F}},\overline{\mathbf{B}}) \in \mathcal{S}^c_{rc}, \end{cases} \tag{9.4.29}$$

where

$$\overline{W}(\overline{\boldsymbol{F}},\overline{\mathbf{B}}) = (1-c_1)\widehat{W}(\boldsymbol{F}_1^{(I)},\mathbf{B}_1^{(I)}) + c_1\widehat{W}(\boldsymbol{F}_1^{(II)},\mathbf{B}_1^{(II)}), \tag{9.4.30}$$

and where $\boldsymbol{F}_1^{(q)}$ and $\mathbf{B}_1^{(q)}$, for $q = I, II$, as defined by Eqs. (9.4.12)-(9.4.13), are determined from the stationary conditions associated with Eq. (9.4.11). It is interesting

to note that if we let

$$\boldsymbol{S}_1^{(q)} = \frac{\partial \widehat{W}(\boldsymbol{F}_1^{(q)}, \mathbf{B}_1^{(q)})}{\partial \overline{\boldsymbol{F}}}, \quad \mathbf{H}_1^{(q)} = \frac{\partial \widehat{W}(\boldsymbol{F}_1^{(q)}, \mathbf{B}_1^{(q)})}{\partial \overline{\mathbf{B}}}, \tag{9.4.31}$$

for $q = I, II$, the stationary condition with respect to ω_1^{me} reads

$$c_1(1-c_1)[\overline{\boldsymbol{F}}\mathbf{M}_1] \cdot [(\boldsymbol{S}_1^{(II)} - \boldsymbol{S}_1^{(I)})\mathbf{N}_1] = 0 \tag{9.4.32}$$

while the stationary condition with respect to ω_1^{mag} reads

$$c_1(1-c_1)(\mathbf{H}_1^{(II)} - \mathbf{H}_1^{(I)}) \cdot \mathbf{M}_1 = 0 \tag{9.4.33}$$

As $\mathbf{N}_1$ represents the normal to a material interphase (between phases I and II), we note that the stationary conditions with respect to ω_1^{me} and ω_1^{mag} are nothing more than the jump conditions for the tractions and true magnetic field across the interphase, respectively. Upon differentiating $R_1\widehat{W}$ with respect to either $\overline{\boldsymbol{F}}$ or $\overline{\mathbf{B}}$, and using again the stationary conditions, we find that the average first Piola-Kirchoff stress of the rank-one lamination $R_1\widehat{W}$ is given by

$$\begin{aligned}\overline{\boldsymbol{S}}_1 &= \frac{\partial R_1\widehat{W}(\overline{\boldsymbol{F}}, \overline{\mathbf{B}})}{\partial \overline{\boldsymbol{F}}} \\ &= (1-c_1)\boldsymbol{S}_1^{(I)} + c_1\boldsymbol{S}_1^{(II)} + c_1(1-c_1)\omega_1^{me}[(\boldsymbol{S}_1^{(II)} - \boldsymbol{S}_1^{(I)})\mathbf{N}_1] \otimes \mathbf{M}_1 - p\overline{\boldsymbol{F}}^{-T},\end{aligned} \tag{9.4.34}$$

while the average true magnetic field (in the reference configuration) of the rank-one lamination $R_1\widehat{W}$ is given by

$$\overline{\mathbf{H}}_1 = \frac{\partial R_1\widehat{W}(\overline{\boldsymbol{F}}, \overline{\mathbf{B}})}{\partial \overline{B}} = (1-c_1)\mathbf{H}_1^{(I)} + c_1\mathbf{H}_1^{(II)}. \tag{9.4.35}$$

As mentioned earlier, explicit analytical expressions for $R_1\widehat{W}$ are not available in most cases. In fact, $R_1\widehat{W}$ can be evaluated analytically only when $\overline{\mathbf{B}} = \overline{B}_x\mathbf{N}_0$, in

which case

$$R_1\widehat{W}(\overline{\boldsymbol{F}}, \overline{B}_x\mathbf{N}_0) = P_L\widehat{W}(\overline{\boldsymbol{F}}, \overline{B}_x\mathbf{N}_0). \tag{9.4.36}$$

Therefore, we can conclude that

$$R_1\widehat{W}(\overline{\boldsymbol{F}}, \overline{B}_x\mathbf{N}_0) = R\widehat{W}(\overline{\boldsymbol{F}}, \overline{B}_x\mathbf{N}_0) = Q\widehat{W}(\overline{\boldsymbol{F}}, \overline{B}_x\mathbf{N}_0). \tag{9.4.37}$$

In all other cases, we still need to check whether $R_1\widehat{W}$ is rank-one convex in order to determine whether or not $R_1\widehat{W} = R\widehat{W}$. This can certainly be done by checking the generalized loss of ellipticity condition on $R_1\widehat{W}$ as outlined in Section 9.2. However, this would require taking two derivatives of $R_1\widehat{W}$. Such computations can be done numerically, but the results are unreliable due in large part to the sensitivity in determining the optimal values for $\phi_1, c_1, \omega_1^{me}$, and ω_1^{mag}.

The method by which we will check rank-one convexity exploits the fact that once $\phi_1, c_1, \omega_1^{me}$, and ω_1^{mag} are determined, expressions for the first derivatives of $R_1\widehat{W}$ are readily available via Eqs. (9.4.34) and (9.4.35). Upon taking into account plane strain and incompressibility conditions, we first define $\mathbf{N} = [\cos(\theta), \sin(\theta)]^T$, $\mathbf{M} = [\sin(\theta), -\cos(\theta)]^T$, and

$$\begin{aligned} g(\overline{\boldsymbol{F}}, \overline{\mathbf{B}}, t, s, \theta) = {} & R_1\widehat{W}(\overline{\boldsymbol{F}}\left[\boldsymbol{I} + t\mathbf{M}\otimes\mathbf{N}\right], \overline{\mathbf{B}} + s\mathbf{M}) - R_1\widehat{W}(\overline{\boldsymbol{F}}, \overline{\mathbf{B}}) \\ & - t\left(\overline{\boldsymbol{F}}\mathbf{M}\right)\cdot\left(\frac{\partial R_1\widehat{W}(\overline{\boldsymbol{F}}, \overline{\mathbf{B}})}{\partial\overline{\boldsymbol{F}}}\mathbf{N}\right) - s\frac{\partial R_1\widehat{W}(\overline{\boldsymbol{F}}, \overline{\mathbf{B}})}{\partial\overline{\mathbf{B}}}\mathbf{M}. \end{aligned} \tag{9.4.38}$$

Then, by making use of a result proven in Chapter 8, it follows that $R_1\widehat{W}$ is rank-one convex if and only if

$$\inf_{t,s,\theta} g(\overline{\boldsymbol{F}}, \overline{\mathbf{B}}, t, s, \theta) = 0, \text{ for all } \overline{\boldsymbol{F}} \text{ and } \overline{\mathbf{B}}. \tag{9.4.39}$$

Since $\widehat{W}$ is already known to be rank-one convex in $\mathcal{S}_{rc}$, we can restrict our attention to $(\overline{\boldsymbol{F}}, \overline{\mathbf{B}}) \in \mathcal{S}_{rc}^c$. Therefore, in checking whether $R_1\widehat{W}$ is rank-one convex,

we start by fixing $(\overline{\boldsymbol{F}}, \overline{\mathbf{B}}) \in \mathcal{S}_{rc}^{c}$, and calculate the optimal values of $\varphi_1, c_1, \omega_1^{me}$, and ω_1^{mag} that determine both $R_1\widehat{W}(\overline{\boldsymbol{F}}, \overline{\mathbf{B}})$, as well as its derivatives. It then remains to check that $g \geqslant 0$ for every value of t, s, θ. As such, one must also calculate $R_1\widehat{W}$ at $(\overline{\boldsymbol{F}}\left[\boldsymbol{I} + t\mathbf{M}\otimes\mathbf{N}\right], \overline{\mathbf{B}} + s\mathbf{M})$ for every value of t, s, θ, which, due to the sensitivity of the numerical scheme in determining $\phi_1, c_1, \omega_1^{me}$, and ω_1^{mag}, and the large parameter space, proves to be a painstaking process. However, we can greatly reduce the range of values of t, s and θ we need to check by making use of the lower bound obtained in the previous subsection. In particular, upon defining

$$\begin{aligned} g_L(\overline{\boldsymbol{F}}, \overline{\mathbf{B}}, t, s, \theta) = P_L\widehat{W}(\overline{\boldsymbol{F}}\left[\boldsymbol{I} + t\mathbf{M}\otimes\mathbf{N}\right], \overline{\mathbf{B}} + s\mathbf{M}) - R_1\widehat{W}(\overline{\boldsymbol{F}}, \overline{\mathbf{B}}) \\ - t\left(\overline{\boldsymbol{F}}\mathbf{M}\right)\cdot\left(\frac{\partial R_1\widehat{W}(\overline{\boldsymbol{F}}, \overline{\mathbf{B}})}{\partial \boldsymbol{F}}\mathbf{N}\right) - s\frac{\partial R_1\widehat{W}(\overline{\boldsymbol{F}}, \overline{\mathbf{B}})}{\partial \overline{\mathbf{B}}}\mathbf{M}, \end{aligned} \tag{9.4.40}$$

we see that $g \geqslant g_L$ for every $(\overline{\boldsymbol{F}}, \overline{\mathbf{B}}, t, s, \theta)$. Since $P_L\widehat{W}$ is known analytically we only need to calculate numerically the associated values of $\phi_1, c_1, \omega_1^{me}$, and ω_1^{mag} in order to determine g_L. Then, if $g_L \geqslant 0$, $R_1\widehat{W}$ will be rank-one convex, and we can restrict our attention to checking that $g \geqslant 0$, which is more computationally challenging, only for those values of t, s and θ for which g_L fails to be positive. In doing so, we find that g_L remains positive for large values of t and s, and it is only for smaller values that we must rely on g to check rank-one convexity. In fact, we find that when $s = t = 0$, $g = 0$ and for all other values, $g > 0$. Therefore, we conclude that $R_1\widehat{W}$ is rank-one convex, and hence $R_1\widehat{W} = R\widehat{W}$.

9.5 Further results for the relaxation bounds

Using the results from Section 9.4.1 and Section 9.4.2, we have

$$P_L\widehat{W}(\overline{\boldsymbol{F}}, \overline{\mathbf{B}}) \leqslant Q\widehat{W}(\overline{\boldsymbol{F}}, \overline{\mathbf{B}}) \leqslant R\widehat{W}(\overline{\boldsymbol{F}}, \overline{\mathbf{B}}). \tag{9.5.1}$$

We now look to use these bounds to characterize $Q\widehat{W}$. This, in part, will involve studying the stability of the laminate; we will compare predictions for the onset of instabilities as indicated by loss of strict rank-one convexity, loss of strong ellipticity, as well as the predictions associated with $P_L\widehat{W}$. We also look to investigate the behavior of $Q\widehat{W}$ directly, and see how tight of a bound Eq. (9.5.1) provides. Before proceeding, we note that that all results in the remainder of this work will be calculated for a fixed value of shear contrast ratio of $\mu^{(2)}/\mu^{(1)} = 10$, fixed volume fraction $c = 0.3$ and a permeability contrast ratio of $\chi^{(2)}/\chi^{(1)} = .2$ With the former two values, we note that $\lambda_{se}^{me} \approx 1.1225$.

9.5.1 Phase Diagrams

As discussed earlier, we expect that loss of strict-rank one convexity will gives a better estimate for stability than the use of the generalized strong ellipticity condition. To confirm this, we look to characterize the set $\mathcal{S}_{rc}$. We do so by computing the smallest values of $d = d_{rc}$ for which the infimum in Eq. (9.4.11) is identically $\widehat{W}$. Generally, one can define $\mathcal{S}_{rc}$ as a function of $(d, \psi, \overline{B}_x, \overline{B}_y)$, or equivalently as a function of $(d, \psi, \overline{B}, \beta)$; recall that once d and ψ are given, then λ_n is calculated by making use of the incompressibility condition $d\lambda_n \cos(\psi) = 1$. When $\beta = 0$, then $\mathcal{S}_{rc}$ can be written explicitly in terms of only d and $\overline{B}_x = \overline{B}$ via

$$\mathcal{S}_{rc}|_{\overline{\mathbf{B}}=\overline{B}_x\mathbf{N}_0} = \left\{(d, \overline{B}) \,:\, d > (\lambda_{se}^x)^{-1}\right\}, \tag{9.5.2}$$

where the dependence of λ_{se}^x on $\overline{B}$ has been suppressed. This result is similar to what was found in the purely mechanical context in Chapters 6 and 7. When $\beta \neq 0$, we find that $\mathcal{S}_{rc}$ depends on $d, \psi, \overline{B}$ and β. In what follows, we look to compute d_{rc} for various values of $\psi, \overline{B}$ and β, and compare them with d_{se}, the value of d for which the principal solution first loses strong ellipticity. For this discussion, the dependence of d_{rc} and d_{se} on $\overline{\mathbf{B}}$ will we characterized in terms of $\overline{B}$ and β, and, for fixed values of

β, we will present a "phase diagram" in the $\overline{B} - d$ plane that will indicate the stable and unstable regions, as predicted by loss of strict rank-one convexity. For loading conditions located in the stable regions, $R\widehat{W} = \widehat{W}$, whereby no domain formation occurs.

In representing the critical values of $d, \psi, \overline{B}$ and β for which strict rank-one convexity (or strong ellipticity) is lost, we choose to write d_{rc} (or d_{se}) as a function of $(\psi, \overline{B}, \beta)$ in order to make contact with available results in purely mechanical context. However, in general the conditions for loss of strict rank-one convexity (or strong ellipticity) can be thought of as conditions that are satisfied by $d, \psi, \overline{B}$ and β, simultaneously.

In general, $d_{rc}(\psi, \overline{B}, \beta) \neq d_{rc}(-\psi, \overline{B}, \beta)$, and equality holds only when $\beta = 0$ or $\frac{\pi}{2}$. This is due to the fact that $\widehat{\Psi}(d, \psi, \overline{B}, 0)$ and $\widehat{\Psi}(d, \psi, \overline{B}, \frac{\pi}{2})$ are even functions in d, where we recall that $\widehat{\Psi}$ is defined by Eq. (9.3.25). We also recall that (see Chapter 6)

$$d_{rc}^{me} \equiv d_{rc}(\psi, 0, 0) = (\lambda_{se}^{me})^{-1}. \tag{9.5.3}$$

Hence, the condition $d_{rc} < d_{rc}^{me}$ implies that the composite is stabilized by the presence of the magnetic field: a larger compressive load along the layers is needed to induce a macroscopic instability than in the absence of the magnetic field (recall that $d \sim \lambda_n^{-1}$).

Figure 9.2 presents phase-diagrams in the $\overline{B} - d$ plane, for various values of β. In particular, the values of β used in Figure 9.2a-Figure 9.2d are $0, \frac{\pi}{6}, \frac{\pi}{3}$ and $\frac{\pi}{2}$, respectively. The solid black curves represent values for which (strict) rank-one convexity is lost, and the dashed black curves, representing values for which strong ellipticity is lost, are included for comparison. Stable regions are also indicated by lighter shades of gray.

When $\psi = 0$, $d = \lambda_n^{-1}$ and therefore we define

$$\lambda_{rc} = \lambda_{rc}(\overline{B}, \beta) \equiv (d_{rc}(0, \overline{B}, \beta))^{-1} \tag{9.5.4}$$

as the value of λ_n for which $\widehat{W}$ first loses strict rank-one convexity under pure-shear loading; λ_{rc} will also depend on the microstructure through the volume fraction c and the anisotropy ratios $\mu^{(2)}/\mu^{(1)}$ and $\chi^{(2)}/\chi^{(1)}$, and λ_{se} is defined similarly. In comparing results for pure-shear loading we find that

$$\lambda_{se}^{x} \leqslant \lambda_{rc}(\overline{B},\beta) \leqslant \lambda_{se}(\overline{B},\beta) \leqslant \lambda_{se}^{y}. \tag{9.5.5}$$

All of these values converge to λ_{se}^{me} in the limit as $\overline{B} \to 0$, and for $\overline{B} \neq 0$, equality between λ_{rc} and λ_{se} holds only when $\beta = 0$ (in which case both equal λ_{se}^{x} as given by Eq. (9.3.43)) or when $\beta = \frac{\pi}{2}$ (in which case both equal λ_{se}^{y} as given by Eq. (9.3.44)). Therefore, even in pure-shear loading, when $\overline{\mathbf{B}}$ is neither aligned with nor perpendicular to the layers, strict rank-one convexity is lost prior to strong ellipticity; this was not so in the purely mechanical case.

For more general plane strain loading, we start by noticing that, as depicted in Figure 9.2a, and consistent with our findings, when $\beta = 0$, the value of d_{rc} is independent of ψ, and the laminate remains stable so long as d is located above the curve $d = (\lambda_{se}^{x})^{-1}$. Moreover, we find that $d_{rc}(\psi,\overline{B},0) > d_{se}(\psi,\overline{B},0)$ for any $\psi \neq 0$. Therefore, just as in the purely mechanical context (see Chapters 6 and 7), strict rank-one convexity is lost prior to strong ellipticity. In fact, the discrepancy between the two increases with increasing ψ. This trend is seen throughout Figure 9.2. Note also that $d_{rc}(\psi,\overline{B},0) > d_{rc}(\psi,0,0) = d_{rc}^{me}$ for every value of ψ. Hence, a magnetic field perpendicular to the layers will always have a destabilizing effect. This point will be discussed further in the next section

When $\beta \neq 0$, d_{rc} has an explicit dependence on ψ which we capture by plotting curves for various values of ψ for which strict rank-one convexity is lost. Therefore, in Figure 9.2b-Figure 9.2d, upon fixing ψ, the laminate is stable so long as d lies above curve corresponding to that value of ψ. We have indicated stable regions for different values of ψ using various lighter shades of gray, while the dark gray region always corresponds to unstable loading conditions. Note that the dependence of d_{rc} on ψ

increases as β increases. In Figure 9.2b, such a dependence is barely noticeable, and we again find that $d_{se}\left(\psi, \overline{B}, \frac{\pi}{6}\right) < d_{rc}\left(\psi, \overline{B}, \frac{\pi}{6}\right)$, whereby (strict) rank-one convexity is lost prior to strong ellipticity. Similar to what was seen when $\overline{\mathbf{B}}$ is perpendicular to the layers, the magnetic field with $\beta = \frac{\pi}{6}$ has a destabilizing effect on the laminate. Also, it is interesting to note that while $d_{rc}(\psi, \cdot, \frac{\pi}{6})$ monotonically increases, $d_{se}(\psi, \cdot, \frac{\pi}{6})$ does not. In Figure 9.2c, we find that the laminate is still destabilized by the presence of the magnetic field, however, the effect is less so. In fact, we find that, in general, $d_{rc}(\psi, \overline{B}, \cdot)$ is a decreasing function, and that there is a certain value of β^* for which $d_{rc}(\psi, \overline{B}, \beta) < d_{rc}^{me}$, $\forall \beta > \beta^*$, whereby the magnetic field can stabilize the laminate. Such a value of β^* will depend on the microstructural parameters as well as ψ and $\overline{B}$. In Figure 9.2c, we also begin to see the role that ψ plays on stability. In particular, it is seen that $d_{rc}(\cdot, \overline{B}, \beta)$ is a decreasing function, whereby rotating the layers tends to stabilize the laminate. This trend is best seen in Figure 9.2d. Moreover, we find that $d_{rc}\left(\psi, \overline{B}, \frac{\pi}{2}\right) < d_{rc}^{me}$ for all values of ψ, whereby a magnetic field aligned with the layers stabilizes the laminate.

With a better understanding of how $\mathcal{S}_{rc}$ behaves, we now look to compare $\mathcal{S}_{rc}$ and $\mathcal{S}_{pcl}$. In addition to providing a second estimate for stability, this comparison will also give us an initial indication as to how tight the bound is. As we saw above, $\mathcal{S}_{pcl}$ can be written completely in terms of d and $\overline{B}_x = \overline{B}\cos(\beta)$ via Eq. (9.4.24). Moreover, $P_L\widehat{W}(\overline{\boldsymbol{F}}, \overline{B}\mathbf{N}_0) = R\widehat{W}(\overline{\boldsymbol{F}}, \overline{B}\mathbf{N}_0)$, from which we can conclude that $Q\widehat{W}(\overline{\boldsymbol{F}}, \overline{B}\mathbf{N}_0) = R\widehat{W}(\overline{\boldsymbol{F}}, \overline{B}\mathbf{N}_0)$. Therefore, as we see in Figure 9.3a, the phase diagram for $P_L\widehat{W}$ in this case is identical to that of $R\widehat{W}$.

To see how $\mathcal{S}_{rc}$ and $\mathcal{S}_{pcl}$ compare for $\beta \neq 0$, we present in Figure 9.3b-Figure 9.3d the phase diagrams of $R\widehat{W}$ and $P_L\widehat{W}$ in the $\overline{B} - d$ plane. Results are presented for $\beta = \frac{\pi}{6}, \frac{\pi}{3}$ and $\frac{\pi}{2}$ in Figure 9.3b, Figure 9.3c and Figure 9.3d, respectively. As in Figure 9.2, when $\beta \neq 0$, d_{rc} depends on ψ, and we recall that, for a fixed value of ψ, the laminate is stable, and no domain formation is required, so long as $d > d_{rc}$. On the other hand $\mathcal{S}_{pcl}$ is independent of ψ, and hence there is only one curve for a given

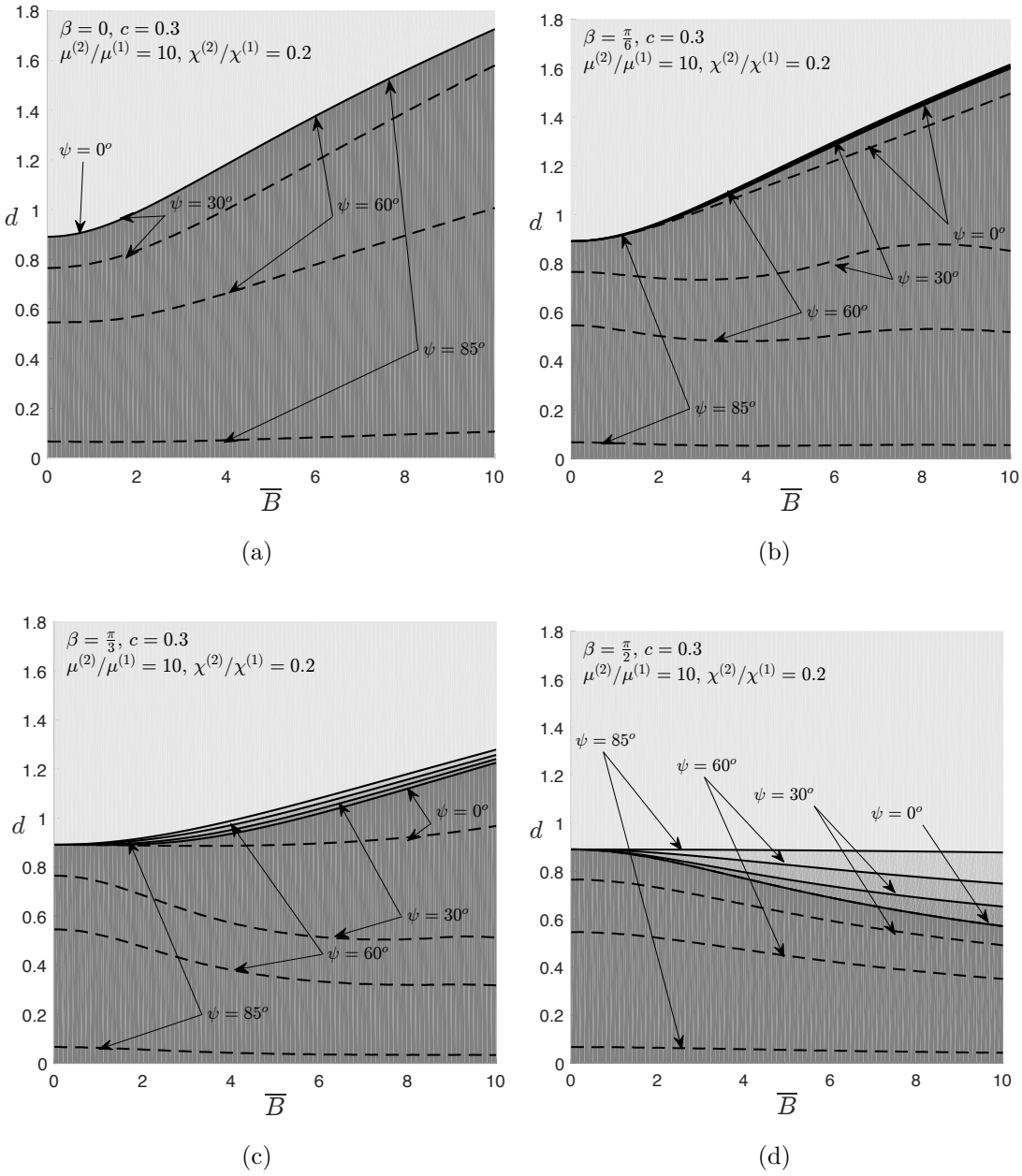

Figure 9.2: Phase diagrams for $\widehat{W}$ in the $\overline{B} - d$ plane, depicting regions of stability as indicated by loss of strict rank-one convexity. The phase diagrams are presented for fixed values of β equal to (a) 0, (b) $\frac{\pi}{6}$, (c) $\frac{\pi}{3}$, and (d) $\frac{\pi}{2}$. Values of d_{se}, depicted by the dashed curves, are included as well. In Figure 9.2b-Figure 9.2d, curves corresponding to values of d_{rc} for fixed ψ are shown. Regions where the principal solution remains strictly rank-one convex are located above such curves. Results are depicted for a fixed shear contrast ratio of $\mu^{(2)}/\mu^{(1)} = 10$, fixed volume fraction $c = 0.3$ and a permeability contrast ratio of $\chi^{(2)}/\chi^{(1)} = .2$.

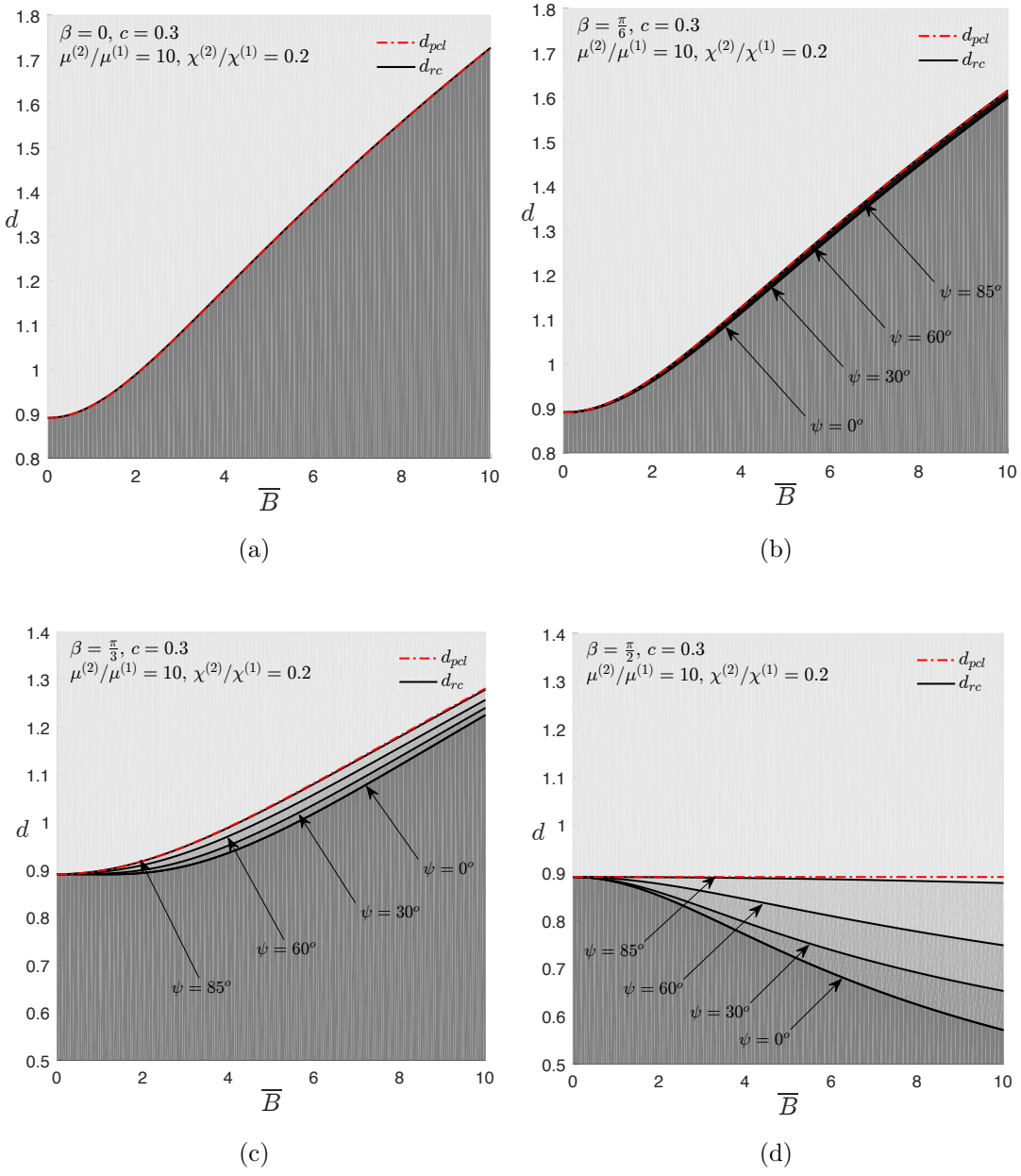

Figure 9.3: Phase diagrams for $\widehat{W}$ in the $\overline{B} - d$ plane, depicting regions of stability as indicated by loss of strict rank-one convexity. The phase diagrams are presented for fixed values of β equal to (a) 0, (b) $\frac{\pi}{6}$, (c) $\frac{\pi}{3}$, and (b) $\frac{\pi}{2}$. Values of d_{pcl}, depicted by the red dashed-dot curves are included as well. Results are depicted for a fixed shear contrast ratio of $\mu^{(2)}/\mu^{(1)} = 10$, fixed volume fraction $c = 0.3$ and a permeability contrast ratio of $\chi^{(2)}/\chi^{(1)} = .2$.

value of β; when $d < d_{pcl}$, $P_L\widehat{W} = \widehat{W}$. As we see, for $\beta \neq 0$, $d_{rc} < d_{pcl}$ for all values of ψ. However, as depicted in Figure 9.3b, the difference between d_{rc} and d_{pcl} is small when β is small. As β increases, d_{rc} and d_{pcl} begin to differ more drastically, due to the fact that d_{pcl} is independent of the component of $\overline{\mathbf{B}}$ parallel to the layers. Indeed, as we see, the larger the value of β, the larger the discrepancy is between d_{rc} and d_{pcl}; this indicates that the difference between $R\widehat{W}$ and $P_L\widehat{W}$ will tend to increase as well. Simultaneously, the difference between d_{rc} and d_{pcl} is largest when $\psi = 0$, and decreases as $\psi \to \frac{\pi}{2}$.

From this analysis, we can expect our bounds to be tight for small values of β, and to a lesser extent when both β and ψ are large. We mention that when $\beta = \frac{\pi}{2}$, $d_{pcl} = (\lambda_{se}^{me})^{-1}$. It is clear from Figure 9.3d that $d_{rc}(\psi, \overline{B}, \frac{\pi}{2}) \leqslant (\lambda_{se}^{me})^{-1}$ for all ψ and $\overline{B}$ (and with equality when $\overline{B} = 0$), and as such, there are a range of loading conditions for which $R\widehat{W}$ predicts no domain formation, i.e. $R\widehat{W} = \widehat{W}$, while $P_L\widehat{W}$ differs from $\widehat{W}$. It follows then that d_{pcl} serves as bound on the stability of the laminate, in that, for a given $\overline{\mathbf{B}}$, $\widehat{W}$ will remain strictly rank-one convex, so that no domain formation is necessary, so long as $d > d_{pcl}$.

9.5.2 Relaxation Estimates

Before proceeding with a direct comparison of $R\widehat{W}$ and $P_L\widehat{W}$, we comment on how our results will be presented. As above, we will analyze the dependence on $\overline{\mathbf{B}}$ by varying $\overline{B}$ and β. On the other hand, when looking at how our results behave for different mechanical loading conditions, we will continue to consider dependence on λ_n, but for more general plane-strain loading conditions, upon fixing λ_n, it will be most convenient to instead look at the dependence on γ, as introduced at the end of Section 9.3. In fact, this will be true for the remainder of this work. We choose to vary γ in lieu of d since it is more closely related to the amount of rotation of the layers, and hence it is easier to interpret our results from a physical perspective later on. Moreover, the effect of the rank-one convexification procedure is more clearly seen

by plotting results as a function a γ. Finally, it allows us to more readily connect with the results of Chapter 6, which are presented as a function of γ. For reference, we recall that $\gamma = d\sin(\psi)$.

A straightforward calculation reveals that, in terms of $\lambda_n, \gamma, \overline{B}$ and β, for a fixed value of $\lambda_n > \lambda_{se}^x$, $P_L\widehat{W}$ begins to differ from $\widehat{W}$ when γ reaches the value of

$$\gamma_{pcl} = \gamma_{pcl}(\lambda_n, \overline{B}, \beta) = \pm\sqrt{(\lambda_{se}^x)^{-2} - \lambda_n^{-2}}, \tag{9.5.6}$$

where it is recalled that λ_{se}^x is a function of $\overline{B}_x = \overline{B}\cos(\beta)$ and is defined by Eq. (9.3.43). As for rank-one convexity, we find that there are in general, two distinct values of γ at which the principal solution loses strict rank-one convexity. This follows from the fact that $\widehat{\Phi}$, as given by Eq. (9.3.35), has a linear term in γ, and is hence an odd function in γ. We denote these two points as $\gamma_{rc}^{\pm}$, and find that in general $\gamma_{rc}^{+} \neq \gamma_{rc}^{-}$. Like γ_{pcl} we take $\gamma_{rc}^{\pm} = \gamma_{rc}^{\pm}(\lambda_n, \overline{B}, \beta)$ as a function of $\lambda_n, \overline{B}$ and β. Since $d^2 = \gamma^2 + \lambda_n^{-2}$, it is clear that

$$\gamma_{rc}^{\pm}(\lambda_n, \overline{B}, \beta) \geqslant 0, \ \forall \ \lambda_n \geqslant \lambda_{rc}(\overline{B}, \beta), \tag{9.5.7}$$

with equality precisely when $\lambda_n = \lambda_{rc}(\overline{B}, \beta)$. From Eq. (9.5.6), we see that the same is true for γ_{pcl}, which equals zero when $\lambda_n = \lambda_{se}^x$.

Now, $\widehat{\Phi}$, as defined in Eq. (9.3.35) is not, in general, a convex function in γ. While this nonconvexity as a function of γ is not equivalent to the lack of rank-one convexity of $\widehat{W}$ as a function of $(\overline{\boldsymbol{F}}, \overline{\mathbf{B}})$, the two are related, and therefore, as mentioned above, the effect of the rank-one convexification is most clearly seen by plotting results as a function of γ. As such, we will fix λ_n and $\overline{B}$ and compare $P_L\widehat{W}$ and $R\widehat{W}$, for varying values of β, as a function of γ. We also include results of $\widehat{W}$ for comparison. Upon fixing, $\lambda_n = 1.6$ and $\overline{B} = 5$, one finds that

$$\lambda_{se}^x = \lambda_{rc}(5, 0) \approx .7806, \quad \lambda_{se}^y = \lambda_{rc}\left(5, \frac{\pi}{2}\right) \approx 1.3724. \tag{9.5.8}$$

Therefore, using from Eq. (9.5.5), it follows that for all $\beta \in \left(0, \frac{\pi}{2}\right)$, $\lambda_{rc}(5, \beta) < 1.6$, so that $\gamma_{rc}^{\pm}$ and γ_{pcl} will differ from 0, whereby $P_L\widehat{W}$ and $R\widehat{W}$ will differ from $\widehat{W}$.

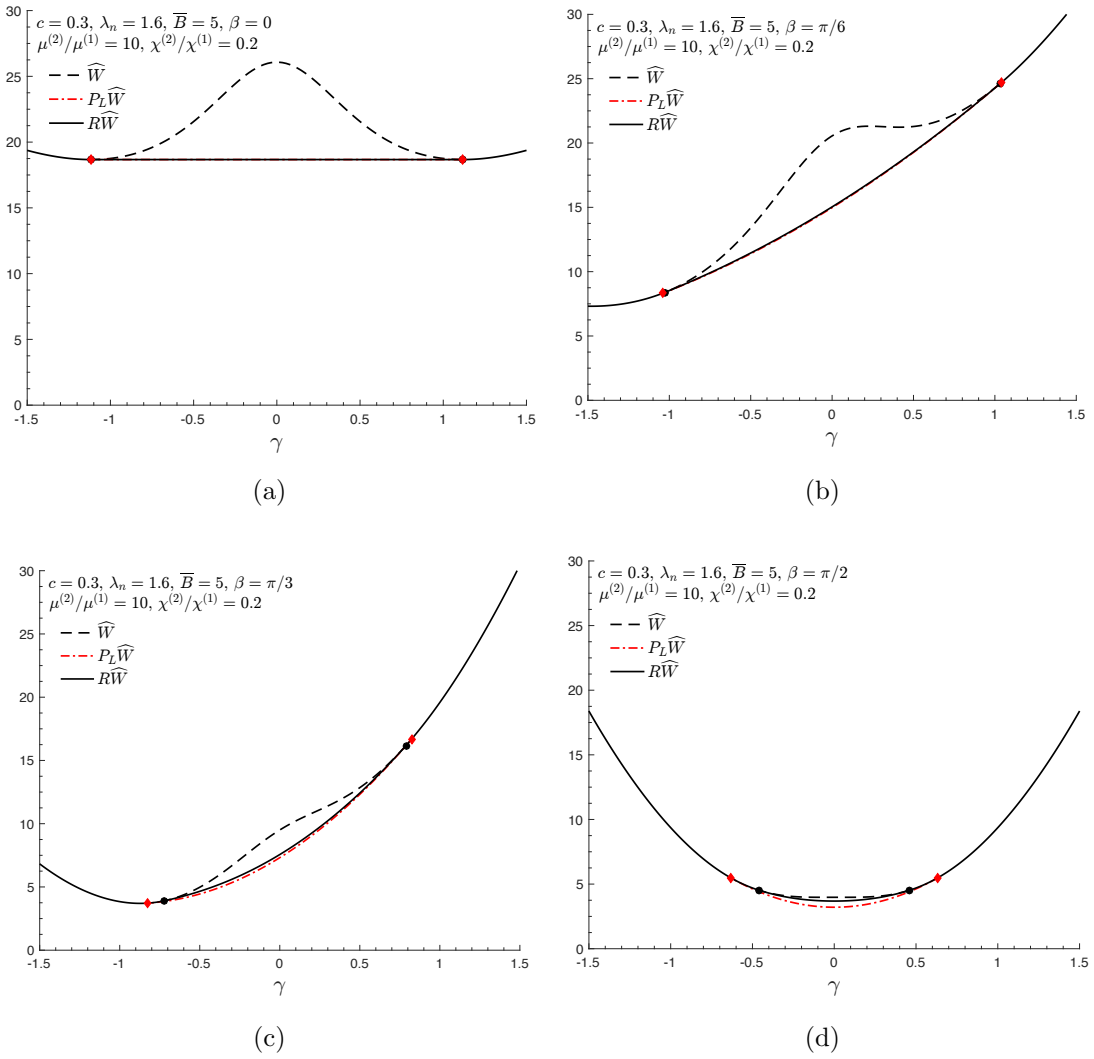

Figure 9.4: Comparison between $\widehat{W}, P_L\widehat{W}$ and $R\widehat{W}$, for (a) $\beta = 0$, (b) $\beta = \frac{\pi}{6}$, (c) $\beta = \frac{\pi}{3}$ and (d) $\beta = \frac{\pi}{2}$. Results are plotted for a fixed shear contrast of $\mu^{(2)}/\mu^{(1)} = 10$, permeability measure contrast of $\chi^{(2)}/\chi^{(1)} = 0.2$ volume fraction $c = 0.3$, $\lambda_n = 1.6$ and $\overline{B} = 5$.

We are now in a position to proceed with the comparison of the bounds, and do so in Figure 9.4. Points where $\widehat{W}$ begins to differ from $R\widehat{W}$ and $P_L\widehat{W}$ are indicated by black circles and red diamonds, respectively. As we saw in Section 9.4.2, $P_L\widehat{W} = R\widehat{W}$

when $\beta = 0$, and hence, in Figure 9.2a, $R\widehat{W}$ corresponds to $Q\widehat{W}$. As anticipated, we see that as β increases, so too does the difference between $P_L\widehat{W}$ and $R\widehat{W}$. For $\beta = \frac{\pi}{6}$, the difference between the upper and lower bounds is hard to distinguish, and hence the bounds give a very accurate approximation to $Q\widehat{W}$. It is only for large enough values of β that we see a significant difference between $P_L\widehat{W}$ and $R\widehat{W}$. This is due to the fact that $\mathcal{S}_{pcl}$ is independent of $\overline{B}_y = \overline{B}\sin(\beta)$, and hence, as $\beta \to \frac{\pi}{2}$, $P_L\widehat{W}$ is unable to fully account for the effects of the component of $\overline{\mathbf{B}}$ parallel to the layers. We recall that the stabilizing effect of the applied magnetic field increases as β increase. It is therefore interesting to note that $Q\widehat{W}$, which lies somewhere between $R\widehat{W}$ and $P_L\widehat{W}$, is better predicted in situations when $\overline{\mathbf{B}}$ destabilizes the laminate. On the other hand, as β increases, the difference between $R\widehat{W}$ and $\widehat{W}$ decreases, and as we see in Figure 9.4d, the difference between $\widehat{W}$ and $R\widehat{W}$ is smallest.

We also look to compare the behavior of these bounds near the points where they transition back to $\widehat{W}$. In particular, in Figure 9.5, we compare the behavior of $R\widehat{W}$ and $P_L\widehat{W}$ as γ approaches $\gamma_{rc}^{\pm}$ and $\pm\gamma_{pcl}$, respectively. In Figure 9.5a and Figure 9.5b, we consider the case when $\beta = \frac{\pi}{6}$. As we see, while the relative distance between $-\gamma_{rc}^{-}$ and $-\gamma_{pcl}$ is larger than that between γ_{rc}^{+} and γ_{pcl}, the behaviors of $R\widehat{W}$ and $P_L\widehat{W}$ are similar, in that their difference is small, and they approach $\gamma_{rc}^{\pm}/\pm\gamma_{pcl}$ at a similar rate. However, as we see in Figure 9.5c and Figure 9.5d where $\beta = \frac{\pi}{3}$, the behavior of the two bounds is qualitatively different depending on whether γ is positive or negative. Indeed, near γ_{rc}^{+} and γ_{pcl}, the difference between $R\widehat{W}$ and $P_L\widehat{W}$ remains relatively small, and both functions approach these points at approximately the same rate. In contrast, near $-\gamma_{rc}^{-}$ and $-\gamma_{pcl}$, the difference between the two bounds is larger, and only diminishes very close to $-\gamma_{pcl}$. As discussed above, this difference is due both to the explicit dependence of $\widehat{\Phi}$ on γ and β, as well as the anisotropy of the laminate itself. Finally, when $\beta = \frac{\pi}{2}$, we see from Figure 9.5e and Figure 9.5f that $R\widehat{W}$ and $P_L\widehat{W}$ behave very differently as they transition back to $\widehat{W}$. Due to the symmetry of $\widehat{\Phi}$ in this case, both $R\widehat{W}$ and $P_L\widehat{W}$ are even functions in γ and symmetric about

$\gamma = 0$, and hence Figure 9.5e and Figure 9.5f depict the same varied behavior. In fact, $R\widehat{W}$ and $\widehat{W}$ behave more similarly than $R\widehat{W}$ and $P_L\widehat{W}$.

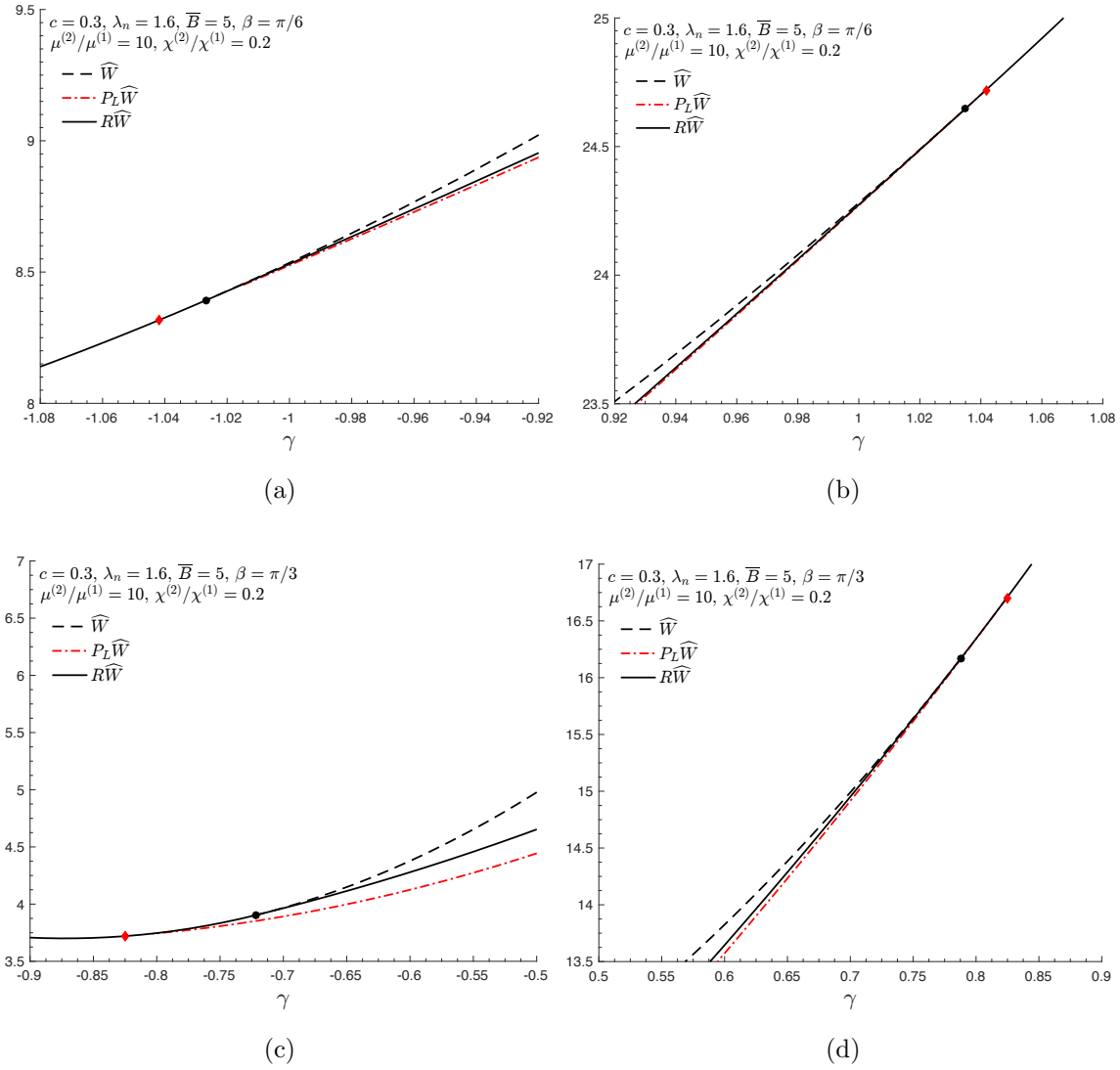

Figure 9.5: Comparison between $\widehat{W}$, $P_L\widehat{W}$ and $R\widehat{W}$, near the points $-\gamma_{rc}^-$ and γ_{rc}^+ for (a) and (b) $\beta = \frac{\pi}{6}$, (c) and (d) $\beta = \frac{\pi}{3}$, and (e) and (f) $\beta = \frac{\pi}{2}$, respectively. Results are plotted for a fixed shear contrast of $\mu^{(2)}/\mu^{(1)} = 10$, permeability measure contrast of $\chi^{(2)}/\chi^{(1)} = 0.2$ volume fraction $c = 0.3$, $\lambda_n = 1.6$ and $\overline{B} = 5$.

In summarizing what we have seen from Figure 9.2-Figure 9.5, we anticipate the difference, both quantitative and qualitative, between $R\widehat{W}$ and $P_L\widehat{W}$ to increase with

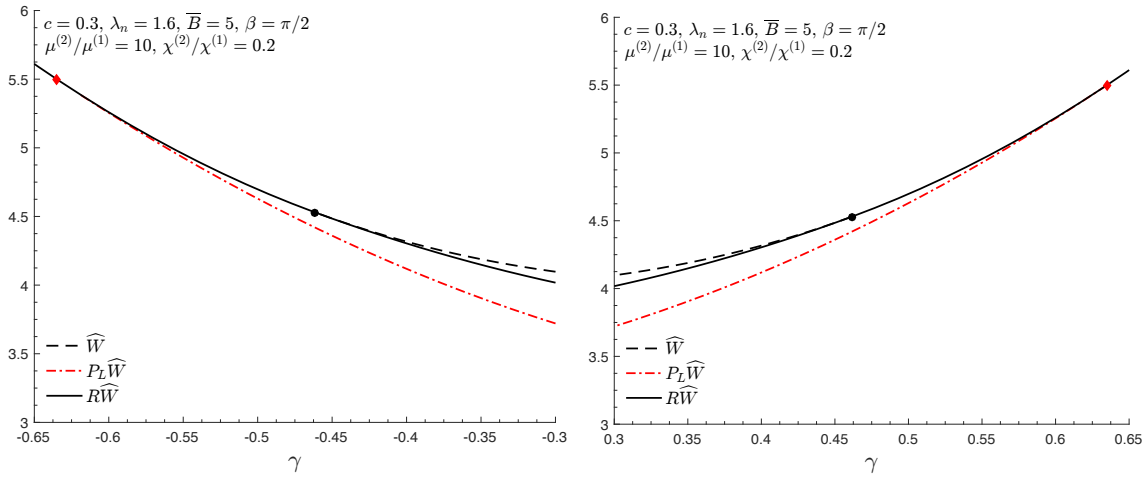

Figure 9.5: Continued

increasing β. Yet, depending on the values of λ_n and $\overline{B}$ considered, this difference will remain small for values of $\beta \leqslant \frac{\pi}{3}$. The range of values of β for which these bounds remain sufficiently tight will also depend on the microstructural parameters (i.e. c, $\mu^{(2)}/\mu^{(1)}$, and $\chi^{(2)}/\chi^{(1)}$), but we can conclude that $R\widehat{W}$ gives a very accurate description of $Q\widehat{W}$ for small to moderate values of β (and is exact for $\beta = 0$). Interestingly, in the cases where $\overline{\mathbf{B}}$ destabilizes the composite, the difference between $\widehat{W}$ and $R\widehat{W}$ is larger, and yet our bounds on $Q\widehat{W}$ are tighter. As β increases, and $\overline{\mathbf{B}}$ begins to stabilize the composite, the difference between $\widehat{W}$ and $R\widehat{W}$ decreases. Although the difference between the bounds increases for large values of β, as we have seen, unlike $P_L\widehat{W}$, $R\widehat{W}$ is more sensitive to the component of $\overline{\mathbf{B}}$ parallel to the layers, and we therefore anticipate that $R\widehat{W}$ will give a better estimate on $Q\widehat{W}$ than $P_L\widehat{W}$ in these cases. In fact, although $R\widehat{W}$ and $P_L\widehat{W}$ differ more as $\beta \to \frac{\pi}{2}$, the relative magnitude of such a difference is smallest in this case. The region between $P_L\widehat{W}$ and $\widehat{W}$ within which both $Q\widehat{W}$ and $R\widehat{W}$ lie is therefore rather narrow, indicating that $R\widehat{W}$ is still, in this case, a good approximation to $Q\widehat{W}$. As such, in the next subsection, we will use $R\widehat{W}$ to estimate the post-bifurcation behavior of the composite, and discuss the

physical implications which arise as a result of the rank-one lamination procedure.

Before proceeding, we make one final comment regarding our bounds. By construction, $P_L\widehat{W}$ represents a lower bound on $P\widehat{W}$. As we have seen, there are certain loading conditions for which $R\widehat{W} = \widehat{W}$ while $P_L\widehat{W} < \widehat{W}$. If $P_L\widehat{W}$ does in fact correspond to the polyconvex envelope of $\widehat{W}$, then, from what we have seen above, there are loading conditions for which $\widehat{W}$ is rank-one convex but *not* polyconvex; this also implies that $R\widehat{W}$ would fail to be polyconvex. While $R\widehat{W}$ and $Q\widehat{W}$ can still coincide, confirming this would require checking that $R\widehat{W}$ is quasiconvex directly, a difficult, if not impossible, task. Nonetheless, if $P_L\widehat{W} = P\widehat{W}$, and $R\widehat{W} = Q\widehat{W}$ this would imply that $Q\widehat{W}$ fails to be polyconvex. We note that, in the purely mechanical context, there do exist cases in which the homogenized potential loses polyconvexity (Braides, 1994) and therefore such findings in regards to $Q\widehat{W}$ are fully consistent with the theory.

9.6 Physical implications of the rank-one convexification

As we have seen in Chapters 6 and 7 in the purely mechanical context, sufficient compression along the stiff layers will trigger an instability. Recalling that λ_n is directly related to the amount of compression of the layers, once $\lambda_n \geqslant \lambda_{rc}$, the composite will form domains to accommodate the load. The mechanism of the instability in the current magneto-elastic setting is still compression along the layers, but as we have seen above, instabilities can either be promoted, or inhibited, by the application of a magnetic field, depending on its orientation.

Now, if the layers are free to rotate, then on average, they will always tend to align themselves with the applied magnetic field. However, in addition to the applied magnetic field, the composite is also subjected to an average macroscopic deformation gradient $\overline{\boldsymbol{F}}$. As $\overline{\boldsymbol{F}}$ fully determines the rotation of the layers of the laminate

(Lopez-Pamies and Ponte Castañeda, 2009), its prescription can result in a nonzero macroscopic magnetization that is unaligned with the applied magnetic field (in the current configuration), which gives way to magneto-elastic contributions to $\overline{\boldsymbol{T}}$; part of these contributions are due to magnetically induced torque. We comment that, having chosen $\mathbf{N}_0 = \mathbf{e}_1$, a smaller value of $\overline{T}_{11} - \overline{T}_{22}$ indicates less compression along the layers. Moreover, $\overline{T}_{11} - \overline{T}_{22} > 0$ corresponds to overall compressive loading, while $\overline{T}_{11} - \overline{T}_{22} < 0$ indicates tensile loading. Thus, under certain loading conditions, the contributions to $\overline{\boldsymbol{T}}$ from the magneto-elastic coupling can create sufficient compression to initiate an instability.

With all of this in mind, we now take a look at the physical implications of the rank-one convexification procedure, and show how the laminate behaves after the onset of a macroscopic instability. We will consider the two extreme cases, namely when $\overline{\mathbf{B}}$ is perpendicular to and aligned with the layers. We once again recall that all results have been calculated for a fixed value of shear contrast ratio of $\mu^{(2)}/\mu^{(1)} = 10$, fixed volume fraction $c = 0.3$ and a permeability contrast ratio of $\chi^{(2)}/\chi^{(1)} = .2$

To help visualize the results, we have included in Figure 9.1b a schematic of the post-bifurcation response of the laminate under combined magneto-elastic loading conditions. Upon losing strict rank-one convexity, the laminate finds stability in the formation of domains which appear in the figure as layers with alternating orientations. Each domain, denoted Layer I and Layer II, are subjected to $\boldsymbol{F}_1^{(q)}$ and $\mathbf{B}_1^{(q)}$ for $q = I, II$, and the constitutive response in the domain is characterized by $\widehat{W}$; this is a consequence of the rank-one convexification procedure, defined through Eqs. (9.4.29)-(9.4.30). As shown in Figure 9.1b, the domains are rotated by angles which we denote here as $\varphi^{(I)}$ and $\varphi^{(II)}$. Note that these angles, in general, are different from the angle ψ. In the two cases to be considered below, it turns out that $\varphi^{(I)} = -\varphi^{(II)}$, and we denote the macroscopic rotation of layers by φ. Due to the form of $\overline{\boldsymbol{F}}$ as given by Eq. (9.3.33), it turns out that $\psi = -\phi$, but more generally, ψ is related to, but not exactly, the rotation of the layers. Now, for magnetic fields with $\beta \neq 0$ or

$\beta \neq \frac{\pi}{2}$, it is possible for $\varphi^{(I)} \neq -\varphi^{(II)}$. Moreover, in the schematic above, the direction of lamination, which we recall is defined through the angle ϕ_1, as introduced at the beginning of Section 9.4, has been taken to be equal to $\frac{\pi}{2}$. While this is true for $\beta = 0$, it is not more generally. Nonetheless, the schematic gives a general sense of the post-bifurcation response, and is meant to aid in the understanding of the laminates behavior.

Before proceeding it is helpful to recall the following expressions given previously in Section 9.3:

$$\tan(\beta_{\overline{\mathbf{b}}}) = \frac{\tan(\beta)}{\lambda_n^2 + \tan(\beta)\tan(\psi)}, \tag{9.6.1}$$

$$\tan(\beta_{\overline{\mathbf{h}}}) = \tan(\beta_{\overline{\mathbf{b}}}) \left(\frac{\breve{\chi}\tan(\beta) - \widetilde{\chi}\lambda_n^2 \cos^2(\psi)\tan(\psi)}{\breve{\chi}\tan(\beta) + \widetilde{\chi}\lambda_n^2 \cos^2(\psi)\tan(\beta_{\overline{\mathbf{b}}})} \right), \tag{9.6.2}$$

$$\overline{\tau} = \frac{(\breve{\chi} - \overline{\chi})\overline{B}^2}{2} \left(\lambda_n^2 \cos^2(\beta)\sin(2\psi) + \sin(2\beta) \right) \tag{9.6.3}$$

$$\overline{T}_{11} - \overline{T}_{22} = \breve{\mu}\lambda_n^2 + (\tan^2(\psi) - 1)\lambda_n^{-2} \left(\overline{\mu} - \frac{\widetilde{\mu}}{d^4} \right) + \overline{\tau}\sin(2\psi) + \overline{T}_{11}^{mag} - \overline{T}_{22}^{mag}, \tag{9.6.4}$$

$$\overline{T}_{11}^{mag} - \overline{T}_{22}^{mag} = \frac{\overline{B}^2 \sin(2\beta)(\cot(\beta_{\overline{\mathbf{b}}})\cot(\beta_{\overline{\mathbf{h}}}) - 1)}{4\lambda_n^2} \left(2\breve{\chi}\tan(\beta) - \widetilde{\chi}\lambda_n^2 \sin(2\psi) \right), \tag{9.6.5}$$

$$\overline{T}_{12} = \frac{\tan(\psi)}{\lambda_n^2} \left(\overline{\mu} - \frac{\widetilde{\mu}}{d^4} \right) - \overline{\tau}\sin^2(\psi) + \overline{T}_{12}^{mag}, \tag{9.6.6}$$

$$\overline{T}_{12}^{mag} = \frac{\overline{B}^2 \sin(2\beta)\cot(\beta_{\overline{\mathbf{b}}})}{4\lambda_n^2} \left(2\breve{\chi}\tan(\beta) - \widetilde{\chi}\lambda_n^2 \sin(2\psi) \right). \tag{9.6.7}$$

We also recall that $\psi = \arctan(\lambda_n \gamma)$.

9.6.1 $\overline{\mathbf{B}}$ perpendicular to the layers

When $\overline{\mathbf{B}} = \overline{B}\mathbf{N}_0$, we know that $Q\widehat{W}(\overline{\boldsymbol{F}}, \overline{B}\mathbf{N}_0) = P_L\widehat{W}(\overline{\boldsymbol{F}}, \overline{B}\mathbf{N}_0)$, and the relaxation construction is nearly identical to the purely mechanical case considered in Chapter 6. However, there are major differences in how an instability can be initi-

ated. We know from Chapter 6 that under purely mechanical loading, the laminate is stable when $\overline{\boldsymbol{F}} = \mathbf{I}$. However, as depicted in Figure 9.2a, when $\beta = 0$, $\lambda_{rc}(\overline{B}, 0) = (d_{rc}(0, \overline{B}, 0))^{-1}$ can be made less than one for large enough values of $\overline{B}$, whereby pure shear loading with a value of $\lambda_n \leqslant 1$ triggers an instability. In particular, using Eq. (9.3.43), it follows that $\lambda_{rc}(\overline{B}, 0) = 1 \iff \overline{B} = \sqrt{\frac{\breve{\mu}}{\breve{\chi}}}$, which, for the values of the parameters given above, is approximately 2.1177. Hence, when $\overline{\boldsymbol{F}} = \mathbf{I}$, and $\beta = 0$, we find from Eq. (9.6.1) that $\beta_{\overline{\mathbf{b}}} = 0$, while

$$\beta_{\overline{\mathbf{h}}} = \frac{(\breve{\chi} - \overline{\chi}) \tan(\psi)}{\overline{\chi} + \breve{\chi} \tan^2(\psi)}, \tag{9.6.8}$$

and therefore is zero when $\psi = 0$ (as is the case when $\overline{\boldsymbol{F}} = \mathbf{I}$). As such, when $\overline{\boldsymbol{F}} = \mathbf{I}$, i.e. $\lambda_n = 1$, $\gamma = 0$, one finds that

$$\overline{T}_{11} - \overline{T}_{22} = \overline{T}_{11}^{mag} - \overline{T}_{22}^{mag} = \overline{\chi} \overline{B}^2 > 0 \tag{9.6.9}$$

so long as $\overline{B} \neq 0$. Hence, a magnetic field perpendicular to the layers produces compression, even in the absence of any mechanical stresses; this phenomenon is often referred to as magnetostriction. Moreover, so long as $\overline{B}$ is large enough, this compression is sufficient to cause an instability, indicating once again that a magnetic field perpendicular to the layers will destabilize the composite.

We now present results in Figure 9.6, for the energy, the rotation of the domain layers, the normal stress difference, and true magnetic field intensity (in the current configuration) of $Q\widehat{W}$ under pure-shear loading conditions and compare them with the predictions of $\widehat{W}$. In each figure, results are included for different values of $\overline{B}$. As mentioned above, when $\overline{\boldsymbol{F}} = \boldsymbol{I}$, a value of $\overline{B} \approx 2.1177$ is large enough for $\widehat{W}$ to lose strict rank-one convexity. It is at this point that there is sufficient compression along the layers, and the composite finds stability via the formation of domains. While under pure-shear loading there is no macroscopic rotation of the layers, there is in fact a drastic rotation of the domain layers, as depicted in Figure 9.6b; in this plot,

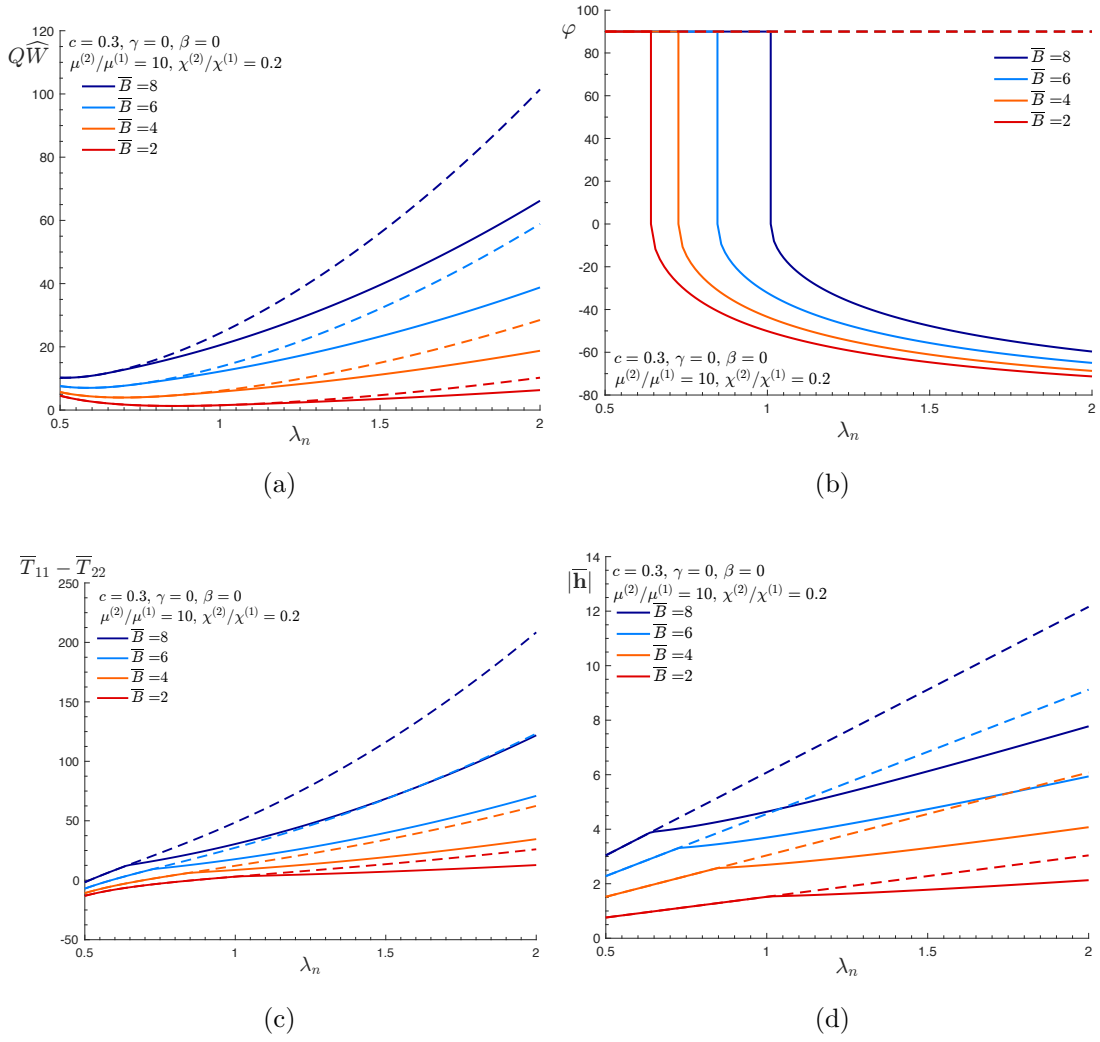

Figure 9.6: Comparison of (a) the energy, (b) the rotation of the domains, (c) the normal stress difference, and (d) the true magnetic field intensity in the current configuration, under pure-shear loading conditions with $\beta = 0$. The principal solution, depicted by the dashed curve, is included for comparison. Results are plotted for a fixed shear contrast of $\mu^{(2)}/\mu^{(1)} = 10$, permeability measure contrast of $\chi^{(2)}/\chi^{(1)} = 0.2$ volume fraction $c = 0.3$.

only the rotations of one domain is shown, with the other domain rotating in an equal and opposite amount. We see that $\varphi < 0$ after the onset of an instability. Note that as λ_n increases, the layers tend to rotate more. It is also interesting to note that, for a fixed value of λ_n, φ increases as $\overline{B}$ increases. This indicates that the layers within the domains tend to become more aligned with $\overline{\mathbf{B}}$ as its intensity increases.

Now, this layer rotation is accompanied by a decrease in overall energy, as shown in Figure 9.6a. Although $Q\widehat{W}$ and $\widehat{W}$ are both increasing functions in λ_n, $Q\widehat{W}$ grows at a slower rate. As the normal stress difference $\overline{T}_{11} - \overline{T}_{22}$ under pure shear, depicted in Figure 9.6c, can be related to the derivative of $Q\widehat{W}/\widehat{W}$ with respect to λ_n, we see that the domain formation associated with the lamination procedure leads to a reduction in the normal stress difference relative to the estimate given by $\widehat{W}$, resulting in a softening effect. This softening is connected to softening in $|\overline{\mathbf{h}}|$, as depicted in Figure 9.6d.; the decrease in $|\overline{\mathbf{h}}|$ decreases the contribution of $\overline{T}_{11}^{mag} - \overline{T}_{22}^{mag}$ to $\overline{T}_{11} - \overline{T}_{22}$ (c.f. Eq. (9.6.4)). We mention also that due to the destabilizing nature of a magnetic field perpendicular to the layers, domain formation occurs earlier as $\overline{B}$ increases, whereby $\lambda_{rc}(\overline{B}, 0)$ is an increasing function, as we have seen in Figure 9.2a.

Due to the fact that macroscopic instabilities can be initiated with $\overline{\boldsymbol{F}} = \mathbf{I}$ and a magnetic field perpendicular to the layers (in the undeformed configuration), it is of interest to investigate the post-bifurcation behavior under simple shear, when $\overline{\boldsymbol{F}}$ can be written as

$$\overline{\boldsymbol{F}} = \begin{bmatrix} 1 & \gamma \\ 0 & 1 \end{bmatrix}. \tag{9.6.10}$$

These results are presented in Figure 9.7, where, in each figure, we have included results for different values of $\overline{B}$. Note that for $\lambda_{rc}(2, 0) < \lambda_n = 1$, whereby the laminate remains strictly rank-one convex for all values of γ. On the other hand, for the values of $\overline{B} > 2$, the results show how the compressive nature of a magnetic field perpendicular to the layers is accommodated. Like in the purely mechanical context, once $\lambda_n \geqslant \lambda_{rc}$, $\widehat{W}$ can regain stability by applying sufficient shear perpendicular to

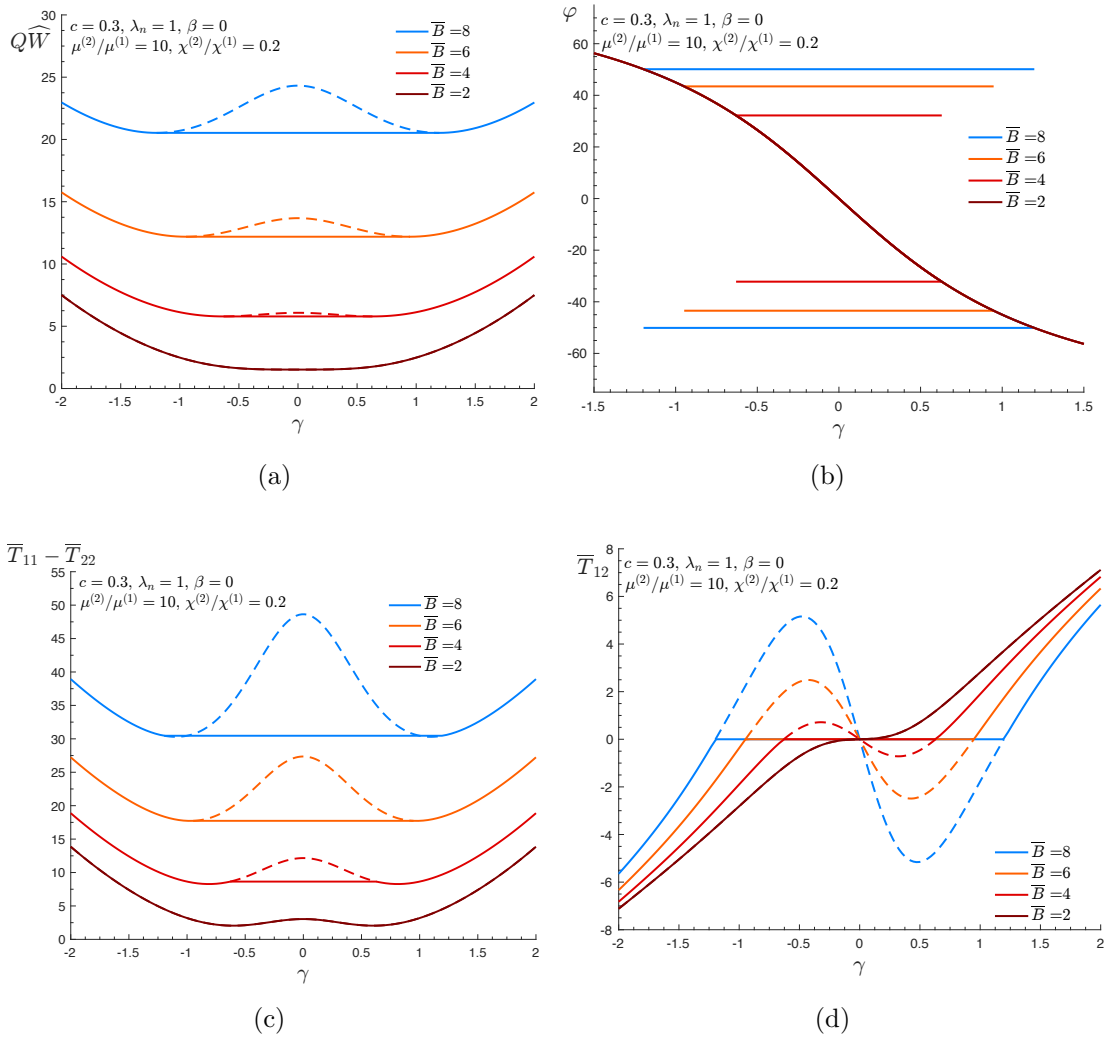

Figure 9.7: Comparison of (a) the energy, (b) the rotation of the layers (c) the normal stress difference, (d) the shear stress, (e) the true magnetic field intensity in the current configuration, and (f) the magnitude of the torque, under plain-strain loading conditions for $\beta = 0$. The principal solution, depicted by the dashed line, is included for comparison. Results are plotted for a fixed shear contrast of $\mu^{(2)}/\mu^{(1)} = 10$, permeability measure contrast of $\chi^{(2)}/\chi^{(1)} = 0.2$ volume fraction $c = 0.3$, and $\lambda_n = 1$.

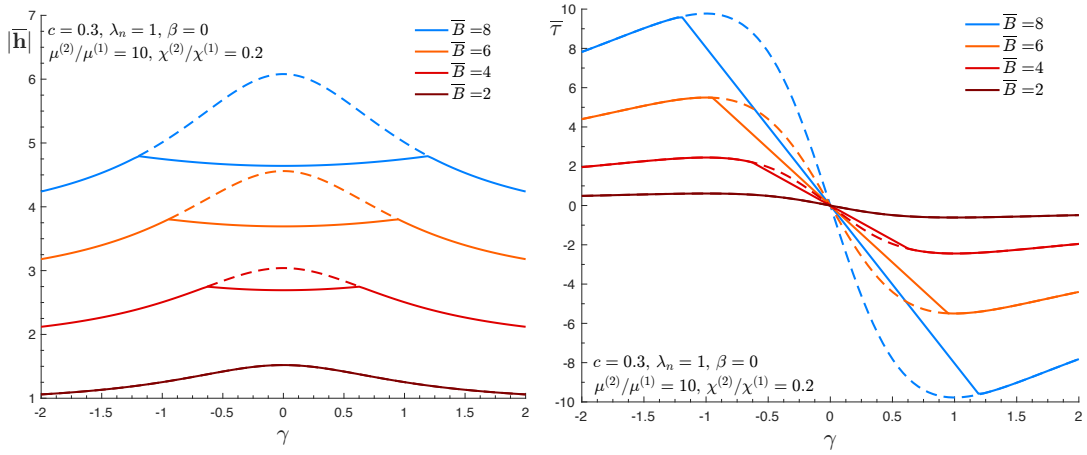

(e) (f)

Figure 9.7: Continued

the layers, as measured by γ; in particular, no domain formation occurs so long as $\gamma > |\gamma_{rc}|$. As mentioned above, for $\beta = 0$, the relaxation construction is nearly identical to the purely mechanical case. Indeed, as we see in Figure 9.7a, $Q\widehat{W}$ is obtained from $\widehat{W}$ by the convexification in the variable γ. Recalling that the value of $\lambda_n = 1$ has been fixed, it is interesting to see that an increase in $\overline{B}$ has the same effect on the energy as an increase in λ_n does in the purely mechanical case (see Figure 6.2a in Chapter 6). This is related to the fact that increasing λ_n and $\overline{B}$ leads to an increase in the overall compression of the layers; the latter does so through magnetostriction.

Now, the Maxwell-type construction associated with $Q\widehat{W}$ is accompanied by a rotation of the domain layers, as depicted in Figure 9.7b. Note that in this case, the domains rotate in equal and opposite amounts, forming a herring-bone structure. The rotation of the domains is shown in Figure 9.7b, whereby, and in reference to Figure 9.1b, the rotation of Layer I corresponds to the constant curve at a positive value of φ, while the rotation of Layer II corresponds to the constant curve at the negative value of φ. As in the case of pure shear, this construction results in softening in both the normal stress difference and the magnitude of true magnetic field (in the deformed configuration), as seen in Figure 9.7c and Figure 9.7e, respectively. In

looking at Figure 9.7d and Figure 9.7f, we see that there is also a softening in $\overline{\boldsymbol{T}}_{12}$ and $\overline{\tau}$. It can be shown that when $\beta = 0$, $\overline{\boldsymbol{T}}_{12}^{mag} = \overline{\tau}$. Therefore, from Eq. (9.6.6), the softening in $\overline{\boldsymbol{T}}_{12}$ is facilitated both by the softening in $\overline{\tau}$ as well as mechanical softening that comes as a direct consequence of the domain formation; the latter occurs in the same way as was seen in the purely mechanical context in Chapter 6.

9.6.2 $\overline{\mathbf{B}}$ parallel to the layers

Here, we consider the case where $\overline{\mathbf{B}} = \overline{B}\mathbf{M}_0$. From Eqs. (9.6.1)-(9.6.3), we find that when $\beta = \frac{\pi}{2}$, then $\beta_{\overline{\mathbf{b}}} = \beta_{\overline{\mathbf{h}}} = \frac{\pi}{2} - \psi$, and $\overline{\tau} = 0$. In other words, when $\overline{\mathbf{B}}$ is parallel to the layers in the undeformed configuration, the true magnetic field $\overline{\mathbf{h}}$ is aligned with $\overline{\mathbf{b}}$ and therefore so too is the magnetization $\overline{\mathbf{m}}$ (in the current configuration). As a result, there are no torques on the system as predicted by $\widehat{W}$, and $\overline{\mathbf{h}}$ will remain aligned with the layers regardless of the amount of shear applied. Moreover, the term proportional to $\overline{\tau}$ in the expression for the normal stress difference (c.f. Eq. (9.6.4)) will also vanish, lowering the normal stress difference, thereby reducing the compression of the layers; this is consistent with the stabilizing effects of a magnetic field parallel to the layers.

To start, we compare in Figure 9.8 the energy, the rotation of the domain layers, the normal stress difference, and true magnetic field intensity (in the current configuration) of $R\widehat{W}$ and $\widehat{W}$ under pure-shear loading conditions. In Figure 9.8a, we see that, once $\widehat{W}$ loses strict rank-one convexity, $R\widehat{W}$ begins to differ from $\widehat{W}$, and while both functions increase as a function of λ_n, $R\widehat{W}$ does so at a slower rate. This is similar to what was seen above, and indicates a softening behavior. Simultaneously, we find that the domain formation leads to an increase in the overall magnetic field intensity, as depicted in Figure 9.8d; this is in contrast to the case of $\beta = 0$. Both of these changes are achieved by a sudden rotation of the domain layers, as seen in Figure 9.8b. Note that while the rotation is more gradual than when $\beta = 0$, for a fixed value of λ_n, φ is still an increasing function in $\overline{B}$. In this case however, this

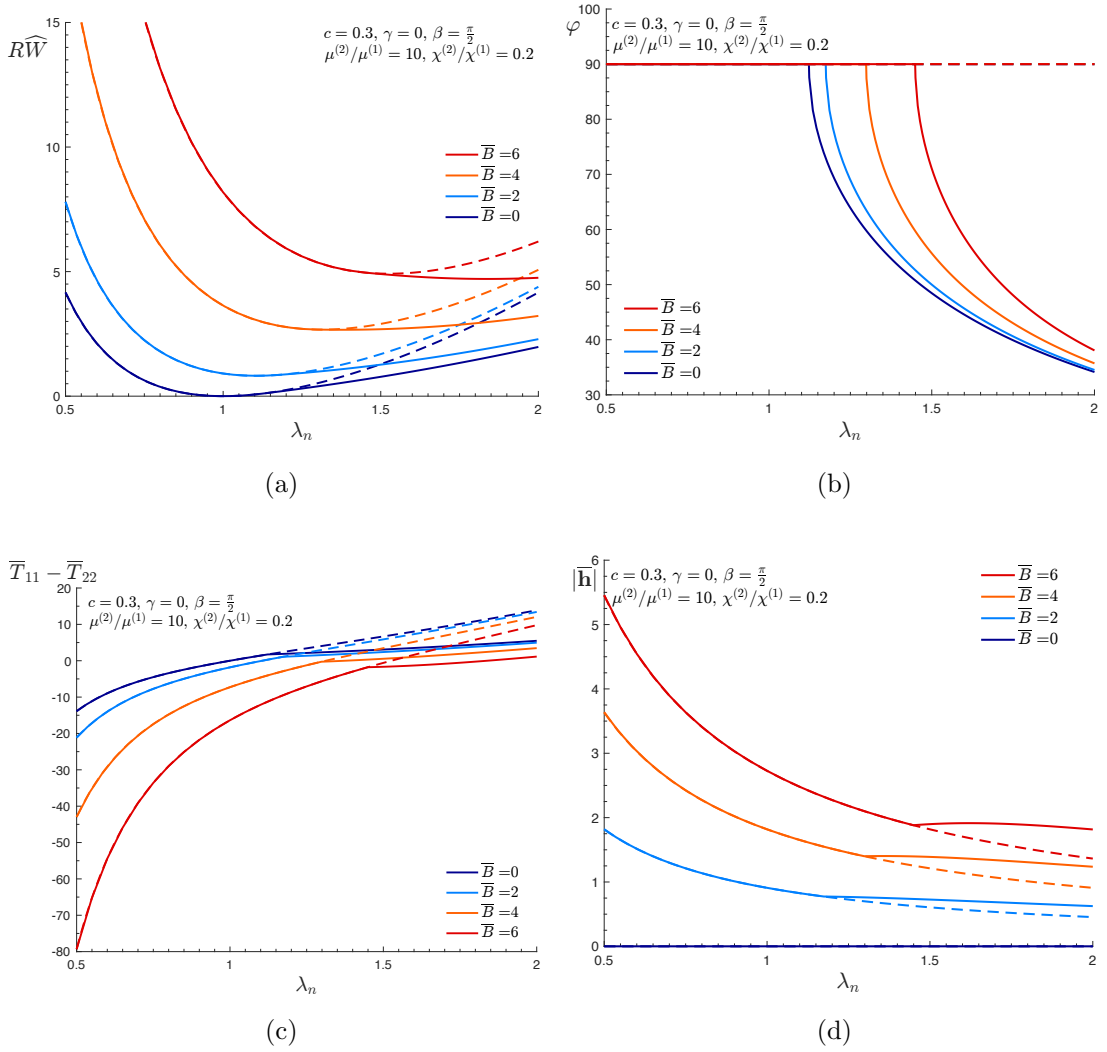

Figure 9.8: Comparison of (a) the energy, (b) the rotation of the domains, (c) the normal stress difference, and (d) the true magnetic field intensity in the current configuration, under pure-shear loading conditions with $\beta = \frac{\pi}{2}$. The principal solution, depicted by the dashed curve, is included for comparison. Results are plotted for a fixed shear contrast of $\mu^{(2)}/\mu^{(1)} = 10$, permeability measure contrast of $\chi^{(2)}/\chi^{(1)} = 0.2$ volume fraction $c = 0.3$.

tends to stabilize the laminate. Keeping in mind Figure 9.1b, when $\beta = 0$, $\varphi < 0$, and as $\overline{B}$ increases, φ increase towards a value of 0, bringing the domain layers more into alignment with $\overline{\mathbf{B}}$. In the current case, $\varphi > 0$, and as $\overline{B}$ increases, φ increases towards a value of $\frac{\pi}{2}$, also bringing the domain layers more into alignment with $\overline{\mathbf{B}}$. That this has a stabilizing effect when $\beta = \frac{\pi}{2}$ and not for $\beta = 0$ can be best understood by simply noting that the less the domains rotate, the less overall compression there is on the laminate.

We now consider more general plane strain loading conditions. Throughout Figure 9.9, a value of $\lambda_n = 1.6$ is used. For the material parameters considered, $\lambda_{rc}(\overline{B}, \frac{\pi}{2}) = 1.6$ when $\overline{B} \approx 7.9584$, at which point $\widehat{W} = R\widehat{W}$. Therefore, when $\overline{B} < 7.9584$, $\lambda_n \geqslant \lambda_{rc}$, whereby $\widehat{W}$ is no longer strictly rank-one convex. Thus, if $\gamma \in (-\gamma_{rc}^-, \gamma_{rc}^+)$, whereby the layers of the laminate have not rotated enough to accommodate the large compression, the composite will undergo a macroscopic instability, and break up into domains. We recall that since $\widehat{\Phi}(\lambda_n, \gamma, \overline{B}, \frac{\pi}{2})$ is an even function in γ, $\gamma_{rc}^- = \gamma_{rc}^+$. Also, we have included results for $\overline{B} = 8$, a value large enough to completely stabilize the laminate, whereby $R\widehat{W} = \widehat{W}\,\forall\gamma$, and no domain formation occurs.

As we see in Figure 9.9a, $R\widehat{W}$ is no longer given as the convexification of $\widehat{W}$ in the variable γ. Upon the initiation of an instability, the composite breaks into domains via the formation of the rotated domain layers, as see in Figure 9.9b. Unlike when $\beta = 0$, we see here that the amount of rotation is not only not constant, but non-monotonic, indicating that, as one goes from $\gamma = -\gamma_{rc}$ to $\gamma = \gamma_{rc}$, the domain will rotate in one direction reaching a minimum (in magnitude) value of φ, and then begin rotating in the other direction. Now, along with the layer rotation, the domain formation leads to a decrease in total normal stress difference, which we see in Figure 9.9c, thereby alleviating the compression of the layers. In fact, for $\overline{B} = 6$, domain formation converts compressive forces into tensile ones, whereby the normal stress difference predicted by $\widehat{W}$ is positive for small values of γ, while $R\widehat{W}$ predicts a

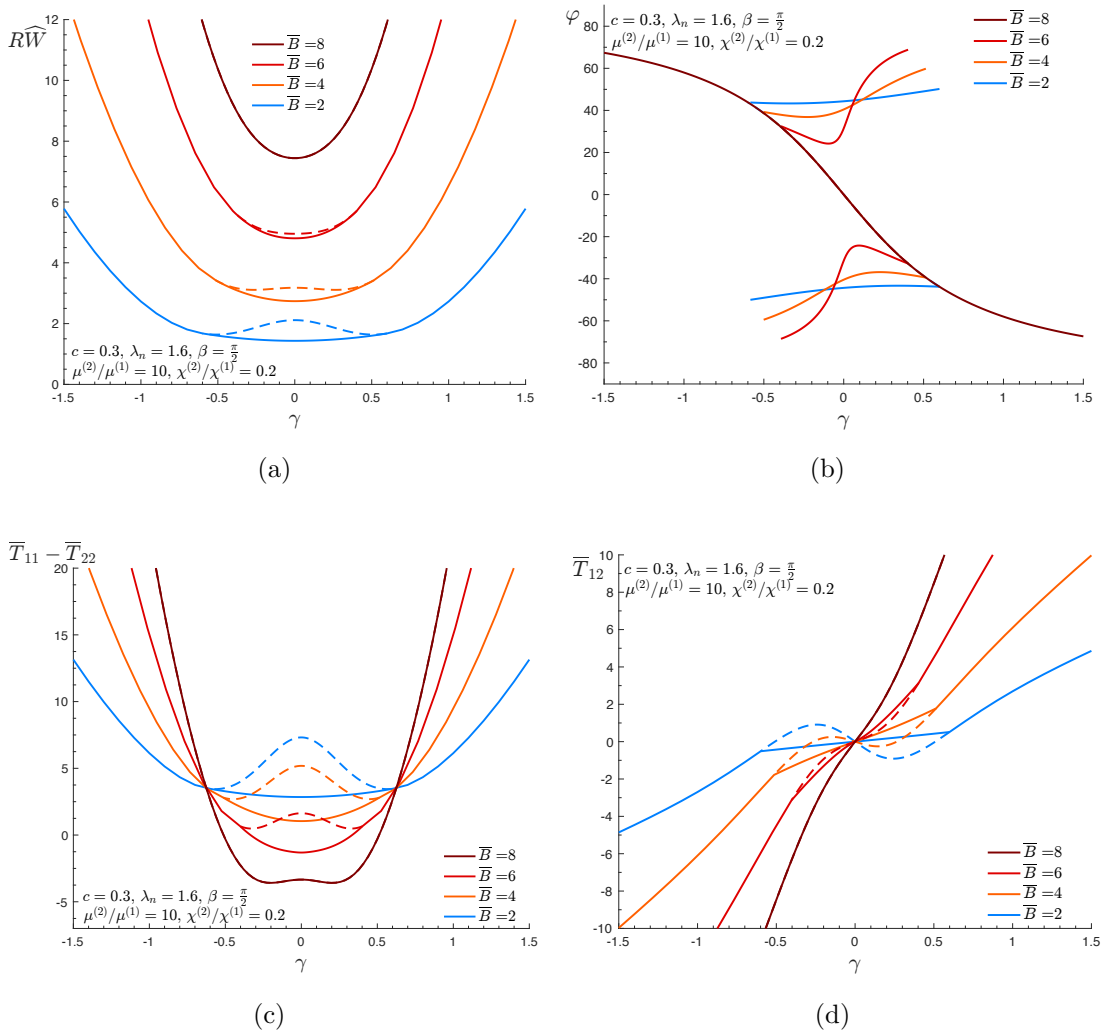

Figure 9.9: Comparison of (a) the energy, (b) the rotation of the layers, (c) the normal stress difference, (d) the shear stress, (e) the true magnetic field intensity in the current configuration, and (f) the magnitude of the torque, under plain-strain loading conditions for $\beta = \frac{\pi}{2}$. The principal solution, depicted by the dashed line, is included for comparison. Results are plotted for a fixed shear contrast of $\mu^{(2)}/\mu^{(1)} = 10$, permeability measure contrast of $\chi^{(2)}/\chi^{(1)} = 0.2$ volume fraction $c = 0.3$, and $\lambda_n = 1.6$.

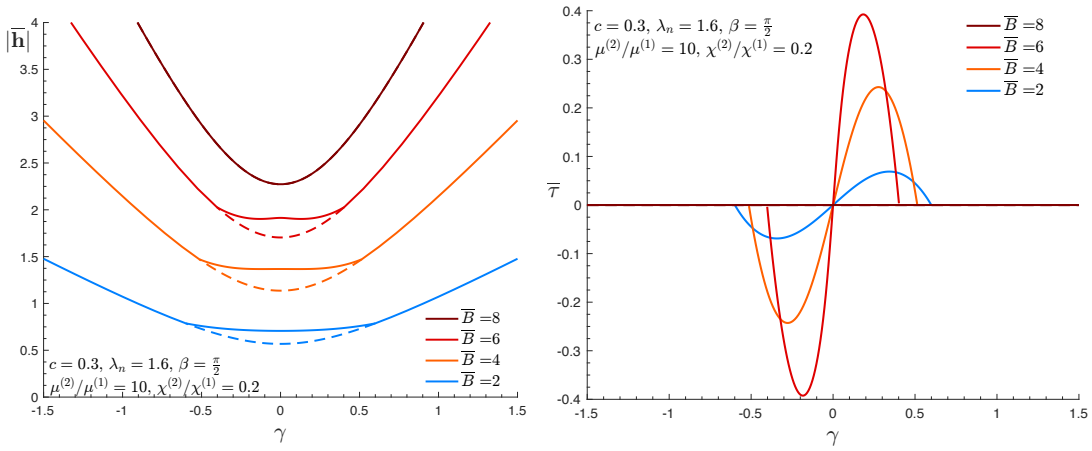

(e) (f)

Figure 9.9: Continued

negative normal stress difference. Note that this dramatic change in stress behavior also affects the shear stresses, as depicted in Figure 9.9d. In the purely mechanical case, as well as when $\beta = 0$, $R\widehat{W}$ has a completely soft mode of deformation, whereby $\overline{T}_{12} = 0$ in the region where $\widehat{W}$ fails to be (strictly) rank-one convex. However, for $\beta = \frac{\pi}{2}$, while $\overline{T}_{12}$ decreases in magnitude and relative to the predictions given by $\widehat{W}$ upon the formation of domains, it is always nonzero for $\gamma \neq 0$. Note also that for $\overline{B} \neq 0$, the sign of the shear stresses predicted by $\widehat{W}$ and $R\widehat{W}$ can be different for certain values of γ.

We recall that when $\beta = \frac{\pi}{2}$, $\overline{\mathbf{h}}$ and $\overline{\mathbf{b}}$ are always aligned and therefore the magnetically induced torques, as predicted by the principal solution, are identically zero. However, we find that $R\widehat{W}$ predicts a sharp increase in the magnitude of the magnetic torque, as depicted in Figure 9.9f. The existence of a magnetic torque coincides with an increase in the overall magnetic field intensity, as depicted in Figure 9.9e; this is to be expected, as $\overline{\tau}$ can be related $|\overline{\mathbf{h}}|$. Interestingly, and in connection to the non-monotonic nature of φ, we find that the torque reaches a maximal value precisely when the domain layers begin to rotate in the opposite direction. These

results indicate that, as a consequence of the rotation of the domains in order accommodate the large compression, the layers within the domains become unaligned with the magnetic field, leading to a nonzero macroscopic magnetic torque. In connection to the schematic depicting the domain formation in Figure 9.1b, this torque can be thought of as a result of the herring-bone structure, whereby the layers within the domain look to realign themselves with $\mathbf{M}_0$.

9.7 Concluding Remarks

In this work, we sought to apply the recent methodology introduced in Chapter 8 for describing the post-bifurcation response of magneto-elastic composites to a model problem. We considered, for analytical ease, a simple laminate consisting of two isotropic neo-Hookean phases that both have linear magnetic responses. Due to the increased complexity of the magneto-elastic coupling, we were unable to obtain an analytical expression for $Q\widehat{W}$ for general magneto-elastic loading conditions; such analytical expressions are only available when the average induction magnetic field is perpendicular to the layers (in the undeformed configuration). Nonetheless, our results still shed light on the behavior of the magneto-elastic laminate both before and after the onset of a macroscopic instability.

The first important conclusion drawn here is that, like in the purely-mechanical context, strict rank-one convexity, in the generalized magneto-elastic setting, of the principal solution is generally lost prior to strong ellipticity, as measured by the generalized strong ellipticity condition that makes use of the incremental magneto-elastic moduli of the principal solution. In fact, only under pure-shear loading with a magnetic field parallel and perpendicular to the layers (in the undeformed configuration) are strong ellipticity and strict rank-one convexity lost simultaneously. For more general loading, rank-one convexity can be lost significantly earlier than strong ellipticity.

While $Q\widehat{W}$ is only known for certain loading conditions, the bounds obtained in

this work remain rather tight so long as the magnetic field is not too aligned with the layers in the undeformed configuration. Even still, the difference between $\widehat{W}$ and $R\widehat{W}$ decreases as $\overline{\mathbf{B}}$ comes into alignment with the layers, whereby $R\widehat{W}$ can give an accurate prediction of $Q\widehat{W}$ for all loading conditions. Now, as we saw, a magnetic field perpendicular to the layers tends to destabilize the composite. It is therefore interesting that our knowledge of $Q\widehat{W}$ is best in these destabilized states.

In investigating the behavior of the laminate, we found that the mechanism of instability, namely sufficient compression along the layers, can either be promoted or inhibited, depending on the orientation of the applied magnetic field. In particular, the component of the magnetic field perpendicular to the layers has a magnetostrictive effect, whereby an instability can be initiated by applying a smaller value of λ_n (relative to the value in the purely mechanical case) in the presence of a magnetic field applied perpendicular to layers of the laminate. In fact, we found that a macroscopic instability can be triggered just by prescribing such a magnetic field, and taking $\overline{\boldsymbol{F}} = \boldsymbol{I}$. Such instabilities resulted in the formation of lamellar domains, and the construction was found to be similar to that in the purely mechanical case. In all cases, stability can be regained through the application of sufficient shear, and the relaxation not only induces mechanical softening, but can also lead to an increase or decrease in the macroscopic magnetic response, depending on the orientation of $\overline{\mathbf{B}}$.

The model used in this work was, admittedly, simple; this choice was made due to the fact that analytical estimates for the principal solution greatly simplify the calculation of $R\widehat{W}$. In particular, our constitutive model is unable to capture magnetic saturation effects, and is therefore most accurate only when the magnitude of the magnetic field is small. Moreover, use of a neo-Hookean potential for the purely mechanical response of the layers cannot capture strain locking behavior. As such, it is of interest going forward to obtain estimates for the principal solution of magneto-elastic composites with more complex material behavior and microstructures; the FOSO method discussed in Chapter 4 would certainly be capable of obtaining such

estimates. From there, we hope to then obtain corresponding estimates for the post-bifurcation response. Certainly, such calculations would be heavily computation, but it should still be possible to, at least numerically, extract $R\widehat{W}$, which will still be a better estimate on the relaxation than $\widehat{W}$, and would account for the onset of an instability.

9.8 Appendix I: Derivatives of $h(\overline{\boldsymbol{F}}, \overline{\mathbf{B}})$

A straightforward calculation shows that, when $(\overline{\boldsymbol{F}}, \overline{\mathbf{B}}) \in \mathcal{S}_{pcl}$,

$$\frac{\partial h}{\partial \overline{\boldsymbol{F}}} = \breve{\mu}(\overline{\boldsymbol{F}}\mathbf{N}_0) \otimes \mathbf{N}_0 + \left(\overline{\mu} - \frac{\left(\widetilde{\mu} + \widetilde{\chi}(\overline{\mathbf{B}} \cdot \mathbf{N}_0)^2\right)}{|\overline{\boldsymbol{F}}\mathbf{M}_0|^4} \right) (\overline{\boldsymbol{F}}\mathbf{M}_0) \otimes \mathbf{M}_0 \tag{9.8.1}$$

and

$$\frac{\partial h}{\partial \overline{\mathbf{B}}} = \frac{\widetilde{\chi}(\overline{\mathbf{B}} \cdot \mathbf{N}_0)}{|\overline{\boldsymbol{F}}\mathbf{M}_0|^2} \mathbf{N}_0. \tag{9.8.2}$$

Therefore, we find that

$$\begin{aligned} \boldsymbol{A} \cdot \frac{\partial^2 h}{\partial \overline{\boldsymbol{F}} \partial \overline{\boldsymbol{F}}} \boldsymbol{A} &= \breve{\mu} |\boldsymbol{A}\mathbf{N}_0|^2 + \frac{4(\widetilde{\mu} + \widetilde{\chi}(\overline{\mathbf{B}} \cdot \mathbf{N}_0)^2)}{|\overline{\boldsymbol{F}}\mathbf{M}_0|^6} [(\overline{\boldsymbol{F}}\mathbf{M}_0) \cdot (\boldsymbol{A}\mathbf{M}_0)]^2 \\ &\quad + \overline{\mu} \left[1 - (\lambda_{se}^x |\overline{\boldsymbol{F}}\mathbf{M}_0|)^{-4} \right] |\boldsymbol{A}\mathbf{M}_0|^2, \end{aligned} \tag{9.8.3}$$

$$\boldsymbol{A} \cdot \frac{\partial^2 h}{\partial \overline{\boldsymbol{F}} \partial \overline{\mathbf{B}}} \mathbf{a} = \mathbf{a} \cdot \frac{\partial^2 g}{\partial \overline{\mathbf{B}} \partial \overline{\boldsymbol{F}}} \boldsymbol{A} = -\frac{2\widetilde{\chi}(\overline{\mathbf{B}} \cdot \mathbf{N}_0)}{|\overline{\boldsymbol{F}}\mathbf{M}_0|^4} (\mathbf{a} \cdot \mathbf{N}_0)[(\overline{\boldsymbol{F}}\mathbf{M}_0) \cdot (\boldsymbol{A}\mathbf{M}_0)], \tag{9.8.4}$$

$$\mathbf{a} \cdot \frac{\partial^2 h}{\partial \overline{\mathbf{B}} \partial \overline{\mathbf{B}}} \mathbf{a} = \frac{\widetilde{\chi}}{|\overline{\boldsymbol{F}}\mathbf{M}_0|^2} (\mathbf{a} \cdot \mathbf{N}_0)^2. \tag{9.8.5}$$

For $(\overline{\boldsymbol{F}}, \overline{\mathbf{B}}) \in \mathcal{S}_{pcl}^c$, we have

$$\frac{\partial h}{\partial \overline{\boldsymbol{F}}} = \breve{\mu}(\overline{\boldsymbol{F}}\mathbf{N}_0) \otimes \mathbf{N}_0 \tag{9.8.6}$$

and

$$\frac{\partial h}{\partial \overline{\mathbf{B}}} = \widetilde{\chi}(\lambda_{se}^x)^2 (\overline{\mathbf{B}} \cdot \mathbf{N}_0) \mathbf{N}_0 \tag{9.8.7}$$

It follows then that

$$\boldsymbol{A}\cdot\frac{\partial^2 h}{\partial\overline{\boldsymbol{F}}\partial\overline{\boldsymbol{F}}}\boldsymbol{A}=\breve{\mu}|\boldsymbol{A}\mathbf{N}_0|^2, \tag{9.8.8}$$

$$\boldsymbol{A}\cdot\frac{\partial^2 h}{\partial\overline{\boldsymbol{F}}\partial\overline{\mathbf{B}}}\mathbf{a}=\mathbf{a}\cdot\frac{\partial^2 g}{\partial\overline{\mathbf{B}}\partial\overline{\boldsymbol{F}}}\boldsymbol{A}=0, \tag{9.8.9}$$

$$\mathbf{a}\cdot\frac{\partial^2 h}{\partial\overline{\mathbf{B}}\partial\overline{\mathbf{B}}}\mathbf{a}=\frac{\widetilde{\chi}\widetilde{\mu}}{\overline{\mu}}(\lambda_{se}^x)^6(\mathbf{a}\cdot\mathbf{N}_0)^2. \tag{9.8.10}$$

9.9 Appendix II: Loss of Strong Ellipticity of $\widehat{W}$

We look to apply the generalized strong ellipticity condition to $\widehat{W}$, whereby we check that

$$\Big(\mathbf{m}\cdot(\widehat{\boldsymbol{Q}}\mathbf{m})\Big)\Big(\mathbf{n}^{\perp}\cdot(\widehat{\boldsymbol{E}}^c(\mathbf{n})\mathbf{n}^{\perp})\Big)-(\mathbf{n}^{\perp}\cdot\widehat{\boldsymbol{R}}^T\mathbf{m})^2>0$$
$$\forall\,\mathbf{n},\mathbf{m},\mathbf{n}^{\perp}\text{ such that }|\mathbf{n}|=|\mathbf{m}|=|\mathbf{n}^{\perp}|=1,\text{ and }\mathbf{m}\cdot\mathbf{n}=\mathbf{n}^{\perp}\cdot\mathbf{n}=0, \tag{9.9.1}$$

where $\widehat{\boldsymbol{Q}}$, $\boldsymbol{E}^c$ and $\widehat{R}$ are defined by Eqs. (9.2.18) and (9.2.19), as applied to $\widehat{W}$. Therefore, we start by calculating the associated magnetoelastic moduli. As the incompressibility condition is enforced by making use of the push-forward of the moduli, we only need to take derivatives of the finite part of $\widehat{W}$, as given in Eq. (9.3.9). We find that

$$\frac{\partial\widehat{W}}{\partial\overline{\boldsymbol{F}}}=\breve{\mu}\overline{\boldsymbol{F}}\mathbf{N}_0\otimes\mathbf{N}_0+\overline{\mu}\overline{\boldsymbol{F}}\mathbf{M}_0\otimes\mathbf{M}_0+\breve{\chi}\overline{\boldsymbol{F}}\,\overline{\mathbf{B}}\otimes\overline{\mathbf{B}}-\frac{\widetilde{\mu}+\widetilde{\chi}(\overline{\mathbf{B}}\cdot\mathbf{N}_0)^2}{|\overline{\boldsymbol{F}}\mathbf{M}_0|^4}\overline{\boldsymbol{F}}\mathbf{M}_0\otimes\mathbf{M}_0, \tag{9.9.2}$$

$$\frac{\partial\widehat{W}}{\partial\overline{\mathbf{B}}}=\breve{\chi}\overline{\boldsymbol{C}}\,\overline{\mathbf{B}}+\frac{\widetilde{\chi}(\overline{\mathbf{B}}\cdot\mathbf{N}_0)}{|\overline{\boldsymbol{F}}\mathbf{M}_0|^2}\mathbf{N}_0, \tag{9.9.3}$$

where $\overline{\boldsymbol{C}} = \overline{\boldsymbol{F}}^T\overline{\boldsymbol{F}}$ is the right Cauchy-Green tensor. It then follows that the push-forward of the magnetoelastic moduli, as defined by Eq. (9.2.19), are given by

$$\begin{aligned} L^c_{ijkl} &= \delta_{ik}\left(\breve{\mu}(\overline{\boldsymbol{F}}\mathbf{N}_0)\otimes(\overline{\boldsymbol{F}}\mathbf{N}_0) + \overline{\mu}(\overline{\boldsymbol{F}}\mathbf{M}_0)\otimes(\overline{\boldsymbol{F}}\mathbf{M}_0) + \breve{\chi}(\overline{\boldsymbol{F}}\,\overline{\mathbf{B}})\otimes(\overline{\boldsymbol{F}}\,\overline{\mathbf{B}})\right) \\ &\quad + \frac{\widetilde{\mu}+\widetilde{\chi}(\overline{\mathbf{B}}\cdot\mathbf{N}_0)^2)}{|\overline{\boldsymbol{F}}\mathbf{M}_0|^6}(\overline{\boldsymbol{F}}\mathbf{M}_0)_j(\overline{\boldsymbol{F}}\mathbf{M}_0)_l\left(4(\overline{\boldsymbol{F}}\mathbf{M}_0)_i(\overline{\boldsymbol{F}}\mathbf{M}_0)_k - \delta_{ik}|\overline{\boldsymbol{F}}\mathbf{M}_0|^2\right), \end{aligned} \tag{9.9.4}$$

$$M^c_{ijk} = \breve{\chi}(\delta_{ik}(\overline{\boldsymbol{F}}\,\overline{\mathbf{B}})_j + (\overline{\boldsymbol{F}}\,\overline{\mathbf{B}})_i\delta_{jk}) - \frac{2\widetilde{\chi}(\overline{\mathbf{B}}\cdot\mathbf{N}_0)}{|\overline{\boldsymbol{F}}\mathbf{M}_0|^4}(\overline{\boldsymbol{F}}\mathbf{M}_0)_i(\overline{\boldsymbol{F}}\mathbf{M}_0)_j(\overline{\boldsymbol{F}}^{-T}\mathbf{N}_0)_k, \tag{9.9.5}$$

so that the corresponding acoustic tensors, as defined by Eq. (9.2.18) take the form

$$\begin{aligned} \boldsymbol{Q}^c(\mathbf{n}) &= \big\{\breve{\mu}[(\overline{\boldsymbol{F}}\mathbf{N}_0)\cdot\mathbf{n}]^2 + \overline{\mu}[(\overline{\boldsymbol{F}}\mathbf{M}_0)\cdot\mathbf{n}]^2 + \breve{\chi}[(\overline{\boldsymbol{F}}\,\overline{\mathbf{B}})\cdot\mathbf{n}]^2 \qquad (9.9.6) \\ &\quad - \frac{\widetilde{\mu}+\widetilde{\chi}(\overline{\mathbf{B}}\cdot\mathbf{N}_0)^2}{|\overline{\boldsymbol{F}}\mathbf{M}_0|^4}[(\overline{\boldsymbol{F}}\mathbf{M}_0)\cdot\mathbf{n}]^2\big\}\boldsymbol{I} \\ &\quad + 4\frac{\widetilde{\mu}+\widetilde{\chi}(\overline{\mathbf{B}}\cdot\mathbf{N}_0)^2}{|\overline{\boldsymbol{F}}\mathbf{M}_0|^6}[(\overline{\boldsymbol{F}}\mathbf{M}_0)\cdot\mathbf{n}]^2\left(\overline{\boldsymbol{F}}\mathbf{M}_0\right)\otimes\left(\overline{\boldsymbol{F}}\mathbf{M}_0\right), \qquad (9.9.7) \end{aligned}$$

$$\boldsymbol{R}^c(\mathbf{n}) = \breve{\chi}\boldsymbol{I}(\overline{\boldsymbol{F}}\,\overline{\mathbf{B}}\cdot\mathbf{n}) + \breve{\chi}(\overline{\boldsymbol{F}}\,\overline{\mathbf{B}})\otimes\mathbf{n} - 2\frac{\widetilde{\chi}(\overline{\mathbf{B}}\cdot\mathbf{N}_0)}{|\overline{\boldsymbol{F}}\mathbf{M}_0|^4}[(\overline{\boldsymbol{F}}\mathbf{M}_0)\cdot\mathbf{n}](\overline{\boldsymbol{F}}\mathbf{M}_0)\otimes(\overline{\boldsymbol{F}}^{-T}\mathbf{N}_0), \tag{9.9.8}$$

$$\boldsymbol{E}^c = \breve{\chi}\boldsymbol{I} + \frac{\widetilde{\chi}}{|\overline{\boldsymbol{F}}\mathbf{M}_0|^2}(\overline{\boldsymbol{F}}^{-T}\mathbf{N}_0)\otimes(\overline{\boldsymbol{F}}^{-T}\mathbf{N}_0). \tag{9.9.9}$$

Due to the plane-strain conditions, $\mathbf{n}$, $\mathbf{n}^\perp$ and $\mathbf{m}$ can be restricted to 2 dimensions. Therefore, the orthogonality conditions $\mathbf{n}\cdot\mathbf{n}^\perp = \mathbf{n}\cdot\mathbf{m} = 0$ along with the constraint that each vector has unit length, imply that $\mathbf{n}^\perp = \mathbf{m}$. Therefore, in order to check strong ellipticity, we introduce the generalized best ellipticity constant (Geymonat et al., 1993)

$$\widehat{\Lambda}(\overline{\boldsymbol{F}},\overline{\mathbf{B}}) = \inf_{\substack{\mathbf{n},\mathbf{m} \\ \mathbf{n}\cdot\mathbf{m}=0,\,|\mathbf{n}|=|\mathbf{m}|=1}} \mathcal{F}(\overline{\boldsymbol{F}},\overline{\mathbf{B}},\mathbf{n},\mathbf{m}), \tag{9.9.10}$$

where

$$\mathcal{F}(\overline{\boldsymbol{F}},\overline{\mathbf{B}},\mathbf{n},\mathbf{m}) = \left(\mathbf{m}\cdot(\widehat{\boldsymbol{Q}^c}\mathbf{m})\right)\left(\mathbf{m}\cdot(\widehat{\boldsymbol{E}^c}\mathbf{m})\right) - (\mathbf{m}\cdot\widehat{\boldsymbol{R}^c}^T\mathbf{m})^2. \tag{9.9.11}$$

We recall that $\widehat{(\cdot)} = \widehat{\boldsymbol{I}}(\cdot)\widehat{\boldsymbol{I}}$, where $\widehat{\boldsymbol{I}} = \boldsymbol{I} - \mathbf{n}\otimes\mathbf{n}$. Upon plugging Eqs. (9.9.7)-(9.9.9) into Eq. (9.9.11), and using the fact that $(\overline{\boldsymbol{F}}\mathbf{M}_0)\cdot\mathbf{n} = (\overline{\boldsymbol{F}}^{-T}\mathbf{N}_0)\cdot\mathbf{m}$, we find that

$$\begin{aligned}
&\mathcal{F}(\overline{\boldsymbol{F}},\overline{\mathbf{B}},\mathbf{n},\mathbf{m}) = \\
&\mathbf{m}\cdot\left(\left[\widehat{\boldsymbol{Q}}^c_{me} - \frac{\widetilde{\chi}(\overline{\mathbf{B}}\cdot\mathbf{N}_0)^2}{|\overline{\boldsymbol{F}}\mathbf{M}_0|^4}(\overline{\boldsymbol{F}}^{-T}\mathbf{N}_0)\otimes(\overline{\boldsymbol{F}}^{-T}\mathbf{N}_0)\right]\mathbf{m}\right)\left(\breve{\chi} + \frac{\widetilde{\chi}((\overline{\boldsymbol{F}}\mathbf{M}_0)\cdot\mathbf{n})^2}{|\overline{\boldsymbol{F}}\mathbf{M}_0|^2}\right) \\
&+ \frac{\breve{\chi}\widetilde{\chi}((\overline{\boldsymbol{F}}\mathbf{M}_0)\cdot\mathbf{n})^2}{|\overline{\boldsymbol{F}}\mathbf{M}_0|^2}\left((\overline{\boldsymbol{F}}\,\overline{\mathbf{B}})\cdot\mathbf{n} + \frac{2(\overline{\mathbf{B}}\cdot\mathbf{N}_0)(\overline{\boldsymbol{F}}\mathbf{M}_0\cdot\mathbf{m})}{|\overline{\boldsymbol{F}}\mathbf{M}_0|^2}\right)^2, \qquad (9.9.12)
\end{aligned}$$

where $\widehat{\boldsymbol{Q}}^c_{me}$ is the acoustic tensor (in the current configuration) associated with the purely mechanical problem and is given by (see Chapter 6)

$$\begin{aligned}
\widehat{\boldsymbol{Q}}^c_{me} &= \left\{\breve{\mu}[(\overline{\boldsymbol{F}}\mathbf{N}_0)\cdot\mathbf{n}]^2 + \overline{\mu}[(\overline{\boldsymbol{F}}\mathbf{M}_0)\cdot\mathbf{n}]^2 - \frac{\widetilde{\mu}}{|\overline{\boldsymbol{F}}\mathbf{M}_0|^4}[(\overline{\boldsymbol{F}}\mathbf{M}_0)\cdot\mathbf{n}]^2\right\}\boldsymbol{I} \\
&+ 4\frac{\widetilde{\mu}}{|\overline{\boldsymbol{F}}\mathbf{M}_0|^6}[(\overline{\boldsymbol{F}}\mathbf{M}_0)\cdot\mathbf{n}]^2\left(\overline{\boldsymbol{F}}\mathbf{M}_0\right)\otimes\left(\overline{\boldsymbol{F}}\mathbf{M}_0\right). \qquad (9.9.13)
\end{aligned}$$

Chapter 10
Closure

This thesis presents a number of results from studying problems in nonlinear homogenization. Each group of chapters is concerned with a specific topic (i.e. linear comparison methods, hyperelasticity, and magneto-elasticity), and can be considered independently. Before summarizing the findings of the various parts of the thesis, as well as discussing future avenues for continued research, it is important to discuss what this thesis, in its entirety, has shown as it pertains most generally to the study of nonlinear homogenization. As we have seen, convexity, or the lack thereof, plays a major role. While convexity can be utilized directly to obtain bounds and ensure that solutions remain "well behaved," a lack of it leads to a much richer set of problems that require more sophisticated tools in order to solve them. This also highlights the importance that the physics of the underlying system to be modeled plays; physical considerations may necessitate a constitutive model that makes use of a non-convex energy potential.

We end this thesis by discussing the chapters individually. In Chapters 2 and 3, we started by investigating the VHS bounds, and in particular, we showed that these nonlinear bounds are optimal. While they provide rigorous bounds on the class of statistically isotropic microstructures, we exploited the degeneracy of the linear bounds to show that the VHS bounds are optimal instead over the class of anisotropic non-

linear composites with linearly isotropic response. This degeneracy means that linear bounds do not rely on higher order statistical information of the underlying microstructure. In particular, the same bounds that hold for random, or periodic, linear materials can be attained by a finite-rank laminate, a material whose microstructure is neither random, nor periodic. Therefore, in order to improve on these bounds, it would be necessary to somehow exclude these undesirable microstructures, *a priori*. While it would still be preferable to generate bounds by making use of an LCC, this degeneracy may be difficult to overcome within the context of linear comparison bounds.

Having seen how VHS bounds failed to fully utilize all available information from the LCC, in Chapter 4, we introduced the FOSO method, which can be used to generate estimates on the effective response of nonlinear materials. The method is based on estimates of Ponte Castañeda (2016), and both yield fully optimized results that are exact to second-order in the heterogeneity contrast of the system. The difference between the two lies in the form of the potential used to characterize the LCC. The symmetric FOSO version works in such a way that the results are the same regardless of the formulation one starts with (i.e. a strain based versus a stress based formulation); this was not the case with the previous FOSO method. Moreover, the symmetric FOSO version is in some sense more robust, as there is more freedom in the choice of stationary points. In application, the FOSO method is able to predict complex physical phenomena, and is in good agreement with available experimental and computational results. One issue that requires further consideration is the choice of the parameter $\alpha^{(r)}$. In the application section, we chose a value of $\alpha^{(r)} = \frac{1}{2}$ out of convenience, but we are unaware of a systematic way for choosing it in general. Recent results suggest that the optimal choice may coincide with the value for which the FOSO method agrees with the weakly nonlinear limiting behavior of the system (see Appendix A).

In Chapters 5 to 7, we turned out attention to investigating the mechanism of

instability in reinforced elastomers, and obtaining estimates for the post-bifurcation behavior in the event that the composite undergoes a macroscopic instability. Chapter 5 was concerned with the theoretical framework for answering such questions, and provided some novel results with regards to the calculation of the rank-one convex envelope of a function, and the implications such a construction has on the relaxation construction. The methodology for extracting the post-bifurcation behavior of a elastomeric system was introduced by Avazmohammadi and Ponte Castañeda (2016), and taken up here to calculate the quasiconvexification $Q\widehat{W}$ of the principal solution of a two-phase laminate consisting of isotropic neo-Hookean phases. A full set of results was obtained for plane-strain loading, in Chapter 6, as well as for more general three-dimensional loading, in Chapter 7. In both cases, it is found that, upon sufficient compression along the layers, the composite finds stability via the formation of domains. This domain formation leads to soft modes of deformation. The calculation in Chapter 7 required the creation of a new set of transversely isotropic invariants that are more physically relevant than the classical $I_1, \ldots, I_5$ invariants. From a mathematical perspective, it is still of interest to determine under what conditions can one conclude that $\widetilde{W} = Q\widehat{W}$. From an engineering point of view, we also would like to study systems with more complex microstructures and constitutive behavior. It is here that the FO-SO method could be utilized to obtain estimates for the principal solution of such systems. These estimates are necessary to study the onset of instabilities, as well as to extract the post-bifurcation response. However, for more complex systems, estimates for $Q\widehat{W}$ would most likely be numerical.

We concluded our work in Chapters 8 and 9, where we looked to generalize the results of the previous three chapters towards the setting of magneto-elasticity. In Chapter 8, we were indeed able to rigorously extend the tools from the calculus of variations to the magneto-elastic setting. While we argue that $\widetilde{W}$ (which is defined in the periodic context using a definition generalizing the one given by Müller (1987) for purely mechanical composites) is quasiconvex, this fact remains to be proven, and

is a possible direction for future work. We then applied the results of Chapter 8 in Chapter 9 to the same neo-Hookean laminate under plane-strain we considered in Chapter 6, but with the added assumption that each phase is magnetically susceptible. Due to the added complexity of the coupled magneto-elastic response, we were unable to obtain general analytical estimates for $Q\widehat{W}$; we were only able to do so for specific loading conditions. We were also unable to obtain analytical results for $R\widehat{W}$. Nonetheless, we obtained a complete numerical description of $R\widehat{W}$, which we used to estimate the post-bifurcation response. We found that the mechanism of instability was, like in the purely mechanical context, related to the compression along the layers. However, such compression can arises either from purely mechanical effects, or from magnetostrictive effects arising from the magneto-elastic coupling. In particular, magnetic fields applied perpendicular to the layers have a destabilizing effect, and can induce instabilities on their own. The post-bifurcation response is again marked by domain formation, and while there is mechanical softening as a result, depending on the orientation of the applied magnetic field, the post-bifurcation magnetic response is either increased (when the magnetic field is parallel to the layers), or decreased (when the magnetic field is perpendicular to the layers). In going forward, like in the purely mechanical context, it is of interest to consider more complex physical systems. From what we have seen for the simple laminate, there is little hope of obtaining analytical results, but numerical results themselves should be sufficient for a full understanding of the post-bifurcation response.

Appendix A

Weakly Nonlinear Composite Cylinder Assemblage

Abstract

In this chapter, we consider Hashin's composite cylinder assemblage (CCA) when both phases are taken to be nonlinear. It is known, for linear phases, that the cylindrical inclusion can be added to the effective medium without perturbing the macroscopic fields. We show that, in the limit of weak nonlinearity, the same property is maintained. We also compare the corrections predicted by various other bounds and estimates.

A.1 Effective Behavior of Nonlinear CCA

We consider a cylindrical material occupying some region $\Omega_0 \subset V_0$, embedded in an effective medium, where V_0 denotes the region occupied by this effective medium. The cylinder's axis is taken to be aligned in the $\mathbf{e}_z$ direction, and we consider the circular cross section of the cylinder, centered at the origin. In the $\mathbf{e}_x - \mathbf{e}_y$ plane, the circular material is composed of a core phase, denoted as phase 1, with inner radius r_i surrounded by a shell phase, denoted as phase 2. The entire core-shell material has a total radius of r_o, so that $c = \left(\frac{r_i}{r_o}\right)^2$ denotes the total volume fraction of core phase (i.e. phase 1), and we let $\Omega_0^{(r)} \subset \Omega_0$ denote the region occupied by phase r. The local

behavior of the material is described by the energy potential

$$w(\mathbf{x}, \mathbf{E}) = \sum_{r=1}^{2} \chi^{(r)}(\mathbf{x}) w^{(r)}(\mathbf{E}) \tag{A.1.1}$$

where $\chi^{(r)}$ denote the characteristic function of phase r, so that $\chi^{(r)}(\mathbf{x}) = 1$ if $\mathbf{x} \in \Omega_0^{(r)}$ and 0 otherwise. As such, the local current density $\mathbf{j}$ is given by

$$\mathbf{j} = \frac{\partial w(\mathbf{E})}{\partial \mathbf{E}}. \tag{A.1.2}$$

We look to determine whether we can embed this material into the effective medium in such a way as to not alter the macroscopic effective behavior. Put another way, we look to determine whether this embedded material can be added in such a way as to not perturb the macroscopic fields. If this is possible, then we can iterate this process, continually replacing the effective medium with the core-shell inclusion, until the entire space is filled. We are then left with a two phase composite with the core phase acting as the inclusion phase, and the shell phase acting as the matrix phase. By letting $\langle \cdot \rangle$ denote the volume average over Ω_0, it follows that

$$\widetilde{w}(\overline{\mathbf{E}}) = \min_{\mathbf{E} \in \mathcal{K}(\overline{\mathbf{E}})} \langle w(\mathbf{x}, \mathbf{E}(\mathbf{x})) \rangle, \tag{A.1.3}$$

where

$$\mathcal{K}(\overline{\mathbf{E}}) = \{\mathbf{E} : \mathbf{E} = -\nabla \phi, \text{ in } \Omega_0, \quad \text{and } \phi = -\overline{\mathbf{E}} \cdot \mathbf{x}, \text{ on } \partial\Omega_0\}, \tag{A.1.4}$$

denotes the set of admissible electric field potentials. Since the composite consists of copies of Ω_0 of varying size, each of which has the same effective property, we only need to look at the effective behavior over Ω_0 itself. It can then be shown that the

average current density $\bar{\mathbf{j}}$ is given by

$$\bar{\mathbf{j}} = \frac{\partial \widetilde{w}}{\partial \overline{\mathbf{E}}}. \tag{A.1.5}$$

Solving Eq. (A.1.3) is the same as solving the associated boundary value problem defined by

$$\begin{cases} \nabla \cdot \mathbf{j}(\mathbf{x}) = 0 & \mathbf{x} \in \Omega_0 \\ \phi(\mathbf{x}) = -\overline{\mathbf{E}} \cdot \mathbf{x} & \mathbf{x} \in \partial\Omega_0 \end{cases} \tag{A.1.6}$$

where it is recalled that $\mathbf{j}$ is defined through the constitutive relation (A.1.2). Any solution to Eq. (A.1.6) must also satisfy

$$[[\mathbf{j}]] \cdot \mathbf{n} = 0, \quad [[\phi]] = 0 \tag{A.1.7}$$

across any material interphase, where $\mathbf{n}$ denotes the unit normal to such an interphase.

A.2 Weakly Nonlinear Limit

To apply the above construction, we consider the case where $w^{(r)}$ is isotropic, and takes the form

$$w^{(r)}(\mathbf{E}) = \frac{\epsilon^{(r)}}{m+1}|\mathbf{E}|^{m+1} \tag{A.2.1}$$

where $E = |\mathbf{E}|$ represents the magnitude of $\mathbf{E}$, $\epsilon^{(r)}$ denotes the conductivity of phase r, and $0 \leqslant m \leqslant \infty$ represents the nonlinearity. Then, the local current density is given by

$$\mathbf{j} = \epsilon(\mathbf{x})|E|^{m-1}\mathbf{E}, \tag{A.2.2}$$

where

$$\epsilon(\mathbf{x}) = \epsilon^{(1)}\chi^{(1)}(\mathbf{x}) + \epsilon^{(2)}\chi^{(2)}(\mathbf{x}). \tag{A.2.3}$$

Since each $w^{(r)}$ is homogeneous of degree $m+1$ in $\mathbf{E}$, the effective potential $\widetilde{w}$ will be as well. Assuming that the effective response is also isotropic, we can write the effective potential as

$$\widetilde{w}(\overline{\mathbf{E}}) = \frac{\widetilde{\epsilon}}{m+1}\overline{E}^{m+1}, \tag{A.2.4}$$

where $\overline{E} = |\overline{\mathbf{E}}|$, and $\widetilde{\epsilon}$ defines the effective conductivity. While the CCA construction is not anticipated, in general, to hold for any nonlinearity m, we are interested in the case when $m = 1 + \delta$ and $\delta << 1$. We note that the CCA construction works in linear case ($m = 1$) and moreover, the effective behavior of the composite is known to saturate the Hashin-Shtrikmann bounds on the effective conductivity of two-phase isotropic composites.

Now, from Eqs. (A.1.3) and (A.2.4), it follows that

$$\frac{\widetilde{\epsilon}|\overline{\mathbf{E}}|^{2+\delta}}{2+\delta} = \langle w(\mathbf{x}, \mathbf{E}^*)\rangle, \tag{A.2.5}$$

where $\mathbf{E}^* = -\nabla\phi$ is the solution to Eq. (A.1.6). We take $\overline{\mathbf{E}} = \overline{E}\mathbf{e}_x$, so that $\widetilde{\epsilon}$ corresponds to the effective transverse conductivity. We assume that $\widetilde{\epsilon}$ can be expanded via

$$\widetilde{\epsilon} = \widetilde{\epsilon}_0 + \widetilde{\epsilon}_1\delta + O(\delta^2), \tag{A.2.6}$$

so that ϕ takes the form

$$\phi = \phi_0 + \phi_1\delta + O(\delta^2), \tag{A.2.7}$$

which implies that

$$\mathbf{E}^* = \mathbf{E}_0 + \mathbf{E}_1\delta + O(\delta^2) \tag{A.2.8}$$

where $\mathbf{E}_i = -\nabla\phi_i$. From this, we find that

$$|\mathbf{E}^*|^2 = |\mathbf{E}_0|^2 + 2\mathbf{E}_1 \cdot \mathbf{E}_0\delta + O(\delta^2). \tag{A.2.9}$$

Using the identity

$$\frac{d}{dx}\left[f(x)^{g(x)}\right] = f(x)^{g(x)}\left(\frac{dg(x)}{dx}\log(f(x)) + \frac{g(x)}{f(x)}\frac{df(x)}{dx}\right), \tag{A.2.10}$$

it follows from Eq. (A.2.2) that

$$\mathbf{j} = \mathbf{j}_0 + \mathbf{j}_1\delta + O(\delta^2), \tag{A.2.11}$$

where,

$$\mathbf{j}_0 = \epsilon(\mathbf{x})\mathbf{E}_0, \quad \mathbf{j}_1 = \epsilon(\mathbf{x})(\mathbf{E}_1 + \mathbf{E}_0\log(E_0)). \tag{A.2.12}$$

Therefore, expanding Eq. (A.2.5) and equating terms of order δ, we have

$$\widetilde{\epsilon}_0\overline{E}^2 = \langle\epsilon(\mathbf{x})|\nabla\phi_0|^2\rangle, \tag{A.2.13}$$

$$(\widetilde{\epsilon}_1 + \widetilde{\epsilon}_0\log(\overline{E}))\overline{E}^2 = \left\langle \epsilon(\mathbf{x})\left[2(\nabla\phi_0)\cdot(\nabla\phi_1) + \frac{1}{2}|\nabla\phi_0|^2\log\left(|\nabla\phi_0|^2\right)\right]\right\rangle. \tag{A.2.14}$$

Hence, in order to obtain the first-order correction $\widetilde{\epsilon}_1$, we must find the solutions ϕ_0 and ϕ_1 to the boundary value problem defined by Eq. (A.1.6). We now adopt the cylindrical coordinate basis $\{\mathbf{e}_r, \mathbf{e}_\theta, \mathbf{e}_z\}$. For reference, we note that $\mathbf{e}_x = \cos(\theta)\mathbf{e}_r - \sin(\theta)\mathbf{e}_\theta$, while $\mathbf{e}_y = \sin(\theta)\mathbf{e}_r + \cos(\theta)\mathbf{e}_\theta$. We assume that ϕ does not vary in the $\mathbf{e}_z$ direction, and therefore we can treat this problem in two-dimensions. In this setting, we note that

$$\Omega_0^{(1)} = \{(r,\theta) \,:\, 0 \leqslant r \leqslant r_i,\, \theta \in [0, 2\pi]\}, \tag{A.2.15}$$

$$\Omega_0^{(2)} = \{(r,\theta) \,:\, r_i \leqslant r \leqslant r_o,\, \theta \in [0, 2\pi]\}. \tag{A.2.16}$$

Moreover, at each level of the perturbation, we assume that

$$\phi_k(r,\theta) = \begin{cases} \phi_k^{(1)}(r,\theta) & 0 \leqslant r \leqslant r_i \\ \phi_k^{(2)}(r,\theta) & r_i \leqslant r \leqslant r_o \end{cases}. \tag{A.2.17}$$

for $k = 0, 1, 2, \ldots$.

A.2.1 Solution to 0^{th} order

Starting with the zeroth order term, Eqs. (A.1.6)-(A.1.7) can be used to show that

$$\begin{cases} \Delta\phi_0^{(r)} = 0,\ r = 1, 2, \\ \phi_0^{(1)}(r_i, \theta) = \phi_0^{(2)}(r_i, \theta), \\ \mathbf{j}_0^{(1)}(r_i, \theta) \cdot \mathbf{e}_r = \mathbf{j}_0^{(2)}(r_i, \theta) \cdot \mathbf{e}_r, \\ \phi_0^{(2)}(r_o, \theta) = -\overline{E} r_0 \cos(\theta), \end{cases} \tag{A.2.18}$$

where, from Eq. $(A.2.12)_1$,

$$\mathbf{j}_0^{(r)} = -\epsilon^{(r)} \nabla \phi_0^{(r)}. \tag{A.2.19}$$

Eq. $(A.2.18)_1$ corresponds to the equilibrium equation, Eqs. $(A.2.18)_2$-$(A.2.18)_3$ correspond to the jump conditions, and Eq. $(A.2.18)_4$ enforces the boundary condition.

From Eq. $(A.2.18)_1$, it follows that $\phi_0^{(r)}$ take the form

$$\phi_0(r, \theta) = \begin{cases} \left(a_1 r + \frac{b_1}{r}\right) \cos(\theta) & 0 \leqslant r \leqslant r_i \\ \left(a_2 r + \frac{b_2}{r}\right) \cos(\theta) & r_i \leqslant r \leqslant r_o. \end{cases} \tag{A.2.20}$$

Note that in general,

$$\varphi(r, \theta) = \sum_{n=1}^{\infty} (g_n r^n + h_n r^{-n}) \cos(n\theta) \tag{A.2.21}$$

satisfies $\Delta\varphi = 0$, but for simplicity, we choose to only consider the first term of the sum. Continuity of ϕ_0 at the origin requires that $b_1 = 0$, while continuity at r_i implies that

$$a_1 r_i \cos(\theta) = \left(a_2 r_i + \frac{b_2}{r_i}\right) \cos(\theta). \tag{A.2.22}$$

As would be done in analyzing a complete power series expansion of the form in Eq.

(A.2.21), we multiply Eq. (A.2.22) by $\cos(\theta)$, and integrate from 0 to 2π to find that

$$a_1 = a_2 + \frac{b_2}{r_i^2}. \tag{A.2.23}$$

.

Now, from Eq. (A.2.20), we find that

$$\boldsymbol{E}_0(r,\theta) = -\begin{cases} a_1(\cos(\theta)\mathbf{e}_r - \sin(\theta)\mathbf{e}_\theta) & 0 \leqslant r \leqslant r_i \\ \left(a_2 - \frac{b_2}{r^2}\right)\cos(\theta)\mathbf{e}_r - \left(a_2 + \frac{b_2}{r^2}\right)\sin(\theta)\mathbf{e}_\theta & r_i \leqslant r \leqslant r_o. \end{cases} \tag{A.2.24}$$

Therefore, Eq. $(A.2.18)_3$ implies that

$$\epsilon^{(1)} a_1 = \epsilon^{(2)}\left(a_2 - \frac{b_2}{r_i^2}\right), \tag{A.2.25}$$

while Eq. $(A.2.18)_4$ yields

$$a_2 + \frac{b_2}{r_o^2} = -\overline{E}. \tag{A.2.26}$$

Eqs. (A.2.23),(A.2.25), and (A.2.26) constitute a system of linear equations, which can be solved to give

$$a_1 = \frac{-2\epsilon^{(2)}\overline{E}}{(\epsilon^{(1)} + \epsilon^{(2)}) - c(\epsilon^{(1)} - \epsilon^{(2)})}, \tag{A.2.27}$$

$$a_2 = \frac{-(\epsilon^{(1)} + \epsilon^{(2)})\overline{E}}{(\epsilon^{(1)} + \epsilon^{(2)}) - c(\epsilon^{(1)} - \epsilon^{(2)})}, \tag{A.2.28}$$

$$b_2 = \frac{r_i^2(\epsilon^{(1)} - \epsilon^{(2)})\overline{E}}{(\epsilon^{(1)} + \epsilon^{(2)}) - c(\epsilon^{(1)} - \epsilon^{(2)})}. \tag{A.2.29}$$

Substituting into Eq. (A.2.13), we find that

$$\widetilde{\epsilon}_0 = \epsilon^{(2)}\frac{(\epsilon^{(1)} + \epsilon^{(2)}) + c(\epsilon^{(1)} - \epsilon^{(2)})}{(\epsilon^{(1)} + \epsilon^{(2)}) - c(\epsilon^{(1)} - \epsilon^{(2)})}, \tag{A.2.30}$$

which is exactly the Hashin-Shtrikman result. To check that the addition of such an

inclusion does not perturb the macroscopic fields to zeroth order, we must check that the current density satisfies the continuity condition $[[\mathbf{j}_0(r_o,\theta)]]\cdot\mathbf{e}_r = 0$. Indeed, we find that

$$\mathbf{j}_0(r_o,\theta)\cdot\mathbf{e}_r = -\epsilon^{(2)}\left(a_2 - \frac{b_2}{r_o^2}\right)\cos(\theta) = \widetilde{\epsilon}_0\overline{E}\cos(\theta) = (\widetilde{\epsilon}_0\overline{\mathbf{E}})\cdot\mathbf{e}_r = \overline{\mathbf{j}_0}\cdot\mathbf{e}_r \quad \text{(A.2.31)}$$

A.2.2 Solution to 1^{st} order

We now move to the first-order equations, which, using Eqs. (A.1.6)-(A.1.7), read as

$$\begin{cases} \Delta\phi_1^{(r)} + \frac{(\nabla\phi_0^{(r)})\cdot D^2\phi_0^{(r)}(\nabla\phi_0^{(r)})}{|\nabla\phi_0^{(r)}|^2} = 0,\ r = 1,2, \\ \phi_1^{(1)}(r_i,\theta) = \phi_1^{(2)}(r_i,\theta), \\ \mathbf{j}_1^{(1)}(r_i,\theta)\cdot\mathbf{e}_r = \mathbf{j}_1^{(2)}(r_i,\theta)\cdot\mathbf{e}_r,, \\ \phi_0^{(2)}(r_o,\theta) = 0, \end{cases} \quad \text{(A.2.32)}$$

where $[D^2\phi_0^{(r)})]_{ij} = (\phi_0^{(r)}))_{,ij}$, and where from Eq. $(\text{A.2.12})_2$

$$j_1^{(r)} = -\epsilon^{(r)}\left(\nabla\phi_1^{(r)} + \frac{1}{2}\nabla\phi_0^{(r)}\log\left(|\nabla\phi_0^{(r)}|^2\right)\right). \quad \text{(A.2.33)}$$

We note that Eq. $(\text{A.2.32})_4$ arises from the fact that to first order in δ, the average electric field is simply $\overline{\mathbf{E}}$, i.e. there is no correction.

A straightforward calculations shows that $(\nabla\phi_0^{(1)})\cdot D^2\phi_0^{(1)}(\nabla\phi_0^{(1)}) = 0$, and so

$$\Delta\phi_1^{(1)} = 0. \quad \text{(A.2.34)}$$

Upon enforcing continuity of ϕ_1 at the origin, we find that

$$\phi_1^{(1)} = c_1 r\cos(\theta),\ 0 \leqslant r \leqslant r_i. \quad \text{(A.2.35)}$$

On the other hand, it can be shown that

$$\phi_1^{(2)}(r,\theta) = \left(c_2 r + \frac{d_2}{r}\right)\cos(\theta) - \frac{\phi_0^{(2)}}{4}\log(|\nabla\phi_0^{(2)}|^2). \tag{A.2.36}$$

Following a similar analysis as above, we find that c_1, c_2 and d_2 must satisfy the equations

$$c_1 - \left(c_2 + \frac{d_2}{r_i^2}\right) = \frac{\epsilon^{(2)}\overline{E}}{D}\left[\log(|a_2|) + \frac{z}{2}\right], \tag{A.2.37}$$

$$\epsilon^{(1)}c_1 - \epsilon^{(2)}\left(c_2 - \frac{d_2}{r_i^2}\right) = \frac{\epsilon^{(2)}\overline{E}}{D}\left[2\epsilon^{(2)}\left(\epsilon^{(1)}\log(|a_1|) - \frac{\epsilon^{(2)}z}{2}\right) - \epsilon^{(1)}\left(\log(|a_2|) + \frac{z}{2}\right)\right], \tag{A.2.38}$$

$$c_2 + \frac{d_2}{r_o^2} = \frac{-\overline{E}}{2}\left[\log(|a_2|) + \frac{cz}{2}\right], \tag{A.2.39}$$

where

$$z = \frac{\epsilon^{(1)} - \epsilon^{(2)}}{\epsilon^{(1)} + \epsilon^{(2)}}, \quad \tau = \frac{2\epsilon^{(2)}}{\epsilon^{(1)} + \epsilon^{(2)}}, \quad \text{and} \quad D = (\epsilon^{(1)} + \epsilon^{(2)}) - c(\epsilon^{(1)} - \epsilon^{(2)}), \tag{A.2.40}$$

and where use was made of the integrals derived in Appendix A.5. Solving this system of equations, we find that

$$c_1 = \frac{(1-c)\overline{E}}{D}\left[\frac{2\epsilon^{(2)}}{D}\left(\epsilon^{(1)}\log(\tau) - \frac{(\epsilon^{(1)} - \epsilon^{(2)})}{2}\right) + \frac{\epsilon^{(2)}z}{2}\right], \tag{A.2.41}$$

$$c_2 = \frac{-\overline{E}}{D}\left[\frac{2c\epsilon^{(2)}}{D}\left(\epsilon^{(1)}\log(\tau) - \frac{(\epsilon^{(1)} - \epsilon^{(2)})}{2}\right) + \frac{(\epsilon^{(1)} + \epsilon^{(2)})}{2}\left(\log(|a_2|) + \frac{cz}{2}\right)\right], \tag{A.2.42}$$

$$d_2 = \frac{r_i^2\overline{E}}{D}\left[\frac{2\epsilon^{(2)}}{D}\left(\epsilon^{(1)}\log(\tau) - \frac{(\epsilon^{(1)} - \epsilon^{(2)})}{2}\right) + \frac{(\epsilon^{(1)} - \epsilon^{(2)})}{2}\left(\log(|a_2|) + \frac{cz}{2}\right)\right]. \tag{A.2.43}$$

Plugging into Eq. (A.2.14), we obtain the first-order correction for $\widetilde{\epsilon}$, as given by

$$\begin{aligned}\widetilde{\epsilon}_1 =&\widetilde{\epsilon}_0 \log\left[\frac{(\epsilon^{(1)}+\epsilon^{(2)})}{(\epsilon^{(1)}+\epsilon^{(2)})-c(\epsilon^{(1)}-\epsilon^{(2)})}\right]+\\ &\frac{c\epsilon^{(2)}}{((\epsilon^{(1)}+\epsilon^{(2)})-c(\epsilon^{(1)}-\epsilon^{(2)}))^2}\left(4\epsilon^{(1)}\epsilon^{(2)}\log\left[\frac{2\epsilon^{(2)}}{\epsilon^{(1)}+\epsilon^{(2)}}\right]+(1-c)(\epsilon^{(1)}-\epsilon^{(2)})^2\right).\end{aligned} \tag{A.2.44}$$

Moreover, it can be readily checked that,

$$\mathbf{j}_1(r_o,\theta)\cdot\mathbf{e}_r=(\widetilde{\epsilon}_1+\widetilde{\epsilon}_0\log(\overline{E}))\overline{E}\cos(\theta), \tag{A.2.45}$$

i.e., to first order, the addition of such an inclusion to the effective medium does not perturb the fields. Therefore, Eq. (A.2.44) corresponds to an exact result, to first order in the nonlinearity, for the effective conductivity of the CCA.

A.2.3 Further Properties of Weakly Nonlinear Response

In solving the equilibrium equations directly, we now have access to information about the local fields in the composite. This allows us to calculate the first and second moments of the electric fields and current densities in the phases. In calculating the moments, by letting $\langle\cdot\rangle^{(r)}$ denote the volume average integral over phase r, we define, for example

$$\overline{E}^{(r)}=\langle\mathbf{E}\cdot\mathbf{e}_x\rangle^{(r)},\quad \text{and}\quad \langle\overline{E}^2\rangle^{(r)}=\langle(\mathbf{E}\cdot\mathbf{e}_x)^2\rangle^{(r)}. \tag{A.2.46}$$

so that the fluctuations are defined as

$$\mathbb{C}_E^{(r)}=\langle\overline{E}^2\rangle^{(r)}-(\overline{E}^{(r)})^2. \tag{A.2.47}$$

Taking into account Eq. (A.2.8) we see that

$$\mathbb{C}_E^{(r)}=\mathbb{C}_{E_0}^{(r)}+\delta\mathbb{C}_{E_1}^{(r)}+O(\delta^2) \tag{A.2.48}$$

where

$$\mathbb{C}_{E_0}^{(r)} = \langle \overline{E}_0^2 \rangle^{(r)} - (\overline{E}_0^{(r)})^2, \quad \text{and} \quad \mathbb{C}_{E_1}^{(r)} = 2\left[\langle (\mathbf{E}_0 \cdot \mathbf{e}_x)(\mathbf{E}_1 \cdot \mathbf{e}_x) \rangle^{(r)} - (\overline{E}_0^{(r)})(\overline{E}_1^{(r)}) \right]. \tag{A.2.49}$$

Similar expressions are obtained for $\mathbb{C}_{j_0}$ and $\mathbb{C}_{j_1}$.

The first observation to make is that both the electric field and current density are uniform in the inclusion phase, to first order. Therefore, the corresponding fluctuations will vanish. Starting with the moments of the field to zeroth order, we find that

$$\overline{E}_0^{(1)} = \frac{2\epsilon^{(2)}\overline{E}}{(\epsilon^{(1)} + \epsilon^{(2)}) - c(\epsilon^{(1)} - \epsilon^{(2)})}, \quad \text{and} \quad \overline{E}_0^{(2)} = \frac{(\epsilon^{(1)} + \epsilon^{(2)})\overline{E}}{(\epsilon^{(1)} + \epsilon^{(2)}) - c(\epsilon^{(1)} - \epsilon^{(2)})}, \tag{A.2.50}$$

$$\overline{j}_0^{(1)} = \frac{2\epsilon^{(1)}\epsilon^{(2)}\overline{E}}{(\epsilon^{(1)} + \epsilon^{(2)}) - c(\epsilon^{(1)} - \epsilon^{(2)})}, \quad \text{and} \quad \overline{j}_0^{(2)} = \frac{\epsilon^{(2)}(\epsilon^{(1)} + \epsilon^{(2)})\overline{E}}{(\epsilon^{(1)} + \epsilon^{(2)}) - c(\epsilon^{(1)} - \epsilon^{(2)})}, \tag{A.2.51}$$

$$\mathbb{C}_{E_0}^{(1)} = 0, \quad \text{and} \quad \mathbb{C}_{E_0}^{(2)} = \frac{(\overline{E} - \overline{E}_0^{(2)})^2}{2c}, \tag{A.2.52}$$

$$\mathbb{C}_{j_0}^{(1)} = 0, \quad \text{and} \quad \mathbb{C}_{j_0}^{(2)} = \frac{(\overline{j} - \overline{j}_0^{(2)})^2}{2c}. \tag{A.2.53}$$

As expected, we see that

$$c\overline{E}_0^{(1)} + (1-c)\overline{E}_0^{(2)} = \overline{E}, \tag{A.2.54}$$

while

$$c\overline{j}_0^{(1)} + (1-c)\overline{j}_0^{(2)} = \widetilde{\epsilon}_0\overline{E} = \overline{j}_0. \tag{A.2.55}$$

Using Eqs. (A.2.35) and (A.2.36), it is a straightforward matter to show that

$$\overline{E}_1^{(1)} = -\frac{(1-c)\overline{E}}{D}\left[\frac{2\epsilon^{(2)}}{D}\left(\epsilon^{(1)}\log(\tau) - \frac{(\epsilon^{(1)} - \epsilon^{(2)})}{2}\right) + \frac{\epsilon^{(2)}z}{2}\right] \tag{A.2.56}$$

$$\overline{E}_1^{(2)} = -\frac{c}{1-c}\overline{E}_1^{(1)}, \tag{A.2.57}$$

which implies that

$$c\overline{E}_1^{(1)} + (1-c)\overline{E}_1^{(2)} = 0 \tag{A.2.58}$$

confirming that there is no correction to the average electric field. From a lengthier calculation, we obtain that

$$\mathbb{C}_{E_1}^{(1)} = 0, \quad \text{and} \quad \mathbb{C}_{E_1}^{(2)} = \frac{(\overline{E} - \overline{E}_0^{(2)})^2}{24c}(z^2(c^2+c+1)-6) - \frac{\overline{E}_1^{(2)}(\overline{E} - \overline{E}_0^{(2)})}{c}. \tag{A.2.59}$$

Finally, upon recalling that $\mathbf{j}_1^{(r)} = \epsilon^{(r)}(\mathbf{E}_1^{(r)} + \mathbf{E}_0^{(r)}\log(E_0^{(r)}))$, we have

$$\begin{aligned}\overline{j}_1^{(1)} = -\frac{\epsilon^{(1)}\overline{E}}{D}\Bigg(&\frac{2(1-c)\epsilon^{(2)}}{D}\left[\epsilon^{(1)}\log(\tau) - \frac{(\epsilon^{(1)}-\epsilon^{(2)})}{2}\right] \\ &+\frac{(1-c)\epsilon^{(2)}z}{2} - 2\epsilon^{(2)}\log\left(\frac{2\epsilon^{(2)}\overline{E}}{D}\right)\Bigg),\end{aligned} \tag{A.2.60}$$

$$\begin{aligned}\overline{j}_1^{(2)} = \frac{\epsilon^{(2)}\overline{E}}{D}\Bigg[&\frac{2c\epsilon^{(2)}}{D}\left[\epsilon^{(1)}\log(\tau) - \frac{(\epsilon^{(1)}-\epsilon^{(2)})}{2}\right] \\ &+\frac{\epsilon^{(1)}cz}{2} + (\epsilon^{(1)}+\epsilon^{(2)})\log\left(\frac{(\epsilon^{(1)}+\epsilon^{(2)})\overline{E}}{D}\right)\Bigg],\end{aligned} \tag{A.2.61}$$

so that

$$(1-c)\overline{j}_1^{(1)} + c\overline{j}_1^{(2)} = (\widetilde{\epsilon}_1 + \widetilde{\epsilon}_0\log(\overline{E}))\overline{E} = \overline{j}_1, \tag{A.2.62}$$

as anticipated. As for the second moments, we have

$$\mathbb{C}_{j_1}^{(1)} = 0, \quad \text{and} \quad \mathbb{C}_{j_1}^{(2)} = \frac{(\overline{j}_0 - \overline{j}_0^{(2)})^2}{24c}(6 - z^2(c^2+c+1)) + \frac{(\overline{j}_0 - \overline{j}_0^{(2)})(\overline{j}_1 - \overline{j}_1^{(2)})}{c}. \tag{A.2.63}$$

A.3 Comparison with Estimates and Bounds

Suquet and Ponte Castañeda (1993) derived an exact result for the effective conductivity of a two-phase composite to second order in the heterogeneity. It was found

that

$$\widetilde{\epsilon} = \langle \epsilon \rangle - \frac{\delta + 1}{2\delta} \left(1 - \frac{1}{\sqrt{\delta + 1}} \right) \frac{(\langle \epsilon^2 \rangle - \langle \epsilon \rangle^2)}{\epsilon_0}, \tag{A.3.1}$$

where $\epsilon^{(1)} = \epsilon_0$ and $\epsilon^{(2)} = \epsilon_0 + \Delta\epsilon$. A straightforward calculation reveals that the expansion of $\widetilde{\epsilon}_0 + \delta\widetilde{\epsilon}_1$, to second order in $\Delta\epsilon$, coincides with the expansion of Eq. (A.3.1) to first order in δ, and is given by

$$\widetilde{\epsilon} \approx \langle \epsilon \rangle - \frac{(\langle \epsilon^2 \rangle - \langle \epsilon \rangle^2)}{2\epsilon_0} \left(1 - \frac{\delta}{4} \right). \tag{A.3.2}$$

Next, we compute the first-order correction of some available estimates and bounds and compare them the exact solution obtained above. For simplicity, we will consider the cases of perfectly insulating inclusions ($\epsilon^{(1)} \to 0$); the case of perfectly conducting inclusions ($\epsilon^{(1)} \to \infty$) can be treated similarly. In particular, we will compare with the rigorous nonlinear variational bounds (VAR) (Ponte Castañeda, 1992b), tangent second order estimates (TSO(W) and TSO(U)) (Ponte Castañeda, 1996; Ponte Castañeda and Kailasam, 1997), the fully optimized second order estimates (FOSO) (Ponte Castañeda, 2016; Furer and Ponte Castañeda, 2018b), as well as the exact results for infinite-rank laminated microstructures (LAM) (Idiart and Ponte Castañeda, 2013).

To start, we note that when $\epsilon^{(1)} \to 0$, the exact result for the correction simplifies to

$$\frac{\widetilde{\epsilon}_1}{\epsilon^{(2)}} = \frac{c(1-c)}{(1+c)^2} - \frac{(1-c)\log(1+c)}{1+c}. \tag{A.3.3}$$

As shown in Appendix A.6, the effective conductivity of the infinite-rank laminate agrees with the exact result to first order in the nonlinearity. In consider the nonlinear variational bounds of the Hashin-Shtrikman type (VAR), as proposed by
Ponte Castañeda (1992b), we have

$$\frac{\widetilde{\epsilon}_{VAR}}{\epsilon^{(2)}} = \frac{1-c}{(1+c)^{(m+1)/2}} \tag{A.3.4}$$

so that

$$\left.\frac{\partial}{\partial m}\frac{\widetilde{\epsilon}_{VAR}}{\epsilon^{(2)}}\right|_{m=1} = -\frac{(1-c)}{2(1+c)}\log(1+c). \tag{A.3.5}$$

Next, we consider the tangent second order bounds of Ponte Castañeda and Kailasam (1997). By making use of duality, this method gives two estimates. One estimate, which we denote TSO(W), corresponding to using an energy principle based on the electric field, while the other, denoted TSO(U), corresponds to using an energy principle based on the current density. The former is preferable when $0 \leqslant m \leqslant 1$, while the latter is used for $1 \leqslant m \leqslant \infty$. The estimates can be written as

$$\frac{\widetilde{\epsilon}_{TSO(W)}}{\epsilon^{(2)}} = (1-c)\left(1+\frac{(m-1)c}{2(\sqrt{m}+c)}\right)\left(\frac{\sqrt{m}}{\sqrt{m}+c}\right)^{m}, \tag{A.3.6}$$

while

$$\frac{\widetilde{\epsilon}_{TSO(U)}}{\epsilon^{(2)}} = (1-c)\left(1+\frac{(m+1)c}{2m^{3/2}}\right)^{-m}. \tag{A.3.7}$$

Remarkably, both estimates predict

$$\left.\frac{\partial}{\partial m}\frac{\widetilde{\epsilon}_{TSO(W)}}{\epsilon^{(2)}}\right|_{m=1} = \left.\frac{\partial}{\partial m}\frac{\widetilde{\epsilon}_{TSO(U)}}{\epsilon^{(2)}}\right|_{m=1} = \left.\frac{\partial}{\partial m}\frac{\widetilde{\epsilon}_{TSO}}{\epsilon^{(2)}}\right|_{m=1} = \frac{c(1-c)}{(1+c)^2} - \frac{(1-c)\log(1+c)}{1+c}, \tag{A.3.8}$$

which is the same as the exact correction for the CCA microstructure.

As discussed by Ponte Castañeda (2016), the original version of the FOSO method yields two estimates, depending on whether one starts with the "u-formulation," which we denote by FOSO(U) and corresponds to the formulation in terms of the current density, or the "w-formulation," which we denote by FOSO(W) and corresponds to the formulation in terms of the electric field. This lack a symmetry is due to the specific choice for the energy potential of the linear comparison composite (LLC) that is used to determine the effective response of the corresponding nonlinear potential. By using a more symmetric choice for the potential of the LCC, we introduced in Chapter 4 the fully symmetric FOSO method, which predicts the same effective response whether one starts with the u-formulation, or the w-formulation.

In implementing any version of the FOSO method, one must choose a value for the weight-factor $0 < \alpha < 1$. Out of convenience, Ponte Castañeda (2016) chose a value of $\alpha = 0.5$, and in Chapter 4, we used the same value, and suggested that the "optimal" value of α would depend, among other things, on the microstructure, nonlinearity, and properties of the phases. In what follows, we will also be interested in studying the effect that the choice of α has on the estimate. Now, in the case of at hand, when $\epsilon^{(1)} \to 0$, it is known that

$$\overline{j}^{(2)} = \frac{\overline{j}}{1-c}. \tag{A.3.9}$$

Then, upon using the u-formulation,

$$\begin{aligned} \frac{\widetilde{\epsilon}_{FOSO}}{\epsilon^{(2)}} &= (1-c)\left[\operatorname*{stat}_k \left\{(1-\alpha)\widehat{j}^{n+1} + \alpha \breve{j}^{n+1}\right\}\right]^{-1/n} \\ &= (1-c)\left[\operatorname*{stat}_k f(k(n), n)\right]^{-1/n}. \end{aligned} \tag{A.3.10}$$

Here, $k = k(n)$ is the anisotropy ratio of the LCC, and the optimal value k^* is determined as a solution to the equation

$$\frac{\partial f(k^*(n), n)}{\partial k} = 0. \tag{A.3.11}$$

The form of $f(k, n)$ is different depending on whether one uses the FOSO(U) method or the symmetric FOSO method. In the former case, we have

$$\begin{aligned} \widehat{j} &= \sqrt{\widehat{j}_{\parallel}^2 + \widehat{j}_{\perp}^2}, & \breve{j} &= \sqrt{\breve{j}_{\parallel}^2 + \breve{j}_{\perp}^2}, \\ \widehat{j}_{\parallel} &= 1 + \sqrt{\frac{\alpha}{1-\alpha}}\sqrt{\frac{c}{2}}k^{1/4}, & \breve{j}_{\parallel} &= 1 - \sqrt{\frac{1-\alpha}{\alpha}}\sqrt{\frac{c}{2}}k^{1/4}, \\ \widehat{j}_{\perp} &= \sqrt{\frac{\alpha}{1-\alpha}}\sqrt{\frac{c}{2}}k^{-1/4}, & \breve{j}_{\perp} &= -\sqrt{\frac{1-\alpha}{\alpha}}\sqrt{\frac{c}{2}}k^{-1/4}. \end{aligned} \tag{A.3.12}$$

To implement the symmetric FOSO version, one takes $\widehat{j}_{\parallel}$ and $\breve{j}_{\parallel}$ as in Eq. (A.3.12).

The expressions for $\widehat{j}_\perp$ and $\breve{j}_\perp$ are more complicated, and therefore have been excluded, but we mention that $\widehat{j}_\perp$ and $\breve{j}_\perp$ satisfy the equations

$$\widehat{j}_\perp \breve{j}_\perp \left((\widehat{j}_\parallel - \breve{j}_\parallel) + k(1-2\alpha)(\widehat{j}_\parallel + \breve{j}_\parallel) \right) - 2k \left((1-\alpha)\breve{j}_\parallel \widehat{j}_\perp^2 - \alpha \widehat{j}_\parallel \breve{j}_\perp^2 \right) = 0, \quad \text{(A.3.13)}$$

$$4\alpha(1-\alpha)\widehat{j}_\perp \breve{j}_\perp + (1-2\alpha)\left((1-\alpha)\widehat{j}_\perp^2 - \alpha \breve{j}_\perp^2 \right) + \frac{c}{2\sqrt{k}} = 0, \quad \text{(A.3.14)}$$

and are chosen in just a way that $\breve{j}_\perp < \widehat{j}_\perp$. In either case, we make use of Eq. (A.2.10), as well as the fact that $\frac{\partial}{\partial m} = -m^{-2}\frac{\partial}{\partial n}$ to find

$$\begin{aligned}
\frac{\partial}{\partial m}\frac{\widetilde{\epsilon}_{FOSO}}{\epsilon^{(2)}} &= (1-c)\frac{\partial}{\partial m}\left[f(k^*(n),n)\right]^{-1/n} \\
&= -\frac{(1-c)}{m^2}\frac{\partial}{\partial n}\left[f(k^*,n)\right]^{-1/n} \\
&= -\frac{(1-c)}{m^2}\left[f(k^*,n)\right]^{-1/n}\left[\frac{\log(f(k^*,n))}{n^2}\right. \\
&\qquad \left. -\frac{1}{nf(k^*,n)}\left(\frac{\partial f(k^*,n)}{\partial k}\frac{\partial k^*}{\partial n} + \frac{\partial f(k^*,n)}{\partial n}\right)\right]
\end{aligned} \quad \text{(A.3.15)}$$

We mention that the derivative with respect to n is the last line is taken with k^* held fixed, while the term $\frac{\partial f(k^*,n)}{\partial k}$ vanishes on account of Eq. (A.3.11). Using the fact that $k^*(1) = 1$ and $f(1,1) = (1+c)$, we find that

$$\left.\frac{\partial}{\partial m}\frac{\widetilde{\epsilon}_{FOSO}}{\epsilon^{(2)}}\right|_{m=1} = \frac{(1-c)}{(1+c)^2}\left[(1-\alpha)\widehat{j}^{\,2}\log(\widehat{j}) + \alpha\breve{j}^{\,2}\log(\breve{j})\right] - \frac{1-c}{1+c}\log(1+c), \quad \text{(A.3.16)}$$

where $\widehat{j}$ and $\breve{j}$ are given as in Eq. (A.3.12), with $k = 1$. It can be shown that when $k = 1$, the expressions for $\widehat{j}_\perp$ and $\breve{j}_\perp$ using either the FOSO(U) method or the symmetric FOSO method are identical, and hence they will give the same first-order correction. Moreover, it is clear that this correction will agree with the exact result

when α is chosen as to satisfy the equation (c.f. Eqs. (A.3.3) and (A.3.16))

$$2c = (1-\alpha)\left(1+\sqrt{2c}\sqrt{\frac{\alpha}{1-\alpha}}+\frac{\alpha c}{1-\alpha}\right)\log\left(1+\sqrt{2c}\sqrt{\frac{\alpha}{1-\alpha}}+\frac{\alpha c}{1-\alpha}\right)$$
$$+\alpha\left(1+\sqrt{2c}\sqrt{\frac{1-\alpha}{\alpha}}+\frac{(1-\alpha)c}{\alpha}\right)\log\left(1+\sqrt{2c}\sqrt{\frac{1-\alpha}{\alpha}}+\frac{(1-\alpha)c}{\alpha}\right). \tag{A.3.17}$$

The implementation of the w-formulation, which we spell out next, is a bit more complicated, as the average electric field in the phases are unknown. Nonetheless, it can be shown that an estimate for the effective conductivity can equivalently be estimated via

$$\begin{aligned}\frac{\widetilde{\epsilon}_{FOSO}}{\epsilon^{(2)}} &= (1-c)\operatorname*{stat}_{k,\overline{E}^{(2)}}\left\{(1-\alpha)\widehat{E}^{m+1}+\alpha\breve{E}^{m+1}\right\}\\ &= (1-c)\operatorname*{stat}_{k,\overline{E}^{(2)}} g(k(m),\overline{E}^{(2)}(m),m),\end{aligned} \tag{A.3.18}$$

where $\overline{E}^{(2)}$ is the average electric field in the matrix phase. The optimal values of k^* and $\overline{E}^{(2)*}$ are then determined via the equations

$$\begin{aligned}\frac{\partial g(k^*,\overline{E}^{(2)*},m)}{\partial k} &= 0,\\ \frac{\partial g(k^*,\overline{E}^{(2)*},m)}{\partial \overline{E}^{(2)}} &= 0.\end{aligned} \tag{A.3.19}$$

As above the form of $g(k,\overline{E}^{(2)},m)$ is different depending on whether one uses the

FOSO(W) method or the symmetric FOSO method. In the former case, we have

$$\begin{aligned}
\widehat{E} &= \sqrt{\widehat{E}_{\parallel}^2 + \widehat{E}_{\perp}^2}, & \breve{E} &= \sqrt{\breve{E}_{\parallel}^2 + \breve{E}_{\perp}^2}, \\
\widehat{E}_{\parallel} &= \overline{E}^{(2)} - (\overline{E}^{(2)} - 1)\sqrt{\frac{\alpha}{1-\alpha}}\frac{k^{-1/4}}{\sqrt{2c}}, & \breve{E}_{\parallel} &= \overline{E}^{(2)} + (\overline{E}^{(2)} - 1)\sqrt{\frac{1-\alpha}{\alpha}}\frac{k^{-1/4}}{\sqrt{2c}}, \\
\widehat{E}_{\perp} &= -(\overline{E}^{(2)} - 1)\sqrt{\frac{\alpha}{1-\alpha}}\frac{k^{1/4}}{\sqrt{2c}}, & \breve{E}_{\perp} &= (\overline{E}^{(2)} - 1)\sqrt{\frac{1-\alpha}{\alpha}}\frac{k^{1/4}}{\sqrt{2c}},
\end{aligned} \tag{A.3.20}$$

while in the latter case, $\widehat{E}_{\parallel}$ and $\breve{E}_{\parallel}$ are the same, while $\widehat{E}_{\perp}$ and $\breve{E}_{\perp}$ are again related through

$$\widehat{E}_{\perp}\breve{E}_{\perp}\left(k(\widehat{E}_{\parallel} - \breve{E}_{\parallel}) + (1-2\alpha)(\widehat{E}_{\parallel} + \breve{E}_{\parallel})\right) - 2\left((1-\alpha)\breve{E}_{\parallel}\widehat{E}_{\perp}^2 - \alpha\widehat{E}_{\parallel}\breve{E}_{\perp}^2\right) = 0, \tag{A.3.21}$$

$$4\alpha(1-\alpha)\widehat{E}_{\perp}\breve{E}_{\perp} + (1-2\alpha)\left((1-\alpha)\widehat{E}_{\perp}^2 - \alpha\breve{E}_{\perp}^2\right) + (E^{(2)} - 1)^2\frac{\sqrt{k}}{2c} = 0, \tag{A.3.22}$$

and chosen so that $\breve{E}_{\perp} < \widehat{E}_{\perp}$.

Once again, when $m = 1$, so that $k = 1$, the expressions are the same whether one uses the FOSO(W) or symmetric FOSO method. Moreover, using the fact that $\overline{E}^{(2)*}(1) = (1+c)^{-1}$, it can be shown that the w-formulation leads to the same correction as the u-formulation, and the value of α needed to recover the exact result is still given by Eq. (A.3.17).

A.4 Results and Discussion

We are now in a position to begin to compare the results from the various bounds and estimates described above. We start by comparing the correction $\widetilde{\epsilon}_1$, normalized by $\epsilon^{(2)}$, as a function of c in Figure A.1a. The exact result, which is recovered by the TSO method and the infinite-rank laminate, is depicted by the solid black curve. Note

that the variational bound, depicted by the solid red curve, does not recover the exact result for any value of $0 < c < 1$. This is related to the fact that, as was shown in Chapter 2-Chapter 3, the variational bound, while rigorously bounding all composites with statistically isotropic microstructures (like the CCA), is in fact optimal over the larger class of nonlinear anisotropic composites that have linearly isotropic response. We also present estimates on the correction from the FOSO method for various fixed values of α. As we see, the correction is very sensitive to the choice of α, and interestingly is not symmetric about $\alpha = 0.5$, in that he results for $\alpha = 0.75$ and $\alpha = 0.25$ are drastically different.

Note that the curve corresponding to $\alpha = 0.5$ is close to the exact result, but it only agrees in the limit as $c = 0$ and $c = 1$, in which case the correction is 0; this is due to the fact that in these extreme cases, the composite is either entirely phase 2 or entirely phase 1, so that $\widetilde{\epsilon}$ is either $\epsilon^{(2)}$ or $\epsilon^{(1)}$, respectively. In Figure A.1b, we have plotted, as a function of c, the value of α for which the estimate for the first-order correction $\widetilde{\epsilon}_1$ as predicted by the FOSO methods recovers the exact result. Indeed, the value of α is different for every choice of c. Nonetheless, we see that the choice of $\alpha = 0.5$ considered in Chapter 4 was reasonable, in that the exact value is never far from this choice. We note that these values of α are correct only in the perfectly insulating case. We expect the value of α to also depend on the properties of the phases, and so when $\epsilon^{(1)} \neq 0$, the curve will certainly look different.

Next, we look at the effect α has on not just the weakly nonlinear behavior, but also the behavior for large nonlinearities. Such a comparison is done in Figure A.2 where, for a fixed value of $c = 0.2$, the effective conductivity is plotted as a function of nonlinear m. We have included results for the variational bounds (VAR), depicted as the solid red curve, tangent second-order estimates (TSO(U) and TSO(W)), depicted as the solid and dashed blue curves, the asymmetric FOSO methods (FOSO(U) and FOSO(W)), depicted as the dashed and dashed-dot black curves, the symmetric FOSO method, depicted as the solid black curve, as well as what we have called the

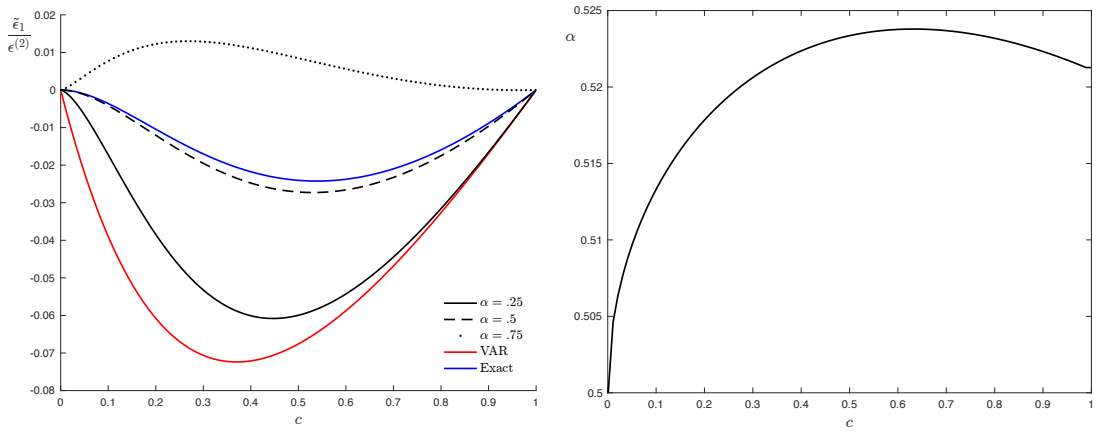

(a) (b)

Figure A.1: (a) A comparison of the first-order correction $\widetilde{\epsilon}_1$, normalized by $\epsilon^{(2)}$. (b) The value of α for which the estimate of $\widetilde{\epsilon}_1$ as given by the FOSO method agrees with the exact result. Both results are given as a function of the volume fraction c of the inclusion phase.

first-order approximation on the effective conductivity, by which we mean the line

$$\frac{\widetilde{\epsilon}_0}{\epsilon^{(2)}} + (m-1)\frac{\widetilde{\epsilon}_1}{\epsilon^{(2)}}, \tag{A.4.1}$$

which is depicted by the solid green curve. We recall that in the current setting

$$\frac{\widetilde{\epsilon}_0}{\epsilon^{(2)}} = \frac{1-c}{1+c}, \quad \text{and} \quad \frac{\widetilde{\epsilon}_1}{\epsilon^{(2)}} = \frac{c(1-c)}{(1+c)^2} - \frac{(1-c)\log(1+c)}{1+c}. \tag{A.4.2}$$

The pair of figures Figures A.2a and A.2b and Figures A.2c and A.2d show, respectively, the effective conductivity for both the entire range of nonlinearities as well as for weak nonlinearities, for $\alpha = 0.5$ and the value of α for which the FOSO estimate recovers the exact result in the weakly nonlinear limit; for the value of $c = 0.2$ considered, $\alpha \approx .51$. We note that the order that the different methods appear in each legend corresponds to the value the method predicts at $m = 0$. In particular, the topmost entry in the legend is the method predicting the largest value of the effec-

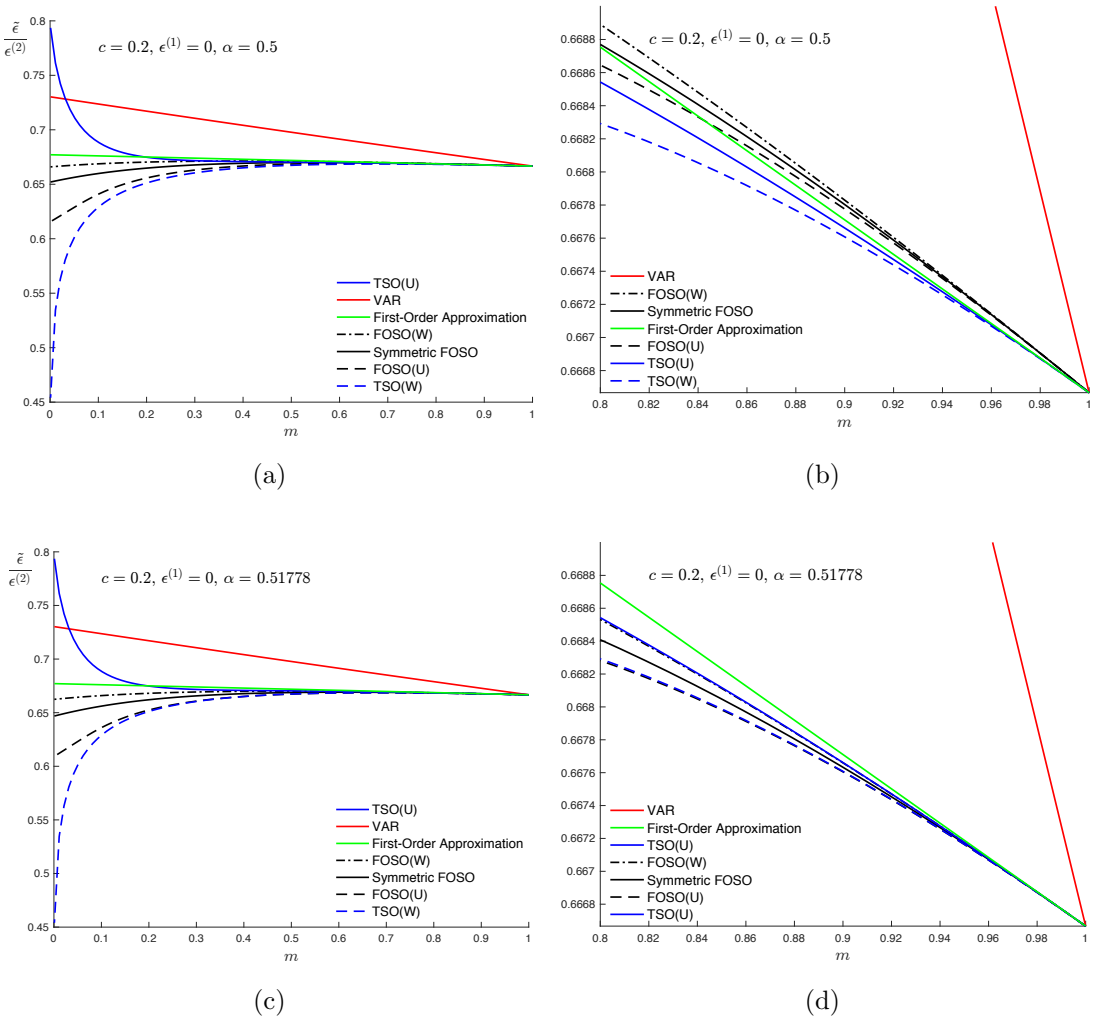

Figure A.2: Estimates for the effective conductivity with α equal to (a)-(b) $\frac{1}{2}$ and (c)-(d) the value for which the FOSO method gives the exact correction. Results are presented as a function of the nonlinear m with a fixed volume fraction $c = 0.2$ of the perfectly insulating phase.

tive conductivity at $m = 0$, while the bottommost entry in the legend is the method predicting the smallest value at $m = 0$.

As was seen in Chapter 4, the FOSO estimate always lies somewhere between the FOSO(U) and FOSO(W) estimates. This trend holds regardless of the value of α, and in looking at the results in Figures A.2a and A.2c, we find that for large

nonlinearities, the effect of changing α is hard to distinguish, but there are in fact some telling differences. A careful inspection reveals that for $m = 0$, when $\alpha = 0.5$, the FOSO method predicts a value of the effective conductivity slightly above 0.65, while for $\alpha \approx .5178$, the FOSO method predicts a value of the effective conductivity slightly below 0.65. Also, we see in Figure A.2a that the FOSO(U) method and the TSO(W) method are rather close for values of $.5 \leqslant m \leqslant 1$, while in Figure A.2c, this agreement continues up to $m \approx 0.2$. Finally, the FOSO(U) estimate crosses above the TSO(W) estimate for $0.3 < m \leqslant 1$ in Figure A.2a for $\alpha = 0.5$, but remains always below it in Figure A.2c when $\alpha \approx .5178$.

Once we look more closely at the weakly nonlinear behavior in Figure A.2b and Figure A.2d, we see how dramatic a difference the choice of α makes. As expected, in both figures, the TSO estimates, which give the exact weakly nonlinear behavior, lie tangent to the first-order approximation in the limit as $m \to 1$. The FOSO methods only due so in Figure A.2d when α is chosen appropriately. In Figure A.2b, we see that all the FOSO estimates lie above the TSO(W) estimate, which, given their behavior for larger nonlinearities (c.f. Figure A.2a), indicates that they all cross the TSO(W) estimate at some intermediate values of m. On the other hand, when α is chosen so that the FOSO methods agree with the exact result in the weakly nonlinear limit, we see in Figure A.2d that the FOSO(U) and TSO(W) appear to agree, as do the FOSO(W) and TSO(U), even for nonlinearities up to $m = .8$. Moreover, the FOSO method tends to lie directly in between. Now, in connection to the comments made above, in every case, the VAR bound is too stiff, even for weak nonlinearities. The FOSO and TSO methods both assume that the underlying microstructure of the composite was statistically isotropic. That the VAR bound is optimal over a much larger class of composites explains this discrepancy.

A.5 Appendix I: Integrals

At various points above, certain integrals must be evaluated analytically. Here, we derive them.

We look to compute

$$I_p = \int_0^{2\pi} \log(a^2 + 2ab\cos(2\theta) + b^2)\cos^p(2\theta)d\theta, \tag{A.5.1}$$

where $0 < b < a$. I_p is used above for $p = 0, 1, 2$. First, we note that

$$\begin{aligned}\log(a^2 + 2ab\cos(2\theta) + b^2) &= \log(a^2 + b^2) + \log\left(1 + \frac{2ab\cos(2\theta)}{a^2 + b^2}\right) \\ &= \log(a^2 + b^2) - \sum_{n=1}^{\infty} \frac{(-1)^n}{n}\left(\frac{2ab\cos(2\theta)}{a^2 + b^2}\right)^n,\end{aligned} \tag{A.5.2}$$

where the power series converges uniformly, since $\left|\frac{2ab\cos(2\theta)}{a^2+b^2}\right| < 1$ for every $\theta \in [0, 2\pi]$. Therefore, we may integrate term by term to find that

$$I_p = 2\pi\log(a^2 + b^2) - \sum_{n=1}^{\infty} \frac{(-1)^n C_{n+p}}{n}\left(\frac{2ab}{a^2 + b^2}\right)^n \tag{A.5.3}$$

where

$$C_n = \int_0^{2\pi} \cos^n(2\theta)d\theta \tag{A.5.4}$$

Now, we can show by induction that

$$C_n = \begin{cases} 0 & n = 2k - 1 \\ 2\pi\frac{(2k)!}{(2^k k!)^2} & n = 2k \end{cases} \qquad \forall k \geqslant 1 \tag{A.5.5}$$

For $k = 1$, it is clear that

$$C_1 = \int_0^{2\pi} \cos(2\theta)d\theta = \frac{1}{2}\sin(2\theta)|_{\theta=0}^{2\pi} = 0. \tag{A.5.6}$$

Upon integrating by parts, we find that

$$C_2 = \frac{1}{2}\sin(2\theta)\cos(2\theta)|_{\theta=0}^{2\pi} + \int_0^{2\pi} \sin^2(2\theta)d\theta = \int_0^{2\pi} \sin^2(2\theta)d\theta \tag{A.5.7}$$

Therefore

$$2C_2 = \int_0^{2\pi} (\sin^2(2\theta) + \cos^2(2\theta))d\theta = 2\pi \implies C_2 = \pi. \tag{A.5.8}$$

Assuming the result holds for all $n' < n$, we note that in general, integration by parts yields

$$\begin{aligned} C_n &= \frac{n-1}{2}\sin(2\theta)\cos^{n-2}(2\theta)|_{\theta=0}^{2\pi} + (n-1)\int_0^{2\pi} \sin^2(2\theta)\cos^{n-2}(2\theta)d\theta \\ &= (n-1)\int_0^{2\pi} \sin^2(2\theta)\cos^{n-2}(2\theta)d\theta \\ &= (n-1)(C_{n-2} - C_n), \end{aligned} \tag{A.5.9}$$

which gives us the recursive relation

$$C_n = \frac{n-1}{n}C_{n-2}. \tag{A.5.10}$$

Therefore, if n is odd, C_n will be proportional to $C_1 = 0$. On the other hand, if $n = 2k$, then

$$\begin{aligned} C_{2k} &= \frac{2k-1}{2k}C_{2k-2} \\ &= \pi\frac{(2k-1)(2k-3)\cdots(3)}{2k(2k-2)\cdots 4} \\ &= 2\pi\frac{2k(2k-1)(2k-2)\cdots(3)(2)}{(2k)^2(2k-2)^2\cdots(4)^2(2)^2} \\ &= 2\pi\frac{(2k)!}{(2^k k!)^2}, \end{aligned} \tag{A.5.11}$$

which proves Eq. (A.5.5).

By repeated multiplication, it is a simple matter to confirm that for any $|x| > 1$,

$$\operatorname{acosh}(x) = \log(x + \sqrt{x^2 - 1}) = \log(2x) - \sum_{n=1}^{\infty} \frac{(2n)!}{(2^n n!)^2} \frac{x^{-2n}}{2n}, \tag{A.5.12}$$

while it is known that

$$\sqrt{x^2 - 1} = -\sum_{n=0}^{\infty} \frac{(2n)!}{(2^n n!)^2} \frac{x^{-2n+1}}{2n-1}. \tag{A.5.13}$$

Therefore, using Eqs. (A.5.3),(A.5.5),(A.5.12) and (A.5.13), we find that

$$I_0 = 4\pi \log(a), \tag{A.5.14}$$

$$I_1 = \frac{2\pi b}{a}, \tag{A.5.15}$$

$$I_2 = \pi \left(2\log(a) - \frac{b^2}{2a^2} \right). \tag{A.5.16}$$

It is also necessary to evaluate another set of integrals. The first is

$$I' = \int_0^{2\pi} \frac{\cos^2(\theta)(b + a\cos(2\theta))}{a^2 + 2ab\cos(2\theta) + b^2} d\theta \tag{A.5.17}$$

By taking $z = e^{i\theta}$, we find that

$$I' = \int_\gamma f(z) dz \tag{A.5.18}$$

where γ is the contour which traces out the boundary of the circle $|z| = 1$ in the complex plane, and

$$f(z) = \frac{(z^2+1)^2(abz^4 + 2b^2z^2 + ab)}{8iz^3(abz^4 + (a^2+b^2)z^2 + ab)}. \tag{A.5.19}$$

ote that $f(z)$ has a pole of order 3 at $z = 0$, and simple poles at $z = \pm i\sqrt{\frac{b}{a}}$, $\pm i\sqrt{\frac{a}{b}}$. Since $0 < b < a$, the only poles satisfying $|z| < 1$ are $z = 0$ and $z = \pm i\sqrt{\frac{b}{a}}$. Therefore,

by the Residue Theorem,

$$I' = 2\pi i \left[\text{Res}(f,0) + \text{Res}\left(f, i\sqrt{\frac{b}{a}}\right) + \text{Res}\left(f, -i\sqrt{\frac{b}{a}}\right) \right]. \tag{A.5.20}$$

Now

$$\text{Res}(f,0) = \frac{1}{2}\lim_{z\to 0}\frac{d^2}{dz^2}[z^3 f(z)] = \frac{b^2+2ab-a^2}{8iab^2}, \tag{A.5.21}$$

$$\text{Res}\left(f, i\sqrt{\frac{b}{a}}\right) = \lim_{z\to i\sqrt{\frac{b}{a}}}(z - i\sqrt{\frac{b}{a}})f(z) = \frac{(a-b)^2}{16iab^2}, \tag{A.5.22}$$

$$\text{Res}\left(f, -i\sqrt{\frac{b}{a}}\right) = \lim_{z\to -i\sqrt{\frac{b}{a}}}(z + i\sqrt{\frac{b}{a}})f(z) = \frac{(a-b)^2}{16iab^2}. \tag{A.5.23}$$

Hence

$$I' = \frac{\pi}{2a}. \tag{A.5.24}$$

We also need to calculate

$$\begin{aligned} J' &= \int_0^{2\pi} \frac{\cos^2(\theta)(b^2+2ab-a^2+2a^2\cos(2\theta))}{a^2+2ab\cos(2\theta)+b^2}d\theta \\ &= (b^2-a^2)\int_0^{2\pi}\frac{\cos^2(\theta)}{a^2+2ab\cos(2\theta)+b^2}d\theta + 2a\int_0^{2\pi}\frac{\cos^2(\theta)(b+a\cos(2\theta))}{a^2+2ab\cos(2\theta)+b^2}d\theta \\ &= (b^2-a^2)J'' + 2aI'. \end{aligned} \tag{A.5.25}$$

In a similar fashion,

$$J'' = 2\pi i \left[\text{Res}(g,0) + \text{Res}\left(g, i\sqrt{\frac{b}{a}}\right) + \text{Res}\left(g, -i\sqrt{\frac{b}{a}}\right) \right], \tag{A.5.26}$$

where

$$g(z) = \frac{(z^2+1)^2}{4iz(abz^4+(a^2+b^2)z^2+ab)}. \tag{A.5.27}$$

Upon simplifying, we find that

$$J'' = \frac{\pi}{a(a+b)}, \tag{A.5.28}$$

from which it follows that

$$J' = \frac{\pi b}{a}. \tag{A.5.29}$$

By making use of the integrals above, we see that

$$\int_0^{2\pi} \frac{\cos^2(\theta)(b-a+2a\cos(2\theta))}{a^2+2ab\cos(2\theta)+b^2} d\theta = 2I' - (a+b)J'' = 0. \tag{A.5.30}$$

The last integral we need to calculate it

$$K' = \int_0^{2\pi} \frac{\cos(2\theta)\cos^2(\theta)(b-a+2a\cos(2\theta))}{a^2+2ab\cos(2\theta)+b^2} d\theta. \tag{A.5.31}$$

The same procedure yields

$$K' = 2\pi i \left[\text{Res}(h,0) + \text{Res}\left(h, i\sqrt{\frac{b}{a}}\right) + \text{Res}\left(h, -i\sqrt{\frac{b}{a}}\right) \right], \tag{A.5.32}$$

where

$$h(z) = \frac{(z^2+1)^2(z^4+1)(az^4+(b-a)z^2+a)}{8iz^5(abz^4+(a^2+b^2)z^2+ab)}. \tag{A.5.33}$$

We find that

$$\text{Res}(h,0) = \frac{1}{4!}\lim_{z\to 0}\frac{d^4}{dz^4}[z^5 h(z)] = \frac{a^3-a^2b+ab^2+b^3}{8iab^3}, \tag{A.5.34}$$

$$\text{Res}\left(h, i\sqrt{\frac{b}{a}}\right) = \lim_{z\to i\sqrt{\frac{b}{a}}}(z - i\sqrt{\frac{b}{a}})h(z) = -\frac{(a-b)(a^2+b^2)}{16iab^3}, \tag{A.5.35}$$

$$\text{Res}\left(h, -i\sqrt{\frac{b}{a}}\right) = \lim_{z\to -i\sqrt{\frac{b}{a}}}(z + i\sqrt{\frac{b}{a}})h(z) = -\frac{(a-b)(a^2+b^2)}{16iab^3}. \tag{A.5.36}$$

Therefore, we conclude that

$$K' = \frac{\pi}{2a}. \tag{A.5.37}$$

A.6 Appendix II: Weakly Nonlinear Infinite-Rank Laminate

The effective transverse conductivity for an infinite rank laminate can by found by solving the Hamilton-Jacobi equation

$$\begin{aligned} &\widetilde{w}_t(\overline{\mathbf{E}}, t) + H(\overline{\mathbf{E}}, \widetilde{w}, \widetilde{w}_t) = 0, \\ &\widetilde{w}(\overline{\mathbf{E}}, 0) = w^{(1)}(\overline{\mathbf{E}}), \end{aligned} \tag{A.6.1}$$

for $t \in [0, -\log(c)]$, where

$$H(\overline{\mathbf{E}}, \widetilde{w}, \bar{\mathbf{j}}) = \widetilde{w} + \max_a \langle a\mathbf{n} \cdot \bar{\mathbf{j}} - w^{(2)}(\overline{\mathbf{E}} + a\mathbf{n}) \rangle_\nu, \tag{A.6.2}$$

and where ν represents the reduced H-measure. For statistically isotropic composites with phase potentials of the form (A.2.1), the effective material has a potential of the form (A.1.3). Letting $r = \frac{\epsilon^{(1)}}{\epsilon^{(2)}}$, and $y = \frac{\widetilde{\epsilon}}{\epsilon^{(2)}}$, we find that y solves

$$y_t + h(y) = 0, \quad y(0) = r \tag{A.6.3}$$

where, for a given nonlinearity m, $h(x) = h_m(x)$ is given by

$$h_m(x) = x + \frac{1}{2\pi} \int_0^{2\pi} \left[(m+1)xa^* \cos(\varphi) - (1 + 2a^* \cos(\varphi) + (a^*)^2)^{(m+1)/2} \right] d\varphi \tag{A.6.4}$$

where a^* satisfies

$$x \cos(\varphi) - (a^* + \cos(\varphi))(1 + 2a^* \cos(\varphi) + (a^*)^2)^{(m-1)/2}. \tag{A.6.5}$$

Noting that $dy = \frac{\partial y}{\partial t}dt = -h(y)dt$, Eq. (A.6.3), can be used to show that y must satisfy

$$\int_r^y \frac{dx}{h(x)} = \log(c). \tag{A.6.6}$$

We look to find the first-order correction to $y = \frac{\widetilde{\epsilon}}{\epsilon^{(2)}}$ by assuming that

$$y = \frac{\widetilde{\epsilon}_0}{\epsilon^{(2)}} + \frac{\widetilde{\epsilon}_1}{\epsilon^{(2)}}\delta + O(\delta^2) = \frac{\widetilde{\epsilon}_0}{\epsilon^{(2)}} + \frac{\widetilde{\epsilon}_1}{\epsilon^{(2)}}(m-1) + O((m-1)^2), \tag{A.6.7}$$

so that

$$\frac{\widetilde{\epsilon}_1}{\epsilon^{(2)}} = \left.\frac{\partial y}{\partial m}\right|_{m=1}. \tag{A.6.8}$$

We first note that

$$a^*(1) \equiv a^*|_{m=1} = (y-1)\cos(\varphi) \implies h_1(y) = \frac{y^2-1}{2}. \tag{A.6.9}$$

Carrying out the integral in Eq. (A.6.6) and simplifying shows that the infinite rank laminate predicts the same behavior as the CCA in the linear limit, with $\widetilde{\epsilon}_0$ taking the same value as in Eq. (A.2.30).

Using Leibniz's rule, upon differentiating Eq. (A.6.6), we find that

$$\frac{\partial y}{\partial m}\frac{1}{h_m(y)} = \int_r^y \frac{\frac{\partial h_m(x)}{\partial m}}{h_m^2(x)}dx, \tag{A.6.10}$$

where

$$\frac{\partial h_m}{\partial m} = \frac{1}{2\pi}\int_0^{2\pi} \frac{\partial}{\partial m}\left[(m+1)xa^*\cos(\varphi) - (1+2a^*\cos(\varphi)+(a^*)^2)^{(m+1)/2}\right] d\varphi$$
$$= \frac{1}{2\pi}\int_0^{2\pi} xa^*\cos(\varphi)$$
$$- \frac{1}{2}(1+2a^*\cos(\varphi)+(a^*)^2)^{(m+1)/2}\log\left[(1+2a^*\cos(\varphi)+(a^*)^2)\right]$$
$$+ (m+1)\left[x\cos(\varphi) - (a^*+\cos(\varphi))(1+2a^*\cos(\varphi)+(a^*)^2)^{(m-1)/2}\right]\frac{\partial a^*}{\partial m}d\varphi$$
$$= \frac{1}{2\pi}\int_0^{2\pi} xa^*\cos(\varphi)$$
$$- \frac{1}{2}(1+2a^*\cos(\varphi)+(a^*)^2)^{(m+1)/2}\log\left[(1+2a^*\cos(\varphi)+(a^*)^2)\right] d\varphi, \quad \text{(A.6.11)}$$

having used Eq. (A.6.5). Recalling Eq. (A.6.9), and using Eq. (A.6.10), we find that

$$\frac{\widetilde{\epsilon}_1}{\epsilon^{(2)}} = 2((\widetilde{\epsilon}_0/\epsilon^{(2)})^2 - 1)\int_r^{\widetilde{\epsilon}_0/\epsilon^{(2)}} \frac{\frac{\partial h_m(x)}{\partial m}\Big|_{m=1}}{(x^2-1)^2}dx, \quad \text{(A.6.12)}$$

where

$$\frac{\partial h_m(x)}{\partial m}\Big|_{m=1} = \frac{1}{2\pi}\int_0^{2\pi} x(x-1)\cos^2(\varphi)$$
$$- \frac{1}{2}\log[\sin^2(\varphi)+x^2\cos^2(\varphi)](\sin^2(\varphi)+x^2\cos^2(\varphi))d\varphi. \quad \text{(A.6.13)}$$

By letting $a = \frac{x+1}{2}$ and $b = \frac{x-1}{2}$,

$$\sin^2(\varphi)+x^2\cos^2(\varphi) = \frac{x^2+1}{2} + \frac{x^2-1}{2}\cos(2\varphi)$$
$$= a^2 + 2ab\cos(2\varphi) + b^2. \quad \text{(A.6.14)}$$

Therefore, using the values of I_0 and I_1 in Appendix A.5, we find that

$$\frac{\partial h_m(x)}{\partial m}\Big|_{m=1} = \frac{x^2-1}{4} - \frac{x^2+1}{2}\log\left[\frac{x+1}{2}\right]. \quad \text{(A.6.15)}$$

Returning to Eq. (A.6.12), we see that

$$\frac{\widetilde{\epsilon}_1}{\epsilon^{(2)}} = \left(\left(\frac{\widetilde{\epsilon}_0}{\epsilon^{(2)}} \right)^2 - 1 \right) \int_r^{\frac{\widetilde{\epsilon}_0}{\epsilon^{(2)}}} \frac{1}{2(x^2-1)} - \frac{x^2+1}{(x^2-1)^2} \log \left[\frac{x+1}{2} \right] dx. \tag{A.6.16}$$

Upon evaluating this integral and simplifying, we find that the expression for $\widetilde{\epsilon}_1/\epsilon^{(2)}$ is identical to the one obtained for the CCA in Eq. (A.2.44).

Bibliography

Agoras, M., Lopez-Pamies, O., Ponte Castañeda, P., 2009a. A general hyperelastic model for incompressible fiber-reinforced elastomers. Journal of the Mechanics and Physics of Solids 57, 268–286.

Agoras, M., Lopez-Pamies, O., Ponte Castañeda, P., 2009b. Onset of macroscopic instabilities in fiber-reinforced elastomers at finite strain. Journal of the Mechanics and Physics of Solids 57, 1828–1850.

Agoras, M., Ponte Castañeda, P., 2013. Iterated linear comparison bounds for viscoplastic porous materials with "ellipsoidal" microstructures. Journal of the Mechanics and Physics of Solids 61, 701–725.

Avazmohammadi, R., Ponte Castañeda, P., 2014a. On the macroscopic response, microstructure evolution, and stability of short-fiber-reinforced elastomers at finite strains: I. analytical results. Philosophical Magazine 94, 1031–1067.

Avazmohammadi, R., Ponte Castañeda, P., 2014b. On the macroscopic response, microstructure evolution, and stability of short-fiber-reinforced elastomers at finite strains: Ii. representative examples. Philosophical Magazine 94, 1068–1094.

Avazmohammadi, R., Ponte Castañeda, P., 2016. Macroscopic constitutive relations for elastomers reinforced with short aligned fibers: Instabilities and post-bifurcation response. Journal of the Mechanics and Physics of Solids 97, 37–67.

Ball, J. M., 1977. Convexity conditions and existence theorems in nonlinear elasticity. Archive for Rational Mechanics and Analysis 63, 337–403.

Ball, J. M., James, R. D., 1987. Fine phase mixtures as minimizers of energy. Archive for Rational Mechanics and Analysis 100, 13–52.

Barchiesi, M., Gloria, A., 2010. New counterexamples to the cell formula in nonconvex homogenization. Archive for Rational Mechanics and Analysis 195, 991–1024.

Bensoussan, A., Lions, J., Papanicolaou, G., 1978. Asymptotic Analysis for Periodic Structures. North-Holland Publishing Co., Amsterdam.

Beran, M., 1965. Use of the variational approach to determine bounds for the effective permittivity in random media. Nuovo Cimento 38, 771– 782.

Bertoldi, K., Boyce, M. C., Deschanel, S., Prange, S. M., Mullin, T., 2008. Mechanics of deformation-triggered pattern transformations and superelastic behavior in periodic elastomeric structures. Journal of the Mechanics and Physics of Solids 56, 2642–2668.

Bertoldi, K., Gei, M., 2011. Instabilities in multilayered soft dielectrics. Journal of the Mechanics and Physics of Solids 59, 18–42.

Bhattacharya, K., 2003. Microstructure of Martensite: Why It Forms and How It Gives Rise to the Shape-Memory Effect. Oxford, New York.

Bhattacharya, K., Kohn, R. V., 1997. Elastic energy minimization and the recoverable strains of polycrystalline shape-memory materials. Archive for Rational Mechanics and Analysis 139, 99–180.

Bobeth, M., Diener, G., 1987. Static elastic and thermoelastic field fluctuations in multiphase composites. Journal of the Mechanics and Physics of Solids 35 (2), 137 – 149.

Borcea, L., Bruno, O., 2001. On the magneto-elastic properties of elastomer-ferromagnetic composites. Journal of the Mechanics and Physics of Solids 49, 2877–2919.

Braides, A., 1985. Homogenization of some almost periodic coercive functionals. Rendiconti della Accademia Nazionale delle Scienze detta dei XL 103, 313–322.

Braides, A., 1994. Loss of polyconvexity by homogenization. Archive for Rational Mechanics and Analysis 127, 183–190.

Braides, A., Fonseca, I., Leoni, G., 2000. $\mathcal{A}-$quasiconvexity: relaxation and homogenization. ESAIM Control, Optimization, and Calculus of Variations 5, 539–577.

Brown, W. F., 1966. Magnetoelastic Interactions. Springer-Verlag, New York.

Bustamante, R., Dorfmann, A., Ogden, R. W., 2008. On variational formulations in nonlinear magnetoelastostatics. Mathematics and Mechanics of Solids 13, 725–745.

Chen, T., Lai, D., 1997. An exact correspondence between plane piezoelectricity and generalized plane strain in elasticity. Proceedings of the Royal Society of London A: Mathematical, Physical and Engineering Sciences 453, 2689–2713.

Cohen, Y., Albalak, R. J., Dair, B. J., Capel, M. S., Thomas, E. L., 2000. Deformation of oriented lamellar block copolymer films. Macromolecules 33, 6502–6516.

Conti, S., 2008. Quasiconvex functions incorporating volumetric constraints are rank-one convex. Journal de Mathématiques Pures et Appliquées 90, 15–30.

Conti, S., DeSimone, A., Dolzmann, G., 2002. Soft elastic response of stretched sheets of nematic elastomers: a numerical study. Journal of the Mechanics and Physics of Solids 50, 1431–1451.

Conti, S., Dolzmann, G., 2015. On the theory of relaxation in nonlinear elasticity with constraints on the determinant. Archive for Rational Mechanics and Analysis 217, 413–437.

Conti, S., Lenz, M., Pawelczyk, M., Rumpf, M., 2018. Homogenization in magnetic-shape-memory polymer composites. Shape Optimization, Homogenization and Optimal Control 169, 1–17.

Dacorogna, B., 1989. Direct Methods in the Calculus of Variations. Springer, New York.

Dacorogna, B., Fonseca, I., 2002. $\mathcal{A}-\mathbb{B}$ quasiconvexity and implicit partial differential equations. Calculus of Variations and Partial Differential Equations 14, 115–149.

Dacorogna, B., Haiberly, J. P., 1998. Some numerical methods for the study of the convexity notions arising in the calculus of variations. Moddlisation mathmatique et analyse numrique 32, 153–175.

Danas, K., Idiart, M., Ponte-Castañeda, P., 2008. A homogenization-based constitutive model for two-dimensional viscoplastic porous media. Comptes Rendus Mecanique 336, 79–90.

Danas, K., Kankanala, S. V., Triantafyllidis, N., 2012. Experiments and modeling of iron-particle-filled magnetorheological elastomers. Journal of the Mechanics and Physics of Solids 60, 120–138.

d'Avila M. P., N., T., G., W., 2016. Localization of deformation and loss of macroscopic ellipticity in microstructured solids. Journal of the Mechanics and Physics of Solids 97, 275–298.

De Giorgi, E., 1975. Sulla convergenza di alcune successioni di integrali del tipo dellarea. Rendiconti di Matematica 6, 277–294.

deBotton, G., 2005. Transversely isotropic sequentially laminated composites in finite elasticity. Journal of the Mechanics and Physics of Solids 53, 1334–1361.

deBotton, G., Hariton, I., 2002. High-rank nonlinear sequentially laminated composites and their possible tendency towards isotropic behavior. Journal of the Mechanics and Physics of Solids 50, 2577–2595.

deBotton, G., Hariton, I., 2002. High-rank nonlinear sequentially laminated composites and their possible tendency towards isotropic behavior. Journal of the Mechanics and Physics of Solids 50 (12), 2577–2595.

deBotton, G., Hariton, I., Socolsky, E. A., 2006. Neo-hookean fiber-reinforced composites in finite elasticity. Journal of the Mechanics and Physics of Solids 54, 533–559.

deBotton, G., Ponte Castañeda, P., 1992. On the ductility of laminated materials. International Journal of Solids and Structures 29, 2329–2353.

DeSimone, A., Dolzmann, G., 2000. Material instabilities in nematic elastomers. Physica D 136, 175–191.

DeSimone, A., Dolzmann, G., 2002. Macroscopic response of nematic elastomers via relaxation of a class of so(3)-invariant energies. Archive for Rational Mechanics and Mathematics 161, 181–204.

Destrade, M., Ogden, R. W., 2011. On magneto-acoustic waves in finitely deformed elastic solids. Mathematics and Mechanics of Solids 16, 594–6042.

Dorfmann, A., Ogden, R. W., 2004. Nonlinear magnetoelastic deformations. Quarterly Journal of Mechanics and Applied Mathematics 57, 599–622.

Dorfmann, L., Ogden, R., 2014. Nonlinear Theory of Electroelastic and Magnetoelastic Interactions. Springer, New York.

Ekeland, I., Téman, R., 1976. Convex Analysis and Variational Problems. American Elsevier, New York.

Ericksen, J., Rivlin, R., 1954. Large elastic deformations of homogeneous anisotropic materials. Archive for Rational Mechanics and Mathematics 3, 281–301.

Fonseca, I., Kinderlehrer, D., Pedregal, P., 1994. Energy functionals depending on elastic strain and chemical composition. Calculus of Variations and Partial Differential Equations 2, 283–313.

Fonseca, I., Müller, S., 1999. $\mathcal{A}-$quasiconvexity, lower semicontinuity, and young measures. SIAM Journal of Mathematical Analysis 30, 527–558.

Francfort, G., 1992. Homogenisation of a class of fourth order equations with application to incompressible elasticity. Proceedings of the Royal Society of Edinburgh 120A, 25–46.

Francfort, G., Murat, F., 1986. Homogenization and optimal bounds in linear elasticity. Archive for Rational Mechanics and Analysis 94, 307–334.

Fredrickson, G. H., Bates, F. S., 1996. Dynamics of block copolymers: Theory and experiment. Annu. Rev. Mater. Sci. 26, 501–550.

Furer, J., Ponte Castañeda, P., 2018a. Macroscopic instabilities and domain formation in neo-hookean laminates. Journal of the Mechanics and Physics of Solids 118, 94–114.

Furer, J., Ponte Castañeda, P., 2018b. A symmetric fully optimized second-order method for nonlinear homogenization. Zeitschrift f ur Angewandte Mathematik und Mechanik 98, 222–254.

Furer, J., Ponte Castañeda, P., 2019. Reinforced elastomers: Homogenization, macroscopic stability, and relaxation. Journal of the Mechanics and Physics of Solids In Press.

Galipeau, E., Ponte Castañeda, P., 2013. A finite-strain constitutive model for magnetorheological elastomers: magnetic torques and fiber rotations. Journal of the Mechanics and Physics of Solids 61, 1065–1090.

Geymonat, G., Müller, S., Triantafyllidis, N., 1993. Homogenization of nonlinearly elastic materials, microscopic bifurcation and macroscopic loss of rank-one convexity. Archive for Rational Mechanics and Mathematics 122, 231–290.

Goshkoderia, A., Rudykh, S., 2017. Stability of magnetoactive composites with periodic microstructures undergoing finite strains in the presence of a magnetic field. Composites Part B 128, 19–29.

Grabovsky, Y., 1993. The g-closure of two well-ordered, anisotropic conductors. Proceedings of the Royal Society of Edinburgh 123A, 423–432.

Gurson, A., 1977. Continuum theory of ductile rupture by void nucleation and growth. Journal of Engineering Materials and Technology 99, 2–15.

Gurtin, M. E., Fried, E., Anand, L., 2010. The Mechanics and Thermodynamics of Continua. Cambridge University Press, New York.

Hariton, I., deBotton, G., 2002. The nearly isotropic behavior of high-rank nonlinear sequentially laminated composites. Proceedings of the Royal Society of London, A. 459, 157–174.

Hashin, Z., 1962. The elastic moduli of heterogeneous materials. Journal of Applied Mechanics 29, 143–150.

Hashin, Z., Rosen, B., 1964. The elastic moduli of fiber-reinforced materials. Journal of Applied Mechanics 31 (2), 223–232.

Hashin, Z., Shtrikman, S., 1962. A variational approach to the theory of the effective magnetic permeability of multiphase materials. Journal of Applied Physics 33, 3125–3131.

Hashin, Z., Shtrikman, S., 1963. A variational approach to the theory of the elastic behaviour of multiphase materials. Journal of the Mechanics and Physics of Solids 11 (2), 127–140.

Hill, R., 1963. Elastic properties of reinforced solids: some theoretical principals. Journal of the Mechanics and Physics of Solids 11, 357–372.

Hill, R., 1964. Theory of mechanical properties of fiber-strengthened materials: I. elastic behavior. Journal of the Mechanics and Physics of Solids 12, 199–121.

Hill, R., 1965. Continuum micro mechanics of elasto-plastic polycrystals. Journal of the Mechanics and Physics of Solids 13 (2), 89–101.

Hill, R., 1965. A self-consistent mechanics of composite materials. Journal of Mechanics and Physics of Solids 13, 213–222.

Hill, R., 1972. On the constitutive macro variables for heterogeneous solids at finite strain. Proceedings of the Royal Society of London A 326, 131–147.

Honeker, C. C., Thomas, E. L., Albalak, R. J., Hadjuk, D. A., Gruner, S. M., Capel, M. C., 2000. Perpendicular deformation of a near–single crystal triblock copolymer with a cylindrical morphology. 1. synchroton saxs. Macromolecules 33, 9395–9406.

Hutchinson, J. W., 1976. Bounds and self-consistent estimates for creep of polycrystalline materials. Proceedings of the Royal Society of London A: Mathematical, Physical and Engineering Sciences 348 (1652), 101–127.

Idiart, M., 2006. Macroscopic behavior and field statistics in viscoplastic composites. Ph.D. thesis, University of Pennsylvania.

Idiart, M., Ponte Castañeda, P., 2013. Estimates for two-phase nonlinear conductors via iterated homogenization. Proceedings of the Royal Society A 469, 20120626.

Idiart, M. I., 2008. Modeling the macroscopic beavior of two-phase nonlinear composites by infinite-rank laminates. Journal of the Mechanics and Physics of Solids 56 (8), 2599–2617.

Idiart, M. I., Moulinec, H., Ponte Castañeda, P., Suquet, P., 2006. Macroscopic behavior and field fluctuations in viscoplastic composites: Second-order estimates versus full-field simulations. Journal of the Mechanics and Physics of Solids 54, 1029–1063.

Idiart, M. I., Ponte Castañeda, P., 2007a. Field statistics in nonlinear composites. I.– theory. Proceedings of the Royal Society of London A: Mathematical, Physical and Engineering Sciences 463 (2077), 183–202.

Idiart, M. I., Ponte Castañeda, P., 2007b. Field statistics in nonlinear composites. II.– applications. Proceedings of the Royal Society of London A: Mathematical, Physical and Engineering Sciences 463 (2077), 203–222.

Idiart, M. I., Ponte Castaneda, P., 2013. Estimates for two-phase nonlinear conductors via iterated homogenization. Proceedings of the Royal Society of London A: Mathematical, Physical and Engineering Sciences 469 (2153).

Kankanala, S. V., Triantafyllidis, N., 2004. On finitely strained magnetorheological elastomers. Journal of Mechanics and Physics of Solids 52, 2869–2908.

Kohn, R. V., Little, T. D., 1998. Some model problems of polycrystal plasticity with deficient basic crystals. SIAM Journal on Applied Mathematics 59 (1), 172–197.

Kohn, R. V., Strang, G., 1986. Optimal design and relaxation of variational problems. i-iii. Communications on Pure and Applied Mathematics 39, 113–377.

Lahellec, N., Mazerolle, F., Michel, J., 2004. Second-order estimate of the macroscopic behavior of periodic hyperelastic composites: theory and experimental validation. Journal of Mechanics and Physics of Solids 52, 27–49.

Laws, N., 1973. On the thermostatics of composite materials. Journal of the Mechanics and Physics of Solids 21, 9–17.

Leblond, J., Perrin, G., Suquet, P., 1994. Exact results and approximate models for porous viscoplastic solids. International Journal of Plasticity 10, 213–235.

Leroy, Y., Ponte Castañeda, P., 2001. Bounds on the self-consistent approximation for nonlinear media and implications for the second-order method. Comptes Rendus de l'Academie des Sciences, Serie II 329 (8), 571–577.

Levin, V., 1967. Thermal expansion coefficients of heterogeneous materials. Mekh. Tverde. Tela 2, 83–94.

Lipton, R., 1988. On the effective elasticity of a two-dimensional homogenised incompressible elastic composite. Proceedings of the Royal Society of Edinburgh 110A, 45–61.

Lipton, R., Kohn, R., 1988. Optimal bounds for the effective energy of a mixture of isotropic, incompressible, elastic materials. Archive for Rational Mechanics and Analysis 102, 331–350.

Lopez-Pamies, O., Ponte Castañeda, P., 2006a. On the overall behavior, microstructure evolution and macroscopic stability in reinforced rubbers at large deformations: I theory. Journal of Mechanics and Physics of Solids 54, 807–830.

Lopez-Pamies, O., Ponte Castañeda, P., 2006b. On the overall behavior, microstructure evolution and macroscopic stability in reinforced rubbers at large deformations: Ii applications. Journal of Mechanics and Physics of Solids 54, 831–863.

Lopez-Pamies, O., Ponte Castañeda, P., 2009. Microstructure evolution in hyperelastic laminates and implications for overall behavior and macroscopic stability. Mechanics of Materials 41, 364–374.

Lurie, K., Cherkaev, A., 1984. Exact estimates of conductivity of composites formed by 2 isotropically conducting media taken in prescribed proportion. Proceedings of the Royal Society of Edinburgh Section A: Mathematics 99 (1-2), 71–87.

Lurie, K., Cherkaev, A., 1986. Exact estimates of a binary mixture of isotropic components. Proceedings of the Royal Society of Edinburgh 104A, 21–38.

Magnus, J. R., 1985. On differentiating eigenvalues and eigenvectors. Econometric Theory 1, 179–191.

Marcellini, P., 1978. Periodic solutions and homogenization of nonlinear variational problems. Ann. Mat. Pura Appl. 4, 139–152.

Maugin, G., Eringen, A., 1972. Deformable magnetically saturated media. 1. field equations. Journal of Mathematical Physics 13, 143–155.

Michel, J. C., Lopez-Pamies, O., Ponte Castañeda, P., Triantafyllidis, N., 2007. Microscopic and macroscopic instabilities in finitely strained porous elastomers. Journal of Mechanics and Physics of Solids 55, 900–938.

Michel, J. C., Lopez-Pamies, O., Ponte Castañeda, P., Triantafyllidis, N., 2010. Microscopic and macroscopic instabilities in finitely strained fiber-reinforced elastomers. Journal of Mechanics and Physics of Solids 58, 1776–1803.

Michel, J. C., Suquet, P., 1992. The constitutive law of nonlinear viscous and porous materials. Journal of the Mechanics and Physics of Solids 40 (4), 783–812.

Miehe, C., Vallicotti, D., Teichtmeister, S., 2015a. Homogenization and multiscale stability analysis in finite magneto-electro-elasticity. Gesellschaft für Angewandte Mathematik un Mechanik-Mitteilungen 38, 313–343.

Miehe, C., Vallicotti, D., Teichtmeister, S., 2015b. Homogenization and multiscale stability analysis in finite magneto-electro-elasticity. application to soft matter ee,

me and mee composites. Computer Methods in Applied Mechanics and Engineering 300, 294–346.

Milton, G., 1981. Bounds on the electromagnetic, elastic, and other properties of two-component composites. Physical Review Letters 46, 542–545.

Milton, G., 2002a. The Theory of Composites. Cambridge University Press, Cambridge.

Milton, G., Kohn, R., 1988. Variational bounds on the effective moduli of anisotropic composites. Journal of the Mechanics and Physics of Solids 36, 597–629.

Milton, G., Movchan, A., 1995. A correspondence between plane elasticity and two-dimensional real and complex dielectric equations in anisotropic media. Proceedings of the Royal Society of London A: Mathematical, Physical and Engineering Sciences 450, 293–317.

Milton, G., Phan-Thien, N., 1981. New bounds on the effective moduli of two-component materials. Proceedings of the Royal Society of London A 380, 305–331.

Milton, G. W., 2002b. The Theory of Composites. Cambridge University Press, Cambridge, England.

Milton, G. W., Serkov, S. K., 2000. Bounding the current in nonlinear conducting composites. Journal of the Mechanics and Physics of Solids 48 (6-7), 1295–1324.

Morrey Jr., C. B., 1952. Quasi-convexity and lower semicontinuity of multiple integrals. Pacific Journal of Mathematics 2, 25–53.

Moulinec, H., Suquet, P., 1998. A numerical method for computing the overall response of nonlinear composites with complex microstructure. Computer Methods In Applied Mechanics and Engineering 157 (1-2), 69–94.

Müller, S., 1987. Homogenization of non convex integral functionals and cellular elastic materials. Archive for Rational Mechanics and Analysis 99, 189–212.

Müller, S., Neukamm, S., 2011. On the commutability of homogenization and linearization in finite elasticity. Archive for Rational Mechanics and Analysis 201, 465–500.

Murat, F., Tartar, L., 1985. Calcul des variations et homogénísation. In: Cherkaev, A., Kohn, R. (Eds.), Les méthodes de l'homogénísation: théorie et applications en physique. Eyrolles, Paris, pp. 319–369.

Nesi, V., Talbot, D. R. S., Willis, J. R., 1999. Translation and related bounds for the response of a nonlinear composite conductor. Proceedings of the Royal Society of London A: Mathematical, Physical and Engineering Sciences 455 (1990), 3687–3707.

Neukamm, S., Schäffner, M., 2018. Quantitative homogenization in nonlinear elasticity for small loads. Archive for Rational Mechanics and Analysis 230, 343–396.

Odgen, R. W., 1978. Extremum principles in non-linear elasticity and their application to composites-i. theory. International Journal of Solids and Structures 14, 265–282.

Ogden, R., 1997. Non-linear Elastic Deformations. Dover, New York.

Ortigosa, R., Gil, A. J., 2016a. A new framework for large strain electromechanics based on convex multi-variable strain energies: Conservation laws, hyperbolicity and extension to electro-magneto-mechanics. Computer Methods in Applied Mechanics and Engineering 309, 202–242.

Ortigosa, R., Gil, A. J., 2016b. A new framework for large strain electromechanics based on convex multi-variable strain energies: Finite element discretisation and computational implementation. Computer Methods in Applied Mechanics and Engineering 302, 329–360.

Ottènio, M., Destrade, M., Ogden, R., 2008. Incremental magnetoelastic deformations, with application to surface instability. Journal of Mechanics and Physics of Solids 90, 19–42.

Parton, V., Buryachenko, V., 1990. Stress fluctuations in elastic composites. Sov. Phys. Dokl. 35, 191–193.

Peigney, B., Peigney, M., 2017. Bounds for nonlinear composite conductors via the translation method. Journal of the Mechanics and Physics of Solids, –.

Peigney, M., 2005. A pattern-based method for bounding the effective response of a nonlinear composite. Journal of the Mechanics and Physics of Solids 53 (4), 923–948.

Pisante, G., 2004. Homogenization of micromagnetics in large bodies. ESAIM: Control, Optimization and Calculus of Variations 10, 295–314.

Ponte Castañeda, P., Tiberio, E., 2000. A second-order homogenization method in finite elasticity and applications to black-filled elastomers. Journal of the Mechanics and Physics of Solids 48 (6), 1389–1411.

Ponte Castañeda, P., 1989. The overall constitutive behavior of nonlinear elastic composites. Proceedings of the Royal Society of London A 422, 147–171.

Ponte Castañeda, P., 1991. The effective mechanical properties of nonlinear isotropic composites. Journal of the Mechanics and Physics of Solids 39 (1), 45 – 71.

Ponte Castañeda, P., 1992a. Bounds and estimates for the properties of nonlinear heterogeneous systems. Phil. Trans. R. Soc. Lond. A 340, 531–567.

Ponte Castañeda, P., 1992b. A new variational principle and its application to nonlinear heterogenous systems. SIAM Journal of Applied Mathematics 52, 1321–1341.

Ponte Castañeda, P., 1996. Exact second-order estimates for the effective mechanical properties of nonlinear composite materials. Journal of Mechanics and Physics of Solids 44, 827–862.

Ponte Castañeda, P., 2001. Second-order theory for nonlinear dielectric composites incorporating field fluctuations. Phys. Rev. B 64, 214205.

Ponte Castañeda, P., 2002. Second-order homogenization estimates for nonlinear composites incorporating field fluctuations: I.– theory. Journal of the Mechanics and Physics of Solids 50 (4), 737 – 757.

Ponte Castañeda, P., 2012. Bounds for nonlinear composites via iterated homogenization. Journal of the Mechanics and Physics of Solids 60, 1583–1604.

Ponte Castañeda, P., 2015. Fully optimized second-order variational estimates for the macroscopic response and field statistics in viscoplastic crystalline composites. Proceedings of the Royal Society of London A: Mathematical, Physical and Engineering Sciences 471 (2184).

Ponte Castañeda, P., 2016. Stationary variational estimates for the effective response and field fluctuations in nonlinear composites. Journal of Mechanics and Physics of Solids 96, 660–682.

Ponte Castañeda, P., Galipeau, E., 2011. Homogenization-based constitutive models for magneto-rheological elastomers at finite strain. Journal of Mechanics and Physics of Solids 59, 194–215.

Ponte Castañeda, P., Kailasam, M., 1997. Nonlinear electrical conductivity in heterogenous media. Proceedings of the Royal Society of London A 453, 793–816.

Ponte Castañeda, P., Siboni, M. H., 2012. A finite-strain constitutive theory for electro-active polymer composites via homogenization. International Journal of Non-Linear Mechanics 47, 293–306.

Ponte Castañeda, P., Suquet, P., 1998. Nonlinear Composites. Advances in Applied Mechanics 34, 171–302.

Ponte Castañeda, P., Willis, J. R., 1995. The effect of spatial distribution on the effective behavior of composite materials and cracked media. Journal of the Mechanics and Physics of Solids 43 (12), 1919–1951.

Ponte Castañeda, P., Willis, J. R., 1999. Variational second-order estimates for nonlinear composites. Proceedings of the Royal Society of London A: Mathematical, Physical and Engineering Sciences 455 (1985), 1799–1811.

Prasman, E., Thomas, E. L., 1998. High-strain tensile deformation of a sphere-forming triblock copolymer/mineral oil. Journal of Polymer Science: Part B: Polymer Physics 36, 1625–1636.

Rice, J. R., 1976. The localization of plastic deformation. In: Theoretical and Applied Mechanics (Proceedings of the 14th International Congress on Theoretical and Applied Mechanics, Delft, 1976, ed. W.T. Koiter). North-Holland, pp. 207–220.

Rogers, R., 1988. Nonlocal variational problems in nonlinear electromagnetoelastostatics. SIAM Journal of Mathematical Analaysis 19, 1329–1347.

Rosen, B. W., 1965. Fiber Composite Materials. American Society for Metals, Metals Park, OH.

Rudykh, S., Bertoldi, K., 2013. Stability of anisotropic magnetorheological elastomers in finite deformations: A micromechanical approach. Journal of Mechanics and Physics of Solids 61, 949–967.

Rudykh, S., Bhattacharya, K., deBotton, G., 2014. Multiscale instabilities in soft heterogeneous dielectric elastomers. Proceedings of the Royal Society A 470.

Rudykh, S., deBotton, G., 2011. Stability of anisotropic electroactive polymers with application to layered media. Zeitschrift für angewandte Mathematik und Physik 62, 1131–1142.

Sanchez-Palencia, E., 1980. Non-Homogeneous Media and Vibration Theory. Springer-Verlag, Berlin.

Schröder, J., Neff, P., 2003. Invariant formulation of hyperelastic transverse isotropy based on polyconvex free energy functions. International Journal of Solids and Structures 40, 401–445.

Serrano, H., 2011. Reiterated homogenization of the vector potential formulation of a magnetostatic problem in anisotropic composite media. Nonlinear Analysis 74, 7380–7394.

Sewell, M. J., 1987. Maximum and Minimum Principles. Cambridge University Press, Cambridge, England.

Siboni, M. H., Avazmohammadi, R., Castañeda, P., 2014. Electromechanical instabilities in fiber-constrained, dielectric-elastomer composites subjected to all-around dead-loading. Mathematics and Mechanics of Solids 20, 729–759.

Silhavý, M., 2018. A variational approach to nonlinear electro-magneto-elasticity: Convexity conditions and existence theorems. Mathematics and Mechanics of Solids 23, 907–928.

Spagnolo, S., 1968. Sulla convergenza della soluzioni di equaziona paraboliche ed ellittiche. Annali della Scuola Normale Superiore di Pisa. Serie III 22, 571–597.

Steigmann, D. J., 2003. Frame-invariant polyconvex strain-energy functions for some anisotropic solids. Mathematics and Mechanics of Solids 8, 497–506.

Steigmann, D. J., 2004. Equilibrium theory for magnetic elastomers and magnetoelastic membranes. International Journal of Nonlinear Mechanics 39, 1193–1216.

Suquet, P., 1987. Elements of homogenization for inelastic solid mechanics. In: Sanchez-Palencia, E., Zaoui, A. (Eds.), Homogenization techniques for composite media. Springer-Verlag, Berlin, pp. 194–278.

Suquet, P., 1993. Overall potentials and extremal surfaces of power law or ideally plastic materials. Journal of the Mechanics and Physics of Solids 41 (6), 981–1002.

Suquet, P., Ponte Castañeda, P., 1993. Small-contrast perturbation expansions for the effective properties of nonlinear composites. Comptes Rendus de l'Academie des Sciences, Serie II 317 (12), 1515–1522.

Talbot, D. R. S., Willis, J. R., 1985. Variational principles for inhomogeneous nonlinear media. IMA Journal of Applied Mathematics 35, 39–54.

Talbot, D. R. S., Willis, J. R., 1985. Variational principles for inhomogeneous nonlinear media. IMA Journal of Applied Mathematics 35 (1), 39–54.

Talbot, D. R. S., Willis, J. R., 1992. Some simple explicit bounds for the overall behavior of nonlinear composites. International Journal of Solids and Structures 29 (14-15), 1981–1987.

Talbot, D. R. S., Willis, J. R., 2004. Bounds for the effective constitutive relation of a nonlinear composite. Proceedings of the Royal Society of London A: Mathematical, Physical and Engineering Sciences 460 (2049), 2705–2723.

Tartar, L., 1978. Quelques remarques sur lhomogénéisation. In: Fujita, H. (Ed.), Functional Analysis and Numerical Analysis. Japan Society for the Promotion of Sciences, Tokyo, pp. 469–481.

Tartar, L., 1985. Estimations fines des coefficients homogénéisés. In: Krée, P. (Ed.), Ennio de Giorgi Colloquium, Research Notes in Mathematics, Vol 125. Pitnam Publishing Ltd., London, pp. 168–187.

Tiersten, H., 1964. Coupled magneto mechanical equations for magnetically saturated insulators. Journal of Mathematical Physics 5, 1298–1318.

Toland, J., Willis, J. R., 1989. Duality for families of natural variational principles in nonlinear electrostatics. SIAM Journal of Mathematical Analysis 20 (6), 1283–1292.

Torquato, S., 1980. Microscopic approach to transport in two-phase random media. Ph.D. thesis, State University of New York, Stony Brook.

Torquato, S., 1991. Random heterogeneous media: Microstructure and improved bounds on effective properties. ASME Applied Mechanics Reviews 44, 37–76.

Triantafyllidis, N., Maker, B. N., 1985. On the comparison between microscopic and macroscopic instability mechanisms in a class of fiber reinforced composites. Journal of Applied Mechanics 52, 794–800.

Triantafyllidis, N., Nestorovic, M., Schraad, M. W., 2006. Failure surfaces for finitely strained two-phase periodic solids under general in-plane loading. Journal of Applied Mechanics 73, 505–515.

Truesdell, C., Toupin, R., 1960. The classical field theories. In: Handbuch der Physik, Vol III. Springer, Berlin, pp. –.

Wellander, N., 2001. Homogenization of the maxwell equations: Case i. linear theory. Applications of Mathematics 46, 29–51.

Wellander, N., 2002. Homogenization of the maxwell equations: Case ii. nonlinear conductivity. Applications of Mathematics 47, 225–283.

Willis, J., 1986. Variational estimates for the overall response of an inhomogeneous nonlinear dielectric. In: et al., J. L. E. (Ed.), Homogenization and effective moduli of materials and media. Springer-Verlag, New York, pp. 247–263.

Willis, J. R., 1977. Bounds and self-consistent estimates for the overall moduli of anisotropic composites. Journal of the Mechanics and Physics of Solids 25 (3), 185–202.

Willis, J. R., 1981. Variational and related methods for the overall properties of composites. Advances in Applied Mechanics 21, 1–78.

Willis, J. R., 1983. The overall response of composite materials. ASME Journal of Applied Mechanics 50 (4B), 1202–1209.

Willis, J. R., 1989. The structure of overall constitutive relations for a class of nonlinear composites. IMA Journal of Applied Mathematics 43 (3), 231–242.

Willis, J. R., 1991. On methods for bounding the overall properties of nonlinear composites. Journal of the Mechanics and Physics of Solids 39 (1), 73–86.

Yin, H. M., Sun, L. Z., 2006. Magneto-elastic modeling of composites containing chain-structured magnetostrictive particles. Journal of the Mechanics and Physics of Solids 54, 975–1003.